The anatomy, ultrastructure and mechanical properties of the locust metathoracic femoral chordotonal organ

by

Matthew E. Walker B.Sc. (Hons)

Department of Zoology
University of Leicester

January 1998

Thesis submitted for the degree of Doctor of Philosophy
at the University of Leicester

ProQuest LLC
789 East Eisenhower Parkway
P.O. Box 1346
Ann Arbor, MI 48106-1346

Statement

The accompanying thesis submitted for the degree of Ph.D., entitled "The anatomy, ultrastructure and mechanical properties of the locust metathoracic femoral chordotonal organ" is based on work conducted by the author in the Department of Zoology, University of Leicester, during the period January 1993 to January 1997.

All of the work recorded in this thesis is original unless otherwise acknowledged in the text or by references. None of the work has been submitted for another degree in this or any other University.

Signed.....

Date.30/1/1998

To Edward, Elaine, Lucy and Emily Walker
and Tom and Kathleen Paskin

ACKNOWLEDGEMENTS

This study was supported by the Biotechnology and Biological Sciences Research Council (formally SERC).

I am indebted to Peter Shelton for his time, patience, encouragement and tolerance in helping me over the last few years.

I would like to thank all those who have made my time at Leicester so rewarding, in particular Ted Gaten, Penny Butler and Jean Liggins who have humoured me on a daily basis. Recognition should also go to Magnus, Rory and Geordie with whom I have shared writing-up blues as well as a special thanks to Emma for suffering my fluctuating moods.

I am especially grateful to my mother and father for giving me the opportunity and encouragement to attend University and to pursue this study.

ABSTRACT

1. This thesis examines the anatomy, ultrastructure and mechanical properties of the metathoracic femoral chordotonal organ (mtFCO) in the locusts *Schistocerca gregaria* and *Locusta migratoria*. Some measurements were also made on the mtFCO of the giant grass hopper *Tropidacris collaris*. The mtFCO is of interest because of its complex mechanical linkages (the apodeme complex, Shelton *et al.*, 1992) and its wide range of receptor response types (Zill, 1985; Field and Pflüger, 1989; Matheson, 1990).

2. Electron microscopy has been used in conjunction with modern image analysis techniques to provide the first comprehensive description of the composition of each of the mtFCO's mechanical linkages.

3. This thesis provides the best evidence so far that the mtFCO of the locust is formed from two fused scoloparia, each of which is innervated by a separate branch of the CO nerve (nerve 5b1). It has been shown for the first time that the neurones of the mtFCO can be subdivided consistently into 6 discrete populations, each of which is innervated by a separate bundle of axons. Neurone size, shape and orientation vary between the populations.

4. The dendrites of the sensory neurones terminate in pairs in specialised scolopale cells in a manner similar to that previously described in other insect COs. This thesis provides the first description of the dendritic distortions which occur upon stimulation of an unfixed sense organ.

5. Biomechanical investigations have revealed that the mtFCO is a viscoelastic system. The results from this thesis suggest that the organ's mechanical properties are likely to be partly or wholly responsible for two documented phenomena common to all COs: hysteresis of the sensory output in response to cyclic elongation/relaxation (Burns, 1974; Matheson, 1990, 1992) and adaptation in firing rate following a step displacement (Usherwood *et al.*, 1968; Theophilidis, 1986).

Contents

Chapter 3: Ultrastructure of the mtFCO mechanical linkages

Chapter 7: Other Proprioceptors within the femur

Chapter 8: Discussion

Chapter 1: Introduction

In order to achieve co-ordinated and efficient movement, animals require sensory feedback from their appendages to determine their positions and patterns of motion. With respect to insect appendages, sense organs associated with each joint provide proprioceptive information that is centrally integrated and is used to generate appropriate motor output. Sensory information concerning the position and displacement of the metathoracic femoro-tibial joint of the locust is derived from a variety of mechanoreceptors. These include: the metathoracic femoral chordotonal organ (mtFCO) (Slifer, 1935; Usherwood *et al.*, 1968); a 'strand' type receptor associated with the mtFCO called the flexor strand (Usherwood *et al.*, 1968; Bräunig, 1985); tactile hairs around the femoro-tibial joint; campaniform sensilla (which signal cuticular stress) (Moran *et al.*, 1976); a muscle tension receptor (Theophilidis and Burns, 1979; Matheson and Field, 1995); and five multipolar sensory cells referred to as 'multipolar joint receptors' (Pflüger and Burrows, 1987) arranged in three groups (Coillot and Boistel, 1968). Of these, the mtFCO is almost certainly the most important source of sensory information concerning rotational movements of the tibia with respect to the femur (Usherwood *et al.*, 1968; Burns, 1974; Field and Rind, 1977, 1981; Hofmann *et al.*, 1985; Hofmann and Koch, 1985; Field and Pflüger, 1989; Matheson and Field, 1990; Matheson, 1990; Büschges, 1994; Kondoh *et al.*, 1995; Matheson, 1997; Newland and Kondoh, 1997a, b).

This thesis is a detailed study of the mtFCO of the locust. It describes its functional connections with other components of the leg; it shows how rotation of the tibia with respect to the femur results in displacement at the level of the mtFCO; it shows that it consists of identifiable groups of sensory neurones; it describes the ultrastructure, and it provides the first account of the way that the dendrites of these sensory neurones are displaced during tibial flexion. In addition, an investigation of the mechanical properties of the mtFCO sheds light on the way in which the neurones are stimulated.

Rotation of the femoro-tibial joint is governed by a neuronal network that modulates activity in the femoral muscles by processing sensory information about tibial position and movement largely provided by

afferents of the mtFCO. In the case of the locust mtFCO, the neurones can be broadly classified into two response types: tonic units which discharge continually at a given leg angle and whose rate may vary depending upon tibia position, and phasic units which discharge in response to changes in tibial position (Usherwood *et al.*, 1968; Zill, 1985a; Matheson 1990; Matheson and Field, 1990; Büschges, 1994; Kondoh *et al.*, 1995). The encoding properties of the locust mtFCO neurones vary across the entire population from units whose output varies with position (position sensitive units), through those that discharge during movement (velocity sensitive units) to those that discharge only at the start or end of displacements (acceleration sensitive units). Between the extremes of purely positional sensitive or purely acceleration sensitive units, there are cells that respond to mixtures of two or three of these parameters (Matheson, 1990; Kondoh *et al.*, 1995). The physiological basis for the differences between neurones is largely unknown (but see Zill, 1985a; Matheson, 1997).

The mtFCO is of particular interest because its morphology appears to play an intrinsic part in its functional operation, (e.g. Field, 1991; Shelton *et al.*, 1992; Nowel *et al.*, 1995). It lends itself to investigation, because it is comparatively large and is structurally complex. In addition, comparative information is available regarding the operation of its pro- and mesothoracic homologues. The study of the mtFCO should help in the understanding of general mechanisms associated with the control of limb position in animals.

1.1 Diversity of function amongst FCOs

Chordotonal organs (COs) in insect appendages each consist of an elastic ligament which spans the joint whose activity it monitors. Joint rotation causes extension or relaxation of the ligament so that bipolar sensory neurones embedded within the strand are induced to fire by the resulting mechanical distortion.

The locust mtFCO contains approximately 100 sensory neurones which form the 'scoloparium' which is located at the proximal end of the elastic strand. Previous studies have shown that the mtFCO is unusual in having a more complex morphology (Field, 1991; Shelton *et al.*, 1992) than that found in the chordotonal organs of the pro- and mesothoracic femora.

Theophilidis (1986a, b) showed that insects in which the limbs have not divergently evolved to perform specialised tasks (such as jumping) have similar COs in all femora. In particular, the common innervation patterns in all three (pro-, meso- and metathoracic) femora of *Decticus albifrons* led Theophilidis (1986a) to propose that in the early stages of orthopteran evolution, the hind legs were similar in structure to those of the pro- and mesothoracic segments, and that they subsequently became modified to meet the behavioural requirements of the insect. In the case of the locust the metathoracic leg is specialised for kicking and jumping. The distinctive morphology of the mtFCO is almost certainly a reflection of this. Since the pro- and mesothoracic legs are least functionally specialised and their FCOs have a simpler organisation, it is assumed that they are closer to the ancestral form.

A comparison of a variety of FCOs (locust- msFCO Burns, 1974; Field and Pflüger, 1989; mtFCO Matheson, 1990; Matheson and Field, 1990; Field, 1991; Shelton *et al.*, 1992: and stick insect- Füller and Ernst, 1973; see Hofmann *et al.*, 1985) has shown that they contain two separate scoloparia (a scoloparium is the name given to an organ containing a group of scolopidial-type receptors). This morphological subdivision of the FCO is often associated with functional specialisation (Kittmann and Schmitz, 1992). Thus, in the mesothoracic leg of the locust one scoloparium with large neurones is involved in mediation of resistance reflexes associated with the motor neurones driving the extensor and flexor tibiae muscles whilst the other one, containing smaller neurones, has been presumed to function as a vibration detector (Field and Burrows, 1982; Zill, 1987).

Similarities between the different insect orders in types and distribution of homologous mechanoreceptors (Finlayson, 1968; Howse, 1968; Wright, 1976) indicate that proprioceptive mechanisms evolved early and were conserved during phylogeny (Bräunig, 1982b). This is also probably true of the FCOs in different legs in spite of the obvious gross differences between the mtFCO and those in the femora of pro- and mesothoracic segments. If the fundamental properties of scolopidial receptors are similar in COs with different functions, it is likely that receptor specificity is heavily dependent upon the ways in which the receptors are mechanically connected to the joints with which they are associated. A significant part of this thesis examines the extent to which the mtFCO's mechanical linkages affect displacement of the receptor cell dendrites.

1.2 Physiological output of the mtFCO

Adrian (1926) was the first to use electrical amplification techniques to detect the pattern of impulses that passes up a sensory nerve when its end-organ is stimulated. The development of intracellular recording and staining techniques has enabled subsequent researchers to characterise the stimulus specificities of identified peripheral neurones and to determine the nature and locations of their central projections (e.g. in the locust: Bräunig, 1982a; Matheson, 1992a; Mücke and Lakes-Harlan, 1995).

The mtFCO is now one of the most intensively studied proprioceptors in insects. Proprioceptive output from the mtFCO is transmitted to the metathoracic ganglia via nerve 5b1 (Campbell, 1961) where synaptic connections are made with spiking (Burrows, 1987a) and non-spiking local interneurones (Burrows, 1987a, b). In addition, sensory neurones from the mtFCO make monosynaptic connections with the motor neurones that innervate the femoral muscles (Burrows, 1987b). Such connections enable the mtFCO to contribute to the reflex control of movements of the tibia (Burrows and Horridge, 1974; Field and Burrows, 1982) and other joints of the same limb (Field and Rind, 1981). For example upon forced flexion of the femoro-tibial joint the activity of the mtFCO results in excitation of the extensor tibiae motor neurones and inhibition of the flexor tibiae motor neurones (Burrows and Horridge, 1974; Field and Burrows, 1982). This results in resistance to imposed joint rotation and provides postural stability. In addition, mtFCO output is carried by intersegmental interneurones to other ganglia (Laurent, 1986; Laurent and Burrows, 1988) to influence reflex movements of adjacent legs (Laurent and Burrows, 1989b).

1.3 Evolution of chordotonal organs

A number of genes are required for the correct differentiation of the precursor cell and specification of sensillum type, one of which is the *'cut'* gene. It produces a homeodomain protein involved in determining cell identity. Manipulation of *cut* (Blochlinger *et al.*, 1991) allowed researchers to transform COs into sense organs that resembled trichoid sensilla and *vice versa*. This demonstrates that the two receptor types and their accessory cells are homologous with one another.

Sugawara (1996) proposed that the ancestral chordotonal organ consisted of an epidermally embedded scolopidium lacking any cuticular apparatus.

Previous authors had also speculated on the evolutionary origins of scolopidial mechanoreceptors. Schmidt and Gnatzy (1984) suggested that free sensory hairs like those found in Crustacea were the original mechanosensilla with scolopidial structure, whilst Rice (1975) suggested that either hair or campaniform sensilla could have been the ancestral form. Sugawara (1996) reasoned that such primitive scolopidia were at some point withdrawn into the body cavity to become chordotonal organs. Whilst the mechanism of mechanoelectric transduction has been investigated in some depth in the case of the epithelial sensilla (Thurm and Küppers, 1980; Erler and Thurm, 1981), there is considerable speculation as to the mechanism of transduction in COs (Moran and Varela, 1971; Rice *et al.*, 1973; Atema, 1973; Moran *et al.*, 1976; Wiederhold, 1976; Moran *et al.*, 1977; Wensler, 1977; Erler and Thurm, 1981; Thurm, 1981; French; 1988). This thesis investigates the ultrastructure of mtFCO sensilla. Comparison of the structure of the primary sensory cells in the mtFCO and epithelial sensilla is used to obtain insights into the possible mechanism of sensory transduction.

1.4 Development of chordotonal organs

Each chordotonal organ is comprised of many sensilla, the cells within each sensillum being derived from a single precursor cell (Bodmer *et al.*, 1987). Each of these precursors differentiates from an individual undifferentiated ectodermal cell (Okabe and Okano, 1997; Brewster and Bodmer, 1995, 1996) and gives rise to four cells: one bipolar neurone and three glial accessory cells (cap, scolopale and ligament) (McIver, 1985; Moulins, 1976). Lineage studies on *Drosophila* (Bodmer *et al.*, 1989; Jan and Jan, 1993) revealed the following pattern of divisions: first the CO precursor cell divides to form a ligament cell and another precursor cell. This precursor divides to give the cap cell and another precursor, which subsequently divides to give rise to the neurone and to a scolopale cell. The scolopale cell and neurone repose end to end, the neurone dendrite inserting into a central cavity that develops within the scolpale cell during development (Bodmer *et al.*, 1989). Initially the organ containing such four cell units begins to differentiate close to the organ's distal site of attachment on the integument. Subsequently the organ becomes proximally elongated so that the sensory cells come to lie in their final position (Hartenstein, 1988). Tibial 'pioneer' axons proceed proximally towards the CNS along specific pathways (Berlot and Goodman, 1984) thought to be based upon chemical gradients (Purves and Lichtman, 1985;

Serafini *et al.*, 1994; Kennedy *et al.*, 1994), cell to cell interactions (Taghert *et al.*, 1982; Bentley and Caudy, 1983; Condic *et al.*, 1989), and growth factors (Purves, 1986; Rohrer, 1990). The path established by the pioneer neurones is followed by subsequent developing afferent and efferent neurones during development (Edwards *et al.*, 1981), including those of the FCO (Klose, 1996).

1.5 The current study

The current study is an investigation of the structure and mechanical relations of the mtFCO in the locust. Most of the investigation concentrated on *Schistocerca gregaria* but comparisons were made with the same organ in *Locusta migratoria*. Some data were obtained from the large tropical grasshopper *Tropidacris collaris*. The study begins with a gross description of the connections of the mtFCO scoloparium with other parts of the leg. The behaviour of each of these connections during tibial rotation was studied using photography of living preparations. This part of the study was designed to characterise the gross input to the mtFCO scoloparium. It was hoped that this would indicate which components of leg displacement the organ is likely to monitor. This study shows that in addition to its linkage with the proximal end of the tibia, the mtFCO is also mechanically coupled to the apodeme of the flexor tibiae muscle via two separate connections. Thus, there is the possibility that the mtFCO responds not only to changing femoro-tibial angle, but also to flexor tibiae muscle tone. This thesis provides the first detailed description of the ultrastructure of the mtFCO's mechanical connections, as well as the ultrastructure of the scoloparium itself. In the past ultrastructural studies of this nature have been shown to provide valuable information regarding the way in which mechanical stimuli are transmitted to the transduction site. Thus, a number of authors have revealed the mechanical filtering role played by the lamella layers of the Pacinian corpusle (Pease and Quilliam, 1957; Loewenstein and Rathkamp, 1958; Loewenstein and Skalak, 1966). Such studies also allow insight into the possible mechanisms of sensory transduction itself. For instance, Moran *et al.* (1977) demonstrated distortion of dendritic cilia in electron micrographs of transversely sectioned dendrites from the pro- and mesothoracic FCOs of the grasshopper *Melanoplus bivittatus* fixed in different states of stimulation.

In the current study, light microscopy was used to show that the neurones of the mtFCO are divided into at least six groups. Neurones in these groups probably correspond to functionally different groups as identified by Matheson (1990) on the basis of their electrophysiological properties. To investigate whether the different neurone groups receive differential stimulation, the neurones were stained with fluorescent dye and visualised using confocal microscopy whilst the femoro-tibial angle was rotated to a range of different positions. The dendrites of each group of neurones was found to undergo characteristic buckling upon extension of the tibia.

There is little known regarding the mechanisms of mechanoreception, although there have been studies on hair receptors both external (Thurm, 1965; Gaffal *et al.*, 1975; Gaffal and Theiss, 1978; French and Sanders, 1979; Gnatzy and Tautz, 1980) and within the vestibular system (Vidal *et al*, 1971; Wilson and Peterson, 1980) and in muscle spindles (Lennerstrand, 1968; Kostyukov and Cherkassky, 1992). In order to reveal the nature of the forces to which the scoloparium is subjected, the mechanical properties of the mtFCO have been characterised using a small strain gauge. These investigations reveal that the mtFCO has viscoelastic properties which are likely to affect the organ's response properties.

In addition to investigating the ultrastructure of the mtFCO scoloparium, the ultrastucture of the neuronal component of the mtFCO flexor strand is described for the first time. The discharge of this receptor has been demonstrated to complement that of the mtFCO scoloparium (Zill, 1985a). In addition, a completely new mechanoreceptor was also revealed during this study. Its structure resembles that of the flexor strand. This receptor is situated distally in the femur at the level at which the mtFCO's cuticular apodeme arises from the proximal tip of the tibia. The receptor's structure suggests that its function may be to monitor the angle between the cuticular apodeme and the tibia as the tibia is rotated.

Chapter 2: Displacement of the mtFCO mechanical connections

2.1 SUMMARY

- *As the input displacement at the femoro-tibial joint is transmitted proximally along the apodeme complex, the magnitude of the displacement corresponding to different ranges of femoro-tibial articulation is reduced differentially. The largest displacements at the level of the scoloparium are over the femoro-tibial range of 60° - 90°.*

- *Despite the fusion between the dorsal and ventral ligaments of the mtFCO, dorsal ligament loop formation causes some degree of differential displacement between them. In addition, the fibres within the ventral ligament are organised so that they tighten sequentially during tibial flexion, further contributing to differential displacement across the apodeme complex ligaments. These phenomena may help to explain why different mtFCO neurones respond over different ranges of joint angle and represent a mechanical mechanism by which range fractionation could occur.*

- *The ventral attachment and the flexor strand both have mechanical roles relating to scoloparium distortion. Morphing maps show that the largest distortions occur in the distal most region of the scoloparium and that the pattern of distortion varies throughout the scoloparium.*

2.2 INTRODUCTION

In order to understand how tibial displacement results in physiologically relevant levels of displacement at the level of the sensory neurones in the mtFCO, it is necessary to characterise the way in which the sensory units are mechanically coupled to the joint. Previous studies of the mtFCO have been incomplete in this respect (Field, 1991; Shelton *et al.*, 1992), and the current work provides the first comprehensive description of the connections of the mtFCO to other parts of the leg and the way in which they are mechanically displaced in response to tibial rotation with respect to the femur.

Slifer (1935) provided one of the earliest accounts of femoral chordotonal organs in a study of the orthopteran *Melanoplus differentialis*. The study was largely concerned with their development in the femora of developing embryos. In addition, the gross morphology of the pro-, meso- and metathoracic organs in the adult was described. Few details of the structure and mechanical attachment of the organs were provided.

Usherwood *et al.* (1968) gave the first detailed description of the mtFCO in the locust. The account included a low resolution study of organ anatomy including a count of the number of sensory neurones present. Conclusive electrophysiological evidence that the function of the mtFCO was to monitor rotation of the tibia with respect to the femur was also provided. However, this description was incomplete and contained several errors. The mtFCO was described as being anchored dorsally via a short ligament to the posterior wall of the femur rather than to the anterior wall (Field and Burrows, 1982). Usherwood *et al.* (1968) also believed that the sensory neurones were mechanically connected to the tibia via a single filamentous apodeme. However, later workers (Field, 1991; Shelton *et al.*, 1992) have shown that the coupling consists of a thin cuticular apodeme arising from the proximal tip of the tibia. Proximally the apodeme is replaced by a pair of closely associated ligaments. This arrangement of twin ligaments and cuticular rod (named the 'apodeme complex' by Shelton *et al.*, 1992) exhibits a characteristic buckling behaviour at some femoro-tibial angles. Usherwood *et al.* (1968) also described the presence of numerous connective ligaments associating the mtFCO apodeme with the tibial extensor and flexor muscles. Shelton *et al.* (1992) found a cluster of these ligaments associated with the apodeme complex just proximal to the buckling region. They called them 'guy-rope fibres' and described them as being attached to unspecified connective tissue elements in the distal femur. The nature of the fibres and their distal termination were not fully understood and are investigated in this thesis. Apodeme complex buckling behaviour has been described in *Locusta migratoria* (Field, 1991) and *Schistocerca gregaria* (Shelton *et al.*, 1992). Comparison of these descriptions suggests that there are differences between the two species with respect to this aspect of mtFCO behaviour. In the current study comparison between the two species were made. It has been suggested that the anatomical arrangement of the apodeme complex provides the mechanical basis for range fractionation at the levels of the sensory neurones (Field, 1991; Shelton *et al.*, 1992). One of the aims of this thesis is to investigate whether the twin ligaments provide differential input to different populations of sensory neurones. Differences in buckling behaviour could affect the way in which differential inputs are generated.

The mtFCO is attached ventrally to the apodeme of the flexor tibiae muscle via a ligamentous ventral attachment (Usherwood *et al.*, 1968; Matheson and Field, 1990; Shelton *et al.*, 1992). The functional implications of

connections between the mtFCO and muscles within the femur have been discussed briefly by several authors (Field, 1991; Shelton *et al.*, 1992) but the role of the ventral attachment ligament has previously been overlooked. The first description of the behaviour of this attachment in response to changes in femoro-tibial angle will be given in this chapter. In addition to the ventral attachment, the mtFCO is also linked to the apodeme of the flexor tibiae by the flexor strand (Usherwood *et al.*, 1968; Field and Burrows, 1982). This strand both transmits displacements to the mtFCO and contains a single extension-sensitive strand receptor (Bräunig, 1985) whose axon joins the chordotonal organ nerve (nerve 5b1: nomenclature of Campbell, 1961). The displacements of the flexor strand are described in this chapter. Its ultrastructure has not been previously described and is discussed elsewhere (see Chapter 7).

For an understanding of how the input displacement causes sensory discharge from the mtFCO neurones, it is necessary to know in what way the sensory dendrites themselves are displaced as the femoro-tibial joint rotates. Although Usherwood *et al.* (1968) counted a population of 24 sensory neurones within the mtFCO, subsequent authors have found increasingly large numbers of neurones by using more critical techniques (Zill, 1985a; Grosch, 1985; Burrows, 1987; Pflüger *et al.*, 1988). Matheson and Field's (1990) study increased the total number of neurones within the mtFCO to approximately 100 and described how the neurones were subdivided into two distinct populations. This led them to conclude that the mtFCO may be composed of two fused scoloparia. The lack of knowledge regarding the displacement of the sensory dendrites has made it impossible to speculate on whether the neurones in the two scoloparia are stimulated over different ranges of joint movement. This thesis addresses the problem by mapping the relative displacement in different regions of the sensory scoloparia and by visualising the dendrites at different femoro-tibial angles.

This chapter contains a description of the behaviour of the main mtFCO mechanical linkages, followed by a quantitative analysis of the way in which the input displacement is transmitted to the sensory cells via the apodeme complex. Most of the description is based upon observations of the mtFCO in *S. gregaria*. Some differences were found between the situation in *S. gregaria* and *L. migratoria* and where these are significant these are described. Rotational movement of the joint results in relatively

large (1.2 mm) proximo-distal displacements of the mtFCO's cuticular apodeme (Field and Burrows, 1982). This report considers the way in which such large displacements of the apodeme lead to relatively small displacements in the vicinity of the sensory neurones. The nature of the input to the mtFCO is examined, and static displacements are used to show how rotation of the joint results in displacements of the mtFCO apodeme complex and the sensory scoloparium.

Previous authors have attempted to characterise the natural input to the mtFCO by analysing the locust walking cycle. Burns (1973) investigated the locust walking cycle using cinematography techniques. However, excessive heat from his cinematography lights almost certainly influenced the animal's behaviour. The walking cycle was investigated in this thesis using modern video image analysis methods.

2.3 METHODS

2.3.1 Dissection

Adult male and female specimens of two genera of locusts, *S. gregaria* and *L. migratoria*, were obtained from laboratory cultures. Metathoracic legs were removed and dissected under a Schott cold light source using a binocular dissecting microscope. The legs were dissected on a glass slide using Plasticine to secure the proximal end of the femur in each case. Insect saline (see Appendix 1) was added at intervals to prevent desiccation. Minimal dissections were performed by removing the cuticle overlying the organ on the anterior side of the femur, whilst leaving the epidermis intact. Some features of the mtFCO could then be observed through the epidermis with the use of strong incident light illuminating from an oblique angle. More extensive dissections were performed by removing a window of cuticle level with the mtFCO from the posterior face of the femur. The mtFCO was revealed lying against the anterior femur wall by the removal of the flexor tibiae muscle and femoral tracheae. Such preparations were viewed using an Olympus compound microscope. Illumination was provided using a single 1 mm diameter fibre-optic light guide attached to the side of the microscope objective by an adjustable collar. Preparations to be photographed were further dissected by removing another window of cuticle level with the organ from the anterior face of the femur. The extensor tibiae muscle, tracheae and

connective tissue were cleared away to give an unobstructed view of the mtFCO which was illuminated using transmitted light.

All preparations for microscopical observation were mounted on a slide, using quick-setting epoxy resin (Araldite) to secure the femur by its proximal end. As the Araldite dried, a Plasticine/Blue-tak bath was constructed on the slide around the leg. The preparation was then flooded with insect saline to prevent desiccation when it was placed on the microscope stage. Before measurements were made, the distal end of the tibia was amputated to make the leg easier to manipulate. A paper protractor aligned with the centre of rotation of the joint, was attached to the underside of the slide and orientated so that the femur lay along the base-line. This arrangement allowed the femoro-tibial angle to be measured over the full range of articulation (full flexion = 0°; full extension = 150°).

To enable displacements of the mtFCO attachments to be measured, fine grade carborundum powder (2 - 5 μm diameter granules) was gently spread onto the organ using a mounted hair. Many of the carborundum grains adhered to the organ and the excess grains were washed away. As the joint was rotated through 10° increments, the carborundum granules enabled displacements of points on the apodeme, ligaments and the scoloparia to be tracked. Displacement of the attachments at different femoro-tibial angles was measured either photographically using x10 and x40 objectives on a Zeiss S.L. photoscope or directly using a long working distance x10 water immersion objective in conjunction with a digital measuring eyepiece. A small Plasticine pellet was used to hold the tibia at 10° intervals of joint rotation. Some preparations were viewed using an inverted epifluorescence microscope equipped with a BioRad Lasersharp MRC 400 confocal laser scanning system fitted with a blue high-sensitive filter block to excite at 488 nm. The autofluorescent emission from the cuticular rod of the apodeme complex was detected at 515 nm and above. Images were stored on optical disc.

2.3.2 Morphing maps

In order to build up a picture of the relative displacements at the level of the sensory neurones, morphing maps were constructed from a series of photographs in which the scoloparia were marked with many carborundum markers. Successive images of the scoloparia at different

femoro-tibial angles were projected onto a sheet of graph paper using a photographic enlarger, and the locations of the carborundum markers were recorded. A grid was then plotted over the outline of the scoloparia at a femoro-tibial angle of 0° in which carborundum grains marked the location of the grid intersects. The grid was then re-plotted at different femoro-tibial angle placing the grid intersects upon the original markers. Differential movement between the markers resulted in two-dimensional distortion of the grid. Not every grid intersect could be associated with a marker. Such grid intersects were relocated after the tibia was rotated by plotting them at a proportional location between existing markers. Morphing maps were constructed at 30° intervals over the full range of femoro-tibial articulation (0° - 150°).

2.3.3 Analysis of the locust walking cycle

Locusts were filmed walking along a narrow runway. To allow filming, one side of the runway was made of Perspex. The floor of the runway was made of rough hardboard to provide a suitable surface to grip. The animals were persuaded to walk by lightly prodding the abdomen with a rod. The enclosure was rearranged vertically to obtain video records of climbing animals. A bench lamp was used to maintain the temperature at approximately 30°C. Video footage was analysed using a Panasonic AG6024 time-lapse video recorder with adjustable picture definition enabling each frame to be displayed as sharply as possible. A 24-inch screen Panasonic Prism A1 high resolution television was used to display the images. The tape was advanced a frame at a time to analyse the walking cycle and determine the maximum and minimum femoro-tibial angles whilst the animals were walking or climbing. These measurements were made on the screen using a protractor and measuring arm.
The sections of video tape that were analysed were selected from periods of continuous walking as both the maximum and minimum femoro-tibial angles decreased as the animals started or stopped.

2.4 RESULTS

2.4.1 General Anatomy

The mtFCO is located dorsally within the femur on the anterior side. The femur is internally organised so that the CO is positioned within an unobstructed longitudinal channel. The channel forms part of the dorsal haemolymph canal (Friedman, 1972a) and extends distally from the

sensory cell region of the organ towards the femoro-tibial joint. Laterally the dorsal haemolymph canal is bounded by the cuticular femur wall on the anterior side and by a trachea associated with the flexor-tibiae muscle apodeme on the posterior side. The CO is confined within the dorsal part of the femur by a septum of connective tissue interconnecting several tracheae which run along the longitudinal axis of the leg (Fig. 2.1). Whilst the mtFCO apodeme complex is dorsal to the septum, the flexor strand is ventral to it within the ventral haemolymph canal.

The main mechanical linkages of the mtFCO with other parts of the distal femur and proximal tibia are shown in Figure 2.2. The main mechanical connection joining the sensory cells of the CO to the tibia across the femoro-tibial joint is formed by the apodeme complex (Shelton *et al.*, 1992). Distally it consists of a cuticular rod that arises from the proximal tip of the tibia. Its origin is adjacent to that of the flexor-tibiae muscle apodeme and is located upon a projected cuticular process (Usherwood *et al.*, 1968; Field and Burrows, 1982). Proximally the cuticular rod tapers and gives rise to a pair of fused ligaments composed of elongated attachment cells. The dorsal ligament forms a continuation of the cuticular rod whist the ventral ligament is attached to the side of the rod near its proximal end.

The most distal elements of the ventral ligament arise approximately 500 μm from the proximal end of the rod and consists of a small cluster of attachment cells. Proximally the ventral ligament is supplemented by additional separate bundles of attachment cells arising from the side of the rod at regular intervals (Shelton *et al.*, 1992). When the apodeme complex is stretched (the tibia is flexed), both the ligaments lie parallel to one another. When the apodeme complex relaxes (tibia is extended), the dorsal ligament buckles to form a loop. Some of the fibres comprising the ventral ligament also slacken when the tibia is extended (Field, 1991; Shelton *et al.*, 1992) (see Figure 2.2). Associated with the apodeme complex is a cluster of approximately 20 guy-rope fibres. These fibres arise from the dorsal ligament immediately proximal to the loop-forming region and run distally to terminate dorsally near the femoro-tibial joint. The exact location of these distal terminations is investigated in Chapter 3.

The mtFCO is anchored dorsally to the anterior femur wall approximately 5 mm from the femoro-tibial joint by a short dorsal attachment. The

dorsal attachment is approximately 500 μm long and contains a muti-terminal receptor (Matheson and Field, 1990). Its role is to provide a proximal anchor point for the organ within the femur against which the remaining mtFCO mechanical linkages work to cause distortion of the sensory scoloparium. A second ligamentous attachment links the CO to the apodeme of the flexor muscle apodeme, ventral to the mtFCO cell body region (Usherwood *et al.*, 1968) (Fig. 2.2). This 'ventral attachment ligament' will be shown to have a variable role in contributing to the displacement of the scoloparium. It buckles over some parts of the femoro-tibial range and is taut over others.

The mtFCO is also associated with the flexor muscle apodeme via the 'flexor strand' (Usherwood *et al.*, 1968) which consists of a strand receptor organ with its cell body located in the metathoracic ganglion (Bräunig, 1982b). The flexor strand arises ventrally from the mtFCO scoloparium region and inserts onto the flexor-tibiae muscle apodeme distally, close to the femoro-tibial joint (Field and Burrows, 1982). The CO is innervated by nerve 5b1 which runs proximally from the organ along the ventral edge of the femur to enter the thorax and form synaptic connections in the metathoracic ganglion (Campbell, 1961).

2.4.2 Displacement of the main mechanical linkages

2.4.2.1 Displacement of the apodeme complex

The following account describes the roles of the components involved in buckling of the apodeme complex during tibial extension in both *S. gregaria* and *L. migratoria*.

S. gregaria

Buckling of the apodeme complex is dependent upon the guy-rope fibres associated with the dorsal ligament. The guy-rope fibres become increasingly stretched as the ligaments are displaced proximally during tibial extension from 0° - 30°. As the guy-rope fibres become increasingly taut, the dorsal ligament distal to their insertion upon it becomes increasingly slack. Upon further extension of the tibia (>30°), this portion of the dorsal ligament becomes fully unloaded and buckles to form the loop whilst the ventral ligament remains under tension (Fig. 2.3). The shape of the loop is determined by the cuticular rod which is displaced along the proximo-distal axis of the femur as the tibia is extended over the

range 0° - 100°. At angles greater than approximately 80° the proximal end of the rod rises up towards the dorsal surface of the femur (Fig. 2.3).

The distal ends of the attachment cells that form the ventral ligament are organised into approximately 20 functional bundles. These bundles (hereafter referred to as crossing fibres) attach at intervals along the proximal 500 μm of the apodeme. The lengths of the crossing fibres between their origins at the rod and their incorporation into the ventral ligament, vary from approximately 8 μm (fibres originating furthest from the mtFCO scoloparium), to approximately 20 μm long (fibres originating nearest the mtFCO scoloparium). This arrangement results in the loop-crossing fibres slackening in a sequential fashion upon extension of the tibia, the most proximal fibres (nearest the mtFCO scoloparium) unloading first. As the tibia is flexed the sequence is reversed, the distal-most fibres first tightening at a femoro-tibial angle of 80° (±10°) and most proximal fibres tightening at a femoro-tibial angle of 45° - 30° (Fig. 2.3).

L. migratoria

Previous descriptions of loop formation have seemed to indicate differences between *S. gregaria* and *L. migratoria*. Whilst parts of the ventral ligament remain under tension at all femoro-tibial angles in the case of *S. gregaria* (Shelton *et al.*, 1992) and only the dorsal ligament goes completely slack, both the dorsal and ventral ligaments become fully unloaded at extreme tibial extension in *L. migratoria* (Field, 1991). To understand the differences in behaviour between the two species, detailed observations were carried out on freshly dissected specimens. In addition to confirming the difference in the unloading of the dorsal and ventral ligaments during tibial extension, it was found that in *S. gregaria*, the cuticular rod rises dorsally above the plane of the apodeme complex as buckling occurs. In *L. migratoria*, the rod dips below the plane of the apodeme complex (Fig. 2.4). Minimal dissection of *L. migratoria* in which a window of cuticle overlying the apodeme complex was removed from the anterior face of the femur, allowed the displacement of the cuticular rod to be observed through the intact epidermis. In such dissections, the cuticular rod does not appear to flip ventrally to the extent observed in more extensively dissected specimens. This could indicate that the dorso-ventral displacement of the apodeme complex in the intact femur is restricted, possibly by a connective tissue septum which separates the dorsal and ventral haemolymph canals. The difference in loop formation

between the two genera is attributable to a morphological difference in the way the mechanical components comprising the apodeme complex are connected together. Although the structure of the loop-forming region of the apodeme complex is similar in both *S. gregaria* and *L. migratoria*, in *S. gregaria* the guy-rope fibres leave the dorsal ligament immediately proximal to the loop forming region. In *L. migratoria* they arise approximately 200 μm proximal to the loop forming region (Fig. 2.4a). This portion of the apodeme complex is relatively unsupported and so twists as buckling occurs allowing the cuticular rod to dip below the plane of the apodeme complex (Fig. 2.4b). These observations have functional implications and suggest differences between the two genera. If both of the ligaments become slack over a significant part of the range of femoro-tibial angles (as in *L. migratoria*), the potential for range fractionation is reduced.

2.4.2.2 Extensibility of the cuticular rod

The cuticular rod of the apodeme complex has been described previously as a purely inextensible structure (Shelton *et al.*, 1992). Field (1991) described the proximal 110 μm of the rod as being hinged. In the present study, the proximal region of the rod was visualised by confocal scanning light microscopy using the autofluorescent properties of the cuticle to reveal its structure. It was found that the terminal 100 μm of the rod is straight when under tension and that it buckles like a spring when the dorsal ligament is slack. This was found to be true in both *L. migratoria* (Fig. 2.5a-d) and *S. gregaria* (not shown). This shows that the rod has limited extensibility at the proximal tip.

2.4.2.3 Ventral attachment ligament

The ventral attachment ligament consists of a short (approximately 700 μm when taut) ligament which inserts onto the apodeme of the flexor-tibiae muscle (Usherwood *et al.*, 1968; Matheson and Field, 1990). When the leg is flexed, the ventral attachment is taut and lies parallel to the CO nerve, opposing distal organ displacement in a similar manner to the mtFCO dorsal attachment. However, unlike the dorsal attachment the ventral attachment has a variable role in contributing to the behaviour of the organ depending on joint angle. It becomes unloaded as femoro-tibial angle increases.

Over the range of femoro-tibial angles 0° - 40° the ventral attachment ligament is gradually unloaded. At femoro-tibial angles in excess of 45°, the ligament becomes slack and buckles. When the tibia is fully extended in *S. gregaria,* the insertion of the ventral attachment ligament onto the flexor tibiae apodeme lies immediately ventral to the sensory scoloparium (Figs 2.6a-d). The ligament buckles under the guidance of several short 'guy-rope' type fibres. These fibres leave the ligament towards its proximal end, and insert onto the apodeme of the flexor tibiae muscle both proximal and distal to the main attachment of the ligament (Figs 2.7a, b).

The degree of displacement of the ventral attachment is determined by the location of the distal insertion of the flexor tibiae apodeme upon the tibia relative to the fulcrum of the joint (Fig. 2.8). The mean range of proximo-distal displacement of the ventral attachment at its insertion onto the flexor tibiae apodeme is 1983.8 μm (±SD 304.3 μm, n=16).
Buckling of the ventral attachment occurs because as the tibia is extended, the apodeme of the flexor tibiae muscle to which this ventral attachment ligament is attached is displaced distally relative to the mtFCO. This shortens the distance between the insertion of the ligament onto the flexor tibiae muscle apodeme and the mtFCO, causing unloading of the ligament.

There are differences between *S. gregaria* and *L. migratoria* in the behaviour of the ventral attachment ligament. It is only taut at femoro-tibial angles of 0° - 40° in *S. gregaria* (Figs 2.6a-d), whereas it becomes taut at both extremes of flexion and extension (femoro-tibial angles 0° - 40° and 135° - 150°) in *L. migratoria* (Figs 2.9a-c).

2.4.2.4 Displacement of the flexor strand

As in the case of the ventral attachment, the ligamentous flexor strand runs distally from the organ to insert onto the apodeme of the flexor tibiae muscle close to the latter's insertion at the base of the tibia (Usherwood *et al.*, 1968). This insertion into the tibia is situated in such a way relative to the distal insertion of the apodeme complex and the centre of joint rotation, that in response to joint rotations the strand organ ligament moves antagonistically with respect to the apodeme complex of the mtFCO (Field and Burrows, 1982). The axial displacement of the flexor strand at different femoro-tibial angles was measured using pairs of carborundum markers located at different proximo-distal levels along its length (Fig. 2.10). Each pair of markers were located 65 μm apart at a femoro-tibial

angle of 0°. When the femoro-tibial angle was changed from 150° the proximal pair of markers moved further apart (17.8 μm) than the distal pair (10 μm), indicating that the flexor strand is more compliant proximally than distally.

2.4.2.5 Combined role of the ventral attachment and flexor strand

In conjunction with the other mechanical connections, the ventral attachment ligament and flexor strand contribute to the displacement of the mtFCO by causing a rotatory displacement of the scoloparium. Over the full range of tibial articulation the scoloparium containing the sensory neurones undergoes a rotatory movement of approximately 20° (Figs 2.11a-e). The displacement of the proximal apodeme complex ligaments, in which the sensory dendrites are located, remains axial. Considering the orientation of the mtFCO scoloparium upon extension of the tibia from a femoro-tibial angle of 0°, slackening of the ventral attachment contributes to the rotational motion over the range of femoro-tibial angles 0° - 40°. Increasing tension within the flexor strand continues the rotation over the remainder of the range of femoro-tibial angles in conjunction with the unloading of the apodeme complex. In *L. migratoria* this rotational motion is further accentuated at extreme tibial extension by the ventral attachment, which becomes taut once again at femoro-tibial angles in excess of 110° and supplements the disto-ventral pull of the flexor strand (Figs 2.9a-c). Since the ventral ligament remains slack at all femoro-tibial angles in excess of 40° in *S. gregaria*, the rotational motion is less pronounced.

2.4.3 Quantitative analysis of the way in which the mechanical input is transmitted to the sensory cells in *S. gregaria*

Discharges of sensory neurones in the mtFCO scoloparium are initiated or modulated by input displacements arising at the level of the femoro-tibial joint. These are transmitted proximally via the mtFCO's mechanical linkages to effect distortion of individual scolopidia. The way in which this occurs and the magnitude of the displacements at the level of the scoloparium has not been characterised previously. Here, the nature of the input and its mechanical transduction to the level of the mtFCO sensory neurones is described.

2.4.3.1 Locust walking cycle

A total of 21 cycles from 7 animals were analysed for each activity to produce a table showing the mean maximum and mean minimum femoro-tibial angles during walking and climbing in *S. gregaria* (Table 2.1).

Table 2.1

Mean femoro-tibial angle (°) ± standard deviation		
	Minimum	Maximum
Walking	29.2° (±9.7°)	76.3° (±9.2°)
Climbing	28.2° (±3.5°)	96.2° (±14.9°)

When walking, the femoro-tibial angle oscillates over a mean range of approximately 47°; whilst the animal is climbing vertically the mean range of femoro-tibial angles is increased to about 68°. The walking cycle is divided into protraction and retraction phases and resembles a saw-tooth wave, showing approximately linear changes in femoro-tibial angle at a mean frequency of 1.6 Hz (Fig. 2.12). During the retraction phase the tibia is elevated and moved forwards relative to the body and the ground in preparation for a step. During the protraction phase the leg moves backwards relative to the body but not the ground. The retraction of the tibia occurs faster (275° sec^{-1}) and occupies a smaller proportion of the walking cycle than the slower (137.5° sec^{-1}) tibial protraction. Thus, approximately 30% of the cycle is represented by retraction and 70% by protraction. This results in the mtFCO apodeme complex being extended at twice the velocity at which it is relaxed. Due to the nature of its mechanical coupling, the organ's ventral attachment to the apodeme of the flexor tibiae muscle will also be pulled taut faster than it is unloaded over the femoro-tibial range of angles 0° - 40° (see Figure 2.8). The converse will be true of the mtFCO flexor strand which will be extended at a slower rate than that at which it is relaxed. These observations have implications regarding the discrimination of proprioceptive information over different parts of the femoro-tibial range. These will be dealt with in the discussion section below. A similar pattern of activity occurs during climbing (results not shown) except that the range of movement is greater.

2.4.3.2 Displacement of the cuticular rod

The input to the mtFCO varies sinusoidally in response to linear angular rotation of the femoro-tibial joint, due to the eccentric location of the

cuticular rod's distal origin (on the tibia) with respect to the centre of rotation of the femoro-tibial joint. The magnitude of the input is determined by the distance between the rod's origin and the centre of joint rotation. Because of the rotatory movement of the femoro-tibial articulation, the input to the apodeme complex has a dorso-ventral as well as proximo-distal component. However, over the range of femoro-tibial angles of the walking cycle, the proximo-distal element of the displacement of the distal attachment of the apodeme complex is approximately linear (Fig. 2.13).

The displacement of the proximal end of the cuticular rod is predominantly proximo-distal because of the supporting influence of the guy-rope fibres (see Figure 2.2). It reflects the proximo-distal component of the input at the distal end of the rod. However, the magnitude of proximo-distal displacement at the proximal end is smaller than that at the distal end due to the influence of the dorso-ventral component of the input displacement at the distal end (Fig. 2.14).

2.4.3.3 Modification of the input due to the properties of the ligaments

Rotations of the femoro-tibial joint result in relatively large displacements (approximately 1000 μm) of the distal apodeme complex. The elasticity of the apodeme complex ligaments at the proximal end of the complex has the effect of decreasing the magnitude of the stimulus displacement as it is transmitted proximally. The displacement of the apodeme complex at different proximo-distal levels in response to rotation of the femoro-tibial joint is shown in Figure 2.15. The range of proximo-distal displacement of the apodeme complex is reduced approximately 30 fold as it is transmitted along the apodeme complex to the level of the mtFCO neurones (Fig. 2.16).

From the level of the guy-rope fibres to the distal-most sensory neurones and over the full range of femoro-tibial rotation, the magnitude of the displacement measured along the mid-line of the apodeme complex ligaments decreases linearly with distance from the femoro-tibial joint (Fig. 2.17). This indicates that the ligaments act as a linear elastic coupling between the cuticular rod and the sensory neurones. Linearity is lost at the level of the sensory neurones.

2.4.3.4 Displacement of the dorsal and ventral ligaments

The ligamentous portion of the apodeme complex is formed by the fusion of dorsal and ventral ligamentous components. These dorsal and ventral components are coupled to the cuticular rod in different ways and this has given rise to speculation that the dorsal and ventral ligaments may behave independently to some degree (Field, 1991; Shelton *et al.*, 1992). Measuring the displacement of the apodeme complex ligaments at their dorsal and ventral margins shows that the two ligaments undergo a degree of differential movement in response to changes in femoro-tibial angle (Fig. 2.18). The degree of differential movement between the dorsal and ventral ligaments decreases proximally as the magnitude of displacements are scaled down. The ventral ligament undergoes a wider range of proximo-distal displacement than the dorsal ligament at most levels. At the most proximal levels (the scoloparium) this trend is reversed, the dorsal ligament having a wider range of proximo-distal displacement than the ventral ligament (Fig. 2.19). These differences are discussed below.

2.4.4 Elastic properties of the dorsal and ventral ligaments

Comparing the maximum displacement of the dorsal and ventral apodeme complex ligaments at different proximo-distal levels shows that the two ligaments have different mechanical properties along their lengths (Fig. 2.19). The dorsal ligament is subject to a smaller range of displacement than the ventral ligament. This can be attributed to the formation of the apodeme complex dorsal loop at femoro-tibial angles greater than 30° - 45°. The range of ventral ligament displacement at increasingly proximal levels is linearly related to position along the ligament. This indicates that the ventral ligament is linearly elastic proximal to the guy-rope fibres. However, the pattern of displacement of the dorsal ligament at different proximo-distal levels indicates that the ligament is more compliant at one end than the other.

This situation was clarified by comparing the distances between pairs of equidistant markers located at the opposite ends of each ligament following an imposed displacement. The markers of each pair were located 191 μm apart when the ligaments were relaxed (femoro-tibial angle 150°). The distance between each pair of markers was measured after the tibia was fully flexed (Fig. 2.20). In the case of the ventral ligament, the distance between the proximal marker pair increased by the same distance as the distance between the distal marker pair as the mtFCO was stretched.

The distance between the dorsal marker pairs increased differentially as the mtFCO was stretched. The distance between the proximal markers increased by more than the distance between the distal markers. This confirms that whilst the ventral ligament is equally elastic at its proximal and distal ends, the dorsal ligament is more compliant proximally than it is distally. This has implications regarding the input to the sensory scoloparium. Scolopidia in series with the more compliant dorsal ligament may be subject to smaller forces than those in series with the ventral ligament for a given tibial displacement. Alternatively, sensory dendrites running into the dorsal ligament may be subject to increased distortion relative to those running into the stiffer ventral ligament.

2.4.5 Other factors affecting the displacement pattern at proximal levels within the apodeme complex ligaments

At the level of the femoro-tibial joint the relationship between proximo-distal displacement of the apodeme complex and femoro-tibial angle is sinusoidal (see Figure 2.13). The following results show that at more proximal levels within the ligaments of the apodeme complex, the displacements diverge from the sinusoidal relationship. A number of factors probably contribute to this including the sequential attachment cell recruitment (ventral ligament) and the loop forming region (dorsal ligament).

This was demonstrated by plotting proximo-distal displacement against femoro-tibial angle at different proximo-distal levels along the apodeme complex. Displacements at each level were then compared to those at the level of the femoro-tibial joint. To make such comparisons, the displacement at each proximo-distal level was scaled such that the range of displacement was of the same magnitude as that at the level of the femoro-tibial joint (Fig. 2.21). The difference between the input displacement curve (the graph of displacement at the joint) and the scaled displacement curve describes the way in which the input signal has been qualitatively modified by the apodeme complex as it is transmitted from the femoro-tibial joint. The input displacement curve was subtracted from the scaled displacement curve to show the degree of modification with femoro-tibial angle.

At the level of the guy-rope fibres, the input displacement is modified such that at femoro-tibial angles between 40° - 110° the ligaments are

undergoing relatively more displacement than over the remainder of the femoro-tibial range. This is the range of femoro-tibial angles involved in the locust walking cycle. This phenomenon represents selective amplification of the input over this range of femoro-tibial angles (Fig. 2.22). At increasingly proximal levels (at the level of the sensory neurones) the degree of selective amplification approximately doubles compared with that measured at the level of the guy-rope fibres. In addition, the femoro-tibial angles over which selective amplification occurs decreases to a bandwidth of approximately 45° over the middle of the femoro-tibial range.

To understand how tibial rotation affects the sensory neurones it is most important to characterise displacements at the level of the scoloparium. To achieve this, the effect of selective amplification upon absolute displacement was measured at four different proximo-distal levels along the mtFCO scoloparium. The range of proximo-distal displacement in response to 30° rotations of the femoro-tibial joint was measured over different parts of the full range of femoro-tibial rotation (0°-30°, 30°-60°, 60°-90°, 90°-120° and 120°-150°) (Fig. 2.23a-d). The series of histograms shows that at more proximal levels within the scoloparium the displacements occurring in response to changes in femoro-tibial angle over the range 60° - 90° are preferentially transmitted to the level of the sensory-neurones (Figs 2.23b-d). Those displacements occurring on either side of this range are selectively reduced. A comparison of the input displacement with the displacement measured in the centre of the scoloparium in a number of preparations shows that the average femoro-tibial angle at which maximum relative amplification occurs is 62.75° ± SD 12.5 (Fig. 2.24). This angle falls in the mid-range of the locust walking cycle.

2.4.6 Analysing the 2 dimensional displacement of the mtFCO scoloparium

The reversible changes in shape of the mtFCO scoloparium with flexion and extension of the tibia show that it has elastic properties. This elasticity is likely to be associated with fibrous sheathing material that surrounds the organ (Shelton *et al.*, 1992). Elastic elements within the scoloparium are also likely to be present. Because of the elasticity within the whole system, rotational movements of the tibia leads to longitudinal displacement of the scoloparium as a whole. However, the meaningful

displacement at the level of the sensory scolopidia is the relative displacement occurring between the tip of the sensory dendrites and the sensory somata. Such displacement provides a measure of the degree to which the sensory units are stretched/distorted.

The relative displacements of different regions of the mtFCO scoloparium at the level of the sensory neurones was characterised by the construction of a series of two-dimensional 'morphing' maps. These maps show how Cartesian co-ordinates projected onto the surface of the scoloparium would be distorted with respect to one another with rotatory displacements of the tibia. The distortion patterns were generated by reference to carborundum markers on the surface of the mtFCO (see Methods, this chapter). The maps also show how the scoloparium as a whole is displaced within the femur during tibial rotation (Figs 2.25a-f).

As the tibia is rotated from 0° to 150° the region of the mtFCO containing the sensory neurones becomes increasingly distorted. Whilst the proximo-distal axis becomes compressed with tibial extension, the dorso-ventral axis becomes increasingly stretched. This is due to the influence of the flexor strand whose tension increases with increasing femoro-tibial angle.

Overlying morph maps representative of the full range of femoro-tibial rotation show the range over which the scoloparium is displaced within the femur (Fig. 2.26). There is a rotatory motion of the sensory neurone-containing region of the mtFCO due to the antagonistic action of the apodeme complex and flexor strand. In addition, the ventral attachment contributes to this rotational displacement as it slackens over the range of femoro-tibial angles 0° - 40° in both *S. gregaria* and *L. migratoria*. In *L. migratoria* the ventral attachment also contributes to the rotational motion over the femoro-tibial range 135° - 150° as previously described (see Figures 2.9a-c).

2.5 DISCUSSION

The mtFCO apodeme complex is arranged so as to convert rotatory input displacement at the level of the articulation of the tibia with the femur into longitudinal displacements along the axis of the femur at the level of the sensory scoloparium. In this respect the role of the apodeme complex

is analogous to that of a linkage between a wheel and piston on a locomotive:

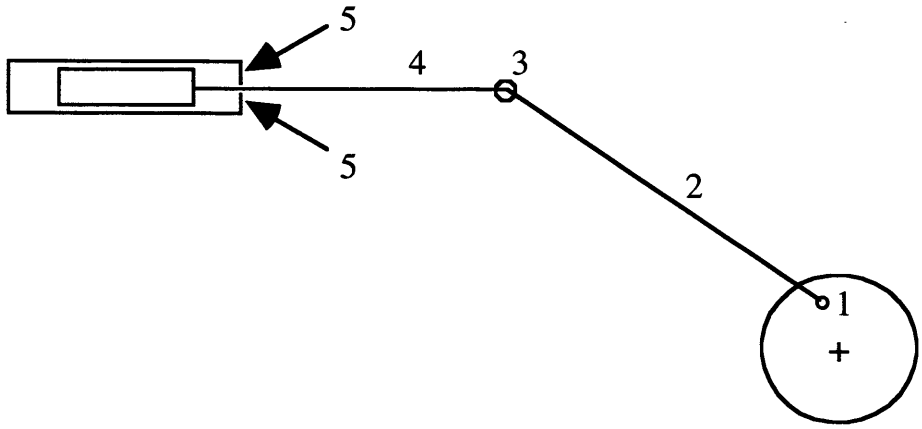

In this model rotational displacement of point 1 as the wheel rotates represents displacement of the distal attachment of the cuticular rod around the centre of rotation of the femoro-tibial joint. This displacement is transmitted along a shaft (2) representing the cuticular rod, to a joint (3), analogous to the junction of the cuticular rod with the ligaments (4). The piston guides (5) effect the conversion of the rotational displacement of the input into longitudinal displacements of the piston and represent the role of the guy-rope fibres. The piston itself represents the mtFCO scoloparium.

2.5.1 Input to the mtFCO

Rotation of the femoro-tibial joint results in relatively large displacements of the distal apodeme complex. Usherwood *et al.* (1968), measured the proximo-distal displacement of the cuticular rod to be 1.9 mm over a 170° range of femoro-tibial angles in female *S. gregaria*. (This large range of tibial rotation may reflect damage or distortion of the femoro-tibial joint). In the current study it was found that the tibia rotates over the range 0° - 150° but that it can be force to move to 160° by distorting the femoro-tibial joint. Subsequent workers measured the range of displacement of the cuticular rod to be 1.2 - 1.3 mm in *S. gregaria* (Field and Burrows, 1982) which is the same as that which was found in this study (femoro-tibial range 0° - 150°). During the locust walking cycle the change in femoro-tibial angle with time resembles a saw-tooth wave comprising short approximately linear changes in femoro-tibial angle. Within each cycle, the mean range of femoro-tibial rotation was found to be 47°. This value is very similar to that observed by Burns (1973) (50°), but greater than that observed by Usherwood *et al.* (1968) (30°). As in the current study, both Burns (1973) and Burrows (unpublished 1994, 1996) observed that tibial

retraction occupies a smaller proportion of the walking cycle than tibial protraction. This results in the mtFCO being stretched faster than it is relaxed. Over the walking range the relationship between femoro-tibial angle and displacement of the distal attachment of the apodeme complex is such that linear angular rotation of the femoro-tibial joint results in approximately linear proximo-distal displacement of the cuticular rod.

The eccentric location of the distal attachment of the cuticular rod (approximately 1 mm from the fulcrum) provides a relatively large input to the mtFCO in response to tibial rotation. This ensures that rotation of the joint produces relatively large displacements whilst any erroneous lateral displacements produced by imperfect femoro-tibial joint articulation result in only small displacements. The mechanical arrangement is almost certainly organised in this way to provide a favourable signal to noise ratio. Such an arrangement necessitates the use of a compliant component coupled in series with the receptors. The compliant element scales down the input to a magnitude appropriate to the transduction mechanism of the sensory cells. A similar arrangement is found in the mtFCO of the cricket *Acheta domesticus* (Nowel *et al.*, 1995). French (1988) speculated that the various coupling structures found in association with different mechanoreceptors would allow a wide range of stimuli to produce similar amplitude movements at the level of their sensory cell membranes. He remarked that this would permit a conservation of structure and function at the level of the sensory cells so that the generation of receptor currents during transduction would take place by similar mechanisms in different systems.

2.5.2 Modification of the mechanical input

As input displacements are transmitted proximally there is a reduction of displacement magnitude due to the compliance of the ligaments. In addition, input displacements are modified differentially over different parts of the femoro-tibial range. Displacements of the cuticular rod over the middle of the range of femoro-tibial angles produce disproportionally large displacements of the ligaments relative to those at the ends of the femoro-tibial range. This is likely to be due to the roles of the dorsal ligament loop and the sequential recruitment of fibres crossing to the ventral ligament. Although in this thesis displacement modification was measured in response to static joint rotations, such modifications may be frequency dependent.

Buckling of the apodeme complex to form the loop occurs in different ways in the two species examined. The physiological consequence of this difference in loop-forming behaviour is unclear, although a combination of two morphological factors may be responsible for it. *L. migratoria* has a more rigid distal insertion onto the tibia than *S. gregaria*. This means that as the distal insertion point moves ventrally when the leg is flexed, there is a tendency for the insertion point to force the cuticular rod downwards. The guy-rope fibres in *L. migratoria* are located at a more proximal level than they are in *S. gregaria*. The result is that a significant length of the ligament component of the apodeme complex is unsupported (Fig. 2.4b). Therefore, as the tibia is extended instead of the apodeme flipping upwards as in *S. gregaria*, local twisting of the ligaments occurs and the cuticular rod flips downwards.

Some evidence was found to suggest that the very large degree of observed ventral deflection of the cuticular rod in dissected specimens of *L. migratoria* may be partially due to the effects of dissection. These result in the rod moving more ventrally than in undissected specimens, particularly at femoro-tibial angles in excess of 90°. A septum separating the dorsal and ventral haemolymph canals of the femur is inevitably damaged during dissection. This septum (also present in *S. gregaria*), although not directly involved with formation of the loops, may limit the range over which the cuticular rod can 'flip' ventrally in undissected legs. In *S. gregaria*, where the rod is always displaced dorsally, the septum has no such role.

Differences in buckling behaviour between the two species may reflect subtle behavioural differences which require differences in the proprioceptive input arising from tibial rotation. Alternatively, the apparent reduction in the range of sensitivity caused by the complete unloading of the apodeme complex ligaments in *L. migratoria* may be compensated for by another mechanical linkage elsewhere in the system such as the ventral attachment which (unlike the situation is *S. gregaria*) becomes taut when the ligaments are fully unloaded.

2.5.3 Implications of differential ligament displacement

Differential displacement between dorsal and ventral apodeme complex ligaments has been noted in the mtFCO of the cricket *Acheta domesticus*

(Nowel *et al.*, 1995). In the present study similar differential displacements were noted between the dorsal and ventral ligaments in *S. gregaria*. It is known that individual mtFCO sensory neurones respond over discrete ranges of femoro-tibial angles (Usherwood *et al.*, 1968; Burns, 1974; Zill, 1985a). Thus, the discharge of the organ at any particular femoro-tibial angle represents the composite of the responses of several neurones whose angular sensitivity ranges overlap. This phenomenon is known as 'the range fractionation principle' (Cohen, 1964).

It has previously been the unspoken assumption that the attachment strands of chordotonal organs stimulate all the sensory units simultaneously. In this case range fractionation would be achieved by a population of neurones having different thresholds for stimulation. The observations made in this thesis and by other recent studies (Field, 1991; Shelton *et al.*, 1992; Nowel *et al.*, 1995) suggest that range fractionation may be due in part to the mechanical properties of the apodeme complex. Differential displacement between the mtFCO ligaments may provide a mechanism by which different populations of sensory neurones having similar electrophysiological properties can be induced to fire over different parts of the femoro-tibial range.

There are three biomechanical factors which provide differential mechanical input to the scoloparium:

1. The guy-rope fibres attached to the dorsal ligament are loaded and unloaded over the course of the walking cycle. Since the ventral ligament is not directly connected to the guy-rope fibres, any influence imposed upon ligament displacement by the guy-rope fibres will affect the dorsal and ventral ligaments to differing degrees.

2. During tibial flexion the attachment cell fibres of the ventral ligament tighten sequentially over the range of femoro-tibial angles 30° to 80° (Fig. 2.3). This results in the attachment cells comprising the ventral ligament being displaced differentially over this part of this femoro-tibial range.

3. Differential elasticity along the length of the dorsal ligament contributes to differential displacement between the two ligaments. If both ligaments are displaced equally at their distal ends, the proximal end of the dorsal ligament would undergo larger displacements than the ventral ligament due to its increased compliance at this level.

2.5.4 Connections to the flexor muscle apodeme

Both the ventral attachment and the flexor strand are connected to the flexor tibiae muscle apodeme so that they provide mechanical input to the mtFCO scoloparium region during movements of the flexor muscle apodeme. Such connections are obviously of considerable importance in contributing to the overall displacement of the mtFCO scoloparia. Connections to a muscle involved in effecting rotation of the joint may also allow the response properties of the mtFCO to be altered depending upon the state of contraction of the muscle (Shelton *et al.*, 1992).

Usherwood *et al.* (1968) speculated that the mtFCO probably also responds to muscle contractions which do not result in rotatory movements of the tibia. Such a situation would involve a simultaneous change in flexor and extensor tibiae muscle tone such that the increased tension developed in the muscles resulted in no tibial rotation. For this to provide information via the mtFCO relating to the state of muscle tone would necessitate either direct interaction of the mtFCO with the muscle fibres, or rely on muscle tension causing distortion of the distal femur. The ventral attachment ligament terminates upon the flexor tibiae amongst numerous muscle fibre bundles and so could provide proprioceptive information either directly regarding the state of contraction of the fibres or indirectly by responding to the displacement of the flexor tibiae apodeme within the femur. In contrast, the mtFCO flexor strand terminates on the flexor tibiae apodeme at a level where no muscle fibres are found. If it were to provide a measure of muscle tone under conditions where the tibia is stationary, this attachment must rely solely upon monitoring the displacement of the apodeme resulting from femoral distortion. There is no evidence that this occurs.

In *S. gregaria* the mechanical influence of the ventral attachment is greatest during extreme tibial flexion when the attachment is held taut. The leg is frequently held in this flexed position for long periods when the locust is at rest, and also immediately prior to jumping. Prior to the jump the tibia remains fully flexed whilst muscle tension in both the flexor and extensor is increased (Brown, 1967). During this process the smaller flexor tibiae muscle is able to oppose the force generated by the larger extensor tibiae by virtue of the mechanical advantage afforded by the fact that the flexor muscle apodeme's distal origin at the tibia is at a greater distance from the fulcrum than that of the flexor tibiae. Since femoro-tibial angle

remains static during this process (0°), the ventral attachment could conceivably have a role in monitoring the state of contraction of the flexor muscle. Certainly the animal is unable to jump when one or both mtFCOs are removed (Usherwood *et al.*, 1968). Burns (1974) recorded the neuronal output from the distal scoloparium in the pro- and mesothoracic locust chordotonal organs. Some units were found to respond strongly to flexor tibiae muscle contraction when the tibia was held in a fixed position. Zill (1985a) obtained similar results in the case of the locust mtFCO (although was unaware of ventral attachement ligament and attributed this activity to distortion of the femoro-tibial joint). These observations strongly implicate the ligaments associating these scoloparia with the flexor muscle apodeme in having a functional role of monitoring muscle tone in the pro- and mesothoracic legs. There is evidence that the mtFCO in the locust is formed from two scoloparia that have fused in the course of evolution (Matheson and Field, 1990; Chapter 4 this thesis). If one of these scoloparia corresponds to the pro- and mesothoracic distal scoloparia the evidence cited above would suggest that the ventral attachment is derived from it. In *L. migratoria*, in addition to being held taut over the femoro-tibial angle range of 0° - 40°, the ventral attachment is also under tension over the angles 135° - 150°. Mechanical input to the mtFCO scoloparium over the latter angles may compensate for the lack of input from the apodeme complex which is completely unloaded over this range of tibial rotation.

Unlike the ventral attachment, the flexor strand remains under tension at all femoro-tibial angles in both *S. gregaria* and *L. migratoria*. With respect to their effects upon distortion of the mtFCO scoloparium, the flexor strand and ventral attachment may have complementary roles, the flexor strand becoming increasingly stretched as the tibia is extended whereas the ventral attachment becomes slack over the majority of the femoro-tibial range. Zill (1985a) showed that when the flexor strand was severed, the increase in mtFCO nerve discharge normally associated with extension of the tibia was almost completely eliminated. This reflects the fact that not only does the flexor strand contribute to the displacement of the scoloparium but that it also contains an extension-sensitive 'strand receptor' (Bräunig, 1985) whose axon runs in the chordotonal organ nerve tract. The latter author speculated that the function of the strand receptor may be to encode some aspect of tibial extension that the mtFCO scoloparium does not monitor.

If the state of contraction of the flexor tibiae muscle modifies the response properties of the chordotonal organ, any modifying influence by virtue of the ventral attachment ligament alone would cease at femoro-tibial angles in excess of 40° in both *S. gregaria* and *L. migratoria*, as the attachment becomes slack over this range. However, the ventral attachment could contribute to distortion of the scoloparium over the range of femoro-tibial angles 135° - 150° in *L. migratoria* as described. In both species, the influence of the ventral attachment holding the system at a higher tension may increase its sensitivity under conditions of extreme tibial flexion although a link between muscle tone and discharge from the organ has yet to be established. However, such associations have been found to exist in crustacean proprioceptor systems (Macmillan *et al.*, 1982). The forces generated by the femoral muscles must be closely monitored by proprioceptors, particularly during jumping, to keep within the capabilities of the load bearing structures (Burrows, 1996).

Recent studies have also shown that muscle tone may be monitored by specialised multipolar receptors, such as that associated with the assessory flexor muscle (Matheson and Field, 1995). Such receptors respond to dynamic components of the muscular contraction contributing to joint rotation. Connections such as the mtFCO ventral attachment ligament and flexor strand may be responsible for providing inputs relating to other aspects of muscular contraction. Such connections certainly would be capable of modifying the responses of some or all the mtFCO sensory units simultaneously by causing distortion of the scoloparium. Such distortion may provide another mechanical mechanism that promotes differential inputs to afferent sensory neurones.

Figure 2.1

The internal organisation of the distal femur is shown in this semi-thin (1 μm) transverse section stained with 1% Toluidine Blue. This figure is a montage built up from multiple greyscale images, captured using a CCD camera and Scion Corporation frame-grabber.

The femur is horizontally divided into dorsal (dhc) and ventral (vhc) haemolymph channels by a thin connective tissue septum (s) interconnecting several large tracheae (t). The cuticular apodemes of the extensor (ext) and flexor (flx) tibiae muscles are located in the dorsal and ventral haemolymph channels respectively. Muscle blocks of the flexor tibiae (ft), accessory extensor (ae) and accessory flexor (af) muscles stain intensely.

The mtFCO is located within the dorsal haemolymph channel on the anterior side of the femur. Laterally the organ is bound by the cuticular femur wall on the anterior side and by the tracheae associated with the flexor-tibiae muscle apodeme on the posterior side (t'). The CO is confined within the dorsal haemolymph channel. The flexor strand (fs) is confined within the ventral haemolymph channel.

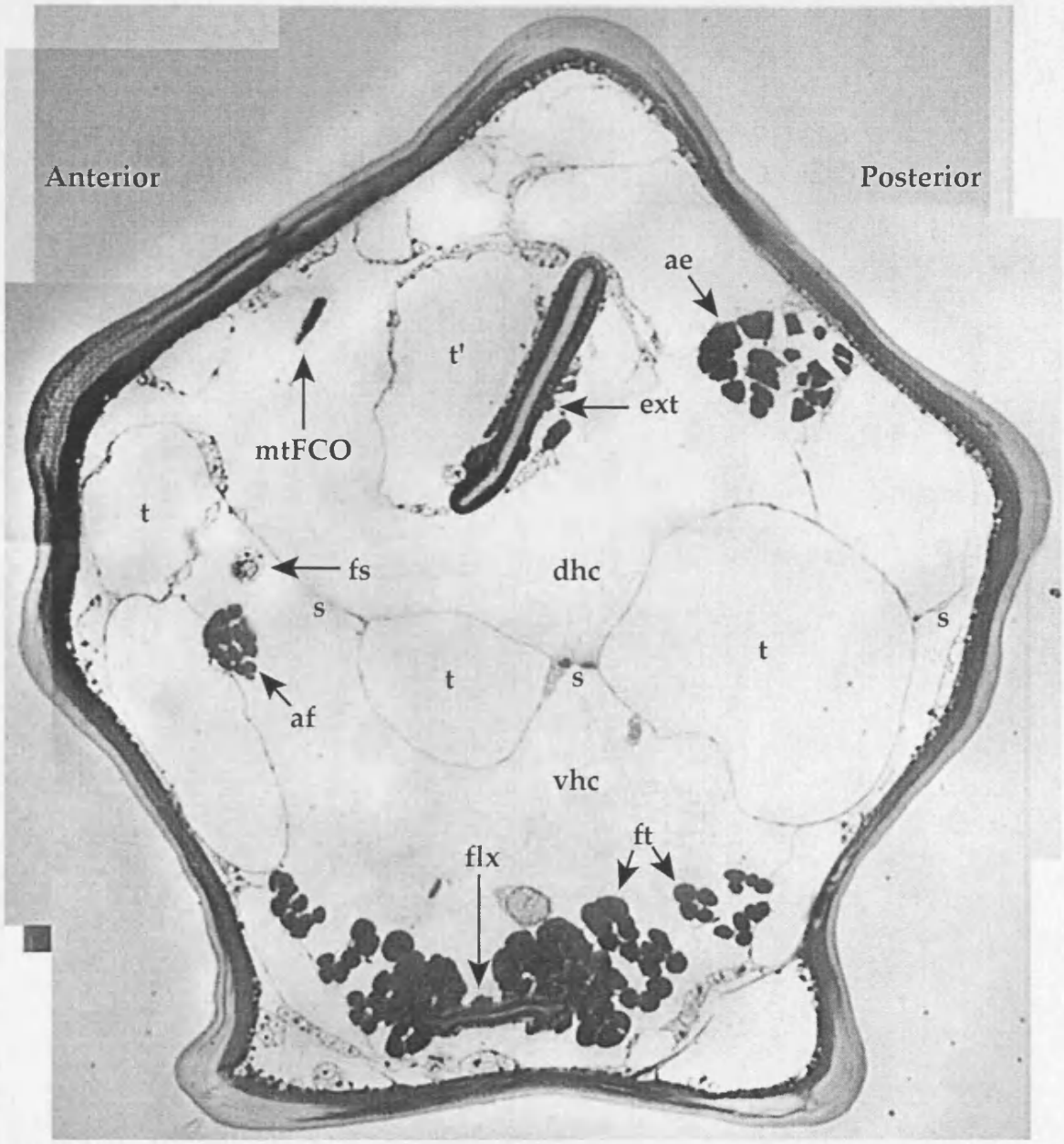

1000μm

Figure 2.2

This semi-schematic diagram shows the general anatomy of the mtFCO and its main mechanical linkages.
The mtFCO is anchored dorsally in the distal femur by a short dorsal attachment (da). Ventrally the organ is connected to the apodeme of the flexor tibiae muscle via two structures; a ventral attachment (va) which arises adjacent to the neurone-containing region of the organ to connect to the flexor tibiae apodeme (f), and the flexor strand (fs) which inserts onto the flexor tibiae apodeme distally near the femoro-tibial joint.

The 'apodeme complex' (ac) forms the main mechanical link across the femoro-tibial joint. Distally it consists of a cuticular rod (r) that arises from the tibia, and proximally it is composed of dorsal (d) and ventral (v) ligaments. Loop formation (l) occurs between the two ligaments as femoro-tibial angle increases (tibial extension). Loop 'crossing fibres' (cf) arise from the side of the cuticular rod at intervals to form the ventral ligament. These fibres are of graded lengths and consequently tighten and slacken sequentially during tibial flexion and extension respectively.
Proximal to the loop-forming regions is a cluster of guy-rope fibres (gf). Similar fibres also occur at intervals between this group and the mtFCO scoloparium (s). Distally the fibres are attached to dorsal connective tissue elements within the femur. The organ is connected to the metathoracic ganglion by nerve 5b1 (n1). It is joined by the cuticular nerve (n2), which arises distally from sense organs in the dorsal femur.

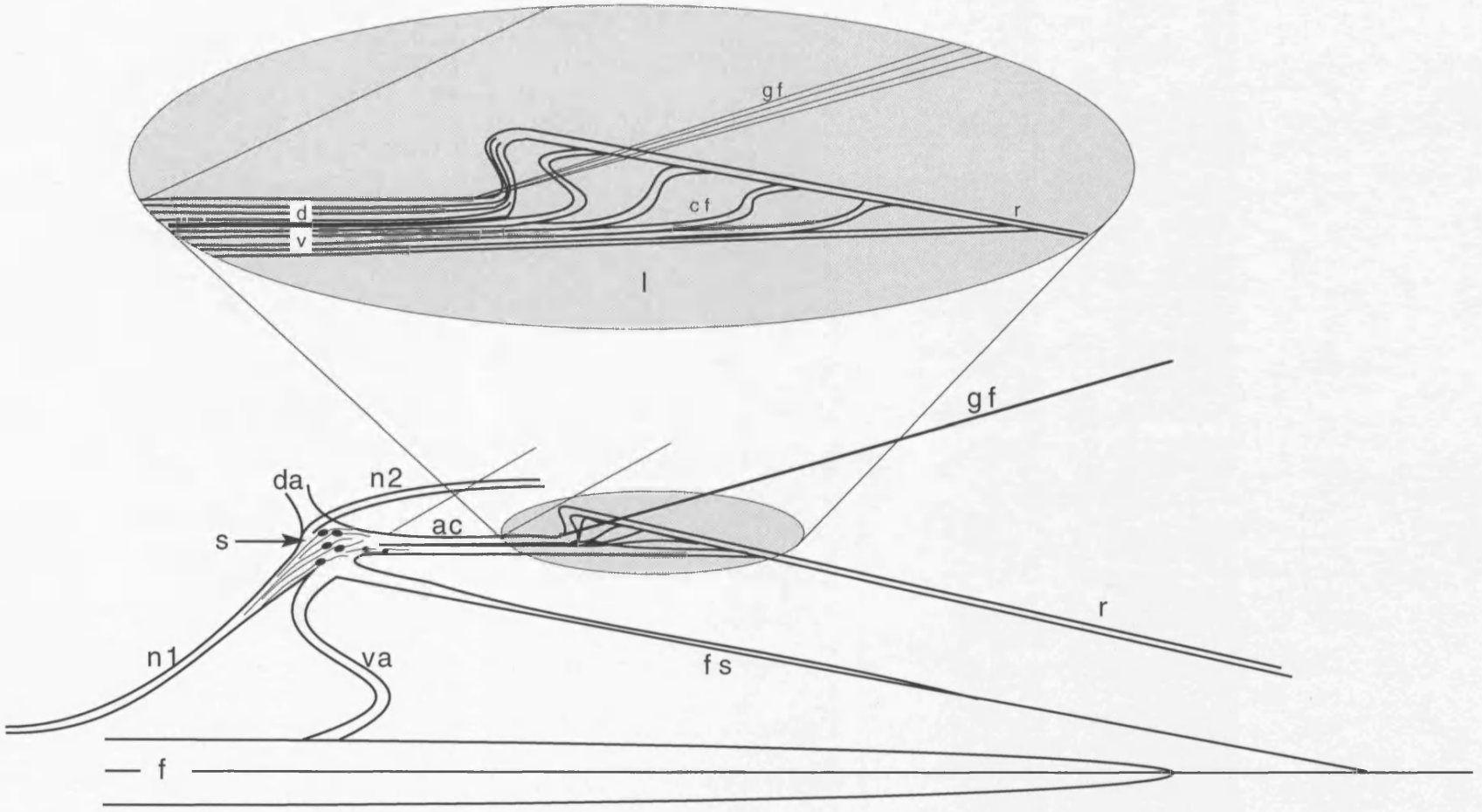
gf
d
v
cf
r
l
gf
da
n2
s
ac
r
n1
va
fs
f

Figure 2.3

A series of light micrographs showing the appearance of the apodeme complex loop in *S. gregaria*, at a series of femoro-tibial angles (indicated). Distal is to the right of the micrographs.
The loop is formed by the cuticular rod (r) which rises above the plane of the apodeme complex. The loop forms due to a slack region of dorsal ligament (l) distal to the guy-rope fibres (g). The crossing fibres (arrows) leave the cuticular rod at intervals to join the ventral ligament. These fibres tighten sequentially upon tibial flexion. At a femoro-tibial angle of 80° the apodeme complex is buckled, the cuticular rod being dorsal to the ventral ligament to form the characteristic loop. The length of dorsal ligament (l) (approximately 150 µm), between the end of cuticular rod and the attachment of the guy-rope fibres, is buckled when the loop is present. The guy-rope fibres leave the dorsal ligament to run distally at an angle of approximately 30° from the plane of the apodeme complex.
The arrows in micrographs 80° to 50° follow the sequential tightening of two individual fibres of the ventral ligament during flexion. The distal-most loop disappears first. The photograph taken at 30° shows the two ligaments (arrows) immediately proximal to the level of the cuticular rod. The appearance of the apodeme complex at each femoro-tibial angle is the same during flexion and extension so that the series of micrographs opposite could represent either a flexion (80° - 30°) or extension (30° - 80°) of the tibia.

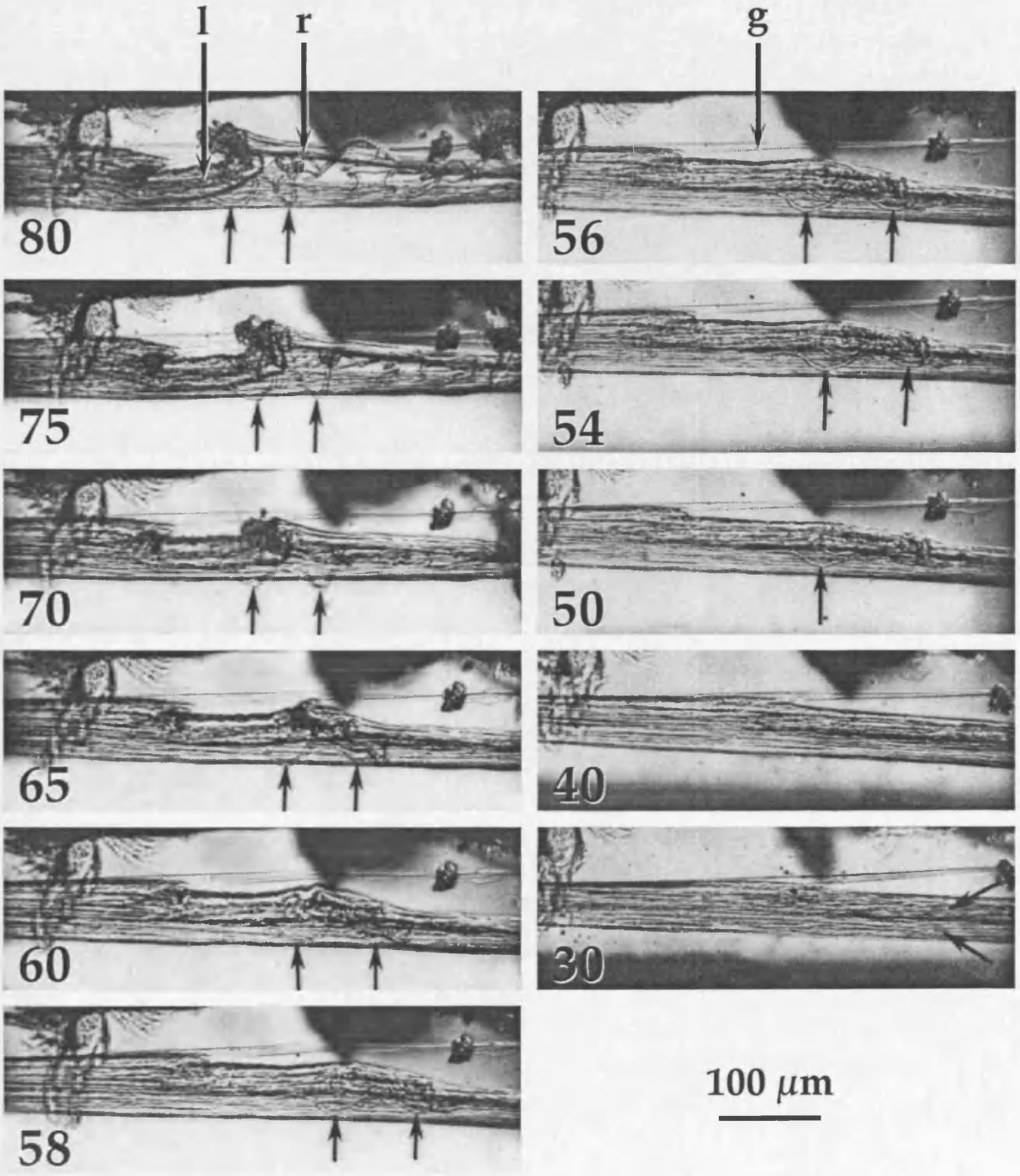
l
r
g
80
56
75
54
70
50
65
40
60
30
58
100 μm

Figures 2.4a, b

These semi-schematic diagrams show the way in which the mechanical connections comprising the apodeme complex are arranged in *L. migratoria*. The dorsal ligament (d) forms a continuation of the cuticular rod (r), whilst the ventral ligament (v) arises from the side of the rod. As is the case in *S. gregaria*, some of the fibres forming the ventral ligament buckle to form loop-crossing fibres (cf) which tighten and slacken in sequential fashion.

a

This diagram shows the junction between the cuticular rod and the ligaments of the apodeme complex at a femoro-tibial angle of 80°. The guy-rope fibres (gf) arise from the dorsal ligament approximately 200 μm proximal to the fusion of the dorsal and ventral ligaments in *L. migratoria*. (This contrasts with the position of the guy-rope fibres in *S. gregaria* where they are located immediately proximal to the loop forming region in *S. gregaria*, indicated in grey).

b

At extreme flexion (150°), the cuticular rod dips below the plane of the apodeme complex causing local twisting (t) in the unsupported region of the ligaments located between the guy-rope fibres and the loop. Both the dorsal and ventral ligaments become fully unloaded distal to the guy-rope fibres. Neither twisting nor full unloading of the apodeme complex are seen in *S. gregaria*.

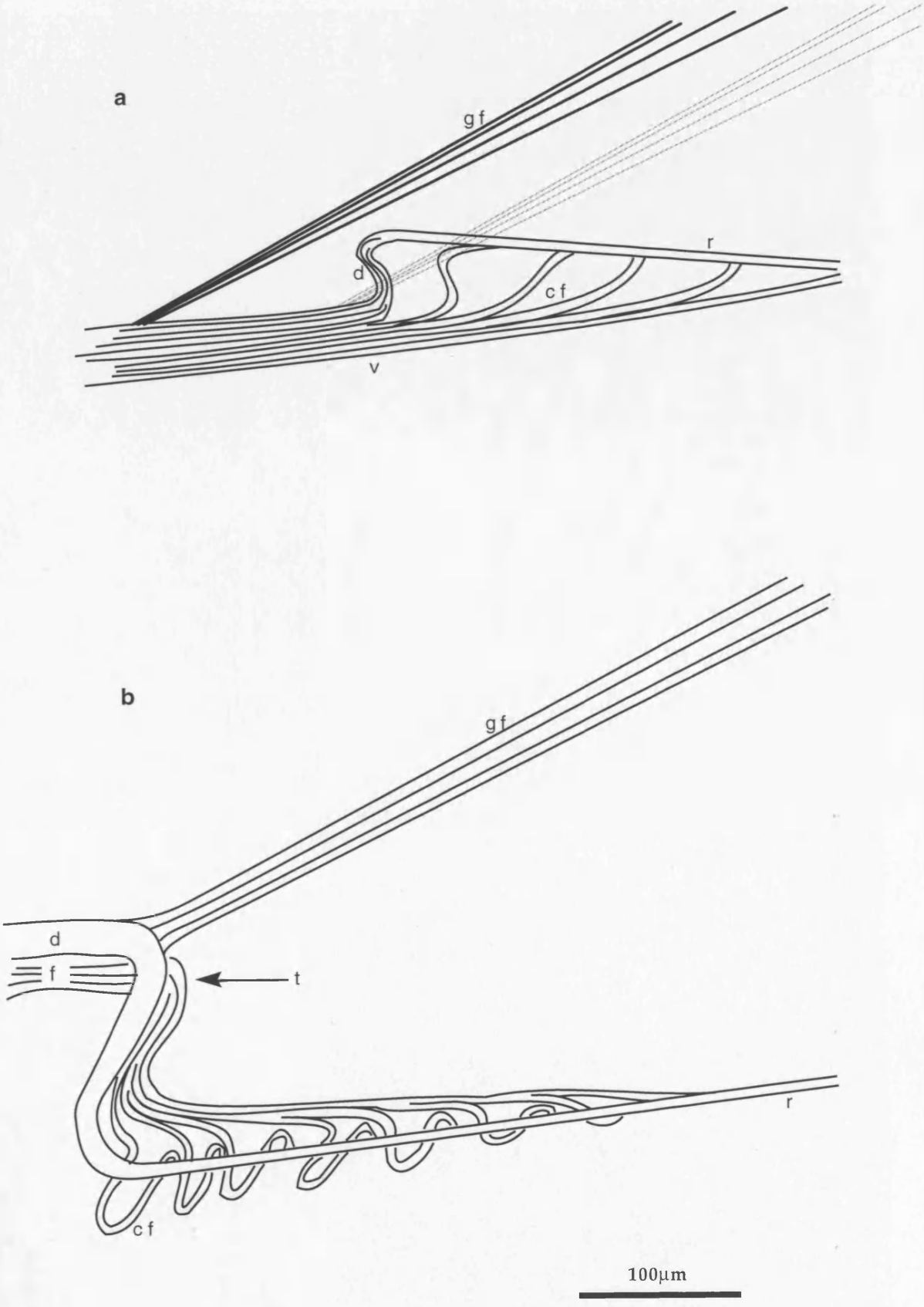
a
g f
r
d
c f
v
b
g f
d
f
t
r
c f
100μm

Figures 2.5a-d

These micrographs show the proximal end of the apodeme complex cuticular rod at different femoro-tibial angles in *L. migratoria*. Using a confocal laser scanning microscope the autofluorescent properties of insect cuticle are utilised to visualise the rod as the tibia is rotated from 0° - 100°. Figure 2.5d is a bright field micrograph taken at a femoro-tibial angle of 100°.

Figure 5a shows the apodeme complex at a femoro-tibial angle of 0°. The cuticular rod appears straight at this leg angle. As the apodeme complex is unloaded (5b, c; femoro-tibial angles 50° and 100° respectively) the proximal 100 μm of the rod buckles like a spring. The light micrograph taken at a femoro-tibial angle of 100° (5d) shows that the portion of the cuticular rod that behaves like a spring is incorporated into the buckling dorsal ligament (arrows in 2.5c,d) as the apodeme complex forms a loop.

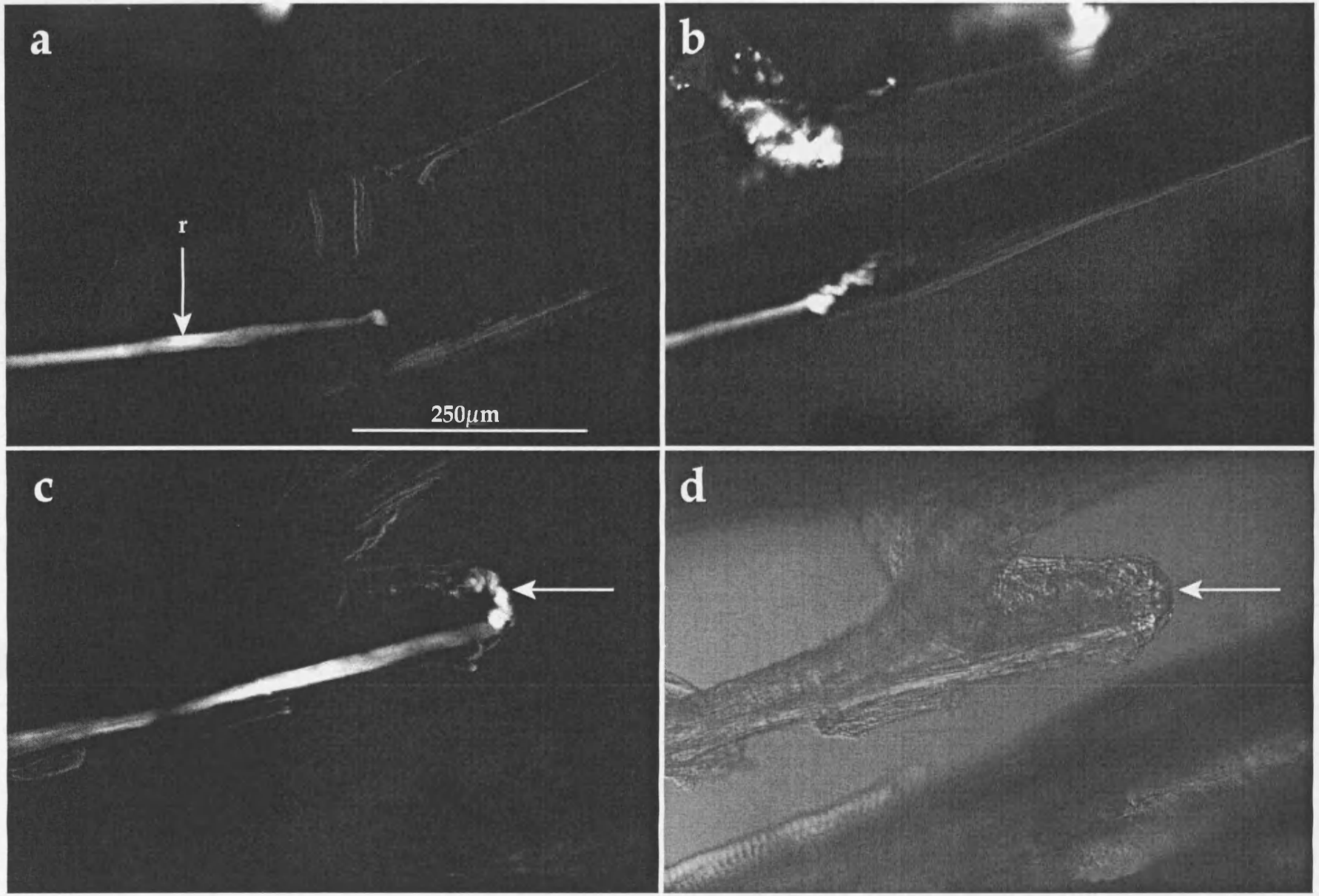
a
r
250μm
b
c
d

Figures 2.6a-d

Series of micrographs showing the position of the ventral attachment ligament at four femoro-tibial angles in *S. gregaria*. Distal is to the right.

The mtFCO scoloparium (s) is partly obscured, but the flexor strand (f), ventral attachment (v) and chordotonal organ nerve 5b1 (n) can be seen.

At a femoro-tibial angle of 0° (Fig. 2.6a), the ventral attachment (v) runs proximally adjacent to nerve 5b1 (n) to insert onto the apodeme of the flexor tibiae muscle.
As the femoro-tibial angle is increased, the ventral attachment becomes gradually unloaded until at femoro-tibial angles in excess of 50° the attachment buckles (Figs 2.6b, c). At a femoro-tibial angle of 150° the insertion of the ventral attachment onto the flexor muscle apodeme lies at the same proximo-distal level as the mtFCO scoloparium (Fig. 2.6d).

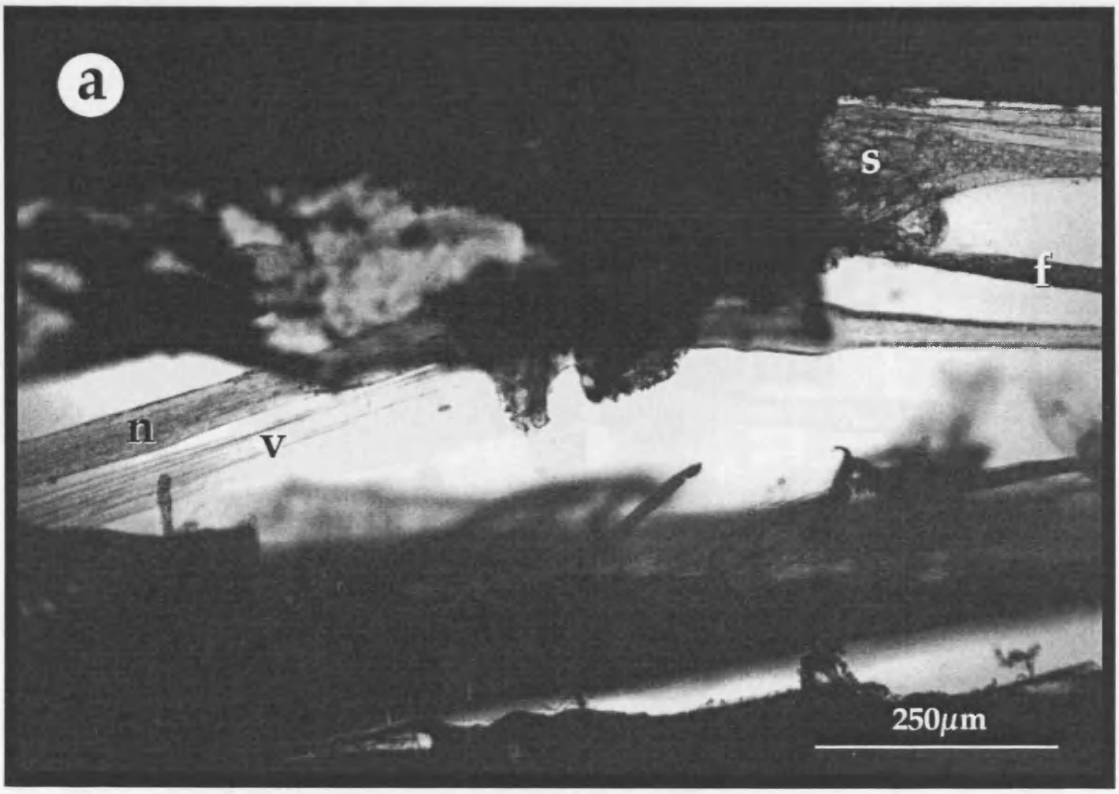
a
s
f
n
v
250μm

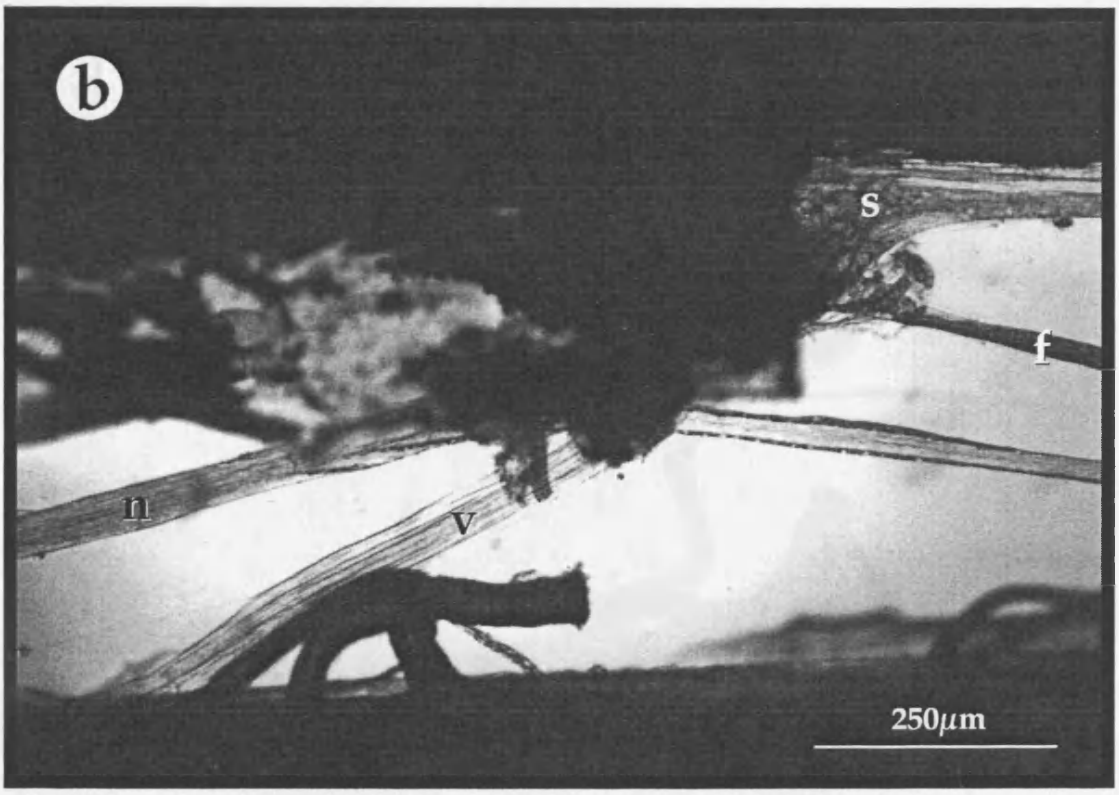
b
s
f
n
v
250μm

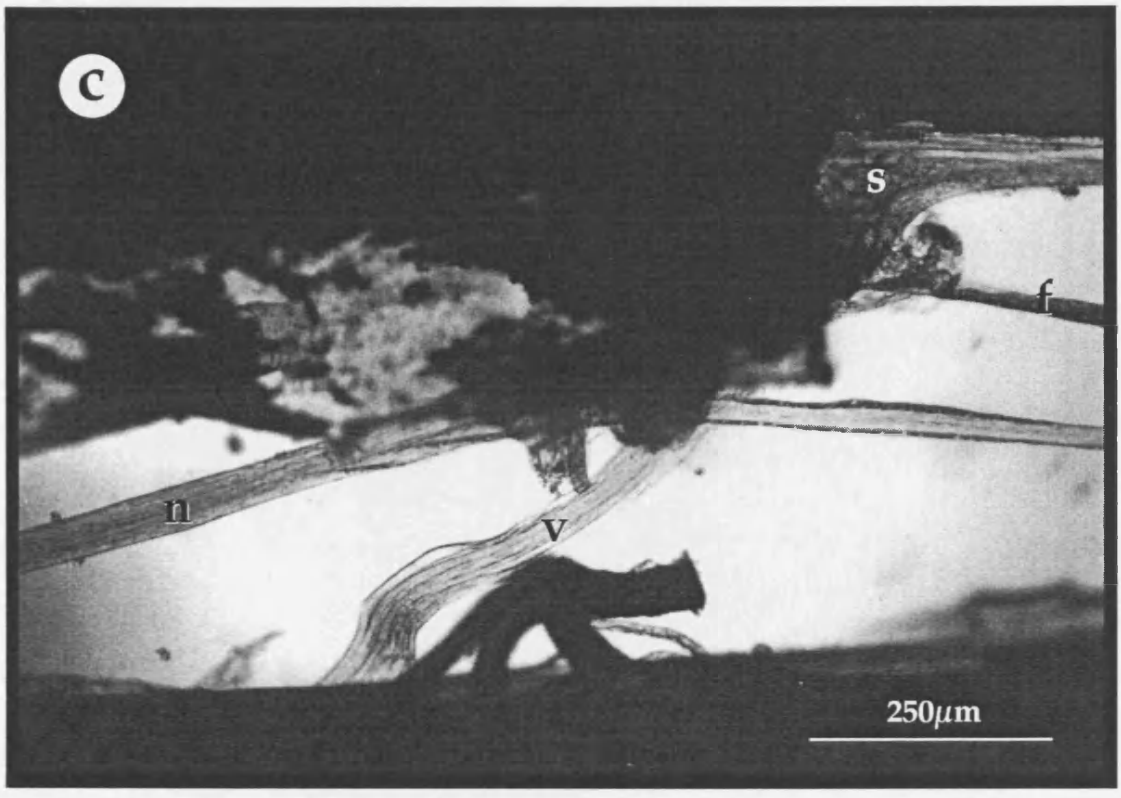
c
s
f
n
v
250μm

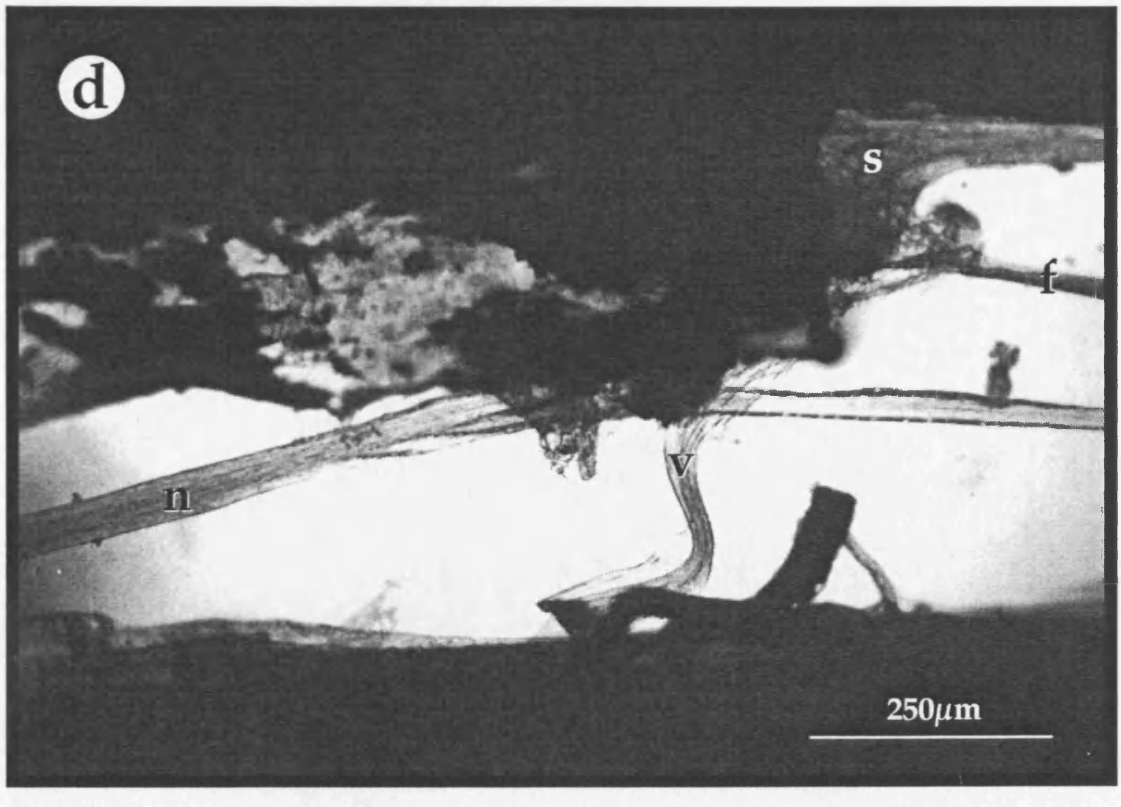
d
s
f
n
v
250μm

Figures 2.7a, b

This pair of light micrographs shows the guy-rope type fibres (arrows) associated with the ventral attachment ligament in *S. gregaria*. Distal is to the right in both cases. Each guy-rope consists of several twisted fibrils (Fig. 2.7a) which control the buckling behaviour of the ligament at femoro-tibial angles greater than 50°. The fibres connect the ventral attachment ligament to the flexor muscle apodeme both distal (Fig. 2.7a) and proximal (Fig. 2.7b) to the ligament's main insertion onto the flexor tibiae apodeme.

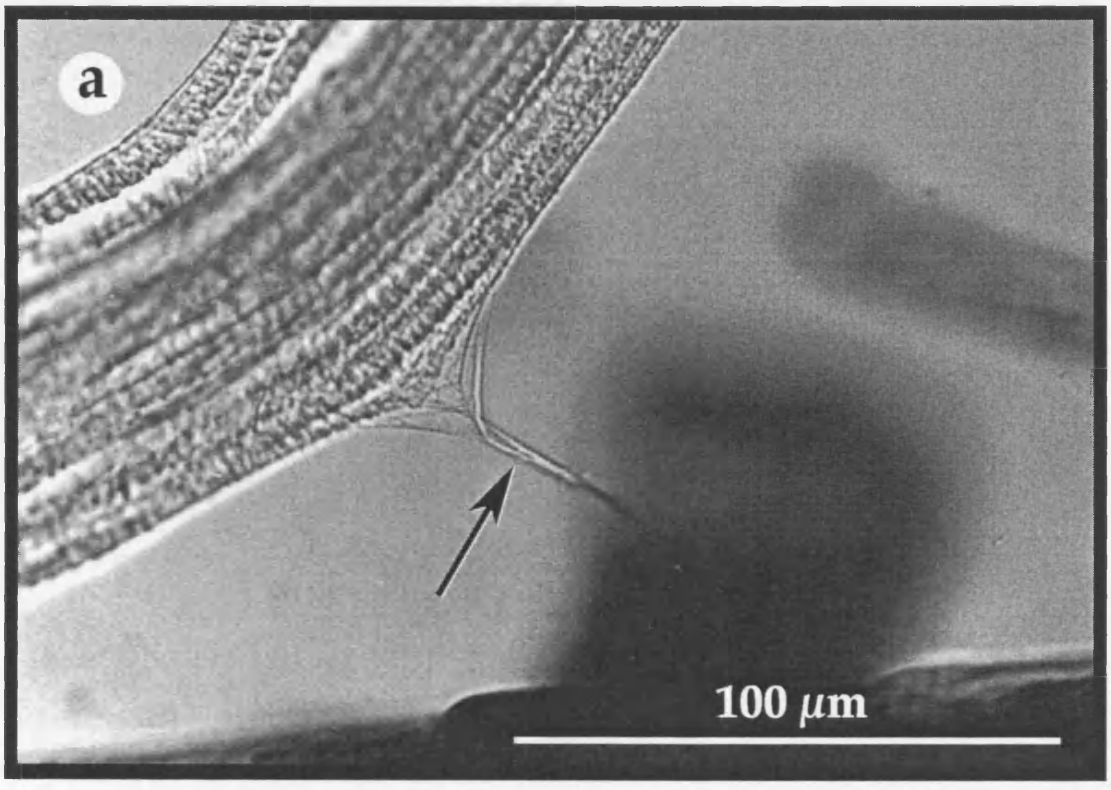
a
100 μm

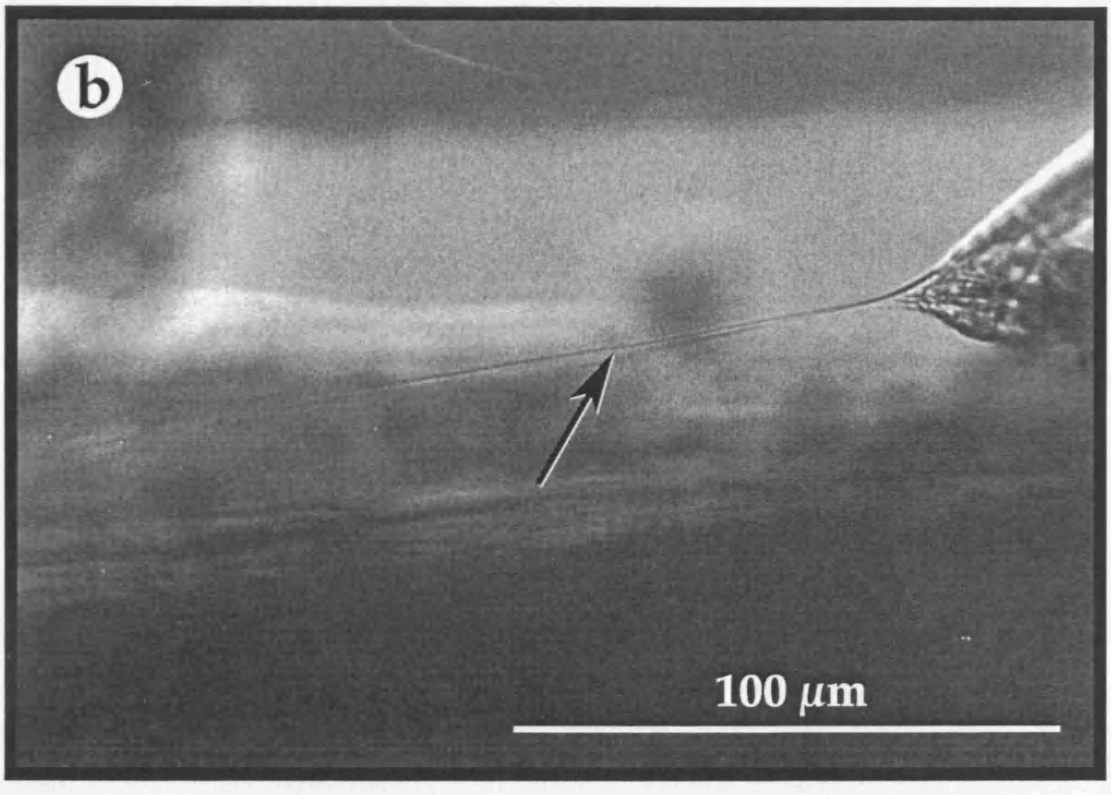
b
100 μm

Figure 2.8

A pair of semi-schematic diagrams to demonstrate the way in which the displacements of the different mtFCO linkages are related in *S. gregaria.*

The distal origin of the apodeme complex cuticular rod (r) is located closer to, and on the opposite side of the centre of rotation (arrow) of the femoro-tibial joint, than the insertion of the apodeme of the flexor tibiae muscle (f). This results in relatively large displacements of the ventral attachment ligament and the flexor strand. They move antagonistically relative to the displacement of the apodeme complex during rotation of the femoro-tibial joint.

F = Femur
T = Tibia
d = dorsal attachment
v = ventral attachment
l = apodeme complex ligaments
r = cuticular rod
b = buckling of the apodeme complex
gf = guy-rope fibres
fs = flexor strand
n = chordotonal organ nerve
f = flexor tibiae muscle

Flexed

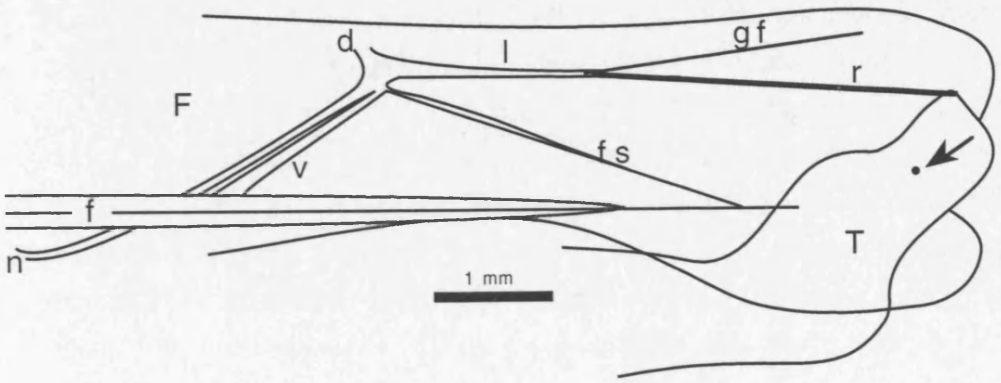

Extended

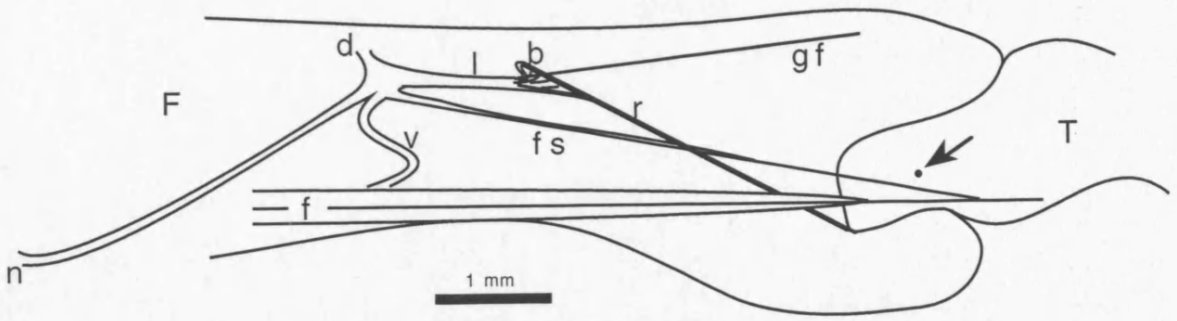

Figures 2.9a-c

These semi-schematic diagrams show the behaviour of the ventral attachment ligament in *L. migratoria* at different femoro-tibial angles.

The ventral attachment of *L. migratoria* behaves similarly to that of *S. gregaria* over the majority of the femoro-tibial range of leg angles, being taut when the tibia is flexed (9a) and buckling at femoro-tibial angles greater than 40° (9b). However, at extreme tibial extension in *L. migratoria*, the ventral attachment ligament becomes taut once again (9c). At femoro-tibial angles of 135° - 150° the taut ventral attachment displaces the mtFCO scoloparium disto-ventrally. The flexor strand also tightens with tibial flexion and supplements the effect of the ventral attachment.

F = Femur
T = Tibia
d = dorsal attachment
v = ventral attachment
l = apodeme complex ligaments
r = cuticular rod
gf = guy-rope fibres
fs = flexor strand
n = chordotonal organ nerve
f = flexor tibiae muscle

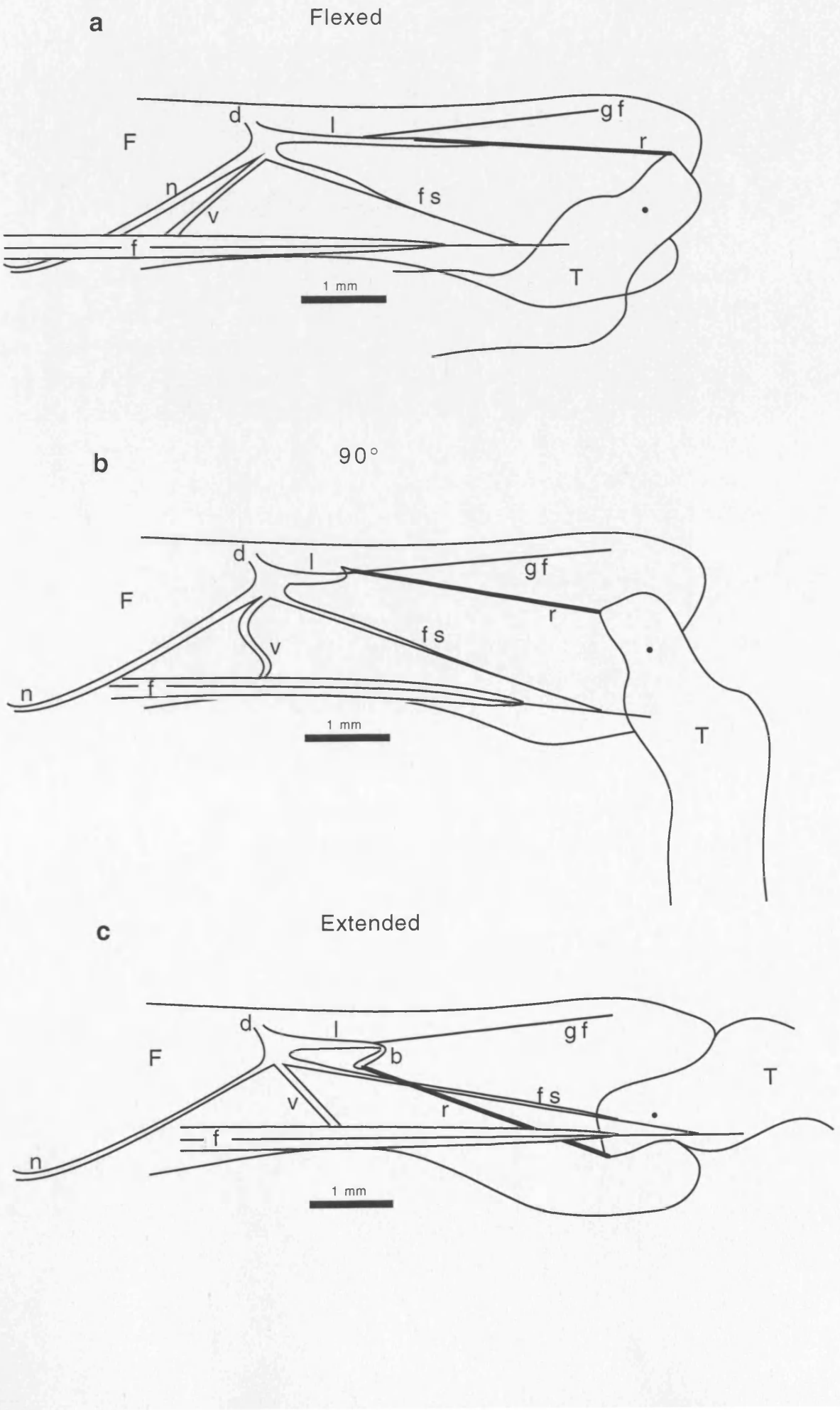
a
Flexed
d
l
gf
F
r
n
fs
v
f
T
1 mm
b
90°
d
l
gf
F
r
fs
v
n
f
1 mm
T
c
Extended
d
l
gf
F
b
T
v
r
fs
f
n
1 mm

Figure 2.10

Histogram showing the relative displacements of two pairs of markers located at different proximo-distal levels along the flexor strand. Each pair of markers were located 65 μm from one another at a femoro-tibial angle of 0°. As the flexor strand was stretched by extending the tibia over the femoro-tibial range 0° - 150°, the distance between each pair of markers increased. The distance between the proximal pair of markers increased by approximately twice that between the distal pair, indicating that the flexor strand is more compliant proximally than distally.

Histogram comparing the displacement of two pairs of equidistant markers over the range of femoro-tibial angles 0° - 150°

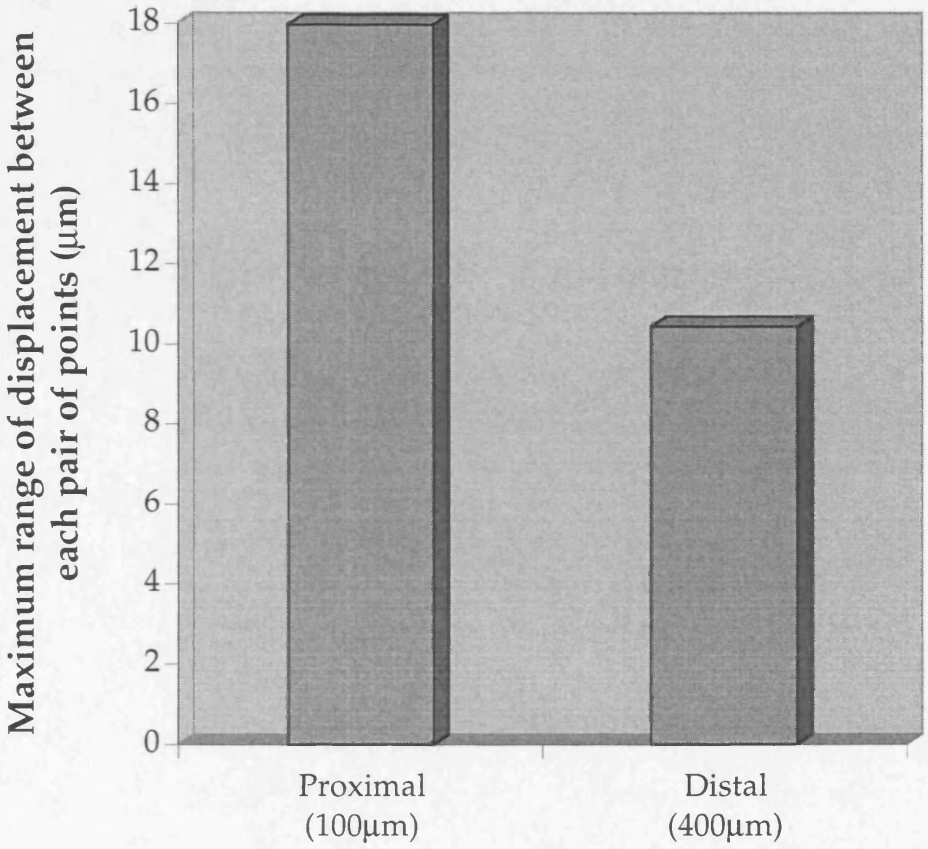

Figures 2.11a-e

This series of light micrographs shows the way in which the mtFCO scoloparium in *S. gregaria* is distorted as the tibia is rotated over the entire range of femoro-tibial angles. Distal is to the right; femoro-tibial angles are given in the top right hand corner of each micrograph.

When the tibia is flexed (Fig. 2.11a) the scoloparium (s) is stretched proximo-distally by the apodeme complex. As the femoro-tibial angle increases (Fig. 2.11b-e), the reciprocal action of the apodeme complex and the flexor strand results in the mtFCO scoloparium undergoing a rotatory displacement of approximately 20° within the femur. The change in scoloparium orientation during tibial rotation is apparent from the rotational displacement of the trachea running across the scoloparium (arrows in Figs 2.11a and 2.11e). fs = flexor strand

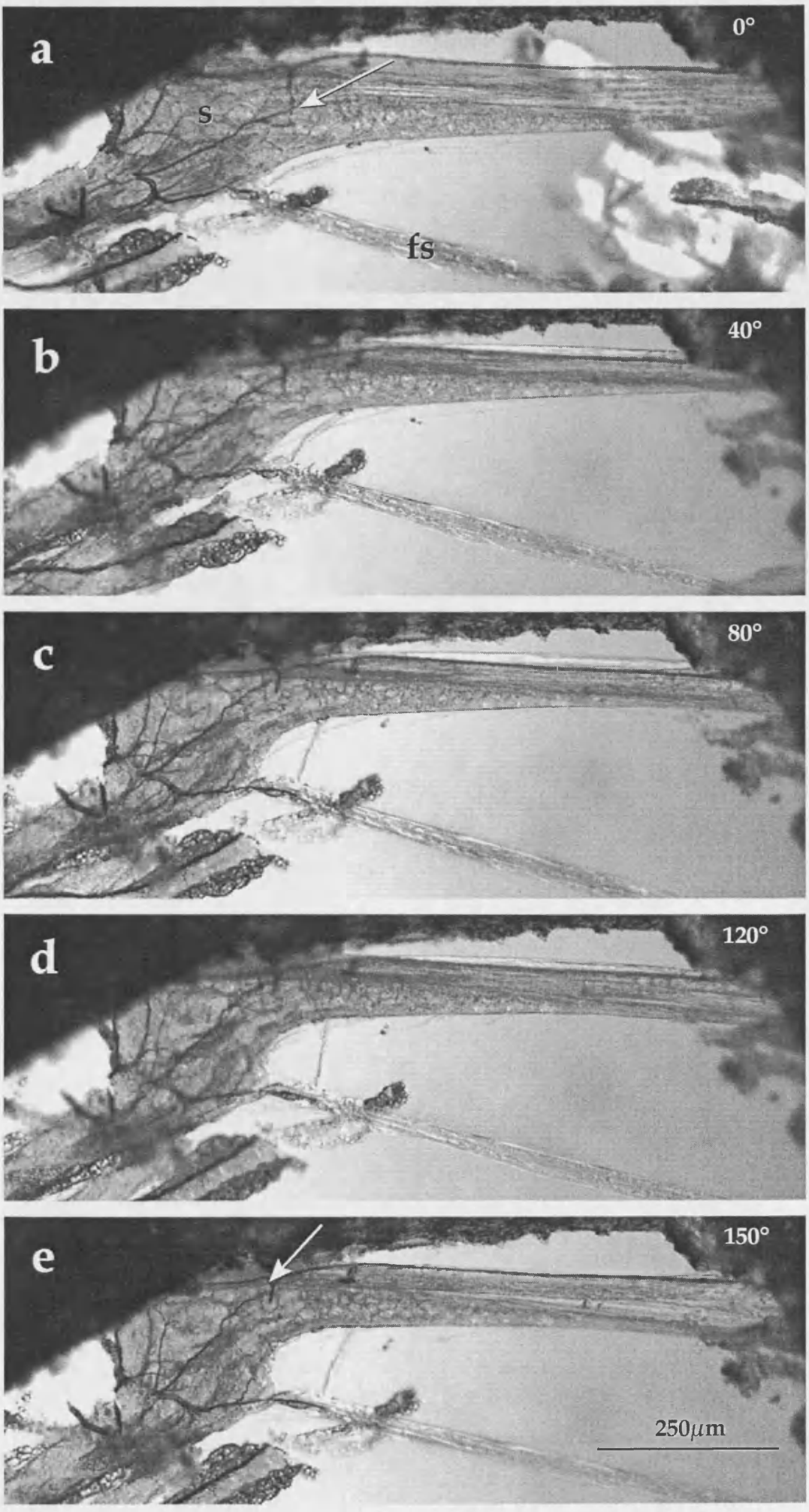
a
0°
s
fs
b
40°
c
80°
d
120°
e
150°
250μm

Figure 2.12

This graph shows the relationship between femoro-tibial angle and time during a period of continuous walking in *S. gregaria*.
The graph is plotted from the mean of 21 cycles analysed from 7 animals.
Each walking cycle is divided into a protraction (stepping) phase and a retraction (recovery) phase. The recovery phase, in which the foot is lifted from the substrate and the tibia is retracted to begin another step, occupies approximately 30% of the walking cycle. Comparison of the gradients of each phase of the mean walking cycle shows that the mean angular velocity of femoro-tibial rotation during retraction (275° sec^{-1}) is twice that during the slower protraction phase (137.5° sec^{-1}).

Graph showing the average walking cycle of the locust *S. gregaria*

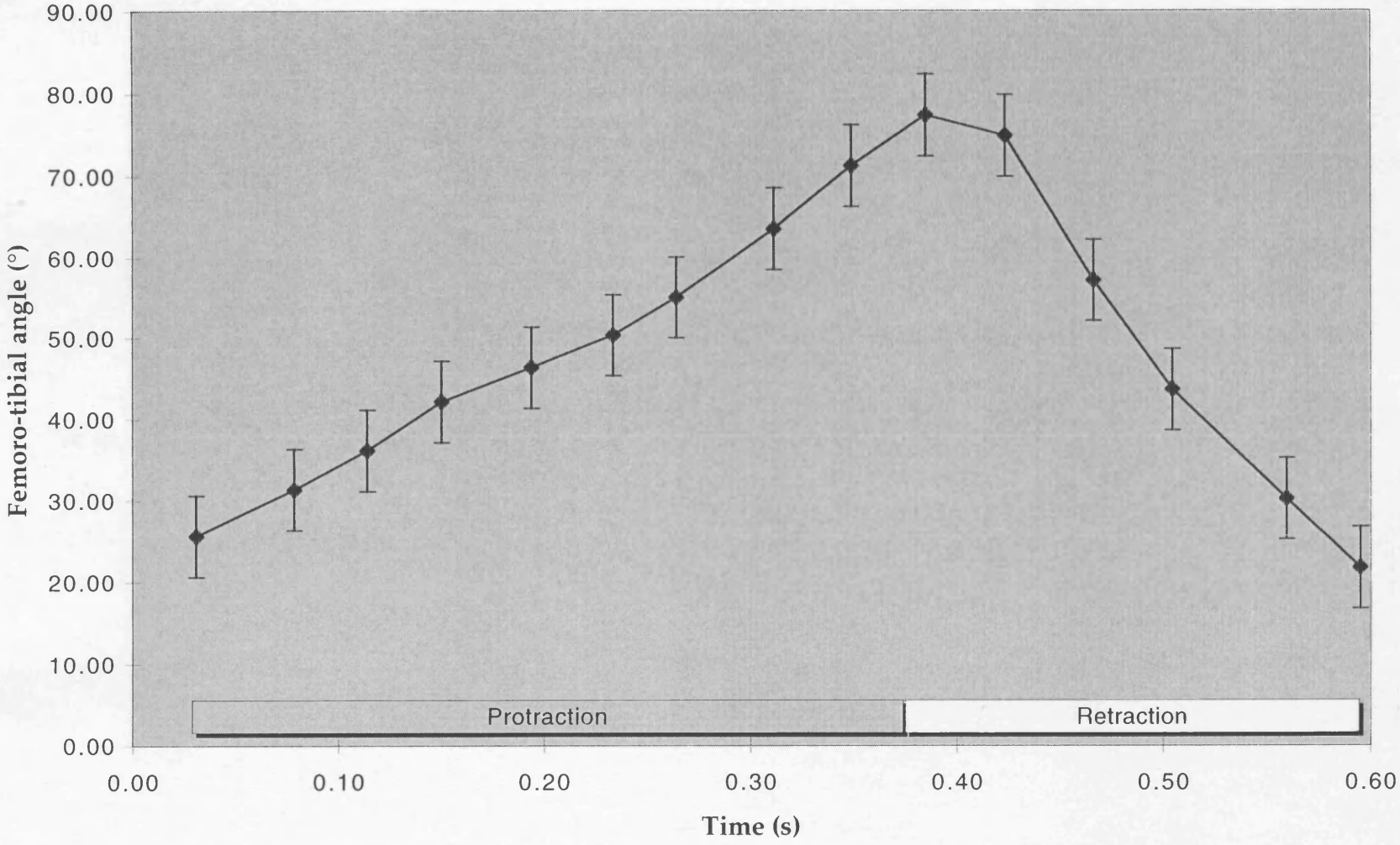

Figure 2.13

This graph shows the displacement of the base of the cuticular rod (where it arises from the tibia) over the full range of femoro-tibial rotation in *S. gregaria*. The range of femoro-tibial angles associated with the locust walking cycle is indicated to demonstrate that the proximo-distal component of the displacement is approximately linearly related to femoro-tibial angle over the walking range.

Graph showing the proximo-distal and dorso-ventral displacement of the cuticular rod where it arises at the tibia

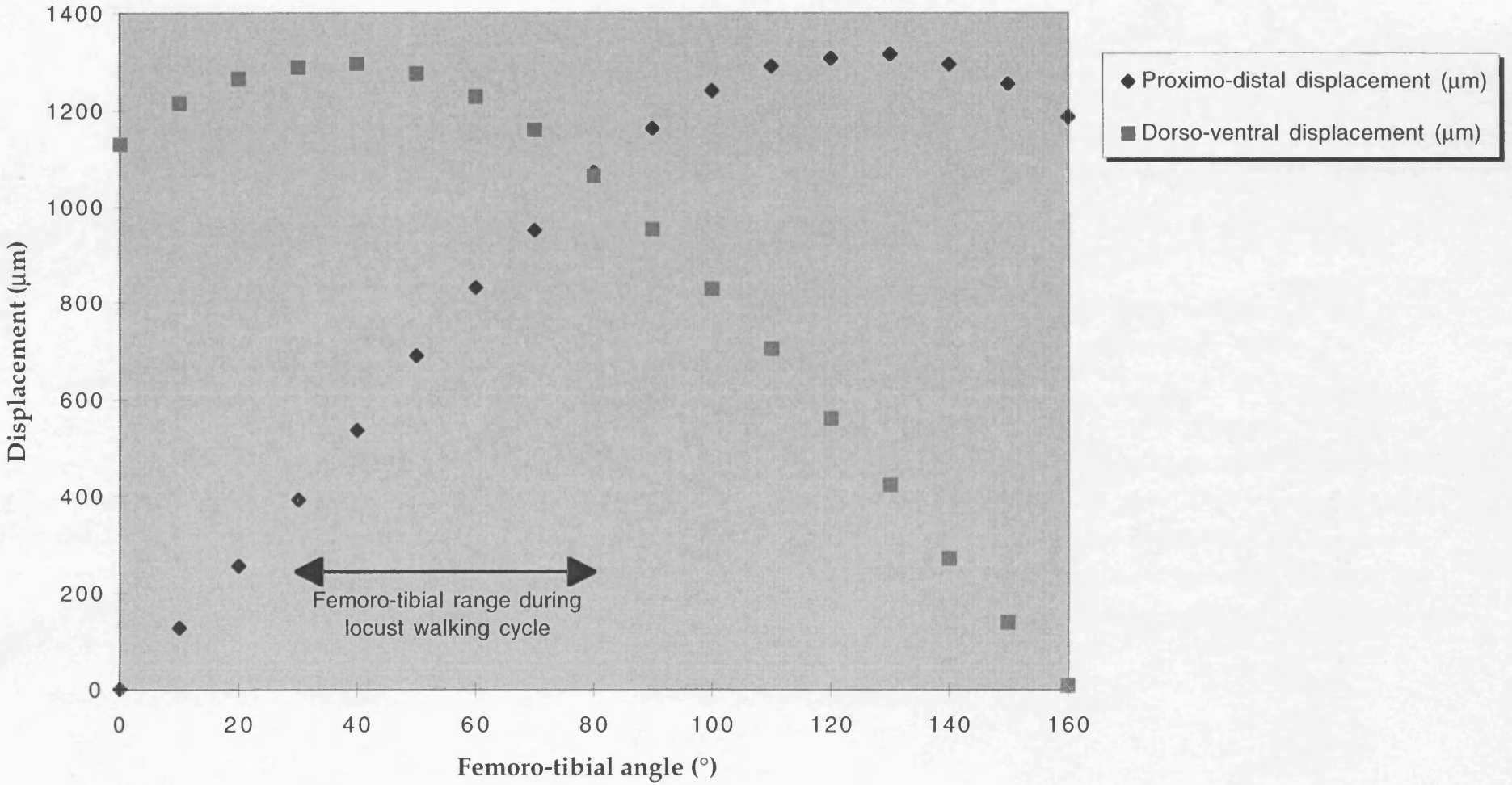

Figure 2.14

This graph contrasts the proximo-distal displacement at both ends of the apodeme complex cuticular rod in *S. gregaria*. The displacement of the distal end of the cuticular rod, where it arises from the tibia, follows a sinusoidal pattern. At the proximal end of the cuticular rod at the level where it connects to the apodeme complex ligaments, the pattern of displacement is similar to that distally, but is modified by the dorso-ventral component of tibial joint rotation. Over femoro-tibial angles 0° - 80° the displacement of the rod is similar at both proximal and distal ends. This is the range of femoro-tibial angles over which the displacement at the level of the femoro-tibial joint is predominately proximo-distal (see Fig. 2.13).

At femoro-tibial angles greater than 80° the displacement of the rod at the level of the femoro-tibial joint is predominantly dorso-ventral which has the effect of reducing the degree of proximo-distal displacement undergone at the proximal end of the cuticular rod over this range.

Graph comparing the displacement of the proximal and distal ends of the apodeme complex cuticular rod

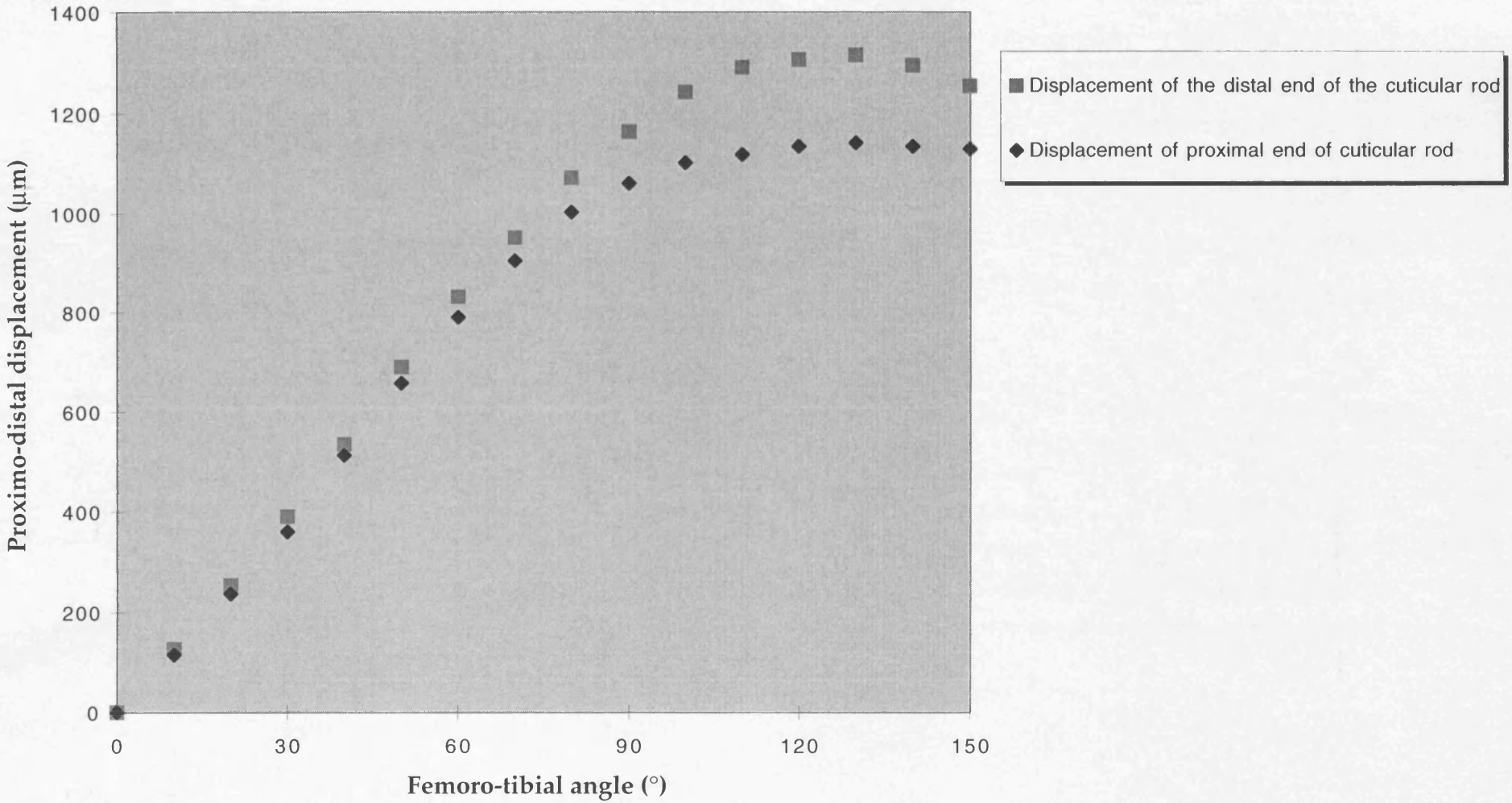

Figure 2.15

Graph showing the proximo-distal displacement of carborundum markers at different proximo-distal levels along the apodeme complex of an individual *S. gregaria* in response to rotation of the femoro-tibial joint. Markers upon the apodeme complex ligaments were located along the mid-line between the fused dorsal and ventral components. Markers undergo a smaller range of displacements with distance from the femoro-tibial joint. The majority of displacement occurs over the femoro-tibial range 0° - 80° at all proximo-distal levels.

Graph showing the displacement of the apodeme complex at different proximo-distal levels over the range of femoro-tibial articulation

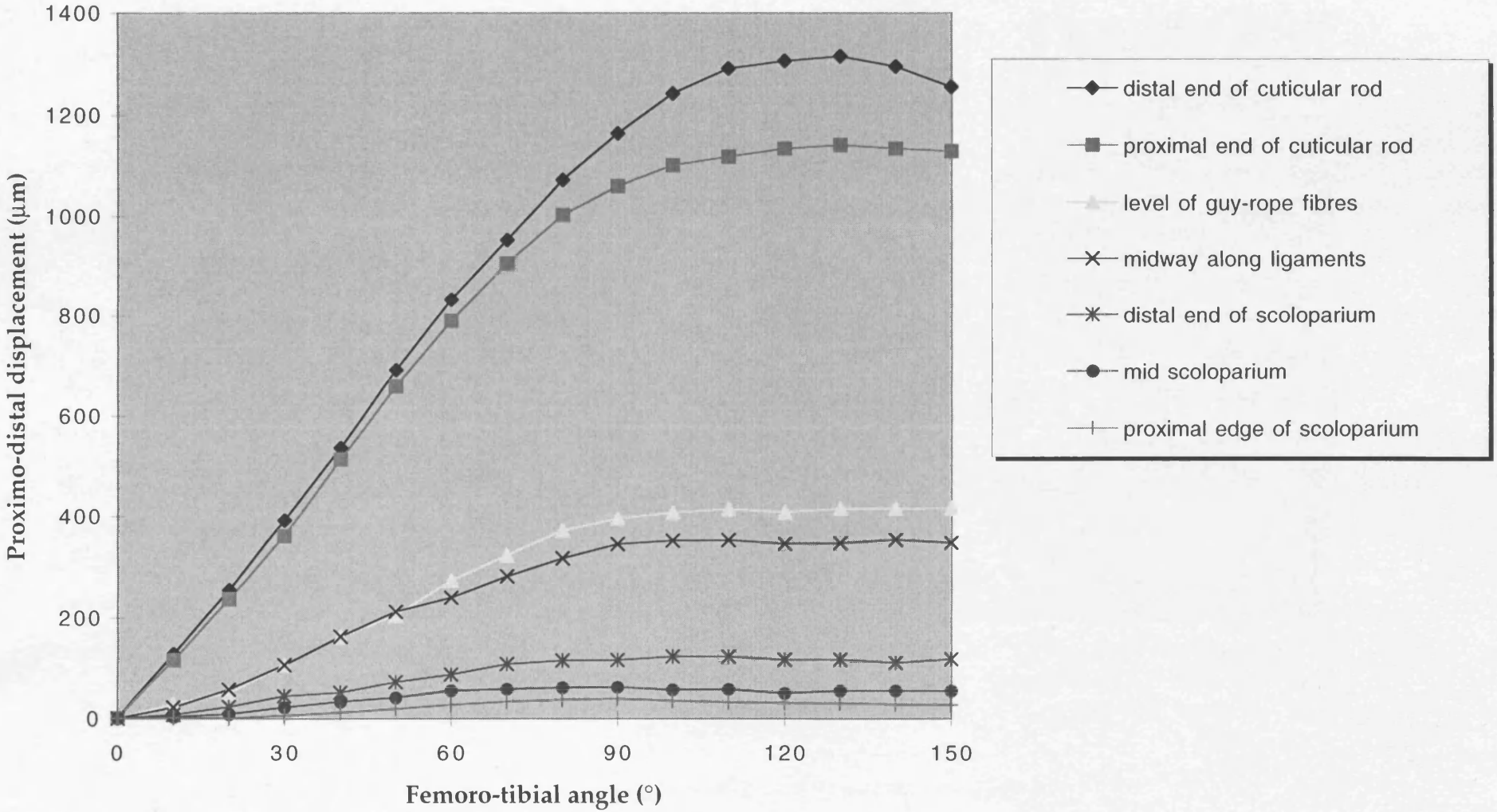

Figure 2.16

Histogram showing the mean range of proximo-distal displacements at different levels along the apodeme complex in *S. gregaria* (n = 4)
The magnitude of the input displacement at the level of the femoro-tibial joint is reduced by 30 times by the time the input is transmitted to the scoloparium.

Histogram showing how the input to the mtFCO sensory neurones is scaled down as it is transmitted from the site of stimulus input to the the sensory region of the organ (n=4)

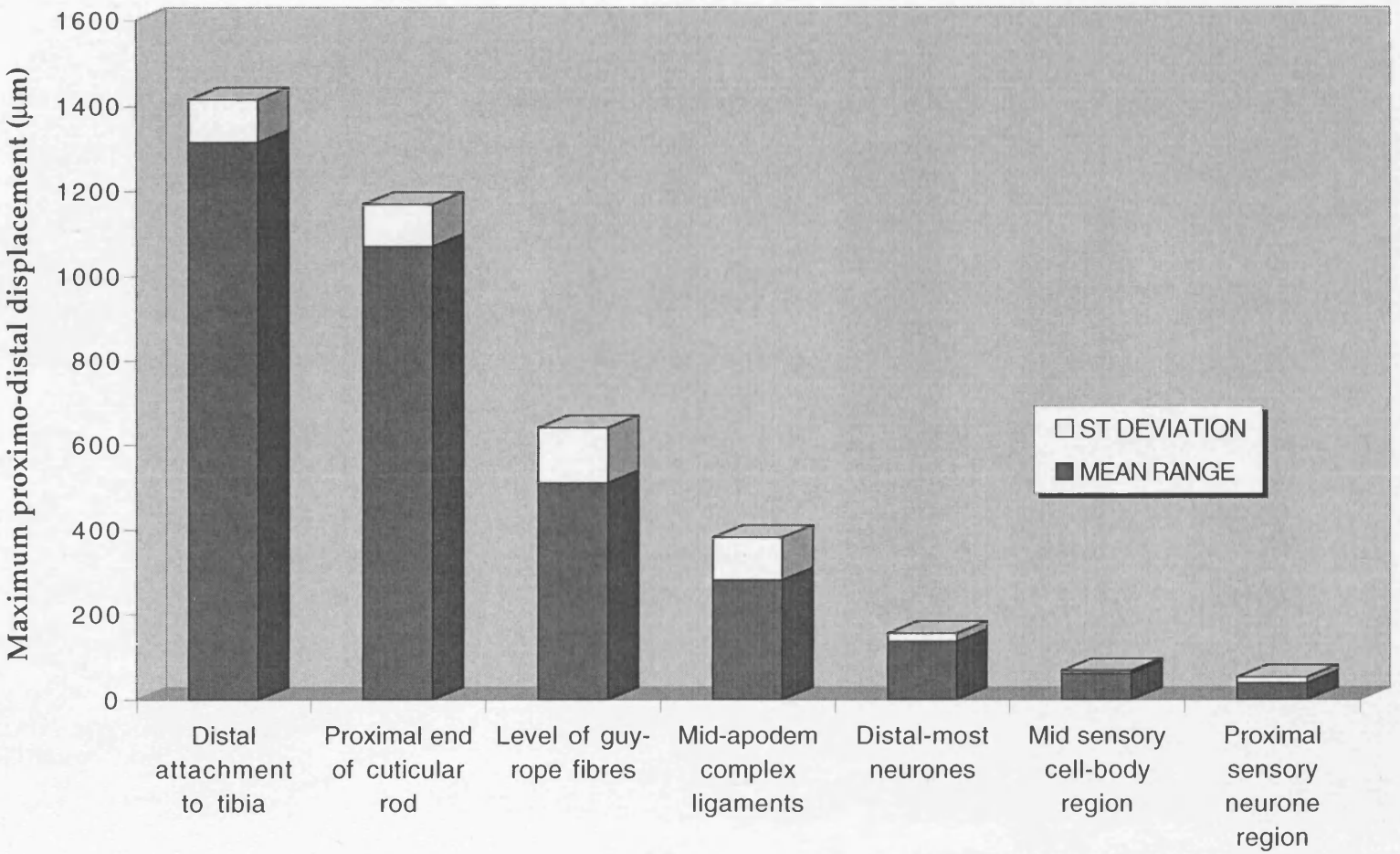

Figure 2.17

This graph shows the maximum range of displacement at several levels along the apodeme complex ligaments in four different preparations of *S. gregaria* (series 1-4). These results show that the magnitude of displacement is linearly related to distance along the ligaments (best fit $r^2 = 0.89$ $P = 0.05$). This demonstrates that the mtFCO ligaments represent a linear elastic coupling between the cuticular rod and the scoloparium, at which level the linearity is lost. The maximum range of displacement decreases by approximately 7% with every 100 μm travelled proximally along the ligaments.

Graph showing that the range of proximo-distal displacement decreases linearly along the length of the apodeme complex ligaments (n = 4)

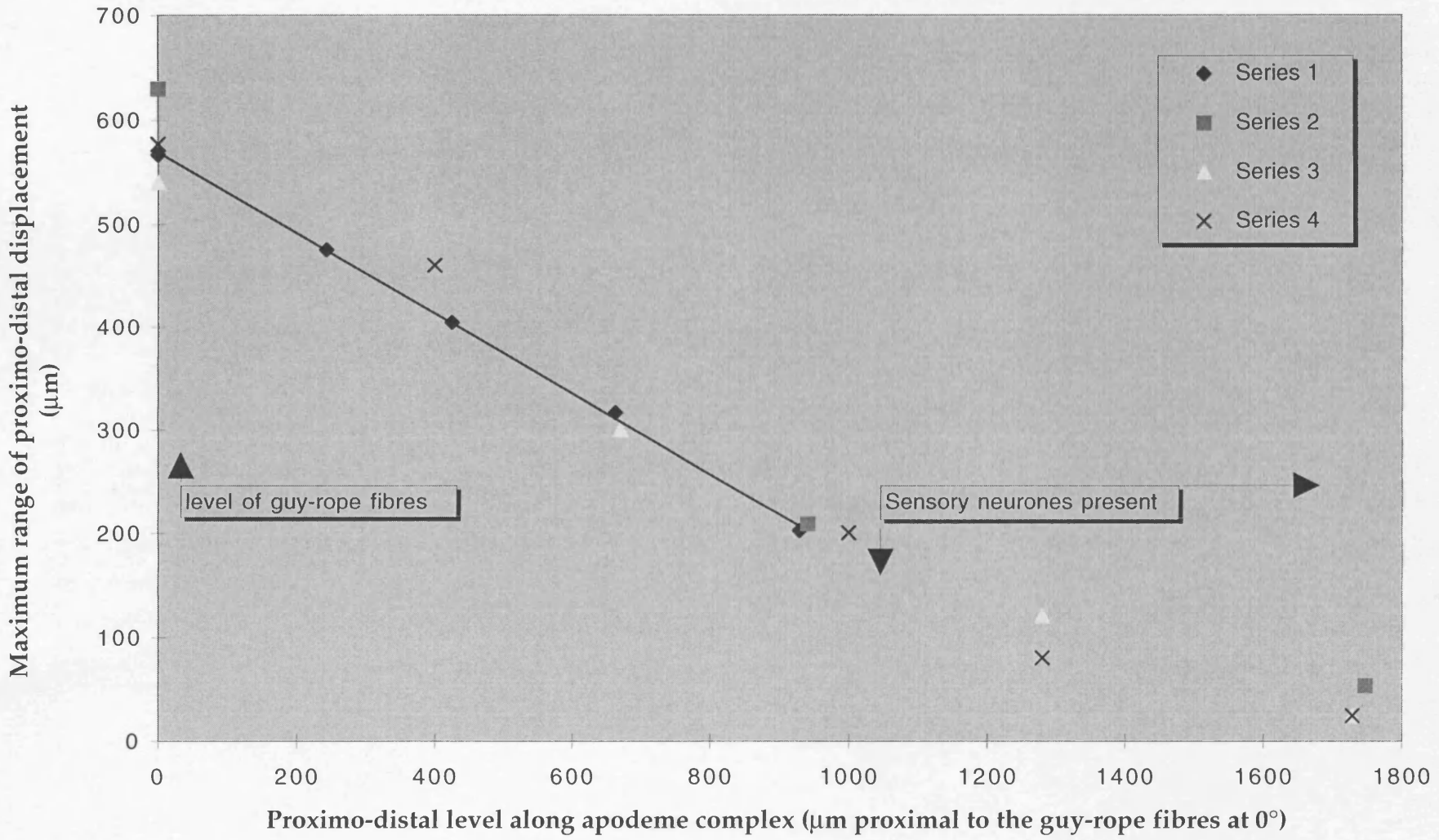

Figure 2.18

This graph contrasts the displacement of the dorsal and ventral ligaments of the apodeme complex at five levels along the ligaments between the guy-rope fibres (pair 1) and the sensory scoloparia (pair 5). The markers were located close to one another but on separate ligaments at a femoro-tibial angle of 0°. The proximo-distal level along the apodeme complex of each pair of markers at this angle is measured on the y axis where 0 μm was the level of the guy-rope fibres and 1000 μm was the level of the distal-most sensory neurones. As the femoro-tibial joint was rotated the markers in each pair were displaced by different amounts, indicating that the dorsal and ventral ligaments undergo differential movement. This phenomenon was especially evident at the level of the guy-rope fibres (pair 1) where the displacements were large. At the level of the sensory scolopidium (pair 5) the range of apodeme complex displacement, and consequently the magnitude of differential displacement between pairs of markers, is reduced.

Graph showing the displacement of pairs of dorsal and ventral markers situated at 5 different proximo-distal levels along the apodeme complex ligaments

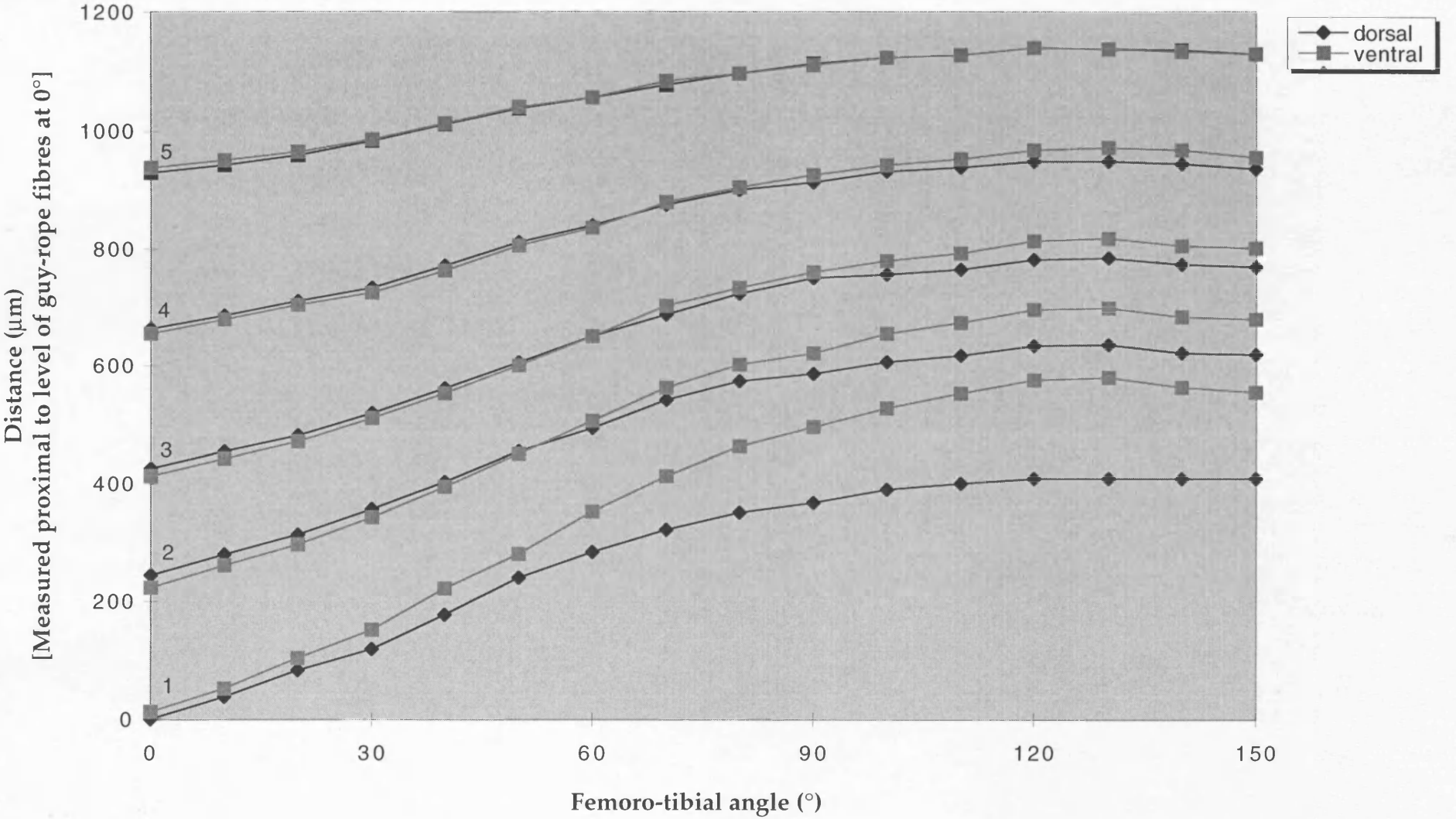

Figure 2.19

The range of displacement of the ventral ligament markers is linearly related to their location along the apodeme complex. This indicates that the ventral ligament is a linear elastic element.
In contrast, the range of displacement of markers located on the dorsal ligament is not linearly related to position along the ligament. This ligament has a smaller range of displacement than the ventral ligament at the level of the guy-rope fibres (due to the loop-forming region), and yet has a comparable range of displacement at the level of the scoloparium. This indicates that the dorsal ligament is not simply a linearly elastic element, but is more compliant at one end than the other.

Graph showing the maximum proximo-distal displacement of the dorsal and ventral apodeme complex ligaments at five proximo-distal levels in response to the full range of femoro-tibial articulation.

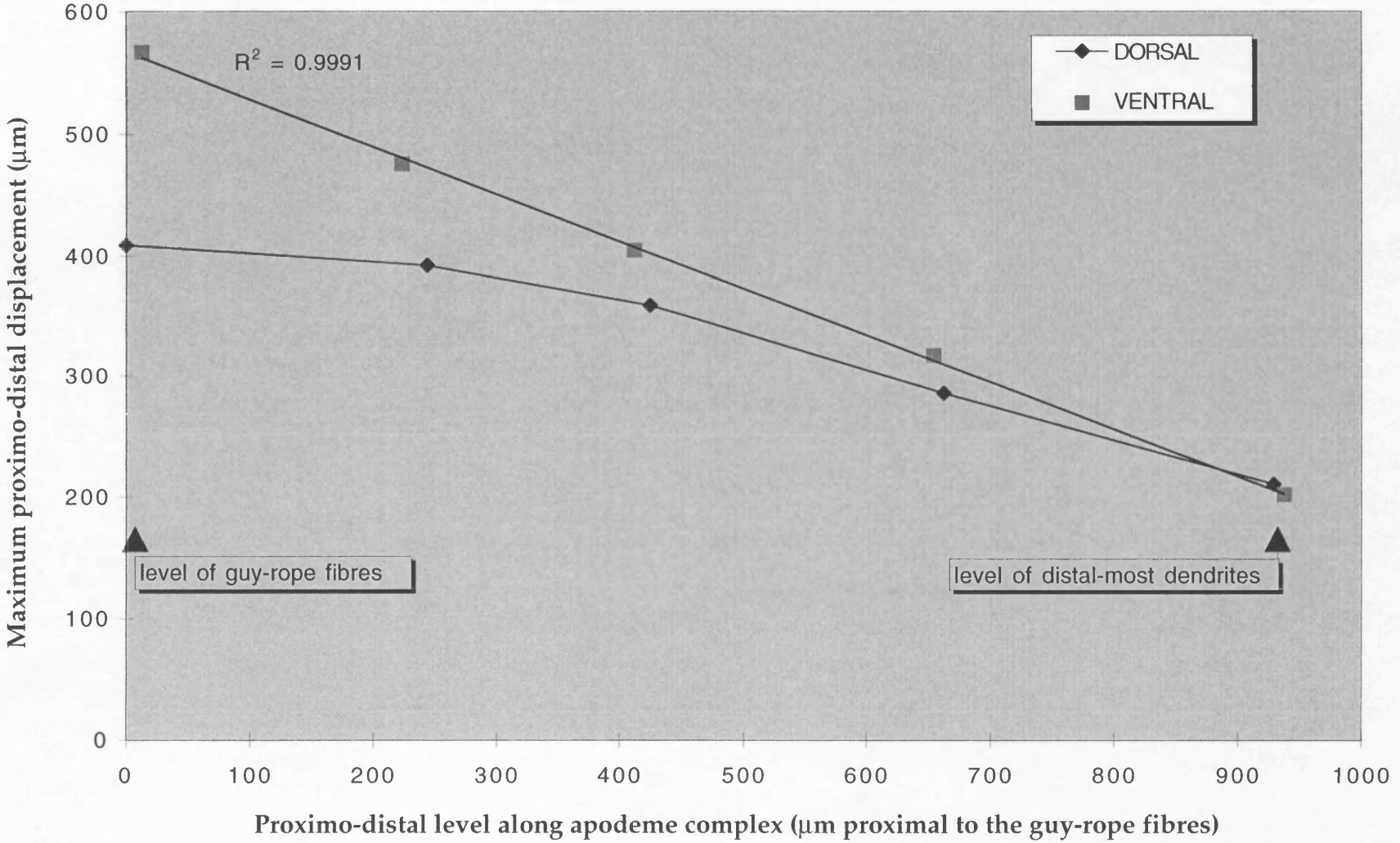

Figure 2.20

Histogram comparing the intervals between equidistant pairs of markers at opposite ends of the dorsal and ventral apodeme complex ligaments before and after the apodeme complex was stretched.
Each pair of markers was located 191 μm apart when the apodeme complex was relaxed. When the apodeme complex was stretched the interval between the marker pairs increased. The interval between the pairs of markers on the ventral ligament increased by a similar amount at both the proximal and distal ends of the ligament. In the case of the dorsal ligament, the distance between the pair of markers at the proximal end of the ligament increased by more than the distance between the pair of markers at the distal end. This indicates that proximal to the guy-rope fibres the ventral ligament in uniformly elastic along its length whilst the dorsal ligament is more compliant proximally than distally.

Histogram showing the distance between pairs of equidistant markers before and after the ligaments are stretched

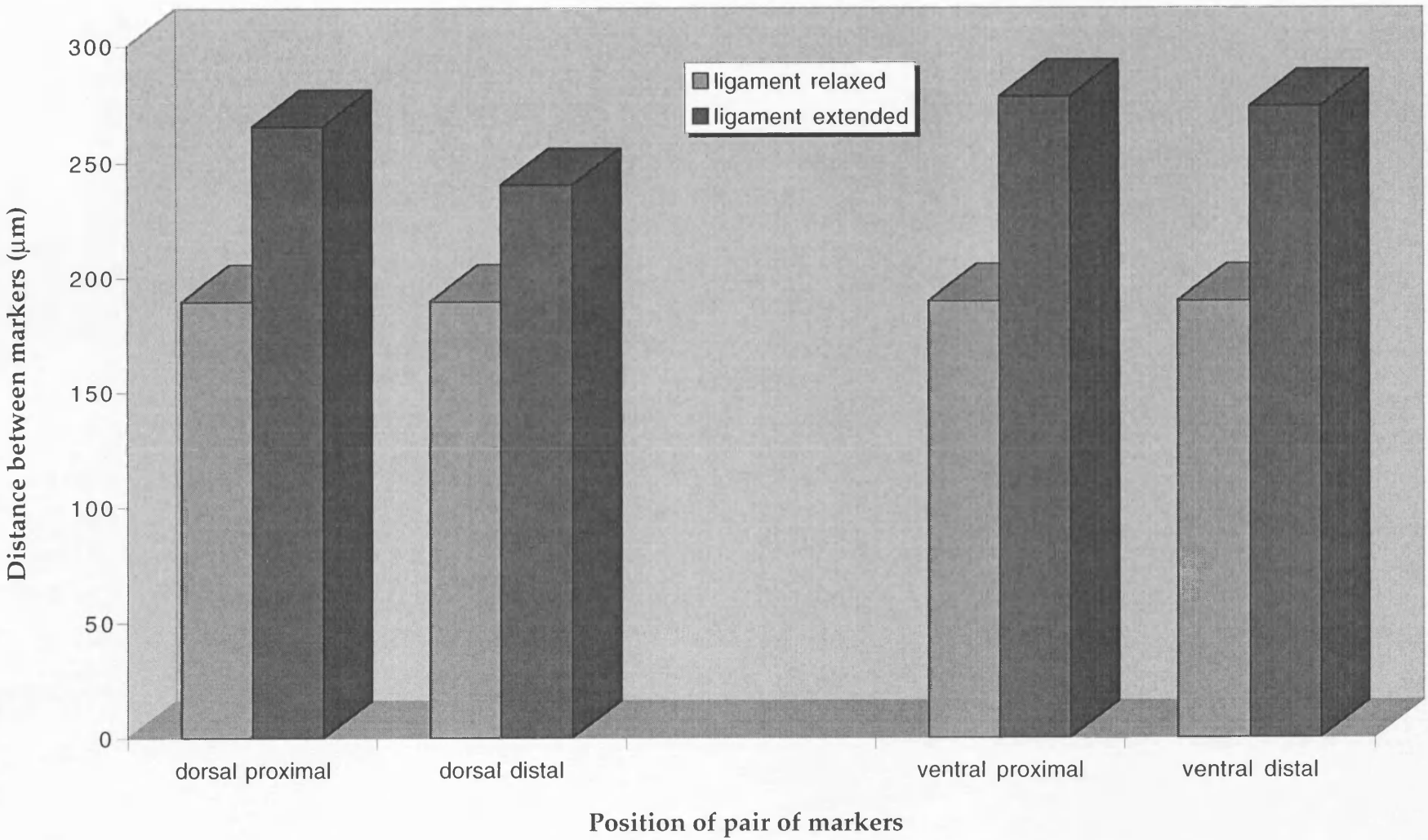

Figure 2.21

Graph demonstrating the way in which the displacement at different proximo-distal levels along the apodeme complex were scaled to allow a standardised comparison with the input displacement at the level of the femoro-tibial joint. In this case the displacement at the level of the guy-rope fibres is plotted before and after scaling so that the maximum displacement is of equal magnitude to that of the distal attachment of the cuticular rod to the tibia. The difference between the curves of input displacement and scaled displacement at the guy-rope fibre level describes the way in which the input has been qualitatively modified during transmission along the apodeme complex to that level.

Graphical demonstration of the way in which the displacement of the apodeme complex at different proximo-distal levels was compared to the input at the femoro-tibial joint

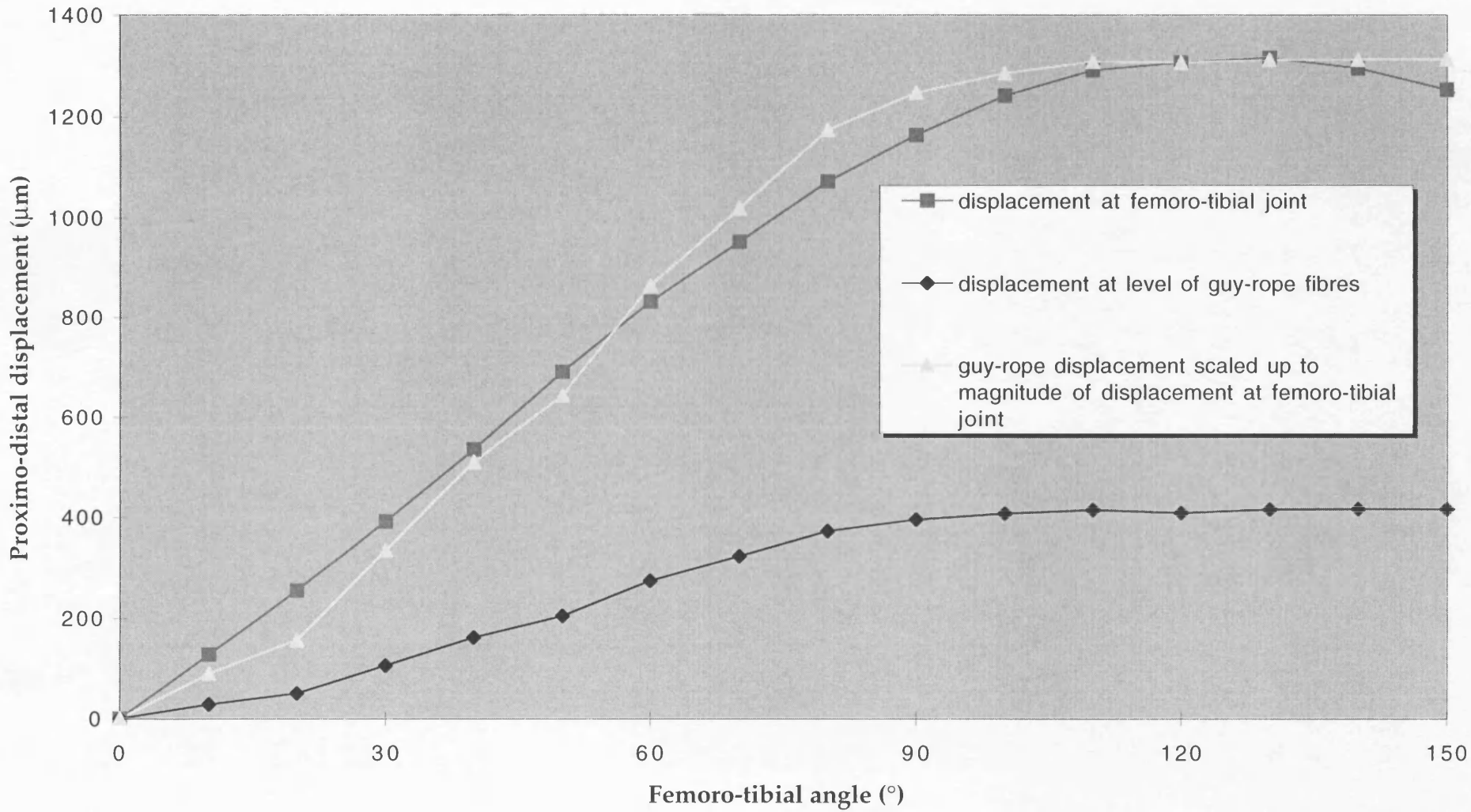

Figure 2.22

Graph showing the relative modification of the input displacement at different proximo-distal levels along the apodeme complex in response to static displacements of the tibia. The curves represent the difference between the displacement at the femoro-tibial joint and the scaled displacements at each proximo-distal level (see Fig. 2.21). Positive values indicate that levels of displacement are larger than would occur if the overall pattern remained sinusoidal. (Negative values indicated that displacements are smaller than would occur under the same conditions). Thus, quantitative modification of the input alone would be represented by a horizontal line intersecting with the y-axis at 0. Deviation from this line represents qualitative modification of displacement whilst being transmitted proximally. The graph shows that displacements at the extremes of the femoro-tibial range are filtered out whilst displacements over femoro-tibial angles 40° - 110° are selectively amplified. At increasingly proximal levels, the degree of differential modification increases, whilst the range of femoro-tibial angles over which selective amplification occurs is reduced.

Graph showing how the input stimulus is qualitatively modified as it is transmitted proximally along the apodeme complex

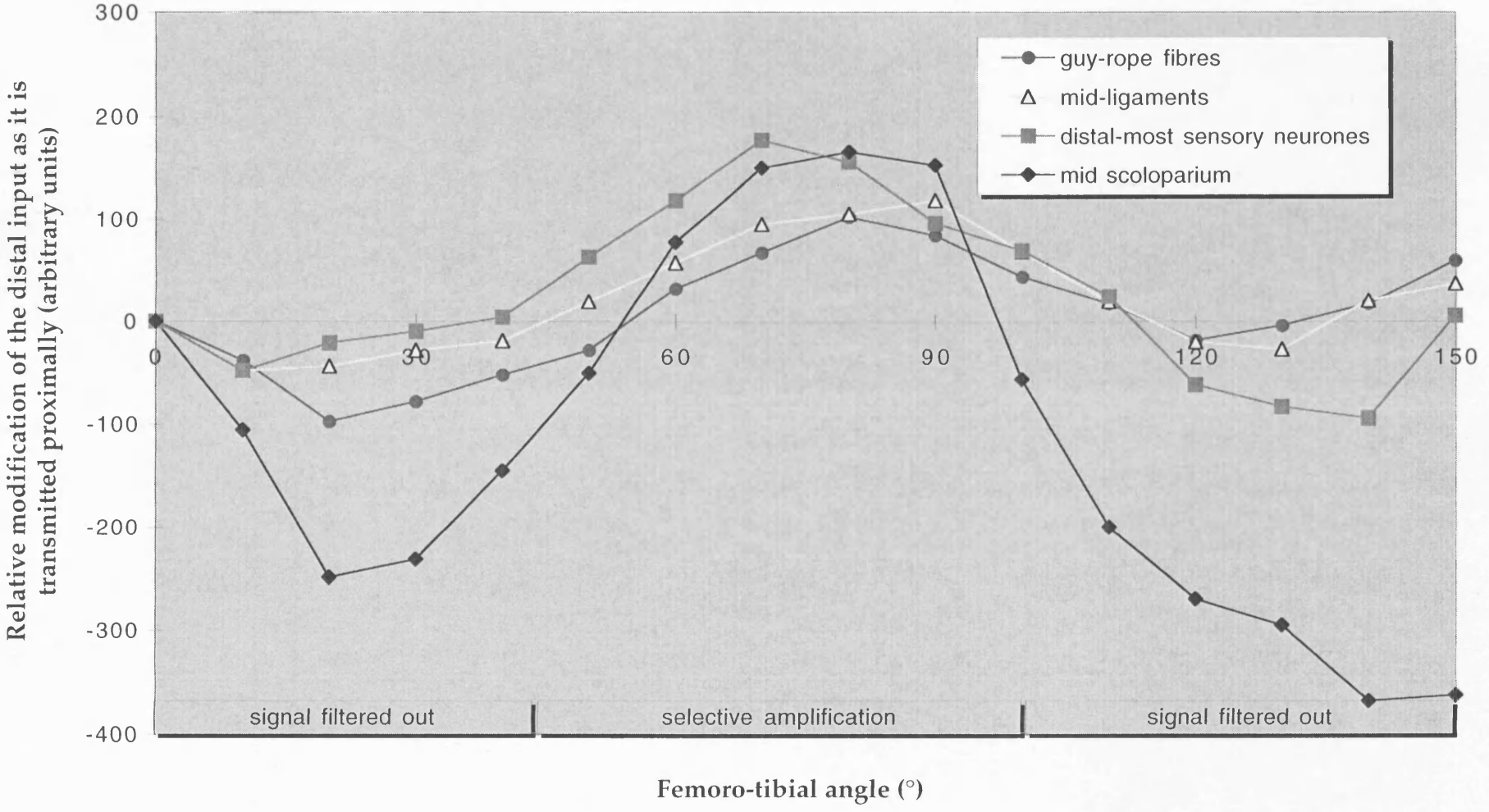

Figures 2.23a-d

This set of four histograms shows the proximo-distal displacement measured over discrete 30° intervals of the femoro-tibial angle range at four proximo-distal levels along the mtFCO scoloparium. The levels are: a) 730μm, b) 630μm, c) 365μm and d) 150μm from the proximal edge of the mtFCO scoloparium when the leg was fully flexed (see semi-schematic diagram below). Displacements measured at the distal-most point (Fig. 2.23a) reflect the sinusoidal shape of the input displacement at the level of the femoro-tibial joint. At increasingly proximal levels the magnitude of the displacements is reduced and the relative displacements occurring over different parts of the femoro-tibial range are modified (Figs 2.23b-d). At the most proximal point, located in the middle of the scoloparium, the majority of the displacement occurs over the 60° - 90° range of femoro-tibial angles (Fig. 2.23d).

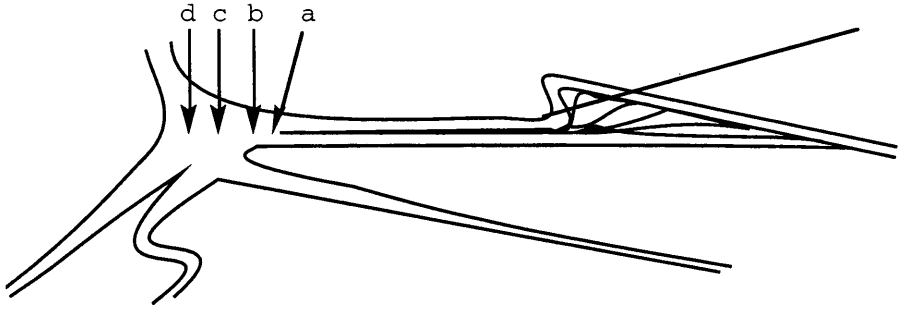

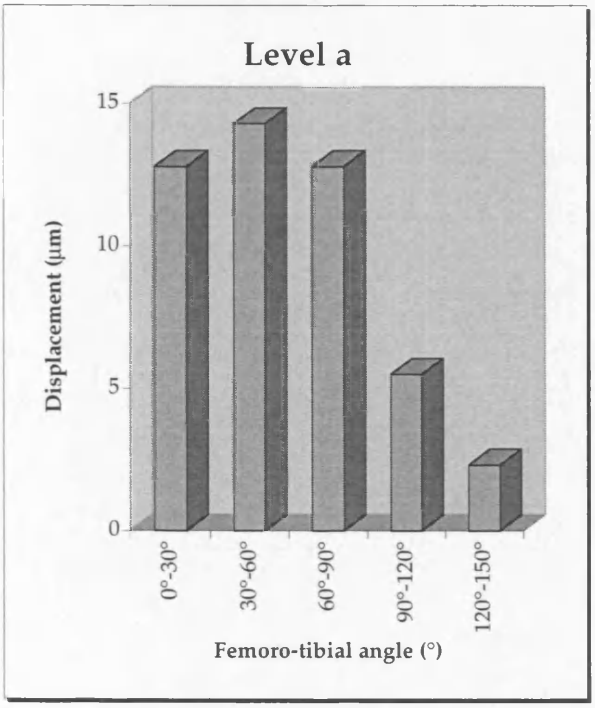
Level a
Displacement (µm)
15
10
5
0
0°-30°
30°-60°
60°-90°
90°-120°
120°-150°
Femoro-tibial angle (°)

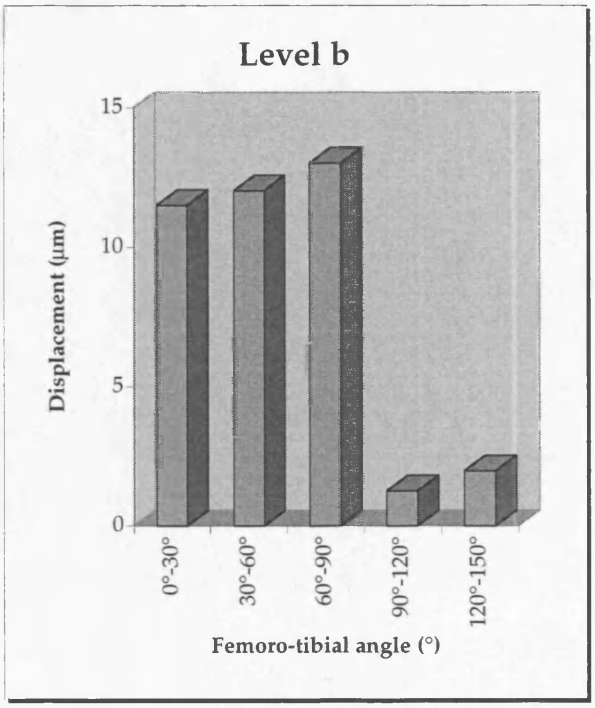
Level b
Displacement (µm)
15
10
5
0
0°-30°
30°-60°
60°-90°
90°-120°
120°-150°
Femoro-tibial angle (°)

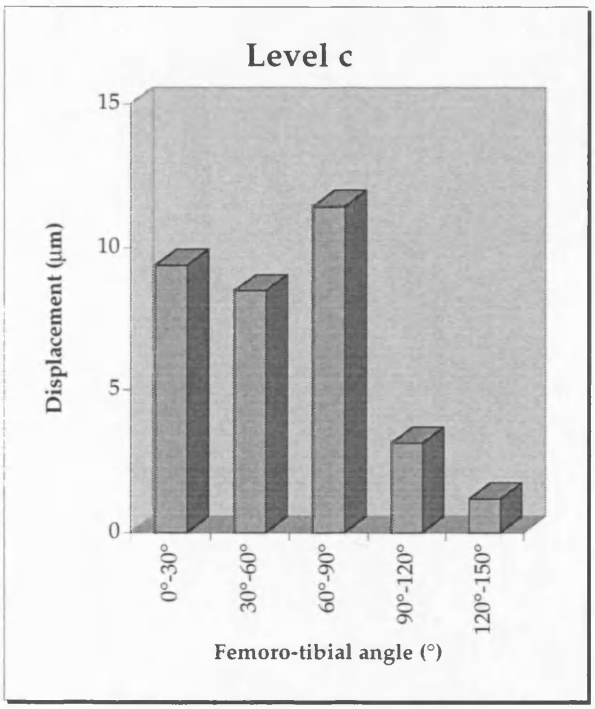
Level c
Displacement (µm)
15
10
5
0
0°-30°
30°-60°
60°-90°
90°-120°
120°-150°
Femoro-tibial angle (°)

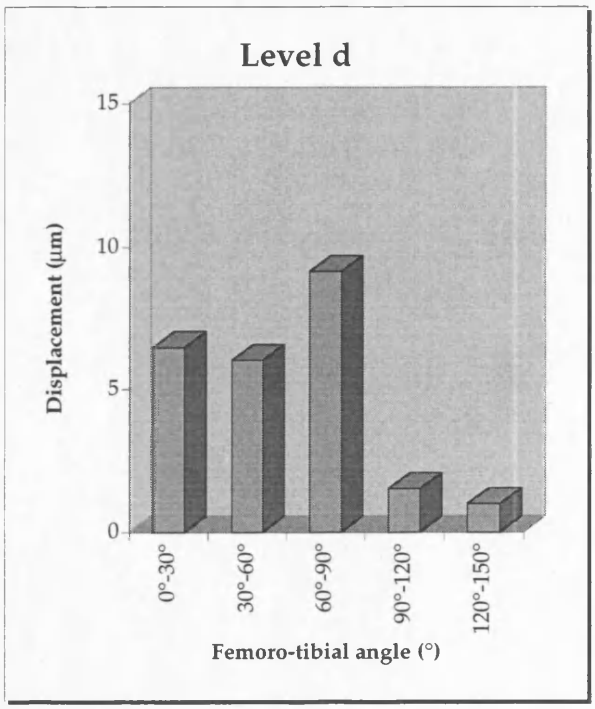
Level d
Displacement (µm)
15
10
5
0
0°-30°
30°-60°
60°-90°
90°-120°
120°-150°
Femoro-tibial angle (°)

Figure 2.24

Graph showing the degree of selective amplification of the input displacement measured at the middle of the sensory scoloparium in four preparations. All four show a similar pattern of displacement modification with the mean maximum amplification occurring at 62.75° ±SD 12.5°.

Graph showing the qualitative modification of the input stimulus between the distal input to the apodeme complex and the level of the mtFCO sensory neurones in 4 preparations

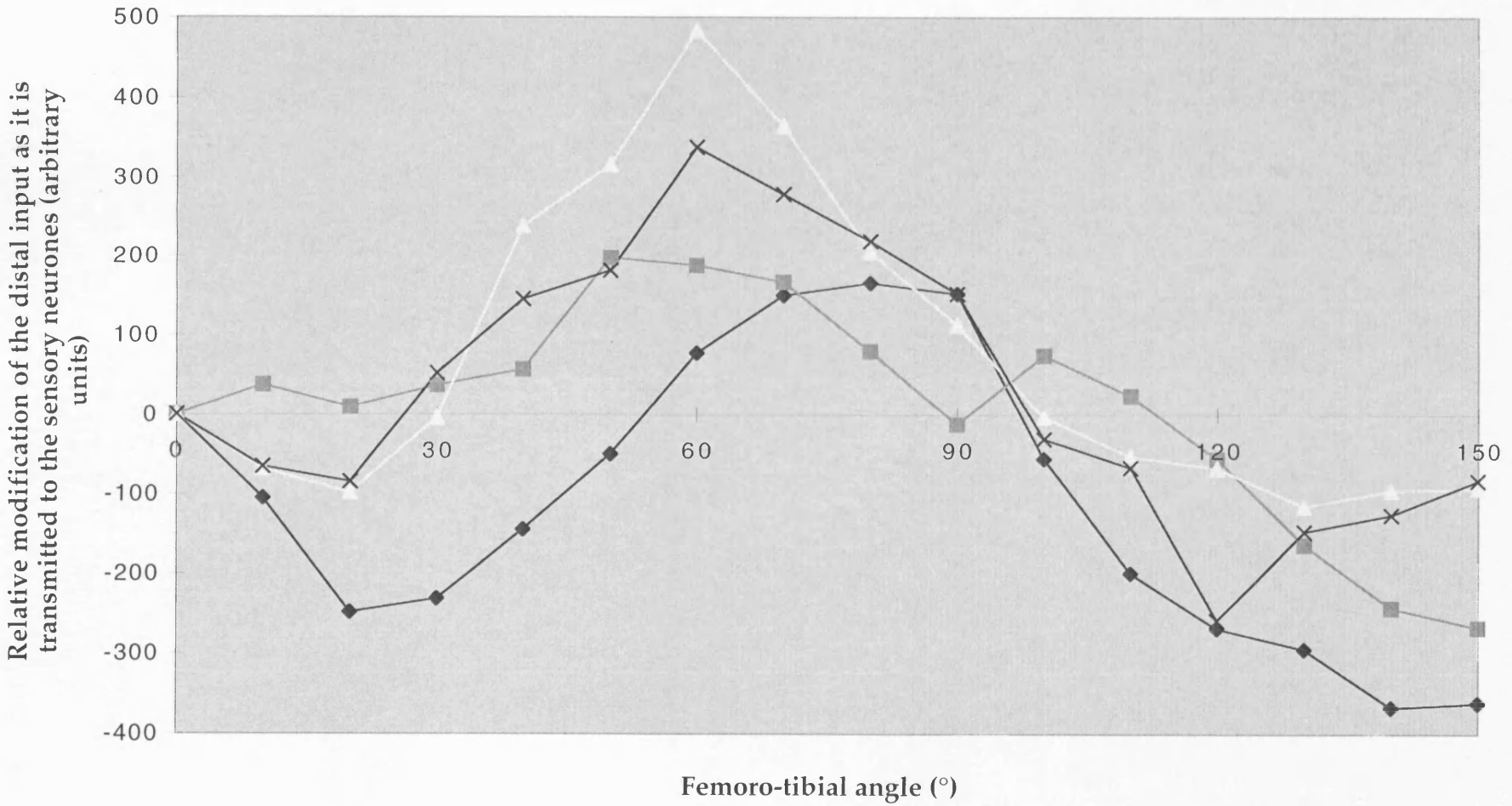

Figures 2.25a-f

Series of morphing maps showing the distortion of the mtFCO scoloparium at 30° intervals across the range of femoro-tibial angles.

As the tibia is extended, the scoloparium becomes proximo-distally compressed due to the elastic recoil of the organ as the apodeme complex is unloaded. The scoloparium also becomes dorso-ventrally elongated due to the increased loading of the flexor strand during tibial extension. This is especially noticeable between the femoro-tibial angles of 60° - 90° (Figs 2.25c, d). A comparison of the maps at extremes of flexion (Fig. 2.25a) and extension (Fig. 2.25f) shows that the distal-most neurones in the scoloparium are likely to be subjected to the most local distortion.

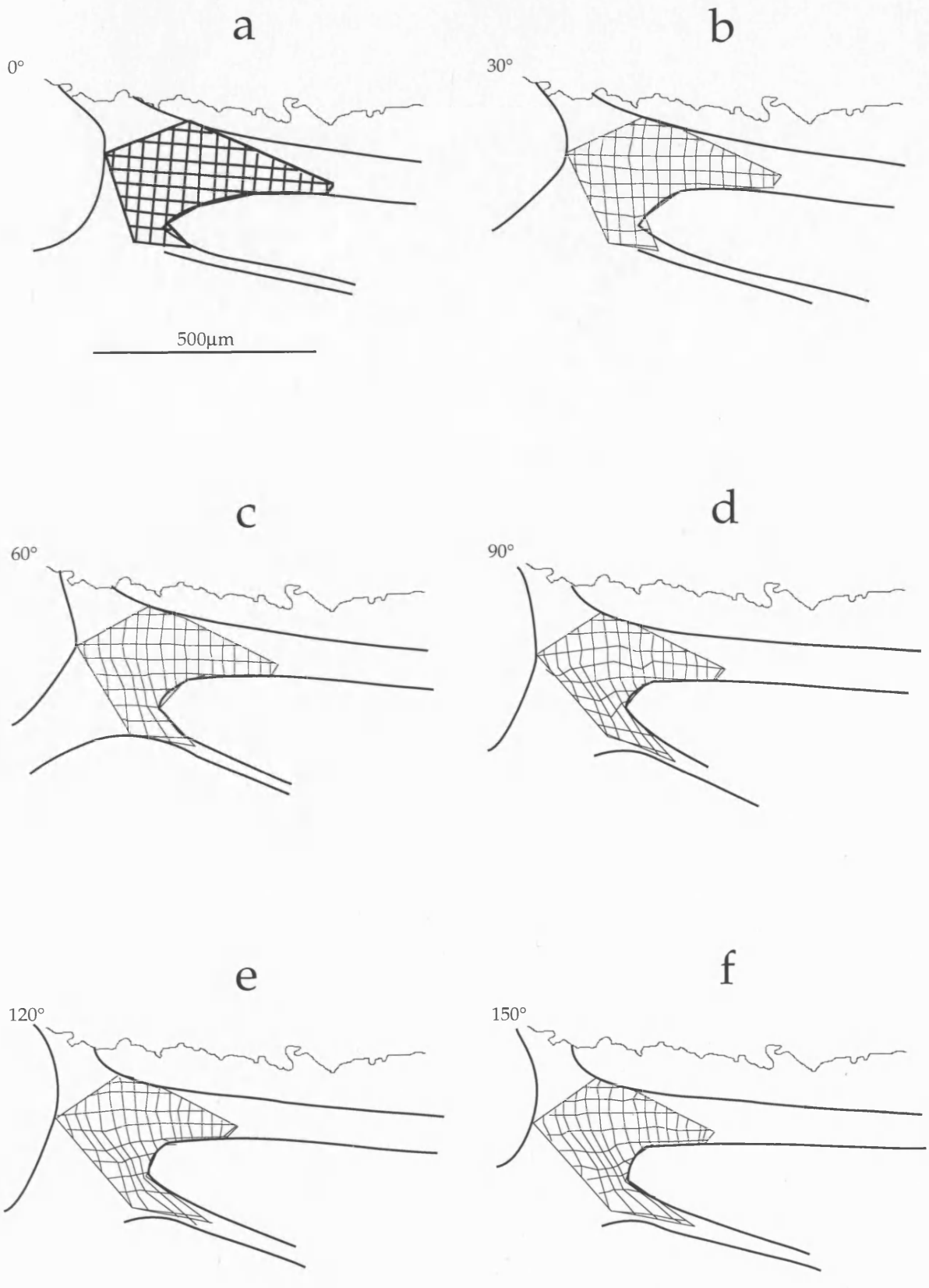
a
0°
b
30°
500µm
c
60°
d
90°
e
120°
f
150°

Figure 2.26

This figure shows the position of the mtFCO scoloparium at three femoro-tibial angles. During tibial extension, the scoloparium is displaced proximally and is slightly rotated due to the combined effects of the ventral attachment ligament and the antagonistic displacements of the apodeme complex and the flexor strand.

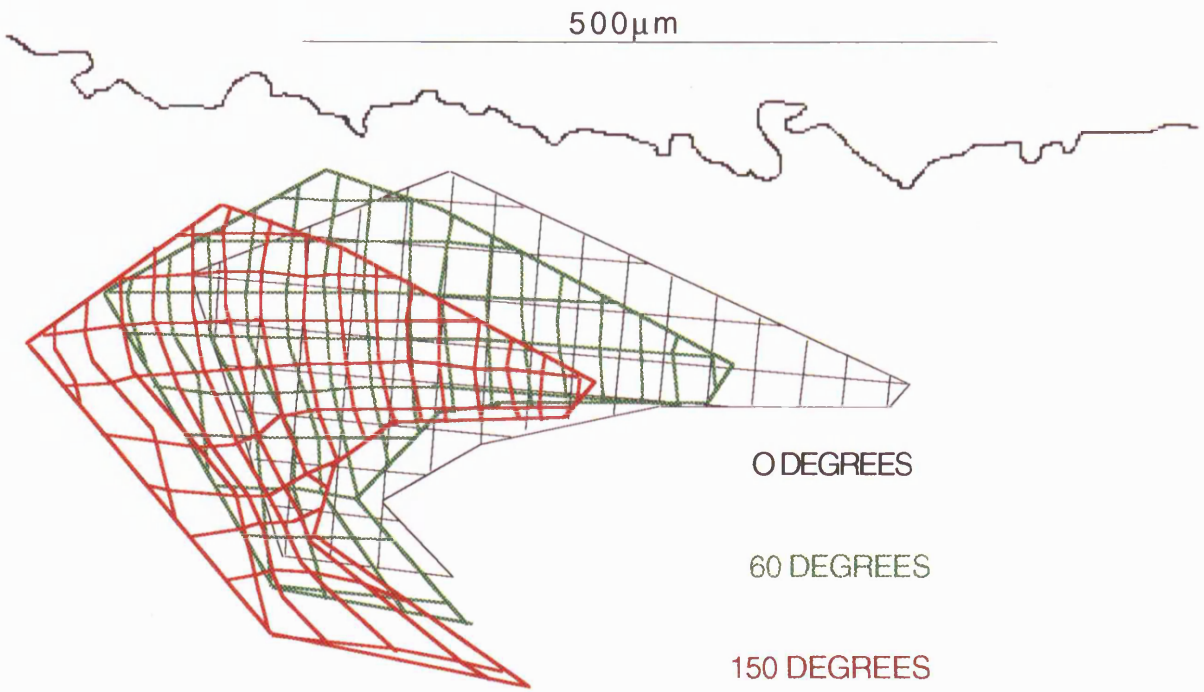
500µm
O DEGREES
60 DEGREES
150 DEGREES

Chapter 3: Ultrastructure of the mtFCO mechanical linkages

3.1 SUMMARY

- *The mtFCO's dorsal attachment, ventral attachment and the ligaments of the apodeme complex, all contain microtubule-packed ligamentous cells associated with differing amounts of extracellular matrix.*

- *The observations in this chapter indicate that the extracellular (Acid Fuchsin-staining) fibres are likely to play an important role, in conjunction with the microtubule-packed attachment cells, in the transmission of mechanical force along the apodeme complex to the mtFCO sensory neurones.*

- *Large (0.5 μm - 1.0 μm diameter) extracellular (Acid Fuchsin-staining) fibres are a common component in all of the organ's mechanical linkages. The guy-rope fibres in particular appear to be composed almost exclusively of this material. In most cases, extracellular fibrils can be found associated with these fibres suggesting that the larger fibres may be formed by the aggregation of fibrils.*

- *It is reasonable to speculate on the grounds of differential distribution of elastic components, the range of attachment cell lengths and the varying diameters and organisation of the attachment cells within the dorsal and ventral ligaments, that the two ligaments will have different mechanical propèrties.*

- *The attachment cells do not appear to be free to slide independently past their neighbours. Instead adjacent attachment cells form desmosome-like junctions, often at the sites of cell to cell interdigitations.*

3.2 INTRODUCTION

Although there are published ultrastructural descriptions of chordotonal organs, none have been comprehensive and few have really considered the structural roles of the different components of the respective systems (Theophilidis, 1986a, b; Field, 1991; Shelton *et al.*, 1992; Yack and Roots, 1992). The present study was designed to identify the ultrastructural features of the mtFCO that are likely to have an important mechanical role.

This chapter includes a description of the mtFCO dorsal and ventral attachments, the ligaments of the apodeme complex and the guy-rope fibres. In addition, the mtFCO flexor strand has been examined at the light

microscope level to reveal its general anatomy. The strand contains a strand-type receptor (Bräunig, 1985) which is associated with both extracellular fibres and fibrils. Further details of the ultrastructure of the strand are investigated in Chapter 7.

Axially oriented extracellular fibres are found throughout the mtFCO and have been reported previously in the apodeme complex of the locust mtFCO (Field, 1991; Shelton *et al.*, 1992) and in the main linkages of similar systems (Nowel *et al.*, 1995: mtFCO of the cricket *Acheta domesticus*). The fibres stain intensely with Acid Fuchsin (Shelton *et al.*, 1992) and phospotungstic acid (Nowel *et al.*, 1995). Similar fibres have been found associated with the nerve cord of insects (Locke and Huie, 1972) and are known to contribute to the elasticity of biological structures (see Nowel *et al.*, 1995). This study shows that such fibres form an integral part of each of the mtFCO's mechanical linkages and that each mechanical linkage has a characteristic distribution of fibres. The results of this chapter show that the extracellular fibres divide the attachment cells into bundles running the length of the apodeme complex ligaments. The distribution of extracellular fibres associated with the mtFCO ligaments has been quantified and in conjunction with other ultrastructural observations suggests that the dorsal and ventral ligaments of the apodeme complex may possess different mechanical properties from one another. Such differences would have functional implications for the sensory neurones lying in series with each ligament.

It is shown that small diameter extracellular fibrils, which exhibit a banding pattern in longitudinal section, are usually found adjacent to the extracellular fibres. In particular, the mtFCO's ventral attachment contains vast numbers of extracellular fibrils. Extracellular fibrils are also present within the dorsal and ventral ligaments and within the organ's dorsal attachment to the femur. This type of fibre is not thought to be collagenous. However, the mtFCO flexor strand is unique in containing an additional class of extracellular fibril that exhibits a distinctive collagen-like banding pattern. The abundance of extracellular fibrils varies between each of the organ's linkages.

The distribution of other components which may influence the mechanical properties of the mtFCO are also examined in this chapter. All

the linkages, with the exception of the flexor strand, feature ligamentous cells that contain axially-orientated microtubules. Axial arrays of microtubules have been proposed by several authors to play a tensile role in the mechanical linkages of proprioceptors (Young, 1970; Moulins, 1976; Yack and Roots, 1992). The organ's dorsal attachment to the femur is exceptional in containing an irregular combination of cellular and acellular components arranged in a complex manner. This has implications regarding its mechanical role.

3.3 METHODS

3.3.1 Dissection and fixation

Adult male and female specimens of the locust, *Schistocerca gregaria* were obtained from laboratory cultures. Isolated metathoracic legs were dissected using a Schott cold light source and a binocular dissecting microscope. Insect saline (see Appendix 1) was used to prevent desiccation of the leg. To reveal the chordotonal organ, windows of cuticle from both the anterior and posterior sides of the femur were removed. The preparations were fixed *in situ* using Karnovsky's (1965) fixative (see Appendix 1) at 4°C for 30 minutes. Short lengths of clean polythene tubing were used to constrain the femoro-tibial joint such that the tibia was held in either the extended or flexed position. Some preparations were postfixed in phosphate buffered 1% osmium tetroxide for 20-30 minutes for TEM analysis.

3.3.2 Embedding

Fixed material was dehydrated in an acetone series before being embedded in EM-grade Araldite. Material to be sectioned serially was embedded in plastic capsules. Wholemount preparations to be examined using conventional light microscopy were mounted on slides using a plastic ring to support a coverslip and retain the Araldite.

3.3.3 Sectioning and staining for light microscopy

Four chordotonal organs were serially sectioned at 1.0 µm using a Huxley ultra-microtome. The sections were mounted in order on subbed slides (subbing solution: 0.1% gelatine + 0.01% chrome alum) and stained with either 1% Toluidine Blue in 1% borax or 5% aqueous Acid Fuchsin (Shelton *et al.*, 1992). Number 0 coverslips were mounted using EM-grade

Araldite. One series of sections was analysed in detail using image analysis techniques.

3.3.4 Analysis of images obtained from serial transverse sections

The semi-thin sections prepared as above were examined using an Olympus Photomicroscope with a x100 oil immersion objective. Image analysis techniques were used to quantify various components within the sections. For this, high resolution (215 pixels/μm^2) images of selected sections were captured using a JVC (TK-1085e) charge-coupled device (CCD) camera and Scion Corporation AG-5 frame-grabber connected to a PowerMacintosh 8100/80 computer with a 17 inch monitor. The images were then displayed and analysed using the public domain software NIH Image (vs. 1.6/ppc) developed at the U.S. National Institutes of Health and available on the Internet at http://rsb.info.nih.gov/nih-image/.
To enable the capture of comparable images from different sections, the camera's built-in automatic gain control was disabled. This enabled the illumination for each section to be manipulated at the microscope without the camera automatically adjusting its sensitivity to compensate. The live video image was displayed on the monitor as the microscope was adjusted. A real time frequency histogram showing the distribution of greyscale values within the image was displayed as the focus and illumination of the section was optimised. The histogram plot was updated frame by frame and showed, for each of the possible 256 greyscale values, the number of pixels in the image that had a particular value. In addition, the software was configured to highlight saturated pixels on the monitor. This made it possible to judge the optimum illumination and ensure good contrast between the stained objects and the background before each image to be analysed was captured.

Images to be analysed were manipulated using a built-in frame averaging function. 16 successive frames were averaged to reduce any background noise in the video signal. The resulting image was saved to disk.
All images were spatially calibrated in μm by assigning the appropriate pixel:μm ratio. Measurements of ligament cross-sectional area were made by manually selecting the area to be measured with an outlining tool. The area of each selection made on the calibrated image was returned in μm^2 and written to a spreadsheet.

Analysis of the cross-sectional areas of stained extracellular fibres was performed using a particle analysis macro routine. The macro automatically counted and measured objects in a binary or thresholded image. It operated by scanning across the image until it encountered the boundary of an object, outlined the object using an outlining routine, measured the object, and then redrew the object at a different (reserved) greyscale level so that each object was only counted once. The macro was configured to ignore particles smaller than a minimum particle size of 4 pixels to avoid counting any specks caused by noise.

Thresholding based on greyscale values was required to discriminate objects of interest from surrounding background. Each image was thresholded using a density slicing mode in which all pixels between an upper and lower threshold were highlighted in red. Background pixels were left unchanged. Threshold levels were manually adjusted so that the objects to be analysed were highlighted. The threshold levels of the density slice were dynamically displayed on a greyscale frequency distribution histogram beside the image window. This enabled the thresholds to be set with respect to the distribution of greyscale values that represented the objects of interest in each image (Fig. 3.1). Setting the thresholds individually for each image in this way allowed for differences in staining intensity between sections whilst maintaining the consistency of regions selected for measuring. The consistency of area selection using this method was in excess of 95% (based upon % error in measured area of 20 images of the same section captured under different optical conditions).

3.3.5 Sectioning, mounting and staining for TEM

Material for examination using transmission electron microscopy (TEM) was sectioned at about 0.1 μm using a glass or diamond knife on a Huxley ultra-microtome. Sections were cut at a range of proximo-distal levels along the mtFCO. The sections were picked up on Pioloform films and mounted on 0.5 mm slot grids. The sections were stained using lead citrate and uranyl acetate or hot (60°C) 2% aqueous phosphotungstic acid (after Locke and Huie, 1972). Stained sections were examined with a Jeol 100CX Transmission Electron Microscope at an accelerating voltage of 80-100 kV.

3.3.6 Carboxyfluorescein staining

To stain fibrous components of the mtFCO, freshly isolated metathoracic legs were injected with 5% 5(6)-carboxyfluorescein (see Appendix 1) and left overnight at 4°C. The mtFCO was then dissected out, rinsed with phosphate buffer and mounted on a slide under a coverslip. Clear nail varnish was painted around the edge of the coverslip to secure and seal it to the slide. These preparations were viewed using an inverted epifluorescence microscope equipped with a BioRad Lasersharp MRC 400 confocal laser scanning system fitted with a blue high-sensitive filter block to excite at 488 nm. The emission was detected at 515 nm and above. Images were stored on optical disc for subsequent image analysis.

3.4 RESULTS

3.4.1 The organisation of the dorsal attachment

Although Usherwood *et al.* (1968) incorrectly described it as attached to the posterior femur wall, the mtFCO is anchored to the antero-dorsal femur wall by a short dorsal attachment (see Shelton *et al.*, 1992). This is approximately 500 μm in length and is enclosed in a sheath that contains extracellular fibres that stain with Acid Fuchsin. Transverse sections through the dorsal attachment reveal it to be a double structure consisting of two ligamentous components. The posterior of the two is the larger in cross-section at most levels along the attachment, and it has a dorsally thickened sheath where it is anchored to the wall of the femur (Figs 3.2a-c). Proximally (with respect to the mtFCO), where the dorsal attachment joins the cell body region, it is the anterior component which is the larger of the two structures (Fig. 3.2d). The anterior and posterior components of the dorsal attachment are mechanically connected to one another along the ventral edge of the attachment by the membranous sheath.

The two components of the dorsal attachment contain ligamentous cells surrounded by various extracellular materials (Figs 3.3). The ligamentous cells form only a small proportion of the cross-sectional area of the dorsal attachment (Fig. 3.3). These cells are packed with microtubules and are surrounded by extracellular matrix (Fig. 3.4a). The dorsal attachment also contains another type of cell that is packed with an amorphous granular material (Fig. 3.4b). The extracellular matrix of the dorsal attachment contains both fibrils (diameter 10 nm - 20 nm) and larger fibres (Fig. 3.3)

that stain with Acid Fuchsin at the light microscope level. The largest Acid Fuchsin-staining fibres (diameter approximately 1 μm) are located dorsally in the attachment sheath, and are found in association with the fibrils (Figs 3.5a, b). The distribution of the extracellular materials within the dorsal attachment is complex. Microtubules, Acid Fuchsin-staining fibres, fibrils and the amorphous-appearing material are all located adjacent to one another within the attachment, with extensive membrane invaginations separating each type of material (Fig. 3.6).

The posterior component of the dorsal attachment is largely composed of fatty deposits. The anterior component contains a ventrally located receptor that is innervated by a branch of nerve 5b1 that extends into the dorsal attachment (Fig. 3.7). Although incompletely described, this sensillum has been identified previously as a multiterminal receptor (Matheson and Field, 1990). The receptor is surrounded by a membranous capsule (Fig. 3.8a) that is completely separated from the dorsal attachment sheath by a layer of glial wrapping (Fig. 3.8b). Its function is unknown. In addition to the multiterminal receptor, the anterior component of the dorsal attachment contains a branch of the cuticular nerve (Fig. 3.7). It does not appear to have any sense organs associated with it in the dorsal attachment and its destination is unknown.

The cross-sectional area of the attachment as a whole increases from 1500 μm^2 at the point of its attachment to the dorsal epidermis to 4000 μm^2 at the level where it joins the sensory cell body region of the organ (the scoloparium). The proportion of Acid Fuchsin-staining material measured at the light microscope level rises nearer to the scoloparium, comprising 5% of the total cross-sectional area at its cuticular attachment and 23% where it enters the region containing sensory cell bodies (Fig. 3.9). This suggests that the dorsal attachment is stiffer close to the mtFCO scoloparium than it is at the level at which it attaches to the femur.

These observations show that the dorsal attachment has a combined mechanical and sensory role. The double nature of the attachment is consistent with the hypothesis that the mtFCO is formed from two scoloparia.

3.4.2 Organisation of the ventral attachment

The ventral attachment ligament consists of fibrous cells containing axially orientated microtubules surrounded by an extracellular matrix which contains extracellular fibres. In addition to extracellular fibres, the extracellular matrix also contains large numbers of extracellular fibrils. These fibrils have characteristic profiles when viewed in cross-section, similar to those of fibrils associated with elastic tissues reported by previous authors (Locke and Huie, 1975). The ventral attachment links the mtFCO to the apodeme of the flexor-tibiae muscle (see Chapter 2: Figs 2.6a-d). Close to its origin at the mtFCO, the ligament has an approximately circular cross-section. At the level at which the attachment inserts onto the apodeme of the flexor-tibiae muscle it is elongated in transverse section, the long axis being orientated along the proximo-distal axis of the leg (Fig. 3.10a, b).

The ventral attachment is enclosed within a thin extracellular sheath and is organised into about twenty subunits. Each one consists of a bundle of up to four ligament cells surrounded by extracellular matrix (Fig. 3.11). Extracellular fibres are located at the periphery of the bundles and within the attachment sheath. These fibres stain with Acid Fuchsin at the light microscope level and phosphotungstic acid at the TEM level (results not shown).

Adjacent ligament cells within each bundle are often closely apposed to one another and are surrounded by numerous extracellular fibrils (diameters 15 nm - 100 nm) (Fig. 3.12a). The ligament cells are packed with microtubules. Small diameter processes orientated axially to the main ligament cells are thought to be finger-like processes arising from them (Fig. 3.12b).

The appearance of the extracellular fibrils in the ventral attachment ligament varies depending upon their location. Fibrils located adjacent to the attachment cells have irregular but relatively simple outlines (diameters approximately 15 nm). Those located towards the periphery of a bundle are more complex with a star-like profile in cross-section (diameters approximately 100 nm) (Figs 3.13a, b). The extracellular matrix in the vicinity of the fibrils often has a very granular appearance. The simple fibrils are packed more densely than those with a star-like profile

(Fig. 3.13c). The fibrils lie parallel to the axis of the ventral attachment and have a repeat banding pattern that can be seen when they are viewed in longitudinal section (Fig. 3.14a). The period of the banding pattern is 16.8 nm. When viewed at higher magnifications each band can be seen to be comprised of two sub-bands (Fig. 3.14b).

Adjacent bundles of ligament cells within the ventral attachment ligament are linked to one another via regions of extracellular matrix. These consist of islands of clear matrix surrounded by fibril-containing material (Fig. 3.15).

The total cross-sectional area of the attachment remains constant along its length at 900 μm^2 ± 25 μm^2 although the proportion of cross-sectional area occupied by ligament cells declines with increasing distance from the mtFCO. This is due to changes in the shapes of the ligament cells along their lengths. At levels close to the point where the ligament joins the flexor tibiae muscle apodeme, transverse sections show that the ligament cells have numerous cytoplasmic extensions giving the cells a characteristic profile quite different from that at more proximal levels (Figs 3.16a,b).

The presence of microtubules packed within the ligamentous cells and the high densities of axially orientated extracellular fibres and fibrils suggests that the ventral attachment ligament performs a tensile role. The lack of neural components within the ventral attachment means that any proprioceptive feedback elicited by the attachment must be mediated by way of is connection to the mtFCO, causing distortion of the mtFCO scoloparium.

3.4.3 The organisation of the apodeme complex

The elements comprising the main mechanical coupling of the organ to the tibia are collectively called the 'apodeme complex' (Shelton *et al.*, 1992). The apodeme complex consists of a distal cuticular rod, dorsal and ventral ligaments and supporting guy-rope fibres.

3.4.3.1 The structure of the cuticular rod

The most distal part of the mtFCO is an apodeme that is in the form of a flattened cuticular rod. It arises from the proximal tip of the tibia and is

approximately 3 mm long in adult *S. gregaria* and *L. migratoria*. The rod has a cross-sectional area of 465 μm^2 ±10 μm^2 along its length before tapering proximally at the level of the origin of the ventral ligament. The rod is inextensible (Shelton *et al.*, 1992) and articulates at the point of origin at the tibia.

3.4.3.2 The organisation of the dorsal and ventral ligaments of the apodeme complex

The ligaments of the mtFCO are composed of bundles of elongated attachment cells organised into distinct units surrounded by thick extracellular fibres that stain positively with Acid Fuchsin at the light microscope level (Shelton *et al.*, 1992). The individual attachment cells are packed with microtubules at a density of approximately 7200 (±345)/μm^2. The density of microtubules appears to be similar at all proximo-distal levels examined in either ligament. Proximally, each attachment cell terminates on a pair of sensory dendrites (Matheson and Field, 1990). The ventral-most attachment cells are the first to terminate on the distal group of ventral neurones, followed by increasingly dorsal attachment cells on dendrites located further proximally. (The nature of the attachment cells' proximal terminations are investigated in Chapter 4.)

The ventral ligament is formed from attachment cells that have their origins on the side of the cuticular rod at its proximal end. The attachment cells are divided into bundles consisting of between one and four cells and are surrounded by axially-orientated extracellular fibres. At the level of its distal origin on the cuticular rod the ventral ligament consists of approximately ten such bundles (Fig. 3.17a). At more proximal levels, additional bundles arise from the cuticular rod and run ventrally to join the ventral ligament in a sequential fashion (Figs 3.17b-f). Each of these 'crossing bundles' contains one or two attachment cells within a membranous sheath associated with thick (diameter approximately 1 μm) extracellular fibres (Figs 3.18a-c).

The dorsal ligament arises from the end of the cuticular rod as a series of separate bundles of attachment cells (Fig. 3.19). More proximally these bundles coalesce to form a single ligament.

Where the attachment cells of the dorsal and ventral ligament join the cuticular rod, the extracellular matrix surrounding them often contains fine fibrils. They are often associated with the larger Acid Fuchsin-staining fibres (Figs 3.20a, b; Fig. 3.21). The function of these fibrils and their constitution remain unknown. However, it is likely that they have a structural role in anchoring the ligament to the rod.

3.4.3.3 Constitution of the extracellular fibres

Ultra-thin sections of material stained with lead citrate and uranyl acetate show the large extracellular fibres (Acid Fuchsin-staining at the light microscope level) have an amorphous internal structure (Figs 3.26a, b). However, the smaller examples of this type of fibre can be seen to be composed of discrete sub-components or 'proto-fibres' associated with densely staining extracellular matrix (Figs 3.27a, b). This suggests that the larger fibres may have arisen by the fusion of smaller fibrils.
The fibrils that form the small Acid Fuchsin-staining fibres are very similar in appearance to those found in the ligaments close to their attachments with the cuticular rod (Figs 3.20a, b; 3.21). Here the smallest Acid Fuchsin-staining fibres are often surrounded by such fibrils.

Proximal to the loop-forming region of the apodeme-complex, the dorsal and ventral ligaments coalesce. They are enclosed in a sheath containing typical Acid Fuchsin-staining fibres that stain intensely with hot phosphotungstic acid. Similar fibres located between attachment cells occur within the ligament itself (Figs 3.22; 3.23).

Evidence was obtained which suggests that individual attachment cells extend along the whole length of the ligaments (approximately 1 mm). A single preparation was examined in detail at three points proximal to the level at which the dorsal and ventral ligaments meet. It was found that the number of attachment cells remained constant, there being 56 attachment cells at all three levels in this preparation (Figs 3.24a, b). Examination of cross-sections at the different levels shows that there is a consistent variation in the size of attachment cells in different parts of the fused dorsal and ventral ligaments. The attachment cells are smaller and more tightly packed in the ventral ligament than in the dorsal ligament (Figs 3.24a; 3.25a, b). In the case of the dorsal ligament, the attachment cells are surrounded by thick layers of extracellular matrix, there being

relatively few junctions between adjacent cells (Fig. 3.25a). Extracellular matrix is less abundant in the ventral ligament resulting in the attachment cells being closely opposed to one another (Fig. 3.25b).

3.4.3.4 Cell junctions between attachment cells and microtubule plaques

Attachment cells are often locally joined to each other by specialised desmosome-like junctions. Specialised areas of adjacent cells extend complementary protuberances towards one another through the extracellular matrix (Figs 3.23; 3.28). Junctions are formed where these protuberances meet, often forming complex interdigitating structures. The junctions may be of the septate variety (Figs 3.28) or more closely resemble non-septate desmosomes (Fig. 3.29). Although no quantitative assessment was made, it was noted that there were more cell juctions between cells of the ventral ligament that there were in the dorsal ligament.

Immediately behind the specialised membrane of these junctions, the cytoplasm appears electron dense due to the presence of intracellular matrix material in which microtubules appear to be embedded (Figs 3.28). Concentrations of microtubules are also found in clusters along the membranes of attachment cells, especially where they come into close proximity to extracellular fibres (Fig. 3.30a, b).

The results discussed above have provided evidence that each attachment cell extends the entire length of the mtFCO ligaments, thus linking the sensory dendrites with the cuticular rod. The structure of the dorsal and ventral apodeme complex ligaments is consistent with the hypothesis that the mtFCO is formed from the fusion two scoloparia, each of which had its own ligamentous attachment to the femoro-tibial joint. It has also been shown that the ligaments contain large numbers of Acid Fuchsin-staining fibres, assumed to have elastic properties (Locke and Huie, 1972; see Nowel *et al.*, 1995). The distribution of these fibres throughout the mtFCO ligaments and the associated implications are investigated in the second half of this chapter.

3.4.3.5 Destination and composition of the 'guy-rope' fibres

The main group of guy-rope fibres arises from the dorsal ligament immediately proximal to the loop-forming region and runs distally to

terminate in the distal femur. The fibres stain with Acid Fuchsin and appear to be composed of the same material as the extracellular fibres found in the ligaments (Shelton *et al.*, 1992). The guy-rope fibres were traced distally through serial 1 μm sections stained with aqueous Acid Fuchsin and were found to terminate in the heavily tanned 'knee' area within the semi-lunar process (Fig. 3.31). The length of the guy-rope fibres is approximately 3 mm (± 500 μm) in an adult locust's femur. Transverse electron micrographs of the guy-rope fibres show them to be composed of a dense amorphous core surrounded by a more lightly-staining peripheral zone (Fig. 3.32). Proximally, close to the insertion onto the dorsal ligament, the guy-rope fibres run closely together, sometimes with several fibres associated together and joined by the lightly-staining material of the peripheral zone. Distally they terminate upon an epidermal in-folding into the femur from its dorsal surface (Fig. 3.33a). At the level at which the guy-rope fibres run into the dorsal epidermis there is a tendency for adjacent fibres to fuse with one another (Fig. 3.33b).

These observations show that the guy-ropes are firmly attached to the surface of the femur. Previous descriptions were inadequate in not identifying this distal termination site (Field, 1991; Shelton *et al.*, 1992).

3.4.4 General morphology of the flexor strand

The flexor strand runs ventrally from the cell-body region of the mtFCO to insert onto the apodeme of the flexor-tibiae muscle close to the femoro-tibial joint (Usherwood *et al.*, 1968; Field and Burrows, 1982). It contains a 'strand-type' receptor which consists of the dendrite of a single sensory neurone with its cell body in the metathoracic ganglion (Bräunig, 1985). The flexor strand leaves the mtFCO from the anterior side, ventral to the sensory cell bodies. The dendrite that innervates the strand leaves nerve 5b1 and travels along the ventral edge of the organ in the connective tissue sheath to reach the flexor strand. The strand's association with the organ is superficial, the connective tissue of the strand attaching to the outer sheath of the organ (Fig. 3.34). Proximally the strand receptor forms the core of the flexor strand and is located loosely within a fatty sheath. Distally the fatty sheath is reduced (Fig. 3.35). The flexor strand contains Acid Fuchsin staining fibres (Fig 3.36a). The combined cross-sectional area of the Acid Fuchsin-staining component remains approximately constant at 22.5 μm^2 (± 5 μm^2) along the length of the strand.

Examination at the transmission electron microscope level shows that there are also two types of striated fibrils embedded within an extracellular matrix which surrounds the dendrite of the strand receptor. These are organised arrays of densely-staining fibrils (diameters 100 - 300 nm) and smaller randomly orientated collagen-like fibres (diameters 10 - 30 nm). The majority of the densely staining fibrils are orientated obliquely, although some are orientated longitudinally with respect to the long axis of the strand (Fig. 3.36b). Here transverse banding is evident. The collagen-like fibrils do not stain intensely, but the 'irregular' periodic banding characteristic of collagens can clearly be resolved (Figs 3.37a, b). The main details of the ultrastructure of the flexor strand are presented elsewhere (see Chapter 7).

The present results show that the strand organ contains both known elastic component and other extracellular fibrils. Their presence suggests that the strand organ has a mechanical role that almost certainly affects the way in which the mtFCO is distorted during dispalcements of the tibia.

3.4.5 Distribution of the elastic (Acid Fuchsin-staining) fibres in the mtFCO apodeme complex

To gain a better understanding of the importance of the Acid Fuchsin-staining fibres in the dorsal and ventral ligaments of the apodeme complex it is necessary to describe their spatial distribution at all levels within them. This was achieved by obtaining a complete series of 1 μm sections of the ligaments and using image processing software to measure the cross-sectional areas of the ligaments at each proximo-distal level and to quantify the amounts of Acid Fuchsin-staining material in different parts of the system. For this part of the study a leg was fixed with the tibia close to the flexed position. The distal-most level at which the ventral ligament was present was denoted as a reference point from which all distances were measured. Proximo-distal level was expressed as the distance (in μm) proximal to this point (see below). For ease of interpretation of the graphs (Figs 3.38 - 3.54) proximal is to the right in this case:

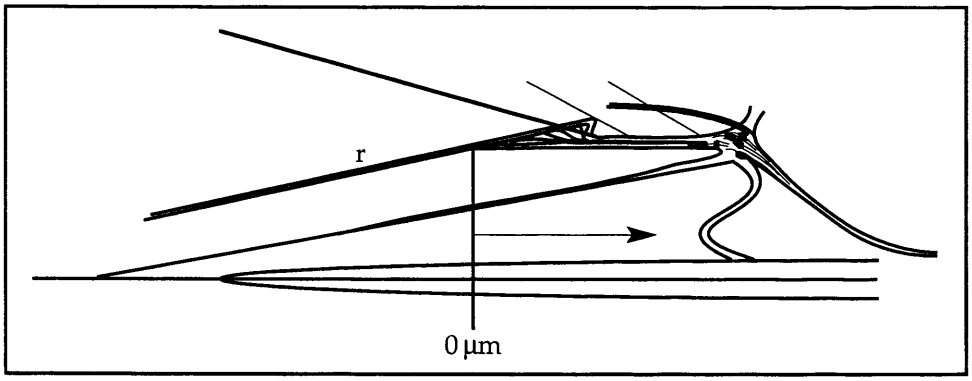

3.4.5.1 Cross-sectional area of the ligaments at different proximo-distal levels

The cross-sectional area of the mtFCO ligaments at a range of proximo-distal levels is shown in Figure 3.38. Proximal to its origin, the cross-sectional area of the ventral ligament increases from 0 to 1000 µm^2 over a distance of 500 µm. This is due to the recruitment of additional ventral ligament fibres arising from the side of the cuticular rod (see Fig. 3.17). The dorsal ligament is not present up to a proximo-distal level of 500 µm. This ligament arises more abruptly, its cross-sectional area rising from 0 - 1000 µm^2 over a distance of approximately 100 µm as it arises from the proximal end of the cuticular rod. Along the length of the apodeme complex lying between the site of guy-rope attachment to the dorsal ligament and the sensory neurones, the cross-sectional area of each ligament remains constant at approximately 1000 µm^2. Conventional calculations used to provide a quantitative measure of a material's mechanical properties (such as Young's Modulus) depend upon a material having a constant cross-sectional area along its length. The variablity in the overall cross-sectional area of the apodeme complex ligaments, especially at their proximal and distal extremes, means that it is not possible to calculate Young's modulus for the system Nevertheless, conclusions regarding the likely mechanical properties of the mtFCO can be drawn if the distribution of the various components is known.

3.4.5.2 Cross-sectional area of the Acid Fuchsin-staining fibres

Whilst the cross-sectional area of the apodeme complex remains relatively constant between the site of guy-rope attachment to the dorsal ligament and the level at which sensory cell bodies occur (625 - 1000 µm), the total cross-sectional area of the Acid Fuchsin-staining component declines proximally. The rate of decline is 10 µm^2/100 µm in the dorsal ligament,

and 4 $\mu m^2/100\ \mu m$ in the ventral ligament (Fig. 3.39). There is more Acid Fuchsin-staining in the ventral ligament than in the dorsal ligament at all proximo-distal levels. This suggests that both ligaments become increasingly compliant proximally, the dorsal ligament more so than the ventral ligament. The situation changes at the proximal end of the ligaments. At the level at which sensory neurones are present within the ventral ligament there is an increase in the cross-sectional area of Acid Fuchsin-staining component. Here the compliance of the ligament would decrease once more. The Acid Fuchsin staining fibres fall into two classes; those fibres lying within the ligaments and those located in the connective tissue sheath surrounding the ligaments.

Dorsal Ligament

In the dorsal ligament there is approximately twice the cross-sectional area of Acid Fuchsin-staining fibres in the outer sheath than within the ligament at all proximo-distal levels (Fig. 3.40). This may indicate that in the case of the dorsal ligament, the majority of its tensile strength lies within the sheath, the centre of the ligament forming of a more compliant core. There is a peak in the cross-sectional area of Acid Fuchsin-staining fibres distally at the level at which ligament buckling occurs (600 μm). Proximally the cross-sectional area of Acid Fuchsin-staining component declines in both the sheath and within the ligament.

Ventral Ligament

Along the first 500 μm of the ventral ligament, as in the case of the dorsal ligament, there is approximately twice the cross-sectional area of Acid Fuchsin-staining component located in the sheath compared with that within the ligament. Between 500 μm and 1000 μm, the cross-sectional area of Acid Fuchsin-staining fibres in the sheath declines. Over the same range, the cross-sectional area of Acid Fuchsin-staining component located within the ligament first increases so that there is equal staining in the sheath and within the ligament at about 800 μm. More proximally the amount of Acid Fuchsin-staining component within the ligament then declines (Fig. 3.41). These observations suggest that the tensile strength of the ventral ligament is likely to be more evenly distributed between the sheath and the core of the ventral ligament than it is in the dorsal ligament. However, at the level at which the ventral ligament comes into contact with the distal-most dendrites of the mtFCO scoloparium

(1100 μm), the cross-sectional area of Acid Fuchsin-staining component situated within the ligament more than doubles. This observation suggests that at the level of the sensory neurones, the core of the ventral ligament becomes stiffer than the ligament sheath.

3.4.5.3 The percentage Acid Fuchsin-staining component in the ligaments

The cross-sectional area of the Acid Fuchsin-staining component can be expressed as a percentage of the total cross-sectional area of the ligaments at any given proximo-distal level. Overall, the % cross-sectional area of Acid Fuchsin-staining component decreases proximally along the length of the ligaments (Fig. 3.42). Distally it accounts for approximately 35% of the apodeme complex cross-sectional area. Proximally it accounts for approximately 5%.

The rate of decline in percentage Acid Fuchsin staining component is initially rapid over the range 0 to 500μm². Over this range only ventral ligament fibres are present and the % Acid Fuchsin-staining component falls from 35% to 10%. Over the range 500-1000 μm the apodeme complex is composed of both dorsal and ventral ligaments. Here, the percentage Acid Fuchsin-staining component in the apodeme complex as a whole declines by 0.86%/100 μm ($R^2 = 0.98$, $P > 0.01$). Most of this decrease can be attributed to the dorsal ligament. The ventral ligament is composed of 10% Acid Fuchsin-staining component at the proximo-distal level at which the sensory neurones begin to occur. The dorsal ligament contains 5% Acid Fuchsin-staining component at this level. Comparison of the relative proportions of Acid Fuchsin-staining material between the two ligaments indicates that the ventral ligament is stiffer than the dorsal ligament at this proximo-distal level.

3.4.5.4 Distribution of Acid Fuchsin staining fibres

Measuring the cross-sectional area of Acid Fuchsin-staining fibres at different proximo-distal levels as above, shows that the quantity of Acid Fuchsin-staining component changes with distance along the ligaments. The number and size distribution of the discrete Acid Fuchsin-staining fibres provides further information as to how this material is spatially distributed in cross section.

Distribution of fibres in the dorsal ligament

There are between 100 and 120 discrete Acid Fuchsin-staining fibres in the dorsal ligament at all proximo-distal levels (Fig. 3.43). At the distal origin of the dorsal ligament (500-600 μm), there are more Acid Fuchsin-staining fibres in the sheath than within the ligament. Proximal to this, over the range 600-900 μm, there are more fibres located inside the ligament than in the ligament sheath. Over this proximo-distal range, the dorsal and ventral ligaments are dorso-ventrally associated with one another and enclosed by a common sheath, thus reducing the ratio of sheath to internal ligament fibres. At the level at which the distal-most sensory neurones are located, the numbers of fibres are distributed approximately equally between the sheath and the inside of the ligament.

Distribution of fibres in the ventral ligament

The total number of Acid Fuchsin-staining fibres in the whole ventral ligament ranges from 20 (at the level of its distal origin) to approximately 150 800 μm along the apodeme complex ligaments (Fig. 3.44). Proximal to its distal origin, the number of Acid Fuchsin-staining fibres in the sheath of the ventral ligament declines (over the range 0-200 μm) before rising again (over the range 200-350 μm) as additional ventral ligament attachment cells arise from the side of the cuticular rod. Further proximally, the number of fibres in the sheath remains constant at approximately 40. The number of Acid Fuchsin-staining fibres located within the ligament (excluding the sheath) rises from 0 to 100 over the range 0 - 800 μm. Proximal to this level, the number of fibres within the ligament declines.

The data described in the above sections allows conclusions to be drawn with respect to the distribution of the Acid Fuchsin-staining component of the ligament at different levels. Conclusions with respect to possible fibre branching can be drawn because an increase in the number of discrete fibres along a ligament whilst the total cross-sectional area of Acid Fuchsin staining component remains constant is indicative of (although not exclusive to) fibre branching. In the case of the ventral ligament there is a marked increase in the number of Acid Fuchsin-staining fibres within the ventral ligament from 60 to 110 over the proximo-distal range 300 μm-800 μm (Fig. 3.44) accompanied by only a modest increase (10 μm^2) in the cross-sectional area of internally located Acid Fuchsin-staining (Figs 3.41).

This suggests that the Acid Fuchsin-staining fibres situated within the ventral ligament branch as they approach the level of the sensory neurones. Changes in the distribution of Acid Fuchsin-staining fibres at different proximo-distal levels along the ligaments are further examined below.

3.4.5.5 Comparing the size-frequency distribution of AFS-fibres in both ligaments as a whole at two proximo-distal levels

The AFSC is distributed throughout the ligaments in a range of fibre sizes. There are large numbers of small fibres and smaller numbers of large fibres. The size frequency distributions of the fibres were compared at the level of the guy-rope fibres (611 μm from the distal origin of the ventral ligament) and at the level of the sensory scoloparium (1071 μm from the distal origin of the ventral ligament) (Fig. 3.45). The size distribution of the fibres is more even distally than proximally; skewness 3.58 and 7.68 respectively. Skewness characterises the degree of asymmetry of a distribution around its mean. Positive skewness indicates a distribution with an asymmetric tail extending towards more positive values. Proximally the number of medium sized fibres in the ligaments (0.6 - 2.0 μm^2) declines, whilst the number of small fibres (<0.4 μm^2) increases.

Size-frequency distribution of AFS fibres in the dorsal ligament

At the proximal end of the dorsal ligament, the range of fibre sizes is smaller than that found at the distal end of the ligament. Proximally, there is an increase in the number of small fibres (<0.4 μm^2) and a reduction in the numbers of larger fibres (>0.4 μm^2) (Fig. 3.46).

Size-frequency distribution of AFS fibres in the ventral ligament

In the ventral ligament there is a fairly similar distribution of fibre sizes at both proximo-distal levels to those found in the dorsal ligament (Fig. 3.47). There are large numbers of small diameter fibres and small numbers of larger diameter fibres at both proximo-distal levels. In the ventral ligament there is a trend towards a proximal reduction in the frequency of medium sized fibres (0.6 μm^2 - 2 μm^2) and an increase in the frequency of smaller (<0.2 μm^2) fibres. The number of fibres <0.2 μm^2 increases proximally by 40%.

Although the trends are generally similar between the dorsal and ventral ligaments, there are some differences in the distribution of fibre sizes between them. Thus, with respect to the numbers of fibres having cross-sectional areas in excess of 1.6 μm^2 there are several fibres between 1.6 μm^2 and 3.0 μm^2 in cross-sectional area at both proximal and distal ends of the ventral ligament (Fig. 3.47). This contrasts with the fibre size distribution found in the dorsal ligament (Fig. 3.46) in which there are no fibres within this size range at the proximal end of the ligament and only 3 such fibres at the distal end.

Comparing size-frequency distribution of AFS fibres between the two ligaments

Distally (611 μm) there are more large fibres (cross-sectional area >1.6 μm^2) in the ventral ligament than in the dorsal ligament (Fig. 3.48). The ventral ligament also has more small fibres (cross-sectional area <1.2 μm^2) than the dorsal ligament at this proximo-distal level. Proximally (1071 μm) the ventral ligament has a wider distribution of fibre sizes than the dorsal ligament (Fig. 3.49). 99% of the AFS-fibres in the dorsal ligament have a cross-sectional area of less than 1.0 μm^2 whilst the ventral ligament contains fibres whose cross-sectional areas are in excess of 2.0 μm^2. This information is of interest because a large number of small fibres are capable of transmitting force more evenly over a large cross-sectional area than a smaller number of large fibres. At both distal (Fig. 3.48) and proximal levels (Fig. 3.49), the ventral ligament has a wider range of fibre sizes than the dorsal ligament.

3.4.6 Organisation of attachment cells into 'functional groups'

The attachment cells of the dorsal and ventral ligaments are grouped into discrete bundles bounded by lightly staining 'perineural' sheath (Field, 1991). The Acid Fuchsin-staining fibres lie in the extracellular matrix between adjacent bundles of attachment cells or 'functional groups'. The number of attachment cells in each functional group is not always constant along the length of the ligaments, although the position of each attachment cell relative to its neighbours is largely conserved (Shelton *et al.*, 1992). These groups can be delimited by the surrounding Acid Fuchsin-staining fibres and were traced through a series of 1 μm serial sections (Fig. 3.50). The number of groups was counted at various proximo-distal levels (Fig. 3.51). The same convention for measuring

proximo-distal level was used as for the previous analysis; the distal-most level at which the ventral ligament was present was denoted as the reference point from which all measurements were taken. The number of functional groups found in the dorsal ligament remains constant at 14 from the level of the guy-rope fibres to the level of the scoloparium (600 μm to 900 μm in this series). Proximal to this region, the number of functional groups begins to fall. Proximal to the level of its origin, the number of functional groups found in the ventral ligament increases. There are approximately 3 additional functional groups/100 μm travelled proximally over the range 0-600 μm. This is due to additional ventral ligament bundles arising from the side of the cuticular rod (see Fig. 3.17). Further proximally (900 μm - 1000 μm), the number of functional groups declines sharply as this is the level in the ventral ligament at which the attachment cells comprising the functional groups terminate on groups of sensory dendrites. Across the apodeme complex as a whole, the functional groups disappear sequentially, the ventral-most groups terminating first followed by increasingly dorsal groups further proximally. This reflects the location of the sensory neurones (Matheson and Field, 1990; Shelton *et al.*, 1992) which extend further distally along the ventral part of the mtFCO.

These results show that the mtFCO attachment cells are not all the same length and that bundles of adjacent attachment cells appear to be consistently grouped together along the length of the ligaments. This gives rise to the possibility that discrete bundles of attachments cells are terminating on subsets of sensory neurones. The mean cross-sectional area of the functional groups varies with proximo-distal level and between the two ligaments, those groups located in the ventral ligament tending to be smaller (Fig. 3.52). This trend is reflected in the cross-sectional areas of individual functional groups traced along the length of the ligaments (Fig. 3.53).

Size-frequency histograms for the functional groups at various proximo-distal levels indicate that the dorsal ligament typically contains fewer and larger functional groups than does the ventral ligament. This can be demonstrated by comparing the size-frequency histograms for the two ligaments at various proximo-distal levels along the ligaments (Fig. 3.54). If the functional groups do terminate on discrete subsets of sensory

neurones, the variation shown between groups and between the dorsal and ventral ligaments may indicate the existence of subtle differences in the transmission of the mechanical stimulus to the different neurone clusters. Elsewhere in this thesis it is shown that adjacent neurones are subjected to different degrees of distortion (see Chapter 5).

3.4.7 Visualisation of the extracellular fibres using confocal microscopy

The Acid Fuchsin-staining extracellular fibres were found to stain preferentially with the dye 5(6)-carboxyfluorescein (CF). Preparations stained with 5% CF were viewed using a confocal laser scanning microscope (Figs 3.55a, b).

3.4.7.1 Extracellular fibre organisation

Manipulation of the optical section depth and the position of the focal plane in the z-axis revealed the organisation of the stained fibres. The extracellular (Acid Fuchsin-staining) fibres run in a predominantly longitudinal direction and appear to undergo some branching The extracellular fibres form a network around the attachment cells (Figs 3.56a-d).

3.4.7.2 Extracellular fibre/neurone interface

Immediately distal to the region containing the mtFCO sensory neurones, the extracellular fibres in the ventral ligament change in appearance and orientation, becoming increasingly branched and irregular in their orientation (Fig. 3.57). The fibres of the dorsal ligament remain orientated along the axis of the organ and retain a uniform appearance. At the level of the dendrites the extracellular fibres become closely associated with the sensory neurones. The fibres surround the dendrites to form a sheath (Fig. 3.58). At the proximal end of the dendrites, there is a marked change in the arrangement of the extracellular fibres. Here they form a mesh-like web at the level at which the dendrites originate from the neurone cell bodies (Fig. 3.59). The extracellular fibres continue to run proximally around each neurone cell body (Fig. 3.60). At this level the fibres appear to branch, forming a reticulated sheath around the sensory neurone cell bodies (Figs 3.61).

These observations show that the extracellular fibres are intimately associated with the neurones themselves and that the mechanical

elements of the system are continuous from the attachment cells to the dendrites and cell somata. The ultrastructure of the attachment cell/sensory neurone interface is described in Chapter 4.

3.5 DISCUSSION

This study has described the distribution of the constituent materials comprising the different mechanical linkages of the mtFCO. This information can be used to indicate the likely role played by each of the linkages and has implications regarding the way in which mechanical stimulation is transmitted to the sensory neurones.

3.5.1 Structure of the dorsal attachment

It has been shown that the mtFCO's dorsal attachment to the femur is surrounded by elastic fibres and fibrils. This indicates that the attachment is likely to undergo some degree of deformation during tibial rotation. This supposition is supported by the presence of a 'multi-terminal' receptor embedded within the attachment. For the first time this attachment has been revealed to be a double structure in transverse section, supporting the hypothesis that the mtFCO is derived from two fused scoloparia (Matheson and Field, 1990). The role of the dorsal attachment appears to be that of a proximal anchor to the sensory units, allowing the distortion of the distal structures of the scolopidia by the forces transmitted from the femoro-tibial joint.

3.5.2 Structure of the ventral attachment

The ultrastucture of the mtFCO's ventral attachment to the flexor tibiae muscle apodeme has been described for the first time. It consists of ligamentous cells packed with axially orientated microtubules. In addition, the attachment is heavily reinforced by numerous elastic fibres and fibrils. The precise function of this attachment has yet to be elucidated, but the implications of its ultrastructure and mechanical coupling to the flexor tibiae muscle apodeme suggests that the muscle's state of contraction may modify the response properties of the chordotonal organ in some way whilst the attachment is held under tension. Burns (1974) suggested that chordotonal organs may have some role in muscle tension reception in his account of the structure of the pro- and mesothoracic chordotonal organs in the locust. In the pro- and

mesothoracic legs the distal scoloparia of the chordotonal organs are attached proximally in the femur to both the cuticle and the flexor-tibiae muscle. The latter connection appears to be analogous to the ventral attachment in the locust mtFCO. It seems likely that the ventral attachment of the mtFCO to the apodeme of the flexor-tibiae muscle may be homologous with these connections in the pro- and mesothoracic limbs. Macmillan *et al.* (1980) proposed that chordotonal organs whose role was attributed to be that of monitoring joint movement and position could also monitor muscle tension. He suggested that this may reflect an evolutionary trend towards an increase in the number of modalities monitored with the internalisation of mechano-receptors.

3.5.3 Ultrastructure of the apodeme complex

The present study has provided the first detailed description of the ultrastucture at all proximo-distal levels along a chordotonal organ's mechanical connection to the site of stimulation. Ultrastructural differences between the dorsal and ventral ligaments revealed in the present study suggest the anatomical basis for variation in mechanical properties both between the ligaments and along the length of each individual ligament. The implications of such observations are that neurones located in series with either the dorsal or ventral ligament, or situated at different proximo-distal levels within an individual ligament, may be subjected to differential stimulation by virtue of their positions in the scoloparium.

3.5.3.1 Differences between the dorsal and ventral ligaments

The dorsal and ventral mtFCO ligaments are distinct in their mode of origin and their structure (Shelton *et al.*, 1992). Dorsal ligament attachment cells share a common distal origin at the proximal end of the cuticular rod whereas the ventral ligament attachment cells originate at a range of different proximo-distal levels. It is known that the attachment cells maintain a relatively constant position within the ligaments with respect to their neighbours, and that their overall position within the ligament is very consistent (Shelton *et al.*, 1992). It has been shown that the dorsal ligament attachment cells are typically larger in cross-sectional area than those in the ventral ligament. In addition, the attachment cells in each ligament have been shown to associate in bundles bounded by axially orientated Acid Fuchsin-staining fibres. These observations suggest

for the first time a mechanism by which discrete groups of sensory neurones, located in series with different attachment cell bundles, may recieve subtly different mechanical stimulation.

3.5.3.2 Anatomy of the guy-rope fibres

The present study has confirmed that the guy-rope fibres of the mtFCO apodeme complex are formed from the same material as the extracellular fibres in the ligaments and stain intensely with Acid Fuchsin. For the first time, the location and nature of the guy-ropes' distal attachment in the femur has been identified. Previously it was not known whether the guy-ropes attached distally to a static femoral component, or to some connective element which was subjected to proximo-distal displacement in response to femoro-tibial rotations. In this study, the guy-rope fibres have been shown to terminate in the distal femur upon an epidermal infolding, providing a static site of attachment. Since the guy-rope fibres are attached exclusively to the dorsal ligament at their proximal ends, whatever mechanical influence they exert upon the apodeme complex will be unevenly distributed across the two ligaments. The dorsal-most attachment cells of the dorsal ligament are lying effectively 'in series' with the guy-ropes. It is reasonable to assume that the mechanical behaviour of such attachment cells would be influenced most strongly by any force exerted by the guy-rope fibres. Any mechanical influence exerted by the guy-rope fibres would have to be transmitted laterally by the attachment cells via cell-to-cell junctions and the extracellular matrix, to influence the displacement of the attachment cells of the ventral ligament. This represents an additional mechanical factor which may contribute towards generating differential displacements between the dorsal and ventral ligaments.

Previous authors (Matheson and Field, 1990) have suggested that the single scoloparium of the mtFCO is derived from the fusion of the twin scoloparia found in the locust pro- and mesothoracic legs (Field and Pflüger, 1989). They proposed that the dorsal ligament of the mtFCO is homologous with the distal scoloparium whilst the ventral ligament is the proposed homologue with the proximal scoloparium. There are also examples of other orthopteran chordotonal organs having double structures, such as the paired scoloparia of the bush cricket *Decticus albifrons* (Theophilidis, 1986a) and the common cricket *Acheta domesticus*

(Nowel *et al.*, 1995). This investigation has shown that, in the case of the locust *S. gregaria*, the twin ligaments linking the mtFCO to the femoro-tibial joint have distinct anatomical characteristics, despite being fused with one another at proximal levels.

3.5.4 Implications of the distribution of different biological materials in the mtFCO's mechanical linkages

The following section evaluates the distribution of the constituent components comprising the mechanical elements that connect the mtFCO with other parts of the leg. These systems link the mtFCO with the cuticle of the femur (dorsal attachment and guy-rope fibres), the tibia (the apodeme complex), and the flexor tibiae muscle apodeme (ventral attachment and flexor strand).

The nature of the components comprising these mechanical couplings will determine how the input stimulus effects changes at the level of the sensory neurones. It is known that each scolopidium is connected distally to an attachment cell along which the displacements occurring at the femoro-tibial joint are transmitted (Matheson and Field, 1990; Field, 1991, Shelton *et al.*, 1992). The way in which these individual mechanical connections are related to their parallel-lying neighbours and the way in which the scolopidia themselves are supported, will govern how a given stimulus causes discharge of action potentials from the sensory neurones. For example, the attachment cells may be able to move independently from one another, or, the response of any one sensory neurone may depend upon the combined input from all the attachment cells distorting the neurone-containing region as a whole. In the following section, the different materials composing the CO's mechanical connections are discussed with reference to the functional implications of the organisation of the organ as a sensory unit.

3.5.5 Properties of the mtFCO's component materials

There are three principal materials which are found in the construction of the CO linkages which must contribute to the mechanical properties of the CO: microtubules, extracellular fibres and extracellular matrix. Each of these materials and their likely mechanical influence upon the mtFCO are discussed individually below.

3.5.5.1 Microtubules

The attachment cells of the dorsal and ventral ligaments are packed with axially orientated microtubules. The ventral attachment and the dorsal attachment also contain of ligamentous cells containing axially orientated microtubules. The following section addresses the possible ways in which microtubules may play a functional role in these structures.

Chemical characteristics of microtubules

Any functional role played by microtubules is likely to be dependent upon their physical characteristics. Because of the way in which microtubules are constructed from their component constituents, microtubules could potentially perform a number of different functions. The building block of the microtubule polymer is the protein tubulin, a 100,000 molecular weight protein consisting of two non-identical subunits a and b (Lee *et al.*, 1973; Luduena *et al.*, 1977; Valenzuela *et al.*, 1981, and Ponstingl *et al.*, 1981). Tubulin is a strongly conserved protein; Farrell *et al.* (1979) suggested the polymer was analogous to a bare skeleton which could be adapted for different tasks by association with other proteins and cofactors. The fact that there are many distinct tubulin genes also presents scope for regulatory complexity (Kemphues *et al.*, 1979; Cleveland, 1979). Microtubules have the ability to assemble-disassemble themselves in a dynamic manner ('treadmilling') by the association and dissociation of their component subunits. Association and dissociation of subunits occurs at both ends of microtubules, but due to differing rate constants each microtubule has polarity; net association occurring at one end and net dissociation at the other (Margolis and Wilson, 1981). A flux rate of 50 $\mu m\ h^{-1}$ was observed *in vitro* by Cote *et al.* (1980). This is consistent with the rate of chromosome movement during anaphase. However, the role played by microtubules in the mtFCO may not necessarily be dependent upon their dynamic assembly/dissasembly properties. Tubulin flux has been shown not to occur in the absence of GTP (Margolis, 1981; Terry and Purich, 1980). In addition, microtubules have other mechanisms for suppressing treadmilling and stabilising themselves, as demonstrated by cilia and flagella outer doublets. Kirschner (1980) hypothesised that the anchorage of a microtubule to a kinetochore or centrosome completely caps the end of the microtubule so that no gain of loss of tubulin can occur. Thus microtubules can be classified on the basis of their stability. Margolis and Wilson, (1981) also pointed out that some

microtubules are completely stable and their function is clearly not linked to their assembly-disassembly properties. They speculated that a microtubule could be modified by association with proteins to create a stable rigid rod, and that the function of such a rod would be mediated by an anchorage-translocation array not coupled to assembly, disassembly or flux. It is likely that the microtubules in the attachment cells of the mtFCO in the adult locust fall into this category. To date there is no evidence of microtubule treadmilling in the mtFCO attachment cells.

Distribution of microtubules in proprioceptors

The distribution of microtubules in a range of proprioceptors can also be used to indicate their likely role in such organs. Microtubules are common constituents of proprioceptors, being found in the sensory processes of campaniform (Moran and Varela, 1971) and hair sensilla (Erler, 1983a, b), as well as the cockroach (Young, 1970), cricket (Theophilidis, 1986a) and locust pro- meso- and metathoracic chordotonal organs. With respect to their role in cells associated with mechanoreceptors, most authors agree that microtubules have a structural role and are present in such large numbers and with a conformity of orientation that they probably act as mechanical linkages analogous to tendons (Moulins, 1976). On the other hand, some authors feel that microtubule-packed cells are notable for their elastic properties (Yack and Roots, 1992; Young, 1970). The characteristics which imply that microtubules have an important mechanical role in the mtFCO are their highly ordered axial orientation and their vast numbers in the attachment cells.

A mechanical role for microtubules

The following section examines evidence obtained from comparable proprioceptive systems which indicates that whilst microtubules may perform a primarily tensile role, they may also be responsible for other important aspects of proprioception. In support of the purely tensile role, Doolan and Young (1981) point out that chordotonal organs are under considerable stress and may require mechanisms to increase the tensile strength of the cells. In the auditory chordotonal organ of *Cystosoma saundersii* they observed interdigitation of adjacent attachment cells and noted that they contained numerous microtubules. The role of microtubules was attributed to one of maintaining the mechanical

integrity of the cells under stress and tension. In the current study, similar interdigitation of attachment cells and associated localisations of microtubules could indicate a similar role. Toh and Yokohari (1985) also implicated microtubules in providing the 'stiffness' in the American cockroach antennal CO sensillum. They described the role of the axially orientated microtubules in the attachment cells as forming a 'characteristic cytoskeleton'. Theophilidis (1986a) found a similar net-like distribution of microtubules in the attachment cells of the pro-, meso- and metathoracic chordotonal organs of *Decticus albifrons*. He hypothesised that the function of the microtubules may be a way of changing the viscoelasticity of the ligaments in order to modify some of the physiological properties (e.g. the adaptation rate) of the different organs. A mechanism by which this might occur was not explained.

The above authors all attribute the role of microtubules in mechano-receptors as purely structural one. However, there is another class of mechano-receptor in which microtubules appear to perform a more diverse range of functions. Although chordotonal organs and campaniform sensilla/hair receptors are fundamentally different in their construction, they are largely composed of the same materials. Comparisons between them may help elucidate the roles these constituent components play in sensory transduction in chordotonal organs. This is especially so in the light of Sugawara's (1996) hypothesis that the different receptors are phylogenetically related. According to him, the chordotonal scolopidia are derived from the other kinds of epidermal sensilla which were withdrawn into the body cavity to become chordotonal organs. Comparisons of the roles of microtubules in chordotonal organs and their roles in campaniform/hair sensilla may reveal whether microtubules in mechanoreceptors always have a common purely 'cytoskeletal' function as proposed by previous authors.

Microtubules present in the modified dendritic sensory processes of insect epithelial mechanoreceptors can be classed into three categories:
a. Densely packed laterally interconnected microtubules of the 'tubular body' (Thurm, 1964) at the apical end of the dendritic tip - the point of stimulus application. **b**. 'Connective' microtubules linking the apical tubular body with the ciliary neck region of the dendrite. These are referred to as 'free' microtubules as they have no specialised

interconnections. They are closely packed and axially orientated within the sensory process which can be as long as 220 μm (Moran *et al.*, 1976). It is these microtubules which bear most resemblance to the microtubules packed in the CO attachment cells. c. 9 doublet microtubules of the 'ciliary body' located at the proximal end of the 'free' microtubules. The dendrite reduces in diameter at this level to form the 'ciliary neck'. There is no direct continuity between the different arrangements of microtubules (Smith, 1969; Wensler, 1977; Keil, 1978). Chordotonal organ sensilla also possess a specialised 9 doublet ciliary structure within their dendritic tips which is presumed to be the site of mechano-electric transduction (Atema, 1973; Moran *et al.*, 1977). Similarities between the arrangement of microtubules in epithelial and chordotonal organ sensilla are immediately apparent: an array of tightly packed microtubules (b) linking the site of stimulus application (a) to a specialised ciliary region (c).

Are the 'free' microtubules in an insect epithelial mechanoreceptor present to transmit the mechanical stimulus towards the ciliary neck?

The hypothesis that 'free' microtubules may have a role in centripetal signal transmission, analogous to the assumed role of the microtubules within the chordotonal organ attachment cells, has been subject to investigation by several authors. Moran and Varela (1971) demonstrated loss of mechanoreceptive function in the cockroach campaniform sensillum when treated with colchicine and vinblastine. They saw large scale disassembly of microtubules in the sensory process and concluded that the 'free' microtubules do play an important role in the process of mechano-sensory transduction (the authors considered interference by the drugs at the level of the metabolic machinery of the neurone's dendrite, cell body or axon as unlikely). They also considered the possibility that the microtubules in the sensory process of the cockroach campaniform sensillum function as 'mechanochemical engines' driven by the force of the stimulus to produce the generator current. They speculated that large numbers of microtubules in the sensory process may serve to increase the gain of the mechanoreceptor, possibly by the release of bound ions caused by a conformational change in the tubulin. Atema (1973) also proposed that distorted microtubules may liberate chemical energy or ions that might control a receptor current. However, contradictory evidence was produced by Moran *et al.* (1976) who strongly supported the hypothesis proposed by Thurm (1965), that sensory transduction occurs at the distal

tip of the sensory process in the campaniform sensilla, rather than amongst the 'free' microtubules. They supported the idea that stimulation of the distal tip of the microtubule-packed sensory process was sufficient to induce the formation of a generator potential utilising the properties of the microtubules associated in the 'tubular body'. They went further and discounted the possibility of the mechanical propagation of the stimulus force via the 'free' microtubules to some proximal transduction site. This view was also endorsed by Erler (1983b) who proved that the 'free' microtubules were not involved in mechanotransduction in tibial hair-mechanoreceptors of *Acheta domesticus*. He demonstrated that the 'free' microtubules could be dissembled with vinblastine (leaving the more stable 'tubular body' intact) without decreasing the mechanical sensitivity of the receptor. This would appear to leave the 'free' microtubules with no specific mechanical role.

Schmidt (1969), Thurm (1982) and Thurm *et al.* (1983) proposed that the microtubules in the 'tubular body' of the cricket tibial hair receptor have a cytoskeletal mechanical support role. The mechanical stress imparted by the stimulus was presumed to distort the cell membrane against the mechanical resistance of the 'tubular body' thus increasing membrane conductance (Rice *et al.*, 1973; Rice, 1975). Erler (1983a) suggested that the packed microtubules in 'tubular bodies' of insect mechanoreceptors may play an essential role in transduction. He showed that as the tubular body is destroyed (using vinblastine) the mechanical sensitivity decays to zero, although the membrane properties of the apical dendritic segment are only slightly altered by this treatment. However, he could not conclusively distinguish between the alternative roles for the 'tubular body' of mechanical transmission of the stimulus or mechano-electric transduction of the stimulus. Nevertheless he favoured a mechanical transmission role because the transducer mechanism still functioned weakly without the tubular body. Other authors have doubts about this proposed role of the tubular body. Kuster *et al.* (1983) suggested that the effects of drugs upon mechanosensitivity did not directly relate to the observed dissociation of microtubules in the tubular body, but were more likely to arise from drug action upon the cell membrane. Thus, the functions of the tubular body, the free microtubules and the ciliary element remain obscure. The microtubular components in each of these regions may be performing a variety of roles. Those of the tubular body

seem to be implicated in the process of stimulus transduction (French, 1988). The microtubules packed between the point of stimulus application (tubular body) and the dendritic cilia have a less clear role. None of the above authors speculated as to the role of the ciliary body microtubules, although the work of Moran *et al.* (1976) and Erler (1983a, b) would seem to rule out any mechanical role for these microtubules in signal transduction.

It seems unlikely the microtubules are directly responsible for mechano-electrical signal transduction in the attachment cells of the locust in the manner suggested by Moran and Varela (1971) or Atema (1973), as there is no evidence that the attachment cells are electrically connected to the dendrites. If any mechano-electric transduction role in attachment cell microtubules is discounted, it has to be assumed that they have a purely structural role. If Sugawara's (1996) theory of chordotonal organ development is correct, the role of microtubules in sensory systems may have changed during the evolution of chordotonal organs. There is the possibility that the microtubules are a redundant component from the sensilla from which they were derived. The fact that they appear to play no particular functional role in mechano-electric transduction is highlighted by the fact that there are examples of chordotonal organ attachment strands whose cells contain no microtubules at all (Theophilidis, 1986a).

There is another reason which might explain why the attachment cells of CO are predominantly packed with microtubules. Matthews *et al.* (1990) used isotype-specific antibodies to localise a85E tubulin protein during the development of *Drosophila melanogaster*. They observed that the embryonic accumulation of a85E tubulin only occurs in support cells of chordotonal organs and the developing musculature of the viscera and body wall. By the late third instar, only non-neural components of chordotonal organs and a subset of nerves stained with anti-a85E. By comparing staining patterns with a cross-reacted polyclonal antibody (P21a85E) they demonstrated that most if not all a-tubulin in chordotonal organs is a85E. Only the ligamentary components of the chordotonal organs are labelled with antibodies to a85E-tubulin; there was no staining in the neural cells or the scolopale cell, both of which do contain tubulin. They showed that cells which express a85E share a requirement for

extensive cell shape changes during development. The observation that tissues which accumulate high levels of a85E all share a developmental program that requires individual cells to achieve a dramatically extended form, suggests that this a-tubulin may have distinct functional properties required to produce and maintain specialised cytoskeletal structures during development. The authors tested this hypothesis by generating a85E$^-$ embryos which survived late into embryogenesis. Defects in the chordotonal organs of a85E$^-$ embryos were observed but so too were defects of the CNS indicating that there were other mutant genes introduced whilst generating the a85E$^-$ embryos, which may have contributed to the abnormal phenotype of the chordotonal organs. Thus no firm conclusion could be drawn regarding the developmental role of a85E-tubulin alone.

The developmental observations of Matthews *et al.* (1990) may provide an indication why microtubules seem to be so widely found in the sensory organs of insects yet lack an obvious functional role. The attachment cells of COs have to extend massively to accommodate the increasing size of the developing animal (estimated to be in the order of 500% (femur length from 4 mm to 22 mm) in the metathoracic leg of the locust). Slifer (1935) also remarked upon this in *Melanoplus differentialis*, the rapid lengthening of the femur during late embryonic and nymphal life results in a corresponding increase in the length of the femoral chordotonal organ. This is demonstrated by her observation that the proximal scoloparium in a 28 day old femoral organ is only slightly longer than it is broad, yet in the adult becomes almost four times as long as its greatest width. Hartenstein (1988) demonstrated that the CO precursor cell (from which the CO originates) is located at its distal site on the integument and that the CO elongates back into its final position during development. Cytoskeletal microtubules unlike other tissues performing a 'connective' function have the ability to break down and re-polymerise in a controlled manner. This property could potentially be exploited to retain ligament integrity in some manner during the moult cycle. Attempts to stain adult structures with antibodies were unsuccessful, so it is unclear as to whether adult COs still contain a85E-tubulin (Matthews *et al.*, 1990).

Implications of microtubule distribution

Authors have remarked that by virtue of the microtubules' orientation in the mtFCO attachment cells, the mechanical stimulus passed to the

sensory cells should be predominantly axial with little or no lateral or shear component (Toh and Yokohari, 1985) (American cockroach antennal chordotonal sensillum). There is nothing in this investigation to support or contradict this hypothesis. However, an equally viable alternative hypothesis would be that depending on the arrangement coupling and/or interaction between the microtubules, there is no reason why microtubules of varying lengths should not be differentially or sequentially recruited across the transverse section of each attachment cell in response to an increase in cell length, thus producing a shearing force across the face of each scolopidium.

Both the dorsal and ventral ligaments of the locust mtFCO are packed with similar densities of microtubules. The precise role of the microtubules is unresolved (see above), but may determine the viscous properties of the ligaments in order to modify some of the organ's response characteristics such as the adaptation rate (Theophilidis, 1986a). Theophilidis (1986a) observed that there were different densities of microtubules in the attachment cells of the proximal and distal scoloparia in the mesothoracic chordotonal organ of the cricket *Decticus albifrons*. He proposed that this may provide a mechanism for differentiating the viscoelastic properties of the two strands and so the responsiveness of the two closely connected scoloparia. Whatever their mechanical influence is, it would be reasonable to expect that the microtubules contribute to some difference in mechanical characteristics between the larger dorsal and smaller ventral attachment cells in the locust. In addition, the attachment cell microtubules in the locust have been shown to localise at the site of cell junctions and become embedded in electron-dense intracellular material. A similar relationship between microtubules and cell junctions was reported in the case of the chordotonal sensillum of the antennal pedicel of the American cockroach (Toh and Yokohari, 1985). In this chordotonal organ the attachment cells are also packed with axially orientated microtubules which end close to the cell membrane where desmosomes occur. The authors observed that microtubules did not end near non-desmosomal membrane and concluded that adhesion of invaginated membranes by microtubule-associated desmosomes in such cells was significant.

Consideration of the role played by mtFCO attachment cell microtubules in the adult locust

In order to speculate as to the role of the attachment cell microtubules in the adult locust, it is nessessary to understand the way in which they are arranged within the cells. The microtubules could potentially be organised in several different functional arrays:

1. Individual microtubules run the length of the attachment cells and are extensible to accommodate changes in cell length.

2. Individual microtubules run shorter distances than the length of the ligaments but remain anchored at both ends to 'attachment plaques', such as the site of desmosomes as observed by Toh and Yokohari (1985). The microtubules would still need to be extensible to allow for changes in length of the attachment cells.

3. Microtubules are anchored within the attachment cell at both ends, but have considerable 'slack' built in. Elongation of the attachment cells would take up the slack.

4. The microtubules polymerise and de-polymerise in response to changes in attachment cell length.

5. The microtubules are anchored at one end only and do not necessarily run the entire length of the attachment cell. In this model one end of each microtubule would be floating free within the cell. The 'free' ends of microtubules anchored at opposite ends of the cell would interdigitate and slide past one another to allow changes in cell length. In such a system individual microtubules could play no direct role in the transmission of axial force, although interactions between large numbers of adjacent sliding microtubules may allow the indirect transmission of force by increasing cell viscosity.

Microtubules are generally considered to be relatively inextensible, (Moulins, 1976; Okuno and Hiramoto, 1979; Toh and Yokohari, 1985). Okuno and Hiramoto estimated the Young's modulus of microtubules (in echinoderm sperm) to be between 2 and 5 x 10^9 Pa, endowing them with properties between those of nylon and wood (Bolton, 1986). In the light of

this, hypotheses 1 and 2 seem unlikely as individual attachment cells of the locust mtFCO undergo length increases of the order of 40% over the physiological range of femoro-tibial rotation. There is no anatomical evidence supporting model 3; the microtubules always appear to be axially orientated whether the preparation is examined flexed or extended. It is difficult to see where any slack microtubules could reside to support model 3 since they are so densely packed within the attachment cells. The scenario in model 4 is particularly unlikely under normal conditions due to polymerisation rate and energetics considerations, and would also preclude the transmission of force. It may however be a consideration during development and at ecdysis. Farrell *et al.* (1979) have shown that tubulin composing stable structures can be dissociated and induced to form treadmilling polymers *in vitro*, demonstrating that tubulin is not restricted to forming either stable or labile polymers. This leaves the possible role of microtubules in the attachment cells of COs to be a cytoskeletal component which may be responsible for contributing to the mechanical characteristics of the attachment cells such as their viscoelasticity (model 5). There is circumstantial evidence that the microtubules are anchored to either the proximal or distal end of the attachment cells. Yack and Roots (1992) reported increased densities in the occurrence of (axially orientated) microtubules at the tapering proximal and distal ends of the attachment strand of the wing-hinge chordotonal organ in the moth *Actias luna* (Lepidoptera, Saturniidae).

3.5.5.2 Extracellular fibres

Extracellular fibres are found in all of the mtFCO's mechanical linkages and range in size from 0.5 nm^2 to 1.5 μm^2 in cross-sectional area. Large Acid Fuchsin-staining fibres are prominent in the dorsal and ventral ligaments of the apodeme complex (including the guy-rope fibres), and are found in association with the sheath of the dorsal attachment, the ventral attachment, and the strand organ. Large Acid Fuchsin-staining fibres in the ligaments of the apodeme complex range from 0.13 μm^2 to 1.5 μm^2 in cross-sectional area. Acid Fuchsin-staining fibres of similar proportions were also found by Nowel *et al.* (1995) in the metathoracic femoral chordotonal organ of the cricket *Acheta domesticus*, ranging from 0.19 to 1.13 μm^2 in cross-sectional area. Nowel *et al.* stated that the elasticity of the cricket chordotonal organ is 'almost certainly' bestowed by these Acid Fuchsin-staining fibres. The larger of these fibres in the locust mtFCO are

often closely associated and coalesce to form dense clumps of AFS material within the ligaments as large as 5 μm^2 in cross-sectional area, and ribbons of AFSC within the sheath of 10 μm^2 cross-sectional area. These fibres are always found embedded in an extracellular matrix. Smaller extracellular fibrils ranging in cross-sectional area from 500 nm^2 to 2000 nm^2 are found at the distal end of the dorsal and ventral ligaments, the dorsal attachment, and are particularly abundant in the organ's ventral attachment ligament. These fibrils closely resemble 'collagen-like' (Gray, 1959) and 'collagen' (Ashhurst, 1982) fibres found in the locust *Locusta migratoria* in both size and appearance. The strand organ has two types of small extracellular fibrils, one type resembling the banded fibrils found in the ventral attachment (Fig. 3.36), and another type with a banding pattern that is strikingly similar to that of previously described collagens. The characteristics of the fibrillar components in this study are tabulated in descending size order (Table 3.1).

A hypothesis linking the various fibre types

Bradfield (1950) noted that there were two extracellular fibre types in insect connective tissue; collagen fibres (for mechanical strength) and fine 'reticular' fibres (to allow plasticity). Whilst pointing out that the two fibre types had distinct chemical compositions, he suggested that they were 'very closely related' to one another because they follow one another in rapid succession in tissue culture (Mallory and Parker, 1927; Mckinney, 1930). It is not clear whether the fibres referred to by Bradfield are the same as those observed in this study, but the possibility that the fibrils are the building blocks of fibres is explored below.

Evidence linking the different sizes of fibres and fibrils

1. Using uranyl acetate and lead citrate all the fibrils in the ventral attachment stain in the same manner with the same intensity and have a fine granular material around their periphery. This granular material resembles the 'microfibres' of Lock and Huie (1972). The 'amorphous' and 'star-like' fibrils observed are distributed in a graded fashion; the smallest fibrils being located closest to the ligament cells and increasingly large and irregular fibrils being found with increasing distance from the cells. These observations suggest that these fibrils are all composed of the same material- the fibrils having a 'star-like' profile possibly being derived from

the association of the smaller fibrils. Representatives from this class of fibril are present in all the mechanical linkages of the mtFCO.

2. Individual fibrils are rarely seen at proximal levels within the ligaments of the apodeme-complex, although they are evident at the distal end of the attachment cells where they arise from the cuticular rod. There is evidence that the smaller Acid Fuchsin-staining fibres are formed by the association of smaller units. These 'sub-fibrils' have a mean cross-sectional area of 973 nm^2 (s.d. = 220 nm^2). The size and profile of these 'sub-fibrils' correspond with those of the fibrils in the ventral attachment, their size and profile being comparable to a fibril which is midway between the 'simple' and 'star-like' stages. In some preparations the 'sub-fibrils' were seen grouped in close association to form small AFS 'units' (Fig. 3.27a). It is proposed that these sub-units then coalesce to form larger AFS fibres as shown in Fig 3.27b. Such AFS fibres have a 'frayed' appearance at the edges as if reflecting the recruitment of smaller units around the periphery. These observations are consistent with the idea that the smallest Acid Fuchsin-staining fibres are composed of a subset of small 'sub-fibrils' whose size and appearance suggest that they may be composed of the same material as the fibrils in the ventral attachment. In the dorsal attachment single small fibrils of the same size and appearance as these 'sub-fibrils' are also evident in the extracellular matrix adjacent to, and possibly interacting with, the larger AFS sheath fibres (Fig. 3.5a).

3. Both the small and large Acid Fuchsin-staining fibres appear to be composed of the same material. Although there is not always consistent staining between the large and small fibres with uranyl acetate and lead citrate (Figs 3.30a, b) there is no such inconsistency when staining with phosphotungstic acid (Figs 3.22 and 3.23). As these figures show, there is a continuous spectrum of Acid Fuchsin-staining fibre sizes present in the ligaments and small individual Acid Fuchsin-staining fibres appear to merge with one another to form larger fibres. The largest of these fibres are often closely associated and coalesce to form dense aggregations of AFSC within the ligaments as large as 5 μm^2 in cross-sectional area and stretches of AFSC within the sheath of 10 μm^2 cross-sectional area. These observations suggest the following hypothesis:

- Small (500-2000 nm²) fibrils are assembled in the extracellular matrix, possibly from lightly-staining granular subunits (Figs 3.13b, c).
- These 'proto-fibrils' associate to form small (Acid Fuchsin-staining) fibres (Fig. 3.27).
- Small fibres merge to form larger fibres.
- The fibres may also be augmented by the association of additional fibrils.

Table 3.1

Location	Description	Banding	Cross-sectional area	Equivalent fibre diameter	Terminology in this study
-apodeme complex ligaments' sheath (Fig. 3.26) -dorsal attachment sheath (Fig. 3.5b) -'guy-rope' fibres (Fig. 3.32)	axially orientated even profile in transverse section.	none	**0.05- 1.5** μm^2	0.26-1.4μm	large Acid Fuchsin-staining fibres
-apodeme complex ligaments (Fig. 3.27) -dorsal attachment sheath (Fig. 3.5a) -ventral attachment (Fig. 3.11) -strand organ	axially orientated densely staining amorphous appearance usually 'ragged' profile in transverse section.	none	**0.0423**μm^2 ±SD 0.035μm^2 (range; 0.040μm^2-0.130μm^2)	0.23μm (0.22-0.41μm)	small Acid Fuchsin-staining fibres
-distal apodeme complex ligaments (Figs, 3.20 and 3.21) -dorsal attachment sheath (Fig. 3.5) -ventral attachment (Fig. 3.13) -Strand organ sheath (Fig. 3.36)	axially orientated. irregular profile; amorphous or 'star-like' appearance depending on location.	regular, evenly spaced banding. 16.8nm inter-band interval. each band possibly consists of paired subperiods	amorphous **509nm**^{2} ±SD 80nm^2 'star-like' **2817nm**^{2} ±SD 700nm^2	25.5nm 59.9nm	Fibrils
-strand organ (Fig. 3.37)	no particular orientation	distinctive asymmetric banding pattern; macroperiod 52-54nm	78.6-491nm^2	**10-25nm**	collagen-like fibrils

Table 3.1 classifies the extracellular fibres/fibrils identified in this study in descending size order. Fibre dimensions are given in both cross-sectional area and equivalent fibre diameter to allow comparisons with previous studies in which fibre diameter was used to quantify the fibre dimensions. The parameters measured in this study are shown in bold.

The above hypothesis is based upon the characteristic fibre sizes, cross-sectional profiles, staining characteristics, location with respect to one another and their orientation. The striated fibrils in the strand organ (Fig. 3.37) are not included in this hypothesis. These fibrils show different

staining characteristics (clearly resolved banding) and do not share the axial orientation common to all the other fibres and fibrils.

Comparison of mtFCO fibres with fibres described by other authors

The characteristics of fibrillar components examined by other authors is tabulated in Table 3.2 in descending size order. A vertebrate collagen is included at the bottom of the table for comparative purposes. It is widely accepted that 64 nm is the repeat macroperiod in 'authentic' collagens; Schmitt *et al.* (1942) characterised collagens from many tissues, also Bear (1942) and Keech (1961). Do the fibrillar components of the mtFCO share any characteristics with previously described fibres which may indicate their composition and possible function?

The Acid Fuchsin-staining component

The Acid Fuchsin-staining fibres examined in this study are the same as those observed by Shelton *et al.* (1992) in the locust apodeme complex and by Nowel *et al.* (1995) in the chordotonal organ of the cricket. Nowel *et al.* histologically identified the Acid Fuchsin-staining fibres in the cricket to be similar to those stained by Locke and Huie (1972) in the neural lamella of the cockroach *Calpodes ethlius*. Locke and Huie went on to demonstrate an additional histological technique to demonstrate the presence of these same fibres (Locke and Huie, 1975) in both the cockroach and the locust *Locusta migratoria*. The Acid Fuchsin-staining fibres in the locust *Schistocerca gregaria* in this study appear to be of comparable size and share the same relative location as those described by Locke and Huie in the neural lamella of *Locusta migratoria* (1975). Locke and Huie also observed (as in this study) uneven fibre staining with uranyl acetate and lead citrate in tissue post-fixed with osmium, which was not evident when the fibres were visualised by staining glutaraldehyde-fixed material with phosphotungstic acid.

3.5.5.3 Extracellular fibrils

The locust neural sheath material described in the study of Locke and Huie (1975) shows another feature also found in the present study. Adjacent to the larger 'elastic fibres' (Acid Fuchsin-staining) are smaller diameter fibres which resemble the 'peroxidase-reactive fibres' of Locke and Huie (1972), or the 'fibrils' referred to in this study. Although present these 'fibrils' were not described by Locke and Huie in their 1975 paper, the

focus of that study being on the staining techniques that were used to resolve the larger elastic fibres. The micrographs in that paper show that the 'fibrils' are arranged in a graded fashion, the 'star-like' appearance of the fibrils near to the edge of the neural lamella contrasting with the increasingly simple profile in cross-section of those fibrils that were embedded deeper. They range in diameter from 25 - 70 nm, this range coinciding almost exactly with the range of 'fibril' sizes in this study. The fibres having a 'star-like' profile can be seen clearly associating with the larger 'elastic fibres' located near the edge of the neural sheath. This supports the hypothesis that the fibrils in the mtFCO associate to form the larger Acid Fuchsin-staining fibres.

The fibrils found in the mtFCO also share the graded size and distinctive mixture of profiles (regular and 'star-like') as those observed in neural connective tissue of *Locusta gregaria* by Gray (1959). He described fibrils of approximately 70 nm diameter with irregular profiles in cross-section as having 'flanges'. In addition, the fibrils he observed exhibited a banding pattern in longitudinal section which led Gray to call them 'collagen-like' fibres. However, although these 'collagen-like' fibrils closely resemble the fibrils observed in this study in both size and appearance, their characteristics differ in two respects. Firstly the fibrils observed by Gray were 'not orientated in any particular direction' unlike the axially arranged fibrils in the mtFCO. Secondly, the period and characteristics of the banding described by Gray contrast with those observed in this study. The 'collagen-like' fibrils he observed had a mean macroperiod of approximately 60 nm, each containing 5 asymmetrically distributed sub-periods. The fibrils observed in this study showed a regular banding with a mean interband interval of 16.8 nm. The fibrils described by Smith and Treherne (1963) located in the neural lamella of the cockroach are also unlikely to be composed of the same material as the fibrils described in the present study. In common with the fibrils characterised by Gray, these fibrils were distributed in a 'meshwork' rather than lying in an axial array and showed asymmetric banding with a 56 nm macroperiod.

Table 3.2

Location	Description	Banding	Fibre diameter	Terminology	Authors
predominantly the sheath of the CO *(Acheta domesticus)*	regular circular profile in transverse section.	not investigated	**0.5-1.2µm**	Acid Fuchsin-staining fibrils	Nowel *et al..*, (1995)
neural lamella of tibio-tarsal CO *(Periplaneta)*	amorphous fibrils	not investigated	**approximately 0.5µm**	electron dense material	Young (1970
neural lamella *(Locusta migratoria)*	amorphous aggregations evidence of smaller subfibres	not investigated	**0.2-0.7µm**	elastic fibres	Locke and Huie (1975)
auditory ganglion connective tissue (*Locusta migratoria*)	amorphous fibres with irregular profiles-particularly, star-like in transverse section. ('flanges'). no particular orientation	asymmetric banding 'typical' of collagens 5 bands/macroperiod mean macroperiod 59.9nm (range 55-64nm)	"fairly uniform" **70nm**	collagen-like	Gray (1959)
ejaculatory duct *(Locusta migratoria)*	smaller diameter amorphous fibres associated with first days after moult larger 'irregular' fibres found 1 week after moult acially arranged	67nm periodicity	**30-70nm**	collagen fibrils	Ashhurst (1982)
neural lamella *(Periplaneta americana)*	multi-directional meshwork	56nm macroperiod	**<60nm**	collagen-like	Smith and Treherne (1963)
neural lamella *(Calpodes ethius)*	amorphous fibres distributed near edge of neural lamella associated with 'microfibres' of diameter **<6nm**	none observed	**40nm**	Peroxidase Reactive Fibres	Locke and Huie (1972)
nervous connective tissue (*Schistocerca gregaria*)	no particular pattern of orientation	asymmetric banding 6 bands/ macroperiod	**25nm (15-40nm)**	collagen	Ashhurst (1965)
surrounding individual attachment cells CO *(Acheta domesticus)*	regular circular profile in transverse section.	not investigated	**50-300nm**	fine Acid Fuchsin-staining fibrils	Nowel *et al.* (1995)
'perilemma' *(Rhodnius prolixus)*	fibres in dense fibrillar layers embedded in neutral mucopolysaccharide	50-60nm macroperiod some evidence of secondary periodicity	**>15nm**	differentially oriented fibres	Smith and Wigglesworth (1959)
neural lamella (connective) wax-moth (*Galleria mellonella*)	intracellular hollow- resembling microtubules	15-20nm banding	**12.5-20nm**	unresolved (possibly collagen; hydroxyproline present)	Ashhurst (1964)
neural lamella *(Calpodes ethius)*	no particular orientation a loose network denser adjacent to cell surface	66nm macroperiod	**13nm**	collagen	Locke and Huie (1972)
neural lamella *(Calpodes ethius)*	associated with peroxidase reactive fibres irregular profile	none observed	**<6nm**	microfibres	Locke and Huie (1972)
neural lamella *(Periplaneta americana)*	axially oriented filamentus layer of elements 0.3µm from lamella surface	none observed	**5nm**	filamentus elements	Smith and Treherne (1963)
sheath of ventral ligament CO *(Acheta domesticus)*	regular circular profile in transverse section. some evidence of fibre fusion	not investigated	**0.5-1.2µm**	thick Acid Fuchsin-staining fibrils	Nowel *et al..*, (1995)
apodeme complex ligaments *(Schistocerca gregaria)*	regular circular profile in transverse section. clear evidence of fibre fusion	not investigated	**0.5-1.25µm**	Acid Fuchsin-staining fibrils	Shelton *et al.*, (1992)
VERTEBRATE (rat)	regular circular profile in transverse section.	597nm (generally accepted to be 64nm in unfixed material)	**40-400nm**	'typical' collagen	Gray (1959)

Table 3.2 summarises the extracellular fibres/fibrils described by previous authors

Evidence for the presence of collagenous fibres in the mtFCO

Although modern studies would almost certainly use antibodies for identifying collagen, virtually all of the relavent work on arthropod sense organ anatomy predates this technology. Matheson and Field (1990) described the fibres of the mtFCO as 'collagenous'. In this study two different types of banded fibril have been observed, distinguishable by their size and banding characteristics. One type of fibril is found in each of the mtFCO's mechanical linkages, the other is exclusive to the flexor strand. Gray (1959) outlined three characteristics which he considered indicative of collagen:

-extracellular non-branching fibrils

-the presence of a series of polarised (i.e. asymmetric) bands in longitudinal section which can be delimited into repeating macroperiods

-the observed banding is of similar periodicity to that of 'authentic' (vertebrate) collagen.

The last of Gray's criteria should be a reliable indicator of the presence of collagen given that the banding pattern is said to be unique to the collagen class of molecules (Schmitt *et al.*, 1955). In practice, the comparison of an observed banding pattern with that of 'authentic' collagen is not easily made, and a variety of methods have been used both alone and in conjunction with one another by various authors to indicate the presence of collagen.

Techniques used by other authors to identify collagen

-Birefringence

Collagen has birefringent properties (Wolman, 1970; Smith *et al.*, 1981). The optical birefringence properties of collagen were characterised and explained by Wolman (1970). Before this time, authors used optical birefringence as an indicator of collagen in conjunction with other techniques. Baccetti (1957) suggested the presence of a collagen-like material in the neural lamella of *Anacridium aegyptium* on the basis of its transmission of polarised light. He reported that the neural lamella showed optical, enzymatic and chemical properties consistent with collagens. Richards and Schneider (1958) similarly demonstrated birefringence in cockroach neural lamella. The ligaments comprising the apodeme complex of the mtFCO show strong birefringence when

illuminated with polarised light *in situ* (results not shown). This suggests the presence of a large number of aligned molecules, but it is not a positive indication of the presence of collagen. This birefringence is equally likely to be a property of the axially-aligned microtubules.

-X-ray diffraction

Low-intensity X-ray irradiation of crystalline collagen produces a distinctive diffraction pattern (Bear, 1942; Schmitt *et al.*, 1942). Some authors have used this technique to present evidence for the presence of collagen in insect tissues. For example Richards and Schneider (1958) used this method to identify collagen in the neural lamella of the cockroach *Periplaneta americana*, which they estimated constituted between 10 - 20% of the total lamella volume. However, Gross (1963) showed in other phyla that not all connective tissue fibres which have the X-ray diffraction pattern and amino-acid composition of collagen possess the typical 64 nm banding periodicity of vertebrate collagen. This, coupled with a difficulty in extracting sufficient pure material for analysis has meant that few other authors have used this technique to localise collagen in insect connective tissue.

-Amino-acid indicators

Presence of the amino-acid hydroxyproline (a characteristic constituent of collagen) has also been provided as evidence for the presence of collagen in insect tissues. To confirm the presence of collagen, Ashhurst (1959, 1961b) identified hydroxyproline in hydrolysates of isolated *Locusta migratoria* neural lamella using chromatographical techniques.

-Banding periodicity

The easily accessible characteristic of banding periodicity is used by the majority of authors (see Table 3.2) to classify a material as collagen or 'collagen-like'. However, there are problems in using the periodicity of the banding to positively identify a fibre as 'authentic' collagen, hence the use of the term 'collagen-like'. The most widespread problem is that of subtle modification of the tissue during the preparation procedure prior to examination. Such procedures include fixation, dehydration and embedding. This problem was encountered by Ashhurst and Chapman (1961) whilst examining 'collagen' fibres in the neural lamella of the locust *Locusta migratoria*. They found that material from the same source

had different characteristics when prepared using different techniques. The fibres in question had a macroperiod of 40-50 nm when examined in thin sections and a macroperiod of 60-65 nm when prepared by heavy metal shadowing of a neural lamella macerate.

Some authors have endeavoured to overcome these 'artifactual' inconsistencies caused by tissue preparation technique. Any changes in macroperiod due to fixation, dehydration and embedding routine can be minimised by treating two contrasting samples in the same manner. Such an approach was used by Gray (1959) when attempting to classify collagen-like material in the neural lamella of the locust *Locusta migratoria*. The comparable treatment of the locust material and a sample of rat-tail collagen allowed him to scale and overlay the macroperiods of the locust onto those of 'authentic' collagen to compare the banding.

In addition to artifacts introduced during tissue preparation, there is the inevitable factor that as a fibre is elongated, such as when it is embedded in an extensible material, the periodicity of the banding changes. This was first observed in collagen by Schmitt *et al.* (1942). They reported that different regions within the macroperiod appeared to increase in length disproportionally to one another. This would preclude the simple scaling of corresponding regions of banding in different preparations to eliminate the factor of preparation artifact/extension when the material was fixed.

Which fibres are composed of collagen?

There is still no convincing evidence that any of the fibres associated with the mtFCO apodeme complex are composed of collagen (Shelton *et al.*, 1992). However, a review of banded fibres in insect nervous tissues by Smith and Treherne (1963) came to the conclusion that all the reports of differently banded fibres were referring to the same material with minor structural modifications within the macroperiod. In particular they pointed out that a common theme in all the accounts of banded fibres in insects was the presence of bands comprised of paired subunits of 'doublets'. This characteristic is clearly shown to be the case in the fibrils of the mtFCO (Figs 3.14b and 3.37b).

The 'collagen-like' fibres observed in the strand organ do show all the characteristics which other authors have deemed necessary to classify the

material as collagen. A 10-25 nm diameter fibre showing a distinctive asymmetric banding pattern in conjunction with a 52-54 nm macroperiod would be sufficient to classify this material as insect collagen in accordance with the criteria of Ashhurst (1965) and Locke and Huie (1972).

What are the remaining extracellular fibres composed of?
Whilst the mtFCO fibrils do show a banding pattern in longitudinal section, the thicker 'Acid Fuchsin-staining' fibres do not. This circumstantially opposes the hypothesis that two classes of fibre are composed of the same material. However, this hypothesis could be realistic if fibres became increasingly cross-linked as they grow larger, so obscuring the banding pattern in some way. There is some evidence that collagens both increase in diameter (Gross, 1950) and using birefringence in conjunction with histological and chromatographic techniques (Tonna and Hatzel, 1967) showed that collagens become increasingly cross-linked with age.

Although there is histological evidence for cross-linking (Locke and Huie, 1975) in the elastic fibres, a resulting loss of periodic banding with increasing fibre diameter is not a property of collagen. Rather than propose that they are all composed of an insect collagen it would seem more likely that the Acid Fuchsin-staining fibres of the mtFCO, and the fibrils with which they are associated, are composed of an unidentified elastic protein. This would exhibit banding in small diameter fibrils which would be subsequently lost in larger diameter fibres.

Why are 'collagen' and AFSC found together in the strand organ?
Although there was no clear evidence for collagen in the mtFCO itself, fibrils with a collagen-like banding pattern were identified in the strand organ. Collagen is a relatively inextensible protein with a high tensile strength (Schmitt *et al.*, 1942; Harkness, 1961; Wainwright *et al.*, 1976). This means that it is capable of storing larger amounts of elastic energy for smaller elongations in comparison to other 'rubbery' proteins such as elastin or resilin. Its properties could endow ligaments with stiffness and prevent shearing, but it seems an unlikely candidate for main elastic components. There are examples of interaction of 'rubbery' protein and 'stiff' fibres to form a 'pliant composite' such as the interaction of elastin and collagen in mammalian artery walls (Gosline, 1980). The role of the

less extensible component in conventional pliant composites is to provide limits to extension which would protect or maintain the integrity of lower modulus components. However, there are examples of systems in which the high tensile component is discontinuous (such as locust arthrodial membrane: Vincent, 1976) serving only as a reinforcing filler. This arrangement allows for large extensions whilst there are no built-in high strain limits (Gosline, 1980). This may be particularly important in the case of the strand organ, as unlike all the other mechanical linkages, it is subject to rising tension during the rapid extension of the tibia associated with the locust jump.

3.5.5.4 Extracellular matrix

The extracellular matrix separates the scolopidia and attachment cells from the haemocoel. Following the terminology of Ashhurst (1959, 1968) and Young (1970) the outer homogenous non-cellular layer is denoted neural lamella whist the term perineurium (or perilemma) is reserved for the underlying 'sheath' cells associated with the neural tissue. Other authors have used these terms less precisely, the term 'perilemma' being applied to the sheath as a whole by some authors (Scharrer, 1939; Pipa and Cook, 1958; Pipa *et al.*, 1959). Ultrastructural studies have shown that the perineurium in insects is continuous with the connective tissue basement membrane overlying all the organs of the body (Ashhurst, 1968). It appears to surround each attachment cell and to bind the ligaments together. Ashhurst (1968) suggests that this 'cementing' property is attributable to the mucopolysacharide content of extracellular matrix (neural lamella). This reflects the view of Bradfield (1950) who related the quantitiy of polysaccharide present in extracellular matrix to the degree of plasticity required of it. The mechanical role of the neural lamella associated with the mtFCO seems to be to hold together the cells and axons of the nervous system whist being flexible enough to allow some movement. The 'binding' role of extracellular matrix is especially apparent in the extracellular material surrounding the dorsal ligament attachment cells where cell to cell contact is minimal and the extracellular matrix fills the intercellular spaces within the ligament.

3.5.5.5 The mechanical role of cell junctions in the ligaments of the apodeme complex

The present study showed that there are considerable numbers of intercellular junctions between attachment cells. Toh and Yokohari (1985) (studying the antennal chordotonal sensillum in *Periplaneta americana*) suggested that the occurrence of invaginated membranes of attachment cells with associated desmosomes contributed to cell rigidity. The relationship between perimeter length and attachment cell cross-sectional area means that the ventral ligament could potentially contain more cell-to-cell junctions per unit cross-sectional area that the dorsal ligament which is composed of bulkier attachment cells. The attachment cells of the ventral ligament appear more closely associated than those in the dorsal ligament and although no quantitative data were obtained there did appear to be more intercellular juctions in the ventral ligament than in the dorsal one. Differences in the numbers of intercellular junctions in the two different ligaments could have mechanical consequences. Further studies are required in this area.

3.5.6 Implications of elastic component distribution in the mtFCO ligaments

Burns (1974) suggested that the elastic properties of the attachment between the apodeme and the proximal scoloparium in the pro- and mesothoracic COs act as a mechanical damper to buffer the delicate sensory area from rapid movements of the tibia. However, the fact that the potentially elastic components are not distributed evenly throughout the apodeme complex suggests that differential elasticity, either between or within the dorsal and ventral ligaments, may also play a functional role in modifying the input stimulus in some way as it is mechanically transmitted to the sensory cells.

Comparing the size-frequency distribution of AFS-fibres between the dorsal and ventral ligaments at two proximo-distal levels shows that the distribution of fibre sizes differs between the two ligaments. This was also observed in the locust by Shelton *et al.* (1992). Proximally in the ligaments as a whole the number of medium sizes fibres (0.6 - 2.0 μm^2) declines, whilst the number of small fibres (<0.4 μm^2) increases (Fig. 3.45). This indicates either a tapering or branching of fibres in one or both ligaments. Examining the individual ligaments separately reveals that the fibres taper

proximally in the dorsal ligament and branch proximally in the ventral ligament.

3.5.5.6 Elastic fibre distribution in the dorsal ligament

In the dorsal ligament, the number of discrete fibres remains relatively constant along its length at between 100 and 120. Over the same range, the cross-sectional area of AFSC in the ligament approximately halves. This shows that the AFS fibres of the dorsal ligament taper proximally along their length. The proximal decrease in AFSC cross-sectional area is similar in both the ligament sheath and within the ligament, indicating that both classes of fibre taper proximally. This is reflected in the range of fibre sizes at different levels. Proximally the range of fibre sizes in the dorsal ligament falls. There is an increase in the number of small fibres ($<0.4\ \mu m^2$) and a reduction in the numbers of larger fibres ($>0.4\ \mu m^2$). The implications of these observations are that the dorsal ligament is likely to have a graded change in compliance as it approaches the mtFCO sensory dendrites. Thus, dendrites terminated at differing proximo-distal levels within the dorsal ligament will be subjected to differing degrees of mechanical force in response to a given tibial rotations.

3.5.5.7 Elastic fibre distribution in the ventral ligament

In the case of the ventral ligament, the increase in both the number and cross-sectional area of Acid Fuchsin-staining fibres over the proximo-distal range 0 - 350 μm reflects the recruitment of ventral ligament attachment cells from the side of the cuticular rod. The cross-sectional area of AFSC along the remainder of the ventral ligament between the loops and the sensory neurones is much more uniform than the equivalent range in the dorsal ligament. Whilst there are consistently more individual fibres located within the ligament than in the ligament sheath, there is a greater cross-sectional area of AFSC in the sheath than within the ligament at the majority of proximo-distal levels. This demonstrates that in the case of the ventral ligament, the internal fibres are smaller than the sheath fibres. In addition, at a proximo-distal level of 800 μm there appears to be a proliferation of Acid Fuchsin-staining fibres within the ventral ligament accompanied by only a modest increase in the cross-sectional area of internally-located Acid Fuchsin-staining fibres. This indicates that the fibres branch within the ventral ligament at the level of the sensory cells. This was confirmed by the 5(6)-carboxyfluorescein staining of the

extracellular fibres. These results indicate that unlike the case in the dorsal ligament fibres, the Acid Fuchsin-staining fibres in the ventral ligament branch proximally rather than taper.

The differential distribution of elastic components in the mechanical linkages of chordotonal organs is not restricted to the locust mtFCO. Nowel *et al.* (1995) described the distribution of Acid Fuchsin-staining fibres in the mtFCO of the cricket. They observed that the Acid Fuchsin-staining fibres in the cricket are much thicker and present in larger numbers proximally than they are distally. In addition there are many more fibres in the ventral ligament than in the dorsal ligament. They remarked that the thinner AFS fibres were the more compliant, implying that the two ligaments attaching the fused scoloparia to the cuticular apodeme have different mechanical properties. The percentage cross-sectional areas of the ligaments composed of AFSC in the cricket and the locust are comparable. Measuring midway between the cuticular apodeme and the sensory cells (cricket data from Nowel *et al.*, 1995) the AFSC comprises approximately 8% of the total cross-sectional area of the ligaments in both species. If the microtubules do play only a limited role in mechanical signal transduction (as suggested previously in this discussion), then the extracellular fibres and the extracellular matrix would be left as the main components transmitting the mechanical stimulus to the sensory cells.

3.5.5.8 Aspects of the extracellular fibre distribution which may have functional implications:

1. There is a gradient of AFSC present along the length of the ligaments. This would suggest that both the ligaments are stiffer distally. This is especially marked in the case of the dorsal ligament which has approximately half as much AFSC proximally than distally.

2. There is more AFSC in the ventral ligament than the dorsal one at all proximo-distal levels. This indicates that the ventral ligament may be stiffer than the dorsal ligament.

3. In the case of the dorsal ligament, there is consistently more Acid Fuchsin-staining material located in the sheath than within the ligament. This raises the possibility that the attachment cells nearer the centre of the

ligament may have different mechanical properties from those closely associated with the sheath.

4. The sheath of the loop-forming region of the dorsal ligament is re-enforced with AFSC. The increase in the cross-sectional area of AFSC over this range is due to a larger number of fibres, not just thicker fibres. This observation indicates that the fibres may have a protective role at this level, preventing excess shear or kinking across the attachment cell membranes. Differential distribution of components in the mtFCO may be a way to differentiate the properties of the two ligaments and so the responsiveness of neurones lying in the dorsal and ventral regions of the scoloparium.

Figure 3.1

This figure demonstrates the image-processing steps used to analyse the distribution of the Acid Fuchsin-staining extracellular fibres in the ligaments of the apodeme complex. The live video image was displayed on the monitor as the microscope was adjusted ('**Pre-capture**' window) (left-hand image). The contrast of each image was optimised and captured using a built-in frame averaging function to reduce any background noise in the video signal ('**Contrast adjusted**' window) (central image). Thresholding was used to discriminate objects of interest from surrounding background based on their greyscale values. Each image was thresholded using density slicing, the selected pixels being labelled in red ('**Density sliced**' window) (right-hand image).

(This figure was grabbed at screen resolution (72 dots-per-inch) for demonstration purposes. Images used for analysis were captured at higher resolution (215 pixels/μm^2)).

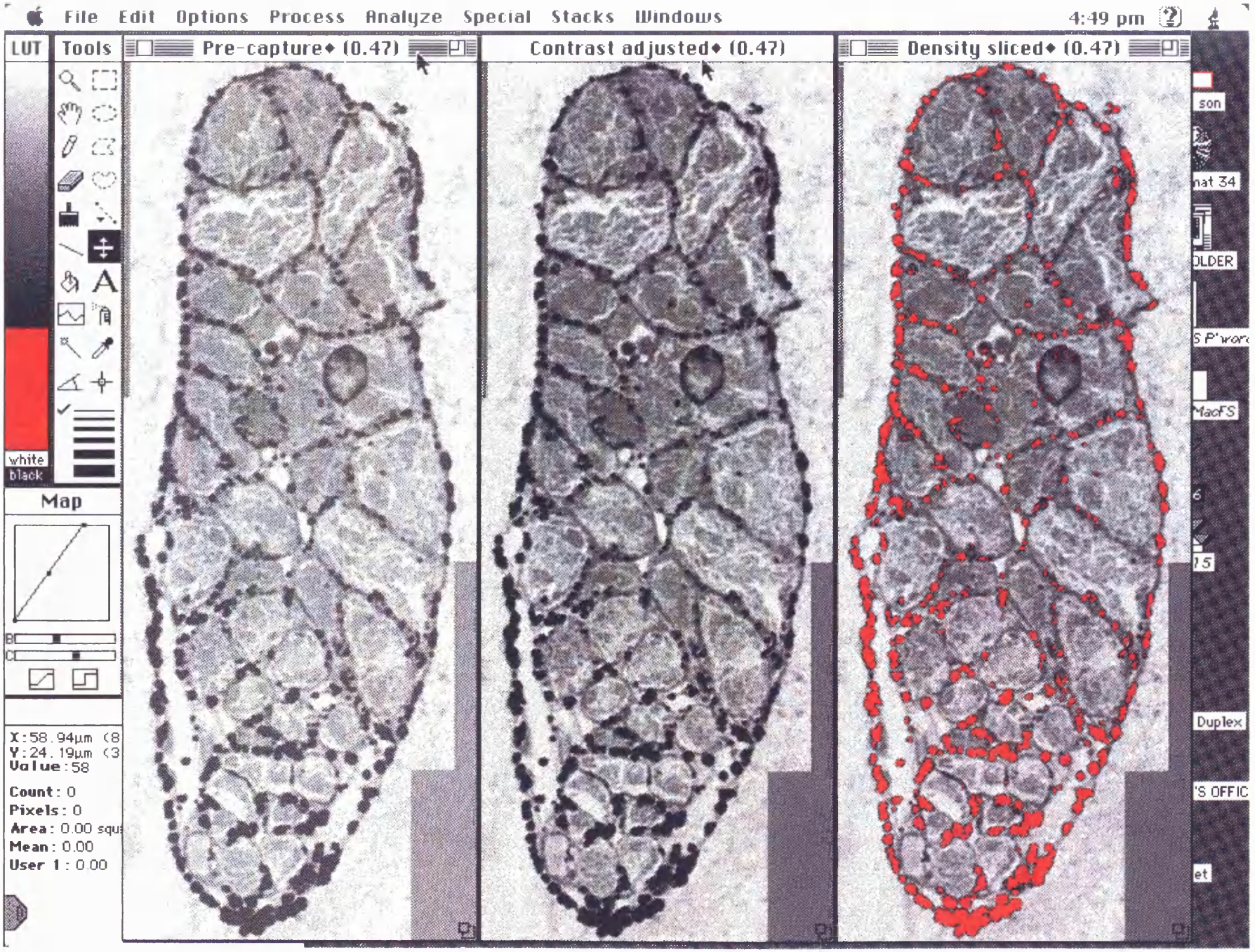
File Edit Options Process Analyze Special Stacks Windows
4:49 pm
LUT
Tools
Pre-capture◆ (0.47)
Contrast adjusted◆ (0.47)
Density sliced◆ (0.47)
white
black
Map
X:58.94µm (8
Y:24.19µm (3
Value:58
Count: 0
Pixels: 0
Area: 0.00 squ
Mean: 0.00
User 1: 0.00
son
nat 34
OLDER
MacFS
Duplex
'S OFFIC
et

Figure 3.2a-d

This figure shows a series of 1 μm transverse sections taken at different levels along the dorsal attachment. The level at which each section was taken is indicated in the inset.

The attachment is a double structure and consists of an anterior (aa) and a posterior (pa) component at all proximo-distal levels. Distally, close to the region where it is attached to the femur wall, the posterior component is the more prominent (Fig. 3.2a). At this level it has a thick dorsal sheath with many extracellular fibres (f) that stain with Acid Fuchsin. At distal levels, the anterior and posterior components of the dorsal attachment are only loosely associated with one another. However, they are anatomically connected to each other along the ventral edge of the attachment at all levels (Figs 3.2a-c). Proximally, where the dorsal attachment joins the cell body region of the mtFCO, the anterior component (aa) is more prominent than the posterior component (pa) (Fig. 3.2d). At this proximo-distal level the branch of the CO nerve (n) which forms the cuticular nerve is sectioned longitudinally.

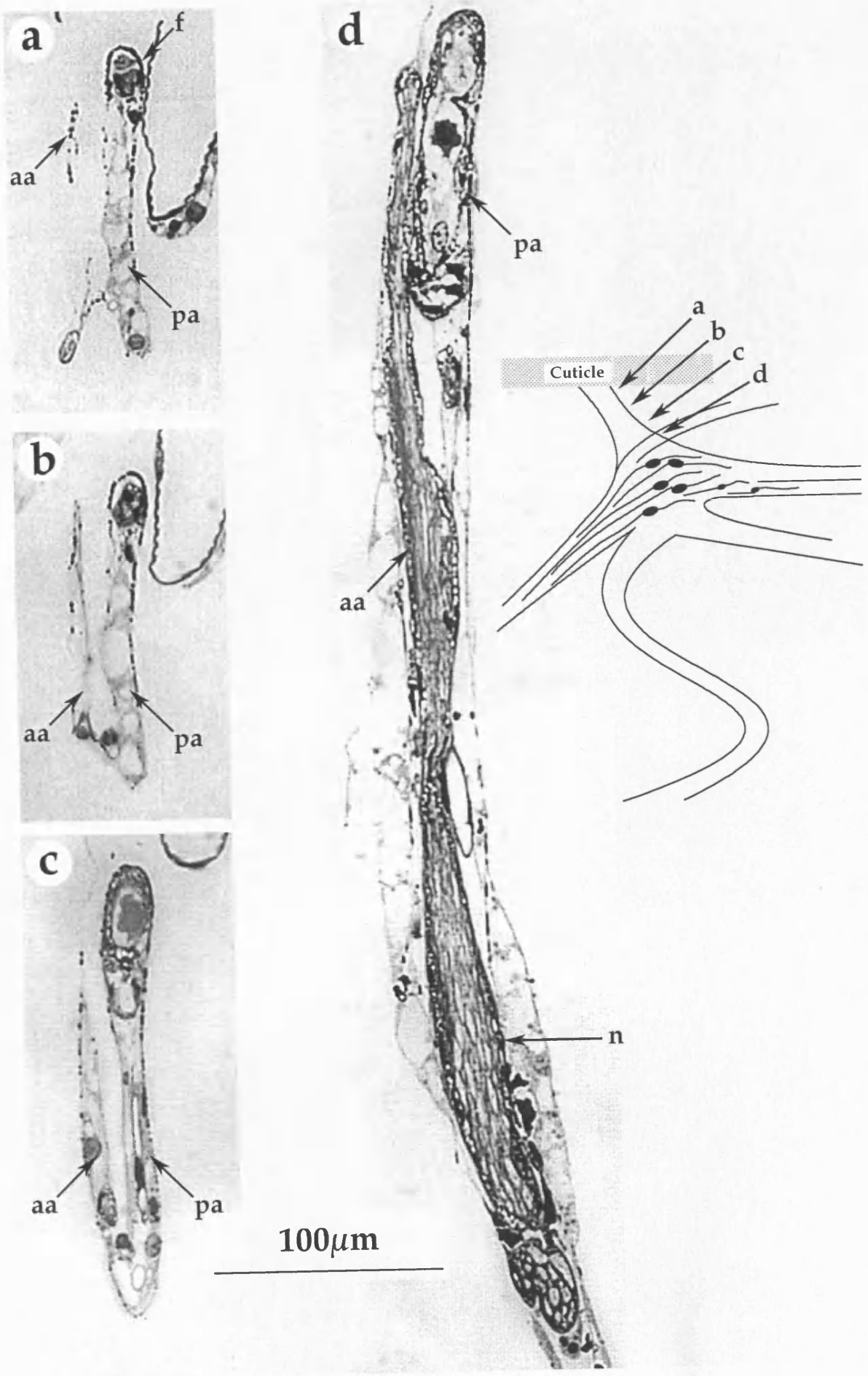
a
f
aa
pa
b
aa
pa
c
aa
pa
d
pa
a
b
c
d
Cuticle
aa
n
100μm

Figure 3.3

Electron micrograph showing distribution of areas within the dorsal attachment that are packed with an amorphous granular material (g). The microtubule-packed ligament cells (l) account for only a small proportion of the dorsal attachment in cross-section. The extracellular matrix contains both fibrils (f) and larger Acid Fuchsin-staining fibres (F). s = dorsal attachment sheath

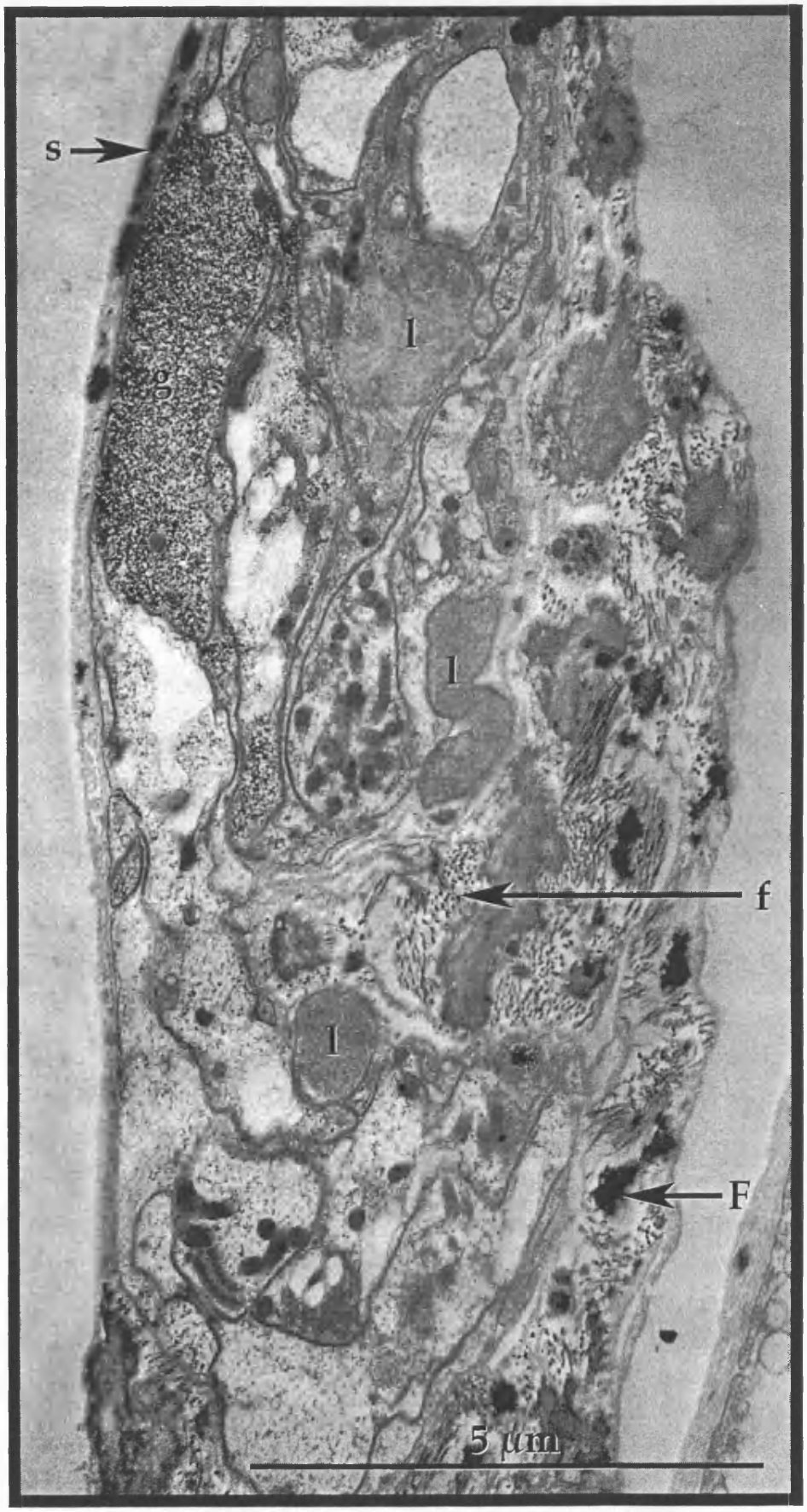
s
g
l
l
f
l
F
5 µm

Figure 3.4a, b

a

Electron micrograph showing that the ligamentous cells of the dorsal attachment are packed with axially orientated microtubules (mt) and are surrounded by extracellular matrix (m).

b

In other areas, amorphous granular material (g) appears to be sequestered within cells bounded by lightly-staining extracellular matrix (m) in which extracellular fibres (F) are embedded.

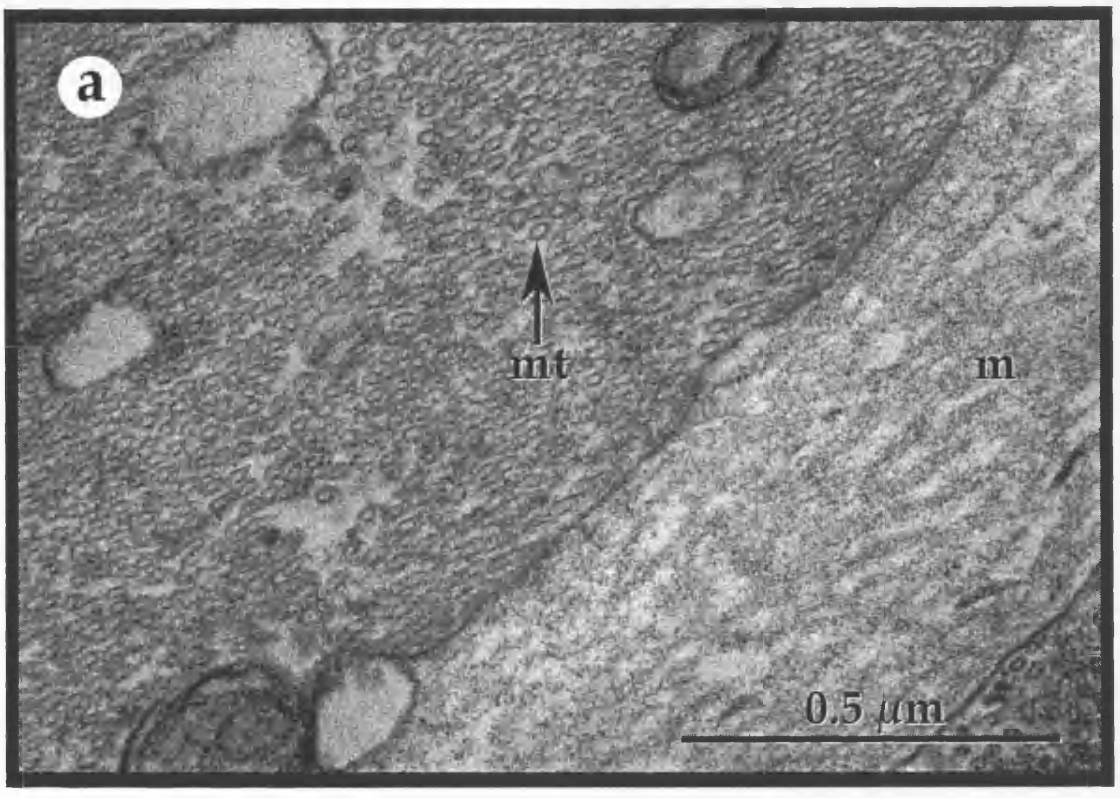
a
mt
m
0.5 μm

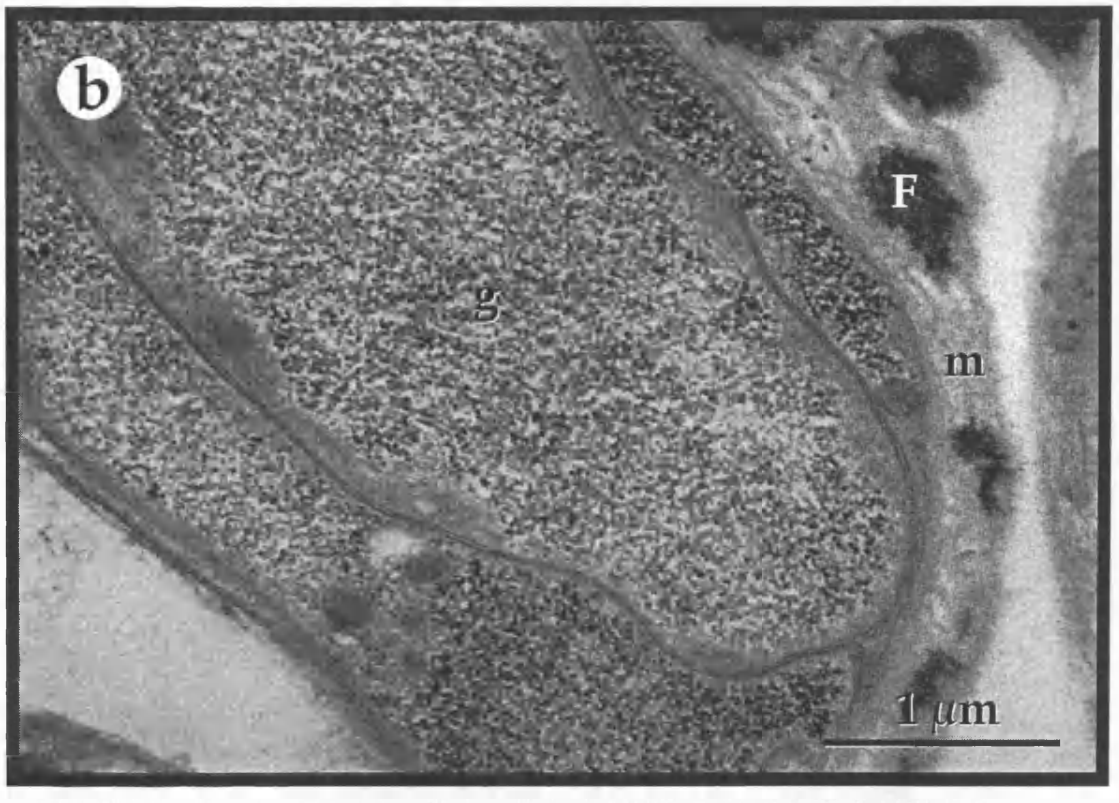
b
F
g
m
1 μm

Figure 3.5a, b

a

The largest Acid Fuchsin-staining fibres (F) associated with the mtFCO dorsal attachment are located in the extracellular sheath (s). They are found adjacent to smaller fibrils (f) embedded in the extracellular matrix. h = haemolymph space

b

There is a continuous spectrum of fibre sizes; some of which are clearly associated with one another (i). F = Acid Fuchsin-staining fibres; f = extracellular fibrils; h = haemolymph space

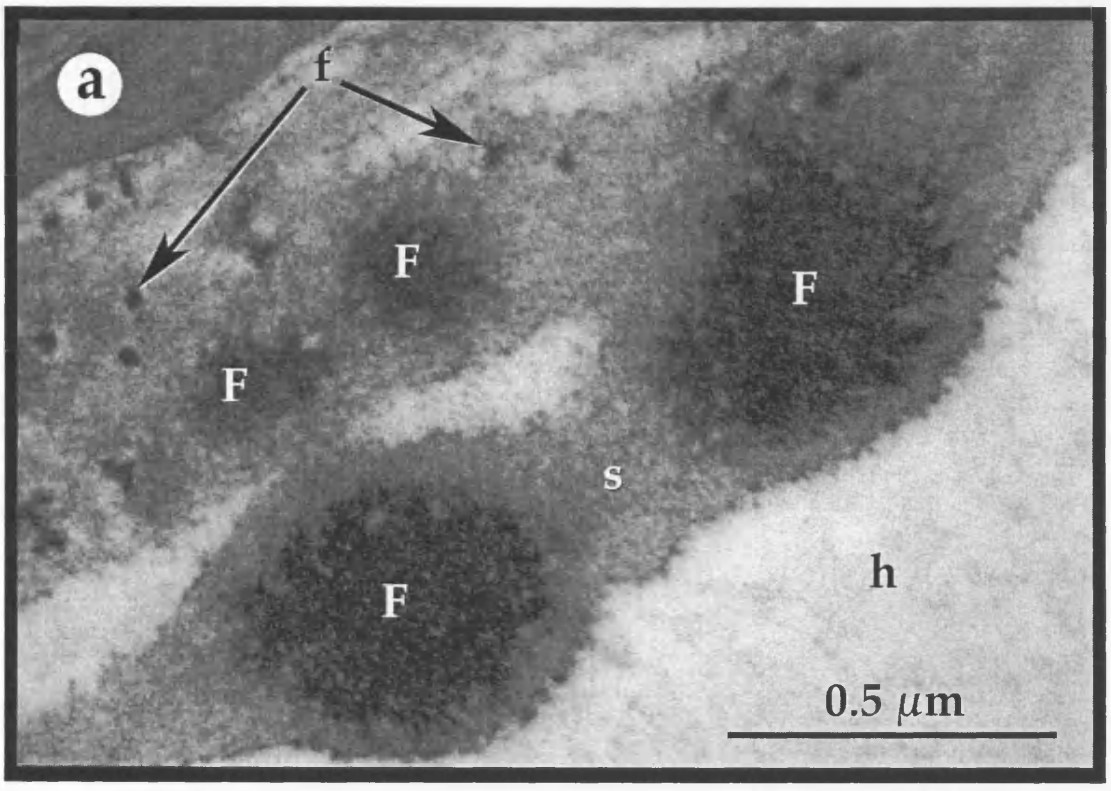
a
f
F
F
F
F
s
h
0.5 μm

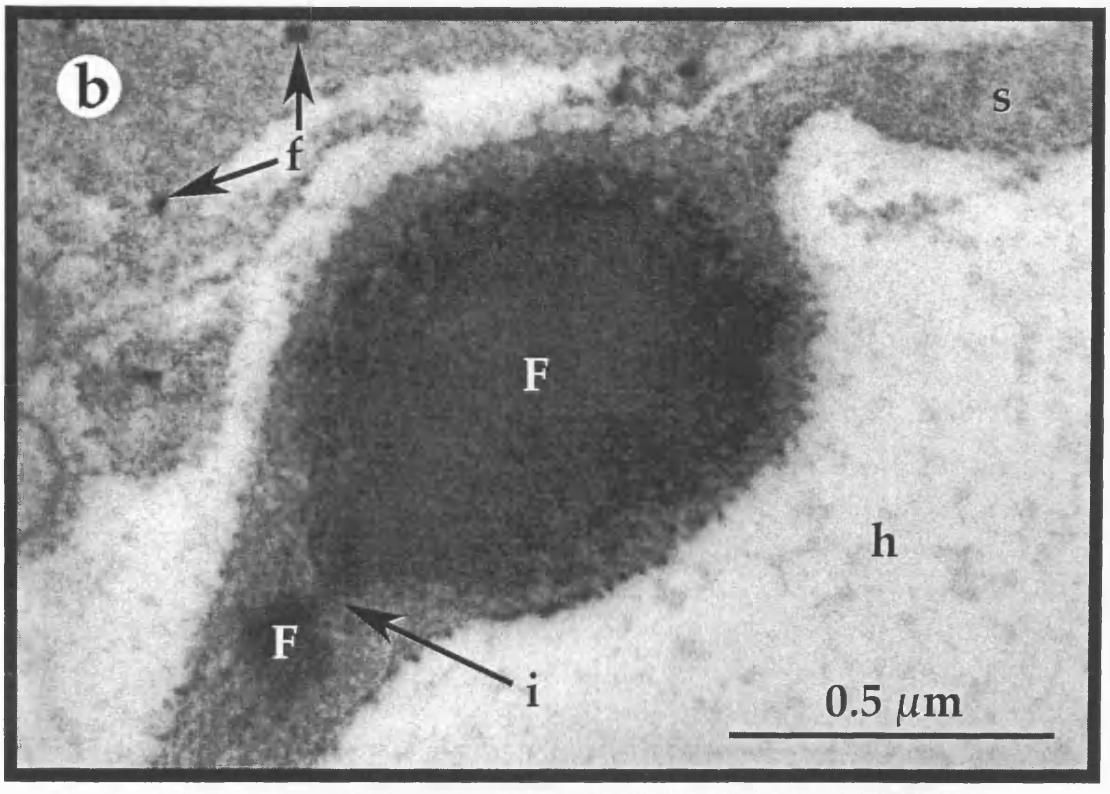
b
f
s
F
h
F
i
0.5 μm

Figure 3.6

Transmission electron micrograph showing the complex distribution of component materials within the posterior component of the dorsal attachment. This micrograph shows microtubules (mt), Acid Fuchsin-staining fibres (F), fibrils (f) and amorphous granular material (g) all located adjacent to one another within the attachment, with extensive membrane interdigitation between each component. There are ladder-like septate desmosomes (sd) forming associations between the interdigitations of a microtubule containing cell (see inset). ecs = extracellular space; mtc = mitochondria

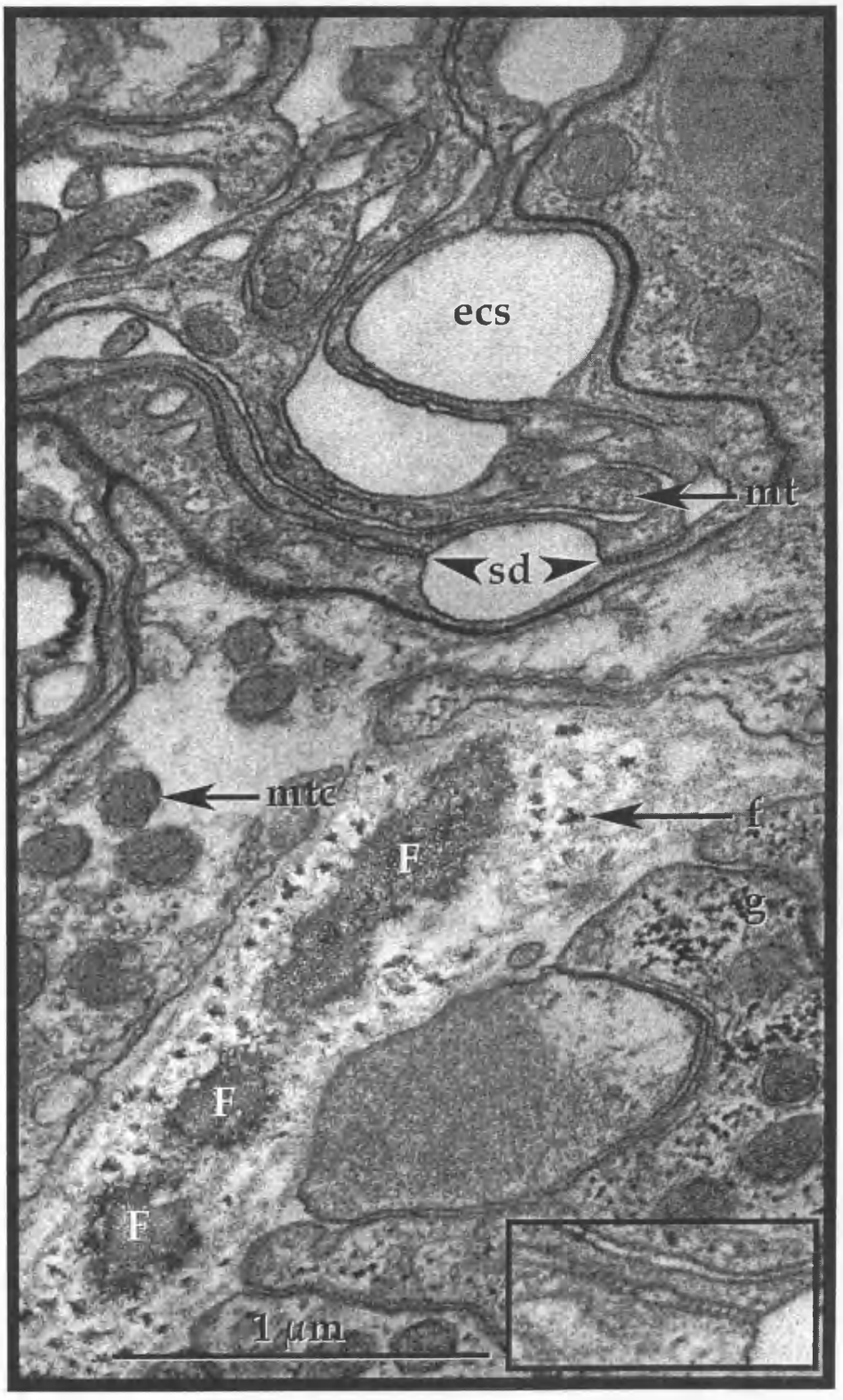
ecs
mt
sd
mtc
f
F
g
F
F
1 µm

Figure 3.7

Line diagram compiled from several electron-micrographs showing the distribution of components within the mtFCO dorsal attachment. The diagram represents a proximo-distal level intermediate between those shown in figures 3.2c and 3.2d.

At this level the cells comprising the posterior component of the dorsal attachment are largely composed of fatty deposits (f) embedded within a network of connective tissue (c). The multiterminal receptor (m) is situated ventrally in the anterior component of the attachment and arises from a branch of nerve 5b1. A second neural component located in the anterior compartment of the dorsal attachment (cut transversely) (n) is a branch of the cuticular nerve; its destination is unknown. s = sheath; c = connective tissue composed of ligamentous cells and extracellular matrix (Figures 3.3 and 3.6); n = longitudinally sectioned nerve; f = fat body; m = multi-polar receptor; cp = capsule surrounding the multiterminal receptor; g = localisation of granular electron-dense material

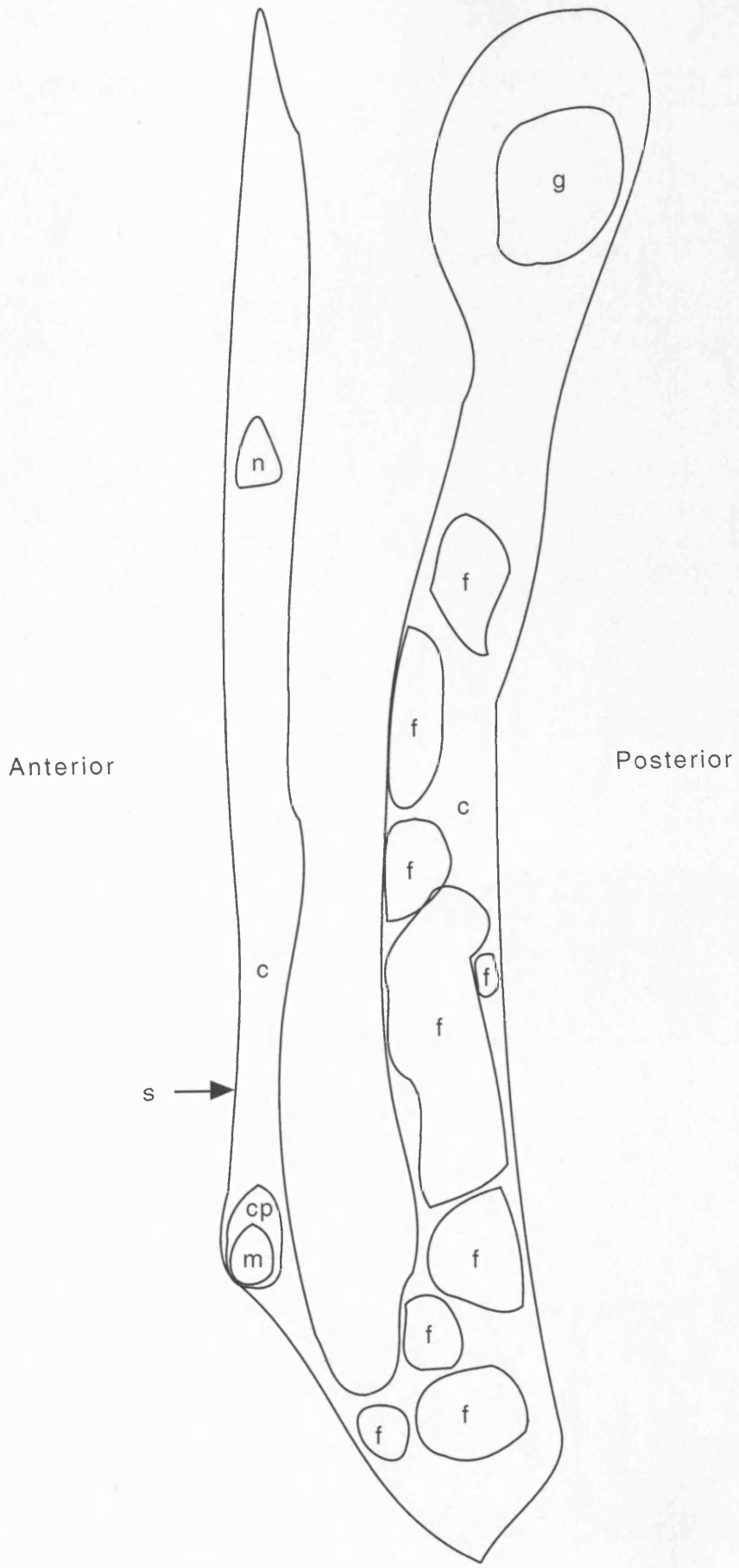
Anterior
Posterior
g
n
f
f
c
f
f
c
f
f
s
cp
m
f
f
f
f

Figure 3.8a, b

a

The multi-terminal receptor is contained within a capsule cell (cp). Branches of the multi-terminal receptor dendrite (d) are wrapped around fingers of membrane-bound cellular material (c) arranged in a loosely radial configuration. The dendritic branches are interspersed with extracellular 'elements' (e). F = extracellular (Acid Fuchsin-staining) fibres; h = haemolymph space

b

Proximally the dendrite (d) of the multi-terminal receptor is surrounded by a layer of glial wrapping (g) which separates the receptor's membranous capsule cell (cp) from the extracellular sheath (s). h = haemolymph space

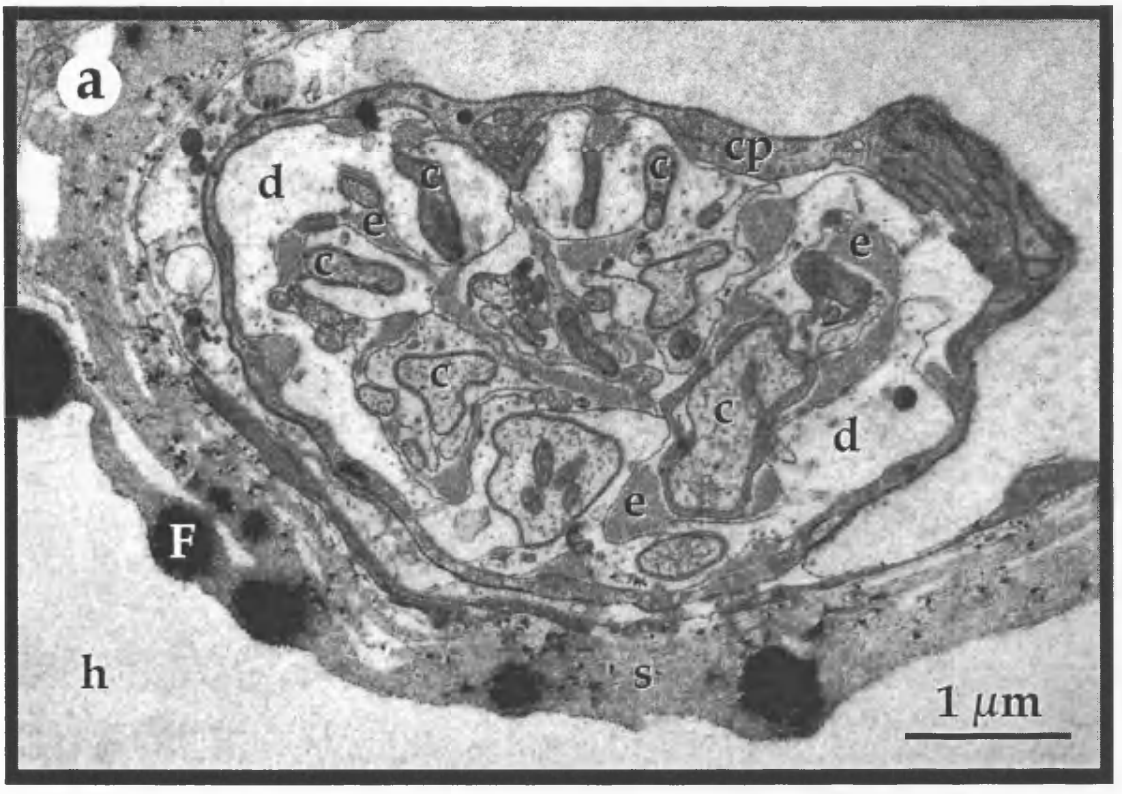
a
d
c
e
c
cp
c
e
c
c
d
e
F
h
s
1 μm

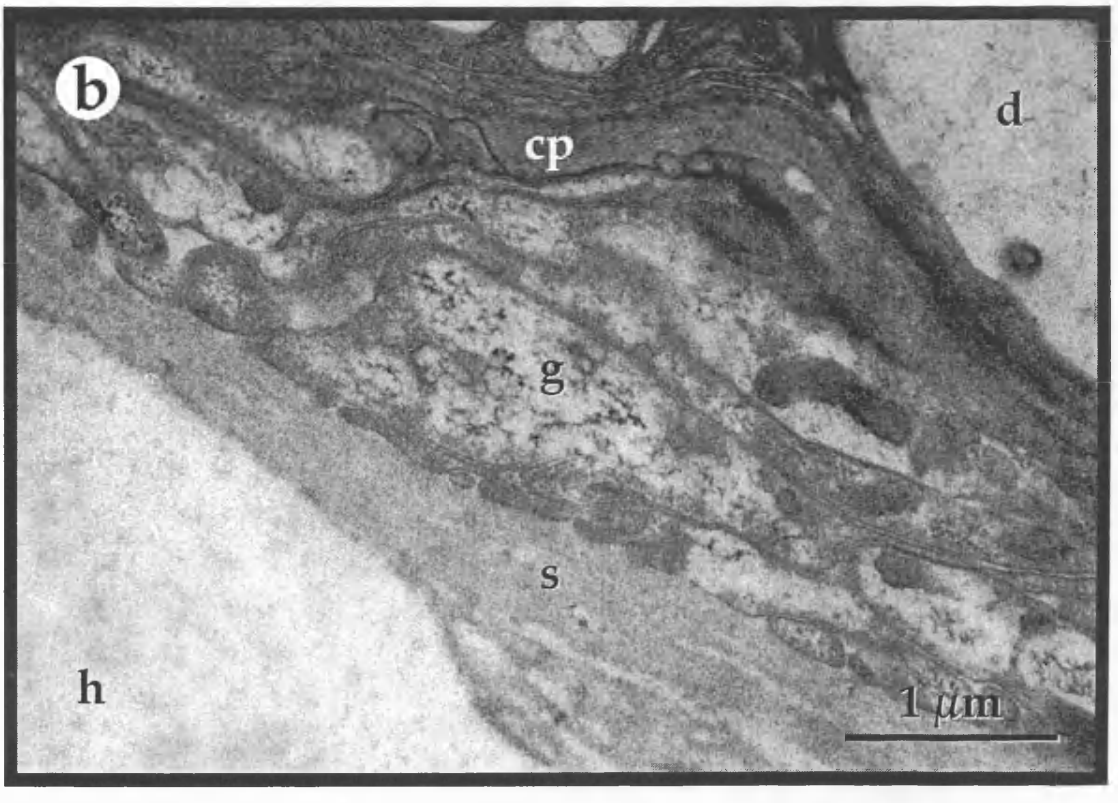
b
cp
d
g
s
h
1 μm

Figure 3.9

The cross-sectional area of the dorsal attachment increases from 1500 μm^2 at the point of its distal attachment to the dorsal epidermis to 4000 μm^2 at the level at which it joins the sensory cell body region of the organ. The cross-sectional area of Acid Fuchsin staining material comprises 5% of the total cross-sectional area at its distal attachment and 23% at the level of attachment to the organ. Error bars = estimated measurement error (10 repeats from each section).

Histogram showing the total cross-sectional area and quantity of Acid Fuchsin-staining component comprising the mtFCO dorsal attachment

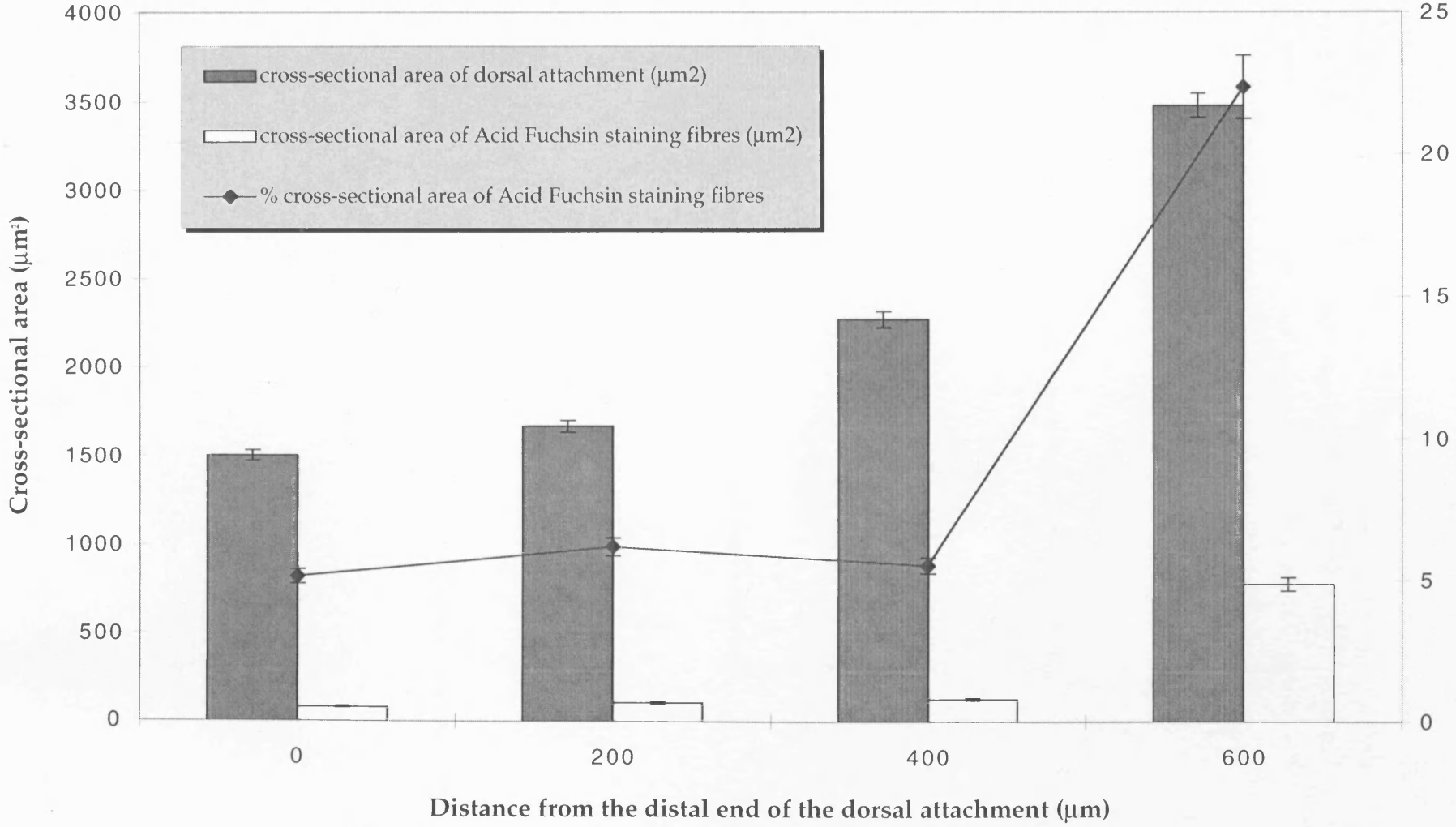

Figure 3.10a, b

The cross-sectional profile of the ventral attachment differs along its length. Figures 3.10a and 3.10b show Toluidine Blue-stained semi-thin (1 μm) sections taken at different proximo-distal levels along the attachment. Sections levels are indicated on the inset diagram (opposite).

a

Dorsally, close to its attachment to the mtFCO, the ligament has a roughly circular cross-section. Nuclei of the ligament cells can be seen (n). Extracellular fibres (F) are located both around the periphery and also within the ligament.

b

At the level where the attachment inserts onto the apodeme of the flexor-tibiae muscle it becomes elongated in transverse section, the long axis being parallel to the apodeme.

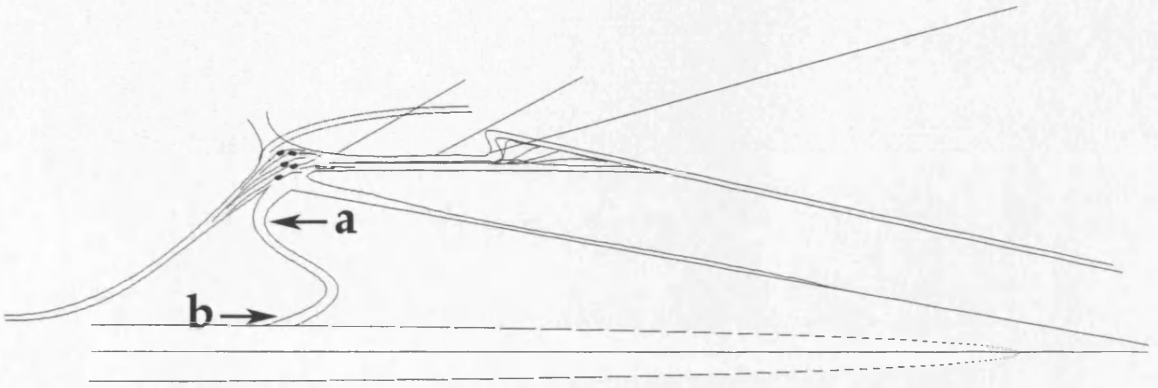

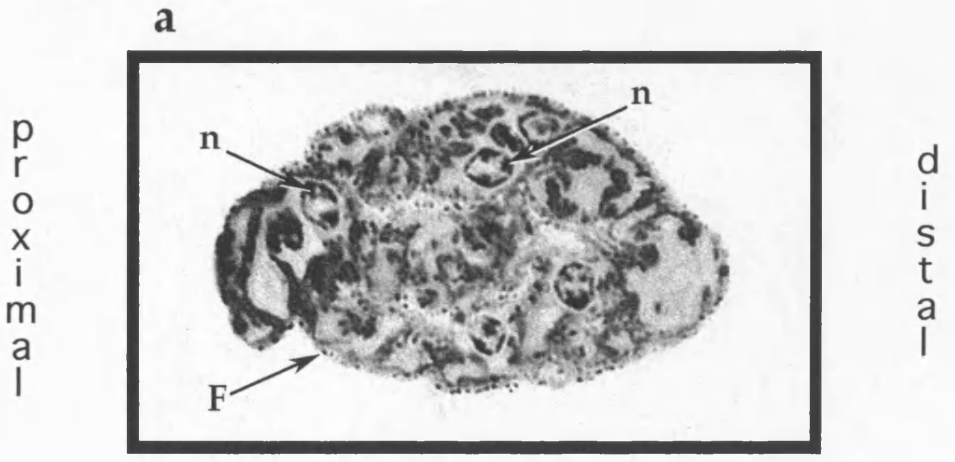

50 μm

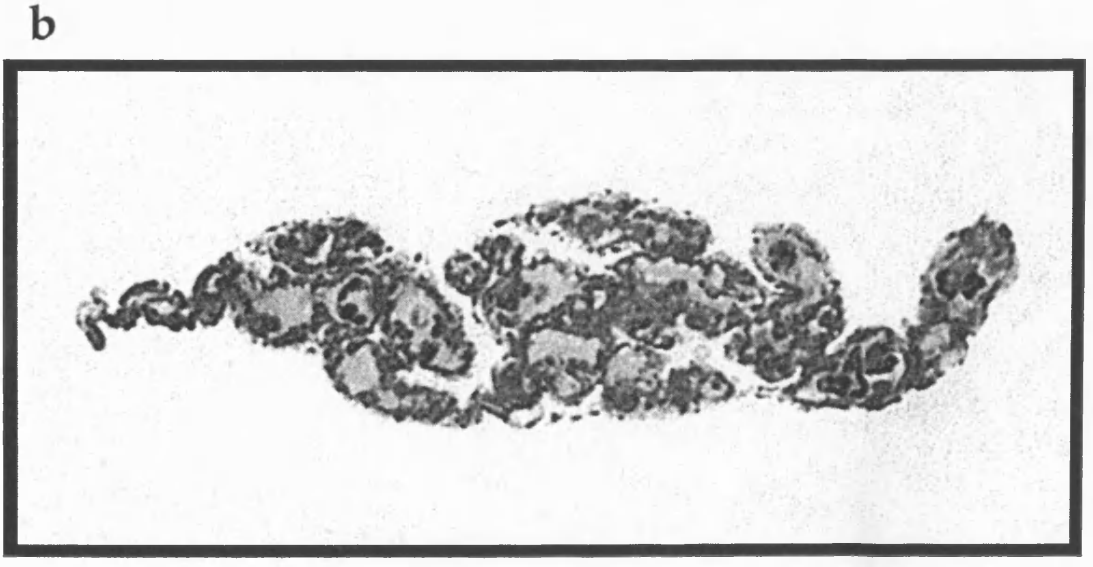

Figure 3.11

This electron micrograph shows that the ligament cells (l) forming the ventral attachment are located in bundles (b) surrounded by thick extracellular matrix (m) which has a granular appearance resulting from fibrillar material being sectioned transversely. The whole ventral attachment is bounded by an extracellular sheath (s). Extracellular fibres (F) are located around the periphery of the bundles and within the extracellular sheath. In this preparation, that has been stained with OsO_4, uranyl acetate and phosphotungstic acid, these fibres stain black. n = ligament cell nucleus

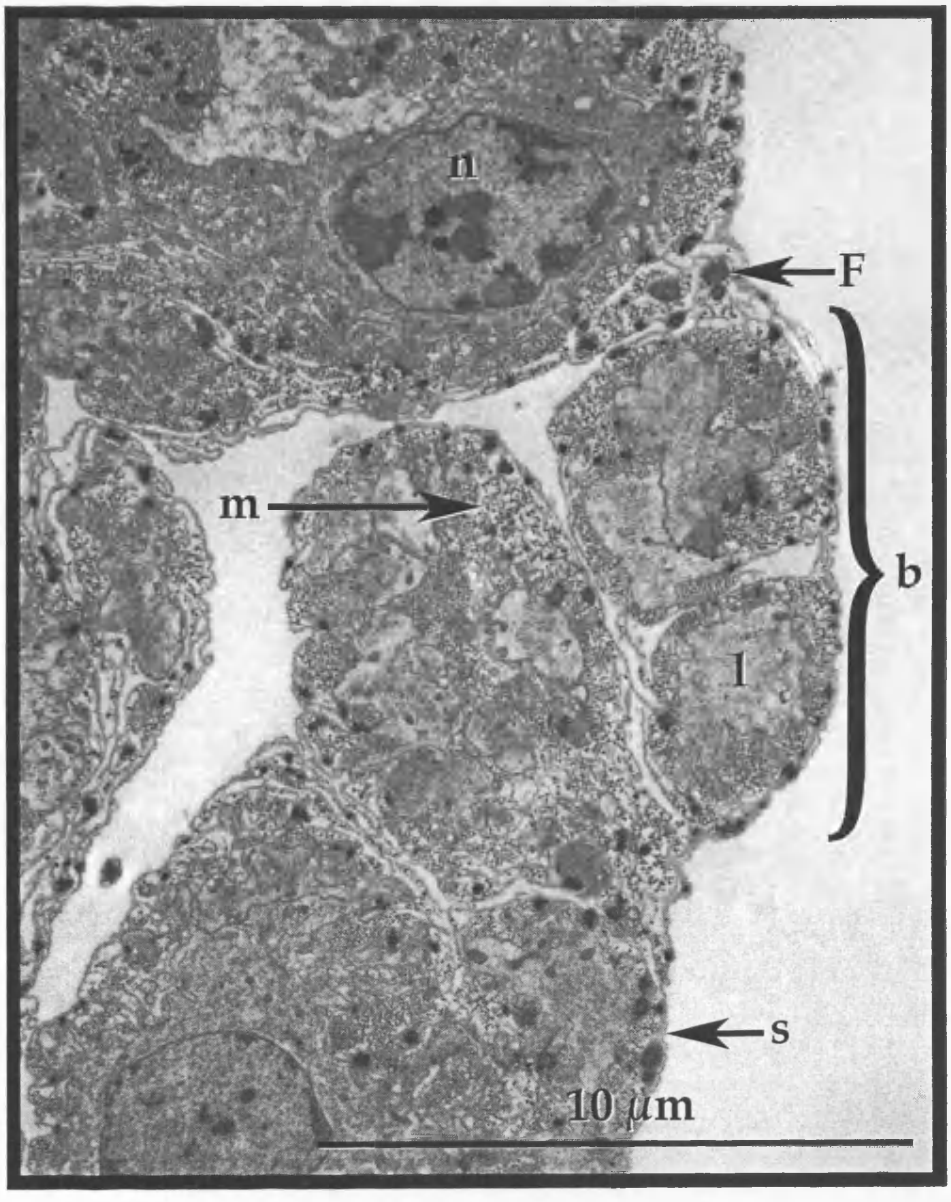
n
F
m
b
l
s
10 μm

Figures 3.12a, b

a

Each bundle (b) within the ventral attachment consists of up to four ligament cells (l), those within the same bundle being closely apposed to one another. The granular appearance of the extracellular material is due to many discrete fibrils (f). F = extracellular fibre

b

The ventral ligament cells (l) are packed with microtubules. Much smaller microtubule-filled processes (p) are orientated parallel to the ligament cells and are assumed to be finger-like protrusions arising from them. The ligament cells are surrounded by extracellular matrix (m).
f = extracellular fibrils

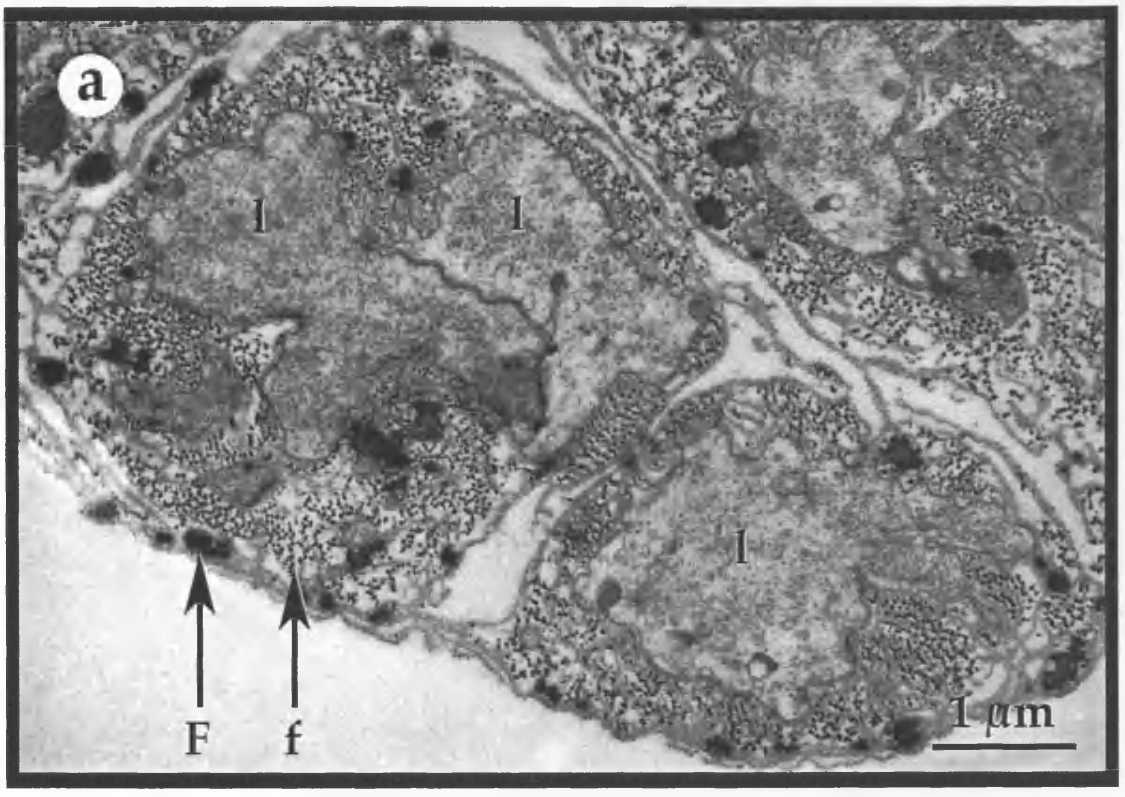
a
l
l
l
F
f
1 µm

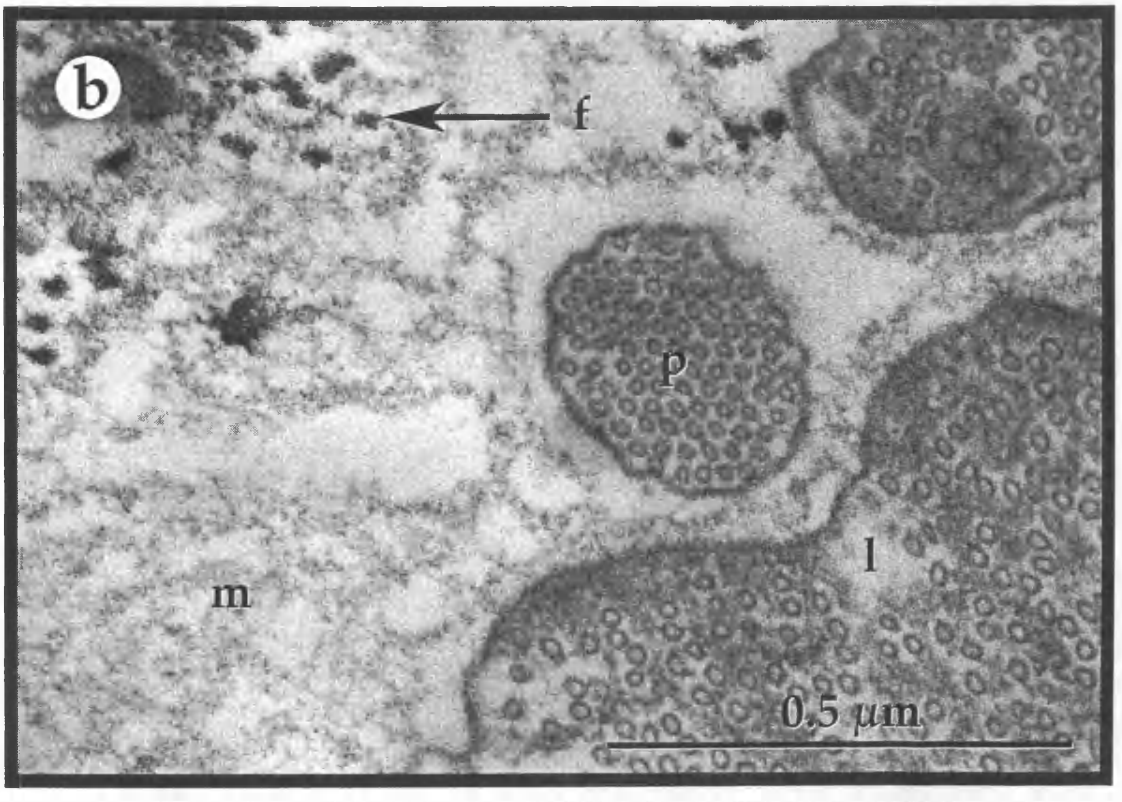
b
f
p
l
m
0.5 µm

Figure 3.13a-c

a, b

The cross-sectional profiles of the extracellular fibrils within the ventral attachment depend upon their locations. Those located adjacent to the ligament cells have a simple profile in cross-section (**a**), whereas those located towards the periphery of a ligament cell bundle have a star-like appearance (**b**). The extracellular matrix in the vicinity of the fibrils is often granular in appearance (g). h = haemolymph space

c

The extracellular fibrils with a simple profile (arrows) are packed more densely than those with a star-like appearance (arrow heads). Especially high densities of fibrils are found associated with the ligament cells where they ramify within the extracellular matrix (m). h = haemolymph space

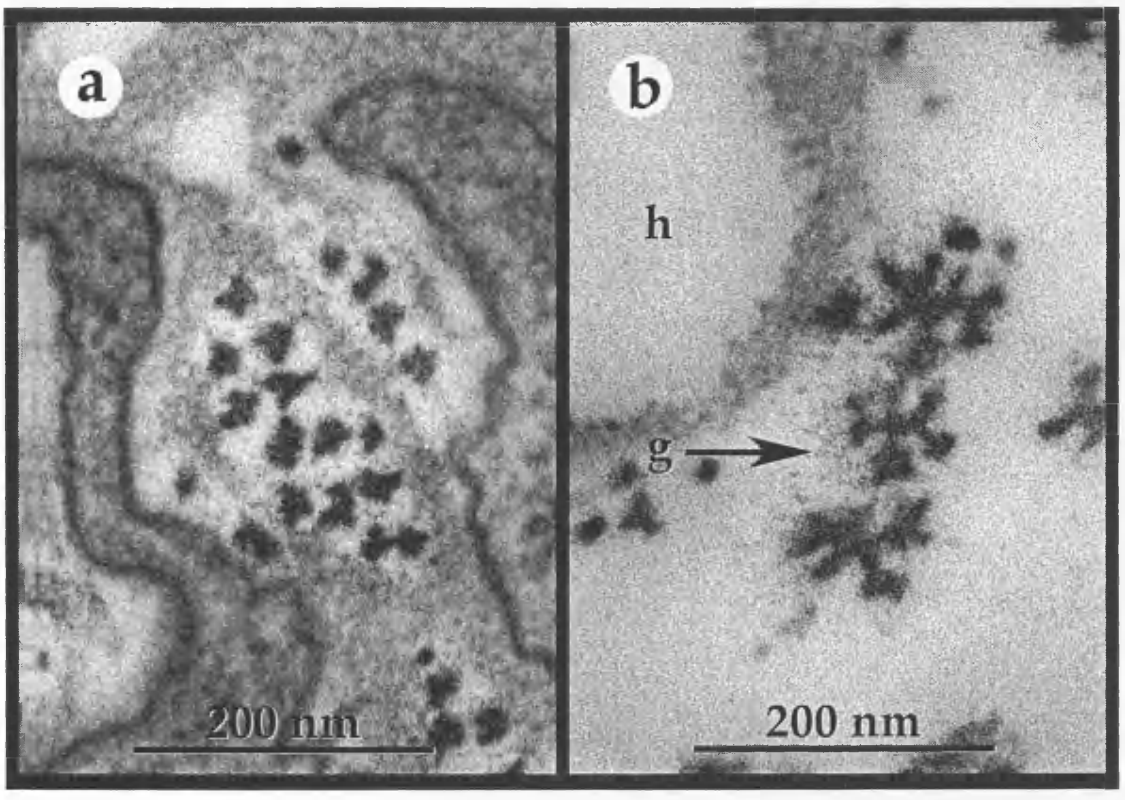
a
200 nm
b
h
g
200 nm

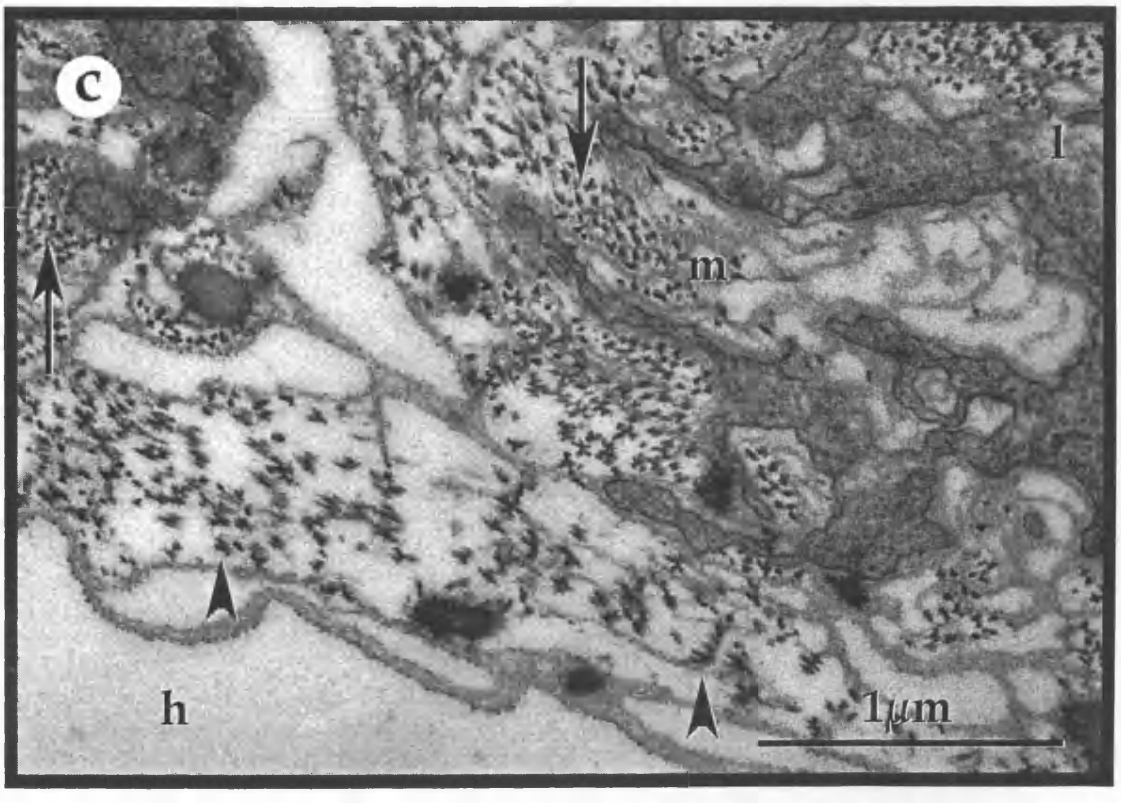
c
l
m
h
1μm

Figure 3.14a, b

a

The extracellular fibrils (f) lie parallel to the long axis of the ventral attachment. There is some evidence of banding (b) when viewed in longitudinal section. m = extracellular matrix; h = haemolymph space

b

When viewed at higher magnifications each band (black arrow) can be seen to be comprised of two sub-bands (white arrows). The period of the banding pattern is 16.8 nm.

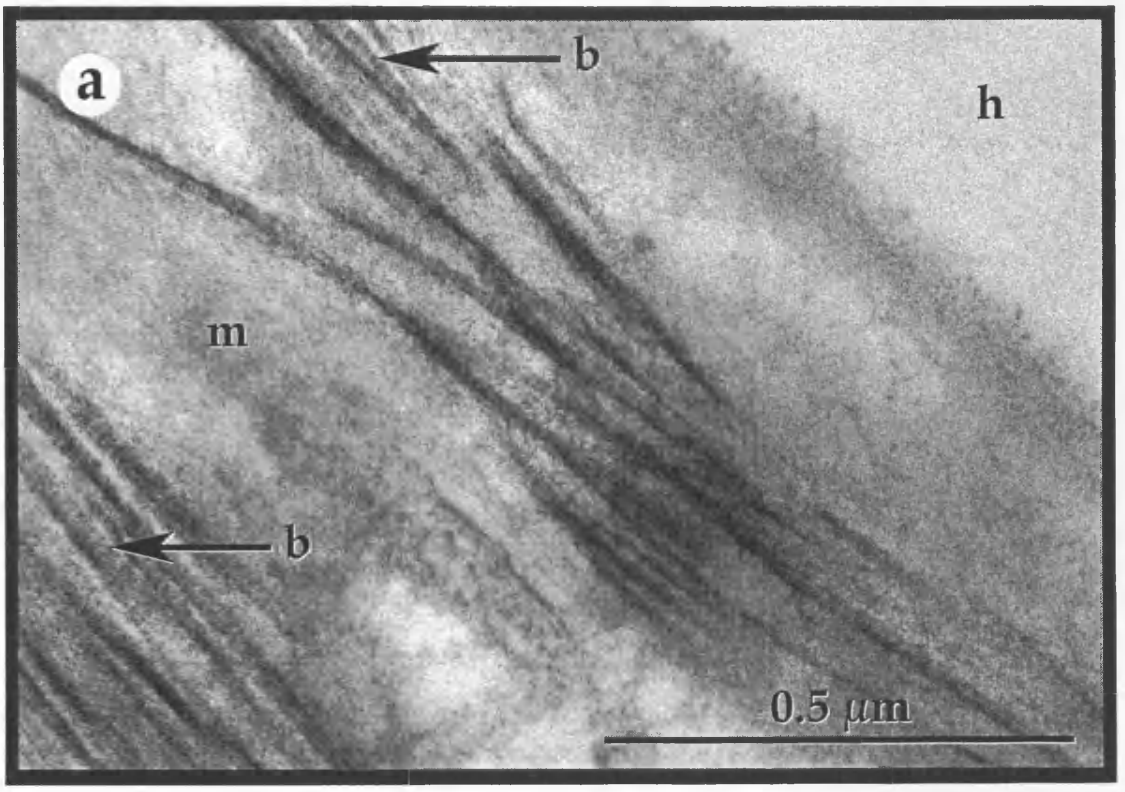
a
b
h
m
b
0.5 μm

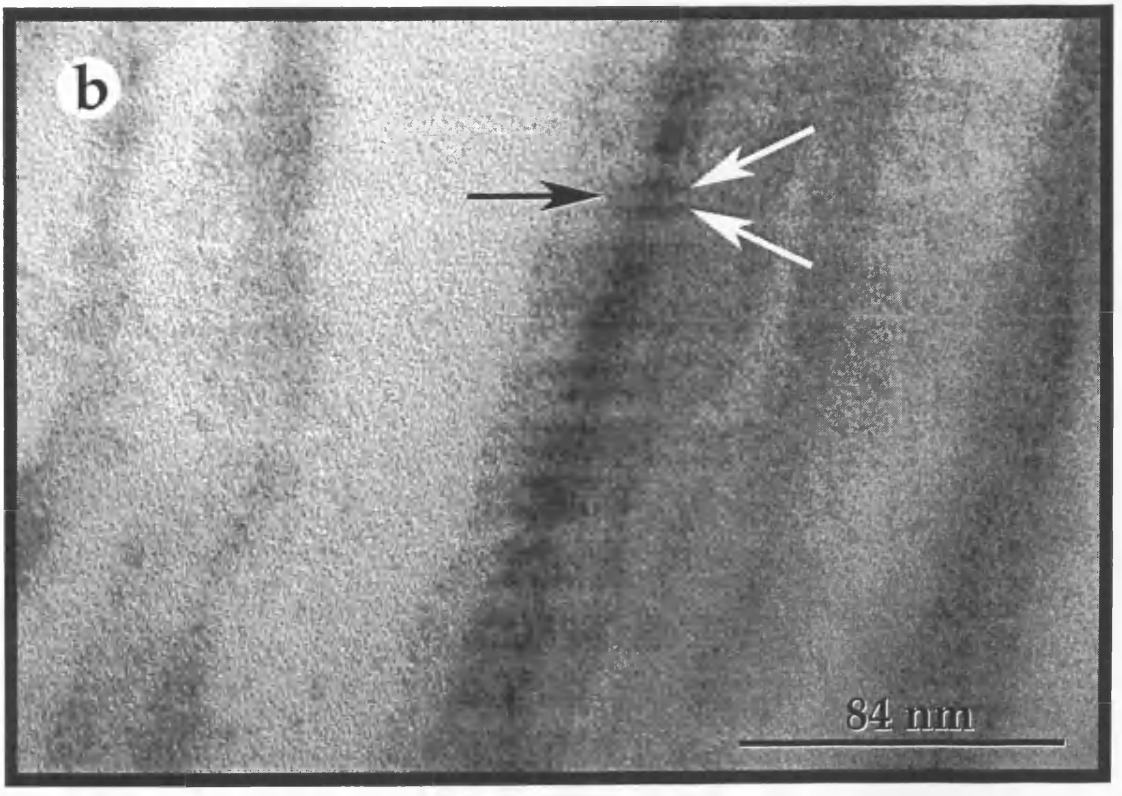
b
84 nm

Figure 3.15

Adjacent bundles within the ventral attachment ligament are associated via the extracellular matrix. Where several ventral attachment bundles are apposed to one another, the extracellular matrix can be seen to consist of islands of electron-lucent material surrounded by denser matrix containing fibrils (arrow heads). l = ligament cell; ecs = extracellular space

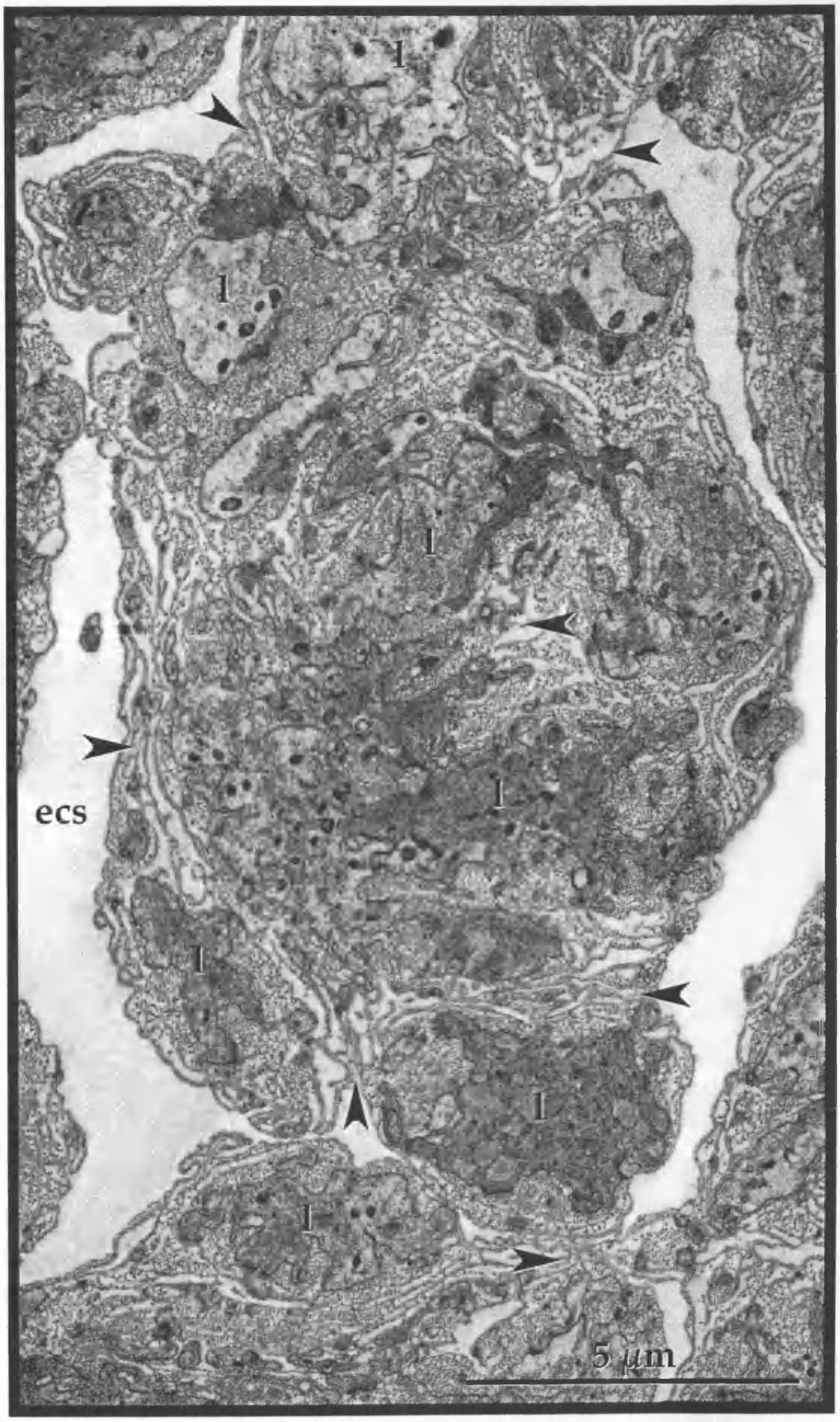
l
l
l
l
l
l
l
ecs
5 µm

Figure 3.16a, b

a

This electron micrograph shows a transverse section of the ventral attachment at a level close to the mtFCO. At this level the ligamentous cells (l) have approximately circular profiles and are surrounded by extracellular matrix (m) which contains numerous extracellular fibrils (f). h = haemolymph space

b

Close to the level where the ventral attachment inserts onto the apodeme of the flexor-tibiae muscle, the ligament cells (l) have an irregular profile. The extracellular matrix (m) appears especially thick between the ligament cell protrusions.

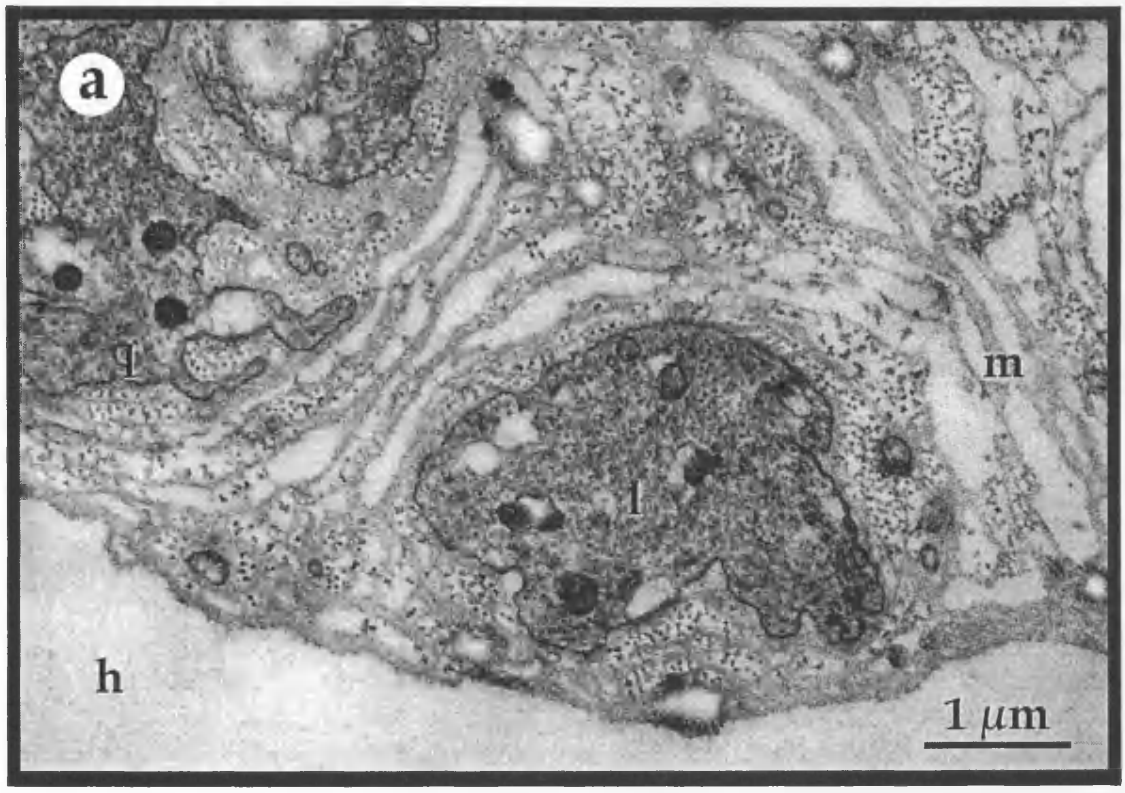
a
q
m
l
h
1 μm

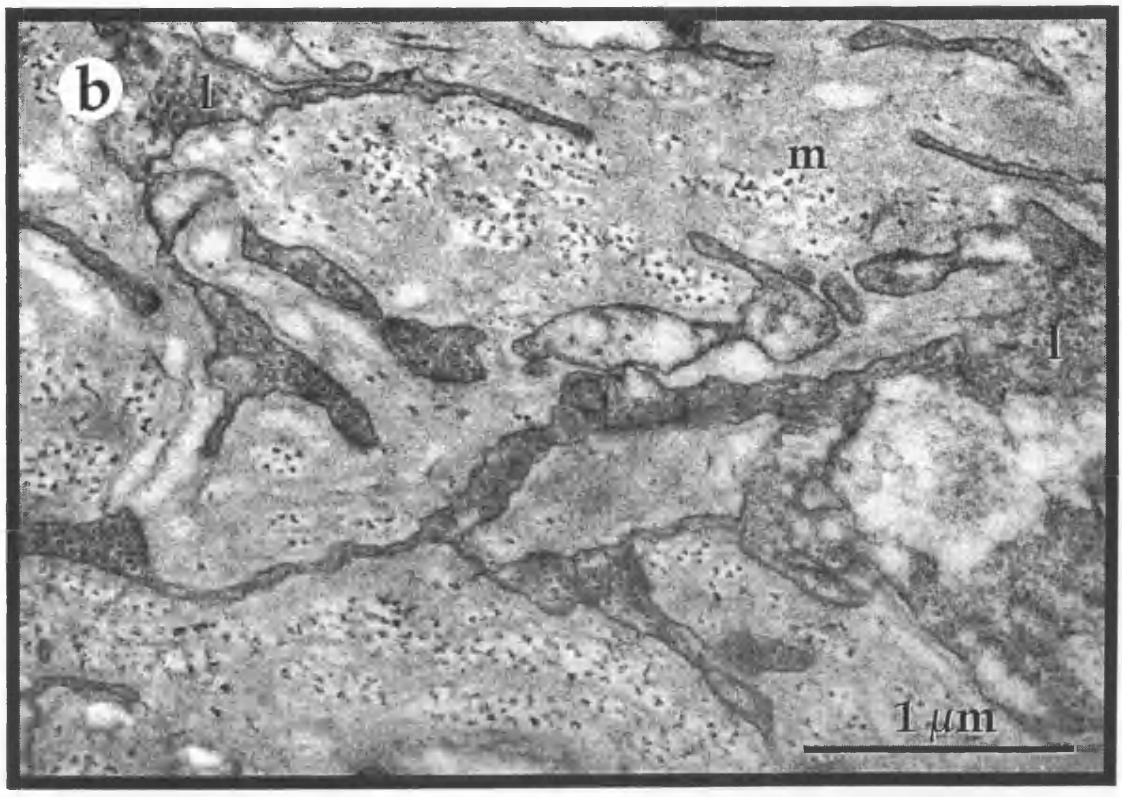
b
l
m
l
1 μm

Figure 3.17a-f

Series of increasingly proximal cross-sections of the mtFCO apodeme complex loop-forming region. These 1 μm sections were stained with Acid Fuchsin which stains the extracellular fibres (F) intensely.

a

The ventral ligament is composed of anatomically distinct units consisting of attachment cells surrounded by extracellular fibres. It arises from the ventral side of the cuticular rod (r) as a bundle of approximately 10 attachment units (v) and associated extracellular fibres (F).

b-d

Proximally the ventral ligament bundle increases in size due to the recruitment of addition ventral ligament units arising from the side of the cuticular rod. A single loop-crossing fibre is followed in this series (arrows).

e-f

The individual units of which the ventral ligament is comprised increase in cross-sectional area proximally. The cross-sectional area of the cuticular rod declines (compare **a** and **f**).

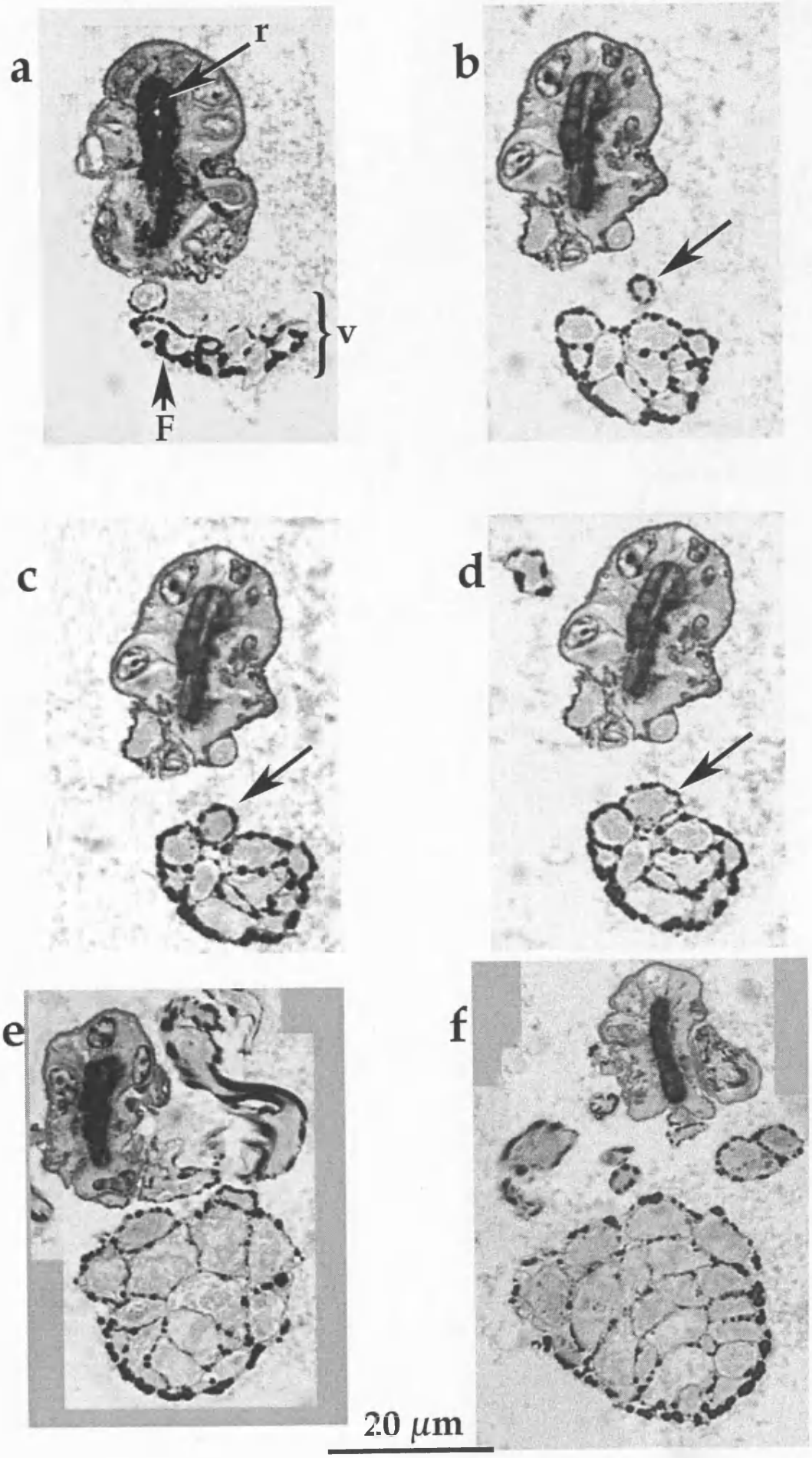
a
r
v
F
b
c
d
e
f
20 μm

Figure 3.18a-c

The loop-crossing fibres which arise from the side of the cuticular rod to augment the ventral ligament (see Figs 3.17b-d) each consist of one or two attachment cells (at) within an extracellular matrix sheath (s) associated with thick extracellular fibres (F).

a

This electron micrograph shows a transverse section through a loop-crossing fibre consisting of one attachment cell (at) surrounded almost entirely by extracellular fibre-material (F).

b

This oblique section through a loop-crossing fibre shows one attachment cell (at) and associated extracellular fibres (F). The appearance of the extracellular fibres differs between the micrographs due to the use of different staining techniques. The sections shown in Figures 3.18a, c were stained with uranyl acetate and lead citrate, whereas the section shown in Figure 3.18b was also stained with hot phosphotungstic acid.

c

This micrograph shows a loop-crossing fibre consisting of two attachment cells (at) bounded by an extracellular sheath (s) in which extracellular fibres (F) are embedded. (The latter stain with Acid Fuchsin at the light microscope level).

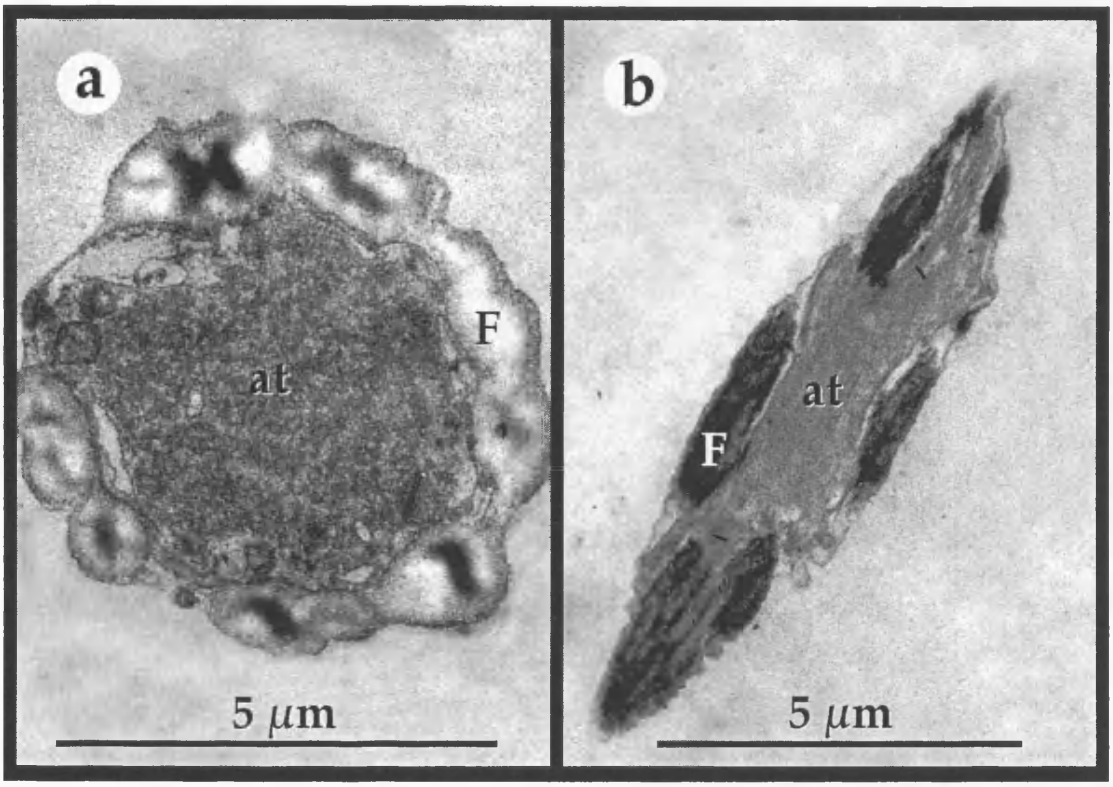
a
F
at
5 μm
b
at
F
5 μm

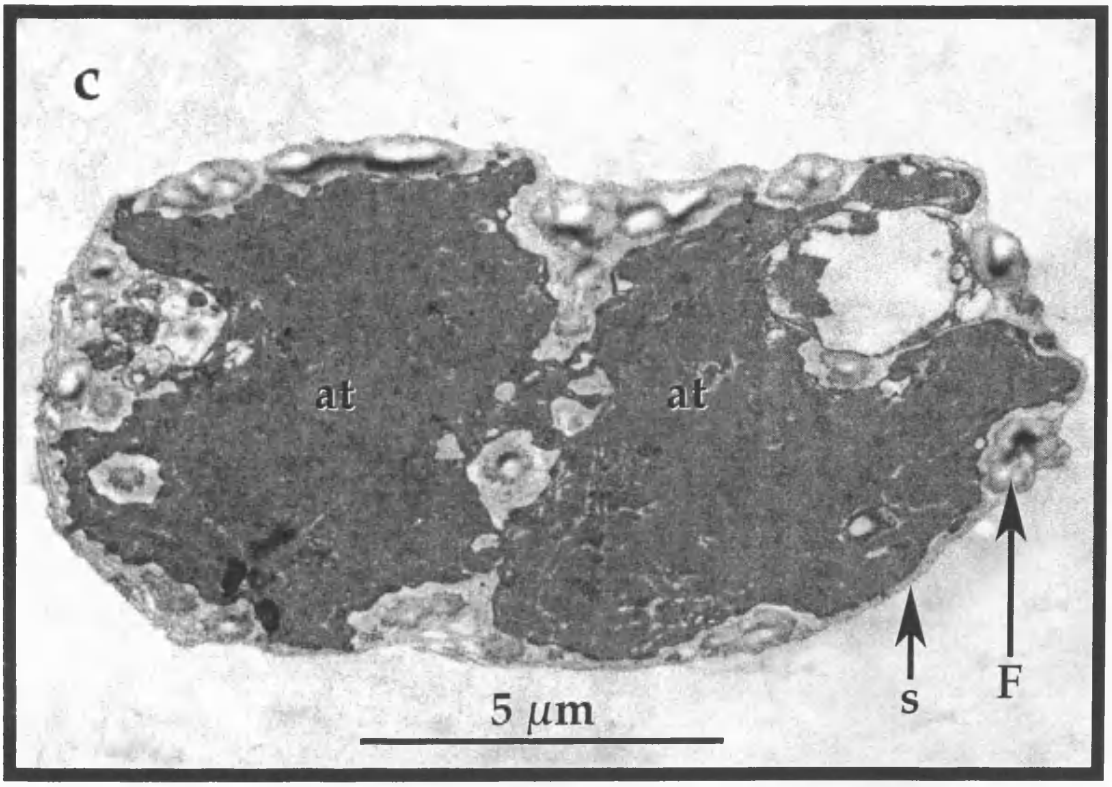
c
at
at
s
F
5 μm

Figure 3.19

This light micrograph of a section stained with Acid Fuchsin shows the organisation of the dorsal (d) and ventral (v) ligaments at a level just proximal to the end of the cuticular rod. At this level the dorsal ligament consists of separate bundles of attachment cells. At more proximal levels they fuse to form a single ligament. Some of the attachment cells comprising the dorsal ligament are associated into clusters (arrow).

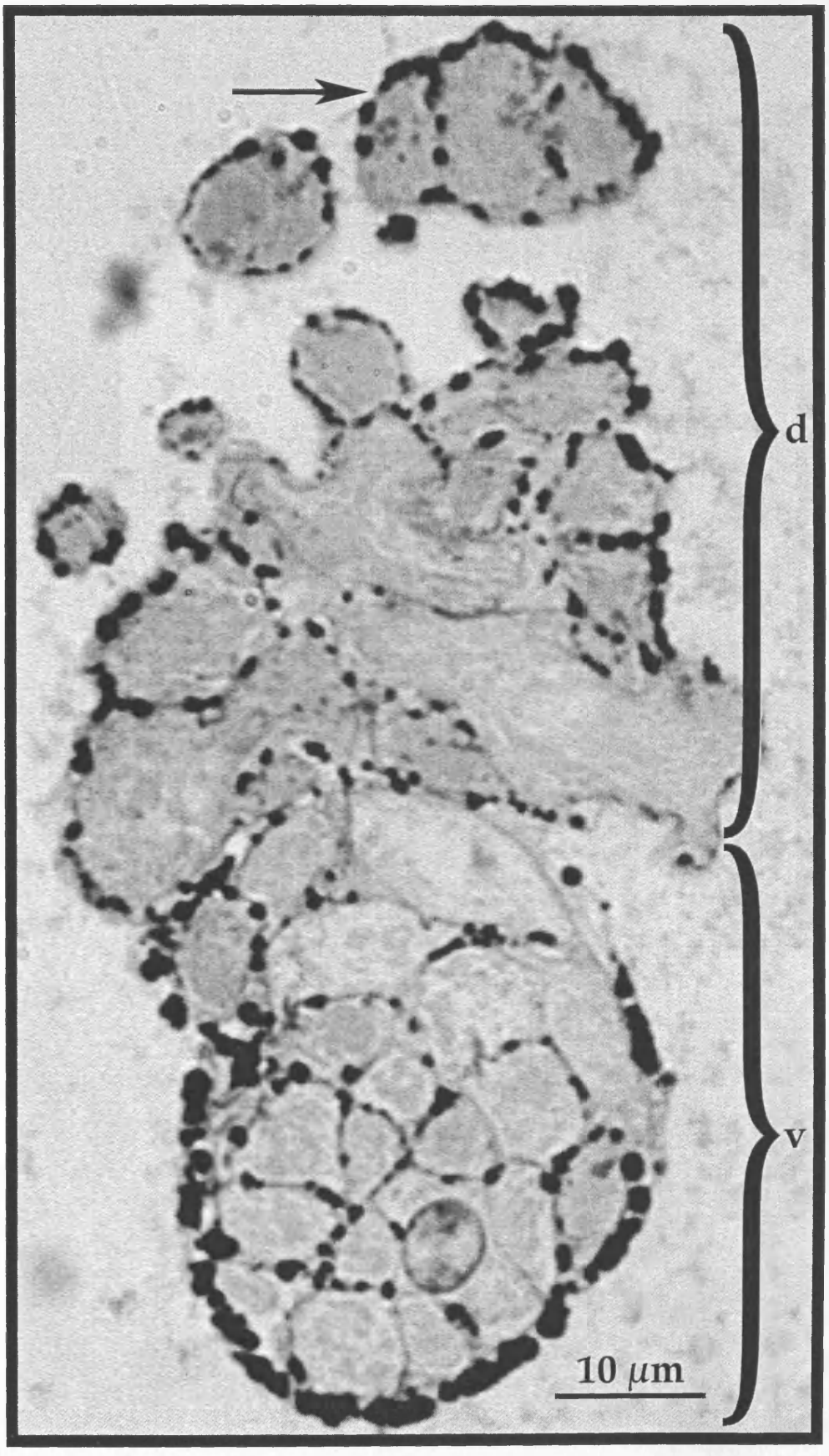
d
v
10 μm

Figure 3.20a, b

a

This electron micrograph of a transverse section through the ventral ligament of the apodeme complex shows large extracellular Acid Fuchsin-staining fibres (F) associated with the attachment cells (at). Close to the point where the attachment cells joint onto the cuticular rod (r), some of the Acid Fuchsin-staining fibres are surrounded by much smaller fibrils (white arrows).

b

This higher power electon micrograph (taken of the region indicated in **a**) shows the appearance of the ventral ligament close to the origin of attachment cells on the cuticular rod (r). Fine fibrils (f) are abundant in the extracellular matrix (m).

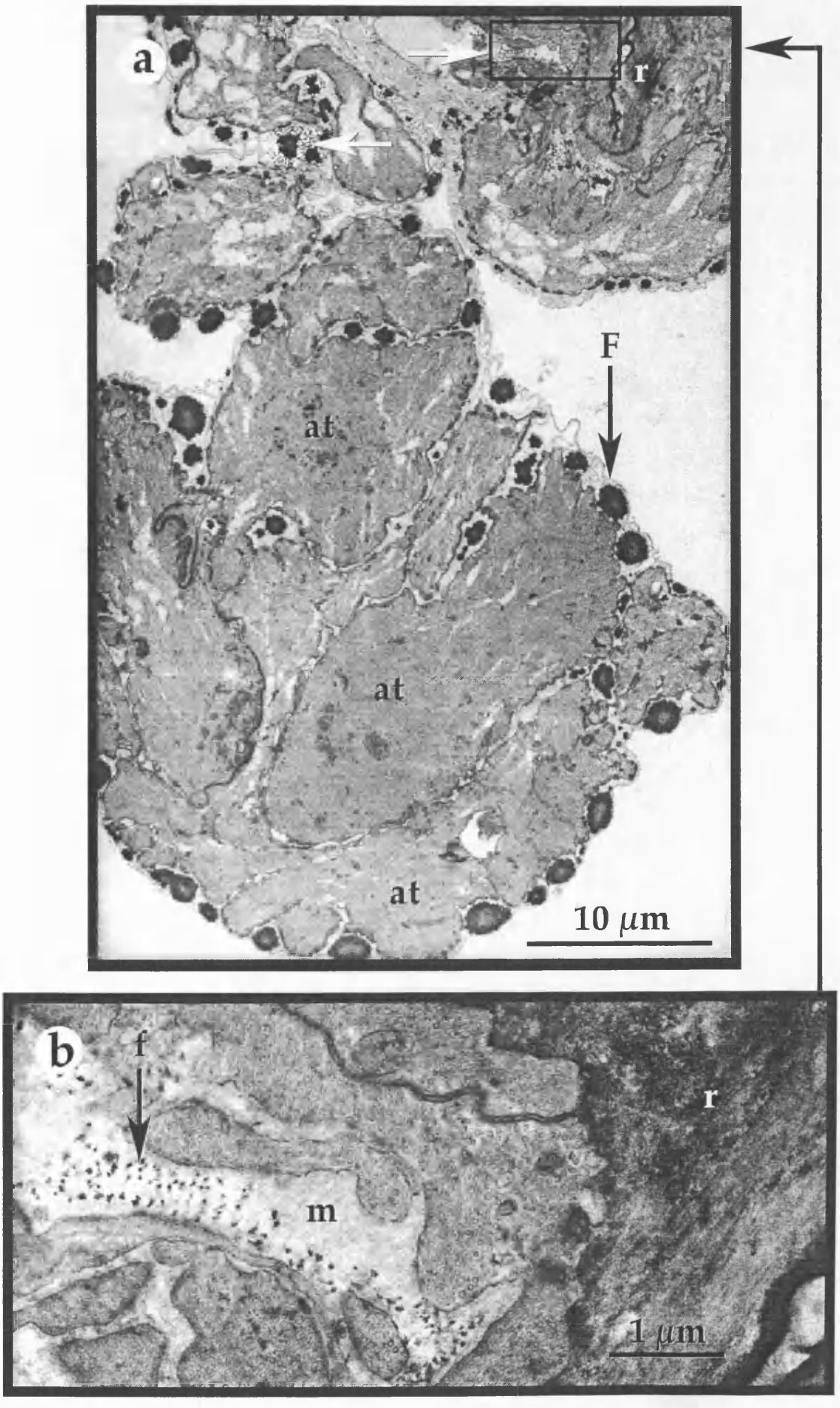
a
r
F
at
at
at
10 μm
b
f
r
m
1 μm

Figure 3.21

This electron micrograph is of a section taken close to the distal end of the dorsal ligament where it is connected to the cuticular rod. Small extracellular fibrils (arrowheads and inset) are present at the distal-most ends of the dorsal ligament attachment cells (at). As in the case of the ventral ligament, these fibrils are often associated with the large extracellular (Acid Fuchsin-staining) fibres (F).

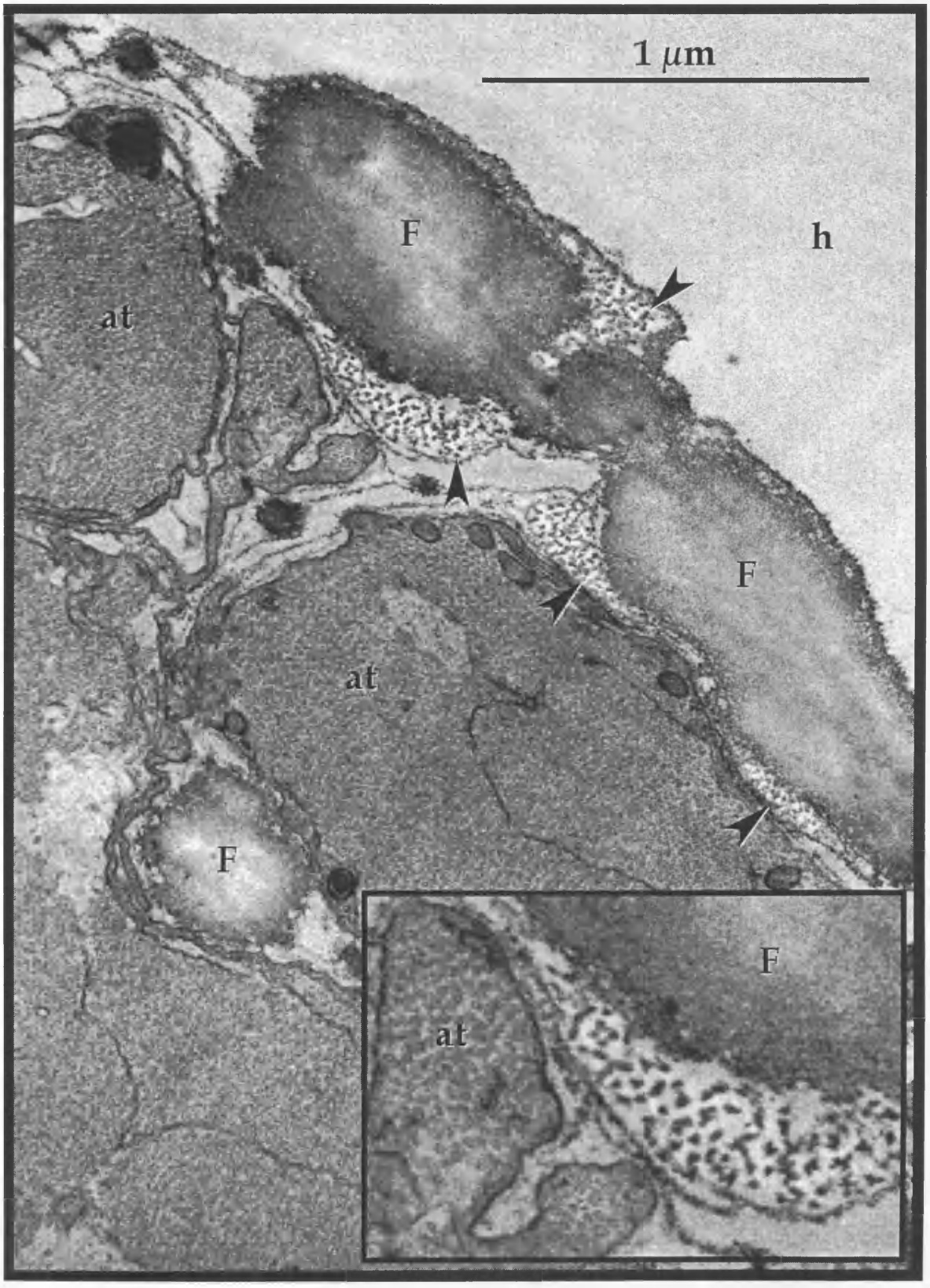
1 μm
F
h
at
F
at
F
F
at

Figure 3.22

The Acid Fuchsin-staining fibres described by Shelton *et al.* (1992) stain darkly with hot phosphotungstic acid (PTA) (Nowel *et al.*, 1995). This electon micrograph of a PTA-stained transverse section shows the fused dorsal and ventral ligaments at a level proximal to the loop-forming region. PTA-staining fibres are found within the ligaments (Fi) and surrounding them in the sheath (Fs). Ventrally the fibres coalesce (Fv) to form a sheet of PTA-staining material.


Dorsal
Fs
Fi
10 μm
Ventral
Fv

Figure 3.23

This micrograph shows a number of PTA-staining fibres (F) within the extracellular matrix (m). Attachment cells (at) are filled with microtubules and connected to each other by prominent desmosome-like junction (d). The preparation was stained with PTA and then post-stained with lead citrate and uranyl acetate to reveal cellular detail.

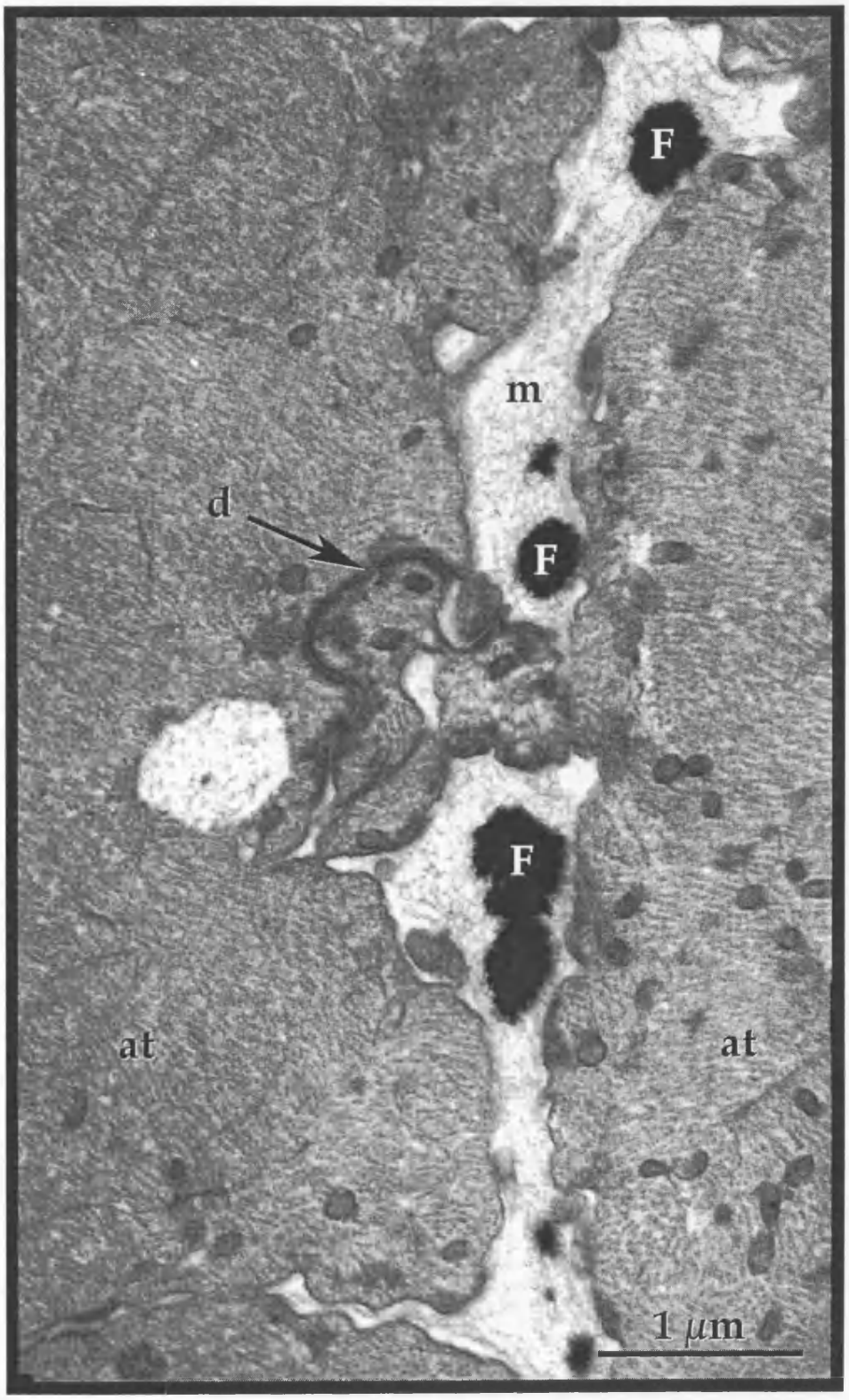
F
m
d
F
F
at
at
1 μm

Figure 3.24a, b

a

Electron micrograph montage showing a transverse section through the apodeme complex ligaments. The section was stained with hot phosphotungstic acid to stain the extracellular fibres (F) and post-stained with lead citrate and uranyl acetate to visualise the attachment cells (at).

b (overleaf)

Outline of individual attachment cells obtained from montages similar to that shown in Figure 3.24a, at three different proximo-distal levels along the ligaments. There were 56 attachment cells at all 3 proximo-distal levels in this preparation. This suggests that within a ligament all attachment cells extend over its whole length. (Note that in this case the cells were numbered separately in each section; individual cells were not traced from section to section).

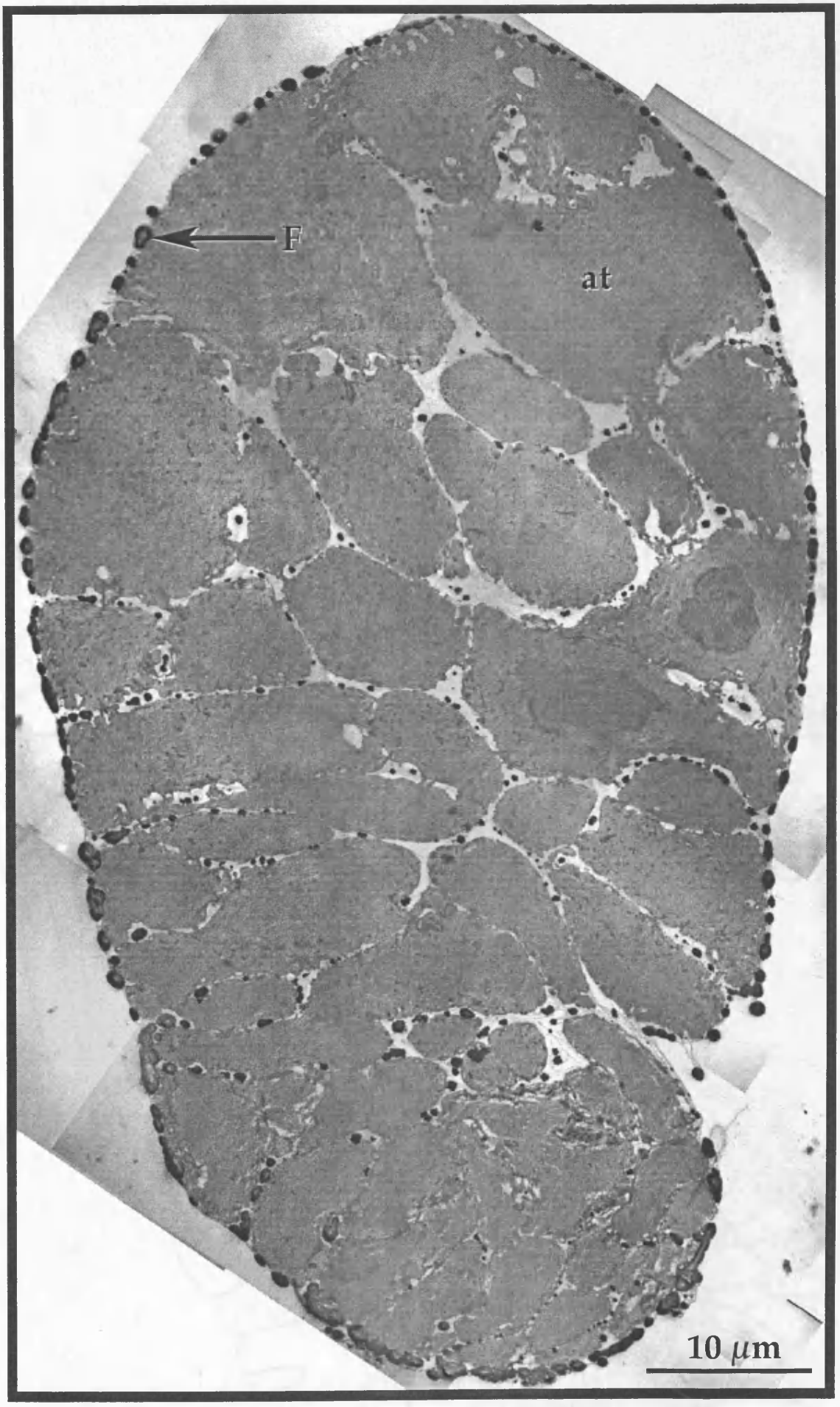
F
at
10 μm

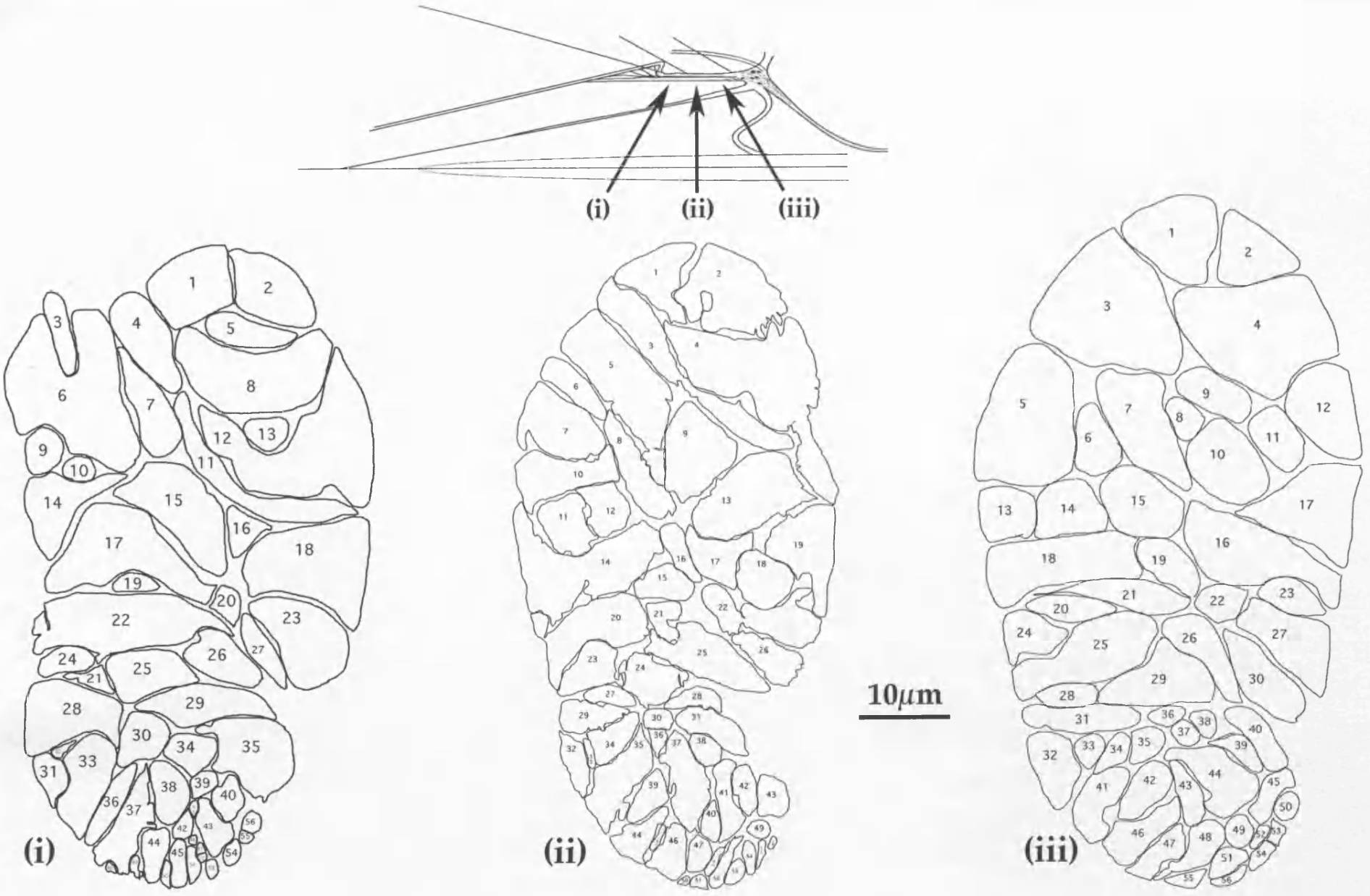
(i)
(ii)
(iii)
10μm

Figure 3.25a, b

a

This electron micrograph shows typical attachment cells (at) of the dorsal ligament. They have a bulky appearance when seen in transverse section and lightly-staining extracellular matrix (m) is found between adjacent cells. The surfaces of the dorsal ligament attachment cells are relatively smooth. F = extracellular (Acid Fuchsin-staining) fibre

b

A micrograph of the ventral ligament shows typical attachment cells (at). They are smaller than those of the dorsal ligament and lightly-staining extracellular matrix (m) is less abundant. The cells are held in closer apposition to one another than in the dorsal ligament. In addition many of the cells have outfolding cellular protrusions at their surfaces (pr). F = extracellular (Acid Fuchsin-staining) fibre

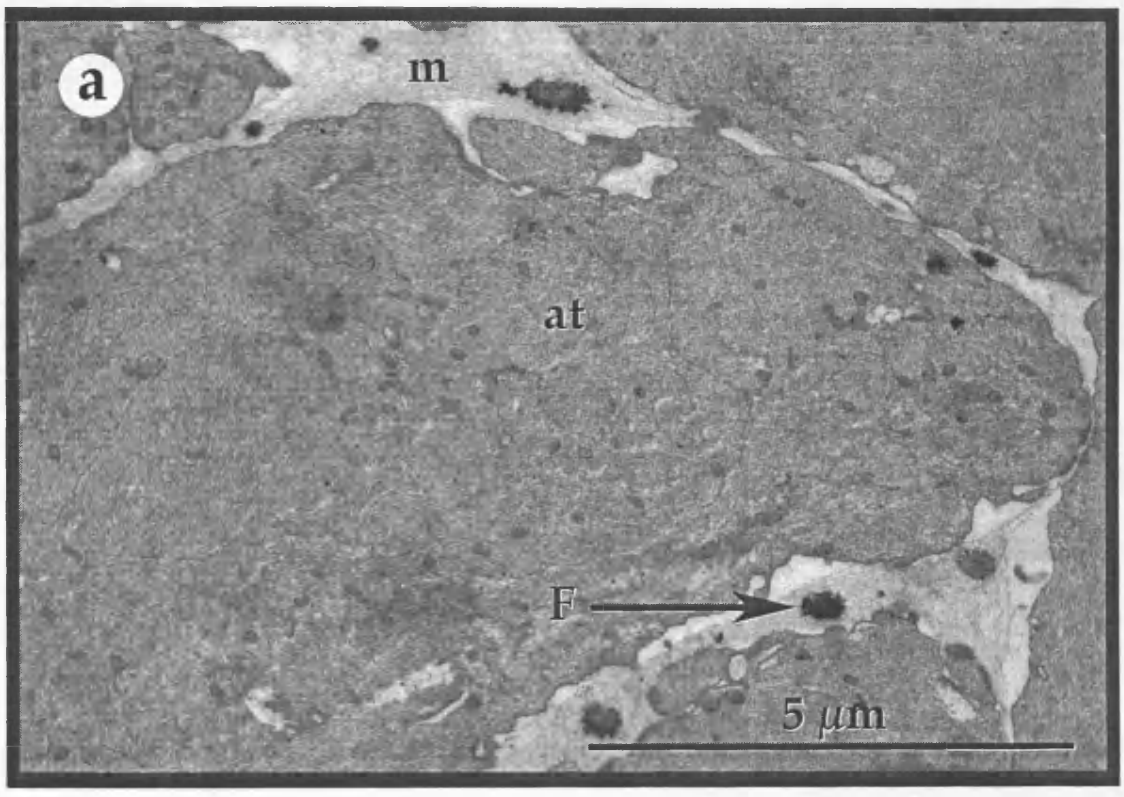
a
m
at
F
5 μm

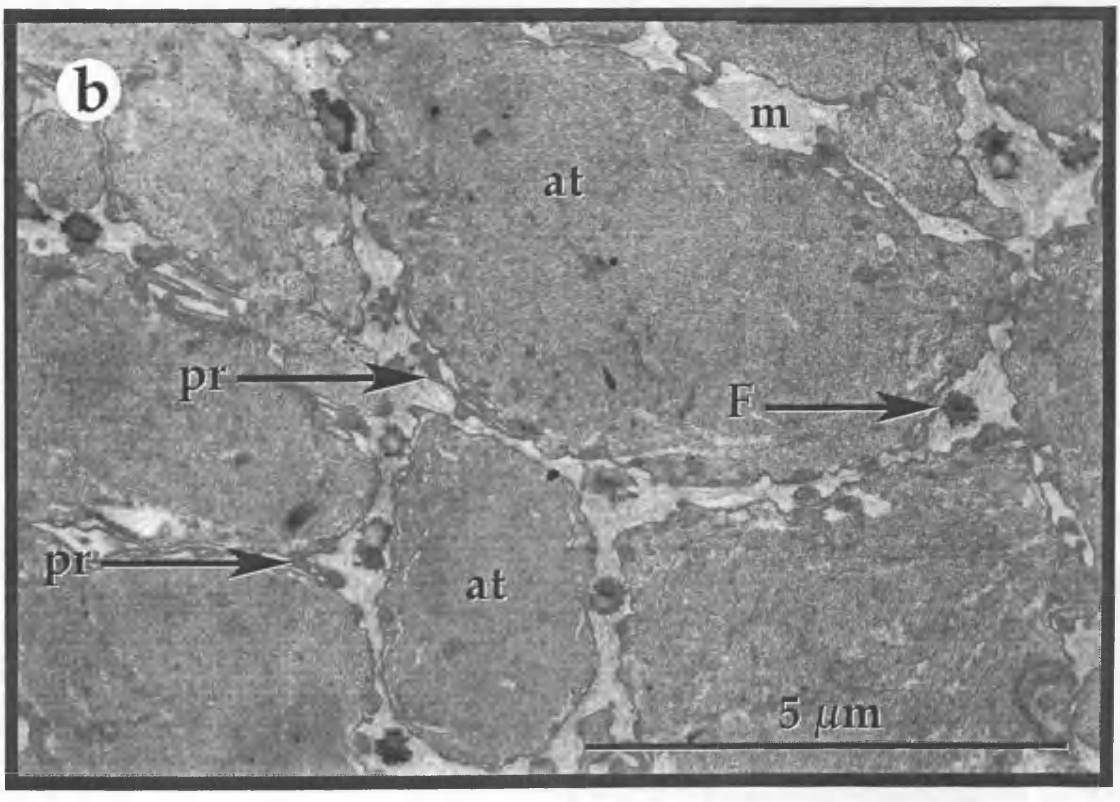
b
m
at
pr
F
pr
at
5 μm

Figure 3.26a, b

a

The larger (Acid Fuchsin-staining) extracellular fibres (F) associated with the ligaments of the mtFCO have an amorphous appearance in preparations stained with lead citrate and uranyl acetate. In transverse section, the fibres (F) are associated with lightly-staining extracellular matrix (m). The extracellular matrix has a granular appearance where it lies adjacent to the fibres.

b

Longitudinal sections of similar material showed the large extracellular fibres (F) have an amorphous constitution along their length, with no evidence of repeat banding. Often but not always, close to the surface of the attachment cells, multiple layers of membrane can be seen (mem).

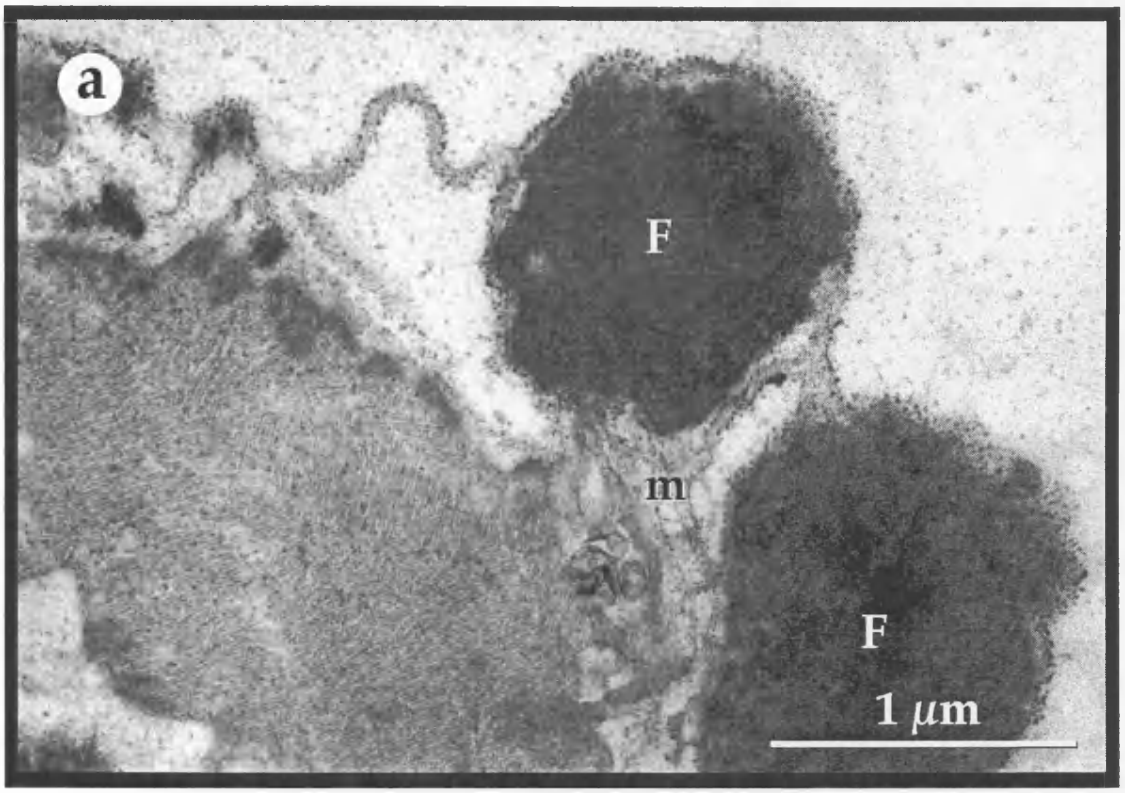
a
F
m
F
1 μm

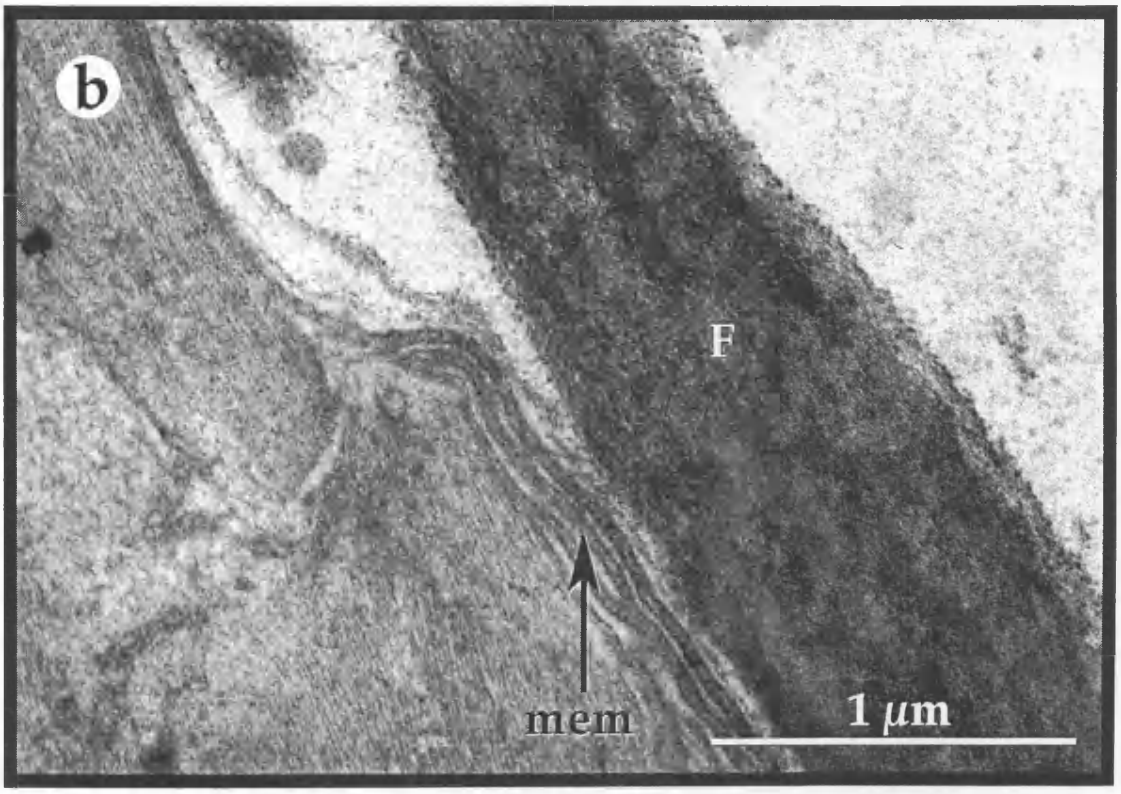
b
F
mem
1 μm

Figure 3.27a, b

a

Acid Fuchsin-staining extracellular fibres (F) are embedded in a lightly-staining extracellular matrix (m) surrounding the attachment cells (at) of the apodeme complex. When viewed in transverse section, the smallest Acid Fuchsin-staining fibres can be seen to be composed of smaller discrete components (pf). Where these discrete components or 'proto-fibres' aggregate, the extracellular matrix (m') appears more electron-dense.

b

Small Acid Fuchsin-staining fibres (Fs) have an irregular profile suggesting that they may be formed by the association of smaller components. Microtubules (mt) within the adjacent attachment cells localise at the cell membrane in the vicinity of the fibre.

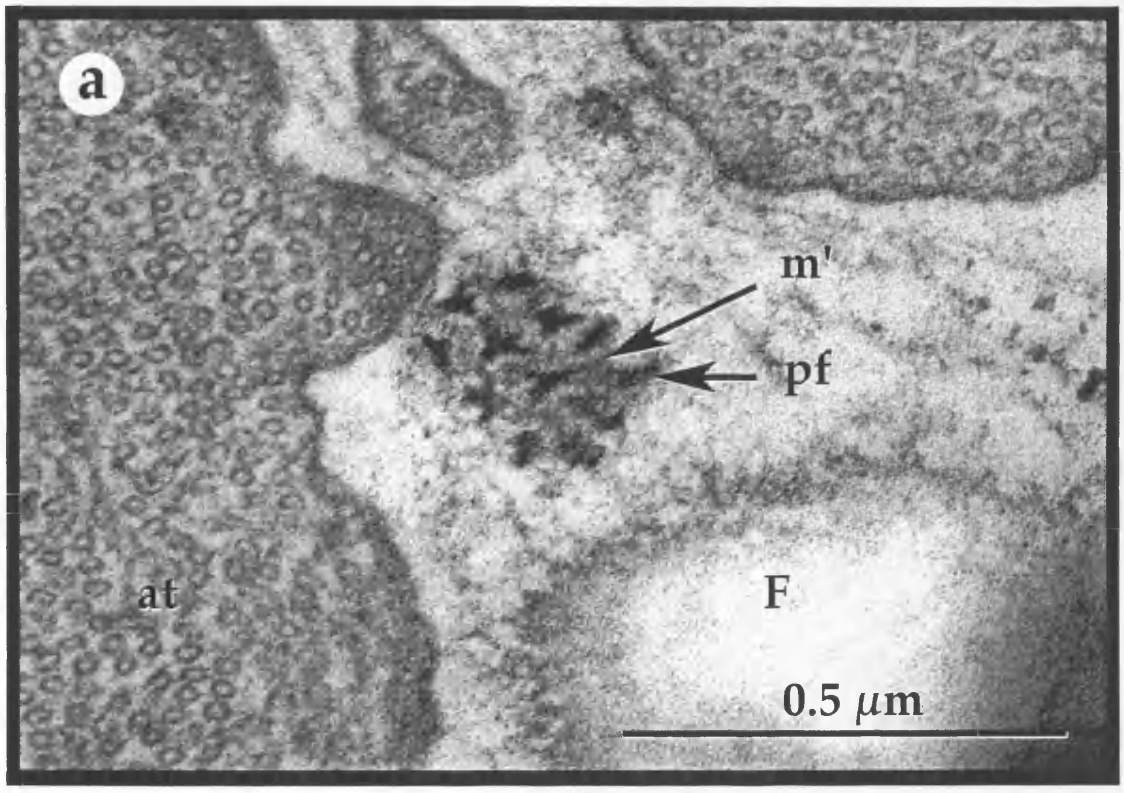
a
m'
pf
at
F
0.5 μm

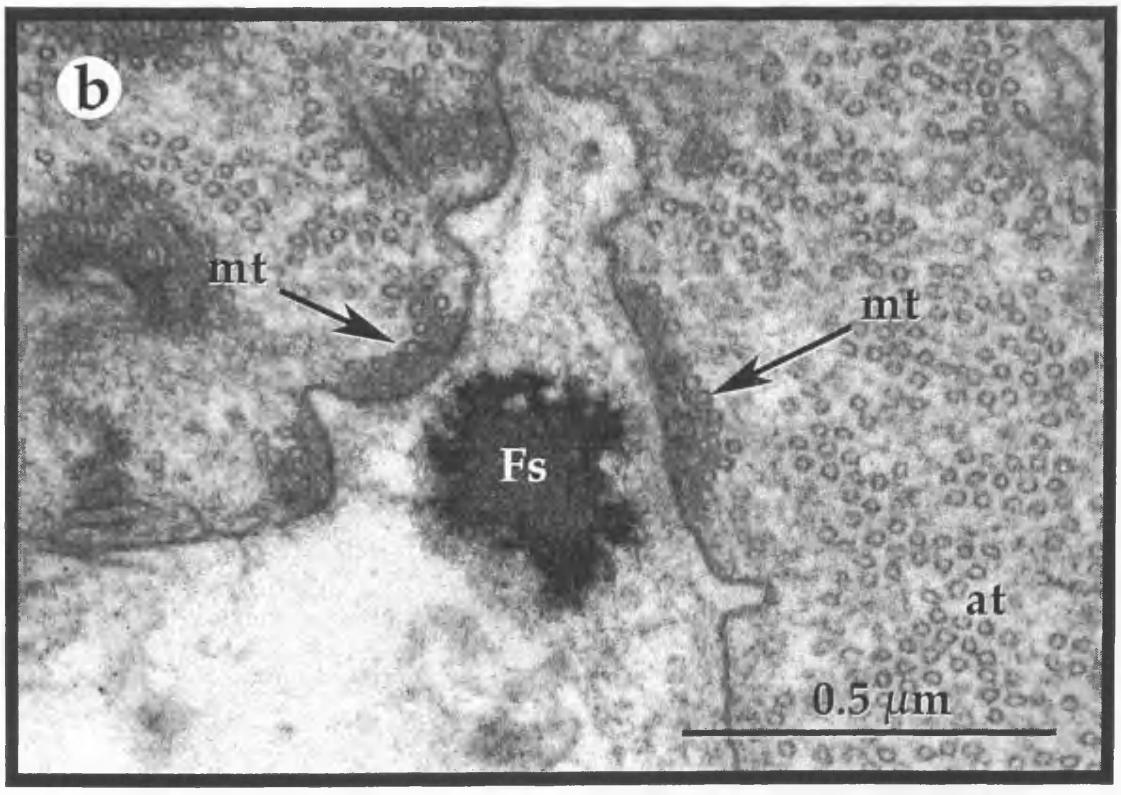
b
mt
mt
Fs
at
0.5 μm

Figure 3.28

Single or multiple intercellular junctions are found where specialised membrane protruberances from adjacent attachment cells (at) appose one another. In this case the junctions (d) are of the septate desmosome variety. Near to these junctions the cytoplasm of the attachment cells often contains an electron-dense intracellular material (mI) between the microtubules (mt). Mitochondria (mtc) are evident in the attachment cells. F = Acid Fuchsin-staining extracellular fibre

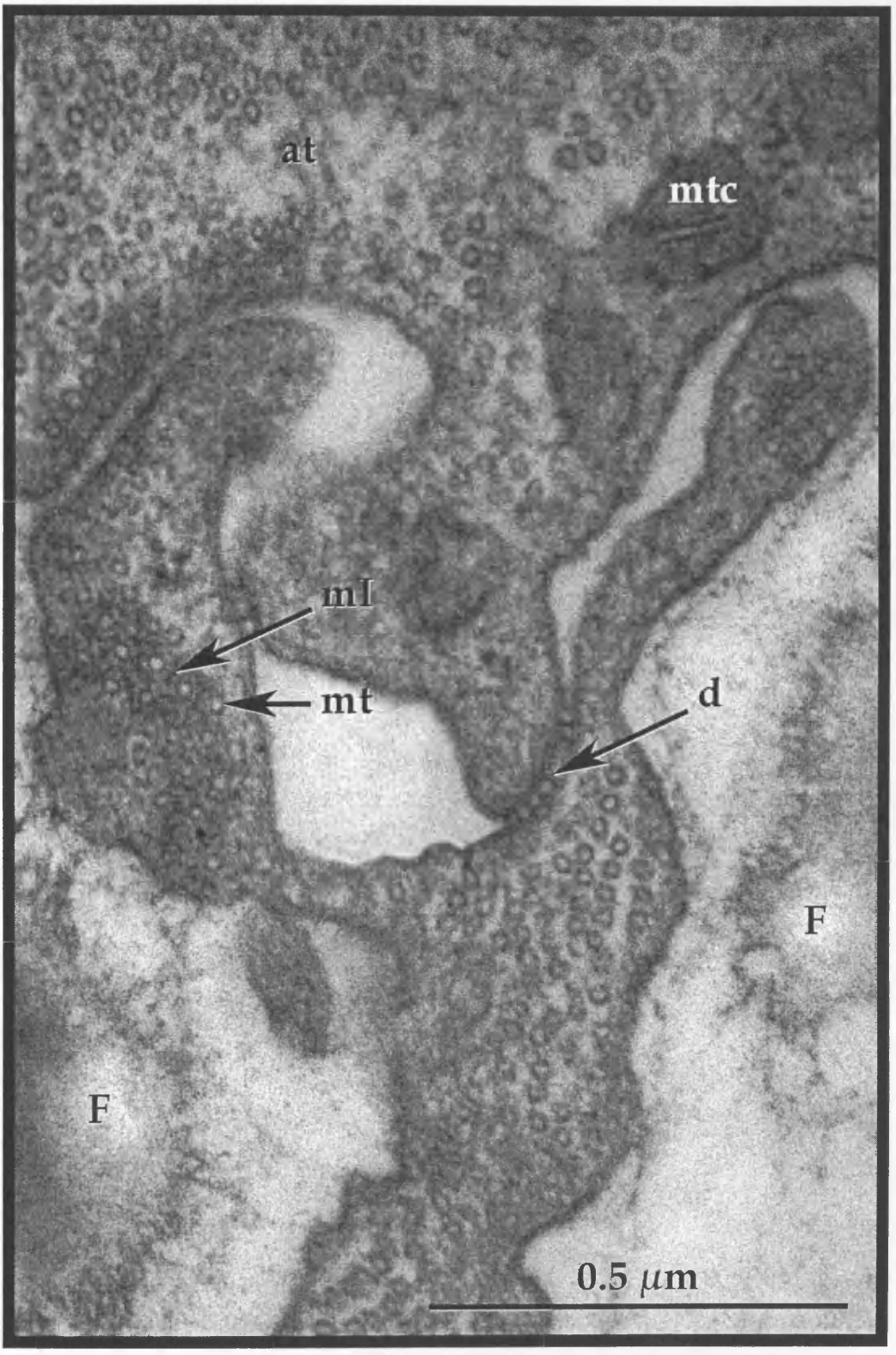
at
mtc
ml
mt
d
F
F
0.5 μm

Figure 3.29

Adjacent attachment cells sometimes form complex interdigitating structures. In this micrograph, a cellular protrusion from one attachment cell (at1) appears to be partially surrounded by a second attachment cell (at2). There are extensive desmosome-like junctions (d) where the two attachment cells are directly apposed to one another. There is a tendency for the microtubules lying adjacent to the cell-to-cell junctions to become aligned in an orderly row along the inside of the cell membranes (arrowheads). Electron-dense intracellular material can also be seen adjacent to the cell junctions.

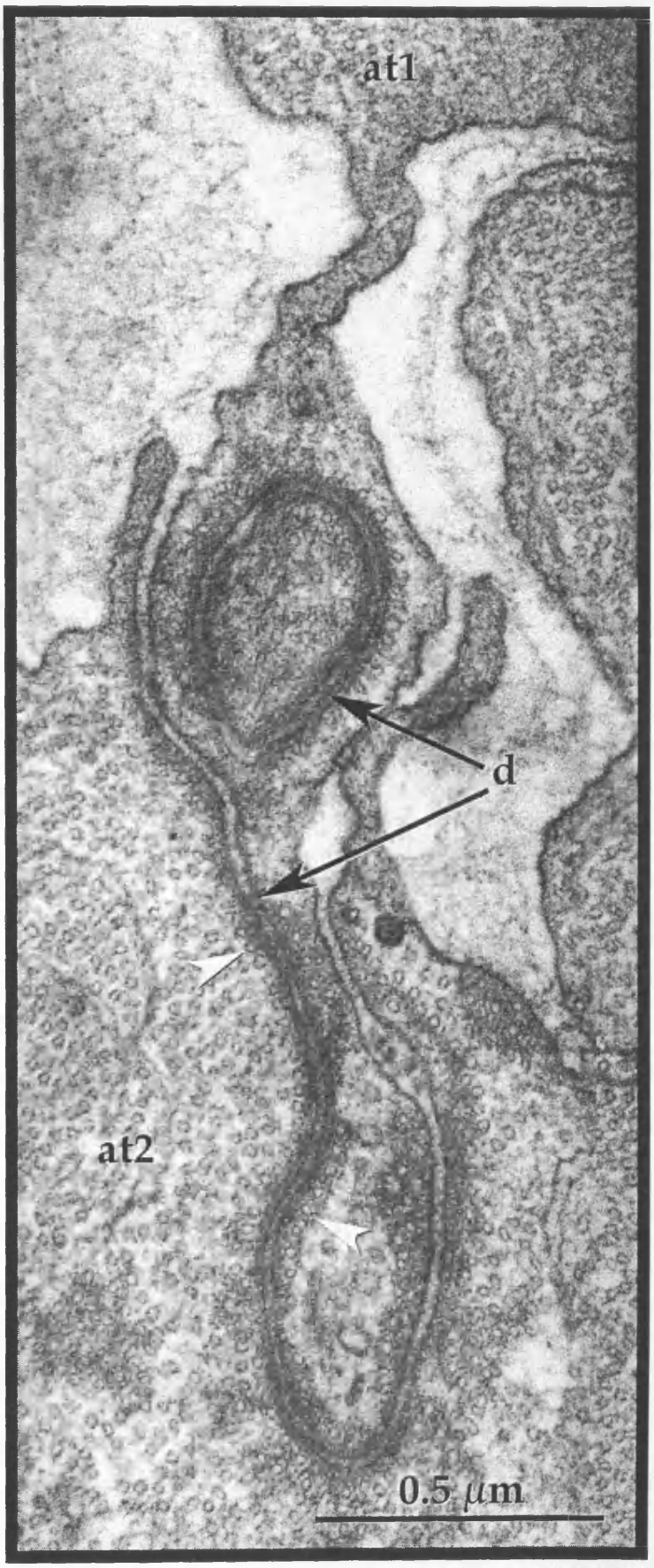
at1
d
at2
0.5 μm

Figure 3.30a, b

a

Electron micrograph showing associations of adjacent microtubules to form clusters or 'plaques' embedded in an electron-dense intracellular material. The microtubule plaques are not always adjacent to the cell membrane but are sometimes well within the cytoplasm of the attachment cell (pI). Plaques associated with the membranes of attachment cells (pM) are usually (but not always) located either in regions of membrane that extend towards neighbouring cells or in regions of membrane adjacent to extracellular fibres (F).

b

This electron micrograph shows a prominent extracellular fibre (F) with a well developed plaque (pM) within the attachment cell to the right. A second plaque (lower left) is opposite a small plaque in the opposite cell (lower right). pI = microtubule plaque not associated with the attachment cell membrane

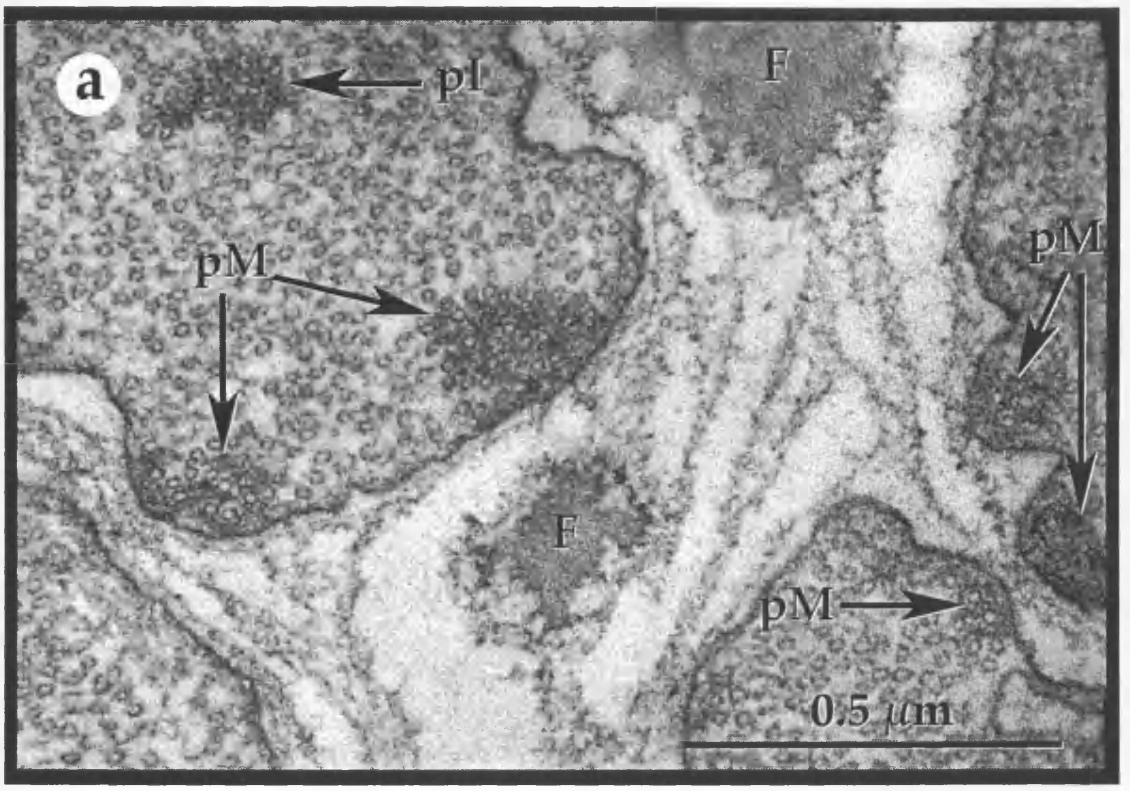
a
pI
F
pM
pM
F
pM
0.5 μm

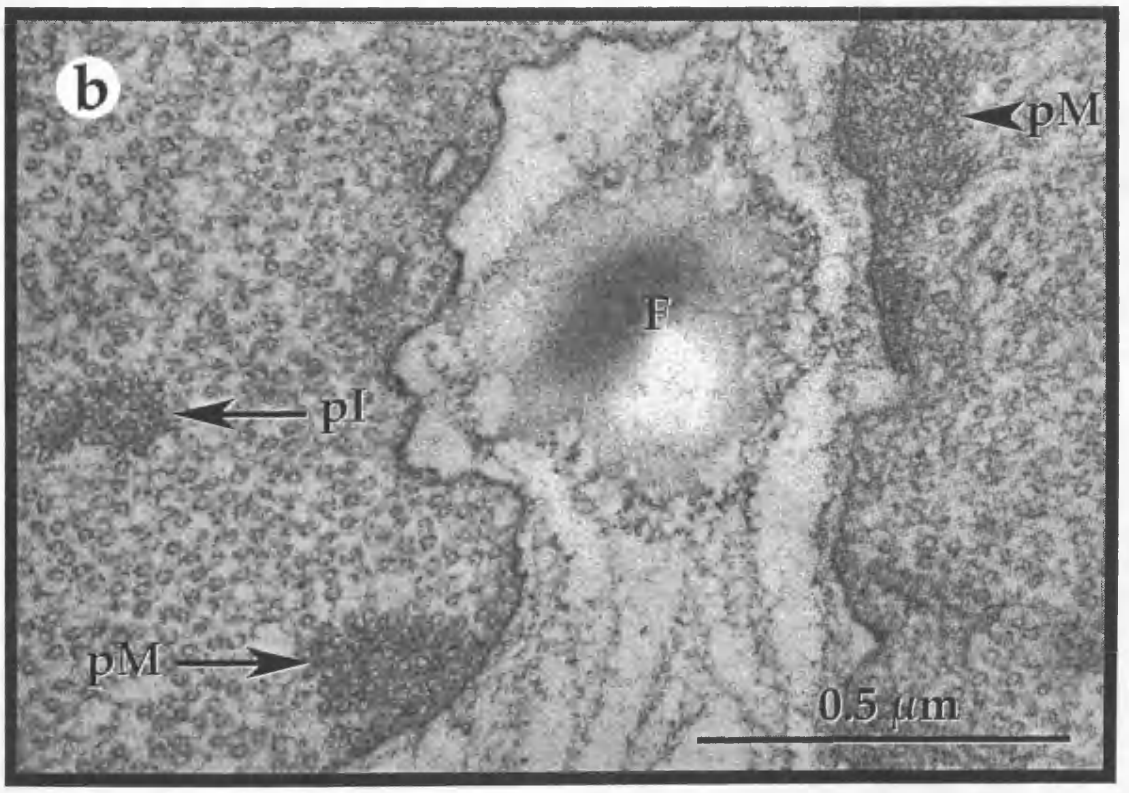
b
pM
F
pI
pM
0.5 μm

Figure 3.31

Scale diagram of the mtFCO showing the location of the guy-rope fibres (gf) in the femur. They extend distally into the heavily tanned knee area. They are approximately 3 mm long (± 500 μm) in an adult locust's femur.

mtFCO = metathoracic femoral chordotonal organ
gf = guy-rope fibres
s = semi-lunar process
f = femur
t = tibia

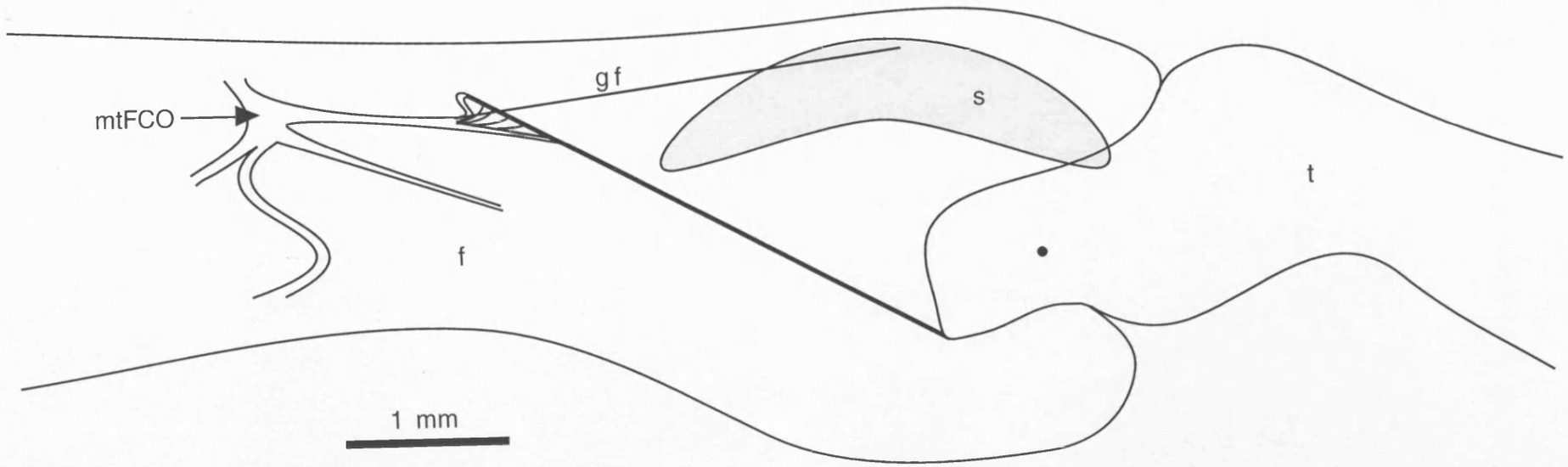
mtFCO
g f
s
t
f
1 mm

Figure 3.32

Transmission electron micrograph showing a transverse section through the guy-rope fibres at the level at which they arise from the dorsal ligament. The fibres have a dense amorphous core (c) surrounded by a more lightly staining periferal zone (m). At this proximal level, several guy-rope fibres run closely together surrounded by a common peripheral zone.

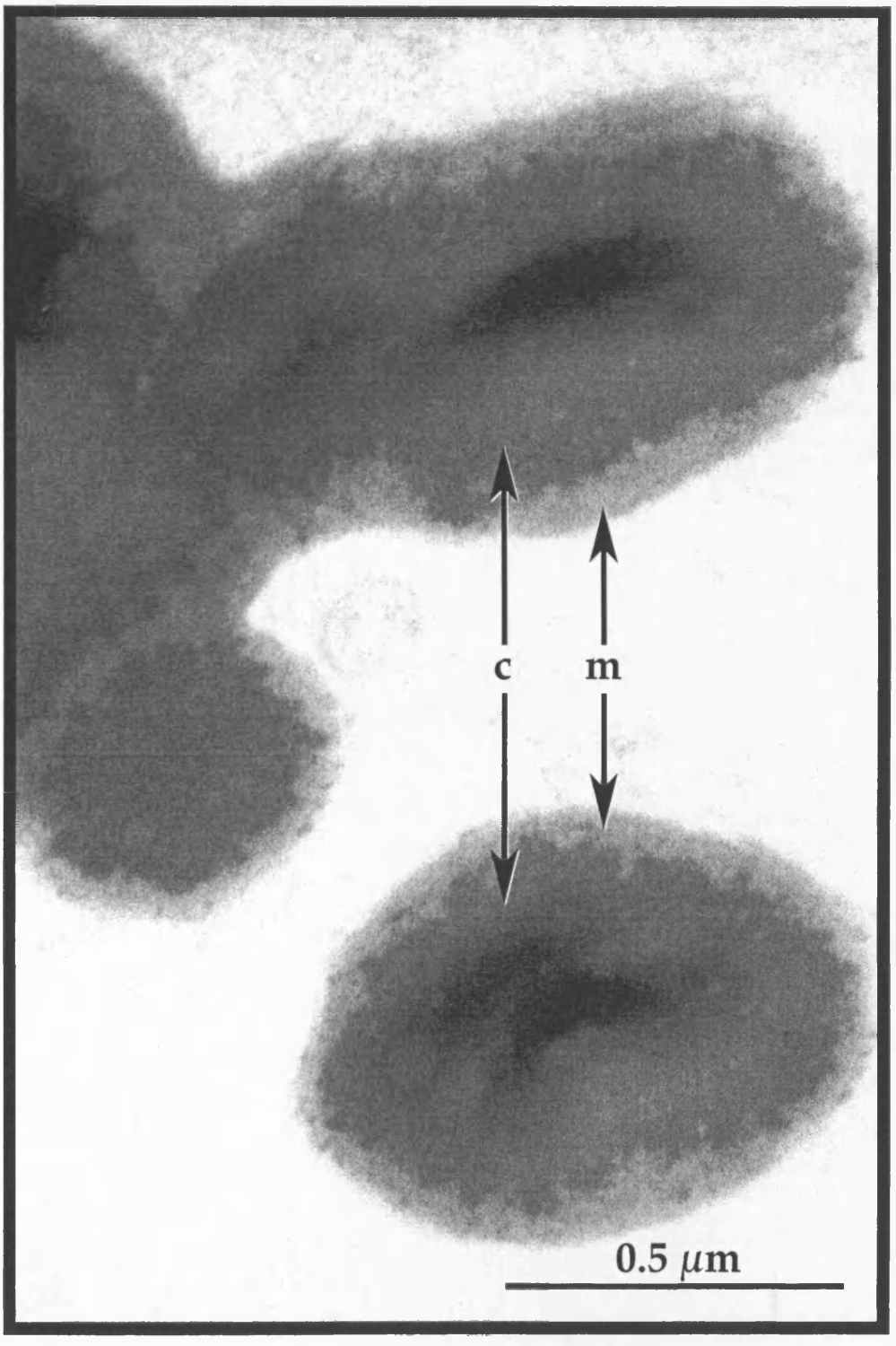
c
m
0.5 μm

Figure 3.33a, b

a

This electron micrograph shows the guy-rope fibres terminating distally in the dorsal femur on an epidermal infolding into the femur cavity (e). The majority of the fibres terminate close to the ventral edge of the epidermal infolding (F), although some fibres terminate further dorsally at regular intervals (arrowheads). n = epidermal cell nucleus

b

This micrograph shows an enlargement of the ventral edge of the epidermal infolding shown above. As the guy-rope fibres run into the dorsal epidermis they fuse with one another to form ribbons (r) of densely-staining material.

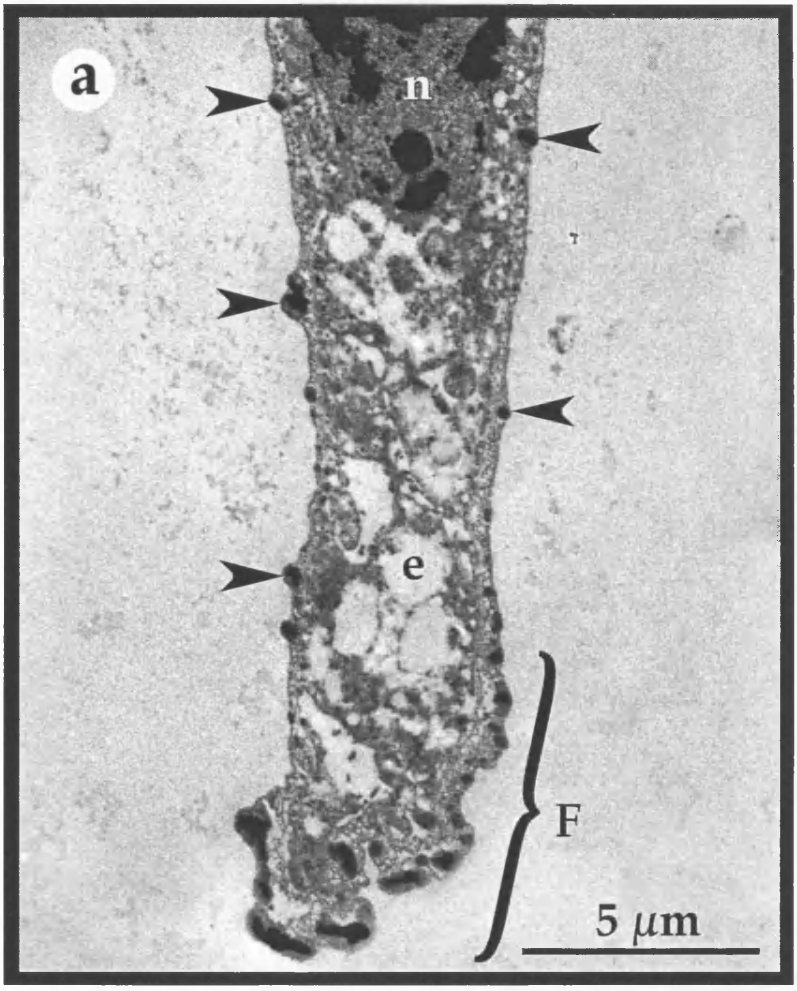
a
n
e
F
5 μm

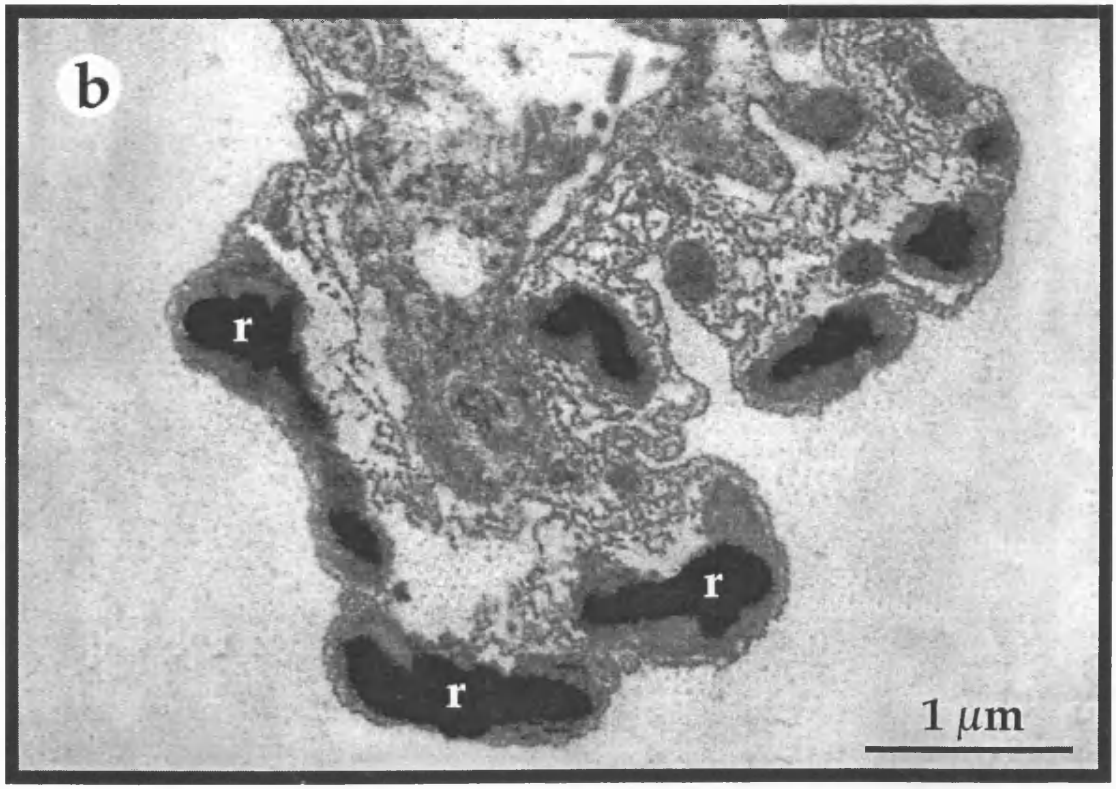
b
r
r
r
1 μm

Figure 3.34

Light micrograph showing the junction of the flexor strand (fs) with the mtFCO scoloparium (s). The strand is reinforced by a fibrous component (f) and attaches to the surface of the mtFCO at two main attachment points (arrowheads). The dendrite (d) that innervates the strand arises from nerve 5b1 at a more proximal level (not shown) and travels along the ventral edge of the mtFCO scoloparium to reach the flexor strand. Distal is to the right.

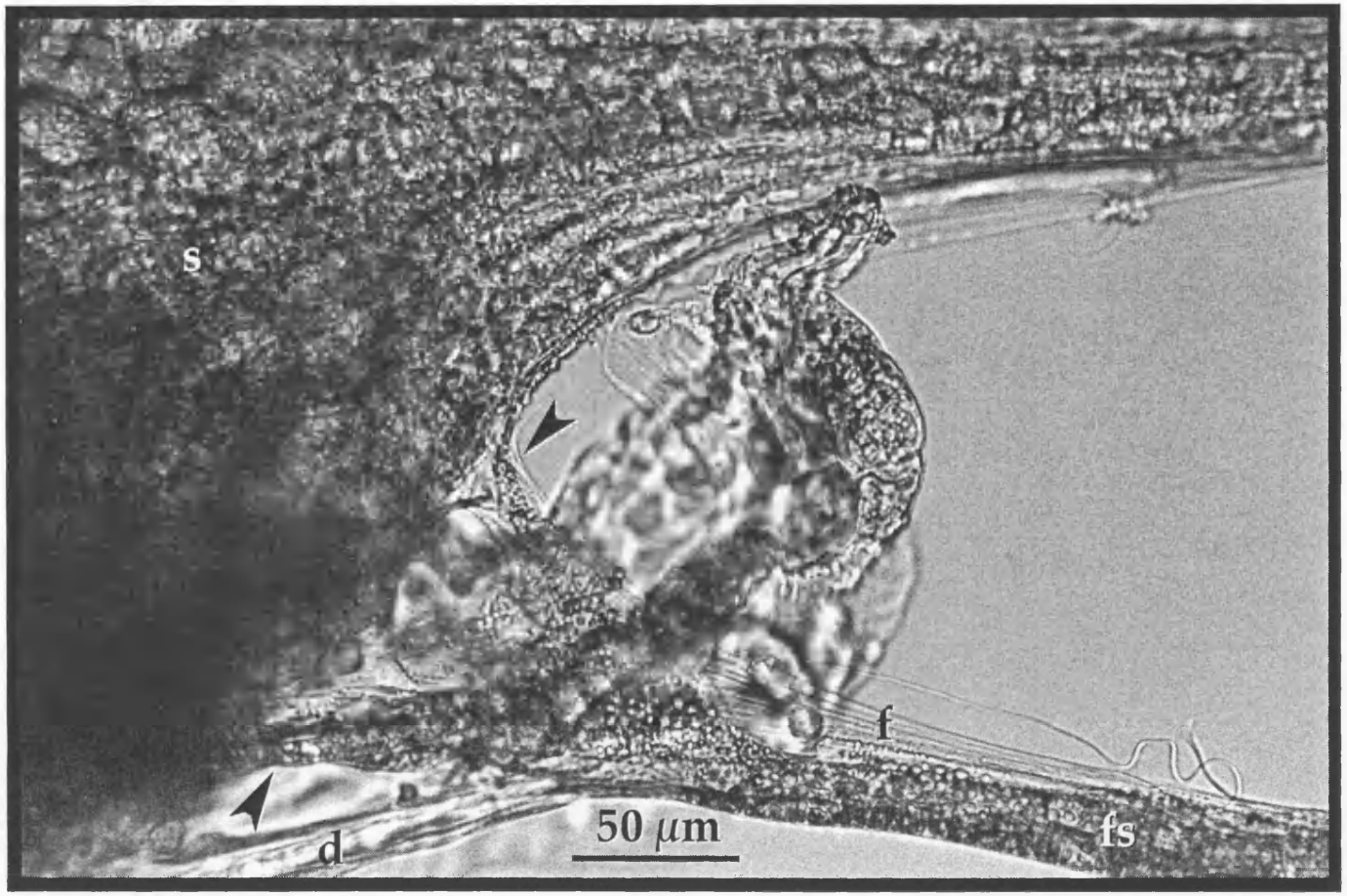
s
f
d
50 μm
fs

Figure 3.35

Series of digital greyscale images of semi-thin (1 µm) sections stained with Toluidine Blue showing the constitution of the flexor strand at different proximo-distal levels (inset). Proximally a strand receptor (sr) (Bräunig, 1982a) forms the core of the flexor strand and is located loosely within a fatty sheath (fs) (levels 1-5). Distally the fatty sheath is reduced (levels 6-8).

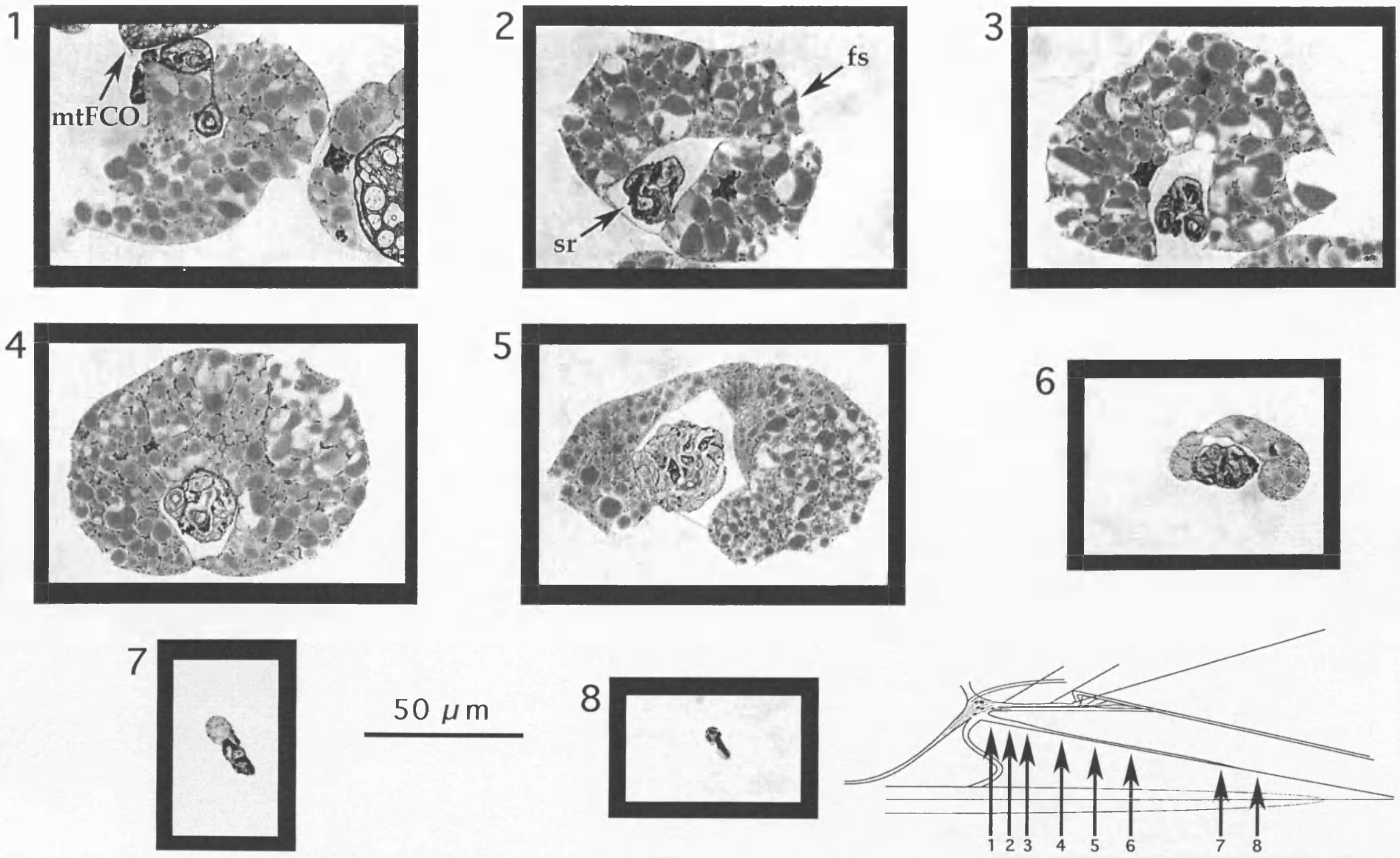
1
mtFCO
2
fs
sr
3
4
5
6
7
50 μm
8
1 2 3 4 5 6 7 8

Figure 3.36a, b

a

This electon micrograph shows that the strand receptor is bounded by a sheath (s) of extracellular matrix in which extracellular fibres (F) are embedded. n = nucleus of strand receptor glial cell. fs = fatty sheath (see Figure 3.35)

b

High power longitudinal section through the strand receptor reveal arrays of densely-staining fibrils embedded in the extracellular matrix (m). The majority of the densely staining fibrils (f) are orientated obliquely along the axis of the strand. Some fibres are orientated longitudinally with respect to the long axis of the strand receptor (arrow) and show a banding pattern.

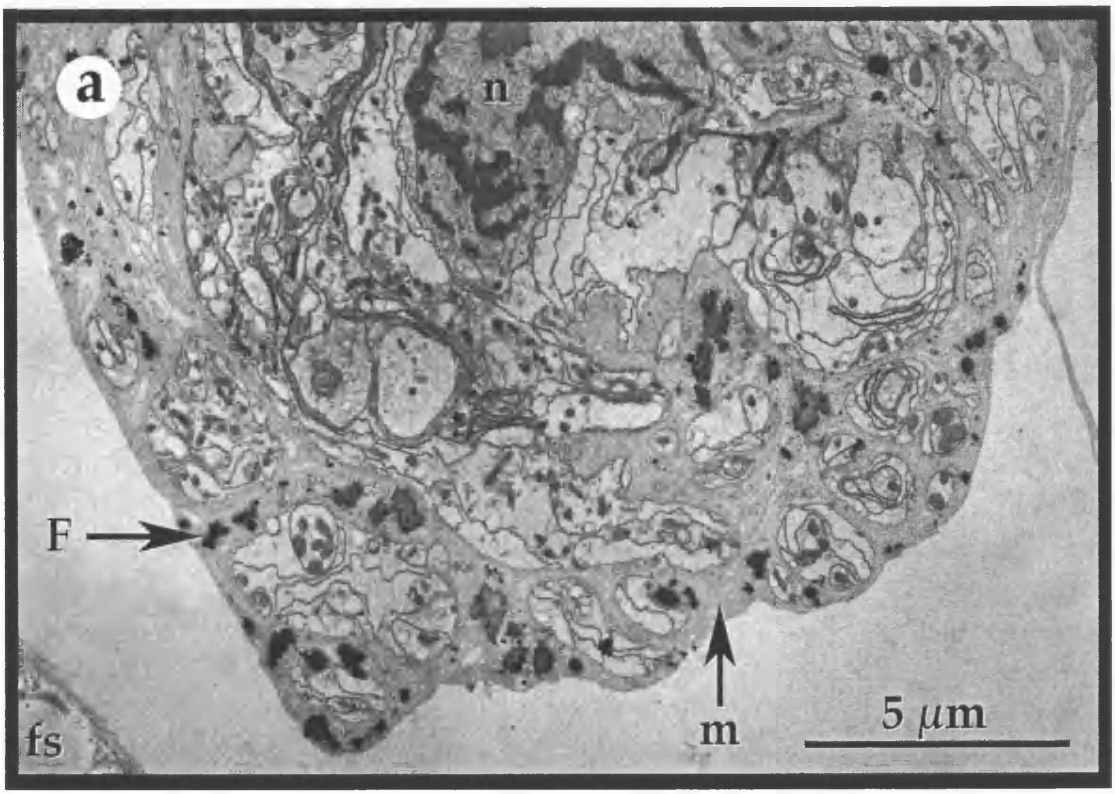
a
n
F
fs
m
5 μm

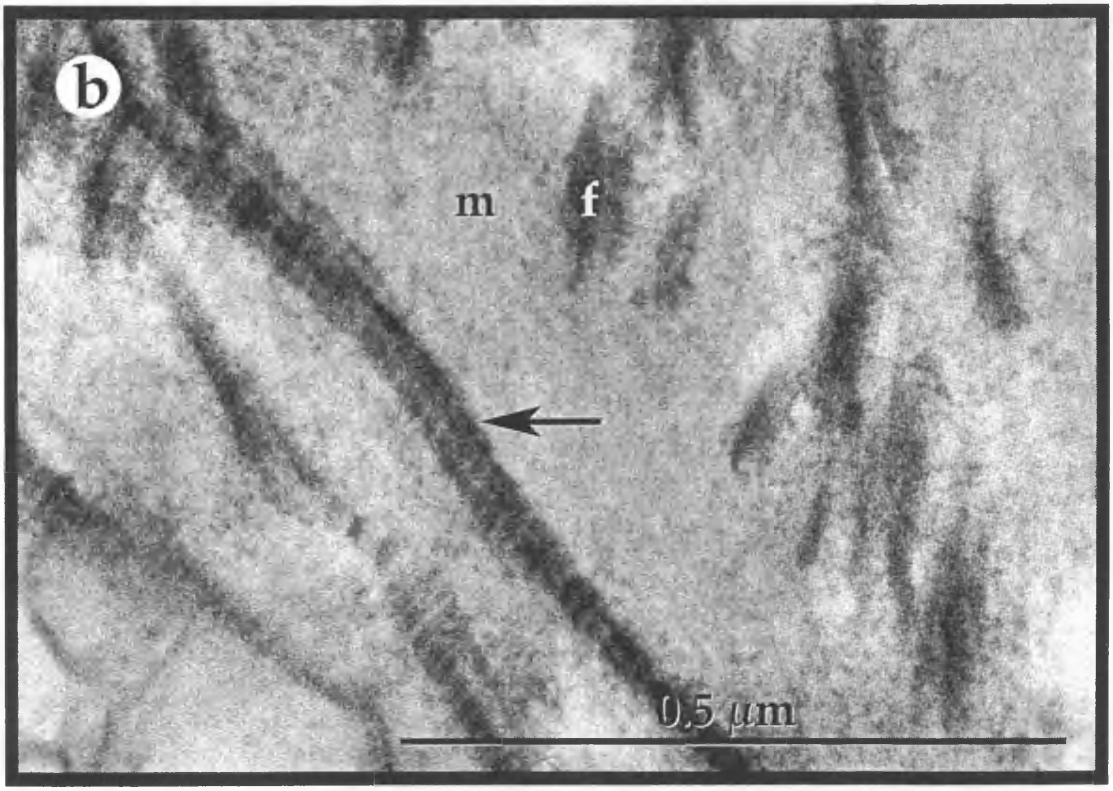
b
m
f
0.5 μm

Figure 3.37a, b

a

The strand receptor has collagen-like fibrils (cf) located within the extracellular matrix sheath (m). Their alignment is not regimented, the fibrils being found at a variety of orientations within the matrix. The outer edge of the extracellular matrix sheath has a beaded appearance (bd) which appears similar in both transverse and longitudinal section.

b

The fibrils do not stain intensely, but the irregular periodic banding characteristic of collagens can clearly be resolved at high magnifications. The macro-period can be delimited by an intensely-staining double band, repeating at 52 nm intervals (indicated).

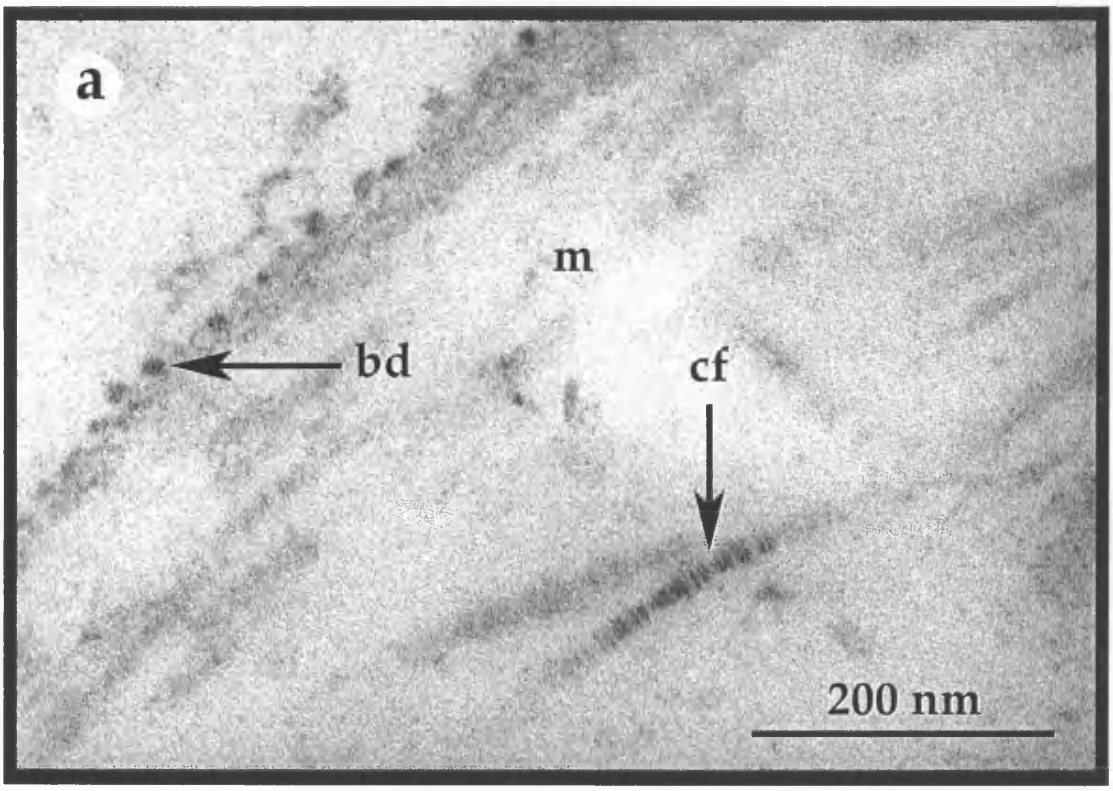
a
m
bd
cf
200 nm

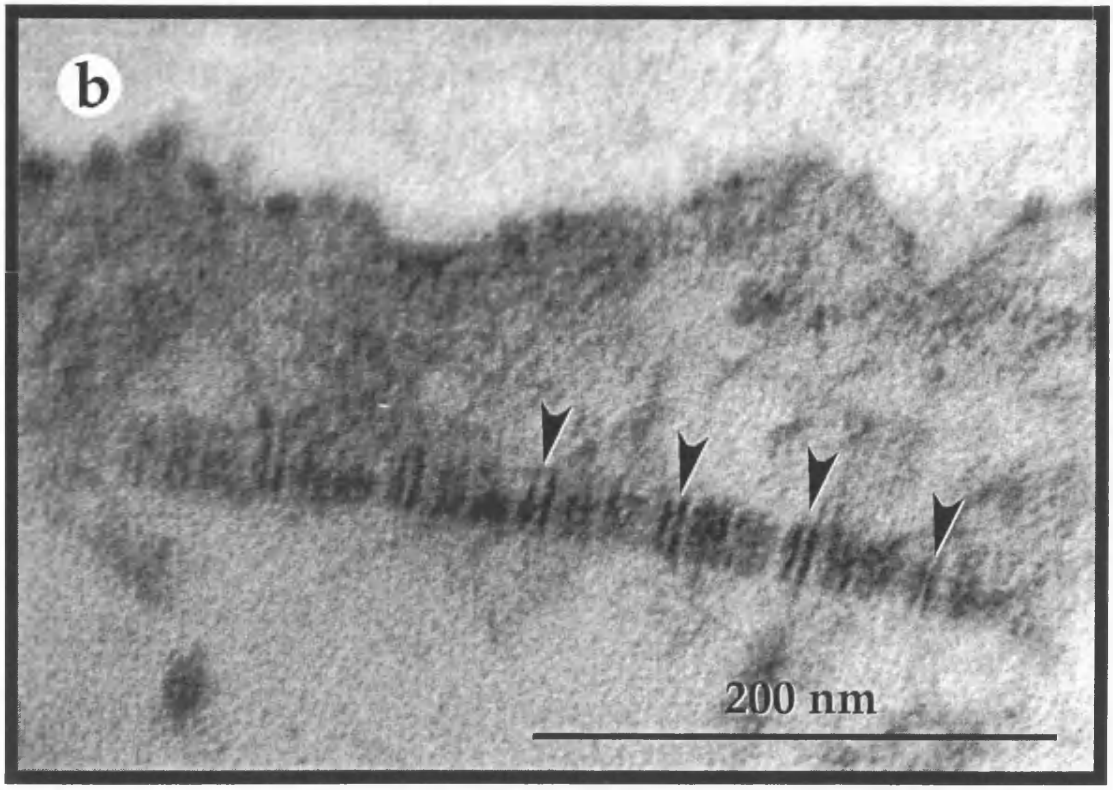
b
200 nm

Figure 3.38

Graph showing the cross-sectional area of the dorsal and ventral ligaments of the apodeme complex at different proximo-distal levels in a preparation where the tibia was in the fully flexed position. Proximal to its point of origin, the cross-sectional area of the ventral ligament increases from 0 μm^2 to about 1000 μm^2 over a distance of 500 μm, reflecting the recruitment of ventral ligament fibres from the side of the cuticular rod. The cross-sectional area of the dorsal ligament rises from 0 - 1000 μm^2 over a distance of approximately 125 μm (500 - 625 μm). In the region of the apodeme complex lying between the loop-forming region and the sensory neurones (625 μm - 1000 μm), the cross-sectional area of each ligament remains constant at approximately 1000 μm^2. The cross-sectional area of the ventral ligament begins to increase once more at its proximal end (at a distance exceeding 1000 μm). This is the proximo-distal level at which the first sensory neurones are encountered. Error bars indicate estimated measurement error based upon 10 repeated measurements from the same image.

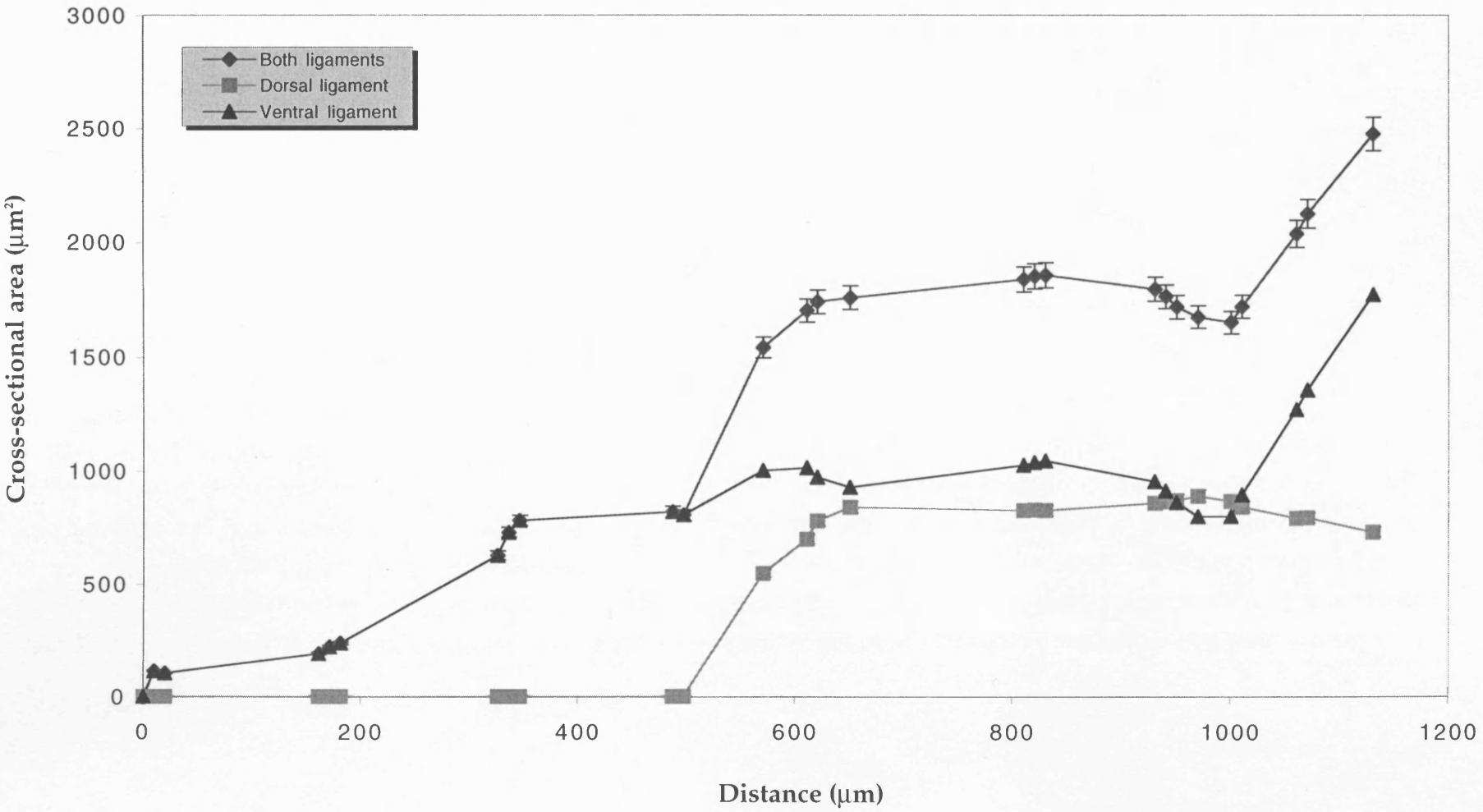
Cross-sectional area of the mtFCO ligaments at different proximo-distal levels
Both ligaments
Dorsal ligament
Ventral ligament
Cross-sectional area (μm²)
3000
2500
2000
1500
1000
500
0
0
200
400
600
800
1000
1200
Distance (μm)

Figure 3.39

This graph shows the total cross-sectional area of the Acid Fuchsin-staining component in the dorsal and ventral ligaments of the apodeme complex at different proximo-distal levels. There is more Acid Fuchsin-staining component in the ventral ligament than the dorsal ligament at all proximo-distal levels. The cross-sectional area of the Acid Fuchsin-staining component declines proximally in both ligaments. Regression lines fitted to the relevant parts of the graphs show that the mean rate of decline is approximately 10 $\mu m^2/100\ \mu m$ in the dorsal ligament, and approximately 4 $\mu m^2/100\ \mu m$ in the ventral ligament. There is an abrupt rise in Acid Fuchsin-staining component at the proximal end of the ventral ligament at the level of the distal-most sensory neurones. Error bars indicate estimated measurement error based upon 10 repeated measurements from the same image.

Total cross-sectional area of Acid Fuchsin-staining component in the mtFCO ligaments at different proximo-distal levels

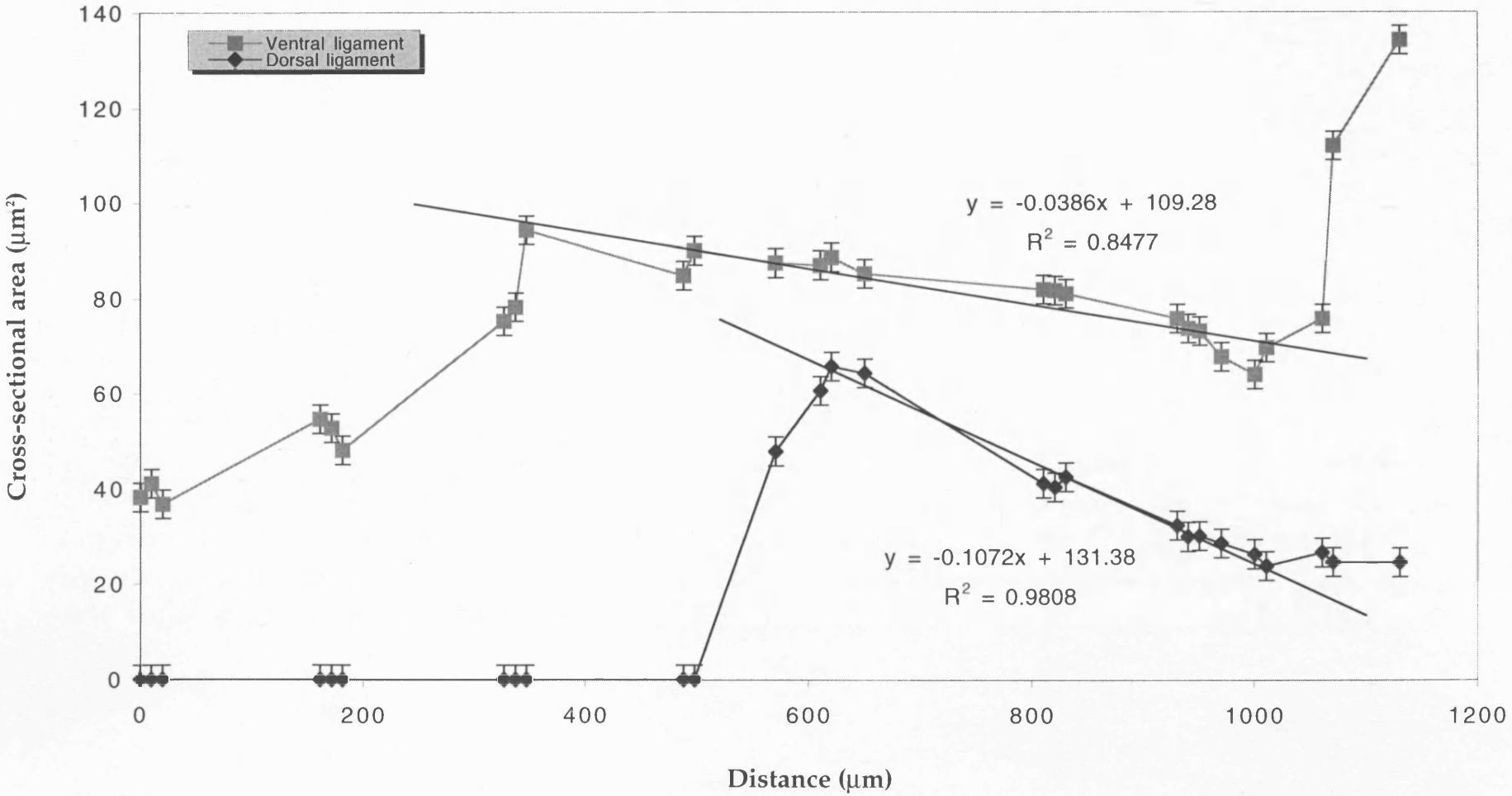

Figure 3.40

Graph showing the proximo-distal distribution of Acid Fuchsin-staining component associated with the dorsal ligament. There is approximately twice the cross-sectional area of Acid Fuchsin-staining component located within the extracellular sheath of the ligament compared with that amongst the attachment cells within the ligament at all proximo-distal levels. There is a large peak in the cross-sectional area of Acid Fuchsin-staining component located in the dorsal ligament sheath at a proximo-distal level of 600 μm. Error bars indicate estimated measurement error based upon 10 repeated measurements from the same image.

Cross-sectional area of Acid Fuchsin-staining component in the dorsal ligament at different proximo-distal levels

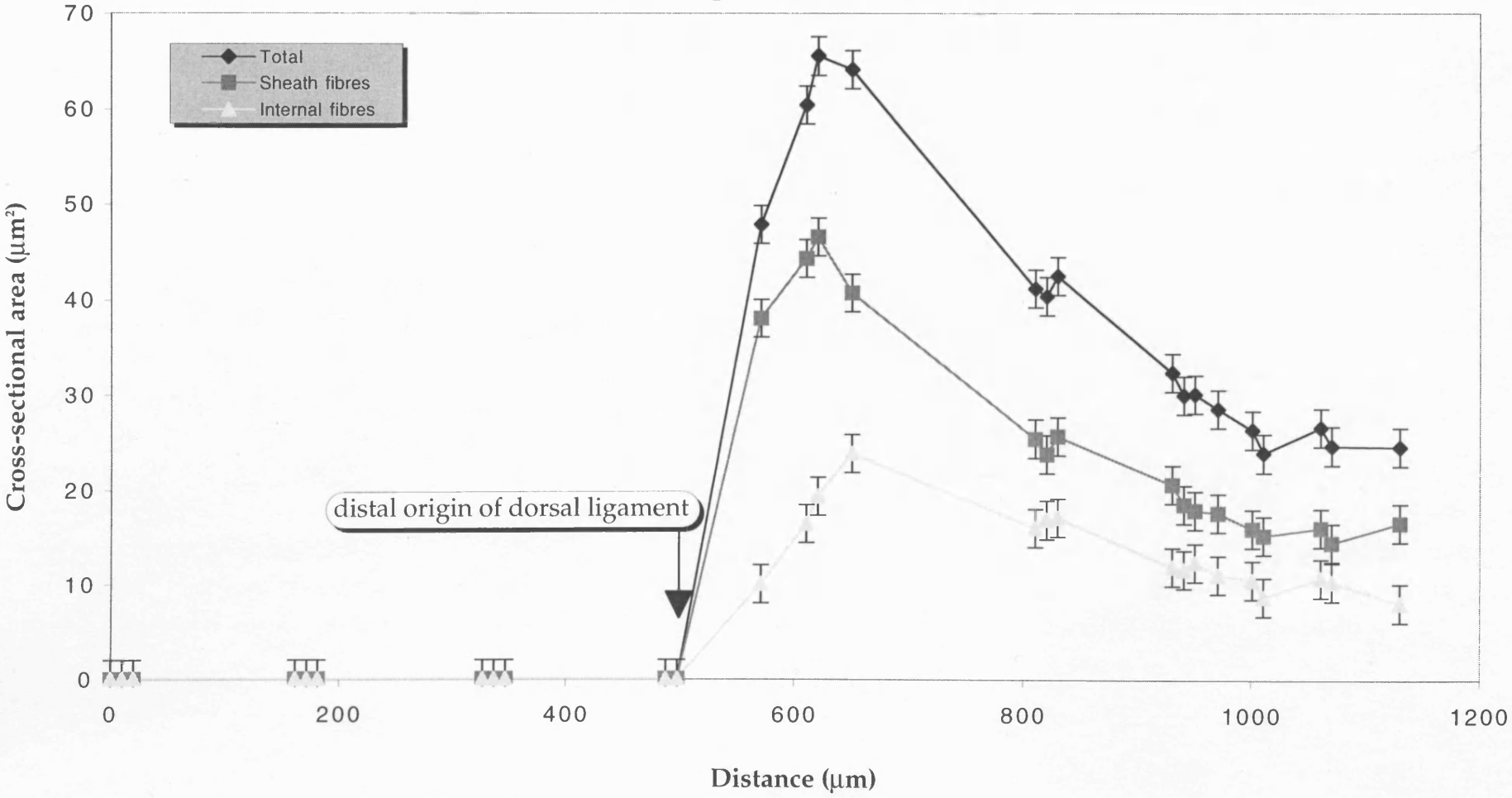

Figure 3.41

Graph showing the proximo-distal distribution of Acid Fuchsin-staining component associated with the ventral ligament. Over the distal-most 500 μm of the ventral ligament there is approximately twice the cross-sectional area of Acid Fuchsin-staining component located in the sheath compared with that within the ligament. Between 500 μm and 1000 μm, the cross-sectional area of Acid Fuchsin-staining component in the sheath declines. Over the same range the cross-sectional area of Acid Fuchsin-staining component located within the ligament first increases so that there is equal staining in the sheath and within the ligament at about 800 μm. At more proximal levels the area of Acid Fuchsin-staining component within the ligament declines so that there is less than there is in the sheath. At the level at which sensory neurones are located within the ventral liagment (1100 μm), there is a marked increase in the cross-sectional area of Acid Fuchsin staining within the ligament. Error bars indicate estimated measurement error based upon 10 repeated measurements from the same image.

Cross-sectional area of Acid Fuchsin-staining component in the ventral ligament at different proximo-distal levels

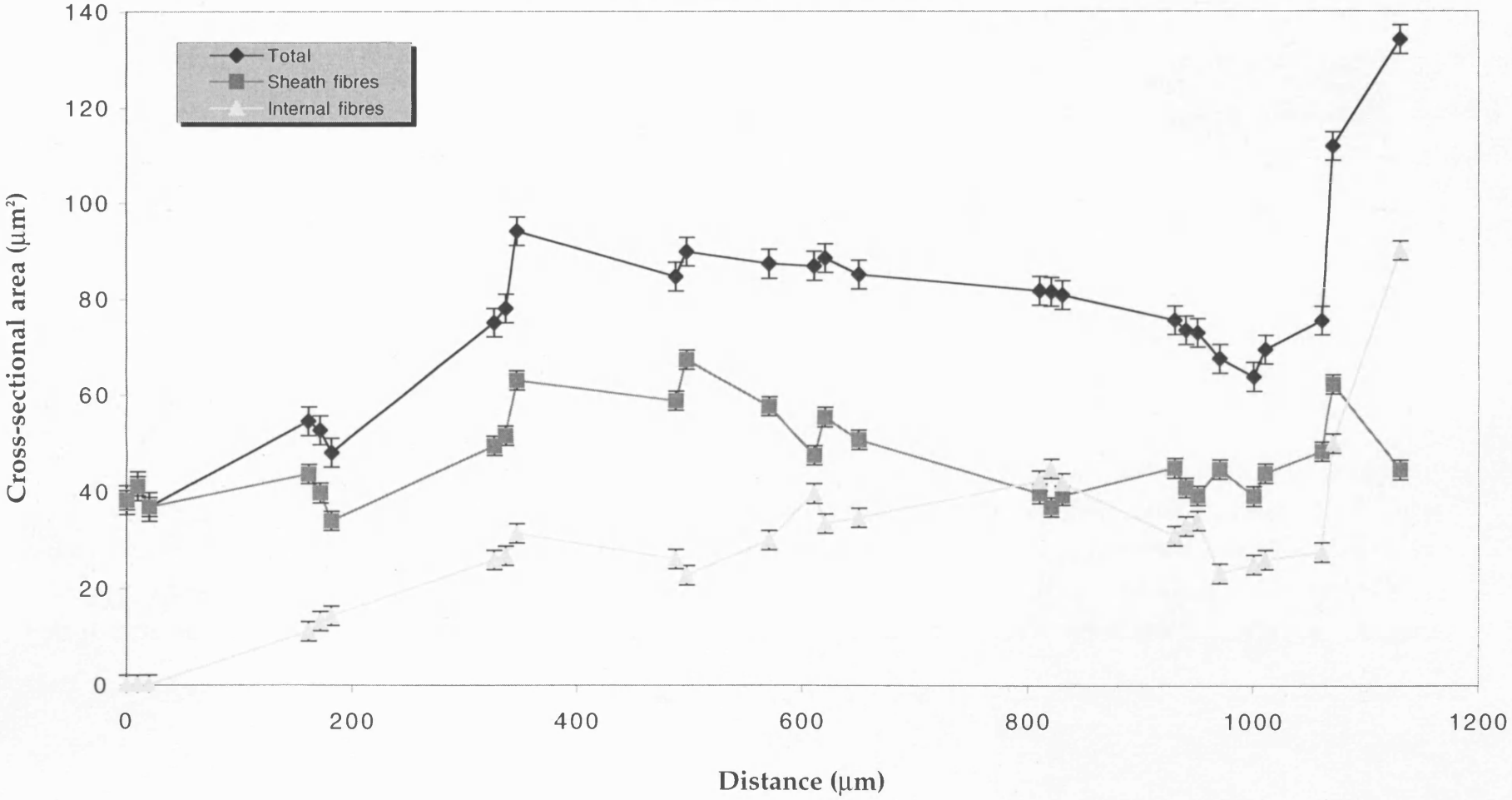

Figure 3.42

The % cross-sectional area of Acid Fuchsin-staining component decreases proximally along the length of the apodeme complex. Distally the Acid Fuchsin-staining component forms approximately 35% of the apodeme complex cross-sectional area. Proximally it forms approximately 5%. Proximal to the distal origin of the dorsal ligament (>600 μm) the % cross-sectional area of Acid Fuchsin-staining component in the ventral ligament remains relatively constant at approximately 8% whilst that of the dorsal ligament approximately halves over the same range. Error bars indicate estimated measurement error based upon 10 repeated measurements upon the same image.

Percentage cross-sectional area of Acid Fuchsin-staining component in the mtFCO ligaments at different proximo-distal levels

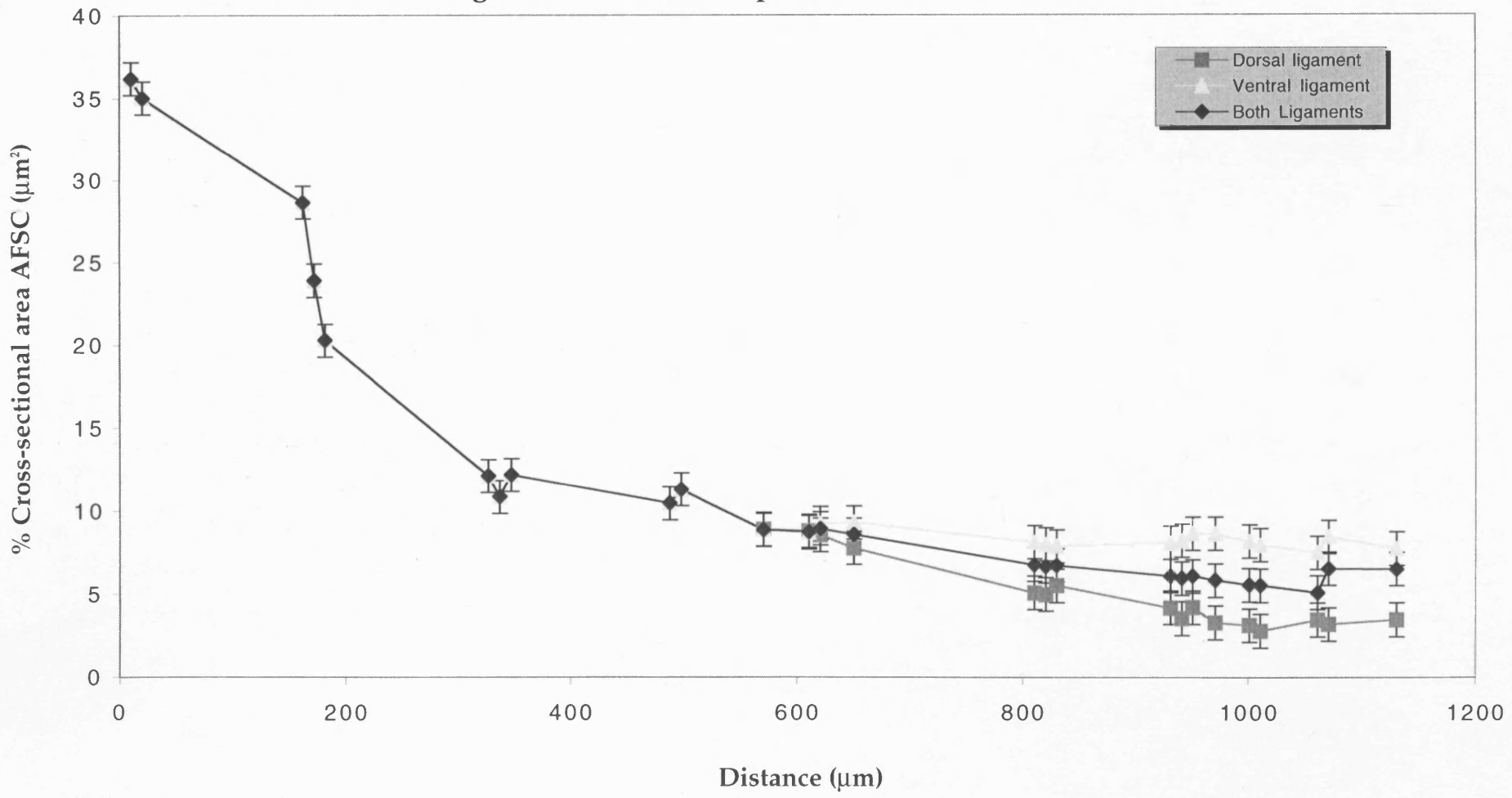

Figure 3.43

Graph comparing the number of discrete Acid Fuchsin-staining fibres located in the sheath of the dorsal ligament with those located within the dorsal ligament at various proximo-distal levels. At the distal end of the dorsal ligament (500-600 μm), there are more AFS fibres in the sheath than within the ligament. This is the region of the dorsal ligament which buckles to form the apodeme complex loop. At this proximo-distal level, the dorsal and ventral ligaments are not associated with one another and the dorsal ligament is surrounded by sheath. Proximal to this, over the range 600-900 μm, there are more fibres located inside the ligament than in the sheath. At the level at which the distal-most neurones are located (>1000 μm), the numbers of fibres are distributed approximately equally between the sheath and the inside of the ligament. Error bars indicate estimated measurement error based upon 10 repeated measurements from the same image.

Distribution of Acid Fuchsin-staining fibres between the sheath and the inside of the dorsal ligament

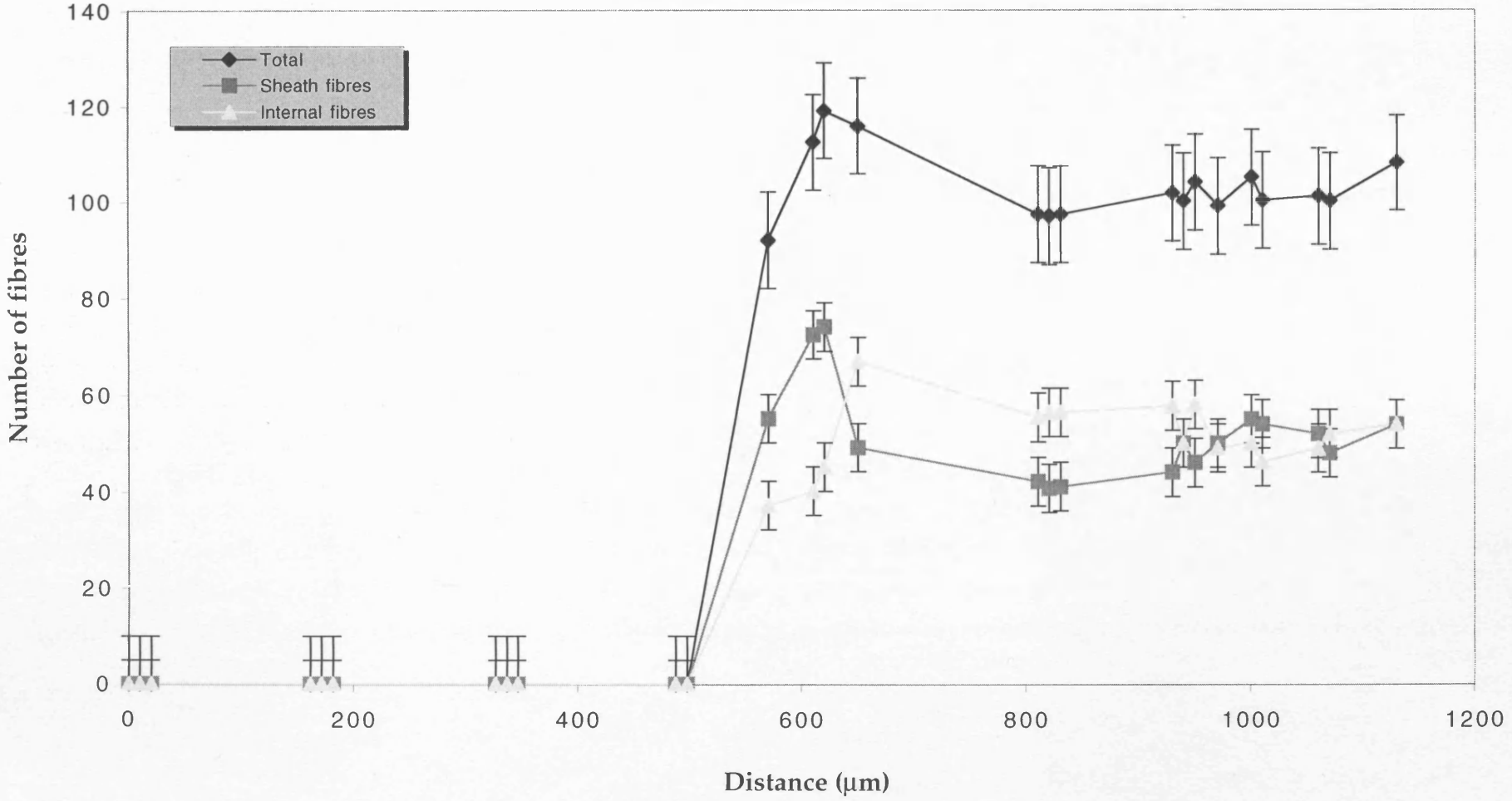

Figure 3.44

Graph indicating the number of discrete Acid Fuchsin-staining fibres located in the ventral ligament sheath and within the ventral ligament at various proximo-distal levels. In the sheath of the ventral ligament the number increases proximally over the range 0-350 μm as the ventral ligament arises from the side of the cuticular rod. Further proximally, the number of sheath fibres remains constant at approximately 40 discrete fibres. The number of Acid Fuchsin-staining fibres located within the ligament rises from 0 to 100 over the range 0-800 μm. Proximal to this level, the number of fibres declines before rising again at the level at which the sensory neurones are located. Error bars indicate estimated measurement error based upon 10 repeated measurements from the same image.

Distribution of Acid Fuchsin-staining fibres between the sheath and the inside of the ventral ligament

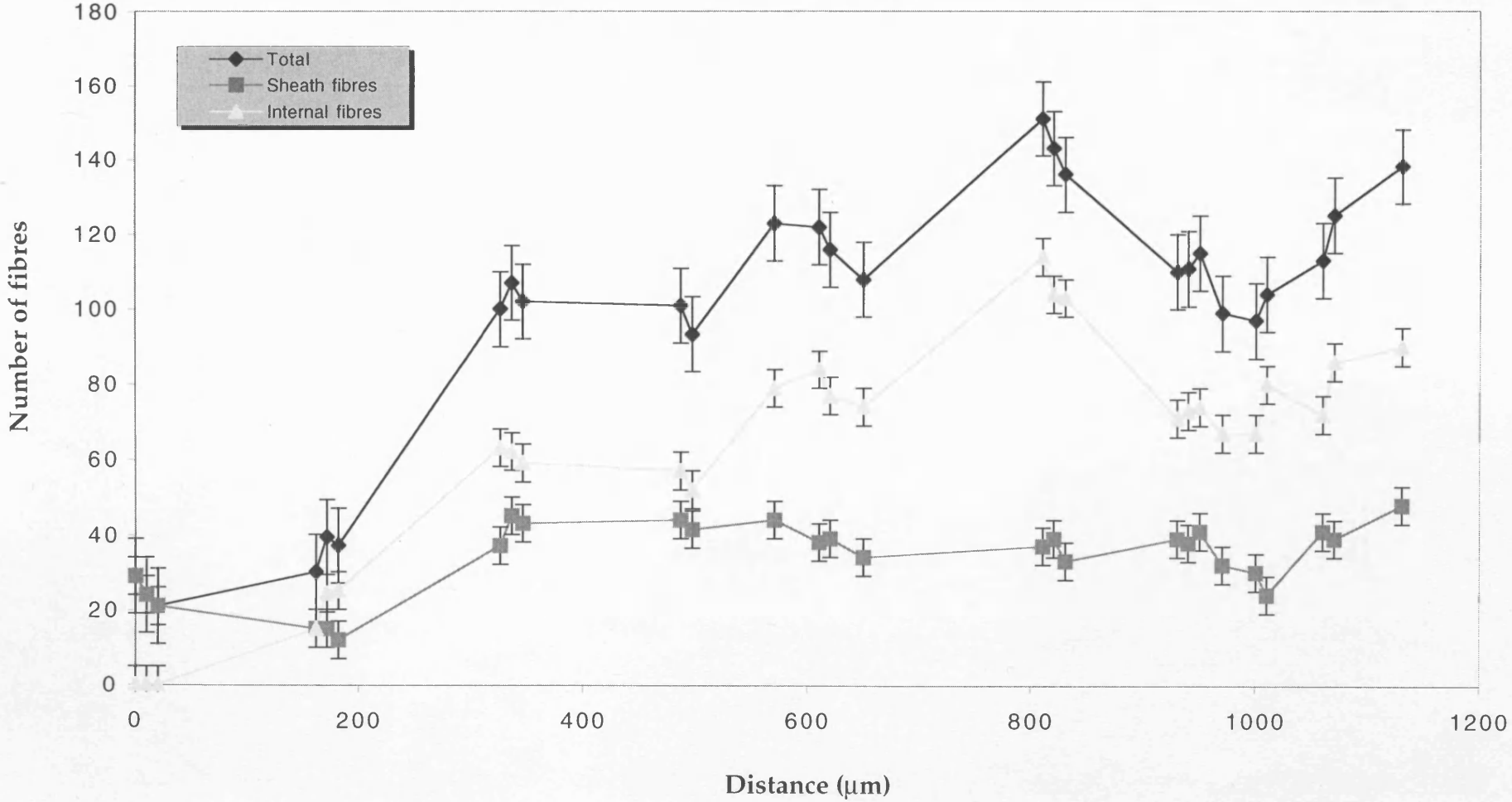

Figure 3.45

Size-frequency histogram showing the distribution of fibre sizes in the apodeme complex (dorsal and ventral ligaments together) at two contrasting proximo-distal levels (inset). The size distribution of the fibres is less skewed distally than proximally; skewness 3.58 and 7.68 respectively. This means that proximally there are fewer large diameter fibres and more small diameter fibres compared to those found distally. Proximally the number of medium sizes fibres in the ligaments (cross-sectional area 0.6 μm^2-2.0 μm^2) declines, whilst the number of small fibres (cross-sectional area <0.4 μm^2) increases.

Histogram showing the size-frequency distribution of all the AFS-fibres at two proximo-distal levels along the mtFCO

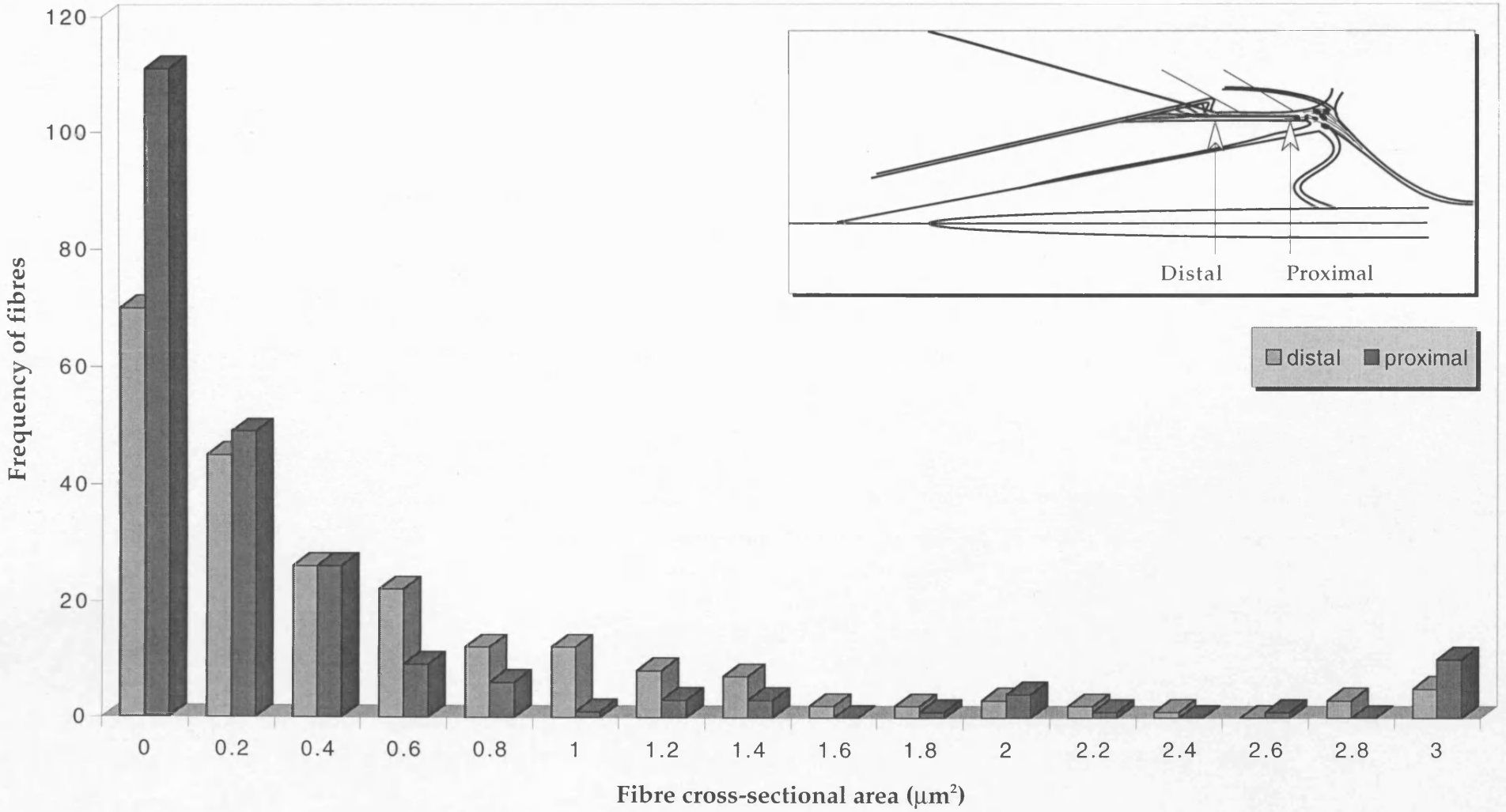

Figure 3.46

Size-frequency histogram showing the distribution of fibre sizes in the dorsal ligament at two proximo-distal levels (inset). The histogram shows that proximally there is an increase in the number of small Acid Fuchsin-staining fibres ($<0.4\ \mu m^2$), and a decrease in the frequency of larger fibres ($>0.4\ \mu m^2$).

Histogram comparing the size-frequency distribution of the dorsal ligament AFS-fibres at its proximal and distal ends

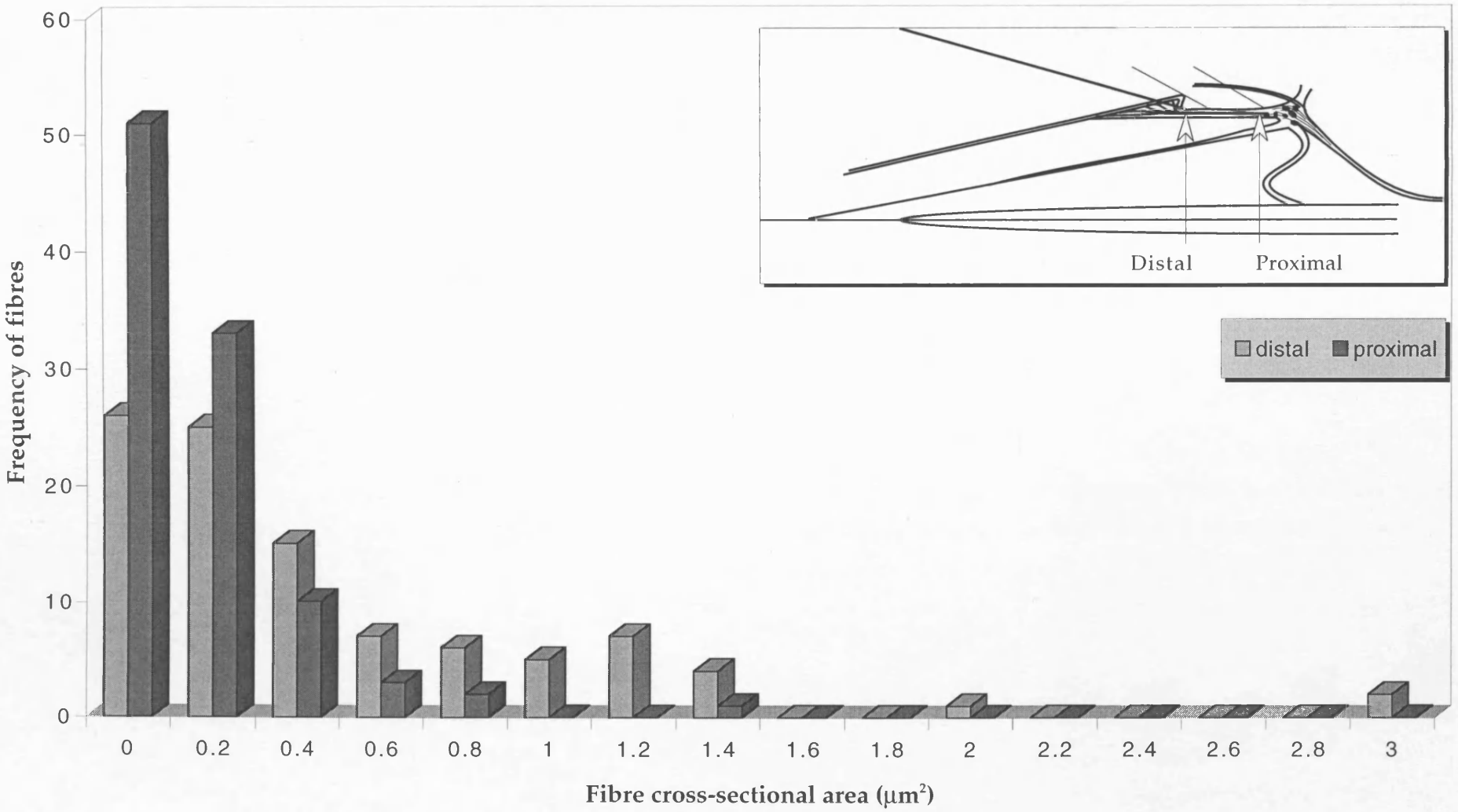

Figure 3.47

Size-frequency histogram showing the distribution of fibre sizes in the ventral ligament at two proximo-distal levels (inset). Proximally the number of medium sized fibres (0.6 μm^2 - 2 μm^2) is reduced, whilst the number of fibres having small cross-sectional areas (<0.2 μm^2) increases. The number of fibres <0.2 μm^2 increases proximally by 40%.

Histogram comparing the size-frequency distribution of the ventral ligament AFS-fibres at its proximal and distal ends

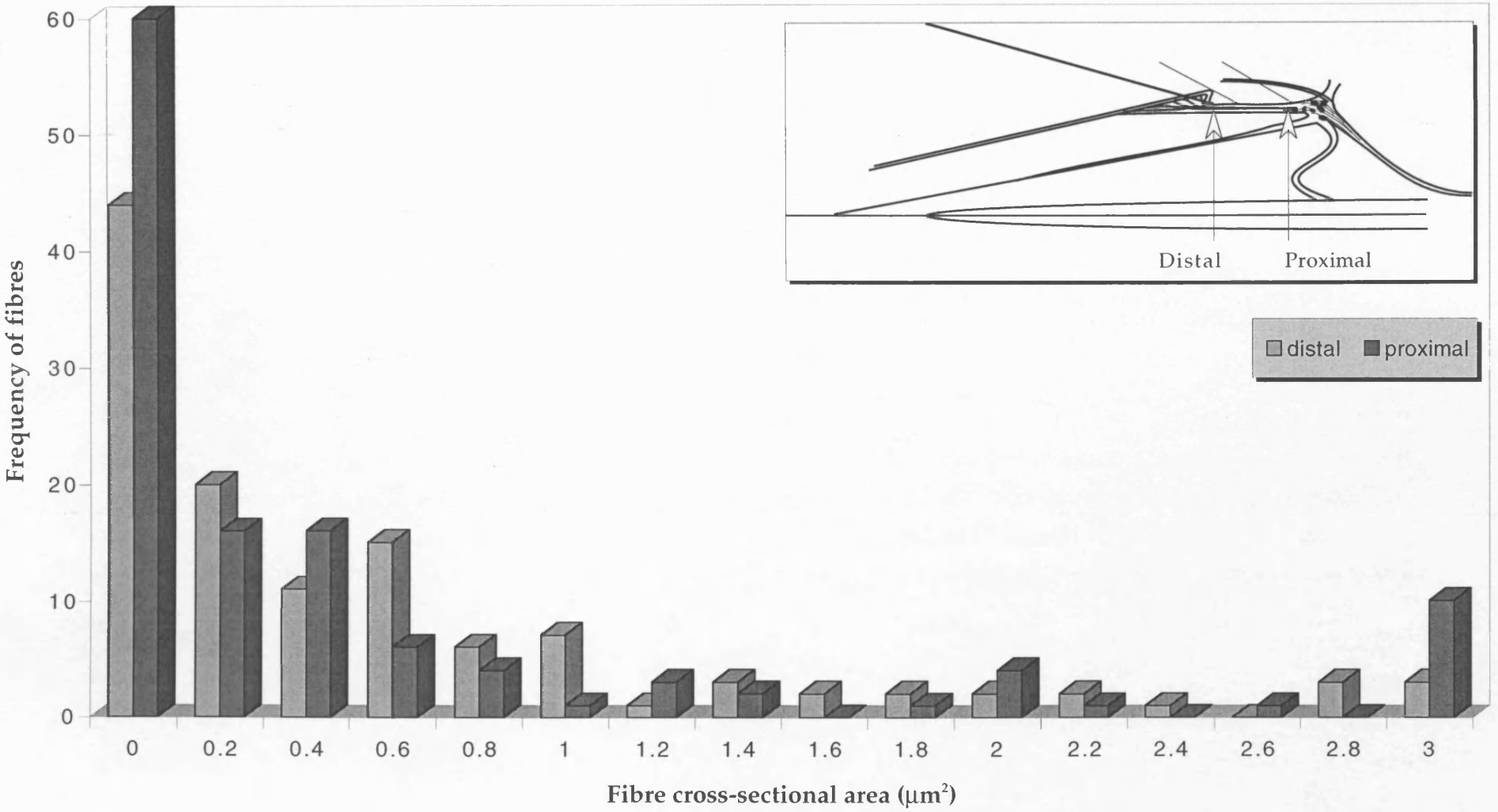

Figure 3.48

Size-frequency histogram contrasting the size-distribution of Acid Fuchsin-staining fibres between the dorsal and ventral ligaments close to their distal ends (inset). There are more large fibres (cross-sectional area >1.6 μm^2) in the ventral ligament than in the dorsal ligament. The ventral ligament also has more small fibres (cross-sectional area <1.2 μm^2) than the dorsal ligament at this proximo-distal level. The range of fibre sizes is similar between the two ligaments at this proximo-distal level.

Frequency histogram comparing the AFS-fibre size-frequency distribution between the dorsal and ventral ligaments at the distal end of the mtFCO ligaments

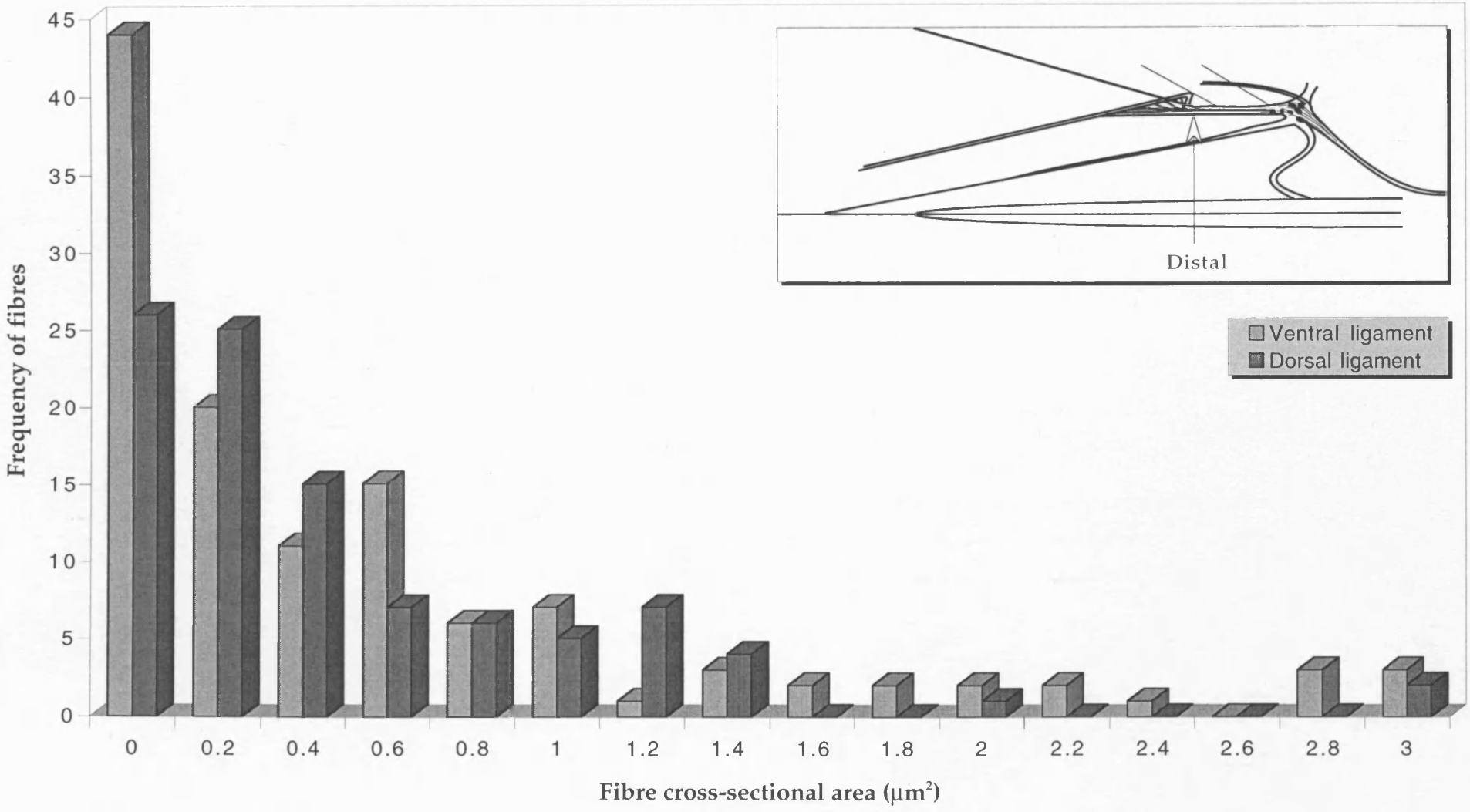

Figure 3.49

Size-frequency histogram contrasting the size-distribution of Acid Fuchsin-staining fibres between the dorsal and ventral ligaments close to the mtFCO scoloparium (inset). The ventral ligament has a wider distribution of fibre sizes than the dorsal ligament; 99% of the AFS-fibres in the dorsal ligament have a cross-sectional area of less than 1.0μm^2 whilst the ventral ligament contains fibres in excess of 2.0μm^2.

Frequency histogram comparing the AFS-fibre size-frequency distribution between the dorsal and ventral ligaments at the proximal end of the mtFCO ligaments

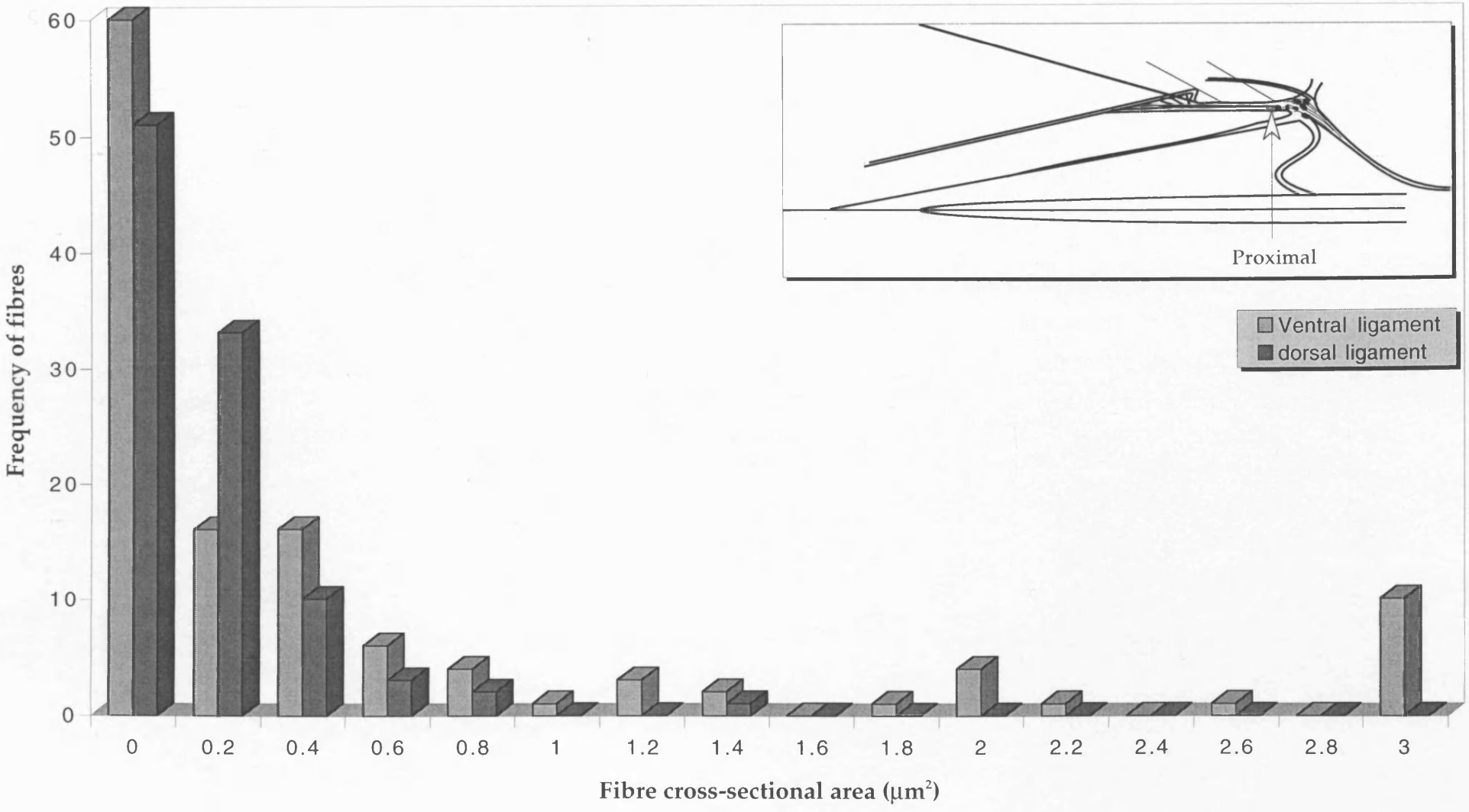

Figure 3.50

Although individual attachment cells cannot be distinguished at light microscope level, the approximately 56 attachment cells (see Figure 3.24) of the apodeme complex can be divided into 'functional groups' surrounded by Acid Fuchsin-staining fibres in semi-thin (1 μm) sections stained with Acid Fuchsin. This figure compares a section taken distally (at a level just proximal to that at which the guy-rope fibres leave the dorsal ligament) with a section taken proximally (at the level of the distal-most sensory neurones). The line diagrams adjacent to each section illustrate the interpretation of the staining patterns. The shaded areas indicate the limits of two dorsally situated functional groups. The dorsally situated areas delimited by Acid Fuchsin-staining fibres tend to be larger than those located ventrally. Proximally the areas defined by the Acid Fuchsin-staining fibres remain evident in the dorsal ligament whilst those in the ventral ligament dissociate at this proximo-distal level as the individual attachment cells terminate on the ventral neurones.

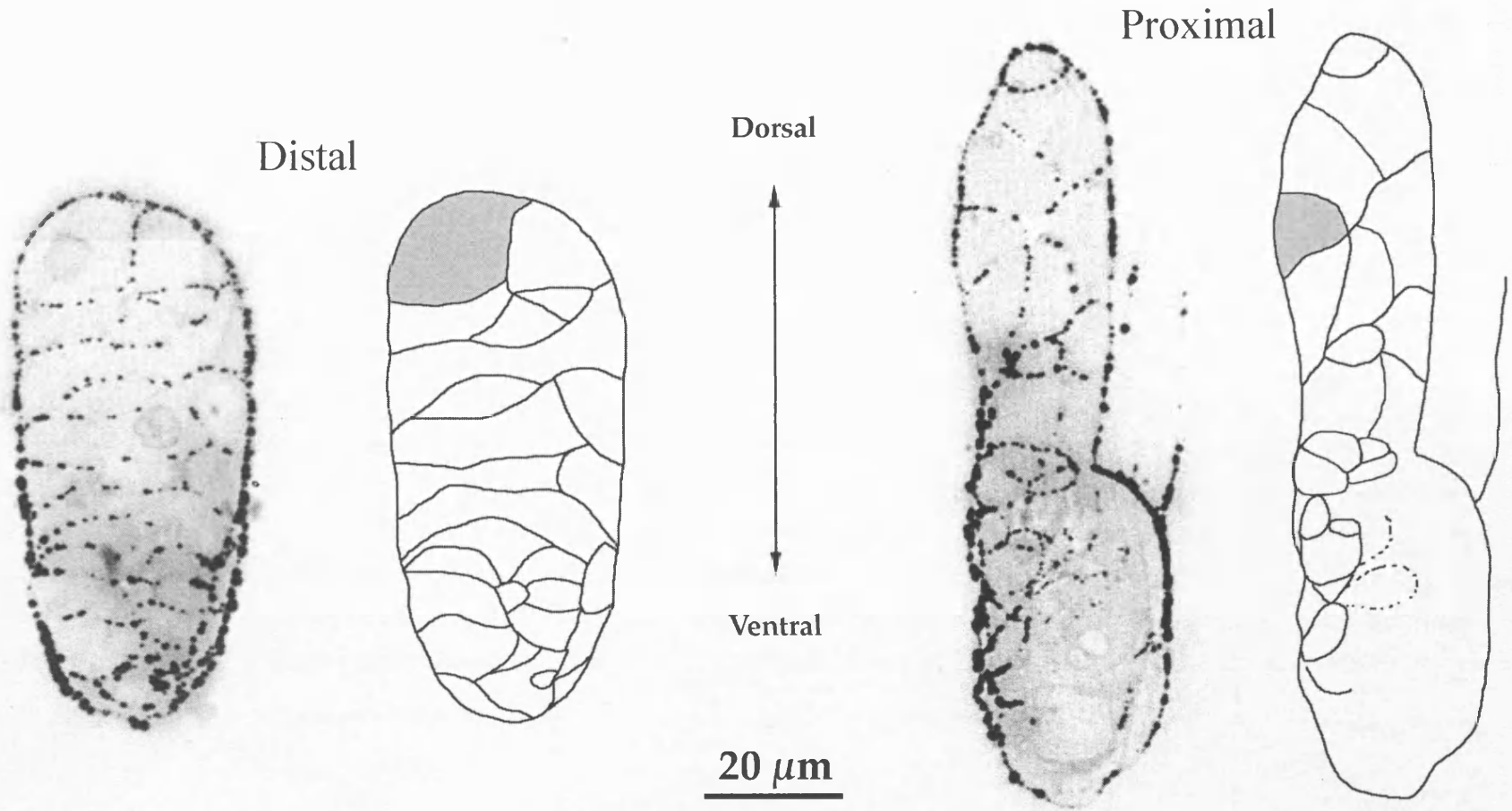
Distal
Dorsal
Ventral
Proximal
20 μm

Figure 3.51

Proximal to the level of its origin, the number of functional groups found in the ventral ligament increases. There are approximately 3 additional functional groups/100 μm travelled proximally over the range 0 μm-800 μm. Further proximally, the number of functional groups in the ventral ligament declines as the attachment cells terminate on the distal-most dendrites of the ventral ligament. The dorsal ligament has a more abrupt distal origin that the ventral ligament, as it arises from the proximal end of the cuticular rod of the apodeme complex. The dorsal ligament can be subdivided into 10-15 functional groups at most proximo-distal levels. Error bars indicate estimated measurement error based upon 10 repeated measurements from the same image.

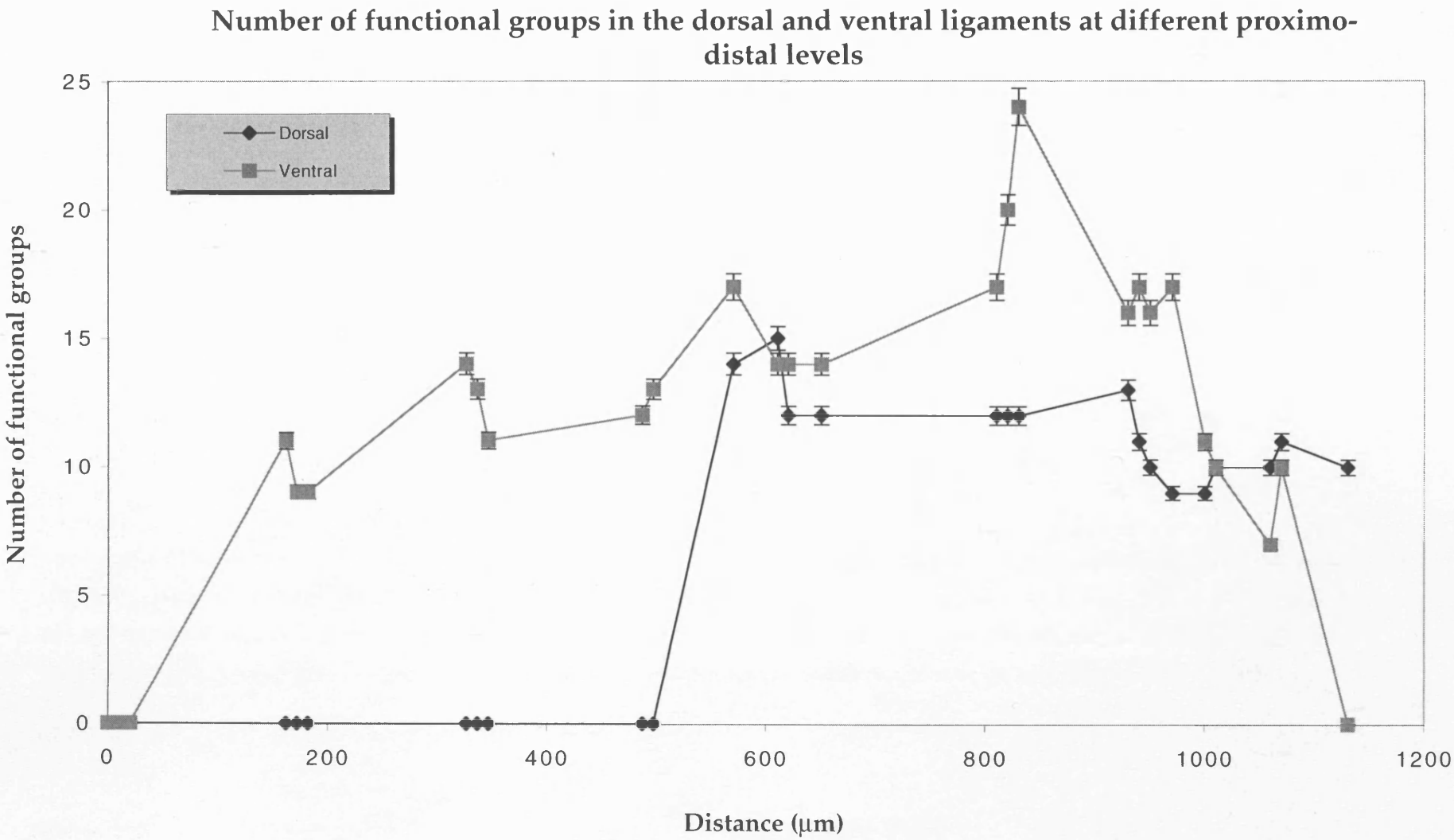
Number of functional groups in the dorsal and ventral ligaments at different proximo-distal levels
Dorsal
Ventral
Number of functional groups
25
20
15
10
5
0
0
200
400
600
800
1000
1200
Distance (µm)

Figure 3.52

The mean 'functional-group' cross-sectional area in the dorsal ligament increases in size proximally, reaching a maximum of approximately 90 μm^2 at a proximo-distal level of 1000 μm. Further proximal to this level, the mean 'functional-group' cross-sectional area declines. In the ventral ligament, the mean functional-group cross-sectional area remains between 50 μm^2 - 70 μm^2 at most proximo-distal levels. Error bars indicate estimated measurement error based upon 10 repeated measurements from the same image.

Functional group's mean cross-sectional areas in the dorsal and ventral ligaments at different proximo-distal levels

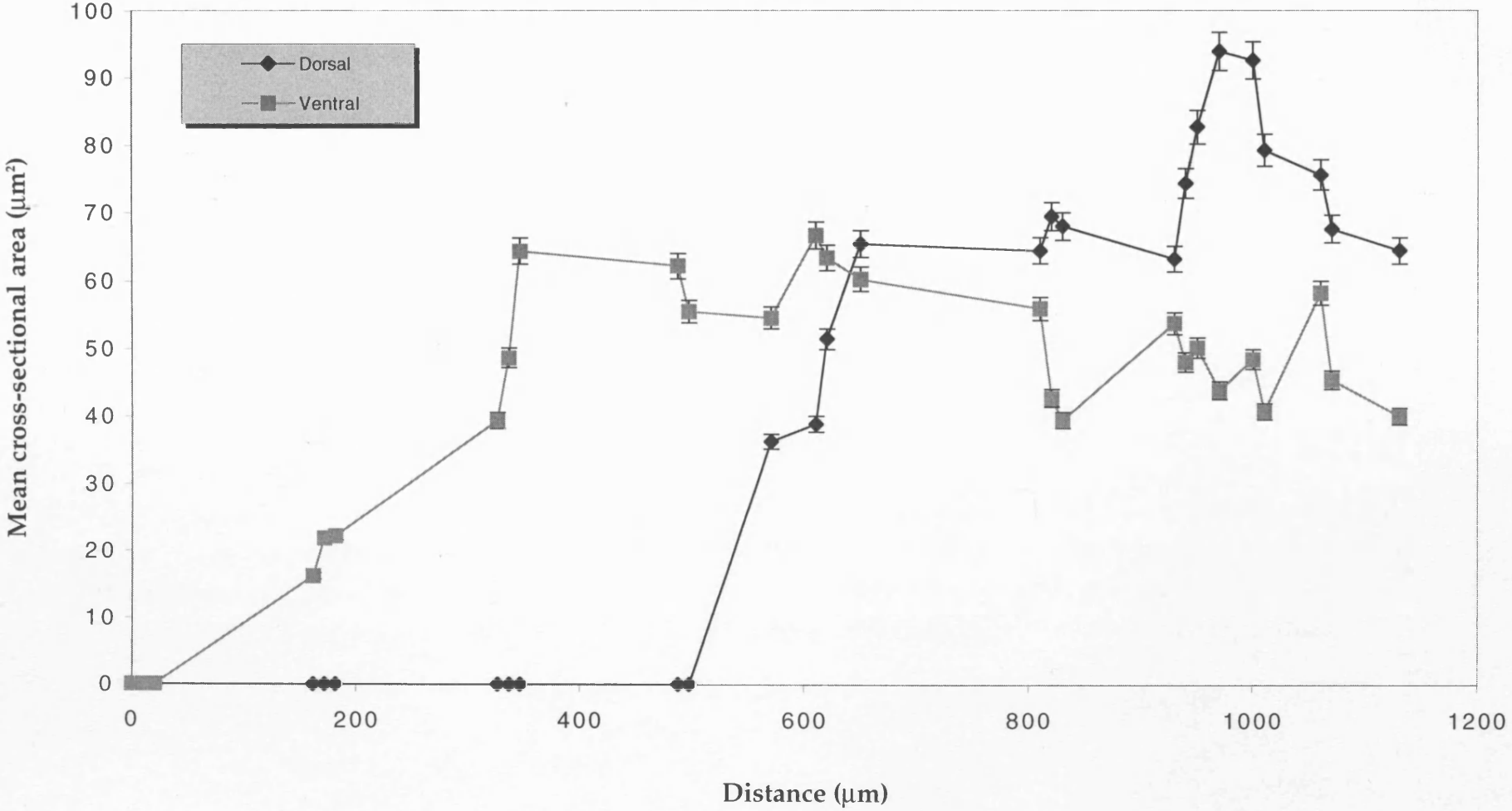

Figure 3.53

Each functional group shown in this graph was traced along the length of the apodeme complex and consisted of two attachment cells at all proximo-distal levels. Both functional groups show increases in cross-sectional area at the proximo-distal levels corresponding to the level at which the attachment cell nuclei were located. The functional group traced along the dorsal ligament is characteristically larger in cross-sectional area than that traced along the ventral ligament.

Cross-sectional areas of two individual functional groups from the dorsal and ventral ligaments at different proximo-distal levels

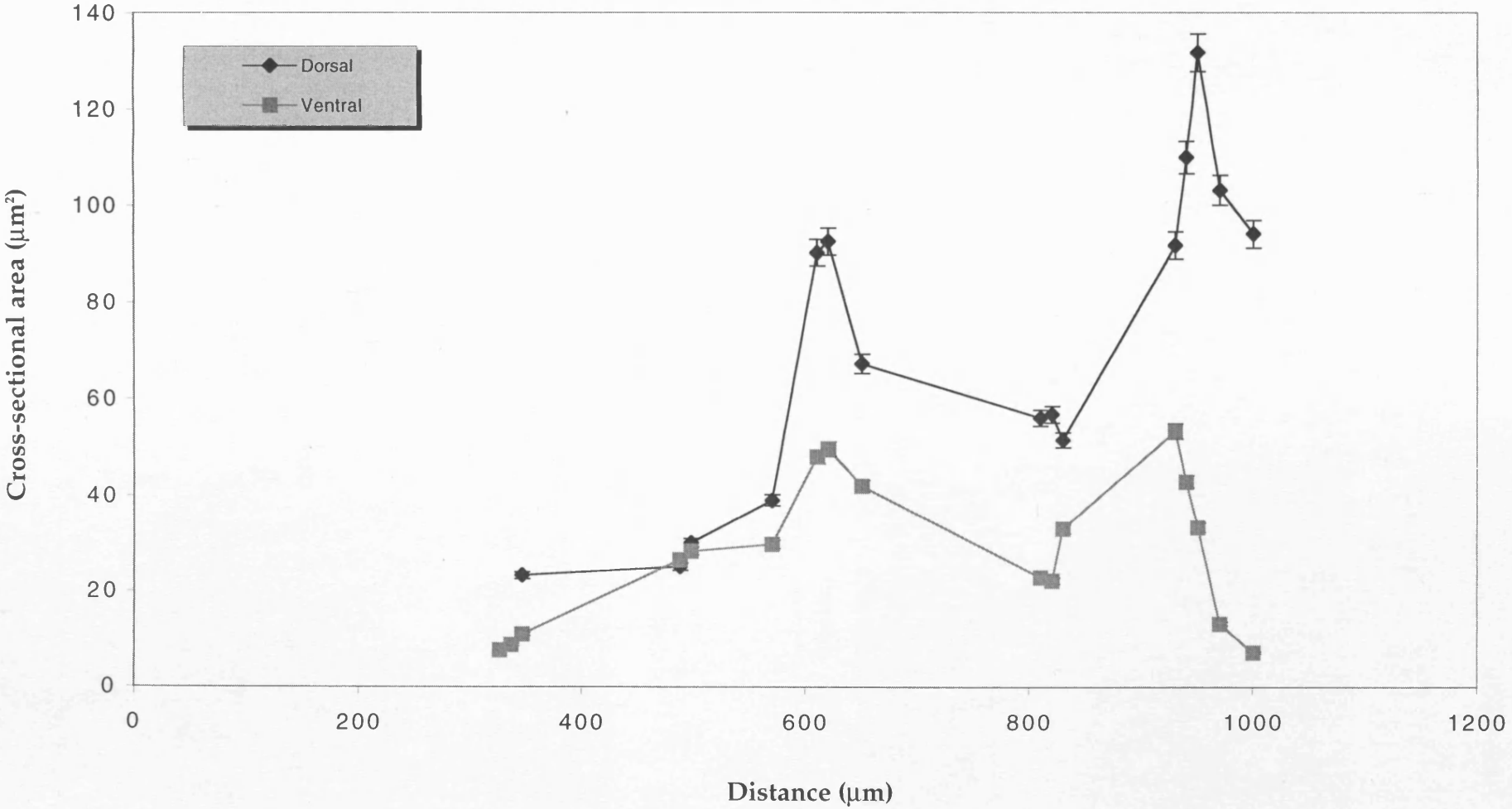

Figure 3.54

This figure consists of a series of size-frequency histograms showing the cross-sectional areas of the functional groups in the dorsal and ventral ligaments of the apodeme complex at four proximo-distal levels (a - d). The histograms show that the dorsal ligament contains fewer and larger functional groups than the ventral ligament at all four levels. The four levels are indicated on the semi-schematic diagram below.

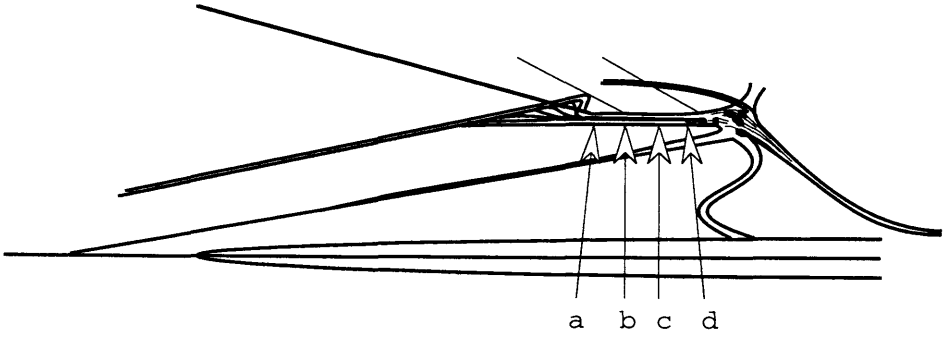

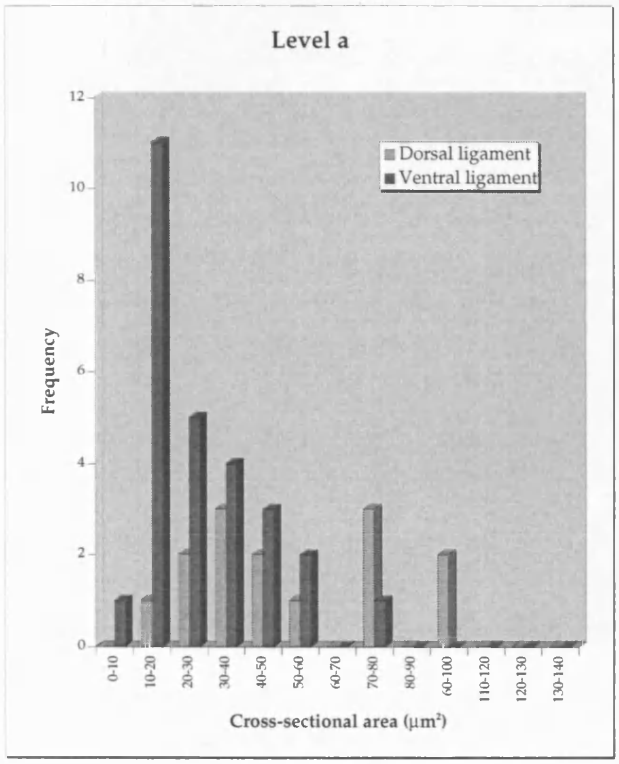
Level a
Dorsal ligament
Ventral ligament
Frequency
Cross-sectional area (μm²)
0-10
10-20
20-30
30-40
40-50
50-60
60-70
70-80
80-90
90-100
110-120
120-130
130-140

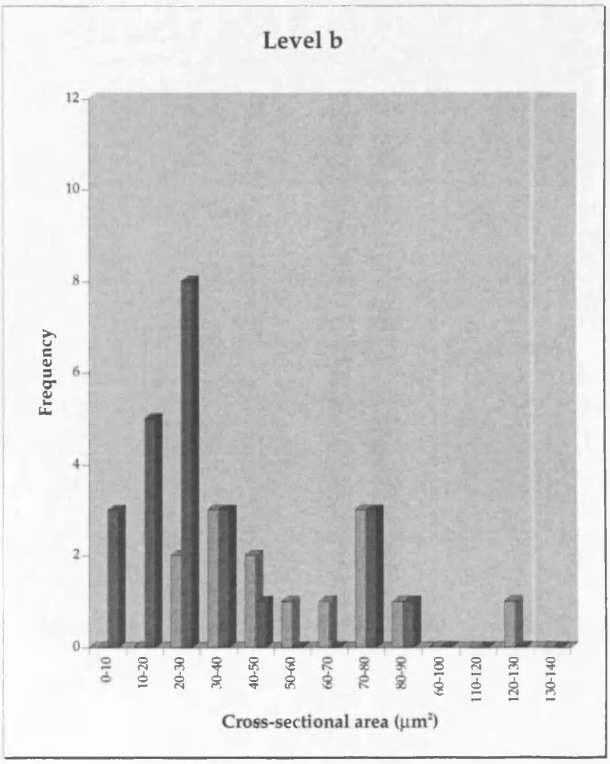
Level b
Frequency
Cross-sectional area (μm²)

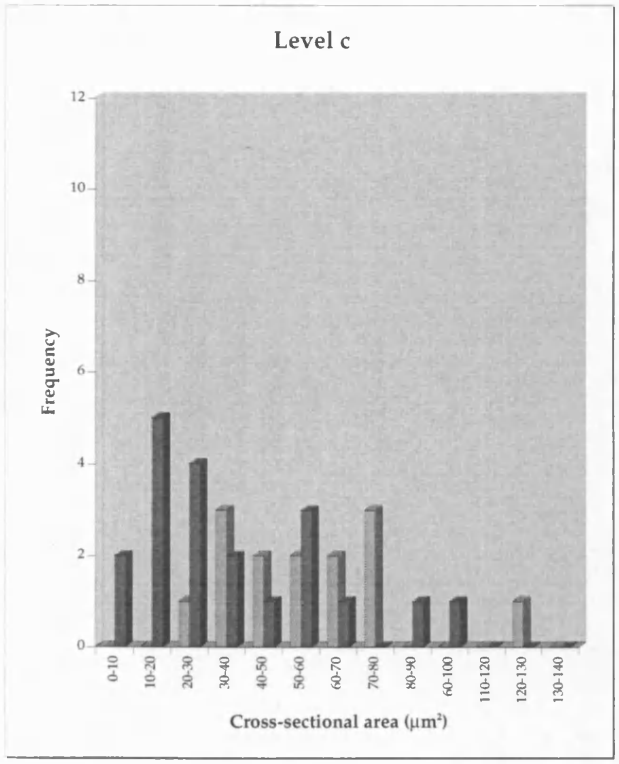
Level c
Frequency
Cross-sectional area (μm²)

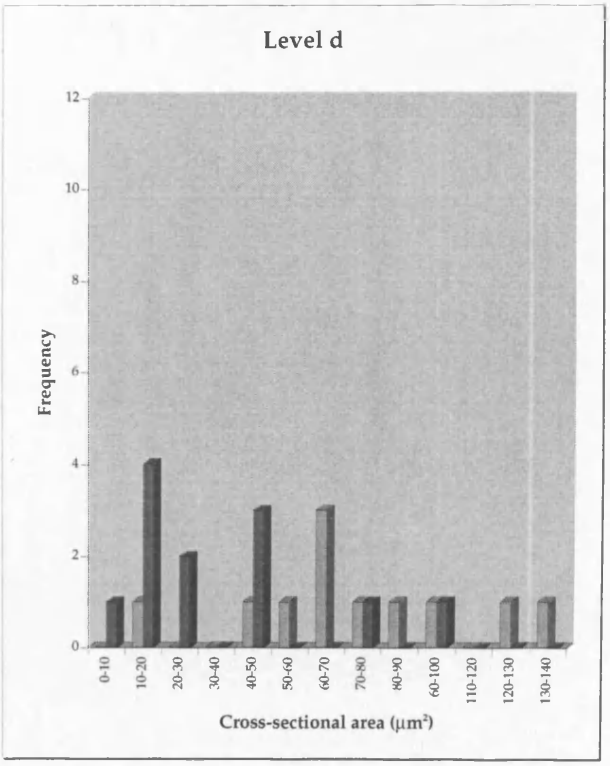
Level d
Frequency
Cross-sectional area (μm²)

Figure 3.55a, b

This figure shows complementary phase contrast (**a**) and confocal fluorescence (**b**) micrographs of the severed end of the apodeme complex. The apodeme complex was severed midway along the length of the ligaments, stained with 5% CF, and gently teased to create a frayed end. Individual extracellular fibres (arrows) can be seen using both microscopical techniques.

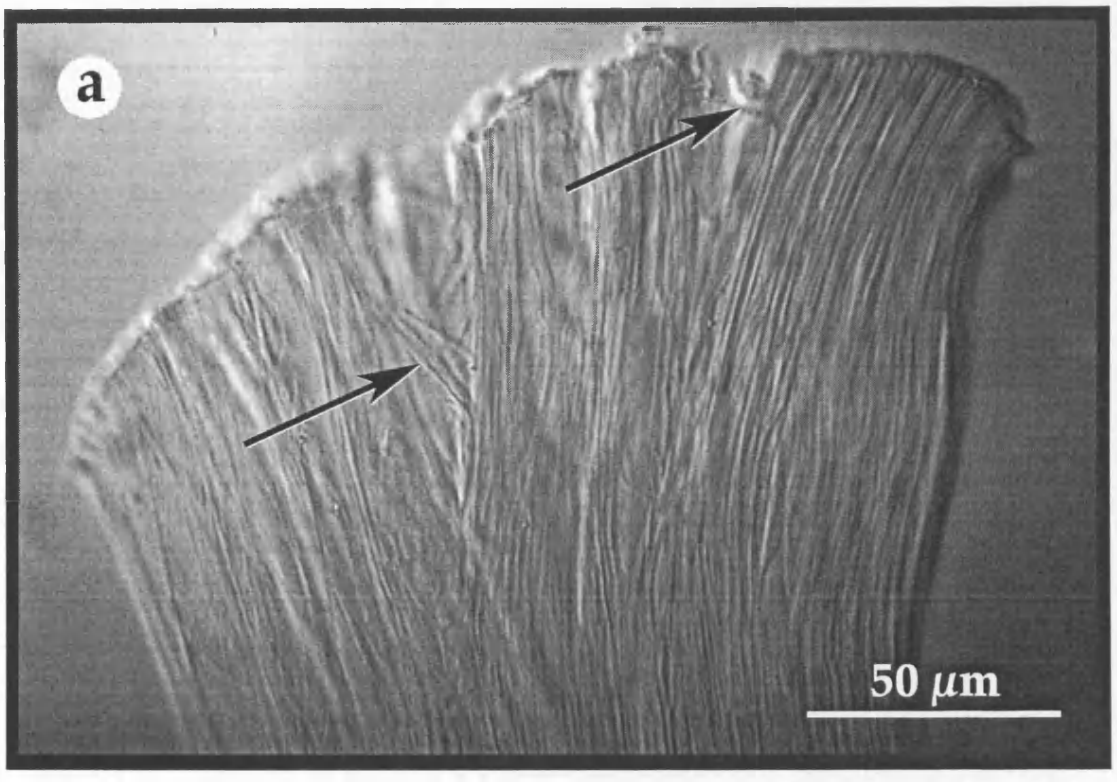
a
50 μm

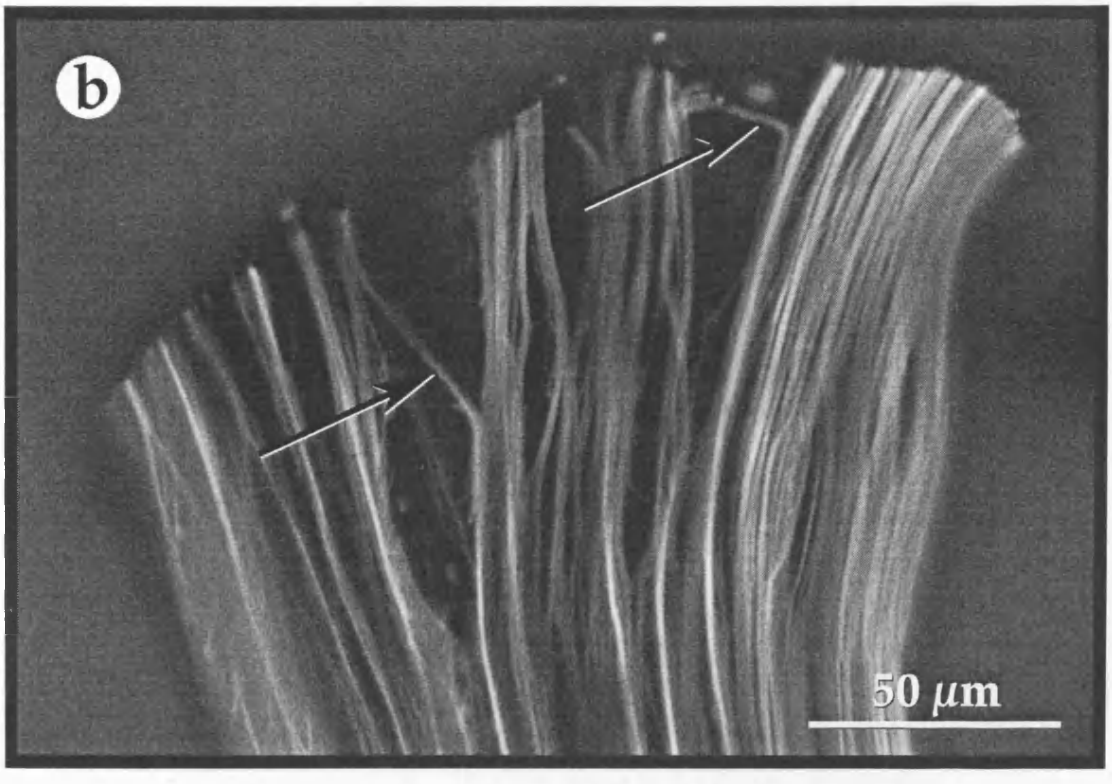
b
50 μm

Figure 3.56a-d

This figure of extracellular fibres in the apodeme complex shows a z-series of confocal micrographs taken with the confocal aperture closed down such that the depth of field was less than the diameter of an attachment cell. This series is taken midway along the apodeme complex ligaments. Proximal is to the upper right and distal is to the lower left of each micrograph.

a

Close to the surface the extracellular fibres in the apodeme complex sheath are numerous and appear to form a meshwork.

b

This optical section is taken a little further into the body of the ligaments. The extracellular fibres which appear most intensely are those located between adjacent attachment cells. Some of the superficial meshwork of sheath fibres can still be detected but appear faint because they are on the limits of the optical section.

c

This optical section is taken from 'within' the ligaments, at a level at which the sheath fibres are outside the focal plane. The extracellular fibres observed in this section are those running longitudinally between adjacent attachment cells, which appear dark (arrowheads).

d

As the focal plane is moved further through the ligaments, the extracellular fibres appear once more as a branching network.

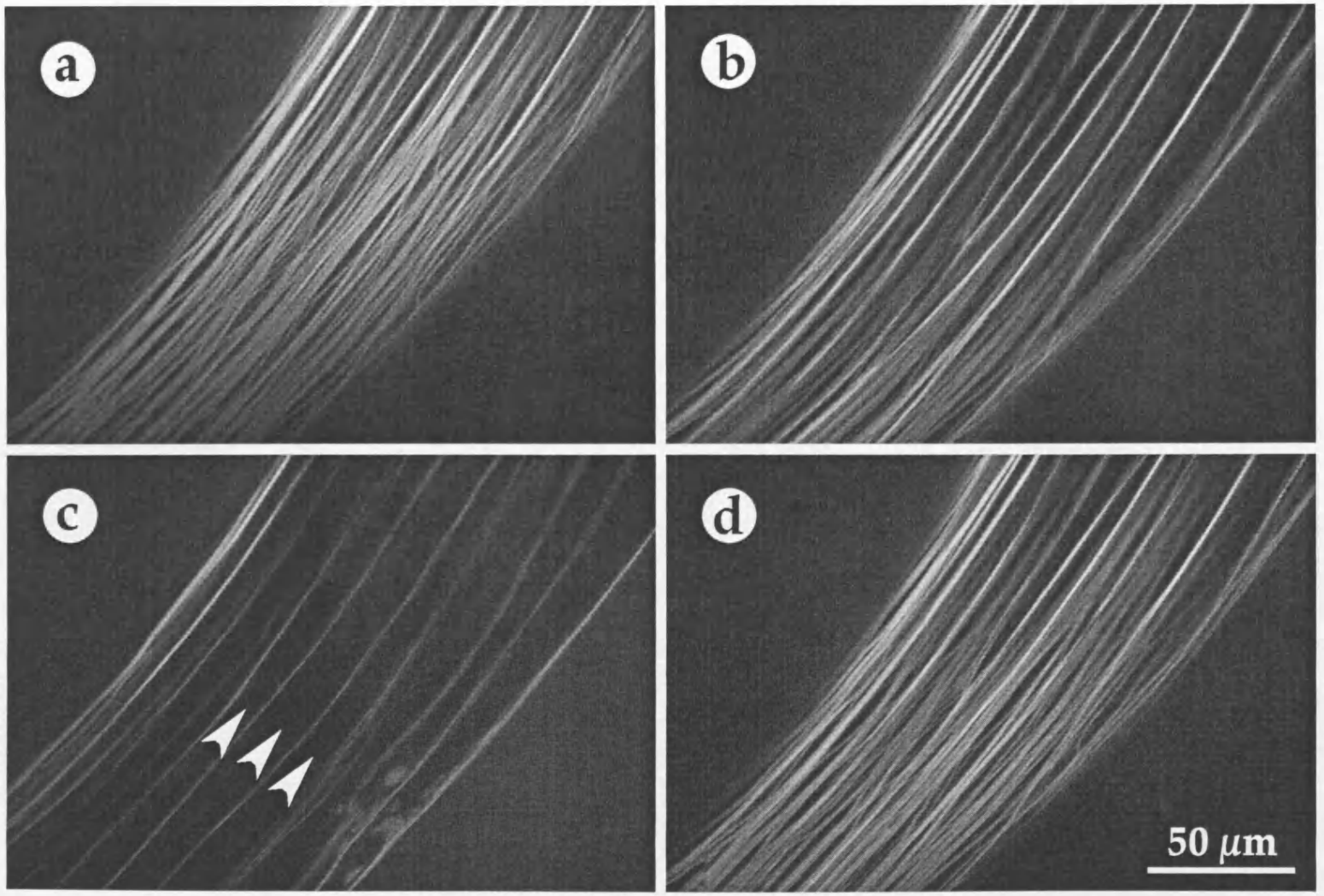
a
b
c
d
50 μm

Figure 3.57

This confocal micrograph shows the extracellular fibres in the dorsal (d) and ventral (v) ligaments immediately distal to the sensory neurones. Distal is to the right. As the fibres enter the cell-body region the extracellular fibres change in appearance and orientation. Whilst the extracellular fibres within the dorsal ligament remain orientated along the axis of the organ and have a uniform appearance with minimal fibre branching, those within the ventral ligament become increasingly branched and irregular in their orientation.

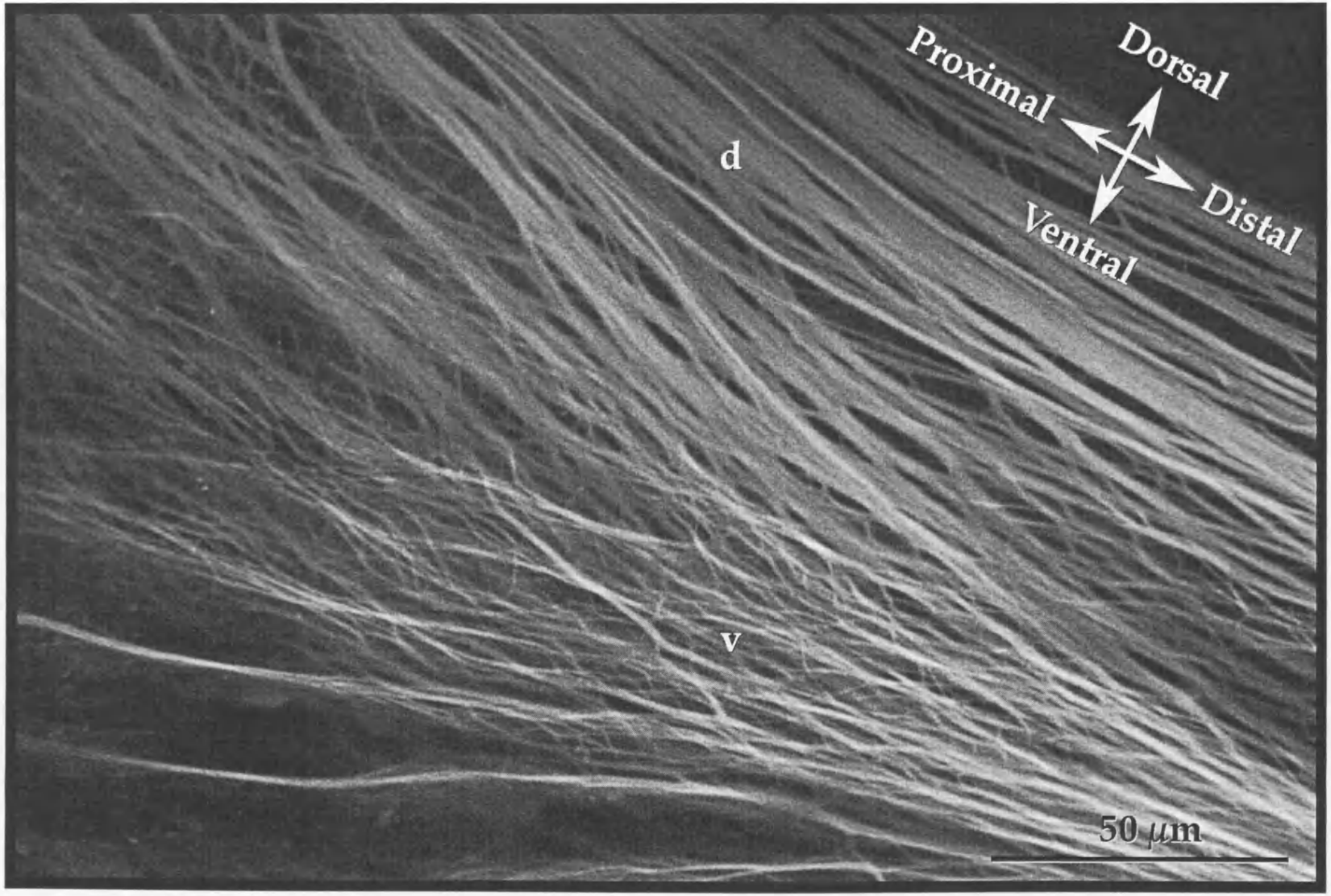
Dorsal
Proximal
Distal
Ventral
d
v
50 μm

Figure 3.58

The CF stained extracellular fibres (F) are shown to associate closely with the sensory neurones in this confocal micrograph. The fibres appear to surround each individual dendrite (d). There is also CF stained extracellular material located between the closely-packed neurone cell somata (cb).

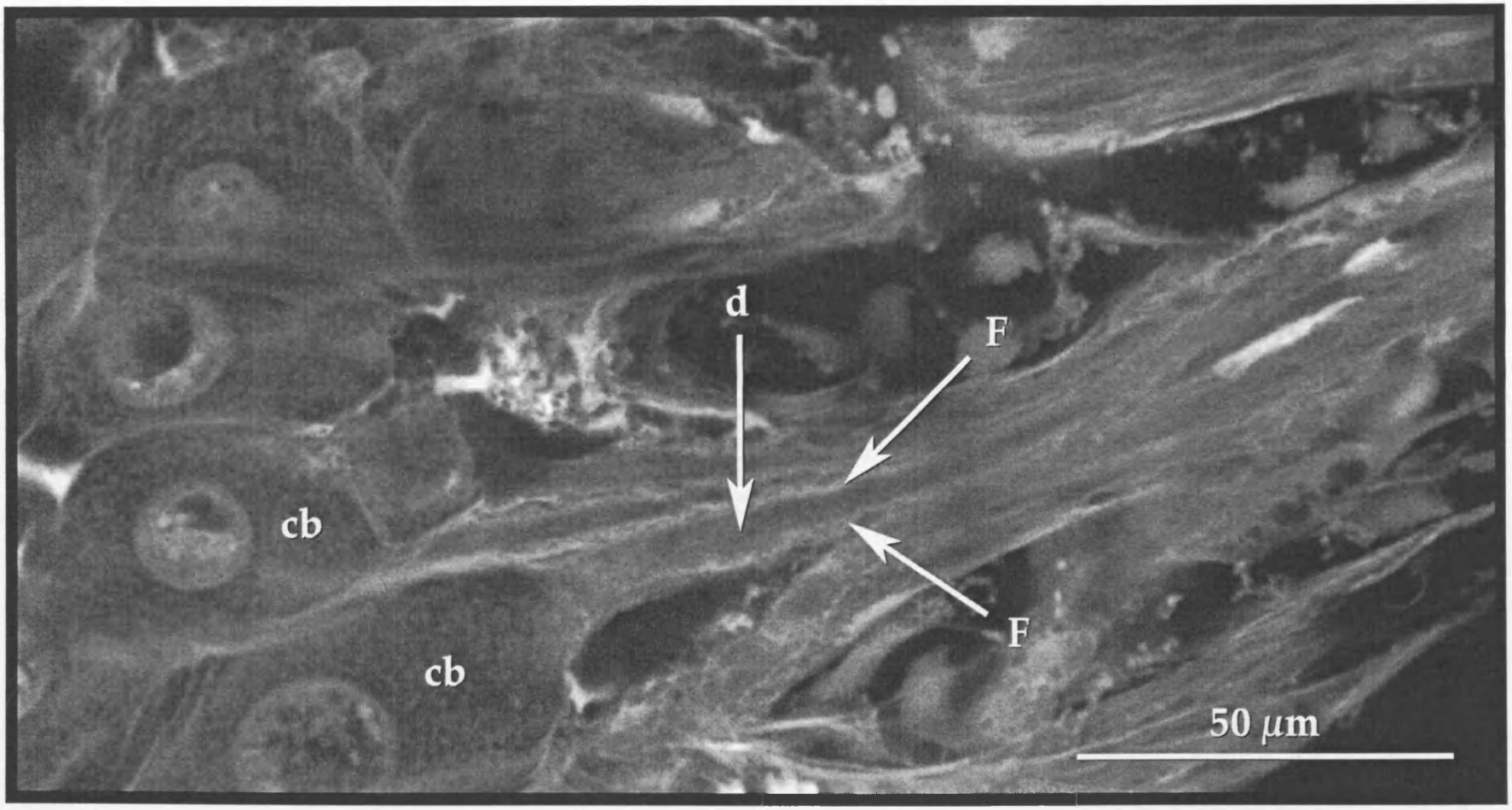
d
F
cb
F
cb
50 μm

Figure 3.59

This confocal micrograph demonstrates the presence of a fibrillar interface at the level at which the sensory dendrites (d) arise from the cell bodies (cb) of the sensory neurones. Distal is to the right. The extracellular fibres (F) are longitudinally orientated as they run along the dendrites (d), whereas they form a mesh-like pattern (Fm) at the level at which they reach the sensory cell bodies.

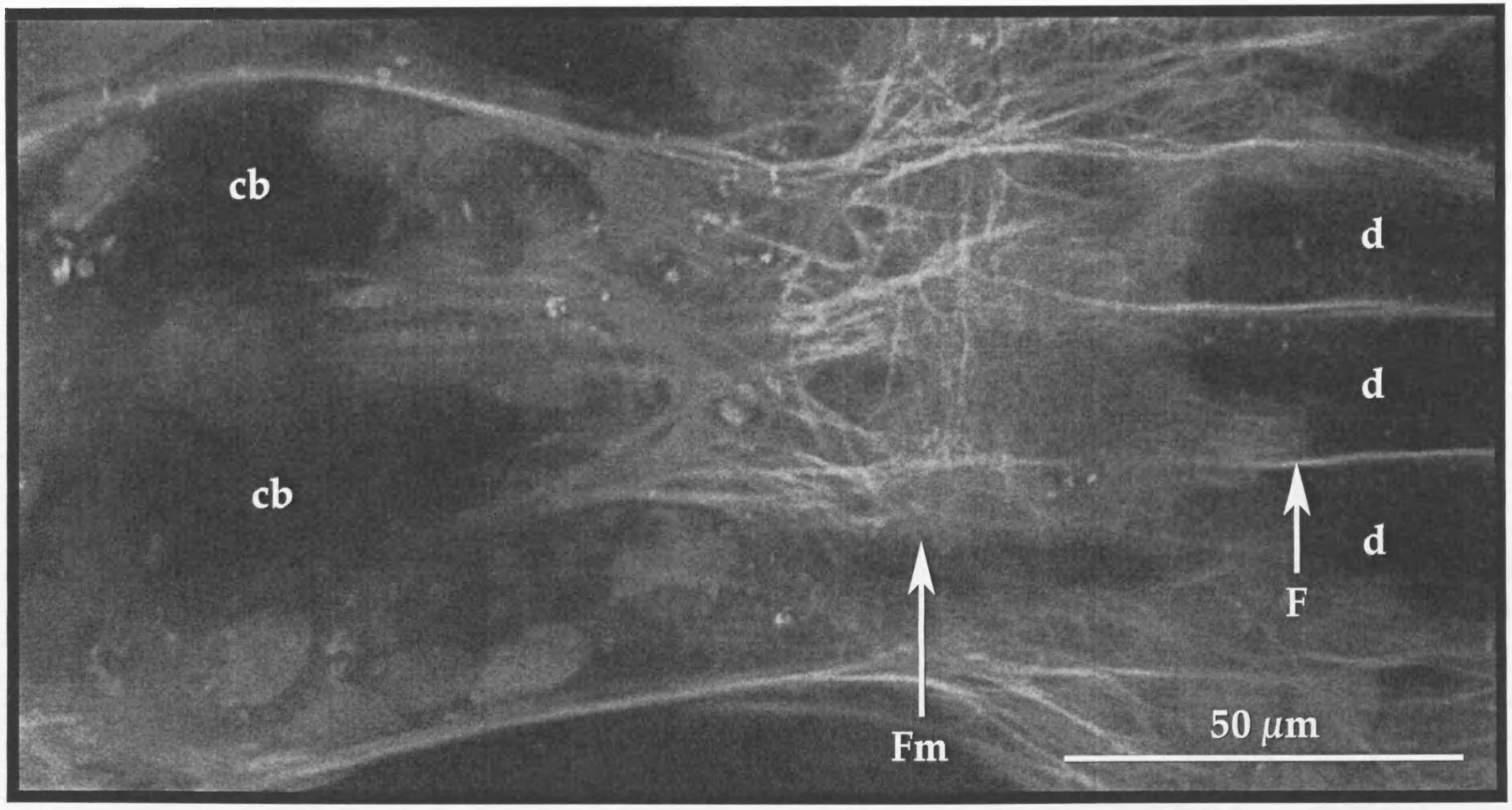
cb
cb
d
d
d
F
Fm
50 μm

Figure 3.60

a

Light micrograph obtained using Nomarski optics of a single large sensory neurone cell body after staining with CF. Distal is to the right. The periphery of the cell body (cb) and the base of the dendrite (d) can be made out.

b

When the same cell is visualised using confocal microscopy, stained extracellular fibres (F) can be seen clearly both at the level of the base of the dendrite and around the periphery of the neurone cell body. To provide an optical section, the confocal aperture was shut down so that the focal plane was less than the diameter of the neurone cell body.

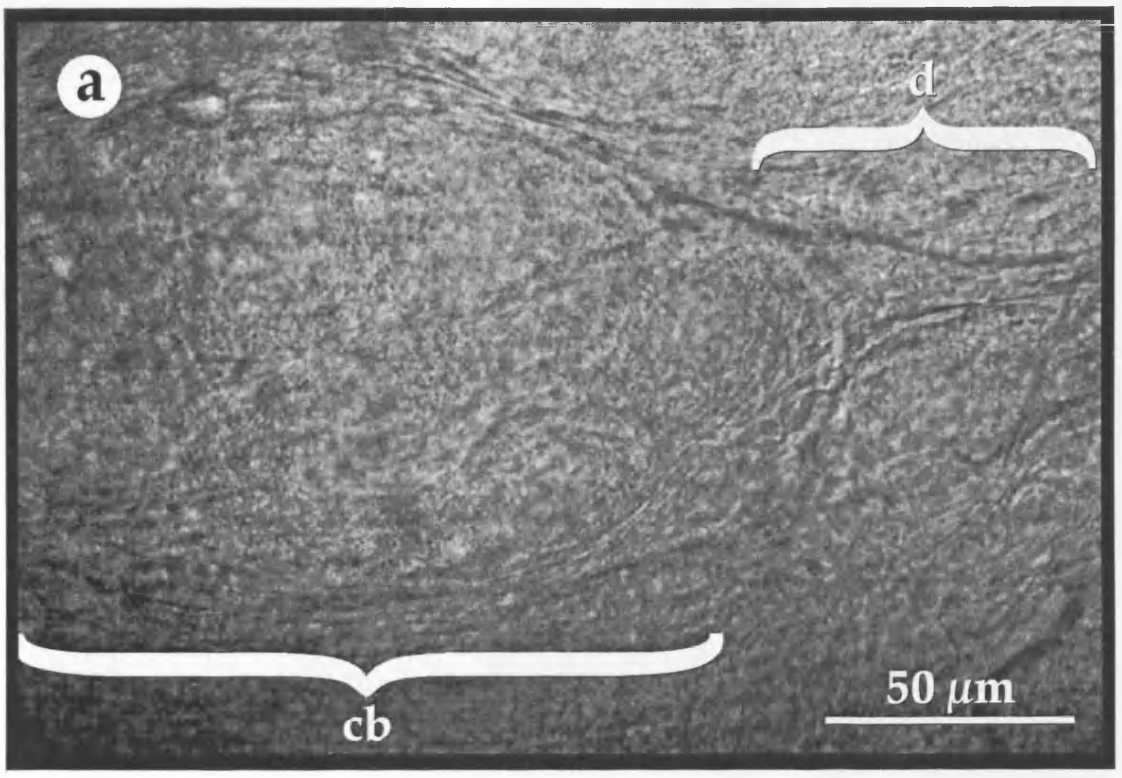
a
d
cb
50 μm

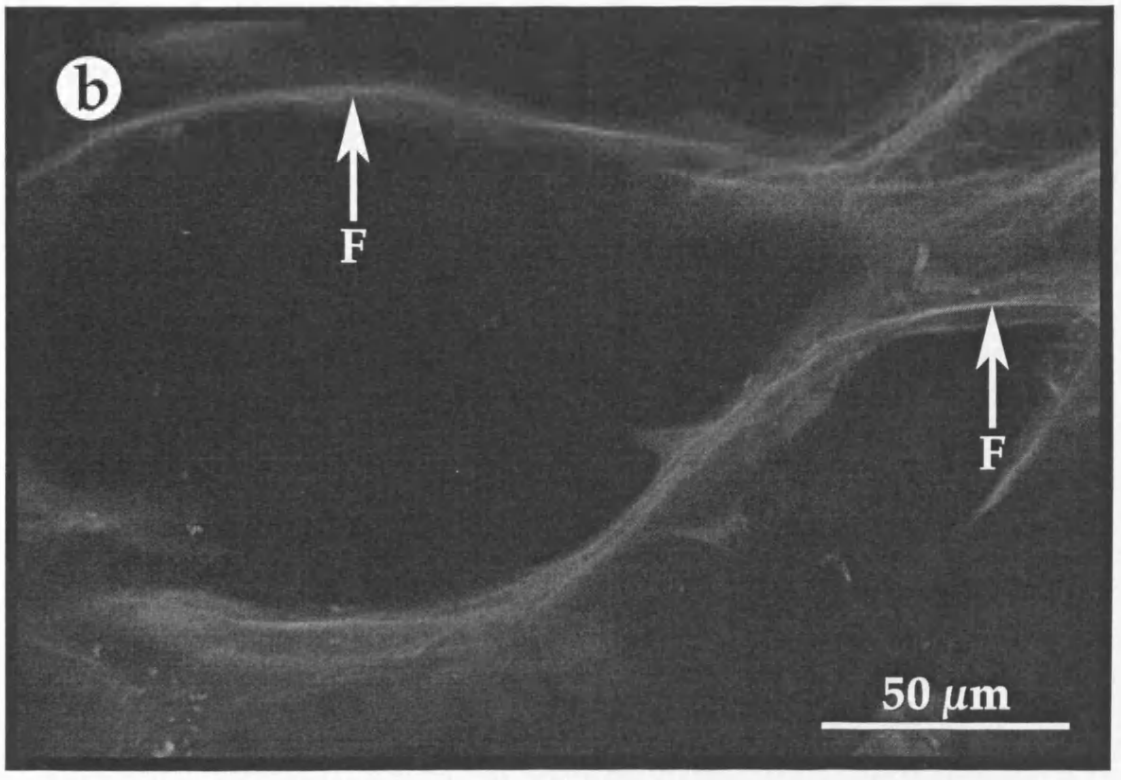
b
F
F
50 μm

Figure 3.61

This pair of confocal micrographs (**a**, **b**) show the location of the cell body (cb) of a single sensory neurone. The two micrographs were taken at slightly different focal planes to demonstrate the reticulated sheath (arrowheads) formed by the extracellular fibres around the somata of the sensory neurone. Distal is to the right.

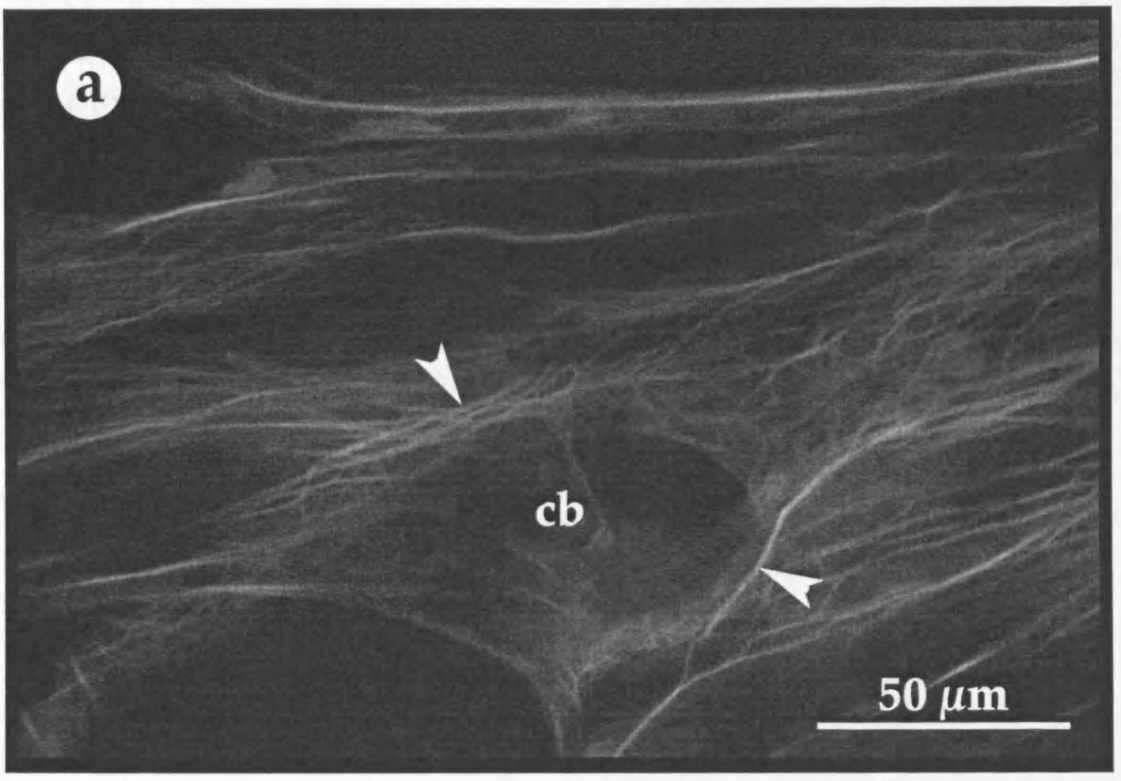
a
cb
50 μm

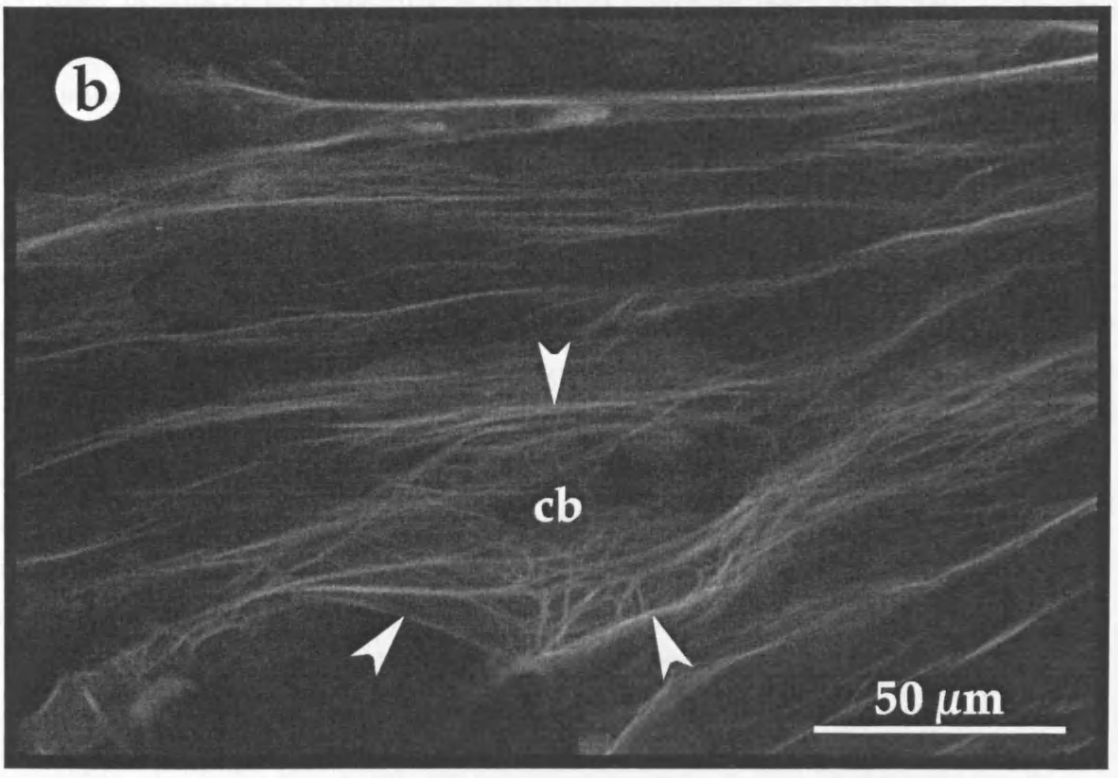
b
cb
50 μm

Chapter 4: Distribution and morphology of sensory neurones in the mtFCO scoloparia of *S. gregaria* and *L. migratoria*.

4.1 SUMMARY

- *Although the neurones comprising the mtFCO superficially appear to be structurally similar, this study shows that six populations of neurones can be identified reliably in all preparations. Some of the six populations may be further subdivided. Comparison of the current results with published descriptions of the distributions of mtFCO neurones of known response types indicates that cell orientation and anatomy may contribute to neurone response characteristics. There is a basis for attributing some of the variation in operational ranges and response types of the mtFCO sensory neurones to their positions and orientations within the scoloparium. However, the situation is complicated as each of the six morphologically identified neurone populations contains representatives from more than one response type.*

4.2 INTRODUCTION

This chapter is concerned with the anatomical characterisation of the mtFCO receptors and investigates whether there is any evidence for regional subdivisions of the scoloparium into identifiable groups of neurones.

For most proprioceptors sensory input is encoded in the form of an action potential discharge that varies with the nature of the sensory stimulation. In the case of the mass response of the locust mtFCO nerve, tonic activity is known to vary with the femoro-tibial joint angle (Runion and Usherwood, 1966). Recordings from single neurones also show that the mtFCO encodes sensory information relating to the velocity and acceleration components of joint rotation (Matheson, 1990). Although he did not use an ideal stimulus regime (he used ramps and steps instead of sinusoids), Matheson's (1990) results provide evidence that the mtFCO sensory units not only respond to position, velocity or acceleration but that many of them respond to combinations of these modalities.

It is known that individual mtFCO sensory neurones respond over discrete ranges of femoro-tibial angles (Usherwood *et al.*, 1968; Burns, 1974; Zill, 1985a, Matheson, 1992b). Therefore, the discharge of the organ at any

particular femoro-tibial angle consists of the combined responses from several neurones whose sensitivity ranges overlap. This allows the proprioceptor to increase its sensitivity range whilst retaining its ability to discriminate small increments within the stimulus range. This phenomenon has been termed 'the range fractionation principle' (Cohen, 1964).

The mtFCO scoloparium is composed of approximately 50 individual scolopidia, each of which consists of a pair of sensory neurones. The paired dendrites of each scolopidium have ciliary structures at their distal tips, and each pair is associated with one attachment cell (Slifer and Sekhon, 1975; Young, 1970; Matheson and Field, 1990). As in other sense organs such as hair sensilla and campaniform sensilla (see French, 1988), the dendritic cilia of COs have a 9+0 configuration of microtubules (Young, 1970; Yack and Roots, 1992).

It remains unclear what mechanism determines the sensitivity range of particular mtFCO neurones and what it is that determines the components of the stimulus (position, velocity, and acceleration) that are effective in generating sensory output. One possibility is that the attachment strands of chordotonal organs stimulate all the sensory units simultaneously and that specificity to different stimuli is achieved by populations of neurones having different physiological properties. Usherwood *et al.* (1968) demonstrated that many of the mtFCO units fire simultaneously, although remarked that they are never all active at the same time. However, Zill (1985a) demonstrated that the neurones could be classified by their electrophysiological characteristics into two main categories (tonic and phasic). His study provided definitive evidence that the physiological properties of individual neurones are important in determining their response characteristics.

More recently (Field, 1991; Shelton *et al.*, 1992; Nowel *et al.*, 1995) suggested that the nature of the mechanical coupling of the sensory units to the femoro-tibial joint may allow distinct populations of neurones to respond over discrete ranges of femoro-tibial articulation. Earlier studies of the locust mtFCO have revealed that the sensory neurones may indeed be arranged in discrete clusters. Usherwood *et al.* (1968) suggested that the 24 neurones he observed could be classified into three groups and although

subsequent authors have been able to visualise increasing numbers of mtFCO neurones (Zill, 1985a; Grosch, 1985; Burrows 1987a; Pflüger, 1988), none of them suggested that there might be more than three groups. Burns (1974) similarly identified 3 neurone clusters in the distal scoloparium of the pro- and mesothoracic chordotonal organs. Theophilidis (1986a) reported that in *Decticus albifrons* the CO nerve is divided into four separate groups of axons at the point where it leaves the main scolopidium. This suggests that there is an anatomical segregation of neurones. Matheson and Field (1990) demonstrated the presence of a substantial group of previously undescribed small neurones extending distally along the ventral ligament. Recalling that the COs of the pro- and mesothoracic legs consist of both proximal and distal scoloparia, Matheson and Field (1990) suggested that the distal population of neurones in the mtFCO is homologous with the proximal scoloparium and that the rest of the mtFCO is homologous with the distal scoloparium.

It has been suggested that differences in the attachment of individual scolopidia to their attachment cells in stretch receptors may allow similar units to respond to different elements of the stimulus by virtue of their mechanical coupling (Moulins, 1976). On the other hand, with respect to the mtFCO there is also the possibility that physiological differences between populations of neurones derived from the proximal and distal scoloparia are responsible for differences in response characteristics between neurones from the two sources. Evidence to support this hypothesis was produced by Zill (1985a) who demonstrated that neurones with different response characteristics exhibited different electrophysiological properties when examined using current injection techniques. This implies that at least some of the neurones have intrinsically different properties which are irrespective of their mechanical coupling.

In an attempt to relate the position of scolopidia in the mtFCO with their neuronal output, Matheson (1990) measured the response properties of individual neurones to a varied stimulus regime before filling the cells with cobalt chloride to reveal their locations. This enabled the compilation of a map of the scoloparium which indicated that at least some neurones with comparable responses are grouped in clusters.

This chapter categorises the sensory neurones into discrete populations using a variety of morphological criteria and characterises their positions relative to the structures coupling the scolopidia to the femoro-tibial joint. These populations are compared with the maps produced by Matheson (1990) on the basis of neurone response characteristics. The ultrastructure of the scolopidia is investigated to reveal whether there is any evidence for anatomical differences between different populations of neurones or the ways in which they are linked to their respective attachment cells.

4.3 MATERIALS AND METHODS

4.3.1 Dissection and embedding

The mtFCO was exposed by the removal of windows of cuticle from the anterior and posterior sides of isolated femora. The extensor tibiae muscle and associated tracheae were dissected out and the preparations were fixed in Karnovsky's (1965) solution at 4°C for 30 - 60 minutes. Some preparations were post-fixed in phosphate buffered 1% osmium tetroxide for 20-30 minutes. The legs were subsequently rinsed in several changes of phosphate buffer, dehydrated through an acetone series, and transferred through several changes of electron microscopy (EM) grade Araldite before final embedding.

MtFCOs for examination using conventional light microscopy were dissected out in Araldite and mounted under number 0 coverslips on cleaned glass slides. Preparations for sectioning were similarly dissected and mounted in softer (see Appendix 1) EM grade Araldite sandwiched between two siliconised (Repelcoted) slides. All mounted material was cured overnight on a 35°C hotplate. The Repelcoted slides were removed from the preparations to be sectioned, leaving the mtFCO embedded within a thin plastic sheet. The plastic was trimmed to allow the mtFCO to be orientated axially within a conventional embedding stub. The stubs were filled with standard EM grade Araldite and cured overnight in an oven at 60°C. Softer (see Appendix 1) Araldite was used during the initial embedding of these preparations to prevent it becoming brittle during the second curing.

Embedded organs were sectioned transversely using a Huxley ultra-microtome. Sections to be viewed using conventional light microscopy

were cut at 1 μm, mounted on subbed slides (see Appendix 1) and stained with Toluidine Blue (see Appendix 1). Number 0 coverslips were then mounted using EM grade Araldite. Material for examination using transmission electron microscopy (TEM) was sectioned at 0.1 μm. Sections were mounted either on hexagonal (200 mesh) 3.05 mm diameter copper grids or were picked up on pioloform (Agar aids) films and mounted on copper slot (0.5 mm) grids. These sections were subsequently stained with uranyl acetate and lead citrate and were viewed using a Jeol 100CX TEM.

4.3.2 Cobalt filling of the sensory neurones

The mtFCO sensory neurones were visualised by retrograde filling of the cells with 45% hexamminecobalt (III) chloride in distilled water (hereafter referred to as cobalt) (after Altman *et al.*, 1980). On each metathoracic leg a small window of cuticle was removed from the anterior face of the mid-femur to expose a length of mtFCO nerve 2-3 mm proximal to the organ. A syringe with a blunt-ended 28 gauge 50 mm needle was used to build a small coiled bath of white non-toxic Vaseline at the edge of the dissection window into which a drop of dye was placed. The CO nerve was severed and the cut end was placed into the bath using a fine glass hook. The exposed nerve was covered with Vaseline to prevent desiccation and a Vaseline cap was added to the bath. To prevent the evaporation of haemolymph, the remainder of the dissection window was also sealed with Vaseline. Preparations were kept in sealed petri-dishes at 4°C for 7-10 days after which the Vaseline baths were removed and the femora with filled nerves were severed from the locusts. Cobalt within the sensory neurones was precipitated using ammonium sulphide and the preparations silver intensified (after Bacon and Altman, 1977). The preparations were then fixed in the flexed position using Karnovsky's (1965) solution before being dissected and mounted as described above.

4.3.3 Image analysis

The positions, sizes and orientations of 1308 cobalt-filled neurones from 18 preparations were characterised using image analysis techniques. Preparations were viewed using an Olympus BH-2 Photoscope coupled to a 8100/80 PowerMacintosh computer equipped with a Scion Corporation AG-5 video rate frame-grabber card. A 63x oil immersion objective and JVC TK-1085E single chip CCD camera were used to capture a real time video image of the preparation which was displayed on a 17 inch

computer monitor using NIH Image (vs. 1.62/ppc) software. Manipulating the microscope stage controls allowed the image to be focused and the preparation to be scanned at high magnification.

Individual neurones were characterised using an adaptation of an existing NIH Image macro written by Bob Rodieck (Department of Ophthalmology, University of Washington, Seattle) (see Appendix 2). The macro executed a routine by which an arbitrarily shaped closed profile could be characterised in a quantitative manner. Each neurone cell body was characterised by the generation of its best-fitting ellipse.
Each generated ellipse had:

- - the same area as the cell body
- - the same centroid as the cell body
- - the same second-order-moments as the cell body (orientation of the ellipse)

The macro was modified to allow the profile of each cell to be indexed, stored and superimposed upon the live video image (see Appendix 2). This enabled neurones that had been characterised to be distinguished from those yet to be measured. Various parameters characterising each neurone profile were measured by the macro and stored with an index number linking each set of measurements to the appropriate cell.

The area of each filled neurone cell body was measured (in μm^2) by tracing its outline with a freehand tool (Fig. 4.1). The execution of the macro plotted the best-fit ellipse and the lengths of the major and minor axes were returned in μm. The ratio of the major and minor axes of the best-fitting ellipse provides an indication of the shape of an object and is defined as the particle's anisometry (Medalia, 1970). The orientation of each neurone relative to the axis of the femur was returned in degrees. A positive value indicated that the distal end of the cell was inclined dorsally with respect to the proximo-distal axis of the mtFCO; a negative value indicated that the inclination was ventral. The rotating stage of the photoscope was adjusted such that the axis of the mtFCO was at 90° to that of the CCD camera. This ensured that the orientations of neurones from different preparations were directly comparable.

4.3.4 Statistics

Statistical comparisons were used to reveal whether the neurone populations identified in this study differed significantly from one another with respect to the sizes, shapes or orientations of their neurones. Each data set was initially tested for normality using either Kolmogorov-Smirnov (n = <50) or Shapiro-Wilk (n = >50) normality tests (Zar, 1984; Shapiro, 1965, 1968). Log-transformation was carried out where necessary in order to normalise the data so that the same statistical techniques could be used in all cases. The degree of variation within and between each neurone population was tested with respect for each parameter (size, shape and orientation) using single factor analysis of variance tests (ANOVA). The distribution of the variance between populations was subsequently determined by Student-Newman-Keuls (SNK) multiple comparisons. Thus, the presence of significant differences between neurone populations were indicated (ANOVA) and the individual populations were then grouped into homogeneous subsets (SNK multiple comparisons).

4.4 RESULTS

4.4.1 Organisation of the scoloparium

Several authors have suggested that the mtFCO sensory neurones fall into discrete populations (Usherwood *et al.*, 1968; Burns, 1974; Zill, 1985a; Matheson and Field, 1990). Whole organs were lightly stained with OsO_4 to see whether there was any evidence for anatomical subdivisions within the scoloparium. It was found that discrete areas of the scoloparium stain differentially with the nerves and cell bodies staining most intensely. Distinct lobes containing cell bodies can be seen to be related to different branches of the mtFCO nerve. These lobes are distributed consistently in all preparations and they were characterised with an outline map (Fig. 4.2). It was found that the CO nerve divides into two main branches at the point at which it enters the mtFCO scoloparium. This suggests that the sensory neurones can be divided into two main groups depending upon whether they are innervated by the dorsal or ventral branch of the nerve.

Preparations in which the neurones had been filled with cobalt confirmed that the regions that stain differentially with OsO_4 represent anatomical features and contain the cell bodies of six different populations of neurones (Fig. 4.3). The sensory dendrites extend distally from these

regions. In some cobalt-filled preparations the populations of sensory neurones could be further subdivided into smaller subgroups on the basis of their anatomical appearance and positions. Thus, groups 1 and 2 were subdivided into 1a, 1b and 2a, 2b respectively (see Fig. 4.3). These subgroups were not identifiable in preparations stained with osmium tetroxide. Using 18 cobalt-filled specimens, the same clusters of neurones were found in both *S. gregaria* and *L. migratoria*. The two species were analysed separately.

The neurones comprising the different populations were characterised upon the basis of the position, size, orientation and anisometry (shape) of their cell bodies. The pattern of cell body size distribution is similar in both species (Fig. 4.4). In groups 1 and 2, the proximal subgroups (1a, 2a) consistently contain larger neurones than the distal subgroups (1b, 2b). Group 1a contains the bulkiest neurones in the entire mtFCO in both species. Groups 1b and 2b consist of similarly sized cells in both cases. Groups 4, 5 and 6 consist of smaller neurones in both species, with a mean profile area of approximately 250 μm^2, the smallest cells being found in *L. migratoria*..

All the mtFCO neurone cell bodies are elongated to some extent (Fig. 4.5). Overall, the neurones of *L. migratoria* tend to be more elongated than those of *S. gregaria*. In *S. gregaria*, the neurones of groups 1a, 2a and 3 are the most elongated, all having a mean anisometry greater than 2. In *L. migratoria*, groups 1a, 2a and 3 are also the most elongated having mean anisometries ranging from 2.4 to 2.6.

The orientation of the sensory neurones is also similar in the two species (Fig. 4.6), although *S. gregaria* has a wider range of cell orientations than *L. migratoria* (±40° and ±30°, respectively). In both species, the group 1a, 1b and 6 neurones cell bodies are all orientated such that their proximo-distal axes are inclined positively relative to the axis of the mtFCO apodeme complex (neurones point dorsally). The cell bodies of the remaining groups are orientated with their proximo-distal axes inclined negatively relative to the axis of the mtFCO apodeme complex (neurones point ventrally). The group 1b and group 4 neurones are orientated most obliquely relative to the axis of the organ in both cases.

These results show that the mtFCO does not consist of a collection of identical scolopidia but that neurones located in different regions of the scoloparium have distinct anatomical characteristics. Thus, the neurones can be classified into different populations upon the basis of their morphological attributes alone. Generally, the mtFCO scoloparium of *L. migratoria* consists of smaller, more proximo-distally elongated cells than that of *S. gregaria*. The largest cells in the scoloparium are located proximally in both species, a trend also found in the proximal scoloparium of the femoral chordotonal organ in the cockroach (Burns, 1974), and the cockroach tibio-tarsal chordotonal organ (Young, 1970).

4.4.2 Comparison with published description of response types

On comparing the locations of these morphologically characterised populations with the locations of groups of neurones identified by Matheson (1990) on the basis of response characteristics, several generalisations can be made. Groups 1 and 2 both contain units that Matheson (1990) claimed were sensitive to combinations of sensory modalities. Many were said to display position sensitivity with levels of tonic activity that changed with femoro-tibial angle. However, all units in groups 1 and 2 also responded to other components of tibial displacement. There are no purely position sensitive units amongst these two groups. Group 1 contains a consistently located cluster of cells that each respond to ramp stimulus flexions at femoro-tibial angles close to 0°. Group 2 contains a similar cluster that also responds during ramp stimuli but in this case those causing tibial extension. Because they respond to ramp stimuli it was implied that such neurones are velocity sensitive (Matheson, 1990).

Neurone group 3, located along the dorsal edge of the organ, contains units that discharge when the tibia is stationary (so-called position sensitivity) and also whose discharge is elevated during ramp stimuli (velocity sensitive). They respond over a wide range of leg angles. This was the most numerous of all the response types Matheson (1990) recorded. This group also contains units that discharge at the beginning of ramp stimuli that mimic tibial extension. They were only sensitive at femoro-tibial angles close to full flexion. Because they discharge at the onset of the stimulus where accelerations are maximal, units of this type were said to be acceleration sensitive (Matheson, 1990). In addition, group

3 is the only group in which purely tonic units (positional sensitivity) were found. Such units are situated proximally in the scoloparium, close to the proximal end of the dorsal attachment.

4.4.3 Correlation between cell morphology and response class

To reveal whether or not neurones with similar discharge patterns share any anatomical characteristics, images of cobalt-filled neurones in *L. migratoria* published by Matheson (1990) were captured and subjected to analysis of their anatomical properties as previously described (size, shape, orientation). For this analysis, units that were directionally sensitive were treated as a single class. Also, the orientation data is rectified such that cell orientation is positive either side of the axis of the organ. In many cases there are too few examples to identify statistically significant differences between groups of neurones. However, there do appear to be some trends present. All the neurone profiles represented by Matheson (1990) appear to have similar profile areas (Fig. 4.7a). This reflects the fact that Matheson did not record from any of the small neurones of groups 4, 5 or 6. However, within one of the clusters of neurones characterised by Matheson, the cells do appear to share certain morphological attributes. From examination of Matheson's drawings it appears that adjacent neurones sharing the same response characteristics have similar cell shapes. The anisometry data shows that units responding only to position or velocity tend to have more circular profiles in cross section than cells responding to more than one modality. Acceleration sensitive neurones have particularly elongated cell bodies (Fig. 4.7b). The profiles of the mtFCO neurones represented by Matheson show a range of orientations relative to the axis of the organ. His drawings show that clusters of cells sharing the same response characteristics tend to be similarly orientated. Neurones encoding all three sensory modalities (position, velocity, acceleration) showed the largest deviation from axial orientation (Fig. 4.7c). The position sensitive cells also showed large deviations from the mtFCO axis. The large variations in the level of deviation seen in this type of cell was probably due to low anisometry (tending towards spherical cell bodies) and the fact that few cells of this response class were represented in Matheson's (1990) study.

These results suggest that the anatomical attributes of the sensory neurones are correlated with their function. Although the results from

this data set are inconclusive it suggests that certain sizes, shapes and particularly orientations of cells are best suited for encoding different modalities of the stimulus (Figs 4.7a-c). However, it is unclear to what degree the diversity of function throughout the mtFCO neurones is due to their anatomical characteristics and how much to their position, mechanical coupling and individual electrophysiological attributes.

4.4.4 Structure of the scoloparium

Matheson and Field (1990) proposed that the locust mtFCO was derived from the fusion of a pair of proximal and distal scoloparia homologous with those found in the pro- and mesothoracic legs. Both cobalt-stained and unstained mtFCOs were serially sectioned at 1 μm in order to show how the different populations of neurones were spatially related to one another. The sections were stained with Toluidine blue. Matheson and Field's (1990) hypothesis that the mtFCO scoloparium consists of two fused scoloparia is strongly supported by the innervation, anatomy and spatial distribution of the sensory neurones (Fig. 4.2) within the scoloparium at different proximo-distal levels (Fig. 4.8a-e). Thus, the mtFCO appears to consist of two laterally fused scoloparia, the 'anterior' scoloparium containing the group 1 and 2 neurones and the 'posterior' scoloparium containing the neurones of groups 3 - 6.

The distal group of small neurones (group 6) that others have proposed is homologous with the proximal scoloparium of the pro- and mesothoracic legs (Matheson and Field, 1990), is situated beneath the dorsal ligament and in series with the ventral ligament of the mtFCO apodeme complex (Fig. 4.8a). Further proximally, the scoloparium containing the group 6 neurones and axons is located posterior to the scoloparium containing the group 1 and group 2 neurones (Figs 4.8d, e). The posterior scoloparium also contains the group 5 axons and is associated with the group 3 neurones. At the level shown in Figure 4.8e, it is difficult to distinguish the anterior and posterior scoloparia from one another. Conformation of the identities of the different neurone populations was obtained by tracing the axons in serially sectioned organs in which the neurones had been filled with cobalt (cobalt fills not illustrated, but see Fig. 4.9). The axons travel proximally to enter the nerve in discrete bundles corresponding to the different neurone groups in the two scoloparia. Although increasingly associated with one another as they approach the mtFCO nerve, the axons

derived from each scoloparium can still be identified (Fig. 4.10a-c). The axons of the cuticular nerve also join those of the neurone groups 3, 4, 5 and 6 to form a dorsal neurone bundle associated with the posterior scoloparium whilst the axons from groups 1a, 1b, 2a, 2b and the strand organ form a ventral bundle associated with the anterior scoloparium. These nerve bundles (4.10c) fuse to form the CO nerve (nerve 5b1). These observations on the internal anatomy of the scoloparium region provide persuasive evidence that the mtFCO is derived from two scoloparia. The fused scoloparia are enclosed by an acellular neural lamella (terminology of Ashhurst, 1959, 1968; Young, 1970) or 'perineural sheath' (terminology of Field, 1991) (Fig. 4.11a, b).

4.4.5 Nature of the scoloparium sheath

The anatomical relations of the neurones to other components of the mtFCO may well have functional importance. All neurones are surrounded by a thin glial sheath and they are separated from the outer perineural sheath by 'scolopidial cells' (Field, 1991). The scolopidial cells may be responsible for secreting the sheath (Field, 1991) which is similar in appearance to that described in other parts of the insect nervous system (Ashhurst, 1959) and is likely to be composed of mucopolysaccharide.

4.4.6 Anatomy of the scolopidia

To compare the structure of the sensory neurones with those of other chordotonal organs and to see if their ultrastructure provides clues as to their function, scolopidial organisation in *S. gregaria* was investigated at the TEM level.

The scolopidia in different parts of the organ are ultrastructurally similar to one another and are comprised of adjacent pairs of sensory neurones (Fig. 4.12). Figure 4.13 summarises the results of the current study of the anatomy of the mtFCO scolopidium and is designed to help with the interpretation of the following description. It is based upon electron micrographs of a non-consecutive series of sections and it demonstrates the ultrastructure of the scolopidia and the way in which they are linked to the attachment cells.

As the attachment cells approach the level of the scolopidia, they show extensive membrane invagination (Figs 4.14a, b). The axially orientated

attachment cell microtubules associate along the membrane invaginations to form regimented rows (Fig. 4.15a). Microtubules which are not immediately adjacent to a membrane invagination associate to form lattices, the smallest units of which consist of individual quartets of microtubules (Fig. 4.15b). Adjacent to the termination of the attachment cells on the scolopidia, the density of microtubules within the attachment cells is reduced (Fig. 4.16a). At this proximo-distal level, the attachment cells are associated in 'functional groups' associated with axially orientated extracellular fibres (Fig. 4.16b). Each attachment cell envelopes the extracellular scolopale cap of its associated scolopidium in which the distal tips of the dendritic cilia are embedded (Figs 4.13, 4.17). Immediately proximal to the scolopale cap, the dendritic cilia are surrounded by a scolopale cell (Fig. 4.18a). The attachment cell surrounds and is closely associated with the scolopale cell which contains electron dense scolopale rods which run longitudinally alongside the dendrites. The dendritic cilia are membrane-bound and are located within an extracellular space in the middle of the scolopale cell (Fig. 4.18b). Internally, the dendritic cilia appear poorly organised at this level. There are both regions of ciliary dilation and a tendency for the 9+0 arrangement to lose its radial symmetry (Figs 4.19a, b). Further proximally the scolopale cell takes on a highly vacuolated appearance and occupies more of the cross-sectional area of the scolopidium as the attachment cell approaches its termination (Fig. 4.20a). Approximately 15-20 μm from the tips of the dendrites, the attachment cell is completely absent and the cilia take on a more symmetrical appearance (Fig. 4.20b) where they adopt a conventional 9+0 arrangement of microtubules (Fig. 4.21). At this level the microtubules are singlets rather than doublets and bear pairs of arms identical in appearance and position to the dynein arms of motile cilia.

Towards the base of the cilia the dendritic membranes lift away from the ciliary microtubules to fill the extracellular space. At this level, the scolopale rods taper and the basal structures of the cilia can be seen (Figs 4.22a, b). The basal body located at the base of the cilia (typical to mechanoreceptive cilia: Young, 1970; Yack and Roots, 1992) has nine-fold symmetry and is associated with the dendritic membrane via faintly staining radial spokes (Fig. 4.22b). At this level, the scolopale cell of the scolopidium is still associated with extracellular elastic (Acid Fuchsin-staining) fibres around its periphery (Fig. 4.23a). Proximal to this level,

ciliary rootlets (see Young, 1970) arise from the ciliary basal body before giving way to a single electron dense ciliary root in each dendrite, whilst the scolopale rods continue to taper (Fig. 4.23b). Eventually the scolopale rod material is lost and at this level mitochondria are found in the dendrites (Fig. 4.24a). The dendrites of neighbouring scolopidia in the same neurone population lie adjacent to one another, each pair sheathed in its own scolopale cell (Fig. 4.24b). Further proximally the scolopale cells taper and loose their vacuolated appearance. At this proximo-distal level the dendrites are wrapped in glial sheath cells (Figs 4.25a). The dendrites of discrete populations of neurones are grouped together and are associated with extracellular elastic (Acid Fuchsin-staining) fibres (Fig. 4.25b). The glial covering of the dendrites continues proximally over the neurone cell bodies which are packed with mitochondria. The cell bodies of the group three and five neurones have a thicker glial covering than those of the other groups.

The twin cilia of each scolopidium are longitudinally offset relative to one another, which is reflected in the fact that the different ciliary structures of each dendrite pair always appear slightly out of step with each other in serial transverse sections. A difference between the two ciliary processes was sometimes apparent in cobalt-filled light microscope preparations (see Figure 4.12). This phenomenon represents the only apparent anatomical difference between dendrite arrangements in the scolopidia.

Proximal to the cell bodies, the axons joint the mtFCO nerve in bundles (see Fig. 4.10). The axons vary in size from 300 nm - 3 μm (Fig. 4.26). The axons of the cuticular nerve also contain a range of sizes of axon (200 nm - 5 μm) (Fig. 4.27a). In all cases, the axons have the typical glial wrapping seen in insects (Fig. 4.27b). Cuticular nerve axons often contain distinct neurotubules. These are a feature of the processes of mechanoreceptive cells (Young, 1970; Yack and Roots, 1992).

4.5 DISCUSSION

4.5.1 Implications of scoloparium organisation

Matheson and Field (1990) proposed that a distal group of smaller sensory neurones (group 6 in this study) was homologous with those of the pro- and mesothoracic proximal scoloparia. The anatomical composition of the

mtFCO confirms that this is the case, the mtFCO scoloparium consisting of two fused scoloparia the sensory neurones of which are innervated separately. The implication of this finding is that the neurones comprising the mtFCO are derived from at least two separate neurone populations which are known to have different response characteristics (Field and Pflüger, 1989).

4.5.2 Distribution of sensory neurones

This thesis has shown that the mtFCO neurones can be further classified into sub-populations on the basis of their anatomical characteristics and innervation. Some of the groups described in this thesis probably correspond to discrete groups of neurones classified by Matheson (1990) on the basis of their response characteristics (Table 4.1):

Table 4.1

Response Characteristics	Group 1	Group 2	Group 3
Position only			✔
Velocity only	✔	✔	(✔)
Acceleration only			✔
Position and Velocity	(✔)	✔	✔
Velocity and Acceleration	✔		
Position, Velocity and Acceleration	✔	(✔)	

Table 4.1 indicates the presence of neurones responding to different components of the stimulus (position, velocity, acceleration) as identified by Matheson (1990) in the discrete populations of neurones identified in this study (groups 1 - 3). Neurones from groups 4 - 6 were not represented in Matheson's (1990) study. The subgroups (1a, 1b; 2a, 2b) are not distinguished. Brackets indicate cells in Matheson's (1990) study which filled only faintly with cobalt.

Although the clusters of neurones characterised by Matheson (1990) on the basis of their response characteristics clearly correspond to the different anatomical groupings of cells classified in this study, the distribution of sensory neurones sharing the same response characteristics is complex. Cells sensitive to both stretch and relaxation are situated in a variety of locations in the sensory scoloparium. However, there is a trend towards increasingly dorsal neurones (group 3) responding over wider ranges of femoro-tibial angles to fewer components of the stimulus, when compared with the ventral-most cells (group 1) which tend to have discrete ranges of operation and respond to a wider range of stimulus components (see Table 4.1).

The combined anatomical and physiological data show that different components of the stimulus are encoded in the sensory scoloparium by clusters of physiologically distinct scolopidia. The fact that some cells responding to similar modalities are located in specific regions of the organ (Matheson, 1990) suggests that certain areas of the scoloparium may be suited to detecting particular stimulus characteristics. This implies that different regions of the scoloparium respond differentially to given patterns of mechanical input. There is also evidence to suggest that the mtFCO attachment cells are arranged into functional groups delimited by Acid Fuchsin-staining fibres (see Chapter 3) and that bundles of neighbouring attachment cells terminate on adjacent scolopidia (Fig. 4.16b). Associations such as this may represent a mechanism by which sub-populations of sensory neurones can be subjected to differential stimulation (Field, 1990). However, according to Matheson's (1990) drawings, dendrites of neurones responsive to different modalities are located adjacent to one another. This suggests that some neurones may not be receiving differential stimulation by virtue of their positions in the scoloparium, but that physiological factors may also be responsible for the response properties of specific sensory units.

Matheson (1990) did not record from any of the smaller distal (group 4, 5 and 6) neurones, and so no conclusions can be drawn about the relationship between their response characteristics and morphology. In addition, Matheson was not aware of the complexity of the apodeme complex and stimulated the organ by gripping this connection with titanium forceps. It is unclear whether the displacement of the dorsal and ventral ligaments or the operation of the loop-forming region was adversely affected by this method of stimulation. It seems likely that this was the case as Matheson stated that a 175 μm displacement of the forceps was equivalent to a femoro-tibial rotation of 20°. A 20° joint rotation elicits a displacement in excess of 200 μm at the level of the apodeme complex cuticular rod. This suggests that the apodeme complex may have been gripped at the level of the compliant ligaments where femoro-tibial rotations elicit smaller displacements (see Chapter 2).

Anatomical differences between neurone populations such as cell body size, dendrite lengths and dendrite diameters may contribute to differences

in cable properties, firing thresholds and ranges of sensitivity. Such factors may result in differential mechano-electric transduction properties between neurone populations.

4.5.3 Structure of the scolopidium

Ultimately the functional anatomy of the scolopidium will determine the effective mechanical stimulus required to induce the firing of the sensory unit. All the mtFCO scolopidia appear structurally similar at an ultrastructural level and the ultrastructure of the mtFCO scolopidium/attachment cell junction is shown in the form of a semi-schematic diagram in Figure 4.13. On the other hand, cell body and dendrite orientations differ between neurone populations.

The structure of the scolopidia in the locust mtFCO is similar to that documented by Young (1970) in the cockroach tibio-tarsal CO. The dendritic cilia are located in an extracellular space flanked by a scolopale cell in which are located intracellular scolopale rods. Apically, the dendrites are capped by extracellular material (the scolopale cap) which forms the interface between the dendrites and the attachment cell. However, the scolopidia of the locust mtFCO differ from those in the cockroach described by Young (1970). The difference is in the way that the scolopidal components are associated. The nature of this junction has implications with respect to the way in which the ciliary components are likely to be distorted by the application of an axial force across the scolopidium.

Young (1970) showed that in the cockroach tibio-tarsal CO, the scolopale cap of each scolopidium interacts extensively with the apical dendrites. This extracellular cap material also completely surrounds the scolopale cell distally, extending to the level of the ciliary dilation. The interaction between the scolopale cap and the scolopale rods is extensive. In addition, Young (1970) showed that the attachment cell extends proximally around the scolopale cell to the level of the base of the cilia. In the locust however, neither the scolopale cap or the attachment cell engulfs the distal ends of the scolopale cell. Instead, the extracellular cap material extends proximally inside the extracellular space. However, the scolopale cap is associated closely with both the dendritic cilia and the scolopale rods (Figs 4.18a, b) in a similar manner to that described by Young (1970).

4.5.4 Effect of axial elongation

The close association between the scolopale cap and the dendritic cilia (Figs 4.17 and 4.18a, b) suggests that distal displacement of the attachment cell could result in the pinching or elongation of the dendrite tips by the extracellular scolopale cap as proposed by previous authors for other mechano-sensilla (Howse, 1968; Thurm, 1965). Young (1970) speculated on the basis of the CO anatomy, that axial elongation of the scolopidium was the most likely result of tibial flexion. However, immunohistochemical studies have since shown that the scolopale rods which flank the dendritic cilia consist of actin and tropomyosin (Wolfrum, 1990, 1991b) and as such were presumed to be inextensible. It is unclear what implications this has with respect to dendritic distortion but it does not exclude the elongation of the cilia themselves in response to axial force across the scoloparium. If the pull were axial, then both dendrites would be subject to similar stimulation. When the system is relaxed, recovery will be effected by the extracellular elastic (Acid Fuchsin-staining) fibres which lie in parallel with the scolopidial unit. The locust mtFCO scoloparium is sheathed by an acellular homogeneous neural lamella which separates the organ from the haemolymph space. The neural lamella is continuous with the basement membrane which overlies all the organs of the body (Pipa and Cook, 1958; Whitten, 1962, 1964; Ashhurst, 1968). This sheath is of variable thickness being thick at the level of the sensory neurones (approximately 0.5 μm) (Fig. 4.11b) and becoming thinner distally (approximately 50 nm) around the mtFCO apodeme complex (see Chapter 3). Peripheral thinning of the neural lamella was also observed by Ashhurst (1961a, b) in the cockroach *Periplaneta americana*. Pipa and Cook (1958) and Ashhurst (1959, 1961b, 1968) speculated about the composition and physical properties of this lamella regarding it as composed of mucopolysaccharide and having a degree of plasticity. Other authors have described various types of fibre within the matrix (Lock and Huie, 1972, 1975). These fibres will also contribute to the mechanical properties of the neural lamella. In the case of the sheath surrounding the mtFCO scoloparium, the matrix contains no discernible fibres. The variable thickness observed in the layer ensheathing the mtFCO may influence the mechanical properties of the scoloparium. However, until its properties are known, the contribution of the neural lamella to the mechanical behaviour of the organ will remain unknown.

4.5.5 Role of the dendritic cilia

The dendritic cilia have been suggested by many authors to be central to the process of mechano-electric transduction (Gray and Pumphrey, 1958; Wiederhold, 1976; Atema, 1973; Varella *et al.*, 1977; Moran *et al.*, 1975, 1977). Gray and Pumphrey (1958) suggested that the conservation of fundamental ciliary structure during the course of phylogeny which incorporated somatic cilia into receptor organs, indicated that some facet of conventional ciliary activity may remain. This suggests that cilia could conceivably play a dynamic role in mechano-transduction by utilising some of the mechanisms which enable them to generate mechanical energy in motile cilia. Subsequent authors have both opposed and supported this premise. Wiederhold (1976) concluded that stiff cilia in mechanoreceptive sensilla act as passive plungers, transmitting mechanical displacement to the site of a basal transducer membrane. Barber (1974) also maintained that the active ciliary model of mechano-sensitivity was unlikely. He suggested that the 9 + 0 configuration of dendritic cilia (rather than the 9 + 2 of motile cilia) and the fact that the sensory endings are stretched during stimulation, implied that simple distortion or piezo-electric current generation were more likely candidates for the mechanism involved in mechano-electric transduction. However, Atema (1973) presented morphological and biochemical evidence to support the active role of cilia in mechano-reception. He proposed that mechanical stimulation at the apical end of the dendrite induced a conformational change in the tubulin polymer comprising the ciliary microtubules. In his model, the conformational change was propagated proximally along the microtubules to activate an ion flux mechanism at a basal site. This mechanism of transduction allowed for amplification of the stimulus energy, producing a generator potential ultimately leading to the production of action potentials at the spike generating site or sites of the cell. Anatomical evidence to support part of the 'ciliary engine' hypothesis was supplied by Varella *et al.* (1977) and Moran *et al.* (1977) who took electron micrographs of transversely sectioned cilia from the pro- and mesothoracic FCOs of the grasshopper *Melanoplus bivittatus* fixed in different states of stimulation. Moran *et al.* (1977) demonstrated the presence of a pronounced bend at the base of cilia in chordotonal sensilla of maximally stimulated organs. They proposed that this kink was a result of active sliding (rather than tubulin

conformational change as suggested by Atema, 1973) between ciliary doublets in response to mechanical deformation at the ciliary tip. They concluded that cilia play an active mechanical role in sensory transduction.

The ciliary dilation and the associated disorganisation of the dendritic microtubules described here and elsewhere (Young, 1970; Yack and Roots, 1992) causes a problem in all models involving an active ciliary mechanism. It is difficult to see what role the ciliary dilation would play in such a mechanism, and how a ciliary 'beat' propagated by a molecular mechanism could pass this region where the 9 + 0 configuration becomes disorganised. Active sliding in motile cilia requires the movement of the dynein arms of one doublet against the adjacent doublet (Warner and Satir, 1974). Therefore, any movement of the scolopale cap would have to cause displacement at the level of the ciliary dilation in order to initiate active microtubule sliding at a more proximal level, since the dynein arms are absent above this point (Doolan and Young, 1981).

Moran *et al.* (1977) conceded that the 9 + 0 arrangement of ciliary microtubules in a sensory sensillum may not be capable of the equivalent of a ciliary beat as produced by motile cilia which have 9 + 2 configurations of microtubules. However, he maintained that the remaining microtubules could retain the ability to actively slide past one another. Crouau (1980) suggested a possible mechanism by which a degree of ciliary motility could be effected in the absence of the central structure and radial spokes associated with conventional motile cilia. He presented electron micrographic evidence showing that the ciliary outer doublets interact with the cell membrane via temporary 'bridges' in the COs of the cave Mysidacea *Antromysis juberthiei*. He demonstrated the sequential formation and breakage of these bridges between the outer arms of the A-subfibre of the doublets with pairs of membrane protuberances. He hypothesised that a cyclic succession of bridging would lead to twisting of the ciliary axoneme when stimulated. Some ultrastructural evidence of doublet/membrane association was observed in this study at the level of the ciliary dilation (Fig. 4.19b). However, Crouau's (1980) model relies upon the ciliary doublets being adjacent to the cell membrane along the length of the cilia which is not always so in the case of the scolopidia of the

mtFCO. No new conclusions can be draws on the evidence of this study regarding the role of the dendritic cilia.

4.5.6 Mechanisms of mechano-electric transduction

Moran *et al.* (1977) described a tilting of the ciliary base in stimulated sensilla which they proposed would result in the distortion of specialised membranes in the region of the ciliary base. They proposed that this distortion would effect a local change in ionic permeability to initiate a generator current. Understanding of the electrophysiology of mechano-sensilla was refined by Thurm and Küppers (1980) and Erler and Thurm (1981), who worked on single sensilla associated with the cuticle of a variety of insects. Using mathematical modelling the latter authors suggested that the apical dendrite was likely to regulate the neurone discharge frequency in response to adequate stimulation via stretch-activated ion channels. This hypothesis, and a possible mechanism of CO sensillum operation, is explored at the end of this thesis.

Figure 4.1

Semi-schematic diagram showing the morphological criteria by which each sensory neurone was characterised. The best-fit-ellipse has the same area as the cell body, and provides a standard uniform profile from which the degree of elongation and attitude of the cell can be measured.

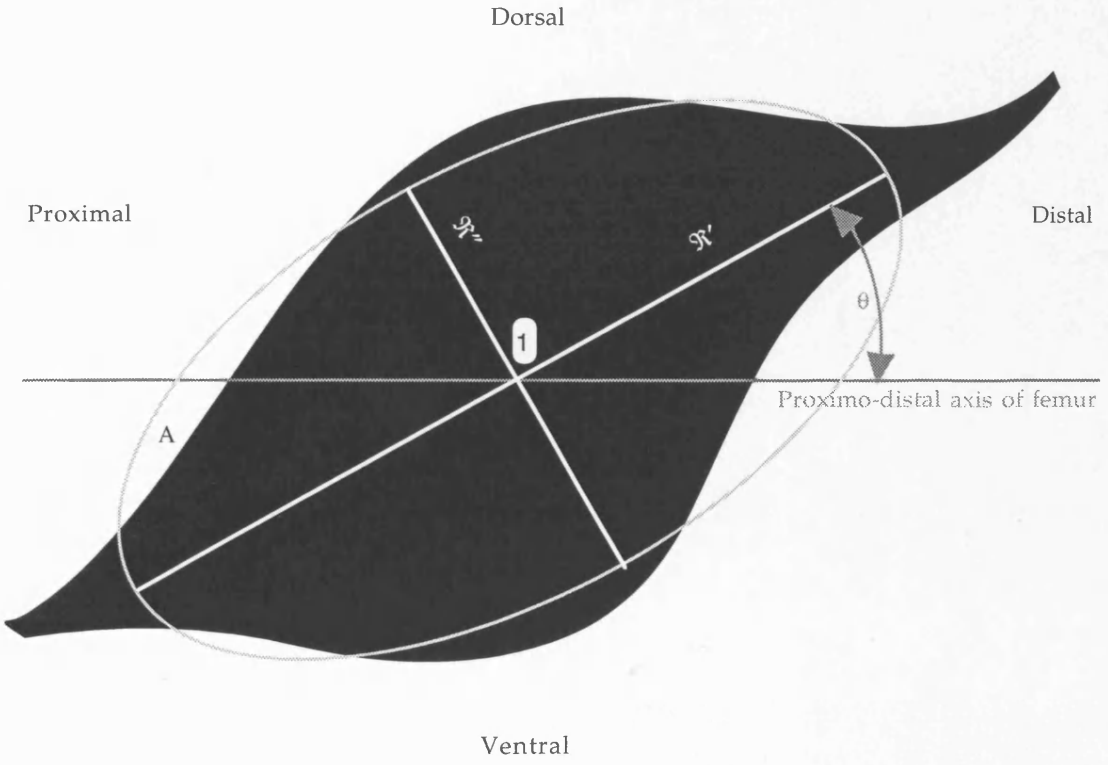

Parameters returned:

cell identification number..... **1**

cell area..... **A**

length of major axis..... $\mathfrak{R}'$

length of minor axis..... $\mathfrak{R}''$

angle between neurone major axis and femoral axis... θ

Figure 4.2

This micrograph shows an isolated mtFCO scoloparium which has been lightly stained (20 mins) with 1% osmium tetroxide. Areas containing nerves and cell bodies stain differentially with osmium. The pattern of staining is consistent in all preparations and reveals discrete lobes within the scoloparium. The overlay shows a line diagram interpreting the differentially stained areas and showing associated branches of the chordotonal organ nerve. The latter is divided into dorsal (d) and ventral (v) branches. The dorsal branch also gives rise to the cuticular nerve.

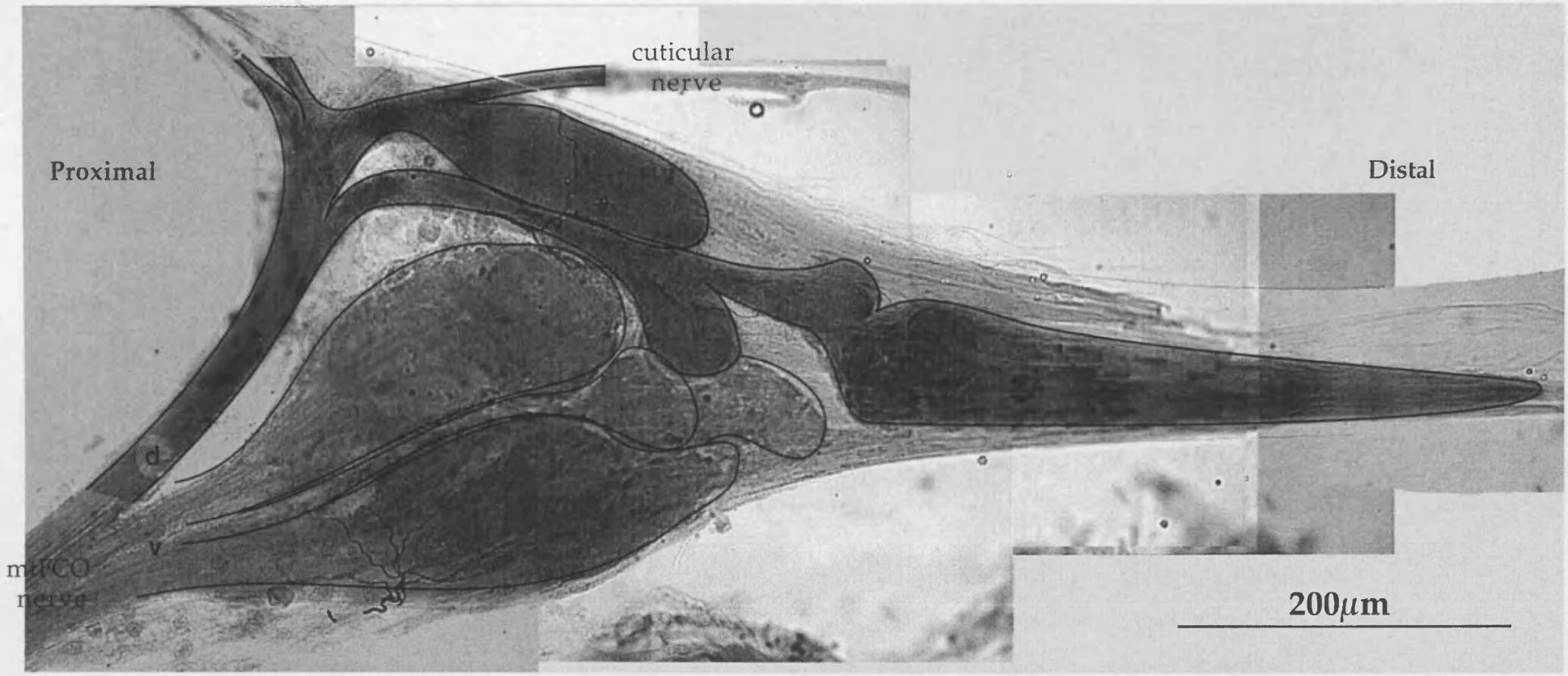
cuticular
nerve
Proximal
Distal
d
v
mtCO
nerve
200μm

Figure 4.3

Light micrograph taken using Nomarski optics showing the mtFCO scoloparium of *S. gregaria* in which the sensory neurones have been stained with cobalt. The overlay indicates 6 neurone populations which correspond with the areas observed to differentially stain with osmium. Groups 1 and 2 can be subdivided into sub-populations (1a, b; 2a, b).

[The arrowhead indicates a proximo-distal level referred to in Figure 4.9]

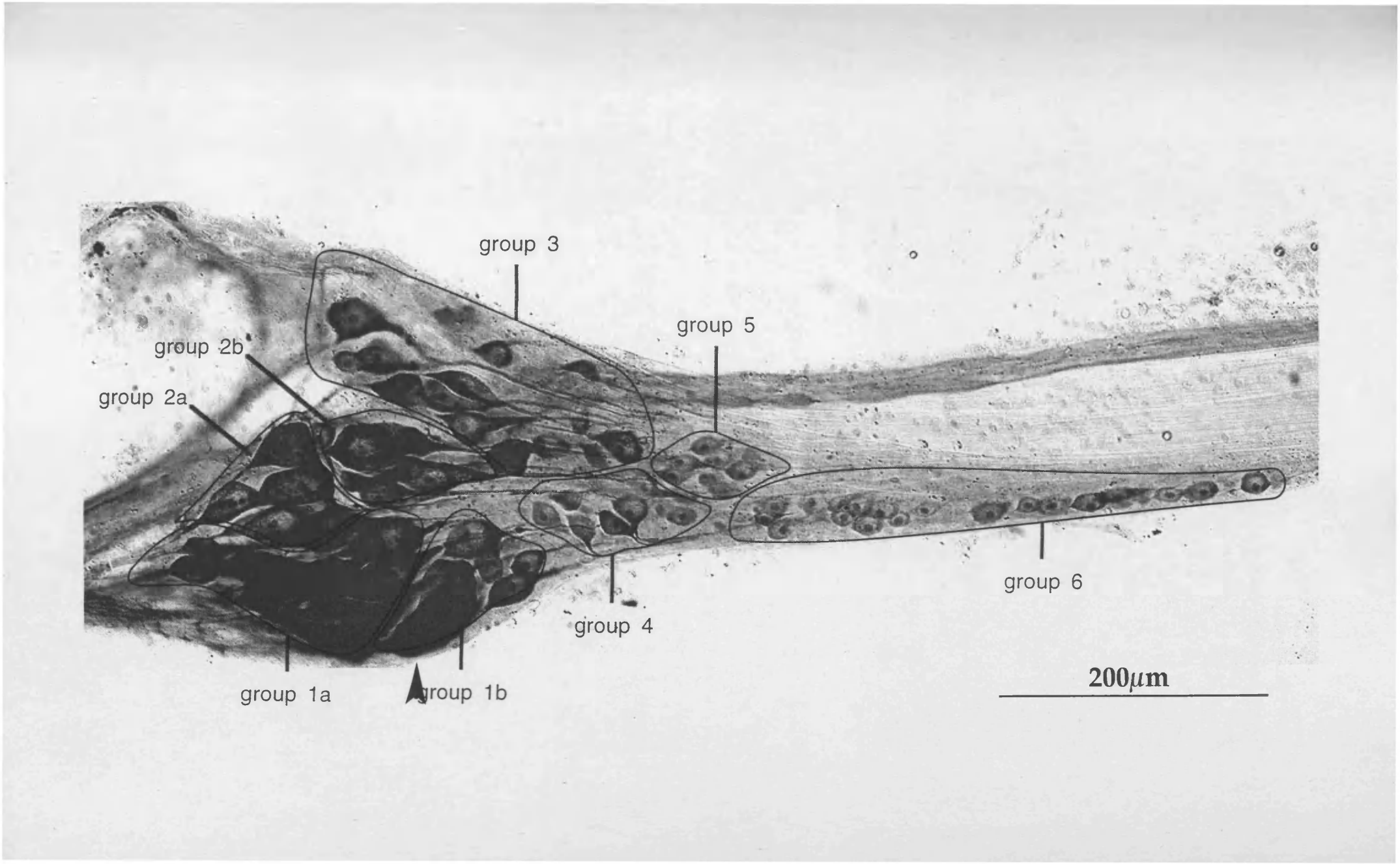
group 3
group 5
group 2b
group 2a
group 6
group 4
group 1a
group 1b
200μm

Figure 4.4

These histograms compare the mean profile areas of different neurone populations of *S. gregaria* (upper) and *L. migratoria* (lower).
The two species have different ranges of cell sizes, the cell body profile areas ranging from 200 μm^2 to 2000 μm^2 in *S. gregaria* and 250 μm^2 to 1100 μm^2 in *L. migratoria*. Significant differences between populations within each species are summarised below.

***S. gregaria* cell profile area**

Single Factor Analysis Of Variance (ANOVA): $F_{41, 43} = 81.77$ $P < 0.05$

Group 5	Group 6	Group 4	Group 1b	Group 2b	Group 3	Group 2a	Group 1a

(bars beneath the groups denote homogeneous subsets)

***L. migratoria* cell profile area**

Single Factor Analysis Of Variance (ANOVA): $F_{79, 105} = 84.38$ $P < 0.05$ df

Group 6	Group 5	Group 4	Group 2b	Group 1b	Group 3	Group 2a	Group 1a

(bars beneath the groups denote homogeneous subsets)

[The line diagram below shows the location of the neurone populations]

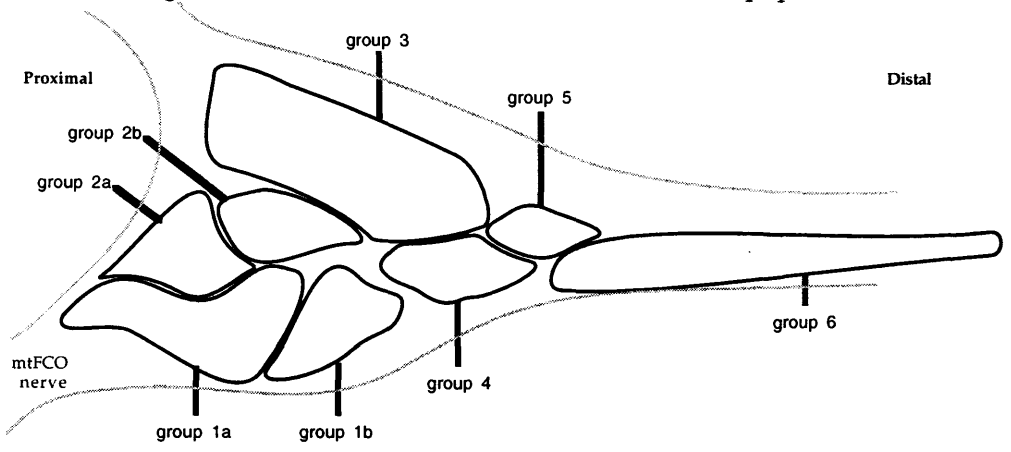

Histogram comparing the mean profile areas of neurones in different groups in *S. gregaria* (total n=482)

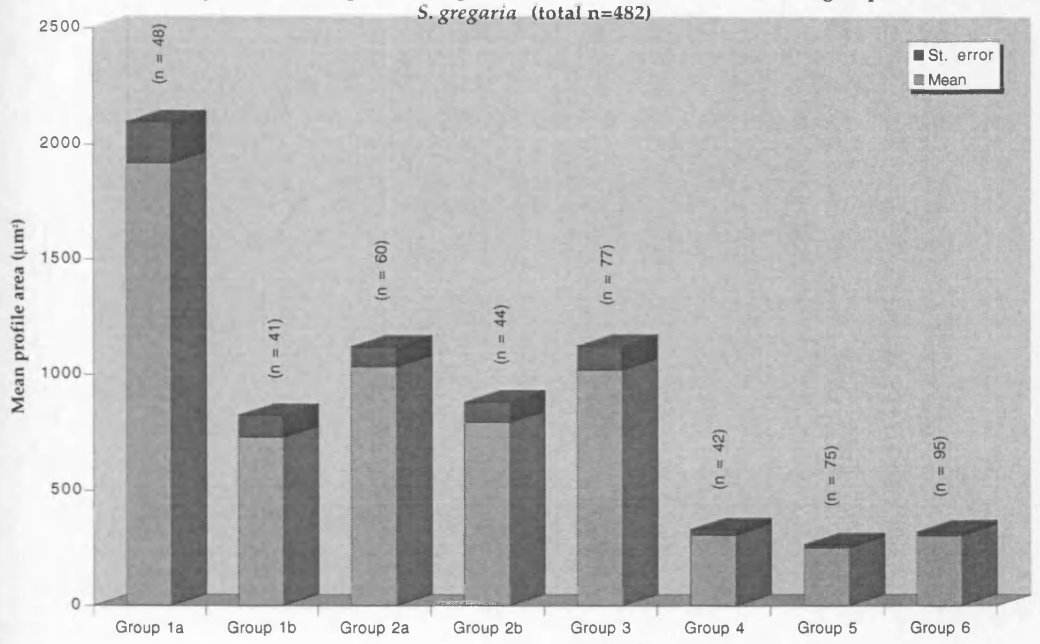

Histogram comparing the mean profile areas of neurones in different groups in *L. migratoria* (total n=826)

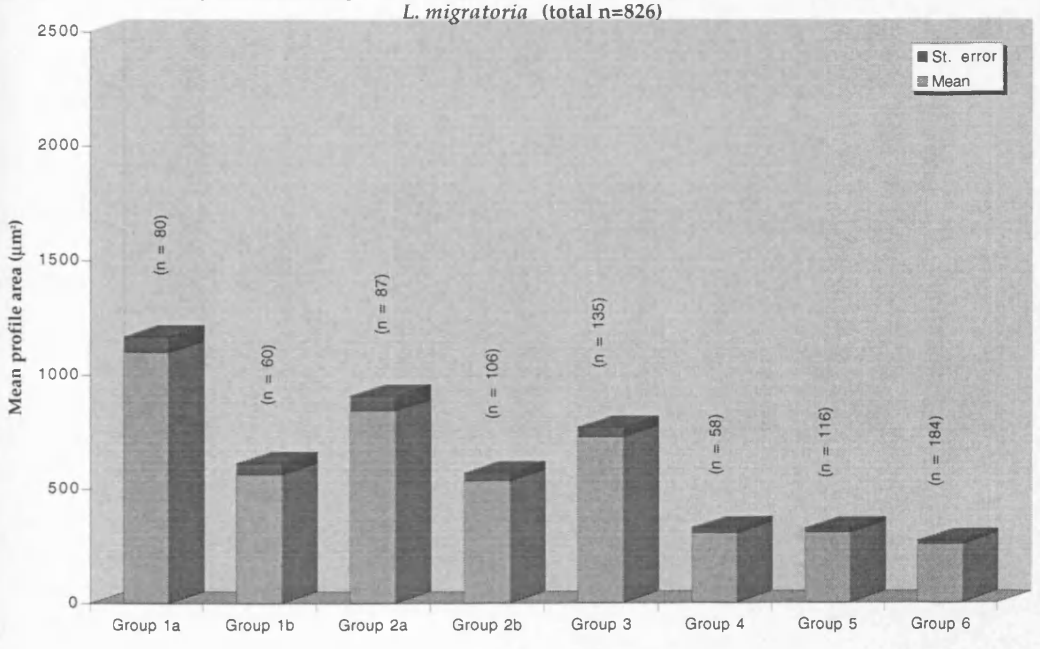

Figure 4.5

Histograms to show the mean cell anisometries of neurones in the different populations in *S. gregaria* (upper) and *L. migratoria* (lower). All sensory neurones in the mtFCO are elongated to some extent (see Figure 4.3), a circular profile having an anisometry of 1. (Values greater that 1 indicate cell elongation).

***S. gregaria* cell anisometry**							
Single Factor Analysis Of Variance (ANOVA): $F_{47,74} = 13.39$ $P < 0.05$							
Group 5	Group 4	Group 1b	Group 2b	Group 6	Group 3	Group 1a	Group 2a
(bars beneath the groups show homogeneous subsets)							

***L. migratoria* cell anisometry**							
Single Factor Analysis Of Variance (ANOVA): $F_{79,57} = 21.14$ $P < 0.05$							
Group 4	Group 5	Group 2b	Group 6	Group 1b	Group 3	Group 2a	Group 1a
(bars beneath the groups show homogeneous subsets)							

[The line diagram below shows the location of the neurone populations]

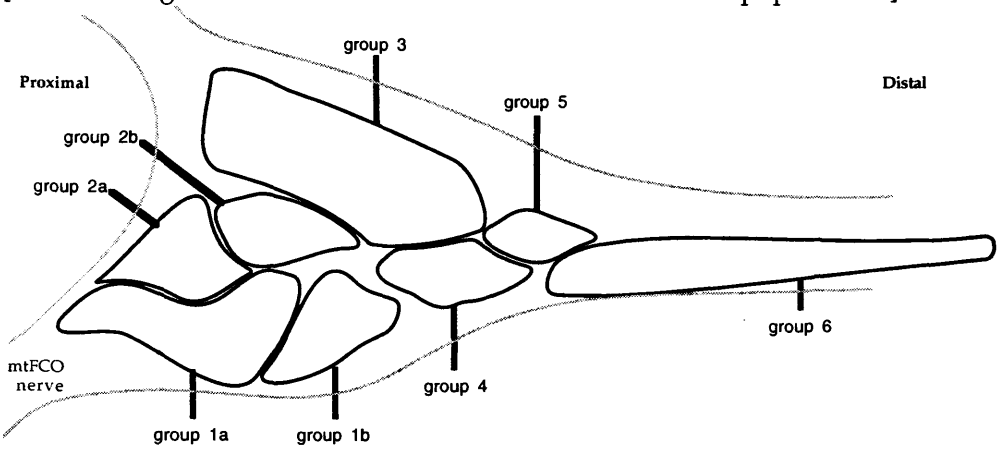

Histogram showing the anisometry of neurones in different groups in *S. gregaria* (total n=482)

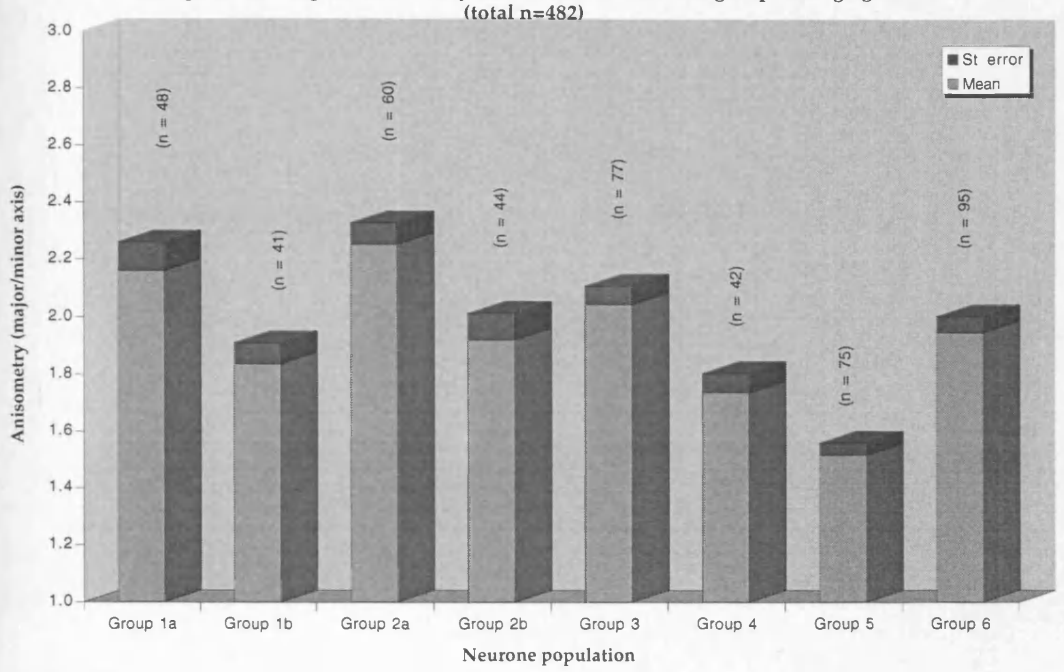

Histogram showing the anisometry of neurones in different groups in *L. migratoria* (total n=826)

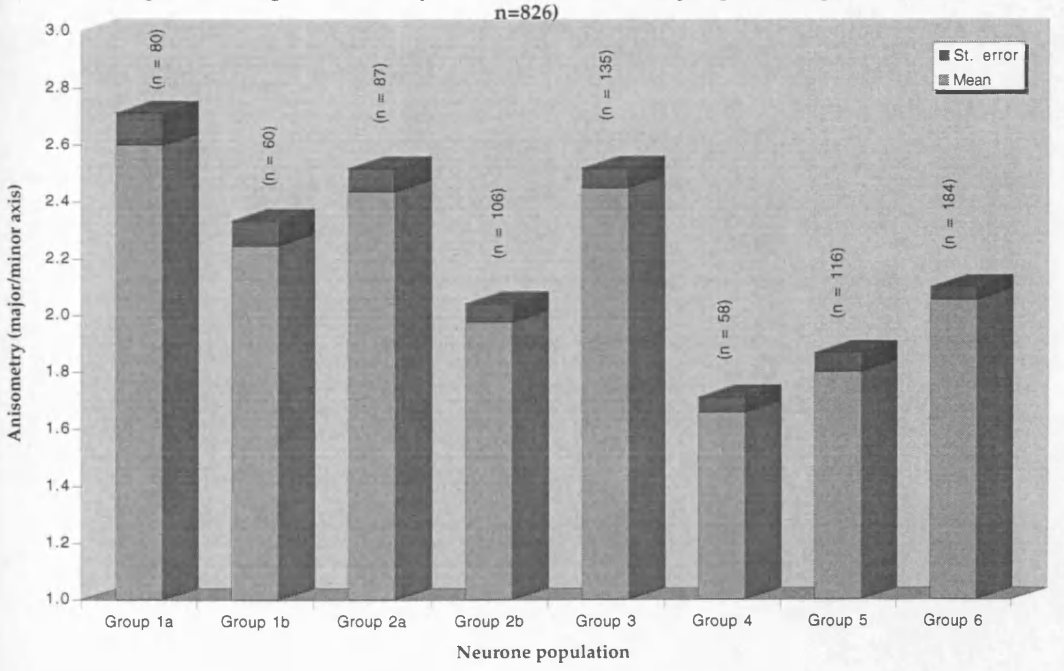

Figure 4.6

These histograms show the mean orientations of the neurones in each population in *S. gregaria* (upper) and *L. migratoria* (lower).
The two histograms show that the overall cell orientation pattern is common to both species, with no neurones lying directly along the axis of the organ (an orientation of 0°). All point obliquely either dorsally (positive values) or ventrally (negative values).

***S. gregaria* cell orientation**

Single Factor Analysis Of Variance (ANOVA): $F_{40, 94} = 107.08$ $P < 0.05$

Group 4	Group 2b	Group 2a	Group 5	Group 3	Group 6	Group 1a	Group 1b

(bars beneath the groups show homogeneous subsets)

***L. migratoria* cell orientation**

Single Factor Analysis Of Variance (ANOVA): $F_{57, 86} = 156.18$ $P < 0.05$

Group 4	Group 2b	Group 5	Group 2a	Group 3	Group 6	Group 1a	Group 1b

(bars beneath the groups show homogeneous subsets)

[The line diagram below shows the location of the neurone populations]

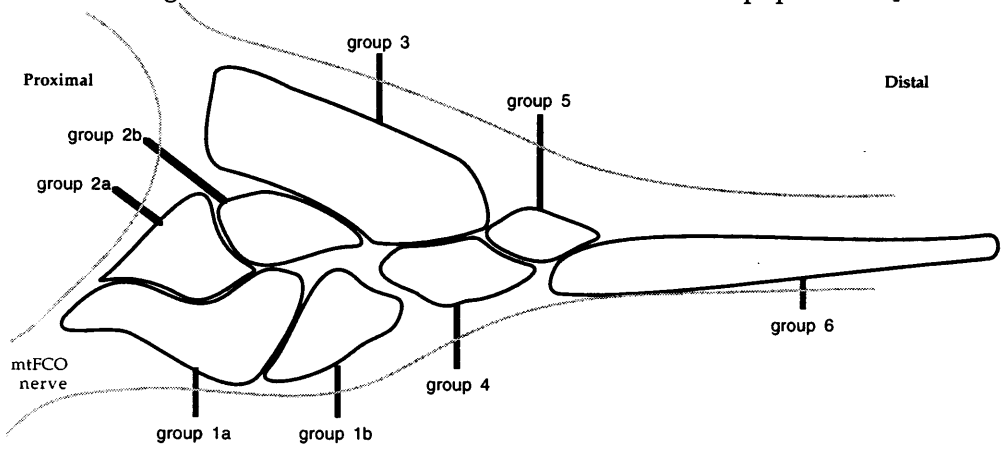

Histogram showing the orientations relative to the axis of the femur of the neurone somata in the different populations in *S. gregaria* (total n=482)

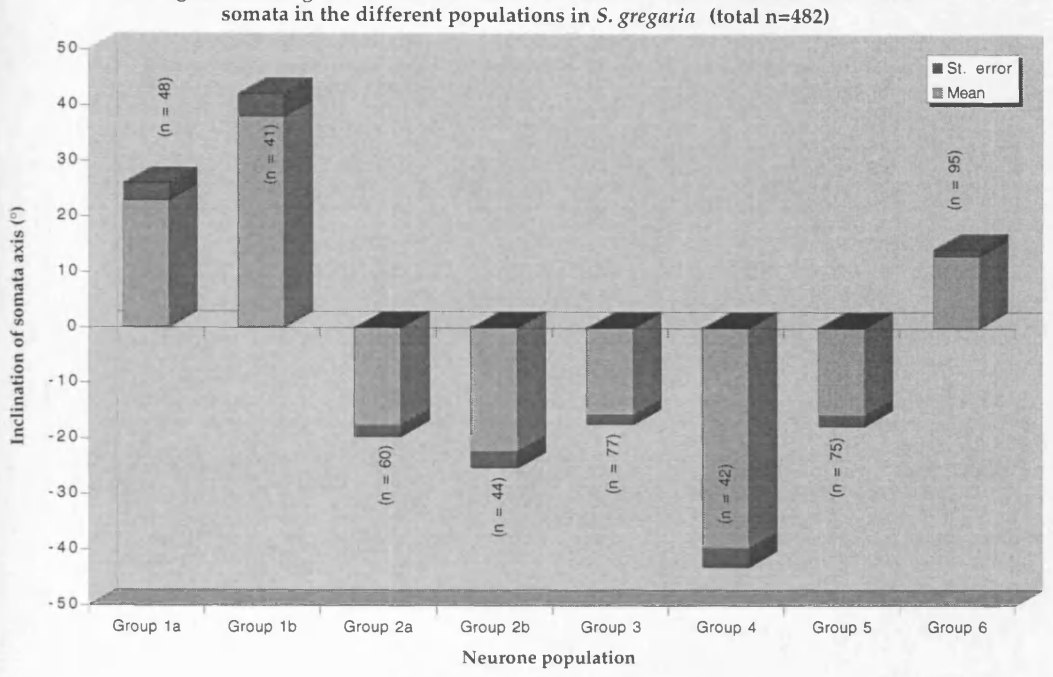

Histogram showing the orientations relative to the axis of the femur of the neurone somata in the different populations in *L. migratoria* (total n=826)

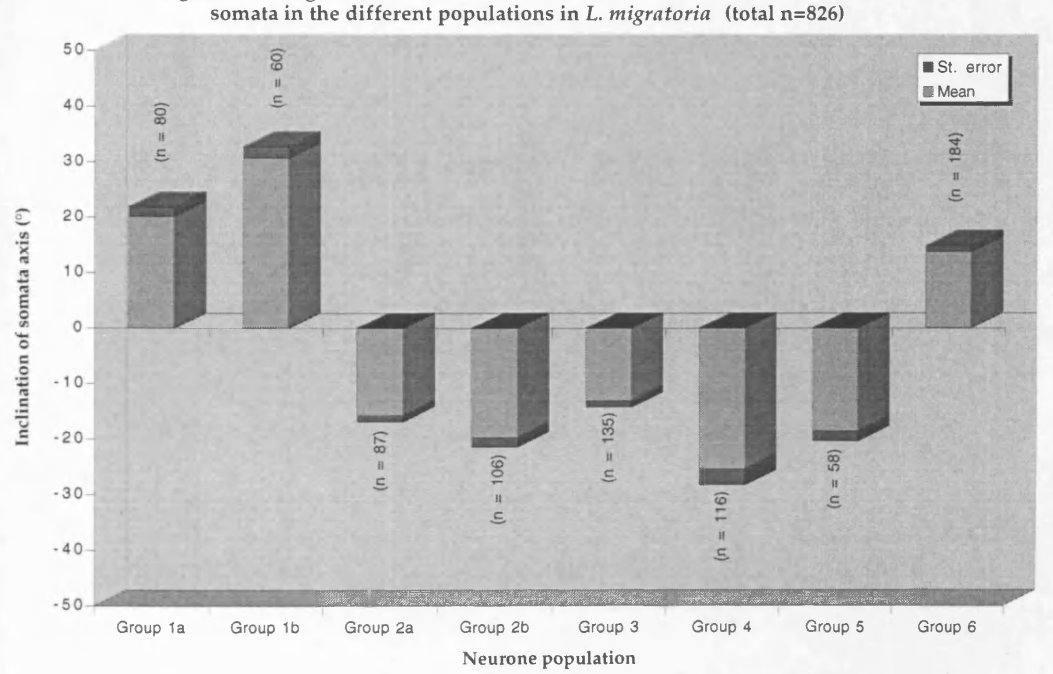

Figures 4.7a-c

These histograms characterise the morphological attributes of mtFCO neurones sharing the same response characteristics as classified by Matheson (1990) in *L. migratoria*.

a

This histogram compares the mean cell body sizes of neurones which respond to different elements of the stimulus. Cell size does not vary significantly across the range of different response types ($F_{5, 54} = 1.68$, $P = 1.56$).

b

This histogram shows the mean anisometries of neurones in the different response classes. The cells sensitive to acceleration appear especially elongated, whilst the cells which encode only the position or only the rotation velocity of the tibia tend to have a more circular profile than the remaining response classes. However, the small sample size means that no significant differences in neurone anisometry can be identified between the response classes ($F_{5, 54} = 2.09$, $P = 2.39$).

c

This histogram demonstrates the orientation of neurone cell bodies in the different response classes.

***L. migratoria* cell orientations, classified by sensory modality**					
Single Factor Analysis Of Variance (ANOVA): $F_{5, 54} = 3.44$, $P < 0.01$					
Acceleration	Velocity	Position and Velocity	Velocity and Acceleration	Position	Position, Velocity and Acceleration
(bars beneath the groups show homogeneous subsets)					

Histogram showing the sizes of the somata of groups of neurones monitoring different sensory modalities

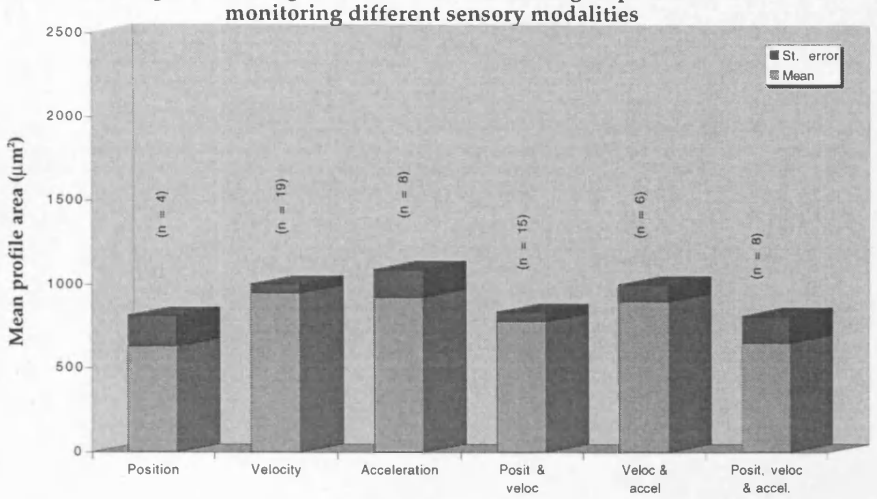

Histogram showing the anisometries of different physiological classes of neurone

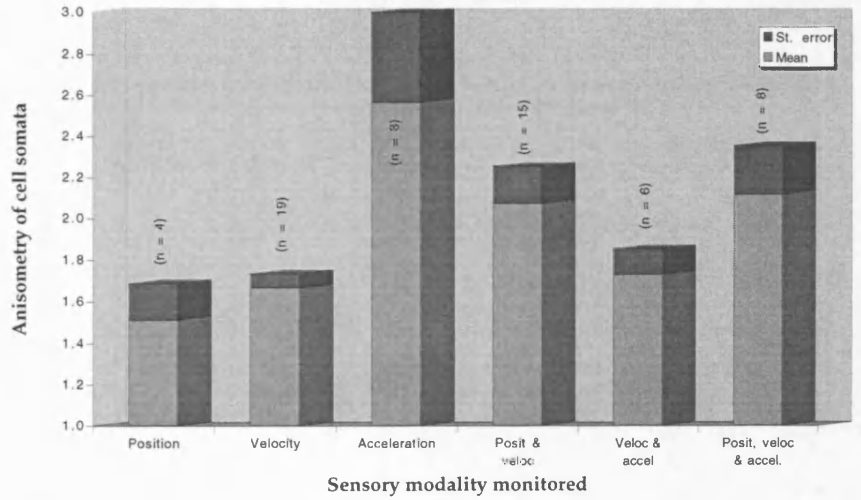

Histogram showing the orientations of cells responding to different sensory modalities

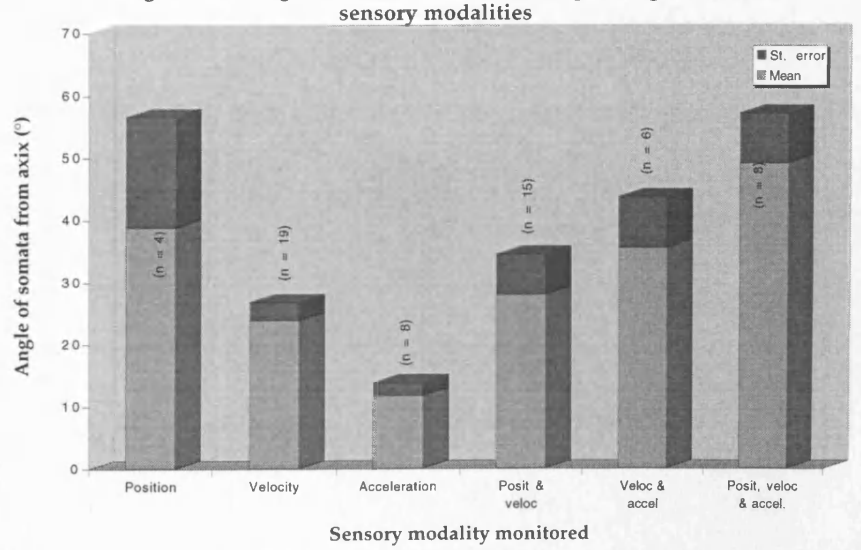

Figures 4.8a-e

This series of semi-schematic diagrams shows the transverse profile of the mtFCO scoloparium at representative proximo-distal levels, and the spatial distribution of the different populations of sensory neurones. For ease of explanation distal is to the left in the upper diagram. Distally, at level **a**, the group 6 neurones extend along the ventral ligament of the apodeme complex. The attachment cells (ac) comprising the dorsal ligament are still present at this level. Proximally, the scoloparium appears 'folded' such that the neurones in series with the ventral ligament come to be positioned adjacent and posterior to the attachment cells of the dorsal ligament. This organisation represents the anatomical sub-division of the mtFCO scoloparium into laterally-fused anterior and posterior scoloparia. Diagrams **b-d** demonstrate the locations of the neurone populations at increasingly proximal levels. Group 5 and 6 neurones are associated with the posterior scoloparium. Proximal to the group 6 cell bodies, their axons travel proximally in a bundle (**c, d, e**). The group 4 neurones are located ventrally and do not appear to fall into either the anterior or posterior scoloparia (although their axons run within the posterior scoloparium proximally). The group 1 and 2 neurones are associated with the anterior scoloparium (**d**). Proximal to this level (**e**) the two scoloparia appear more closely associated with one another. The distal-most group 3 neurones are located on the anterior side of the mtFCO (**d**). However, as the scoloparia become increasingly fused they are located dorsal to the group 4, 5 and 6 axons (**e**). Ventrally, the strand organ (so) is associated with the anterior scoloparium.

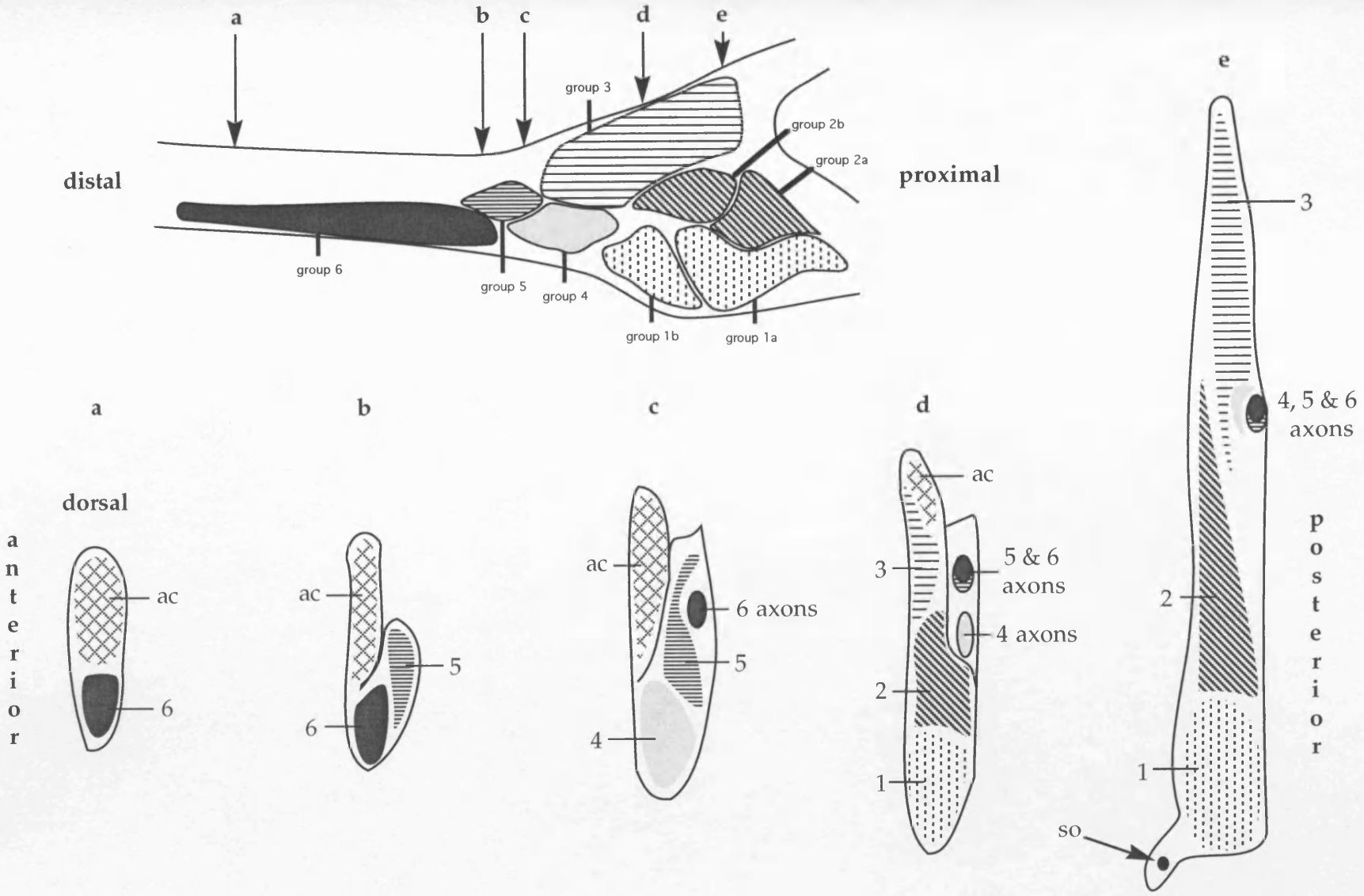
a
b
c
d
e
distal
proximal
group 3
group 2b
group 2a
group 6
group 5
group 4
group 1b
group 1a
a
b
c
d
e
dorsal
anterior
posterior
ac
6
5
4
3
2
1
5 & 6 axons
4 axons
6 axons
4, 5 & 6 axons
so

Figure 4.9

Composite of high resolution digital images of a transverse section of the mtFCO stained with Toluidine blue. This section was taken from a series at the level at which the cuticular nerve joins the mtFCO dorsally, and corresponds to the level indicated in the cobalt-filled organ shown in Figure 4.3. The overlay demonstrates the spatial relations of the different neurone populations at this level. Ventrally, the 1b neurones lie immediately ventral to the 1a neurones. Further dorsally, the 2b neurones lie dorsal to the 2a neurones and extend up the anterior side of the organ. At this level, the dendrites of the group 2a neurones can be seen inserting in pairs (arrow) into individual attachment cells. Dorsally, the group 3 neurones are situated on the posterior side of the organ above a small nerve bundle which contains the axons of both the group 6 and group 5 neurones (see Fig. 4.2). The cuticular nerve (cn) axon bundle can be seen entering the mtFCO dorsally between the anterior and posterior scoloparia at this level.

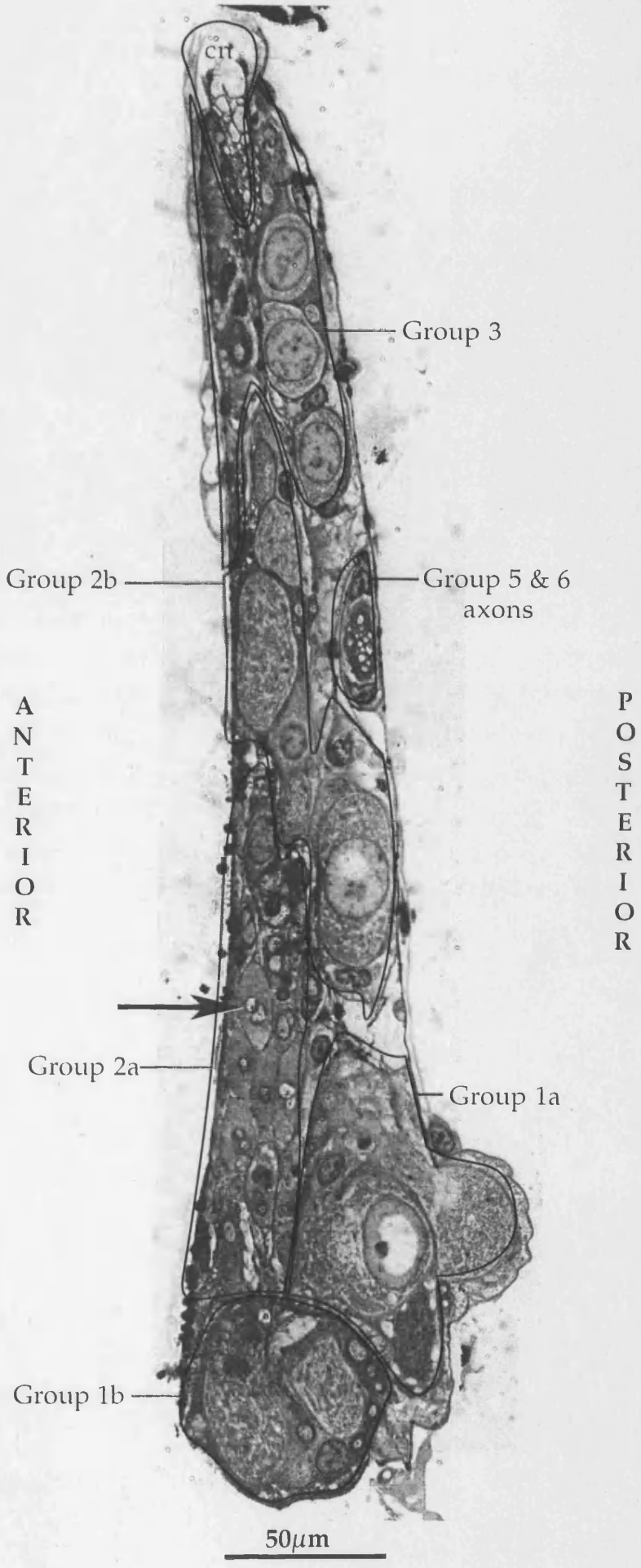
crt
Group 3
Group 2b
Group 5 & 6
axons
ANTERIOR
POSTERIOR
Group 2a
Group 1a
Group 1b
50μm

Figures 4.10a-c

This series of digital images (**a-c**) shows the axons associated with the different mtFCO neurone populations at increasingly proximal levels. The upper image of the mtFCO scoloparium indicates the proximo-distal levels from which the transverse sections were taken. At level **a**, the axons corresponding to each neurone population (indicated) are grouped into discrete bundles. The dorsal-most group is derived from the cuticular nerve (cn). Proximal to this, the axons of adjacent bundles begin to associate. Section **b** shows the fusion of the 1a and 1b axon bundles. Immediately distal to the mtFCO nerve (level **c**) the axon bundles are clearly grouped into two main bundles, one derived from the posterior scoloparium and the cuticular nerve (**P**), and one from the anterior scoloparium (**A**). The axon bundle from the posterior scoloparium includes the group 3, 4, 5 and 6 axons. The axon bundle derived from the mtFCO anterior scoloparium contains the axons of the group 1 and 2 neurones.

[Group 4 axons could not always be traced reliably; they seemed to associate with the posterior scoloparium bundle in most preparations.]

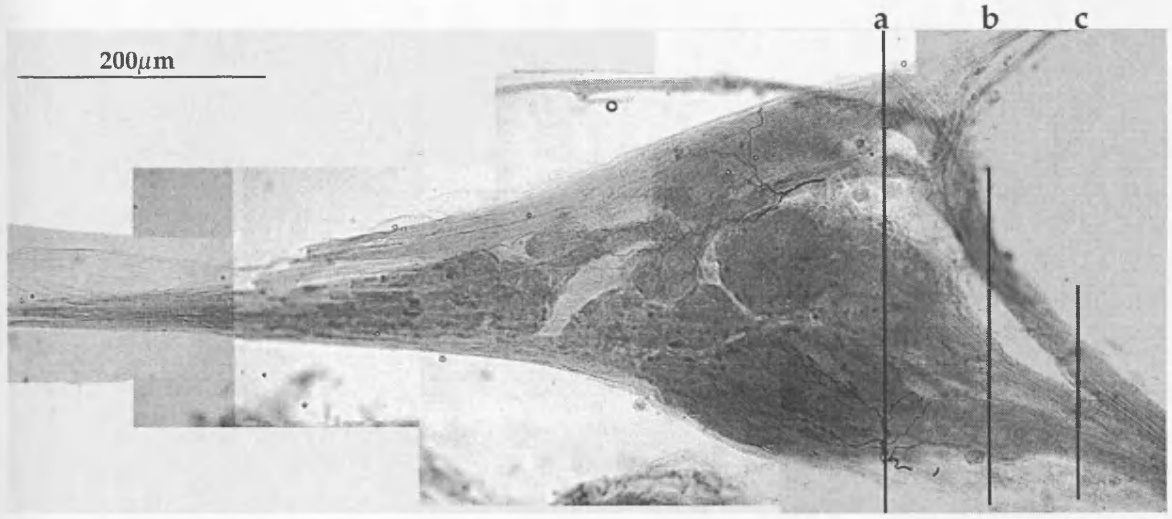
200μm
a
b
c

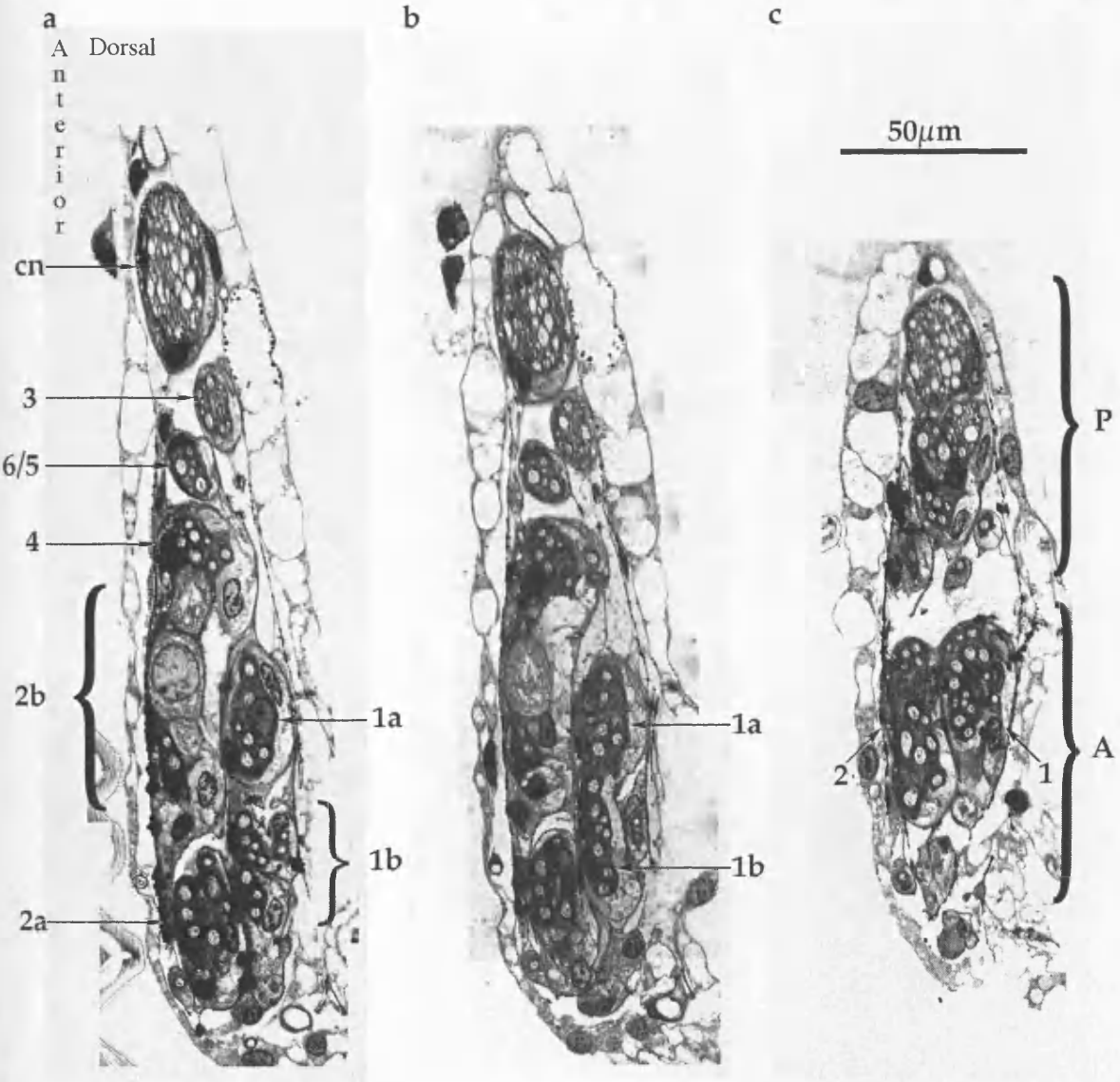
a
b
c
Anterior
Dorsal
cn
3
6/5
4
2b
1a
1b
2a
1a
1b
50μm
P
A
2
1

Figures 4.11a,b

a

The neurone cell bodies (n) have a glial sheath (g) and are surrounded by 'scolopidial cells' (sc) which probably secrete the acellular neural lamella or 'perineural sheath' (p). h = haemolymph space; n' = neurone nucleus

b

The acellular perineural sheath (p) appears homogeneous, although it stains a little darker at its outer edge. It may be formed directly by the scolopidial cells (sc). h = haemolymph space

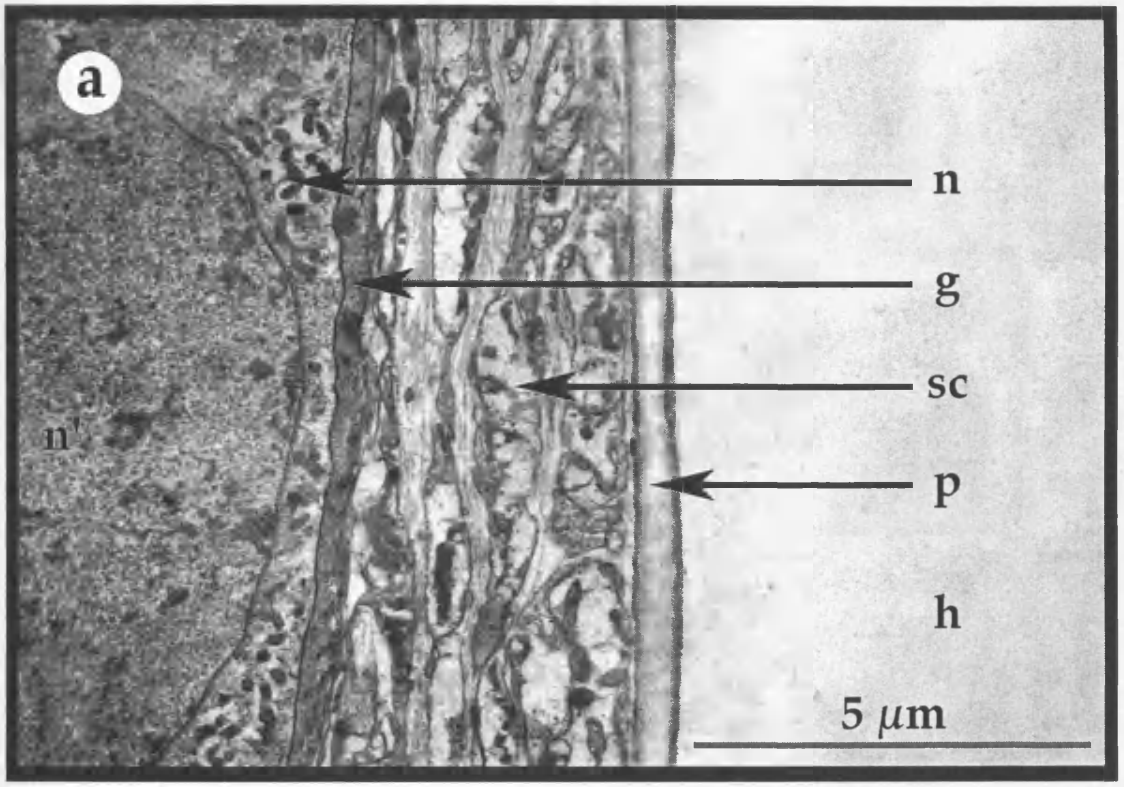
a
n
g
sc
n'
p
h
5 μm

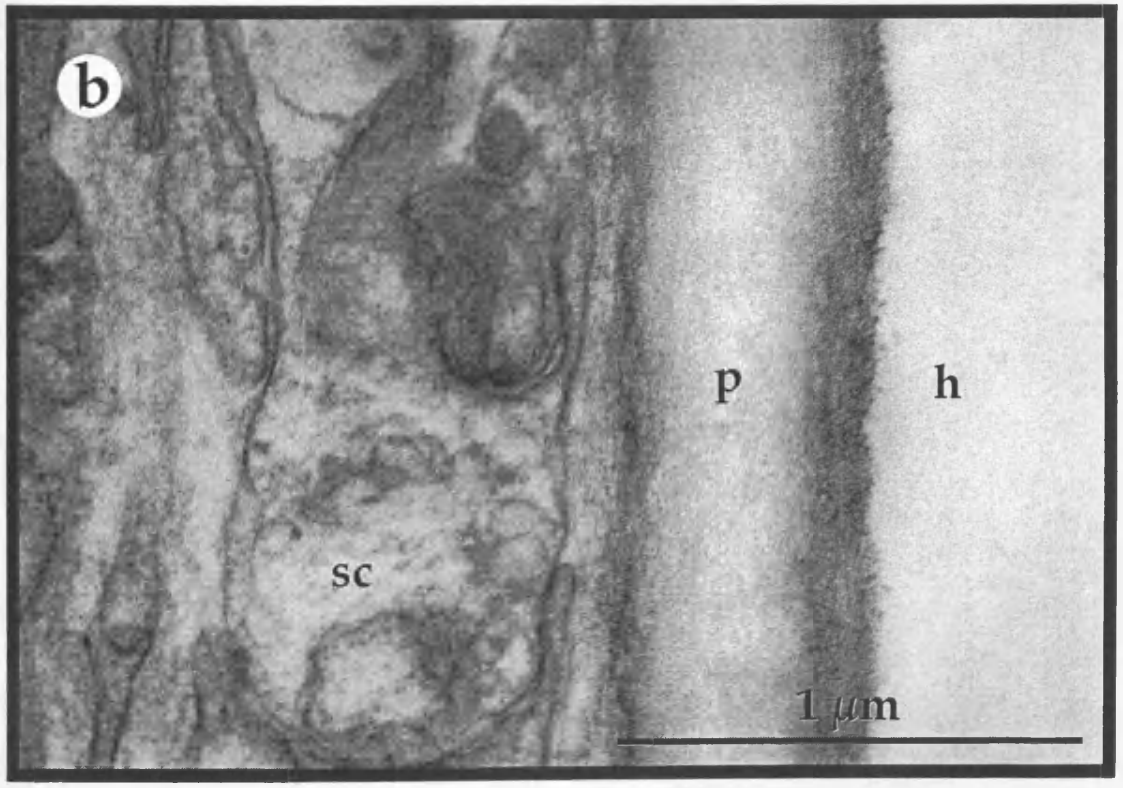
b
p
h
sc
1 μm

Figures 4.12

This image shows a single group 4 scolopidium whose sensory neurones are stained with cobalt. The image is compiled from several greyscale digital images in order to overcome depth of field limitations.
Dendrites (d) travel distally together and terminate in thin ciliary processes (p). The dendrite cilium junctions have different appearances in the two neurones (arrow-heads). Distal is to the right.

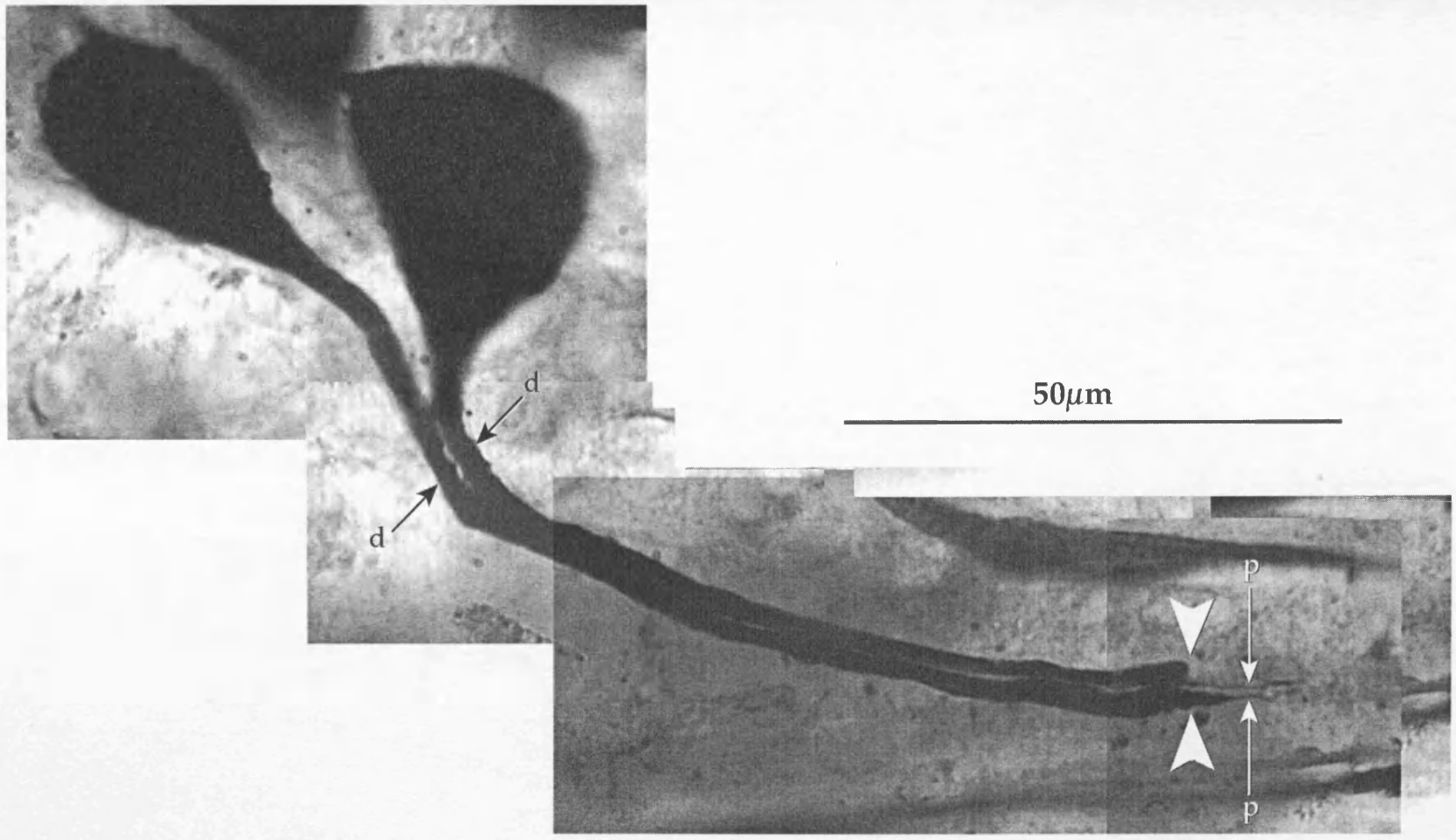
d
d
50μm
p
p

Figure 4.13

This semi-schematic diagram demonstrates the ultrastructure of a scolopidium at the level at which a single attachment cell (at) terminates upon the apical dendrites of twin sensory neurones. The cilia (c) of each dendrite (d) terminate in an extracellular space (ex) flanked by a vacuolated scolopale cell (s) containing electron-dense scolopale rods (sr). Apically, the cilia are embedded in an extracellular scolopale cap (sc). The attachment cells contain axially orientated microtubules (mt) which associate with membranous infoldings of the attachment cell membrane (m). The entire scolopale unit is flanked by extracellular fibres (F) which stain with Acid Fuchsin at the light microscope level. Each dendritic cilium has a ciliary dilation (cd). Basally the cilia terminate on a basal body (b) which is joined to a single ciliary root (rt) by several short rootlets (rl). Proximal to the scolopale cell, the twin dendrites are surrounded by glial wrapping (g). mtc = mitochondria;

[The arrows on the right of the diagram indicate the proximo-distal levels of subsequent figures].

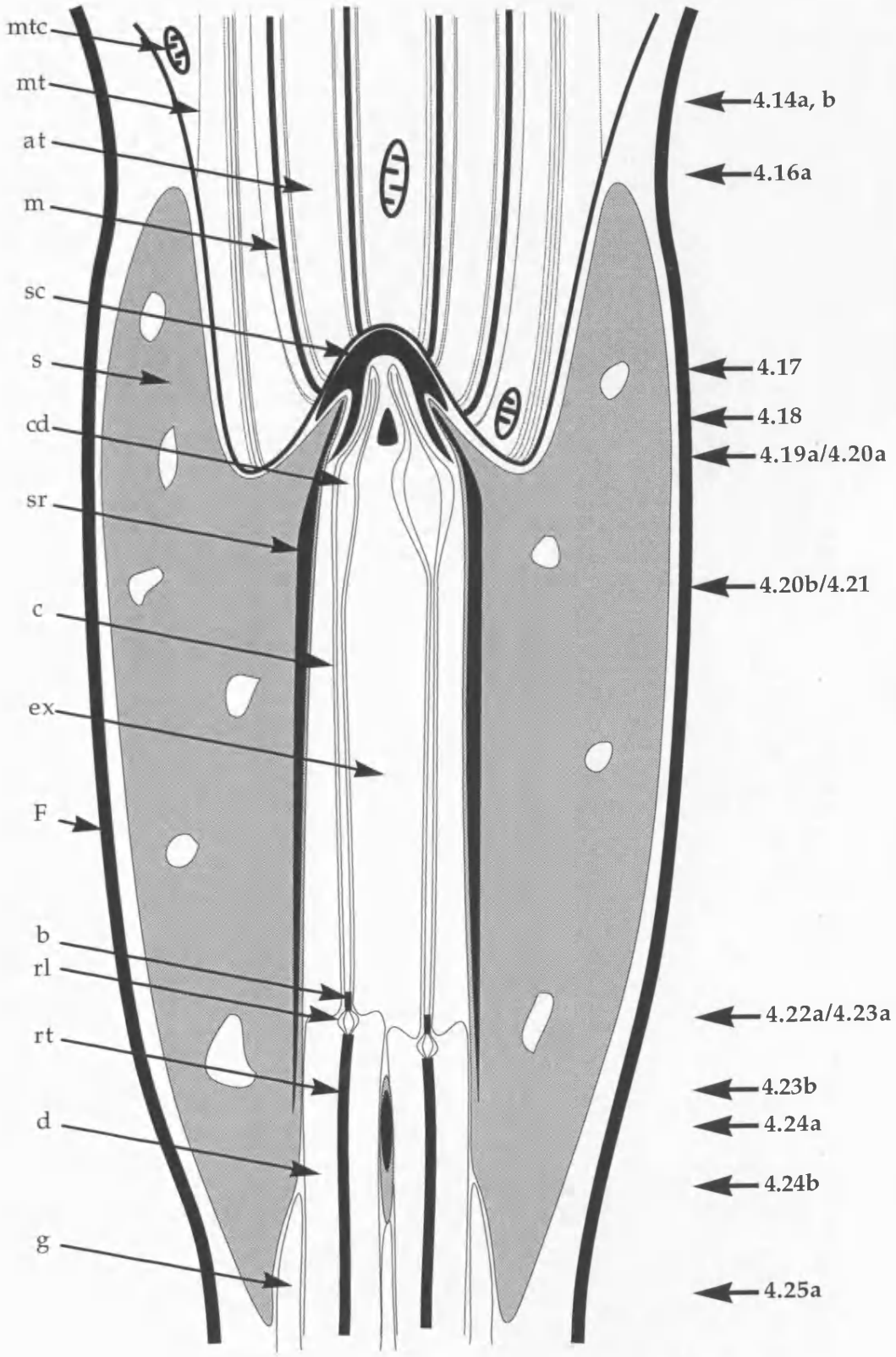
mtc
mt
at
m
sc
s
cd
sr
c
ex
F
b
rl
rt
d
g
4.14a, b
4.16a
4.17
4.18
4.19a/4.20a
4.20b/4.21
4.22a/4.23a
4.23b
4.24a
4.24b
4.25a

Figures 4.14 a, b

a

This electron micrograph shows a transverse section of an attachment cell (at) near to its proximal termination on the mtFCO scoloparium. Whorl-like patterns are formed by folding of the attachment cell membrane.

b

A similar micrograph showing membrane whorls formed by lateral invagination of the attachment cell membrane. Plaques (arrowhead) within the attachment cells (at) are common and high power micrographs (not shown) reveal that they consist of microtubules.

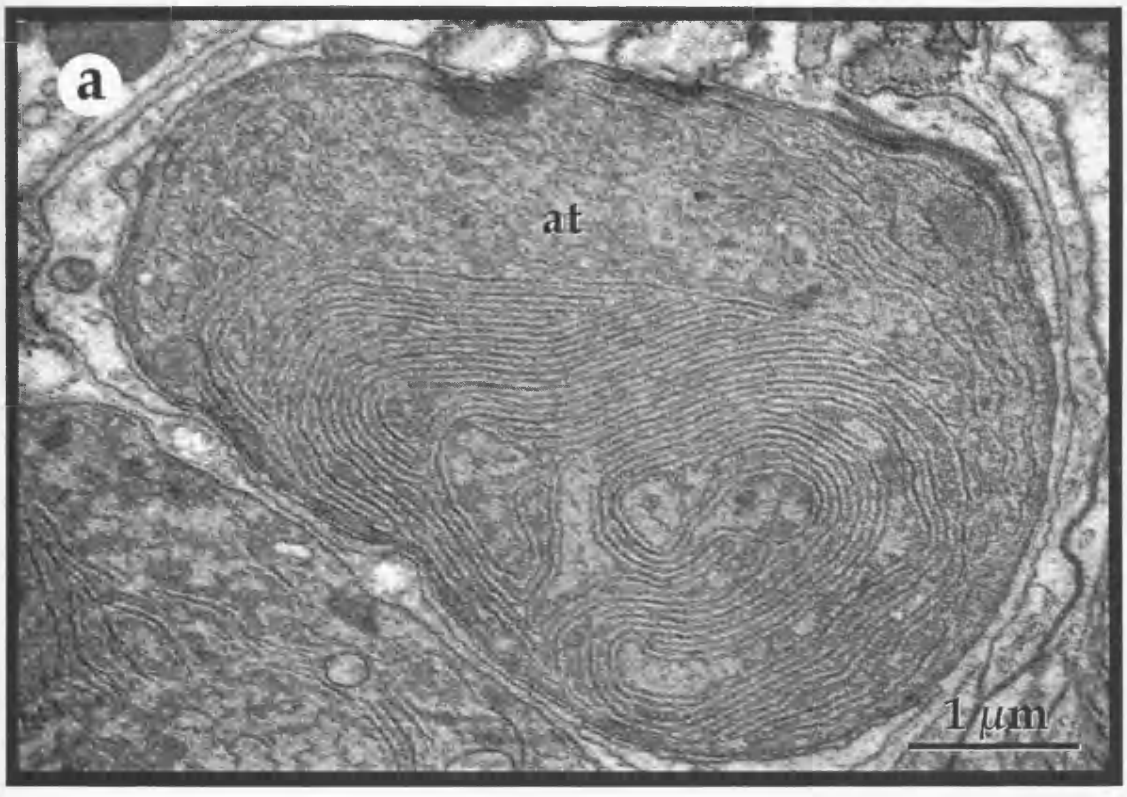
a
at
1 μm

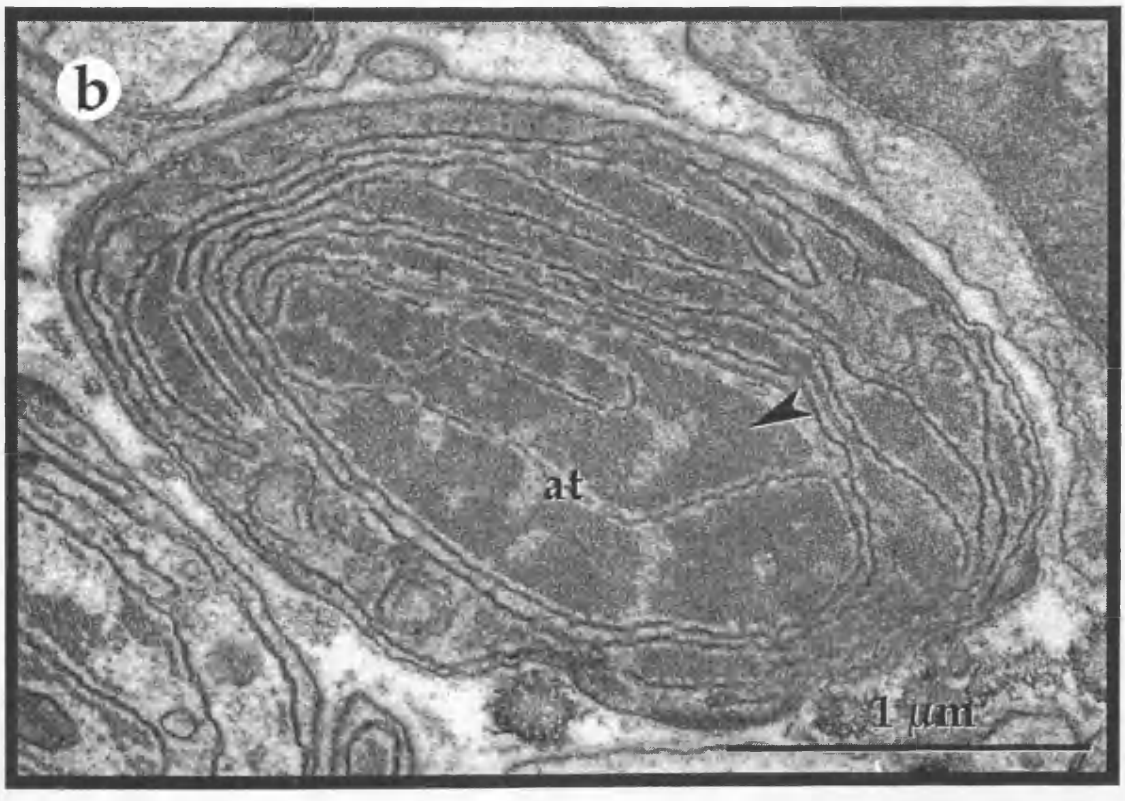
b
at
1 μm

Figure 4.15a, b

a

Electron micrograph showing the association of attachment cell microtubules (m) with the membrane infoldings of the attachment cell whorls (see figure 4.14a) to form ordered rows. The spaces between the infoldings are extracellular (ex). Width of inset = 0.3 μm

b

The microtubules not associated with membranous whorls are often associated with one other. In areas of lower microtubule density, microtubule quartets are common (arrowheads). In areas of high density the microtubules form large plaques in which the microtubules are arranged in a crystalline-like arrays, tens of tubules wide (see Figure 4.13b). F = extracellular fibres; m = attachment cell membrane
Width of inset = 85 nm

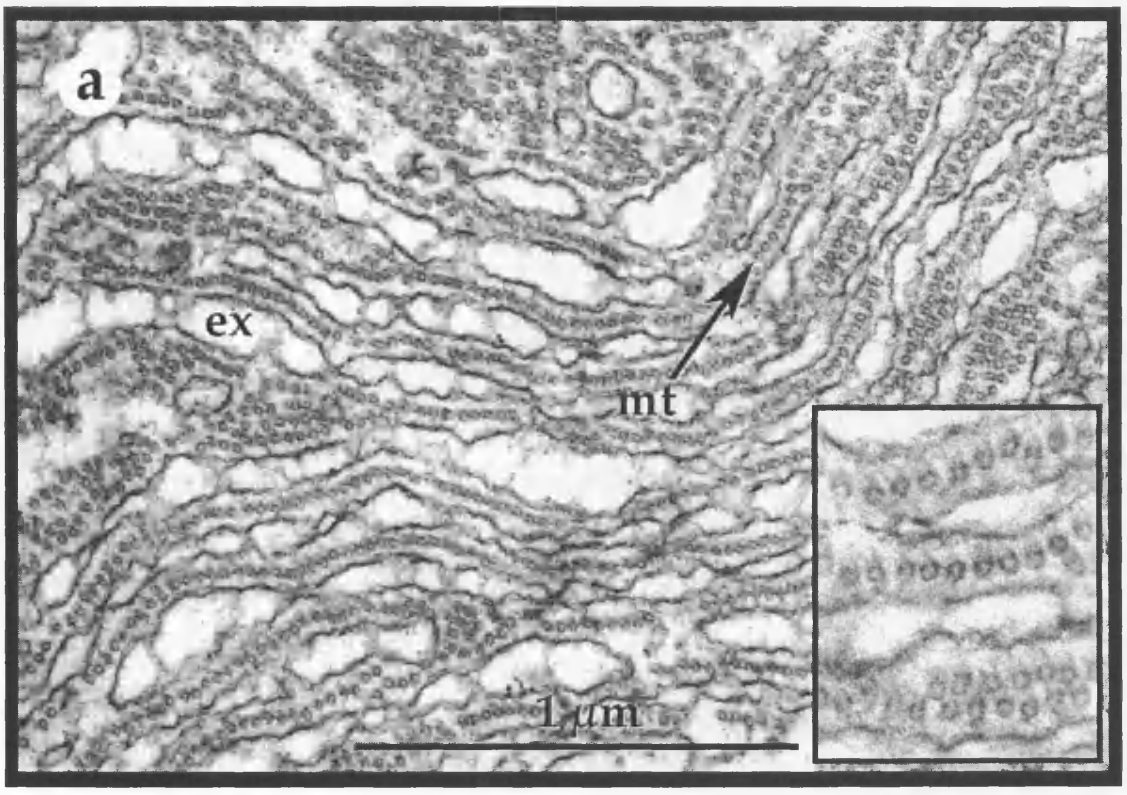
a
ex
mt
1 μm

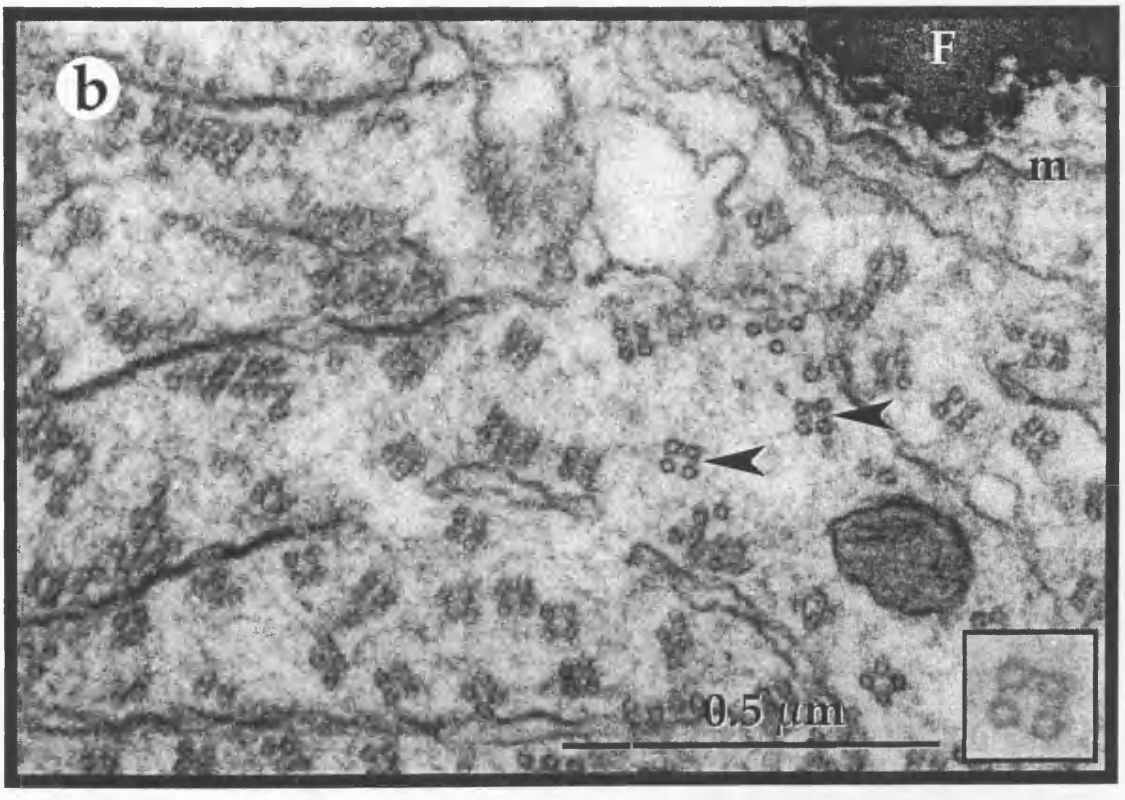
b
F
m
0.5 μm

Figure 4.16a, b

a

This electron micrograph shows an attachment cell immediately adjacent to its proximal termination on a dendrite. The density of microtubules is low in comparison to midway along the apodeme complex ligaments where the attachment cell is packed with microtubules (see Chapter 3). The remaining microtubules (mt) are distributed adjacent to the attachment cell membrane whorls (m). Mitochondria are present at this level (mtc). F = extracellular fibre

b

Low power electron micrograph showing a cluster of four associated attachment cells (numbered) flanked by extracellular (Acid Fuchsin-staining) fibres (arrowheads). h = haemolymph space

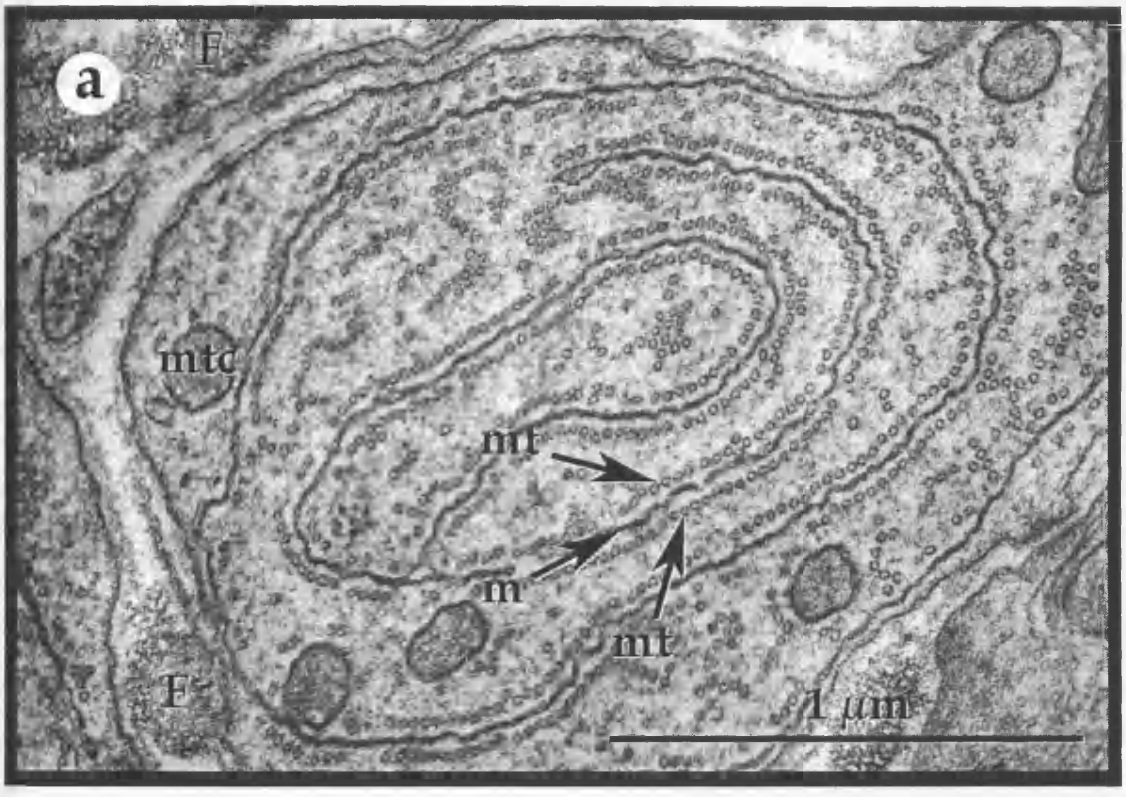
a
F
mtc
mt
m
mt
F
1 µm

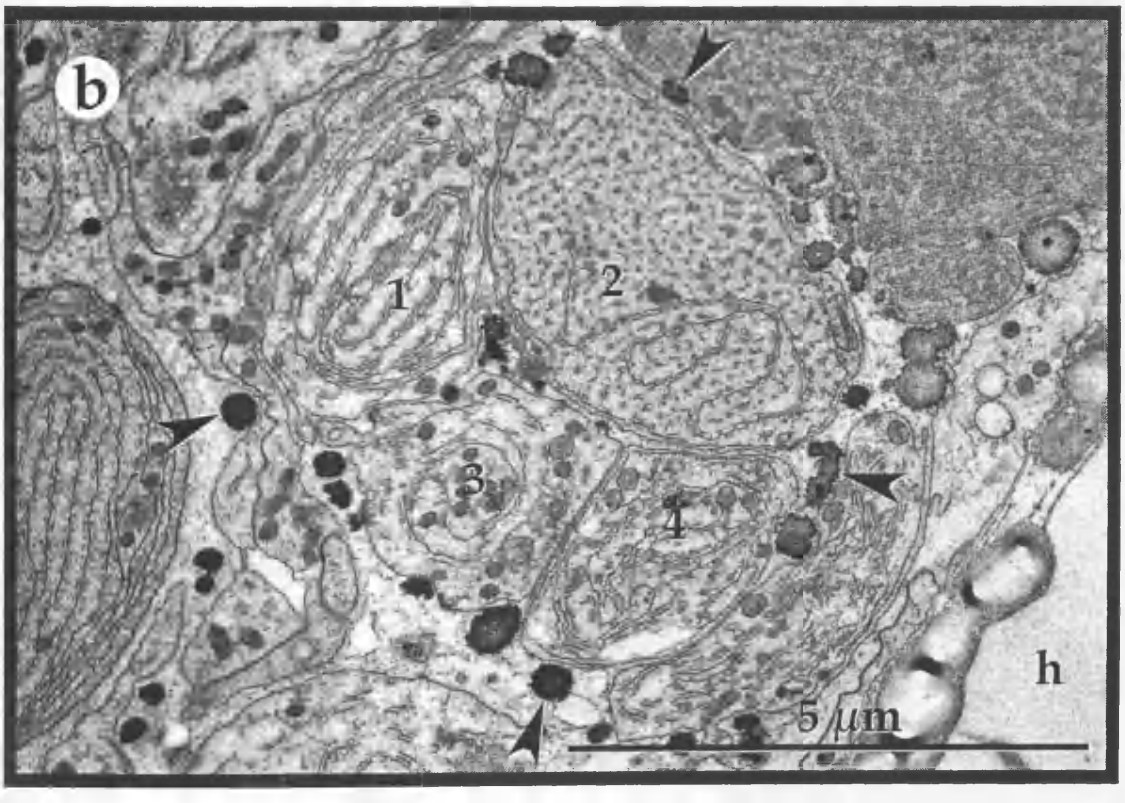
b
1
2
3
4
h
5 µm

Figure 4.17

Transverse section through the extracellular scolopale cap (sc), showing the apical tips of the cilia (c) (inset). The membrane whorl pattern of the associated attachment cell (at) breaks down at this level. F = extracellular fibre

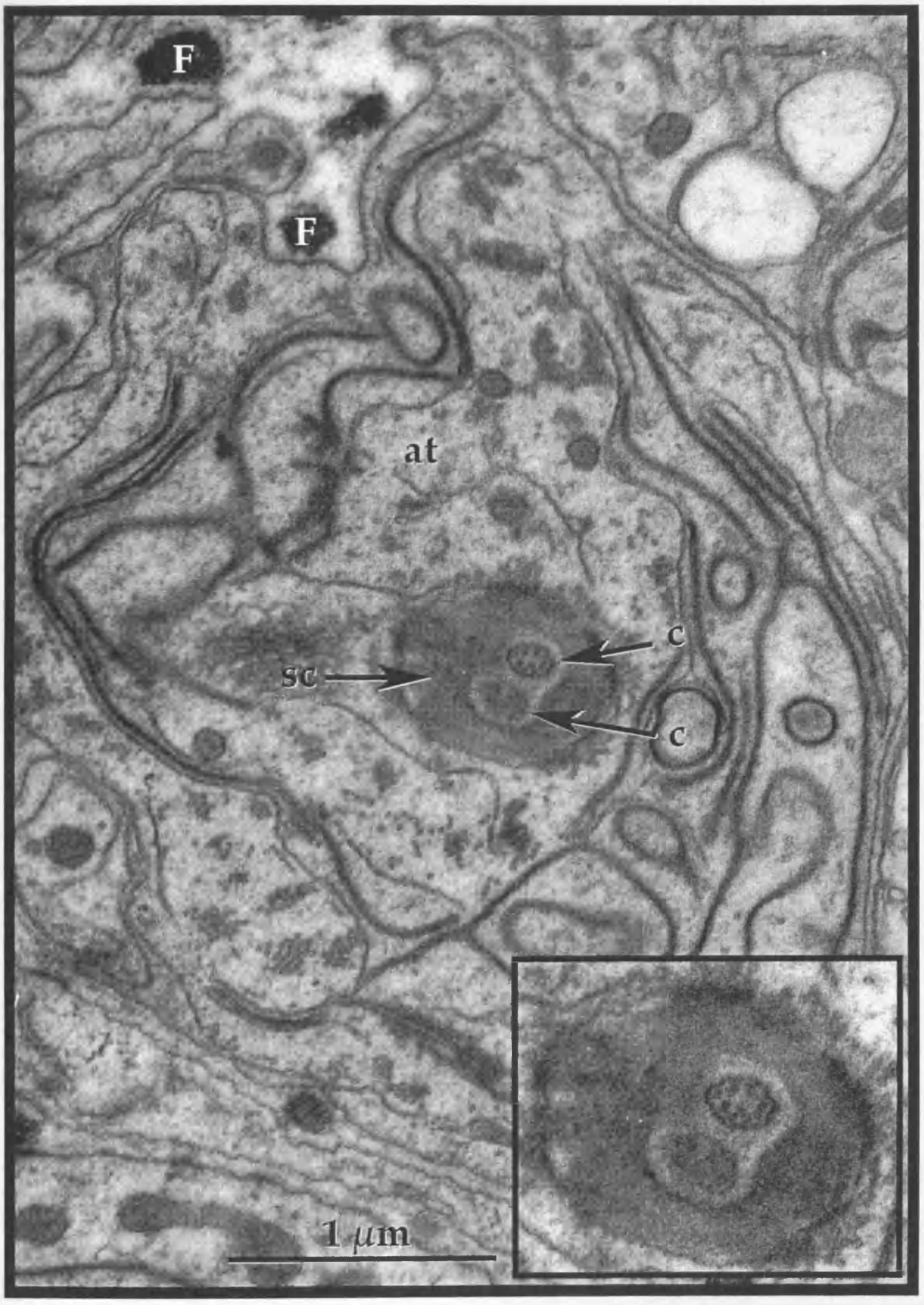
F
F
at
c
sc
c
1 μm

Figures 4.18a, b

a

Proximal to the scolopale cap, the dendritic cilia are surrounded by a scolopale cell (s) containing scolopale rods (sr). Extracellular scolopale cap material (sc) engulfs the scolopale rods and protrudes between the two cilia, largely occluding the extracellular space (ex). The attachment cell (at) surrounds the scolopale cell at this level.

b

This figure shows a higher-power view of 4.18a. The cilia are bound by the dendritic membrane (dm). Each cilium contains axially-orientated microtubules which appear to be arranged into 9 doublets. There are also some individual microtubules located centrally in each cilium. Both cilia are closely associated with the scolopale cap material (sc) located within the extracellular space (ex), the scolopale cap extending radially between the scolopale rods (sr). The rods are also closely associated with the scolopale cap material.

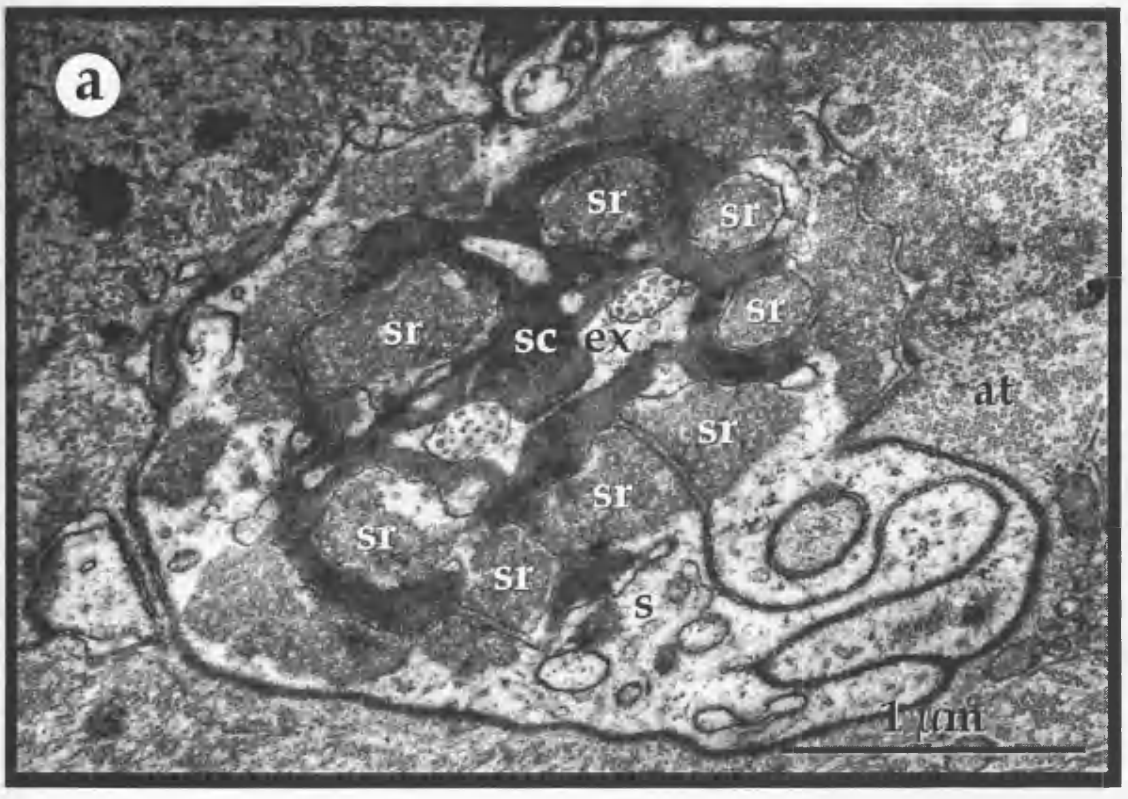
a
sr
sr
sr
sc
ex
sr
at
sr
sr
sr
sr
s
1 µm

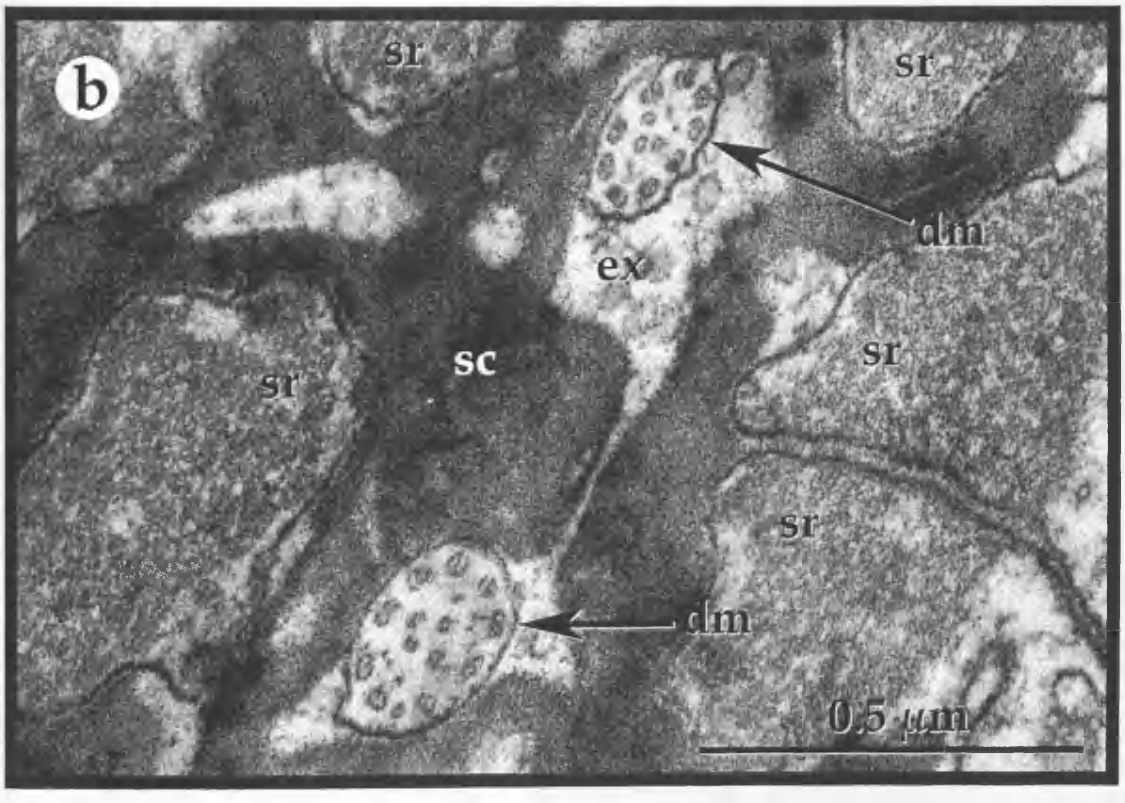
b
sr
sr
dm
ex
sr
sc
sr
sr
dm
0,5 µm

Figures 4.19a, b

a

This electron micrograph shows a cross-section through a single scolopidium at the level of the ciliary dilation. Only one cilium appears dilated at this level. Both cilia have some material at their cores and in the dilated one the doublets are not organised in a regular fashion. The extracellular space is filled with granular material (g) and surrounded by the scolopale cell (s). The scolopale rods (sr) are partially fused with one another. At this proximo-distal level the attachment cell (at) is still present and gives the appearance of concentrically dividing the single scolopale cell into two (see Figure 4.13). m = extracellular matrix; F = extracellular fibre

b

Viewed at higher magnification and at a slightly different level, once more the ciliary dilation can be see to deviate from normal ciliary structure. In each of the cilia, the 9 doublets appear to be associated with some lightly staining granular material. In addition, there is some evidence of close association between the doublets and the dendritic membrane in the narrower cilium because the position of each doublet coincides with a kink in the membrane (arrowheads). A small amount of scolopale cap material (sc) is still visible in this micrograph.

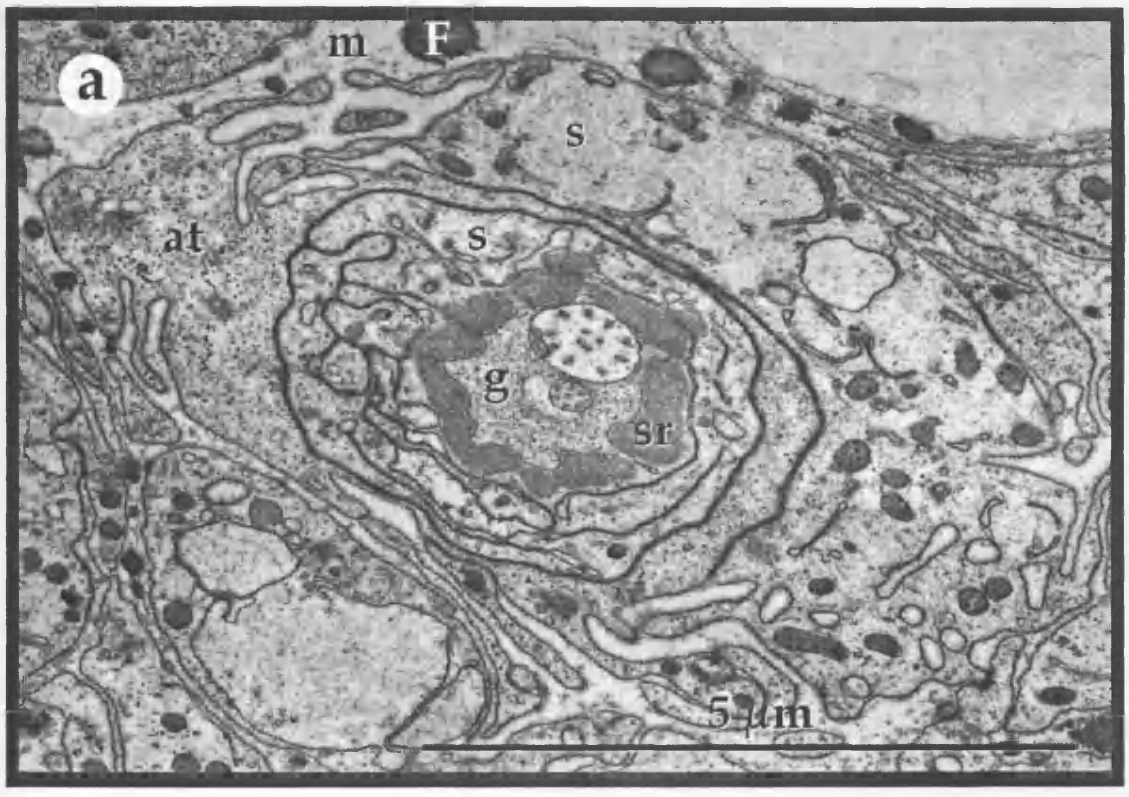
a
m
F
s
at
s
g
sr
5 µm

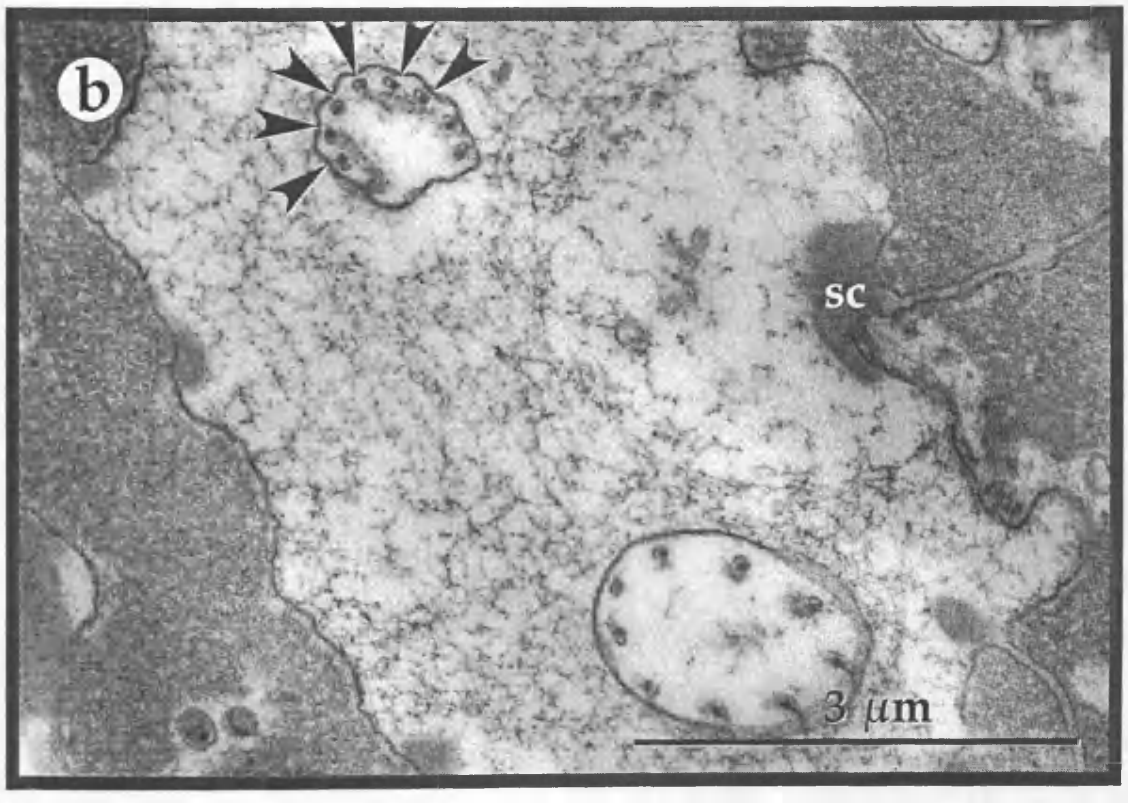
b
sc
3 µm

Figures 4.20a, b

a

At this proximo-distal level, the attachment cell (at) is close to its termination and no longer appears to divide the scolopale cell (s) into two. In this section it is the larger of the two cilia which appears to have infolding of the dendritic membrane adjacent to the ciliary microtubules, which are disorganised (inset). F = extracellular fibre

b

Proximal to the level of the ciliary dilation, the attachment cell is absent and the scolopale cell (s) completely surrounds the dendritic cilia. The latter have a fairly symmetrical cross-sectional appearance at this level. The scolopale cell has a vacuolar cytoplasm with many membranous infoldings. F = extracellular fibre

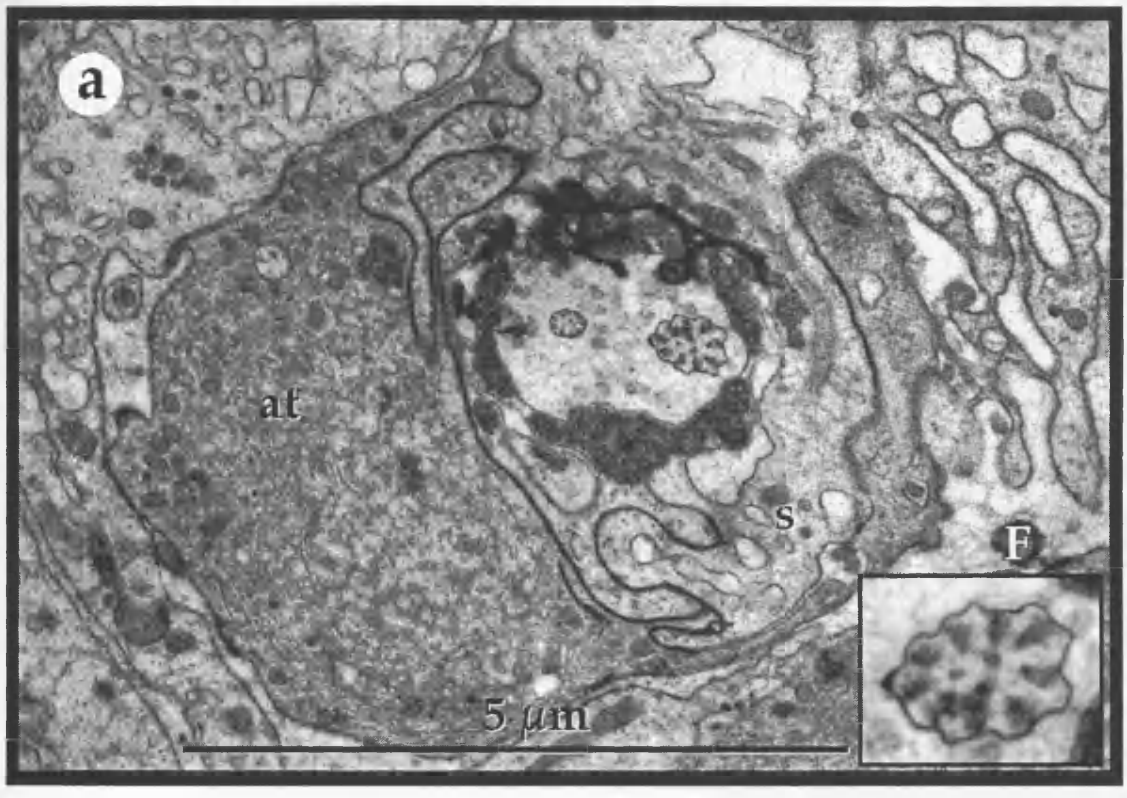
a
at
s
F
5 μm

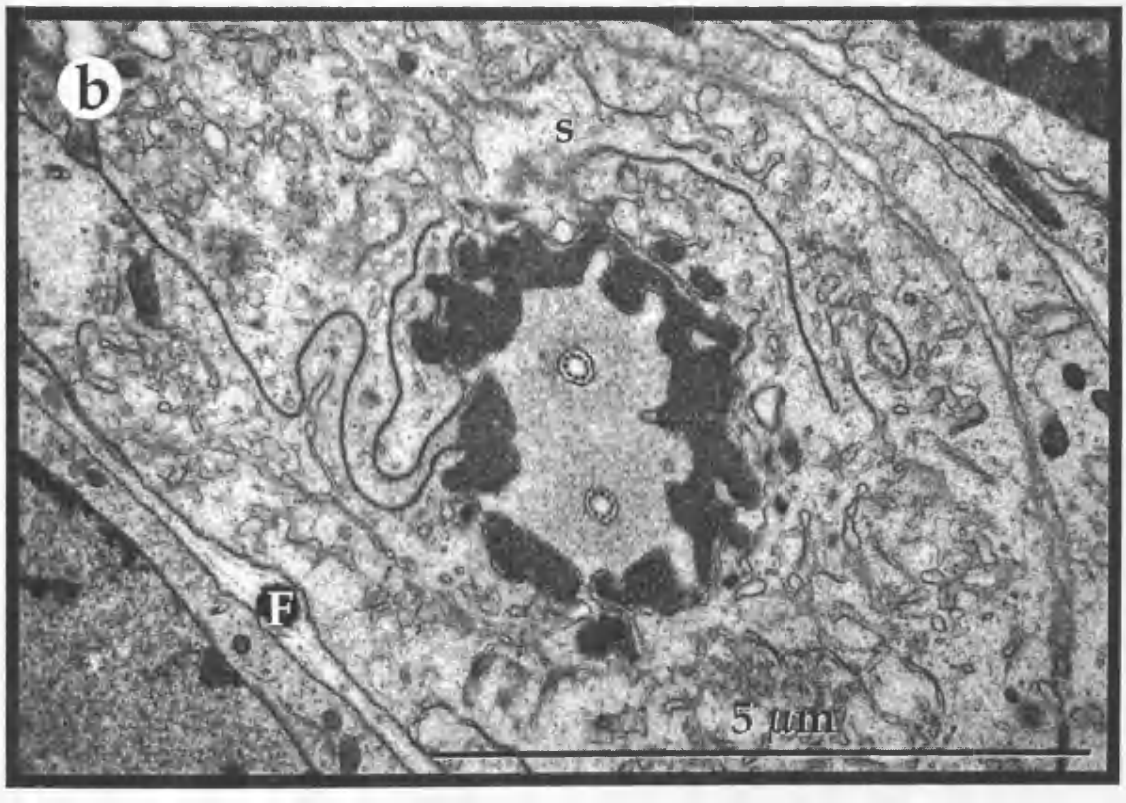
b
s
F
5 μm

Figure 4.21

Proximal to the ciliary dilation, the ciliary microtubules adopt a conventional 9 + 0 arrangement, each bearing a pair of dynein-like arms (arrowheads). The inset shows an enlargement of the two microtubules indicated and demonstrates that the microtubules are singlets at this proximo-distal level. There is no obvious interaction between the microtubules and the dendritic membrane (dm) at this level. ex = extracellular space; sr = scolopale rod material; s = scolopale cell

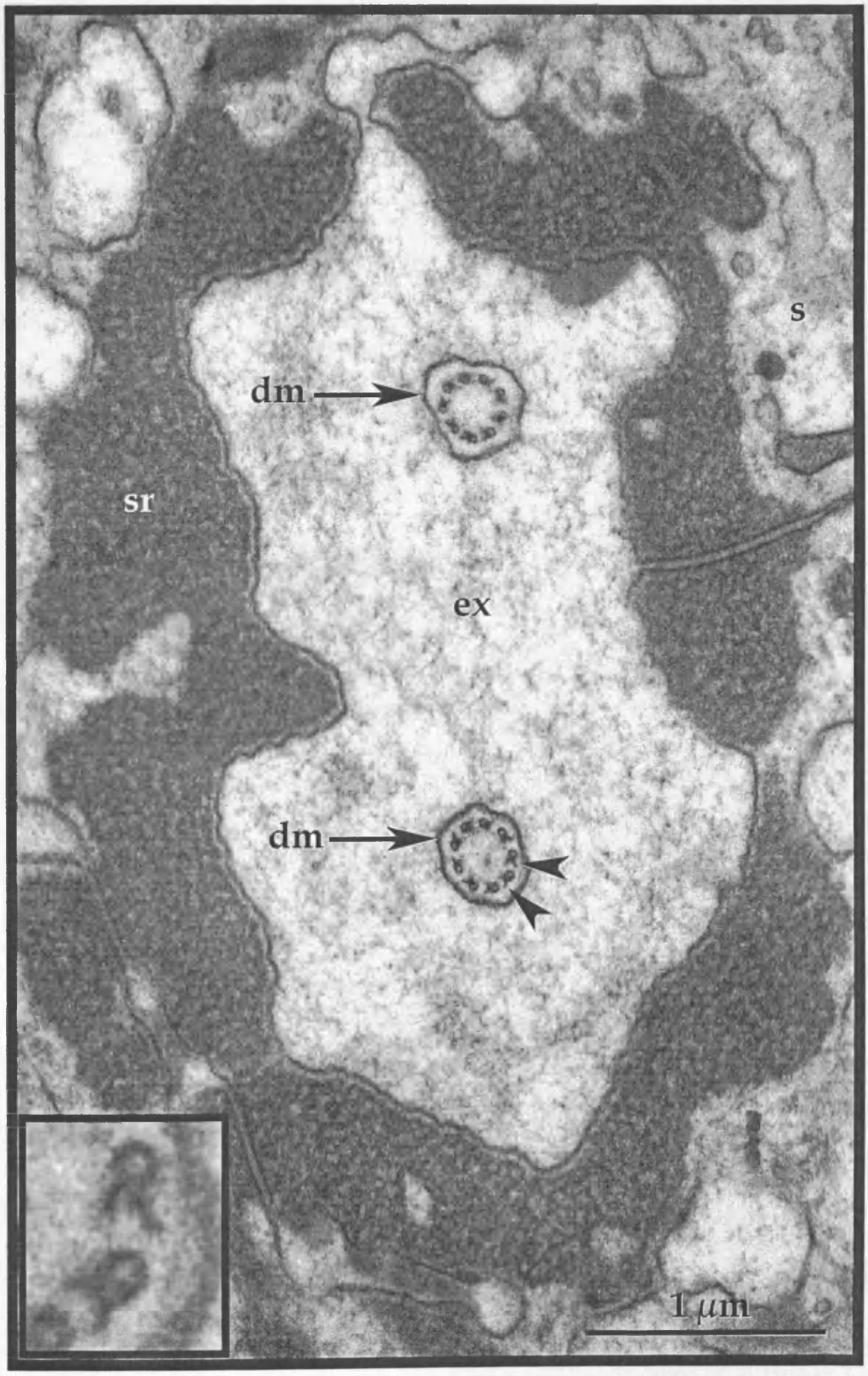
s
dm
sr
ex
dm
1 μm

Figures 4.22a, b

a

Each dendritic cilium terminates proximally at a basal body (bb). At this level, the dendritic membrane (dm) lifts away from the ciliary structures so that the dendrite (d) fills what was previously the extracellular space. Proximally each basal body gives rise to 9 ciliary rootlets (rl). These are visible in the lower of the two dendrites.

b

At higher magnification (lower micrograph) a basal body can be seen to interact with the dendritic membrane (dm) via 9 lightly-staining radial spokes (arrowheads).

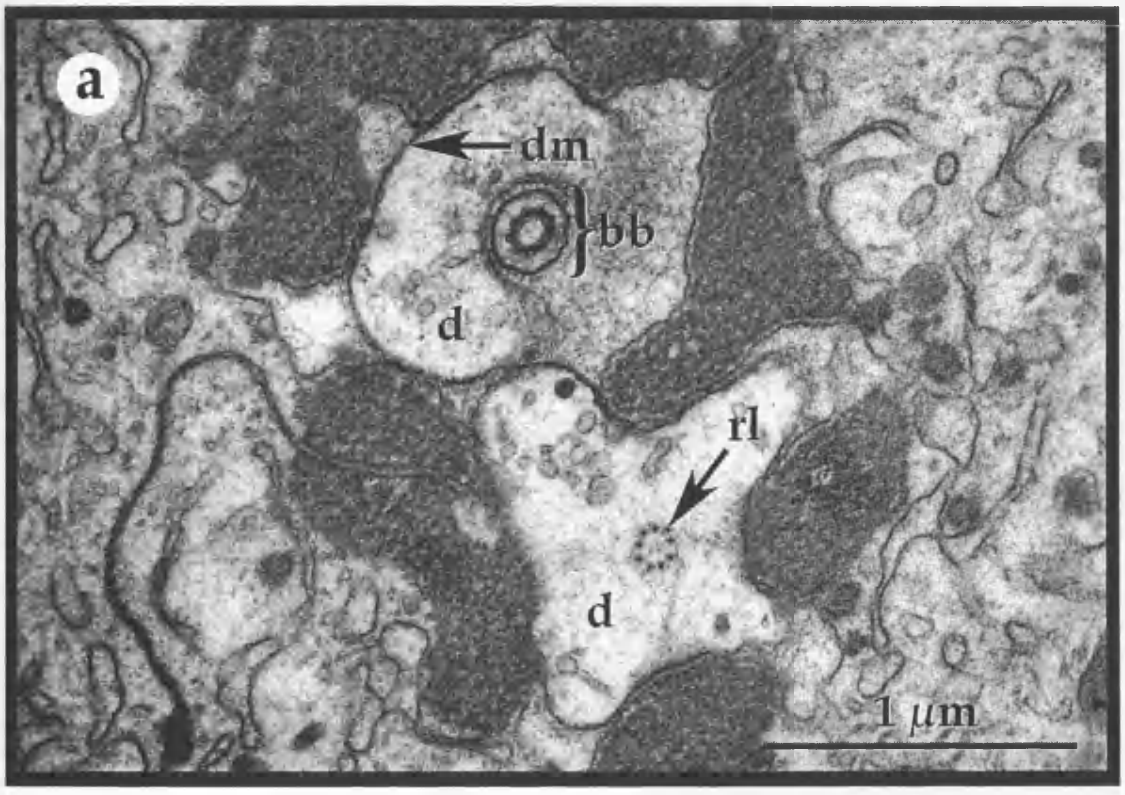
a
dm
bb
d
rl
d
1 μm

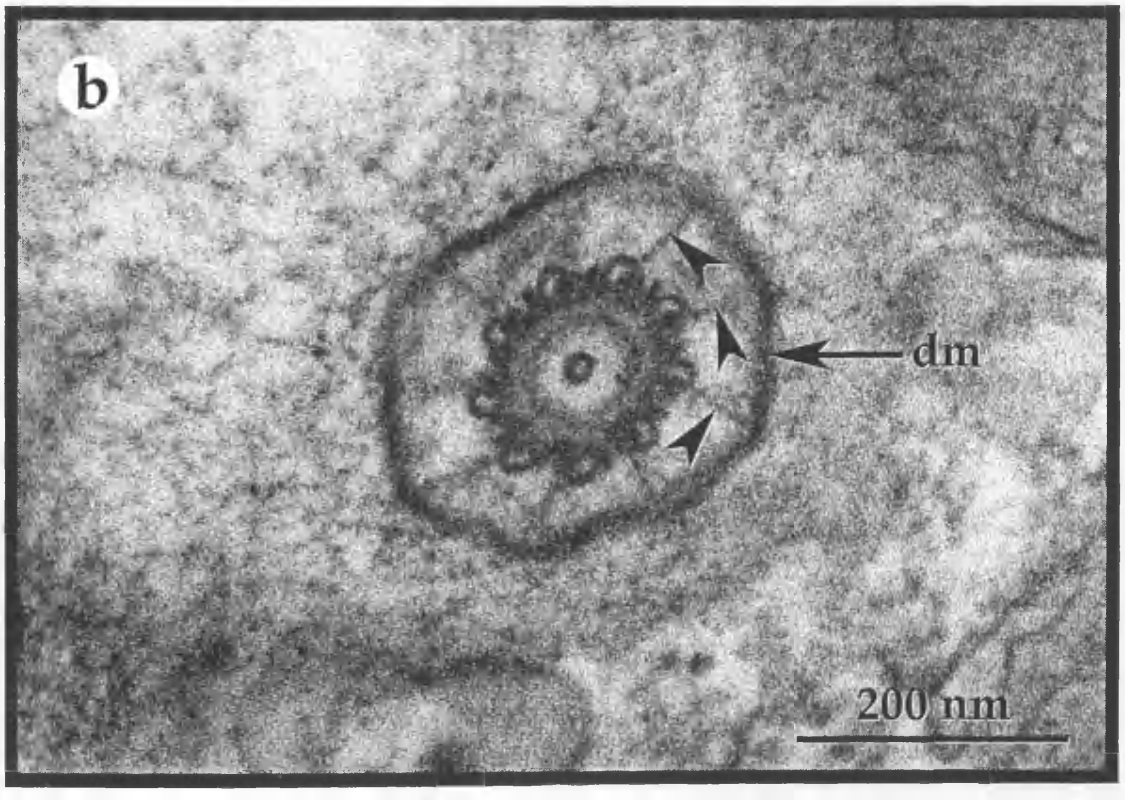
b
dm
200 nm

Figure 4.23a, b

a

Low power electron micrograph showing that the scolopale cell (s) of the scolopidium is surrounded by axially orientated extracellular (Acid Fuchsin-staining) fibres (arrowheads).

b

Micrograph showing the dense ciliary root (rt) proximal to each dendritic cilium. The scolopale rods (sr) are still present at this level, although they are reduced in size.

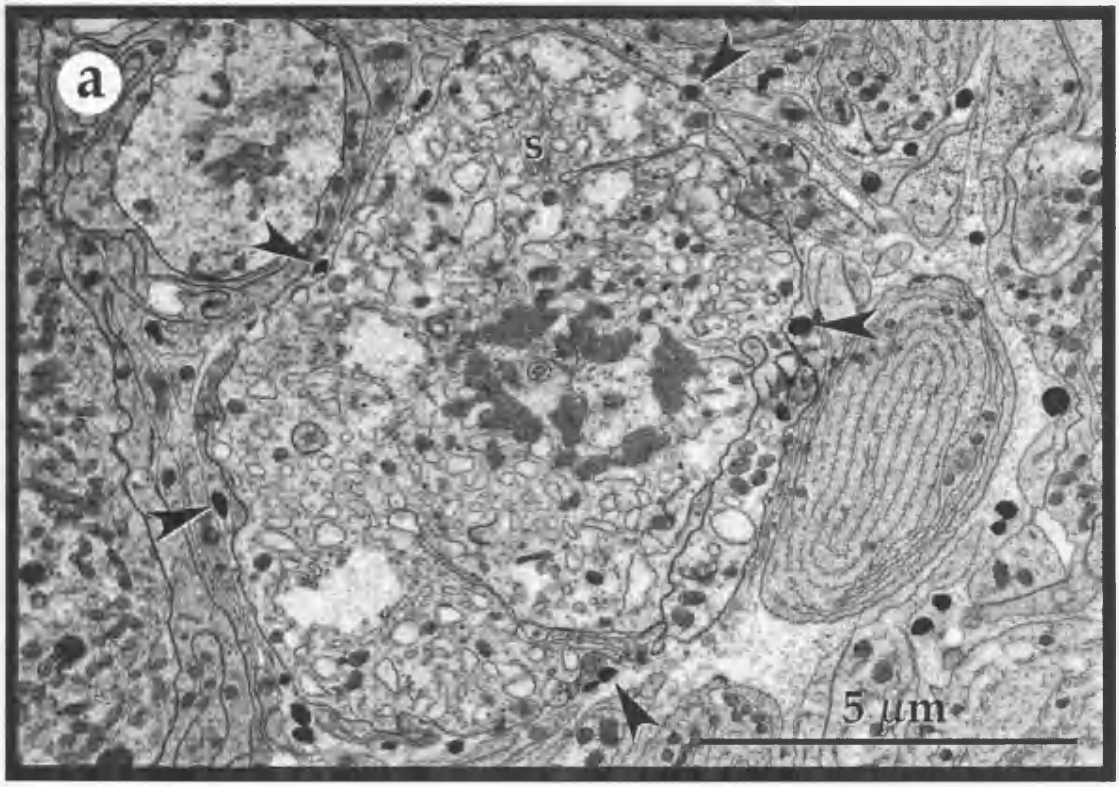
a
s
5 μm

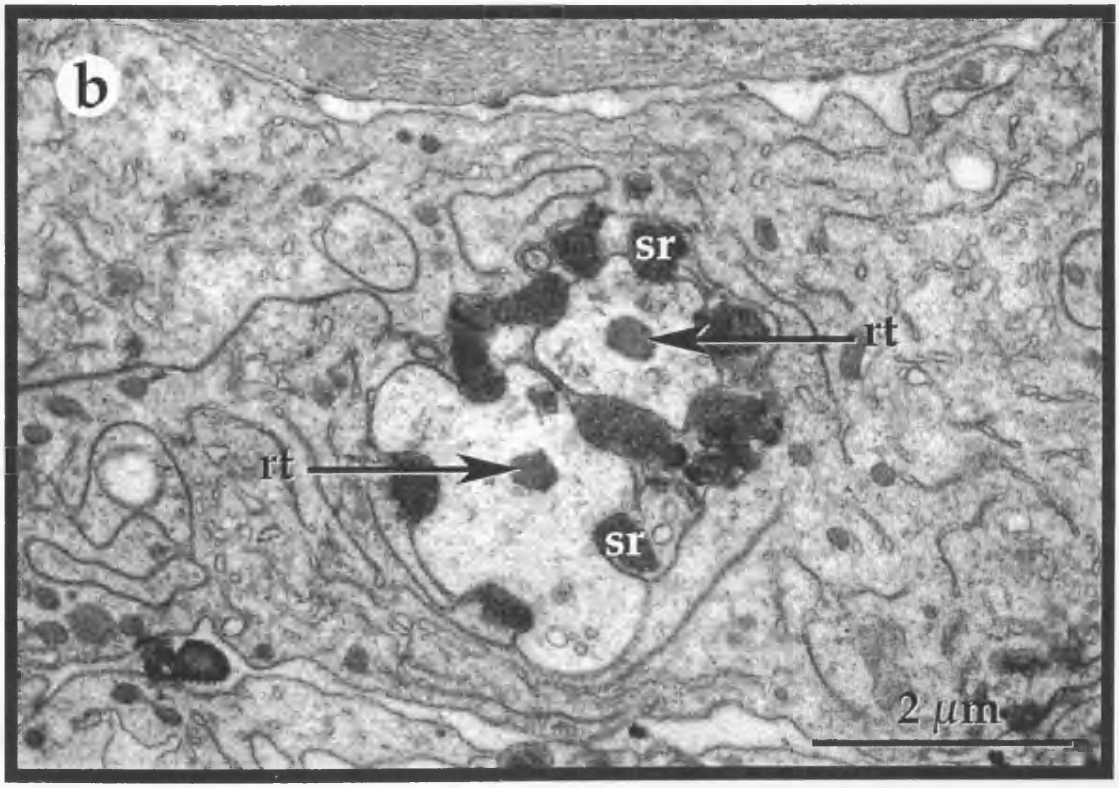
b
sr
rt
rt
sr
2 μm

Figure 4.24a, b

a

This micrograph shows the proximal limit of the scolopale rods. Only a small amount of rod material (sr) remains, which in this case is located between the two dendrites (d). Both dendrites contain many mitochondria (mtc), and the ciliary root in one dendrite is split into 'finger processes' (fp). s = scolopale cell

b

Pairs of dendrites (d) of scolopidia from the same neurone population lie adjacent to one another. Each dendrite pair is surrounded by a single scolopale cell (s). There is no scolopale rod material remaining in the scolopale cells at this level. Each dendrite contains a ciliary root (rt).

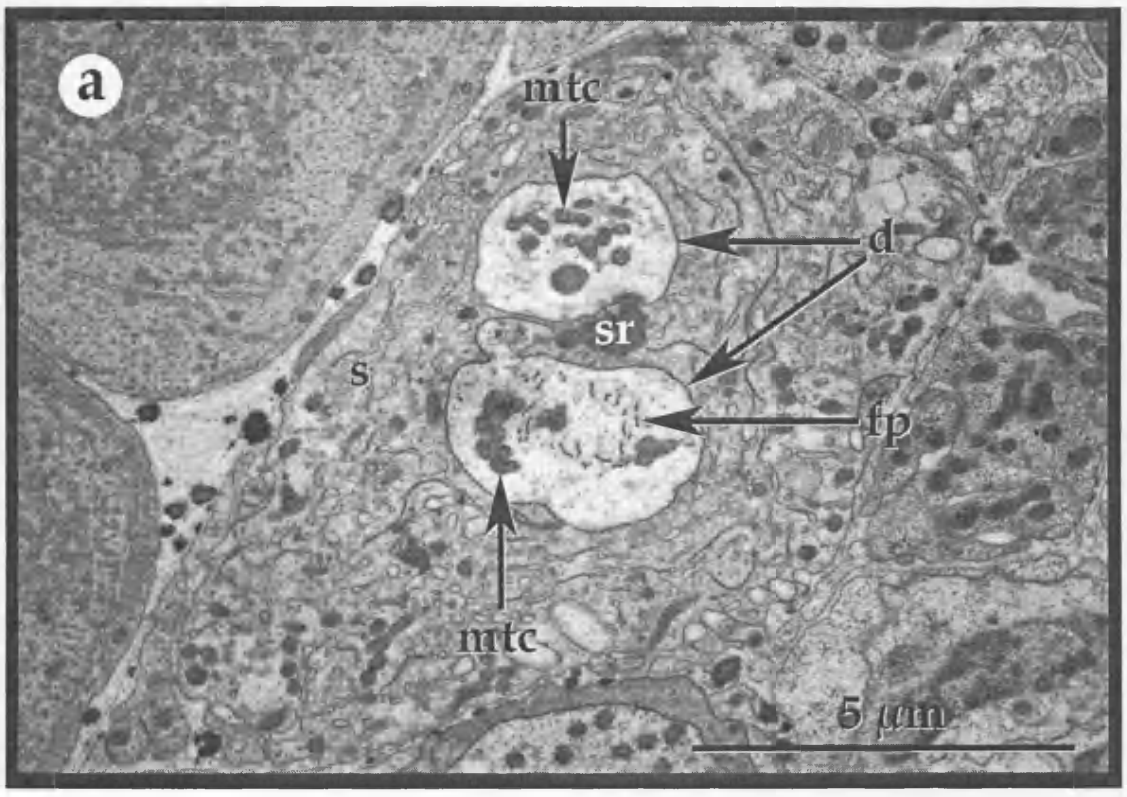
a
mtc
d
sr
s
fp
mtc
5 µm

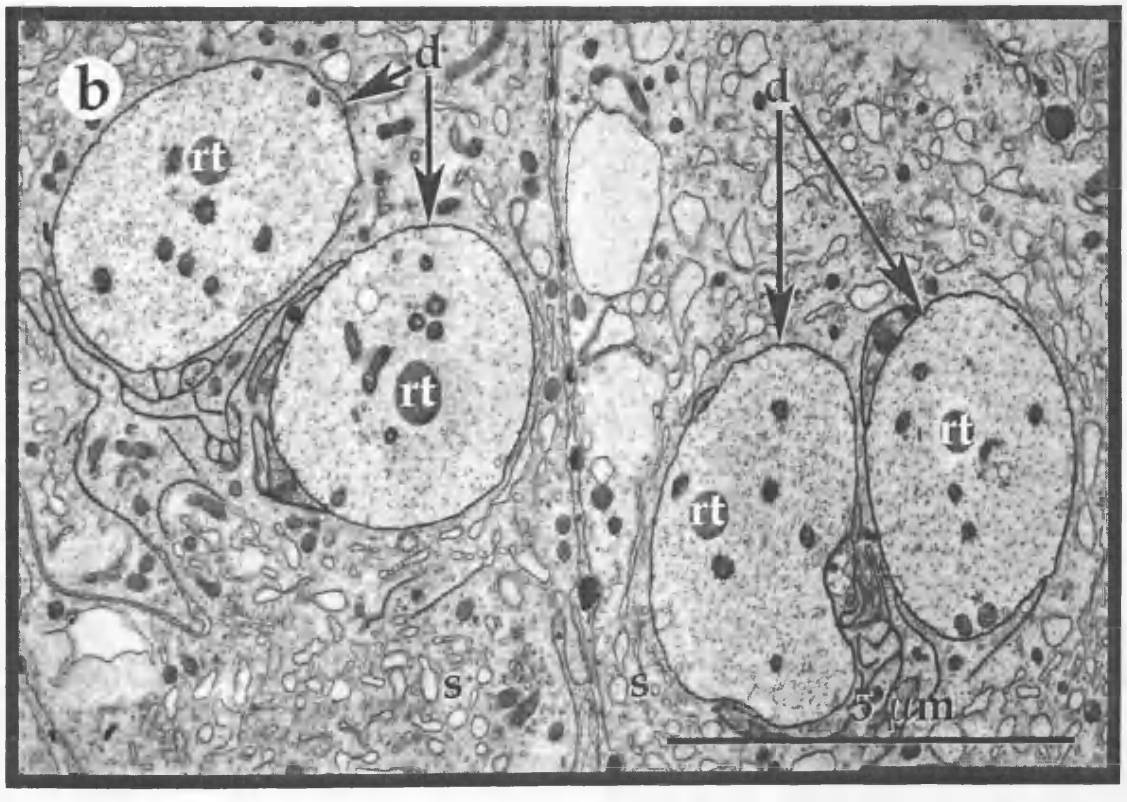
b
d
d
rt
rt
rt
rt
s
s
5 µm

Figure 4.25a, b

a

Proximal to the level of the ciliary roots, the dendrites of each scolopidium travel to their respective neurone cell bodies in pairs. The dendrites are tightly wrapped in a glial sheath cell (g). The scolopale cell (s) is still present although it lacks vacuoles at this level.

b

Low power micrograph showing the presence of extracellular (Acid Fuchsin-staining) fibres (arrowheads) flanking the dendrite pairs of four adjacent scolopidia (numbered).

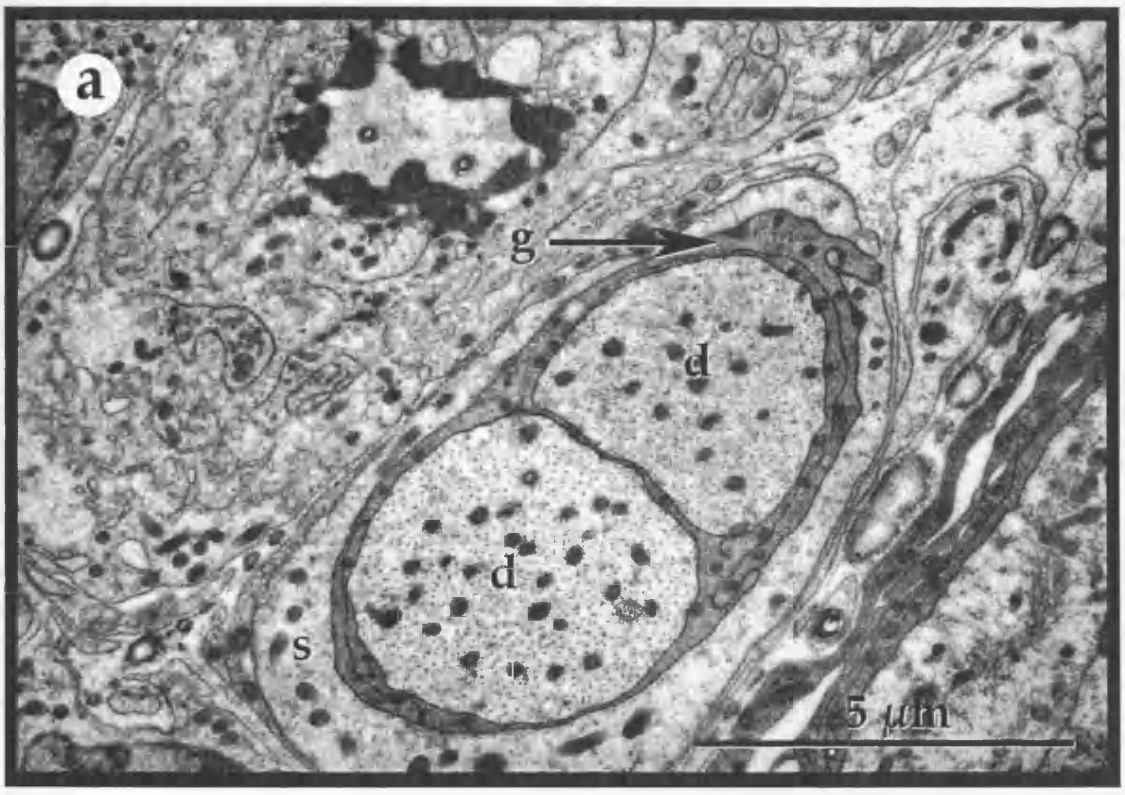
a
g
d
d
s
5 μm

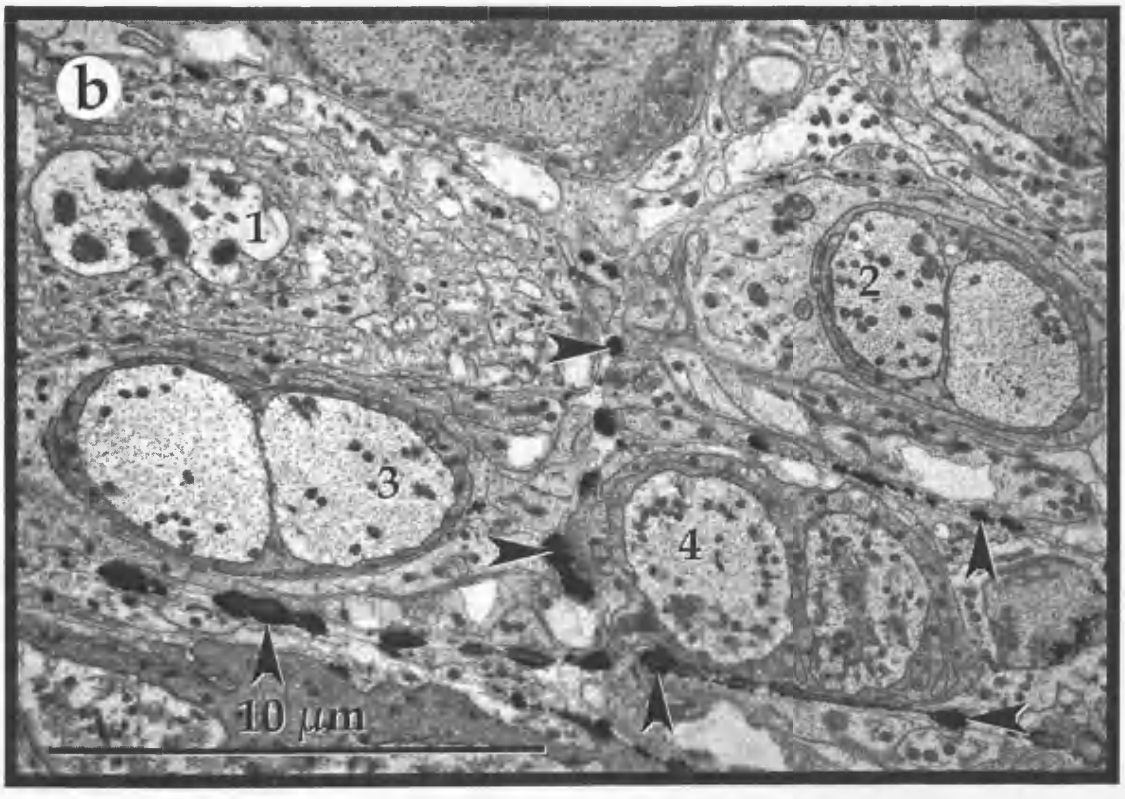
b
1
2
3
4
10 μm

Figure 4.26

This micrograph shows the axons from the group 6 (a6) neurones travelling to the CO nerve in a bundle. Axons from the group 5 neurones (a5) also associate with this bundle. h = haemolymph space

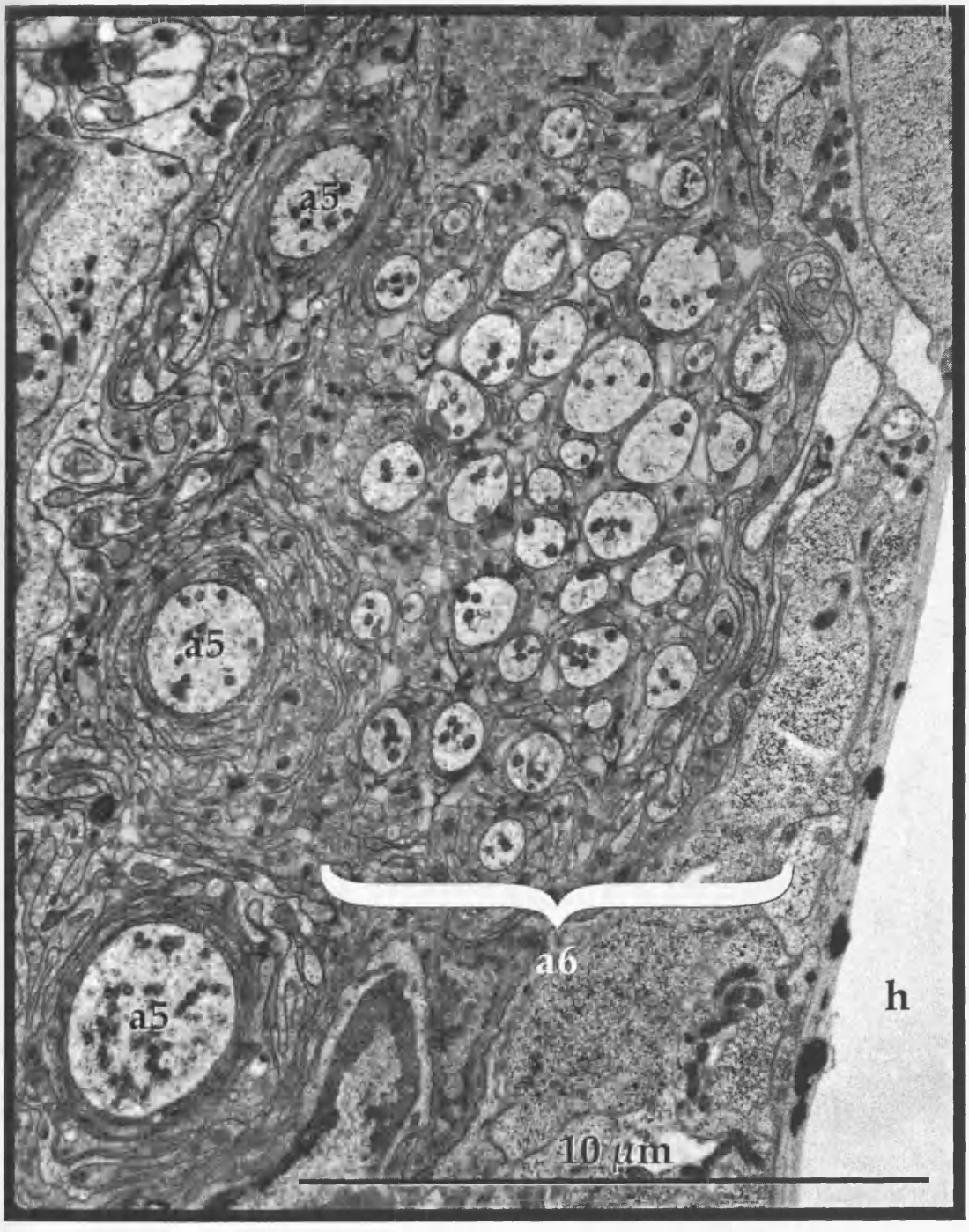
a5
a5
a5
a6
h
10 µm

Figures 4.27a, b

a

Transverse section through the cuticular nerve bundle as it passes through the mtFCO scoloparium to join the CO nerve. There is a range of axon sizes, some of which contain neurotubules (n).

b

The axons (a) of the cuticular nerve bundle are separated from one another by thin glial wrappings (g).

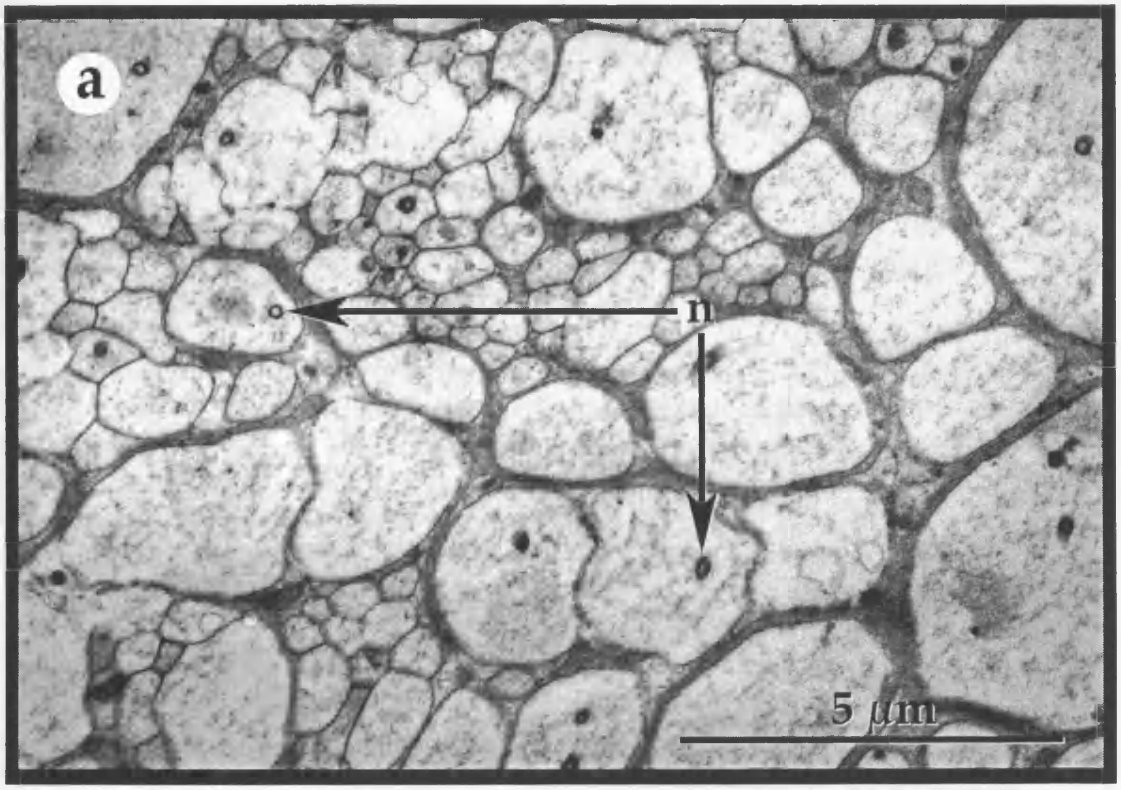
a
n
5 µm

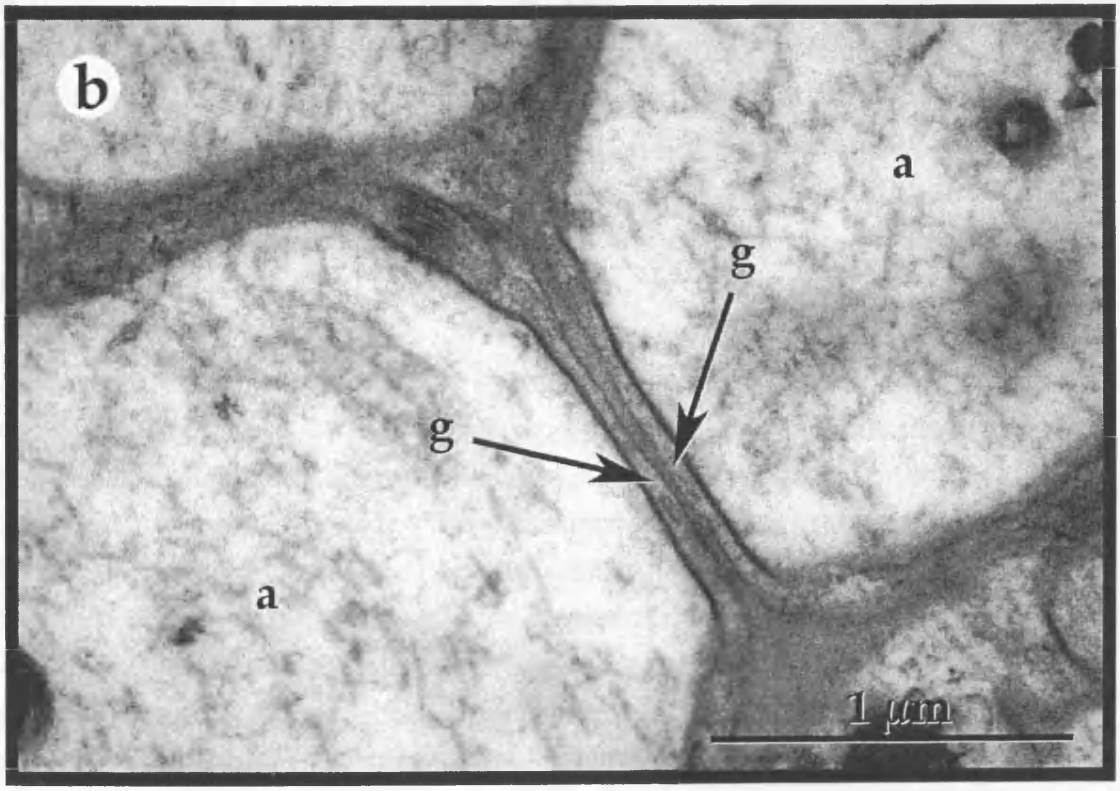
b
a
g
g
a
1 µm

Chapter 5: Displacement of the mtFCO sensory neurones

5.1 SUMMARY

- *When the tibia is in the fully flexed position, the dendrites of the mtFCO neurones are stretched. As the tibia is rotated, the different neurone populations undergo characteristic dendritic buckling. Neurones situated in different regions of the mtFCO scoloparium are subjected to differential displacement across the femoro-tibial angle range. This phenomenon may be partly due to the nature of the mechanical coupling of the scoloparium with the tibia. Measuring the relationship between dendrite length and femoro-tibial angle has shown that whilst some neurones are distorted across the entire femoro-tibial range, others have discrete ranges of distortion.*

5.2 INTRODUCTION

Dendrites are membrane-bound neural processes which allow neurones to interact with other cells or respond to environmental stimuli by virtue of their spatial distribution. In the case of mechano-sensilla one possible role of the dendrite is that it allows the transducer membrane to be positioned in a suitable location to monitor local mechanical displacement, such as that at the base of a sensory hair. Previous authors have speculated about the role of dendrite morphology in contributing to receptor response characteristics (Atema, 1973; see French, 1988). Dendrite orientation has been used to classify the neurones in the mtFCO (Zill, 1985a) and to indicate what the nature of the adequate mechanical stimulus of the receptor might be.

With the exception of a recent study by Nishino and Sakai (1997) on unfixed dye-stained cells of the cricket *Gryllus bimaculatus* FCOs, the way in which the CO receptor cells are mechanically distorted during tibial displacement has been investigated by comparing the morphology of specimens fixed in the stimulated and non-stimulated states (Atema, 1973; Moran *et al.*, 1977). This chapter has employed a method which has allowed the sensory neurones in fresh unfixed preparations to be visualised. Rotations of the tibia about the femoro-tibial joint to new static positions allowed the morphology of the cells to be examined at a range of femoro-tibial angles.

The results of this chapter show that as the tibia is flexed the dendrites are stretched and they undergo characteristic buckling as the tibia is extended. It is also shown that neurones located in different regions of the mtFCO scoloparium are subjected to different degrees of distortion. In addition, dendrites in different regions are shown to undergo characteristic buckling and to have different relationships of dendrite length with femoro-tibial angle. This study has also shown that there is an element of differential movement between the inside of the scoloparium and the organ sheath. Thus, descriptions of scoloparium distortion based solely upon the displacement of surface markers cannot characterise the actual stimulation of the sensory neurones.

5.3 MATERIALS AND METHODS

Retrograde filling of the mtFCO neurones was carried out using a 5% aqueous solution of the fluorescent dye 5(6)-Carboxyfluorescein (see Appendix 1). Femoro-tibial angle was manipulated whilst the stained cells were visualised *in situ* using an inverted epifluorescence microscope fitted with a BioRad Lasersharp MRC 400 confocal laser scanning system. The filling was performed on intact whole animals, the femora being subsequently removed and mounted immediately prior to examination.

5.3.1 Staining and dissection

Individual *S. gregaria* were chilled overnight at 4°C and immobilised in glass petri-dishes using insect wax. The femora of each animal were secured anterior face uppermost. A window of cuticle was removed at mid-femur level to expose the CO nerve, leaving the femoral tracheae intact. The severed end of the CO nerve was held in contact with 5(6)-Carboxyfluorescein dye (CF) by placing it in a sealed Vaseline bath using the same technique as used for cobalt staining (Chapter 4). In some preparations, the severed end of the nerve was lightly teased apart to encourage single isolated neurones to fill with dye. Preparations were kept in petri-dishes at 4°C overnight (12 h) in a saturated atmosphere whilst the dye migrated distally along the axons of the CO nerve to fill the neurones. In some specimens, the Vaseline bath was made at the base of the femur with the metathoracic leg nerves being severed at the point at which they inserted into the metathoracic ganglion. In these cases, the preparations were left in the fridge for 48 h to allow sufficient time for the dye to reach the mtFCO. Following staining, a window of cuticle overlying the mtFCO

was removed from the anterior and posterior faces of the isolated femora as described for transmission light microscopy (see Chapter 2). In some preparations, carborundum granules, used to act as displacement markers, were applied to the surface of the organ using a mounted hair.

5.3.2 Mounting for microscopy

Since the neurones were observed whilst the organ remained *in situ*, special arrangements were needed to mount the isolated legs so as to minimise the problems associated with short working distances set by the microscope objectives. The tibia was severed just below the knee and the leg was mounted anterior face down on a large number 0 cover-slip using rapid Araldite. The coverslip formed the base of a specially made welled slide milled from a single sheet of transparent Perspex (Fig. 5.1). The coverslip was secured to the slide using dental wax to form a water-tight seal. The slide fitted into the standard slide slot on the microscope stage and in addition had an extended plate which lay on top of the stage when the slide was in position. A paper protractor was attached to this plate using double-sided tape (Fig. 5.1). The protractor was aligned with the centre of rotation of the femoro-tibial joint whilst the baseline ran along the axis of the femur. The slide well was subsequently flooded with insect saline (see Appendix 1) to prevent desiccation and provide a suitable optical environment. The preparation was illuminated using laser or conventional light sources. For confocal imaging the preparations were excited at 488 nm and the emission was detected at 515 nm and above. A Plasticine pellet was used to hold the tibia at different angles whilst digital images were captured and saved to optical disk.

5.3.3 Image Analysis

In order to measure the lengths of the neurone dendrites when the tibia was held at different positions, the digital images were imported into the public domain image analysis package NIH Image (vs. 1.62/ppc). Parameters such a dendrite length were measured by tracing over the image with a freehand tool. Lengths were returned in μm.

5.4 RESULTS

Previous authors (Field, 1991; Shelton *et al.*, 1992) have speculated that the sequential tightening of the ventral ligament attachment cells during tibial flexion (see Chapter 2) may present some or all of the mtFCO neurones

with differential stimulation by virtue of their positions in the scoloparium. The pattern of dendrite distortion with changing femoro-tibial angle may also depend upon several other factors. These include:

- The asymmetric attachment of the mtFCO apodeme upon the tibia relative to the centre of rotation of the joint. This results in the organ being subjected to sinusoidal displacement as the tibia is rotated.

- The modifying influence of the mtFCO guy-rope fibres upon apodeme complex displacement over some parts of the femoro-tibial range.

- Differential displacement of the dorsal and ventral ligaments.

- Different mechanical properties of the two ligaments.

- The influence of the mtFCO's ventral attachment to the flexor tibiae muscle.

- The effects of the flexor strand.

Confocal imaging of the mtFCO scoloparium enabled individual dye-filled neurones to be observed over a range of femoro-tibial angles and the characteristic displacement of neurones located in different regions of the scoloparium to be described. In particular, the change in dendrite length over the full range of femoro-tibial angles was measured from representative neurones in each population (groups 1 - 6; see Chapter 4) to see whether or not the patterns of dendritic distortion observed could be correlated with any of the above factors.

5.4.1 Morphology of dendritic distortion

The group 1a neurones, located near the ventral edge of the scoloparium, are subjected to minimal absolute proximo-distal displacements (approximately 20 to 60 μm) as the tibia is rotated. However, as the tibia is extended the influence of the flexor strand causes the mtFCO cell body region to rotate (see Chapter 2), resulting in a change in the orientation of these neurones within the scoloparium. The dendrites of such neurones develop a kink approximately 10 - 20 μm proximal to their dendritic terminations (Fig. 5.2).

Neurones located centrally in the mtFCO scoloparium (groups 1b and 2b) also develop a single distinctive dendritic kink adjacent to their dendritic terminations (Fig. 5.3). In addition to dendritic buckling, group 2a neurones also develop kinks in their axons, proximal to their neurone cell bodies (Fig. 5.4). This phenomenon is not observed in the other neurone populations.

The dendrites of neurones located near the dorsal edge of the scoloparium (dorsal group 3 neurones) buckle in a similar manner, though more extensively, to those dendrites located in the middle of the scoloparium. These neurones develop a series of dendritic kinks along their lengths as the tibia is extended (Fig. 5.5). The dendrites of the most proximal group 3 neurones do not follow this pattern of distortion and instead develop a single large kink upon tibial extension (Fig. 5.6).

The spatial distribution of the neurones with respect to the ligaments of the apodeme complex would suggest that the group 6 neurones, situated in series with the attachment cells comprising the ventral ligament, are the most likely to be subjected to mechanical range fractionation. The dendritic displacements of the group 6 neurones confirm that the architecture of the ventral ligament does result in the differential stimulation of these cells. The distal-most group 6 neurones are subject to considerable (approximately 150 μm) proximo-distal displacement over the range of femoro-tibial angles 0° - 150° with increasingly proximal cells undergoing smaller absolute displacements (approximately 100 μm). Where there are 2 filled cells close together, the proximal one always undergoes a smaller range of displacements (Fig. 5.7). The dendrites of the group 6 neurones project distally along the ventral ligament of the apodeme complex. When the tibia is fully flexed the group 6 dendrites lie in a layered formation, the dendrites of proximal neurones terminating dorsal to those of distal neurones (Fig. 5.8). When the tibia is fully extended, the group 6 neurones bunch closely together as the apodeme complex is unloaded (Fig. 5.9). The dendrites remain in an ordered dorso-ventral sequence within the ventral ligament, and adopt a buckled appearance. The dendrites arising from the distal and ventral-most neurones buckle to a greater extent to those of the proximal cells, and develop a distinct kink (Fig. 5.10).

Viewing the group 6 neurones over a series of femoro-tibial angles, shows that the majority of dendritic displacement occurs over the femoro-tibial angles 0° - 80° and that over this range the distal-most dendrites appear to kink first, followed by the dendrites of increasingly proximal cells (Fig. 5.11).

5.4.2 Quantification of dendritic distortion

In order to correlate dendrite length with position in the scoloparium, the dendrite lengths of neurones belonging to different populations were measured at full tibial flexion (0°) (Fig. 5.12a). There is a tendency for distally located groups to have shorter dendrites than those groups located more proximally in the scoloparium (groups 1, 2 and 3). Within each of the proximal groups there is also a greater variability in dendrite length. That may be because groups 1 and 2 contain neurone sub-populations (1a, 1b; 2a, 2b) which were not differentiated in this instance.

The different neurone populations in different regions of the mtFCO scoloparium were found to exhibit different degrees of mechanical stretch during tibial flexion. The degree of dendritic distortion which occurs within each neurone group over the range 150° - 0° is shown in Figure 5.12b. Variation in % extension of dendrites in different regions of the scoloparium reflects to some extent the variable distortion measured on the surface of the organ. This was shown to vary across the scoloparium, with increasing distortion being found distally (see Chapter 2). The data descibed here shows that the dendrites of neurones situated distally (group 6) tend to become distorted to a greater degree than the dendrites of the increasingly proximal group 5, 4 and 3 neurones. However, there is variability in the degree of distortion measured in the group 1 and 2 neurones which does not fit a simple model of decreasing distortion at increasingly proximal levels.

In an attempt to rationalise dendrite distortion patterns during tibial rotation with anatomical factors, the dendrite lengths of neurones located in different regions of the scoloparium were measured at a range of femoro-tibial angles.

The dendrites of the group 1, 2 and 3 neurones all show generally similar distortion patterns as the tibia is rotated, although there are minor differences. The dendrites of these groups are stretched when the tibia is

held in the flexed position and shorten over the entire femoro-tibial range as the tibia is extended (Figs 5.13, 5.14 and 5.15). From plots of dendrite length against femoro-tibial angle it can be seen that the rate of dendritic shortening is not constant as the tibia is extended from 0° - 150°. The majority of these neurones shorten at a decreasing rate, although there are exceptions to this trend in all three groups (in particular over the femoro-tibial range 0° - 30° in the case of the group 1 neurones). Where it occurs, the decreasing rate of dendritic distortion as femoro-tibial angle increases may reflect the sinusoidal nature of the mechanical input at the joint (see Chapter 2, Fig. 2.13).

The patterns of dendrite length changes seen in the group 4 neurones vary. In some cases the change of length with femoro-tibial angle is more or less linear over the whole range (0° - 150°) and resembles the distortion patterns characteristic of the group 3 neurones (Fig. 5.15). However, Figure 5. 16 shows an example of a group 4 dendrite (neurone 2) which changes in length over the first half of the femoro-tibial range only (0° - 90°). These observations show that neurones in the same group (adjacent neurones) can be subject to both different amplitudes and patterns of mechanical displacement.

Unlike the group 4 neurones, the group 5 neurones undergo a consistent range of dendritic distortion. The group 5 dendrites analysed in this study (n = 4) underwent a total mean change in length of 20.45 μm (±1.03 μm) over the full femoro-tibial range 0° - 150°. However, although their ranges of distortion are similar, the dendrites show a spectrum of different dendrite distortion patterns with changing femoro-tibial angle (Fig. 5.17). The length changes of some dendrites appear to be approximately linearly related to femoro-tibial angle (Fig. 5.17, neurone 2) in a manner similar to that observed in some group 4 neurones. Some dendrites share the same pattern of dendritic distortion as shown by other group 4 neurones, with changes in dendrite length occurring over the initial part of the femoro-tibial range only (Fig. 5.17, neurones 3 and 4). There is also an intermediate pattern of dendritic distortion represented, similar to that shown by some of the group 2 and 3 neurones. Here, dendrite length change occurs over the whole range of femoro-tibial angles but the rate decreases with increasing angle (e. g. Fig. 5.17, neurone 1).

The distortion patterns of the group 6 neurones show two characteristics which may result from their location in the mtFCO scoloparium. There is a characteristic distortion pattern with tibial rotation and a position-dependent graded distortion amplitude. The rate of dendritic shortening with tibial rotation is initially rapid but declines markedly at femoro-tibial angles in excess of 100° (Fig. 5.18). This pattern of distortion reflects the fact that group 6 lies in series with the ventral ligament of the apodeme complex, which unloads rapidly during the sequential slackening of ventral ligament loop-crossing fibres during tibial extension (see Chapter 2). There is no further sequential slackening over femoro-tibial angles in excess of 100°, resulting in the rate of dendrite distortion declining. The dendrites of increasingly dorsal and proximal neurones are deformed to differing degrees depending upon their locations within the ventral ligament (Fig. 5.18, graph 4b), the dorsally located neurones being subjected to wider ranges of dendritic distortion. This reflects the order in which the ventral ligament fibres are unloaded, providing a possible mechanical basis for range fractionation.

To make comparisons between the rates of dendrite distortions between the different neurone populations as the femoro-tibial joint is rotated, the mean rates of dendritic displacement were plotted (Figs 5.19a, b). The mean rate of dendrite extension for each neurone population was calculated as μm dendritic extension/10° rotation of the femoro-tibial joint over the femoro-tibial ranges of 0° - 150° (Fig. 5.19a). The mean dendrite extension rates were also calculated over the femoro-tibial range 0° - 40° (Fig. 5.19b) to avoid producing artificially low rates of distortion for those dendrites which change in length over the first half of the femoro-tibial range only (e.g. Figs 5.16 neurone 3 and 5.17 neurones 3 and 4).

The rates of dendritic distortion were found to be variable between the different neurone populations, although the small sample sizes of the data sets prevented further statistical analysis. The mean rates of dendrite extensions ranged between 1 and 2 μm/10° rotation of the femoro-tibial joint when averaged across the entire femoro-tibial range (0° - 150°) (Fig. 5.20a). When the rates of dendrite extensions were measured over the initial part of the femoro-tibial range (0° - 40°) the increase in length/10° rotation ranged between 2 and 4 μm (Fig. 5.19b). The dendrites of the group 1 and 2 neurones appeared to undergo larger distortions/10° femoro-tibial rotation than those of the other neurone populations

irrespective of whether the rates were measured over the initial part or the femoro-tibial range (0° - 40°) or the entire femoro-tibial range (0° - 150°). This may indicate that the dendrites of these particular neurones are situated in regions of graded compliance within the scoloparium. This would maximise dendrite distortion upon displacement of the scoloparium.

5.4.3 Displacement within the scoloparium relative to the outer sheath

The ability to visualise features located within the mtFCO scoloparium allowed a comparison to be made of internal displacement with the displacement of surface markers on the mtFCO sheath. A series of four surface markers was identified in different regions of the scoloparium. Each marker directly overlaid a discrete neuronal feature when the femoro-tibial angle was 150°. As the tibia was flexed, switching between confocal and conventional light microscope channels allowed the displacement of each pair of points to be plotted at intervals of 30° (Fig. 5.20). These data reveal that there is a degree of differential displacement between the sensory neurones and the mtFCO sheath. In each case, the marker located within the mtFCO scoloparium undergoes a different pattern of displacement from that of the overlying marker positioned on the surface of the scoloparium. This is particularly evident in the dorso-ventral axis, although there are also differences in the proximo-distal axis. This may reflect the role of the the flexor strand which is anchored to the scoloparium sheath (see Chapter 3, Fig. 3.34). These observations indicate that the sheath and the inside of the scoloparium differ in compliance, a possibility that was also indicated by the distribution of the extracellular elastic fibres (see Chapter 3). The implications of this observation are that measurements of mechanical displacement using markers on the outside of the organ cannot completely describe the actual displacements imposed upon the sensory cells themselves.

5.5 DISCUSSION

This study provides the first detailed description of the way in which the dendrites of chordotonal organ neurones are displaced by changes in femoro-tibial angle. Although another recent study has examined the displacement of dye-filled neurones in the FCOs of the cricket (Nishino and Sakai, 1997), that study only described gross displacements of neurone

cell bodies and provided no useful information concerning dendrite behaviours. The current study has shown that whilst there is variability in dendritic displacement throughout the mtFCO scoloparium, some generalisations can be made.

There is a trend towards increasing dendritic distortion towards the periphery of the scoloparium. The dendrites of neurones located at the dorsal, ventral and distal margins of the scoloparium (groups 3, 1 and 6) appear to be subjected to the most severe kinking (Figs 5.6, 5.10 and 5.13). In addition, the axons of the most proximal neurones become buckled as the tibia is extended (Fig. 5.4).

Changes in dendrite length with femoro-tibial angle reveal that neurones located in series with the ventral ligament (group 6) are distorted over limited femoro-tibial ranges (Figs 5.17 and 5.18) whilst other neurones (e. g., group 3) tend to undergo distortion over a wider range of femoro-tibial angles (Fig. 5.15). In addition, differences in the patterns of dendritic buckling may indicate that different populations of neurones are subjected to differing degrees of axial and off-axis forces. This may mean that different neurones respond to different components of mtFCO displacement such as stretch and shear.

The observations made in the present study are not intended to imply the nature of the adequate stimulus, but instead to provide an indication of dendritic strain. All the neurones examined exhibited dendritic buckling during extension of the tibia. Since many are directionally sensitive it is likely that the adequate stimulus for some is stretching whilst for others it is buckling.

5.5.1 Range Fractionation

A number of previous authors have suggested that chordotonal organs may be mechanically organised so that the sensory neurones are differentially stimulated. Burns (1974) observed that the neurones of the pro- and mesothoracic femoral chordotonal organs in the locust are arranged in conical arrays and speculated that each neurone may be maximally sensitive over a different part of the femoro-tibial range. In the metathoracic leg of the locust, both Field (1991) and Shelton *et al.* (1992) implicated the mechanical organisation of the apodeme complex in range fractionation.

This study is the first to demonstrate that the dendrites of the mtFCO scolopidia are distorted in a range of different ways depending upon their locations in the scoloparium. Such a phenomenon was implicit in the suggestion of Field (1991) and Shelton *et al.* (1992) who suggested that the graded attachment cell lengths of the ventral ligament may result in range fractionation at the level of the sensory neurones. The present study describes graded displacements of the group 6 neurone dendrites that can easily be explained in terms of the differential displacement of the ventral ligament attachment cells (see Chapter 2).

However, measurement of dendritic length with changing femoro-tibial angle has shown that the arrangement of the apodeme complex does not affect neurone distortion as might have been expected on the basis of the description of the apodeme complex loop-forming behaviour by Field (1991) and Shelton *et al.* (1992). It would have been reasonable to suppose that neurones lying in series with the dorsal ligament of the apodeme complex might have been subjected to a limited range of displacements due to the slackening of this ligament during loop formation (see Chapter 2). Conversely neurones in series with the ventral ligament appear to be located such that they would be subjected to a wider range of stimulation since the ventral ligament never becomes fully unloaded over the entire range of tibial rotation (in *S. gregaria*). This does not appear to be the case. The dendrites of the group 6 neurones (associated with the ventral ligament) undergo relatively large changes in length over the femoro-tibial angles 0° - 90° but undergo small changes in length over the remainder of the femoro-tibial range. Dendrites of other neurone populations, such as the dorsally-located group 3 neurones associated with the dorsal ligament (Fig. 5.15), change in length over the entire range of tibial rotation.

The fact that dendritic length change occurs over variable femoro-tibial ranges reflects the findings of Matheson (1990) who observed that whilst some neurones fired at different rates across the entire range of femoro-tibial angles, others responded over discrete ranges only. Matheson's (1990) work also revealed a trend towards increasingly dorsal neurones responding over wider ranges of femoro-tibial angles and to fewer sensory modalities. The ventral-most cells tended to have narrower discrete ranges of operation. This trend correlates superficially with the

distribution of dendritic distortion patterns found in this study. However, whilst Matheson (1990) recorded from some neurones which fired only at femoro-tibial angles in excess of 90°, no neurones were observed in this study whose dendrites changed length exclusively over this range. Clearly further work is required before the relevance of the different patterns of dendrite distortion to the physiological properties of the neurones can be fully evaluated.

5.5.2 Applications of dendritic distortion measurements

Dendritic distortion is a useful subjective measure of the relative displacements undergone by neurones in different regions of the mtFCO scoloparium. For example, the measurement of dendrite length with changing femoro-tibial angle shows that the group 6 neurones (associated with the ventral ligament) appear to be subjected to greater mean relative dendrite elongations than those of group 3 neurones (associated with the dorsal ligament) (Fig. 5.12b). Measurement of dendrite distortion also reveals that the group 6 neurones are recruited in a sequential fashion reflecting the graded lengths of the ventral ligament attachment cells. As the tibia is extended, the dendrites of the ventral-most neurones begin to shorten first, followed by the dendrites of increasingly proximal and dorsally located neurones (Fig. 5.11, graph 4b).

Whilst dendritic membrane distortion is generally accepted to be the stimulus which induces mechano-sensilla to generate action potentials (see French, 1988), neither the dendritic stretching nor buckling observed in this study provide a simple explanation for the different discharge patterns observed by Matheson (1990). If this were the case, considerable variation in the range of dendrite distortions might have been expected. The results show that all the dendrites are stretched when the tibia is flexed at 0°, and that upon tibial extension all the dendrites begin to buckle over the range of femoro-tibial angles 0° - 30°.

The fact that all the dendrites are distorted over a broadly similar range of femoro-tibial angles suggests that gross dendrite elongation may be only a part of the adequate stimulus required to elicit neuronal discharge. Other factors such as different membrane properties, thresholds or small structural differences between scolopidia may allow different populations of neurones to respond over different ranges. Such differences may also be

responsible for the fact that different neurones appear to respond to different elements of the stimulus (Matheson, 1990).

Nevertheless, it is reasonable to suggest that dendritic length change provides a useful proportional measure of mechanical input to the neurones. The assumption that the degree of dendritic elongation is proportional to the mechanical input across the spike generating region allows simplistic estimation of the magnitude of the adequate stimulus to an individual neurone. For example if the dendritic cilium is assumed to play a key role in the process of signal transduction, and the relative displacement which it undergoes is assumed to be proportional to that to which its dendrite is subjected, its degree of elongation over the femoro-tibial range can be calculated. Dendrites located in different region of the scoloparium are stretched by 20% - 30% across the femoro-tibial range (Fig. 5.12b). Just how a dendritic cilium would behave when subjected to longitudinal stress is unknown. If it were to have a similar compliance to the dendrite itself, a dendritic cilium of 10 μm length would change in length by 2 - 3 μm over the full femoro-tibial range or by 0.75 μm over the mean walking range of 45°. However, it is unlikely that the mechanical properties of the dendritic cilia with their associated scolopale cell are the same as those of the dendrite itself. Nevertheless, change in dendrite length with leg angle remains the only measure we have at present of the way in which tibial rotation affects scolopidial neurone structure.

5.5.3 Implications of buckling morphology upon possible mechanisms of sensory transduction

The role of gross dendritic distortion in contributing to mechano-electric transduction cannot be dismissed. Pringle (1955) suggested stretching of the dendrites was the transduction mechanism leading to depolarisation in slit sensilla, whilst Barth (1972) favoured dendrite compression in these organs. However, other authors have demonstrated that mechano-sensilla in which the mechanical input stimulates the dendritic tip exclusively, are capable of an extraordinary degree of sensitivity. In addition, compression rather than stretching of the dendrite tip has often been reported as being the effective stimulus. Thurm (1965) demonstrated that dendritic compression was the effective stimulus in the case of hair-plate sensilla. He reported that a lateral 0.1 μm compression (15% of non-stimulated diameter) elicited the maximal response with the threshold stimulus being 3 nm (0.5% non-stimulated diameter). French and Sanders

(1979) similarly measured the threshold deformation and found it to be a 4 nm compression. Both Chapman *et al.* (1975) and Spinola and Chapman (1975) documented a 1 - 10 nm tubular body compression at threshold in campaniform sensilla. Thurm too (1964) found that in the case of a mechanoreceptor in the cuticle of a honey bee, a 0.1 μm compression of the dendritic tubular body was the maximum encountered physiologically and that the organ functioned with a range of mechanical input displacements of less than 0.1 μm.

Such mechanoreceptors evidently do not undergo excessive dendritic distortion, and yet have extreme sensitivity. It seems likely that the dendritic cilia, which chordotonal organ sensilla have in common with these organs, may be largely responsible for the process of mechano-electric transduction. It could be the case in chordotonal organ sensilla that the dendrite simply allows the cilium to be positioned in a suitable region of the mtFCO whilst the cell body remains at a proximal site to avoid excessive shearing. In such a model, the observed dendritic stretching and buckling would play little part in the response of a neurone, although it would reflect the magnitude of distortion at the actual transduction site. Alternatively, dendritic distortion might conceivably change the conduction properties of the portion of the neurone between the transduction site and the cell body. In this case it could play an active role. The nature of that role is not clear although it could be involved in some sort of signal filtering. These ideas remain speculative at present.

5.5.4 Differential sheath displacement

The observation that internal markers can be displaced over a greater range than their externally located counterparts indicates that there is a degree of independent movement between the neural lamella which forms the mtFCO sheath and the neurones themselves. The discrepancy between displacement ranges of internal and external points implies that the compliance of the mtFCO sheath is different from that of the components contained within it. This is consistent with the distribution of the Acid Fuchsin staining component within the scoloparium and in the outer sheath (see Chapter 3).

The present observations provide the first detailed account of the pattern of dendrite distortion in the mtFCO. They show that the patterns of distortion vary between neurones. This implies that the mechanical

inputs to different neurones are subtly different. The fact that some dendrites are distorted over the entire femoro-tibial range whilst others are distorted over discrete femoro-tibial ranges provides an explanation for how range fractionation could occur.

Figure 5.1

This pair of semi-schematic diagrams shows the way in which the mtFCO was mounted on the inverted epifluorescence microscope. Diagram **a** shows an exploded view of the welled slide (w) and the way in which it fitted onto the microscope stage (s). The locust leg (l) was positioned on a large coverslip (c) which formed the base of the slide well. Part of the slide base was shaped to slot into the microscope stage (indicated), whilst leaving the portion of the slide closest to the user sitting on top of the stage. This made room to attach the protractor (p). Diagram **b** illustrates the reason for mounting the femur anterior side downwards in a welled slide. The horizontal line within the femur indicates the position of the mtFCO. The working distance (wd) between the objective lens and the stained neurones is kept to a minimum by the mounting of the femur on a thin coverslip.

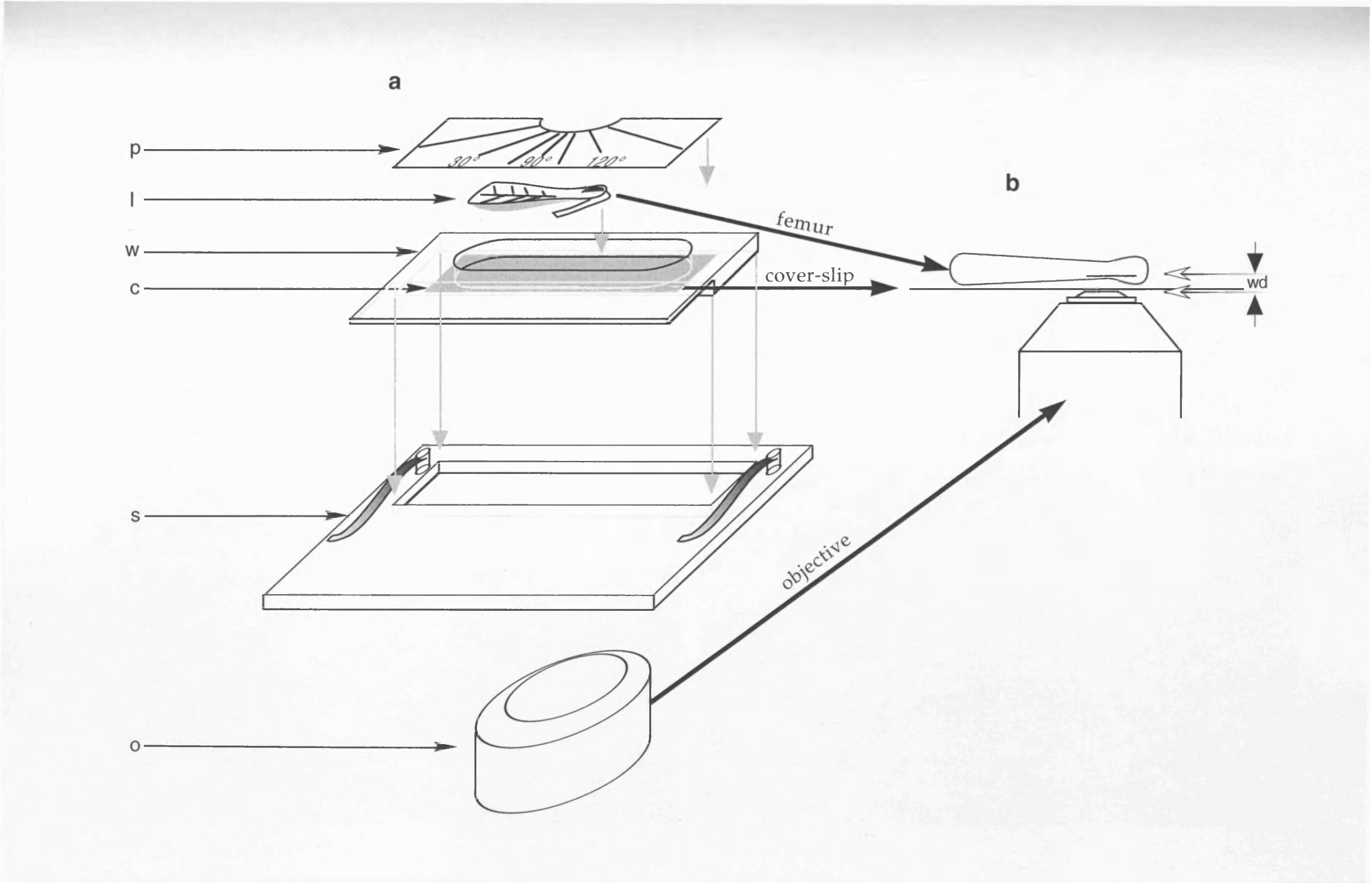
a
b
p
l
w
c
s
o
30°
90°
120°
femur
cover-slip
wd
objective

Figure 5.2

These confocal micrographs show a group 1a neurone at four femoro-tibial angles. This neurone is located close to the ventral edge of the scoloparium (indicated). The edge of the cuticular nerve (cn) is also visible. The dendrite of this neurone develops a single kink approximately 20 μm from its distal tip as the tibia is extended from 0°. The kink continues to become more acute over the entire range of femoro-tibial angles 0° - 150°. The displacement of group 1a neurones is modified due to their close proximity to the attachment of the flexor strand to the mtFCO scoloparium. The angle of this dendrite relative to the neurone cell body changes by approximately 20° over the full femoro-tibial range due to rotation of the organ caused by the influence of the flexor strand. At 150°, the kinked dendrite of another 1a neurone becomes visible (arrowhead), located along the extreme ventral margin of the scoloparium. Distal is to the right of each micrograph.

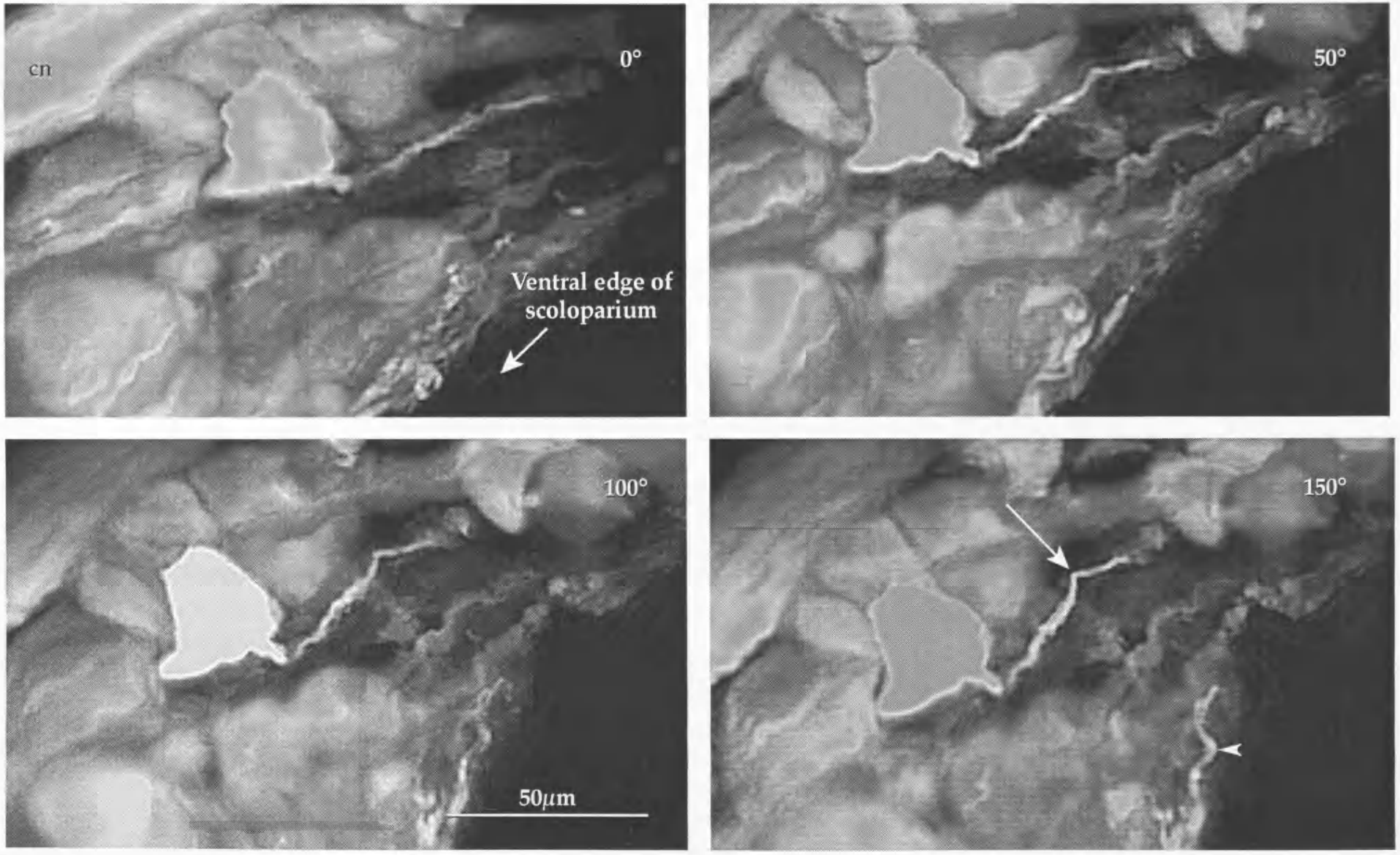
cn
0°
Ventral edge of scoloparium
50°
100°
50μm
150°

Figure 5.3

Series of confocal micrographs taken at different femoro-tibial angles showing centrally located neurones in the mtFCO scoloparium. In this series, group 2b neurones are located dorsally, 1b neurones are located ventrally and the two distal-most neurones belong to group 4 (indicated at 0°). The dendrites visible in this series all develop a characteristic kink (indicated at 50°) approximately 40 μm from their distal terminations over the range of femoro-tibial angles 0° - 50°. The dendrites do not appear to buckle further over the range of femoro-tibial angles 50° - 150°.

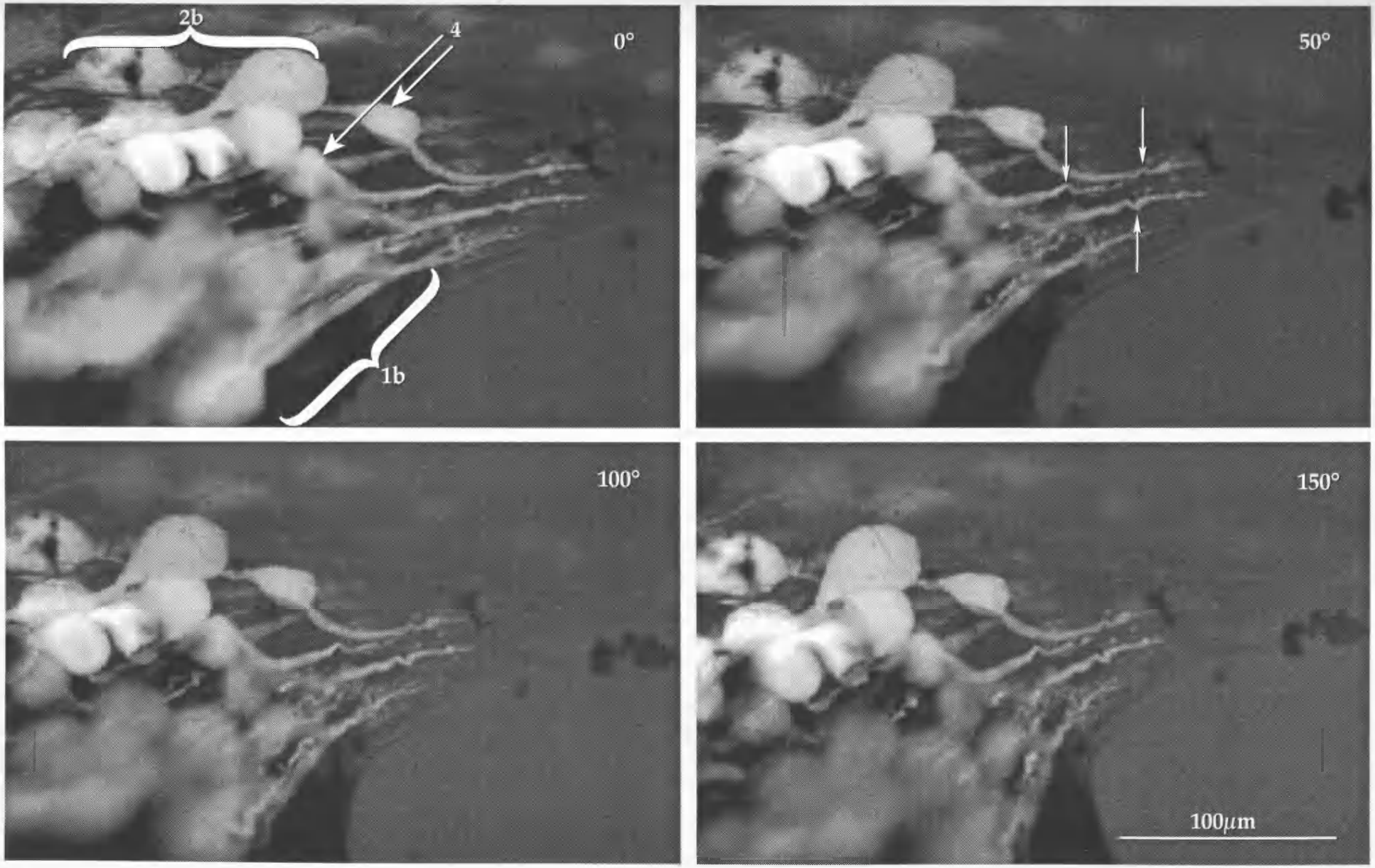
2b
4
0°
1b
50°
100°
150°
100μm

Figure 5.4

Series of confocal micrographs demonstrating the axonal kinking shown by group 2a neurones (dendrites not shown). These neurones are located proximally within the mtFCO scoloparium, close to the cuticular nerve. Some individual axons of the cuticular nerve (cn) are visible at a femoro-tibial angle of 0°. As the tibia is extended, the cell bodies of the neurones are displaced proximally, causing the axons to kink (indicated). Distal is to the right of each micrograph.

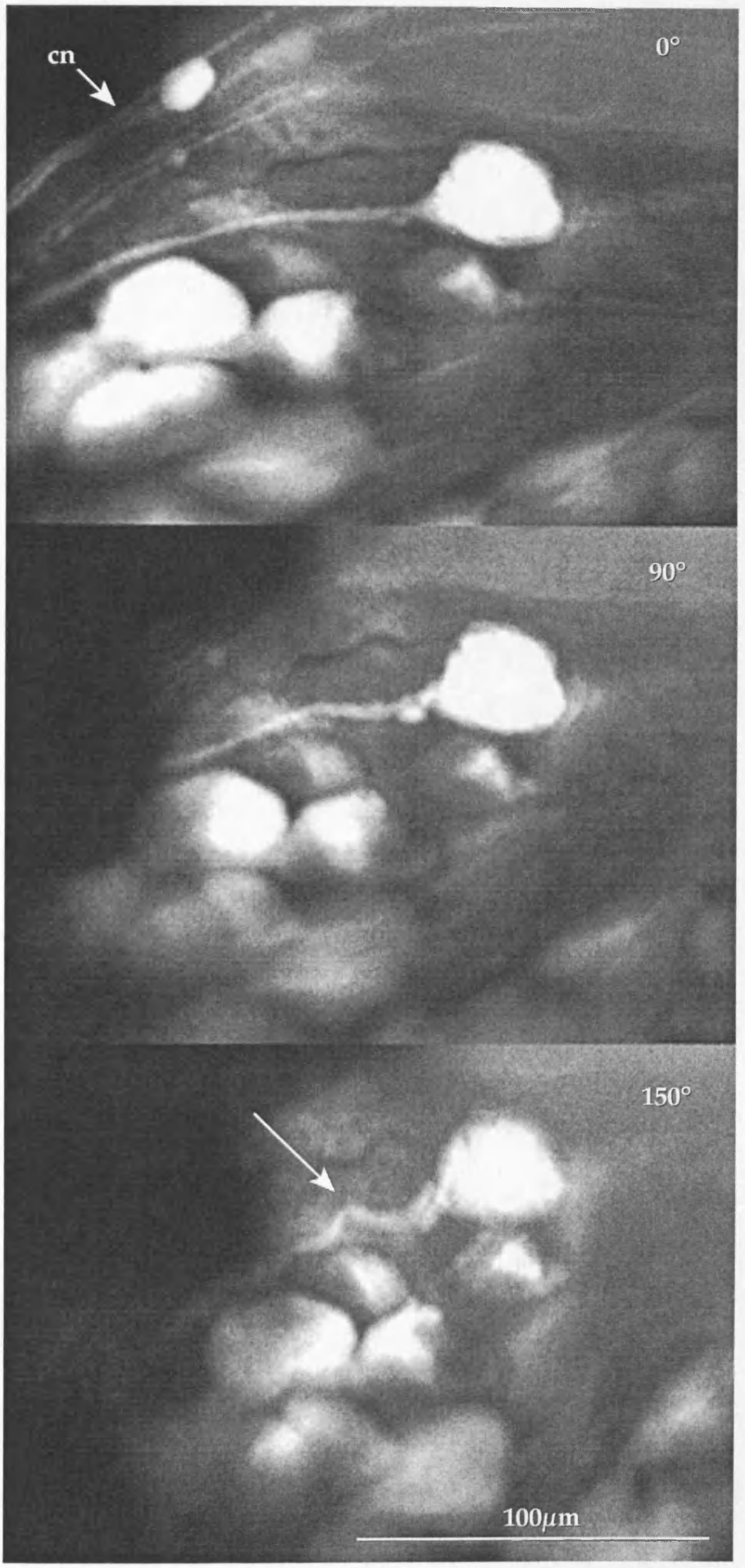
cn
0°
90°
150°
100μm

Figure 5.5

This series of confocal micrographs shows the displacement of a single group 3 neurone over the full range of femoro-tibial angles. Group 3 neurones develop multiple dendritic kinks as the tibia is extended. The larger kinks are located distally and appear first (indicated) as the tibia is extended.

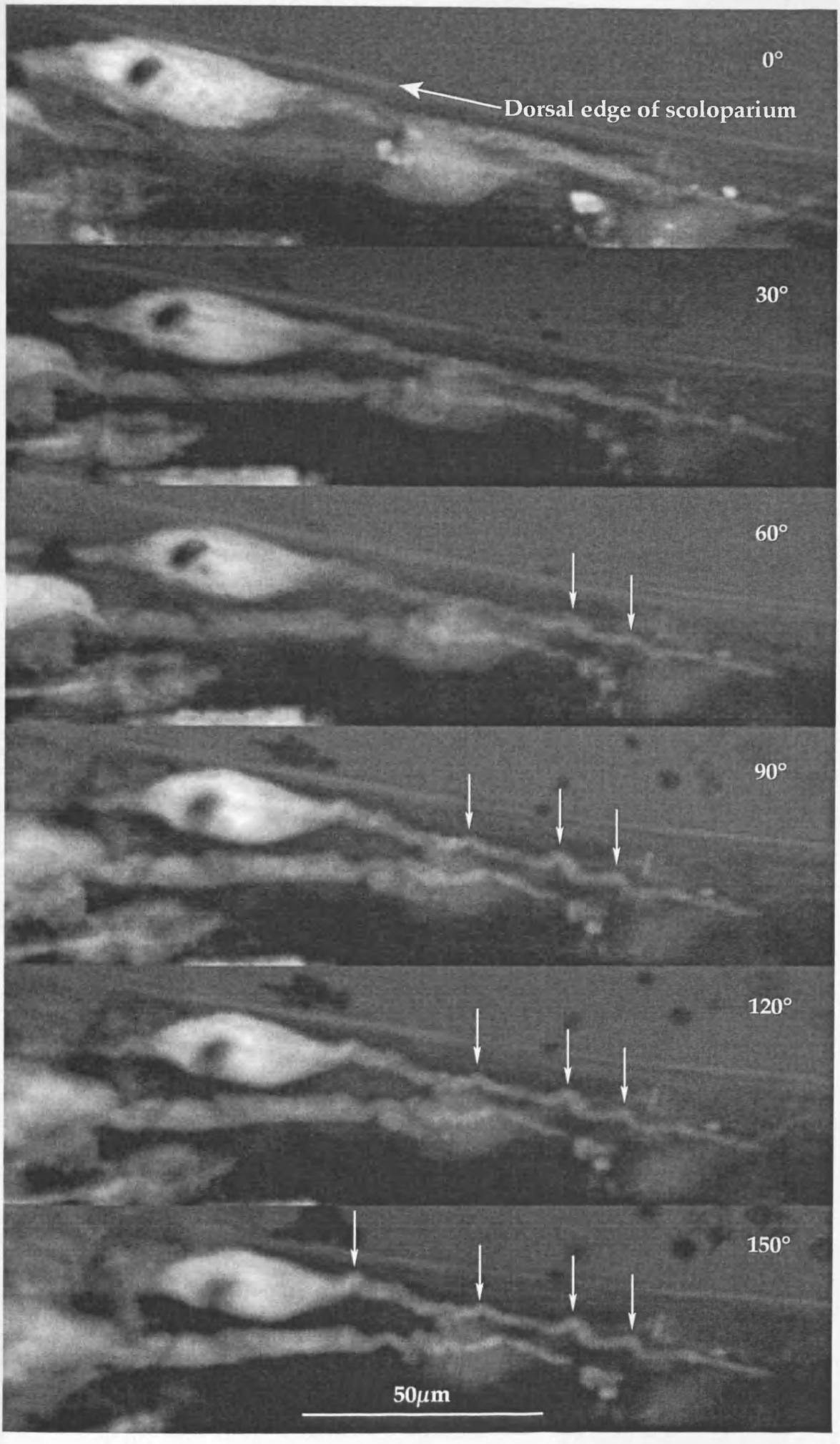
0°
Dorsal edge of scoloparium
30°
60°
90°
120°
150°
50μm

Figure 5.6

The two most proximal group 3 neurones show characteristic dendritic kinking which is unlike that of the rest of the group. This series of confocal micrographs shows one of these cells at three femoro-tibial angles. The dendrite develops a single large kink (indicated) as the tibia is extended. Distal is to the right of each micrograph. cn = cuticular nerve

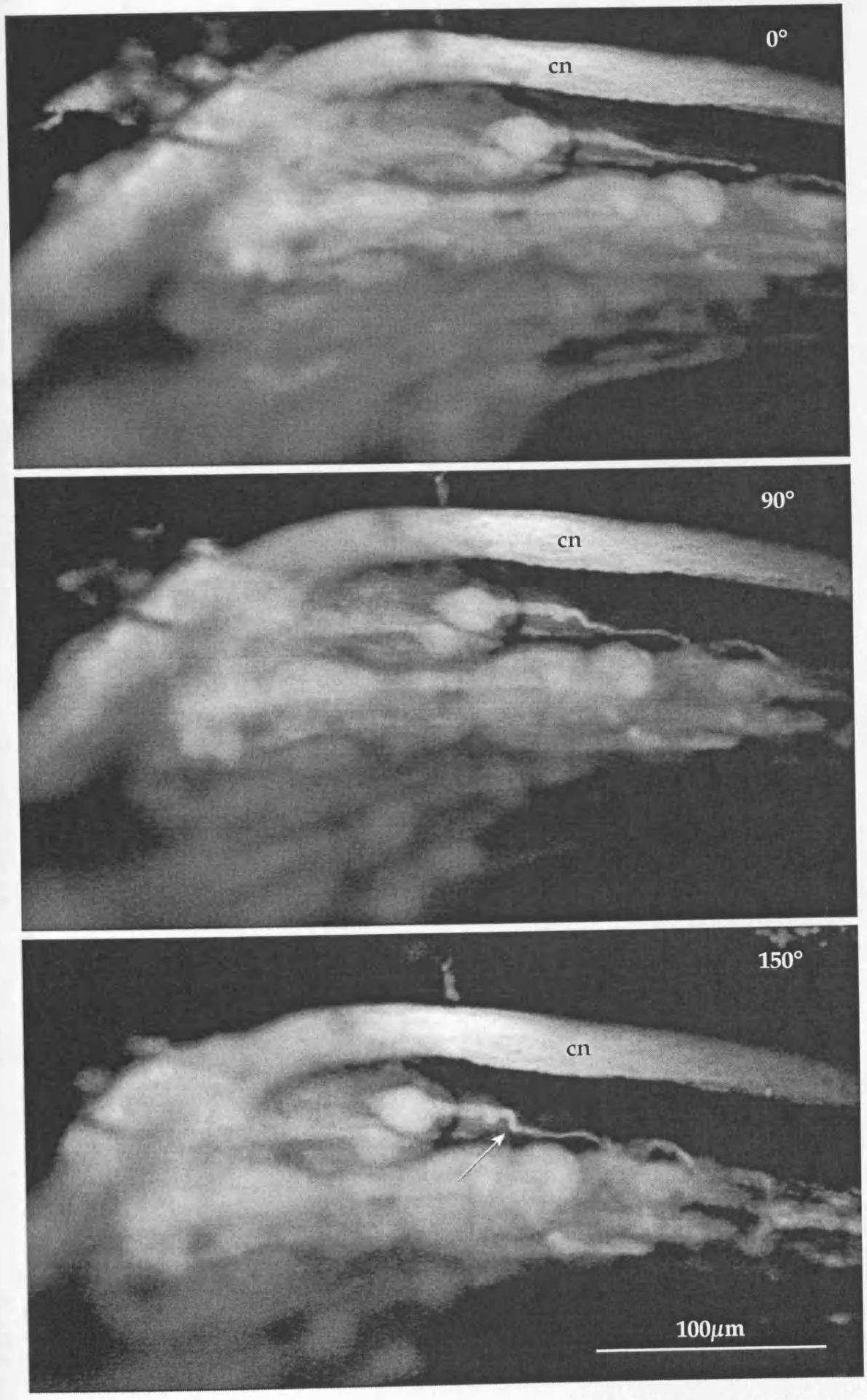
0°
cn
90°
cn
150°
cn
100μm

Figure 5.7

Two pairs of images showing the location of two group 6 neurones (1 and 2) at the extremes of the femoro-tibial range of angles; 0° (upper) and 150° (lower). Each pair of images consists of a bright field micrograph and a confocal micrograph of the same preparation taken at the same femoro-tibial angle. The microscope stage remained in a fixed position as the tibia was manipulated so that proximo-distal level in the femur is unchanged in all micrographs. Distal is to the right.

Group 6 neurones are located in the ventral ligament of the apodeme complex. These figures demonstrate that such neurones are subjected to different ranges of displacement depending upon their proximo-distal levels. The distance between the two labelled cells changes between full tibial flexion (0°) and maximum tibial extension (150°). This is because the ventral ligament is elastic and cell 1 undergoes a greater range of proximo-distal displacement (190 μm) than cell 2 (150 μm). cn = cuticular nerve; fs = flexor strand

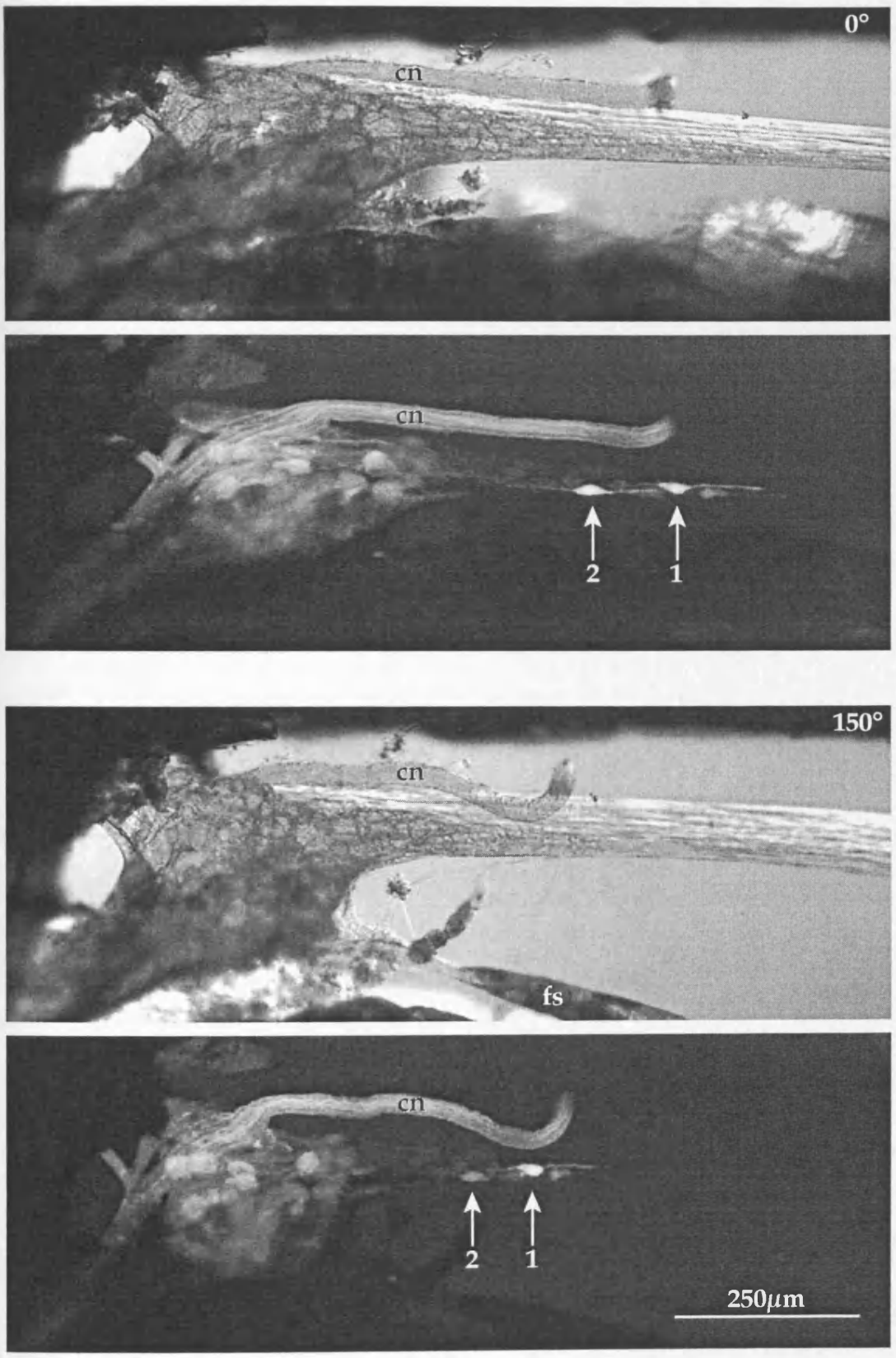
0°
cn
cn
2
1
150°
cn
fs
cn
2
1
250μm

Figure 5.8

Pair of micrographs (bright field, upper; confocal, lower) of the same preparation showing the mtFCO at a femoro-tibial angle of 0°. At this femoro-tibial angle, the dendrites of the group 6 neurones extend distally to terminate at a range of dorso-ventral levels in the ventral ligament. Distal cells have ventral terminations (1) whilst proximal cells have increasingly dorsal terminations (2, 3). Distal is to the right of each micrograph. cn = cuticular nerve; fs = flexor strand; t = trachea

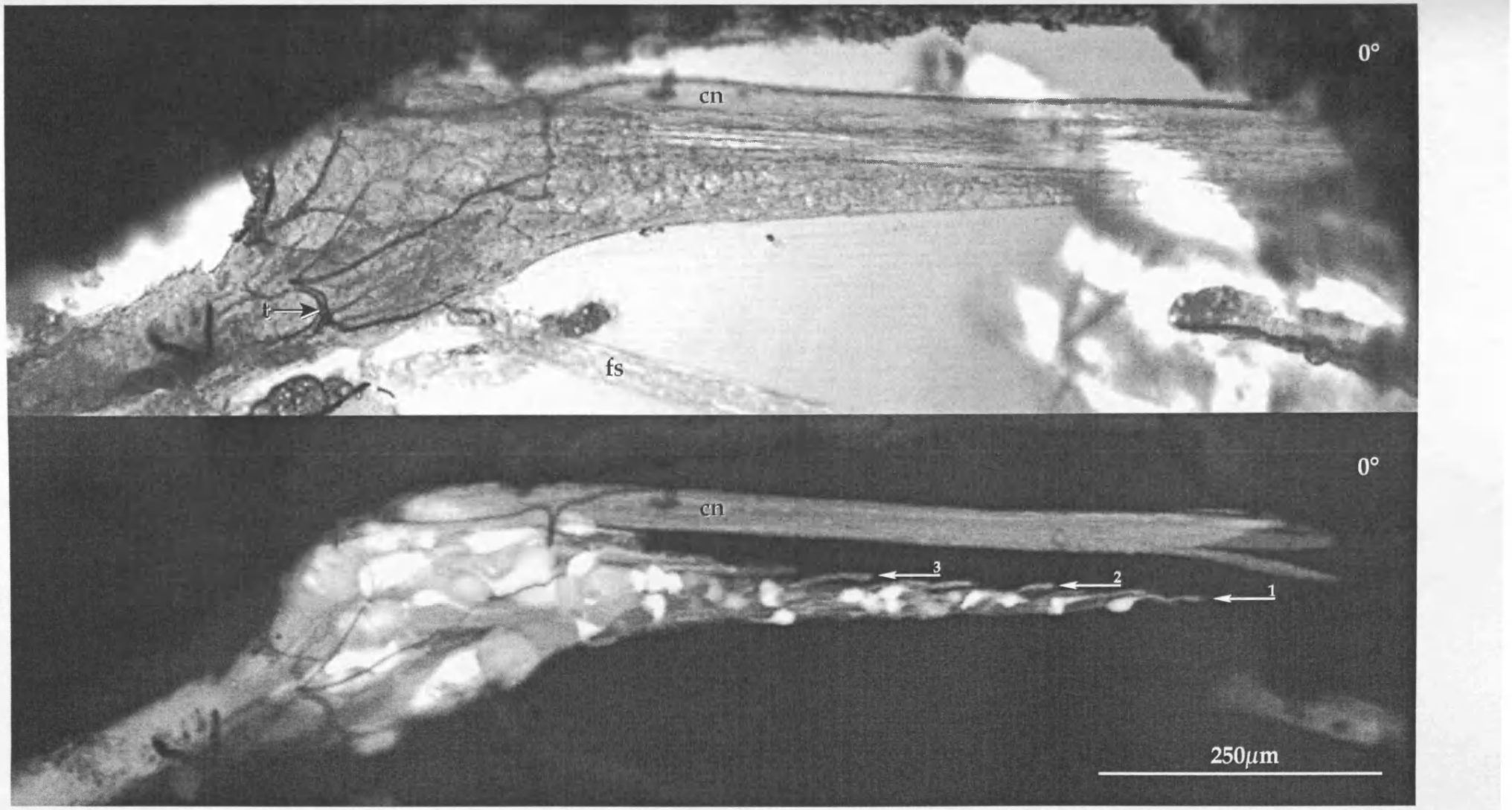
0°
cn
t
fs
0°
cn
3
2
1
250μm

Figure 5.9

Pair of micrographs (bright field, upper; confocal, lower) of the same preparation showing the mtFCO at a femoro-tibial angle of 150°. This is the same preparation as shown in Figure 5.8. When the tibia is fully extended, the dendrites of the group 6 neurones maintain their dorso-ventral relations. The dendrites of the distal-most neurones (1) terminate ventrally, whilst the dendrites of increasingly proximal neurones (2, 3, and 4) terminate at increasingly dorsal levels. The dendrites of the distal-most neurones appear kinked at this femoro-tibial angle. The strand receptor (sr) of the flexor strand (fs) is also visible in these images. Distal is to the right of each micrograph. cn = cuticular nerve; fs = flexor strand; t = trachea

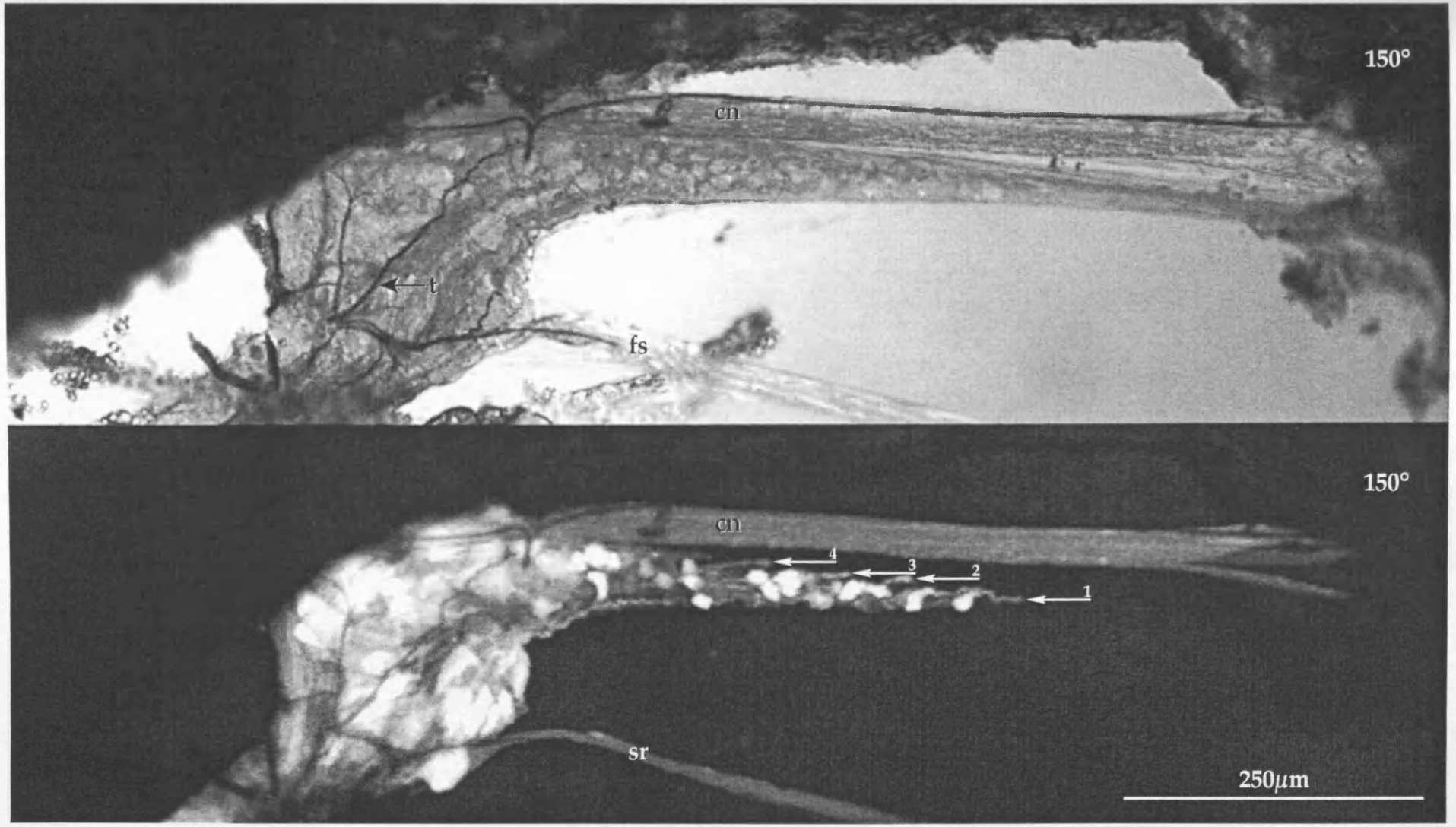
150°
cn
t
fs
150°
cn
4
3
2
1
sr
250μm

Figure 5.10

This confocal micrograph shows the group 6 neurones at a femoro-tibial angle of 150°. When the tibia is in this position, the distal-most neurones appear to be distorted to a greater degree than the more proximally located group 6 neurones. Distinct dendrite kinks are evident (indicated) amongst the distal cells. Distal is to the right.

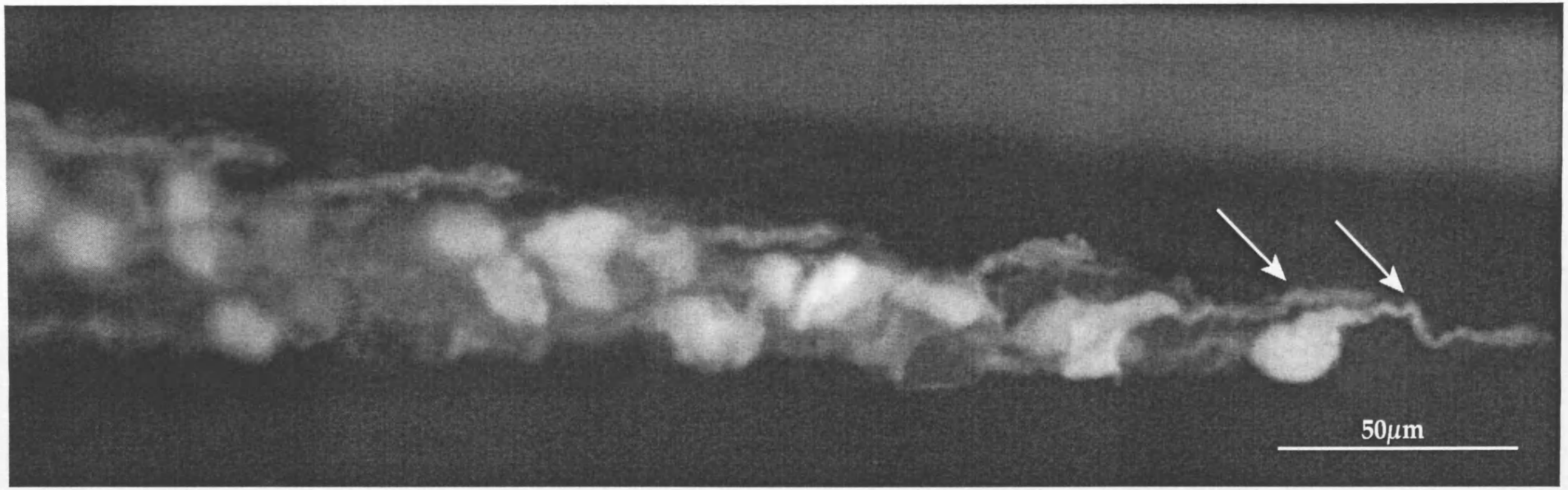
50μm

Figure 5.11

This series of confocal micrographs demonstrating the displacement of the entire mtFCO scoloparium. The location of the microscope stage remained constant as femoro-tibial angle was manipulated so that proximo-distal level in the femur is directly comparable between each image.

Comparing the location of the group 6 neurones in this series shows that the majority of scoloparium displacement occurs over the range of femoro-tibial angles 0° - 80°. As the tibia is extended from full flexion, a difference in dendrite buckling can be observed between distal group 6 neurones. When the tibia is fully flexed (0°), the dendrite of neurone 1 appears slightly kinked, whilst that of neurone 2 is straight. At a femoro-tibial angle of 40°, the dendrite of neurone 1 is clearly kinked whilst that of neurone 2 remains straight. When the tibia is further extended to a femoro-tibial angle of 80°, the dendrites of both neurones appear buckled. This observation indicates that the group 6 neurones may be distorted in a sequential order with the dendrites of increasingly proximal and dorsal neurones buckling as the tibia is extended. Distal is to the right of each micrograph. cn = cuticular nerve; fs = flexor strand

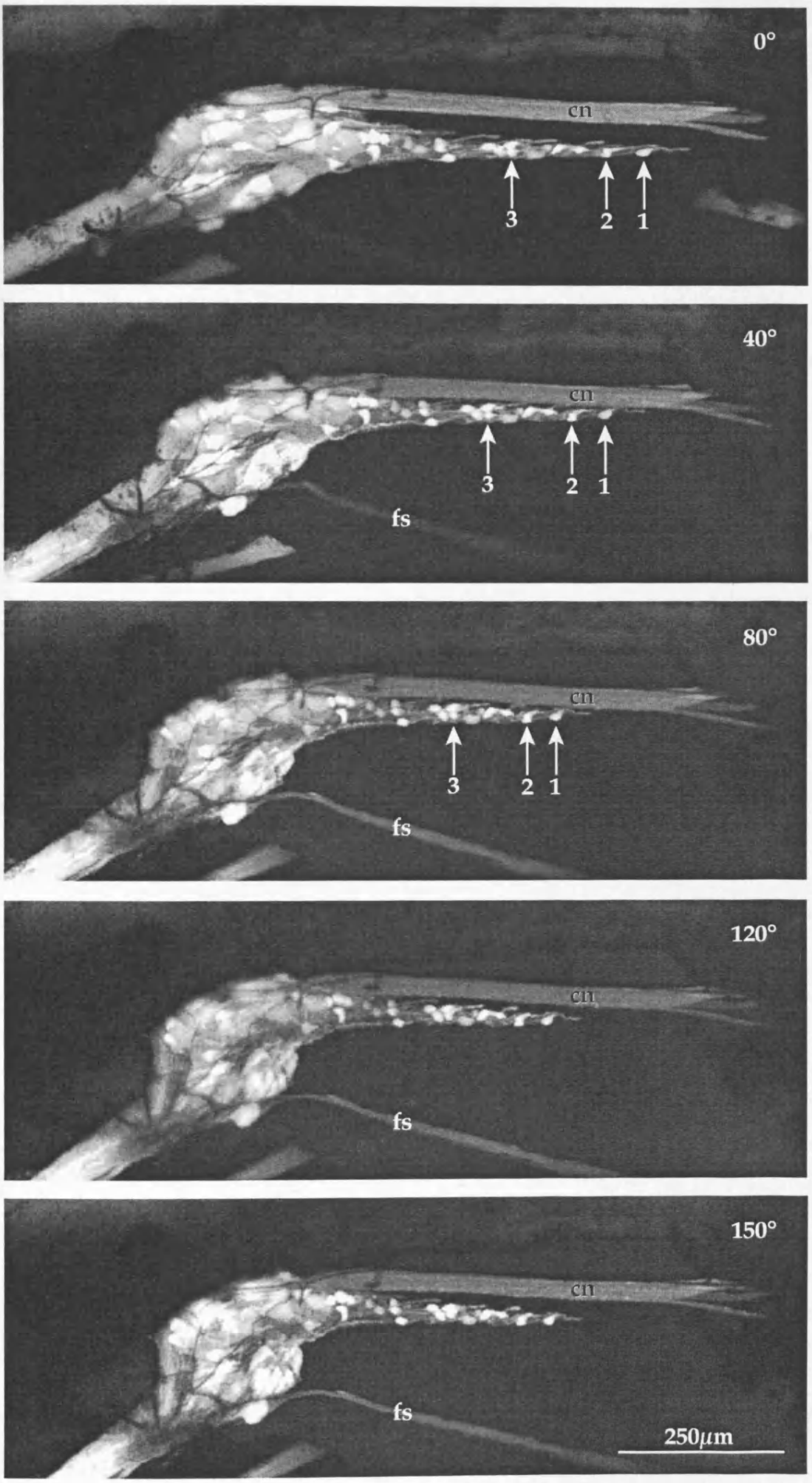
0°
cn
3
2
1
40°
cn
3
2
1
fs
80°
cn
3
2
1
fs
120°
cn
fs
150°
cn
fs
250μm

Figures 5.12a, b

a

This histogram shows the mean maximum dendrite lengths (measured at full tibial flexion) of the different neurone populations. The dendrites of neurones that are located distally in the mtFCO scoloparium (groups 4, 5 and 6) tend to be shorter than those of more proximally situated neurones. The dendrites of the group 6 and group 2 neurones vary significantly from one another in length. The mean dendrite length of the group 2 neurones is twice that of the shorter group 6 neurones:

***S. gregaria* dendrite lengths**

Single Factor Analysis Of Variance (ANOVA): $F_{4,7} = 17.7$ $P < 0.05$

Group 6	Group 4	Group 5	Group 1	Group 3	Group 2

(bars beneath the groups denote homogeneous subsets)

b

This histogram shows the degree of dendrite elongation to which each neurone population is subjected. Dendrite elongation is expressed as the percentage of the length at full extension by which each dendrite is stretched as the tibia is flexed by rotation of the tibia from 150° - 0°. The dendrites of groups 4, 5 and 6 are subjected to increasing degrees of dendritic stretching, reflecting their increasingly distal positions in the scoloparium. The ranges of dendritic distortion are variable amongst the remaining neurone groups. Higher levels of variation within groups 1 and 2 may be because each of these groups contains 2 populations of cells (1a, 1b; 2a, 2b). The small sample sizes prevent further statistical analysis in this instance.

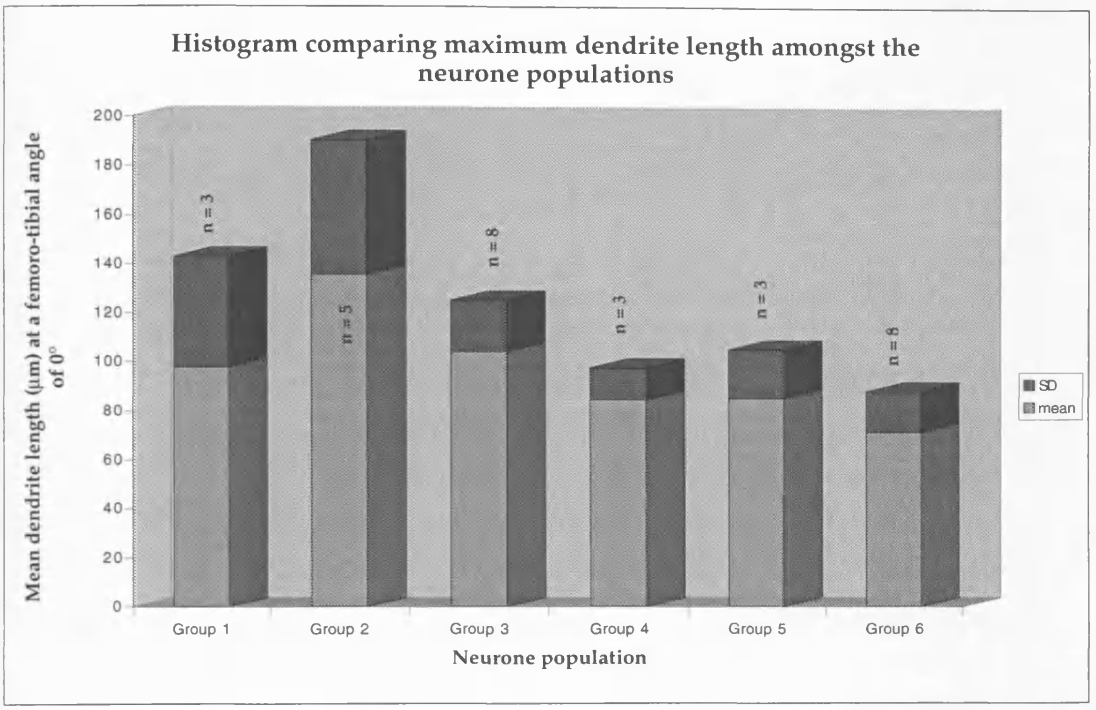
Histogram comparing maximum dendrite length amongst the neurone populations
Mean dendrite length (µm) at a femoro-tibial angle of 0°
200
180
160
140
120
100
80
60
40
20
0
n = 3
n = 5
n = 8
n = 3
n = 3
n = 8
Group 1
Group 2
Group 3
Group 4
Group 5
Group 6
Neurone population
SD
mean

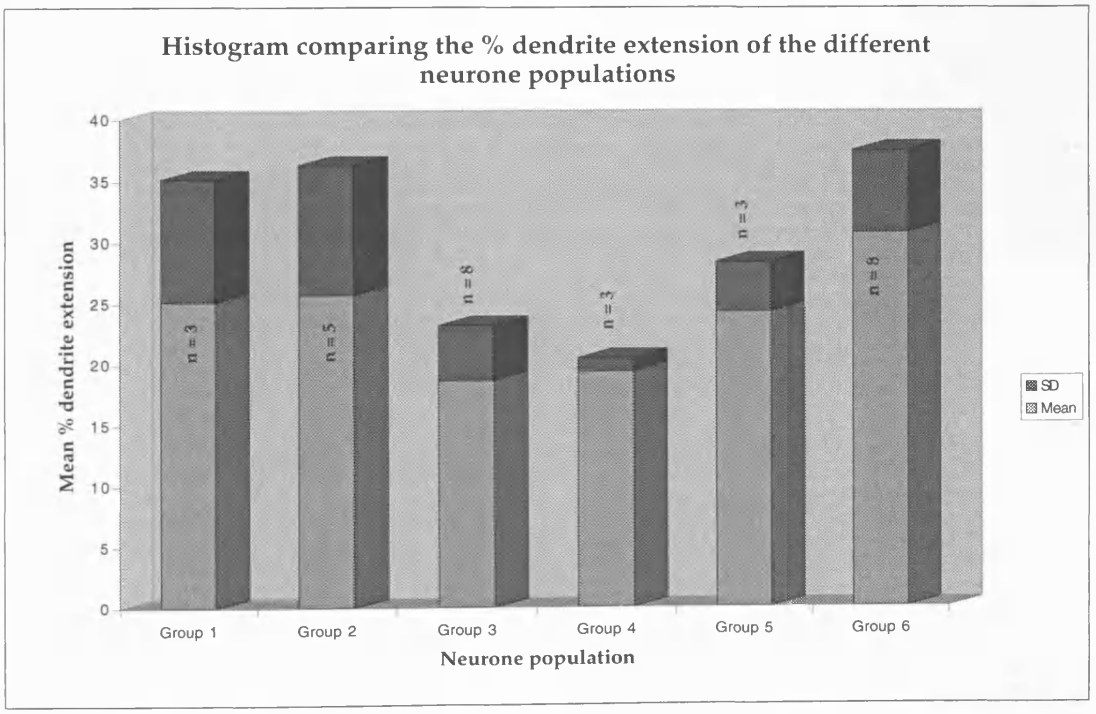
Histogram comparing the % dendrite extension of the different neurone populations
Mean % dendrite extension
40
35
30
25
20
15
10
5
0
n = 3
n = 5
n = 8
n = 3
n = 3
n = 8
Group 1
Group 2
Group 3
Group 4
Group 5
Group 6
Neurone population
SD
Mean

Figure 5.13

This figure shows the locations and dendritic distortion patterns of 3 group 1 neurones during tibial extension. All three of these neurones show changes in dendrite length over the entire femoro-tibial range. Neurone 1 (situated in group 1b) shows an initial increase followed by a decreasing rate of dendritic shortening with increasing femoro-tibial angle. Neurone 2 (group 1b) shows a similar trend although there are some fluctuations in the rate of shortening at angles greater than 50°. The pattern of dendritic distortion shown by neurone 3 (group 1a) is generally similar although there is a particularly small change in length over the range 0° - 30°. Arrows indicate neurones 1 - 3. Distal is to the right in all accompanying confocal micrographs

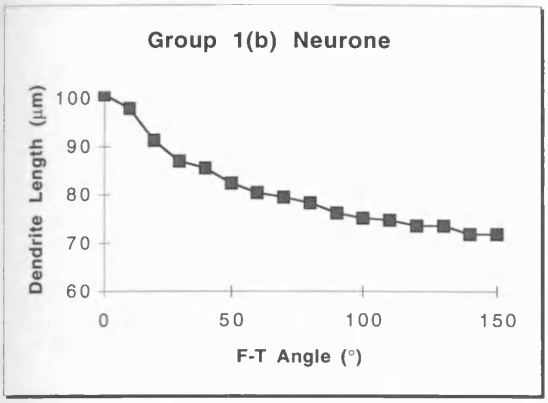
Group 1(b) Neurone
Dendrite Length (µm)
100
90
80
70
60
0
50
100
150
F-T Angle (°)

1

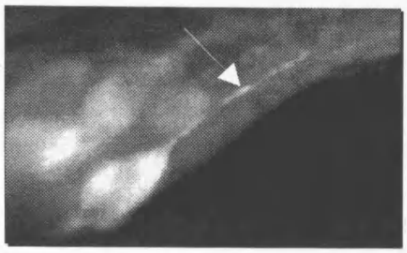

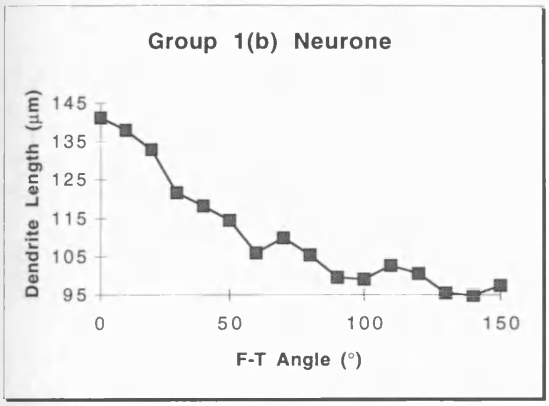
Group 1(b) Neurone
Dendrite Length (µm)
145
135
125
115
105
95
0
50
100
150
F-T Angle (°)

2

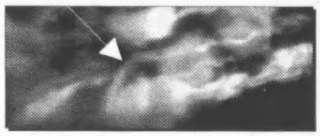

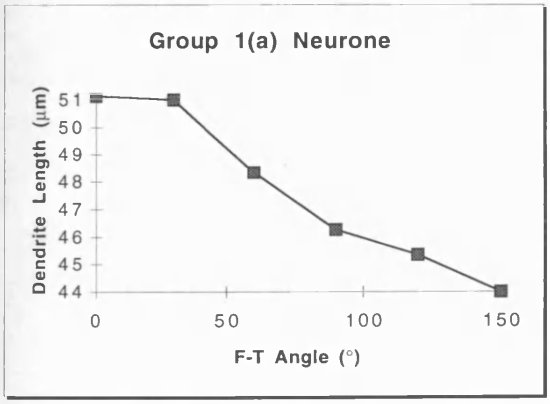
Group 1(a) Neurone
Dendrite Length (µm)
51
50
49
48
47
46
45
44
0
50
100
150
F-T Angle (°)

3

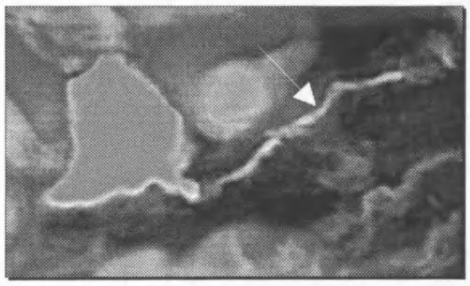

Figure 5.14

These figures show the locations and dendrite distortion patterns of 5 neurones located in group 2. Dendrite length continues to change as the tibia is rotated over the entire femoro-tibial range in all of these neurones. Dendritic length changes at a decreasing rate as femoro-tibial angle increases and as the tibia is extended from full flexion. In this case there is no slower initial phase followed by a more rapid rate of shortening as seen in group 1 neurones. Arrows indicate neurones 1 - 5. Distal is to the right in all accompanying confocal micrographs

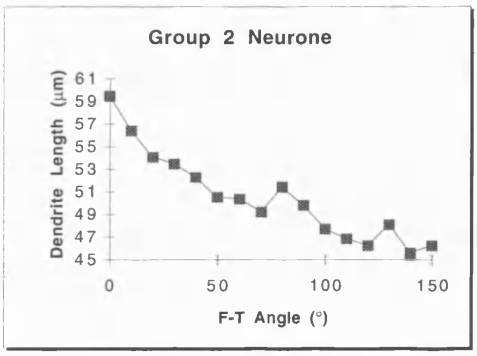
Group 2 Neurone
Dendrite Length (µm)
61
59
57
55
53
51
49
47
45
0
50
100
150
F-T Angle (°)

1

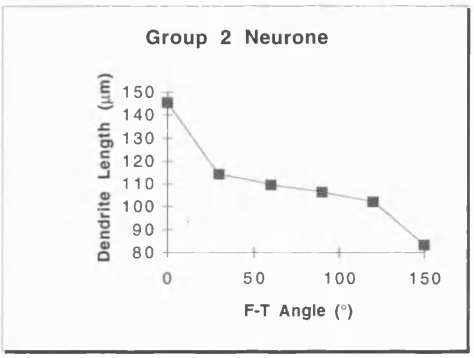
Group 2 Neurone
Dendrite Length (µm)
150
140
130
120
110
100
90
80
0
50
100
150
F-T Angle (°)

2

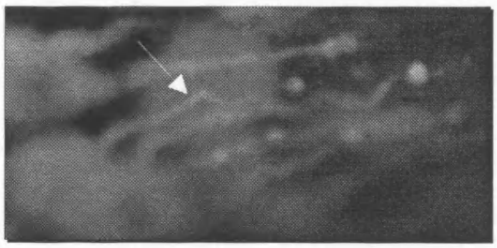

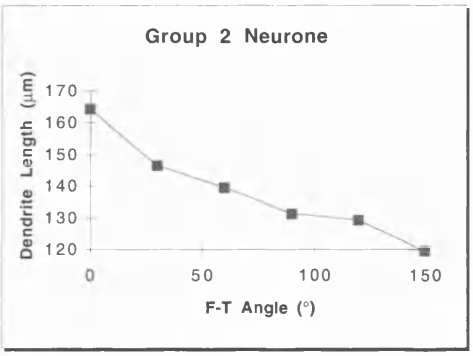
Group 2 Neurone
Dendrite Length (µm)
170
160
150
140
130
120
0
50
100
150
F-T Angle (°)

3

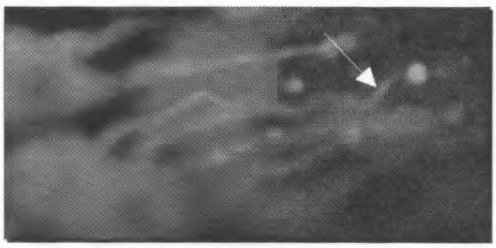

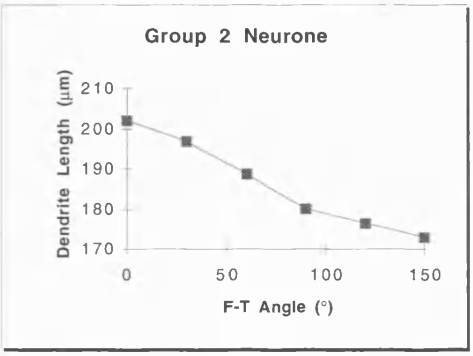
Group 2 Neurone
Dendrite Length (µm)
210
200
190
180
170
0
50
100
150
F-T Angle (°)

4

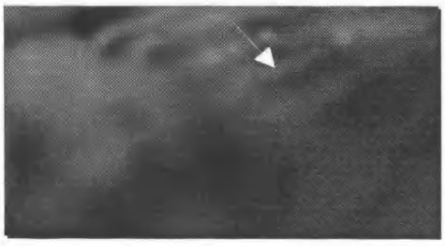

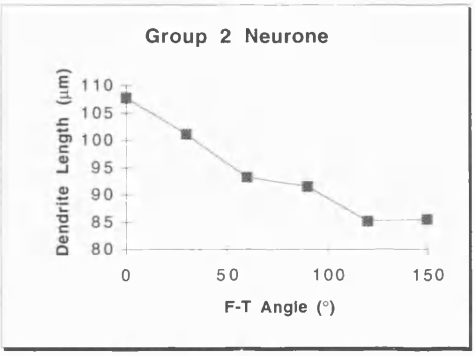
Group 2 Neurone
Dendrite Length (µm)
110
105
100
95
90
85
80
0
50
100
150
F-T Angle (°)

5

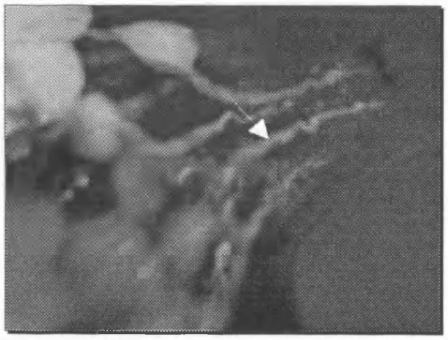

Figure 5.15

The location and dendritic distortion patterns of 8 group 3 dendrites (including 1 pair of dendrites both shown on graph 3) are shown opposite. The group 3 dendrites are subject to changes in dendrite length over the full range of femoro-tibial angles. Most show a tendency to shorten at a slightly decreasing rate as the tibia is extended from the flexed position. The dendrites of two neurones (5 and 6) show an increase in dendrite distortion with tibial rotation over particular parts of the femoro-tibial range; 30° - 60° and 60° - 90° respectively. The relationship between dendrite length and femoro-tibial angle is almost linear in the case of one of the neurones located at the extreme proximal margin of group 3 (neurone 4). Arrows indicate neurones 1 - 7. Distal is to the right in all accompanying confocal micrographs

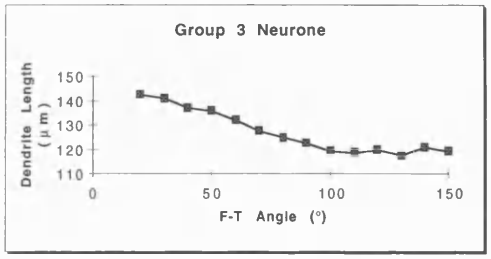
Group 3 Neurone
Dendrite Length (µm)
150
140
130
120
110
0
50
100
150
F-T Angle (°)

1

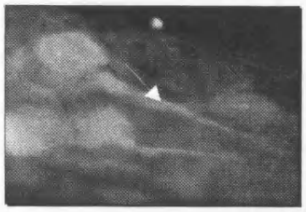

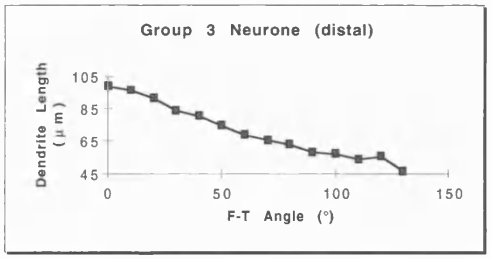
Group 3 Neurone (distal)
Dendrite Length (µm)
105
85
65
45
0
50
100
150
F-T Angle (°)

2

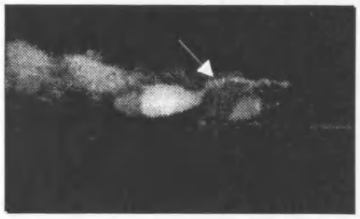

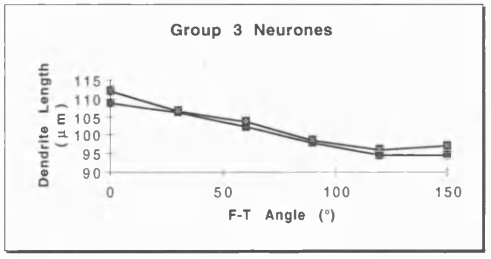
Group 3 Neurones
Dendrite Length (µm)
115
110
105
100
95
90
0
50
100
150
F-T Angle (°)

3

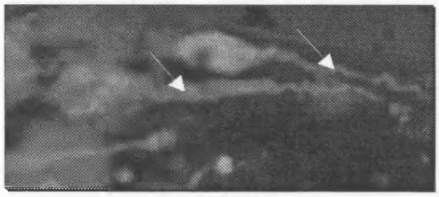

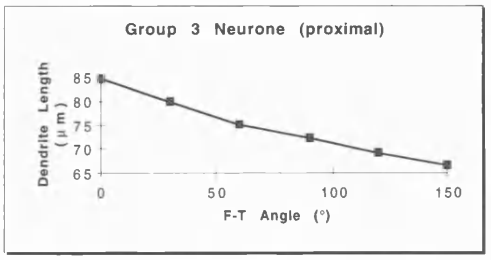
Group 3 Neurone (proximal)
Dendrite Length (µm)
85
80
75
70
65
0
50
100
150
F-T Angle (°)

4

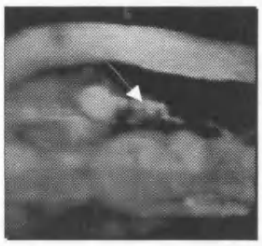

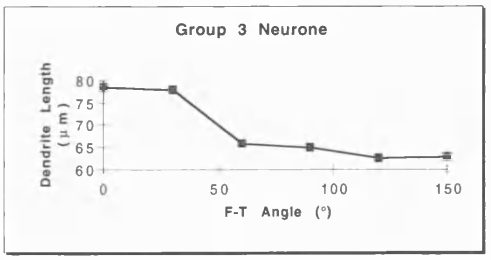
Group 3 Neurone
Dendrite Length (µm)
80
75
70
65
60
0
50
100
150
F-T Angle (°)

5

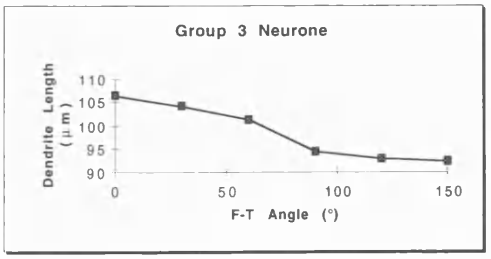
Group 3 Neurone
Dendrite Length (µm)
110
105
100
95
90
0
50
100
150
F-T Angle (°)

6

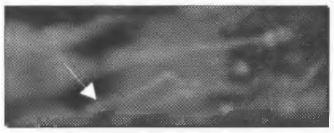

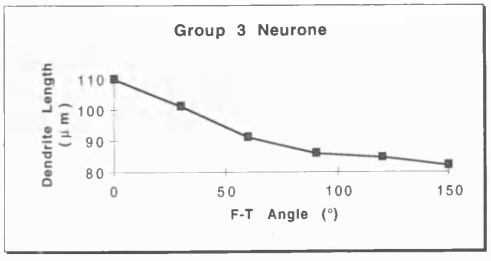
Group 3 Neurone
Dendrite Length (µm)
110
100
90
80
0
50
100
150
F-T Angle (°)

7

Figure 5.16

This figure shows the relationship between dendrite length and femoro-tibial angle of 3 neurones located in group 4. Neurones 1 and 2 are located adjacent to one another in the same preparation, yet show different dendrite distortion patterns. The relationship between dendrite length and femoro-tibial angle is approximately linear for neurone 1. The length of the neurone 2 dendrite changes similarly over the range of femoro-tibial angles 0° - 90°, but remains approximately 57 μm in length over the remainder of the femoro-tibial range. Neurone 3 shows a generally similar dendrite distortion pattern to that of neurone 1, with the dendrite length changing continually over the entire femoro-tibial range. However, length changes are not so linear and dendrite length increases at angles greater than 130°. Arrows indicate neurones 1 - 3. Distal is to the right in all accompanying confocal micrographs

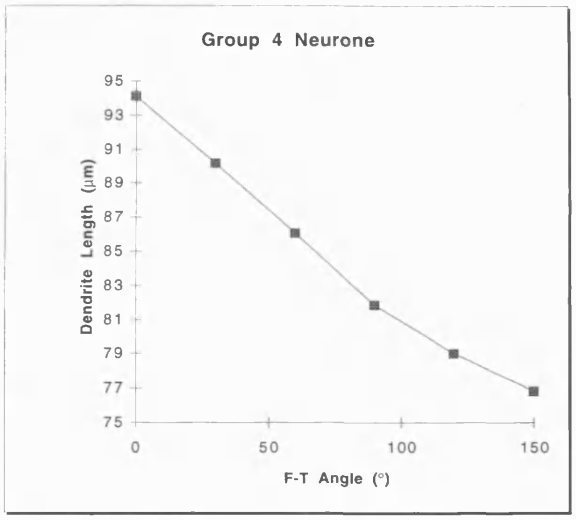
Group 4 Neurone
Dendrite Length (µm)
95
93
91
89
87
85
83
81
79
77
75
0
50
100
150
F-T Angle (°)

1

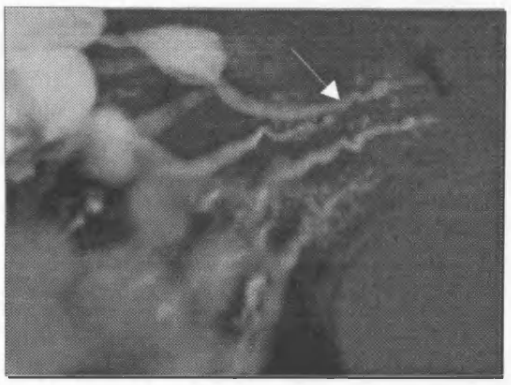

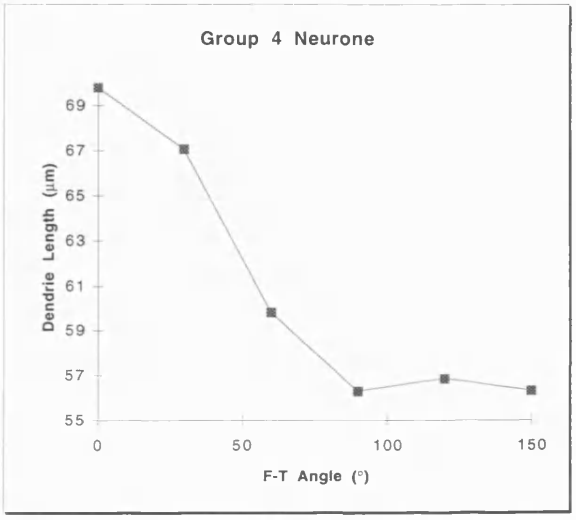
Group 4 Neurone
Dendrie Length (µm)
69
67
65
63
61
59
57
55
0
50
100
150
F-T Angle (°)

2

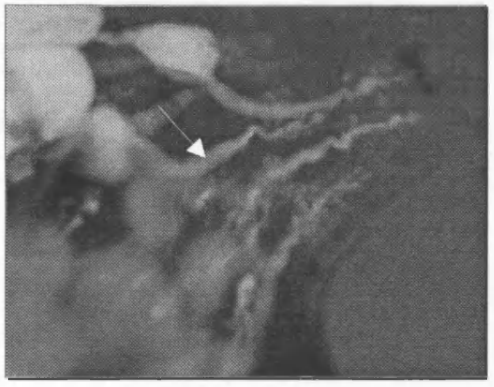

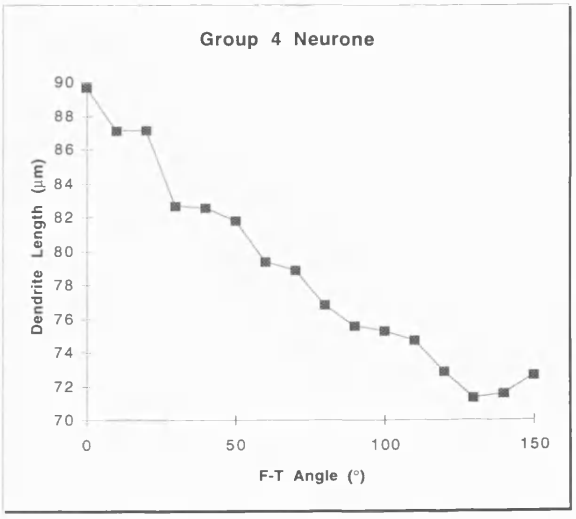
Group 4 Neurone
Dendrite Length (µm)
90
88
86
84
82
80
78
76
74
72
70
0
50
100
150
F-T Angle (°)

3

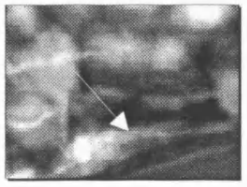

Figure 5.17

This figure shows the relationship between dendrite length and femoro-tibial angle upon tibial rotation from the flexed position for 4 neurones located in group 5. Neurones 1 and 2 both show changes in dendrite length over the entire femoro-tibial range. However, the rate of dendrite length change declines with increasing femoro-tibial angle in the case of neurone 1 whereas neurone 2 undergoes relatively consistent changes in dendrite length with increasing femoro-tibial angle. This situation contrasts with the distortion patterns shown by the dendrites of neurones 3 and 4 . Both of these dendrites show comparatively large changes in dendrite length over the first half of the tibial extension range (0° - 80°) followed by minimal changes in dendrite length over the second half (80° - 150°). Arrows indicate neurones 1 - 4. Distal is to the right in all accompanying confocal micrographs

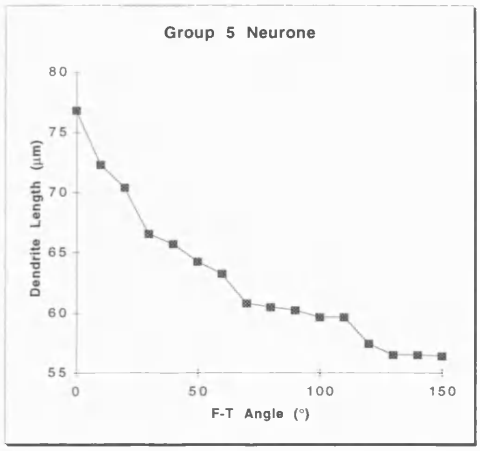
Group 5 Neurone
Dendrite Length (µm)
80
75
70
65
60
55
0
50
100
150
F-T Angle (°)

1

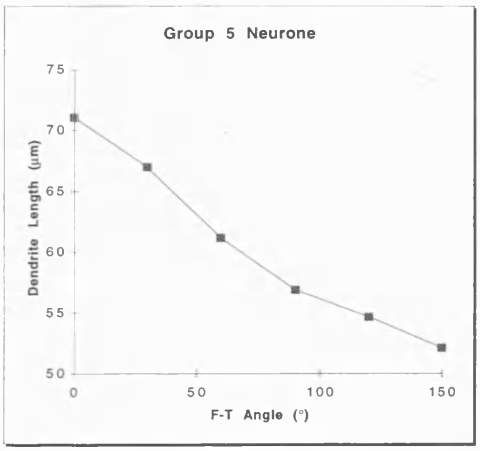
Group 5 Neurone
Dendrite Length (µm)
75
70
65
60
55
50
0
50
100
150
F-T Angle (°)

2

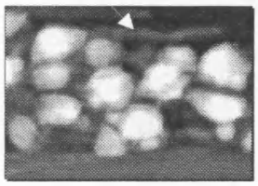

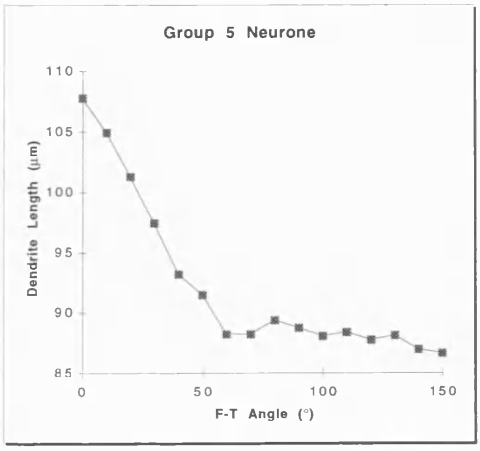
Group 5 Neurone
Dendrite Length (µm)
110
105
100
95
90
85
0
50
100
150
F-T Angle (°)

3

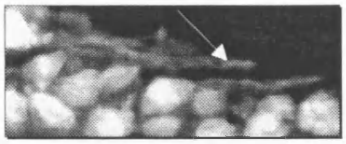

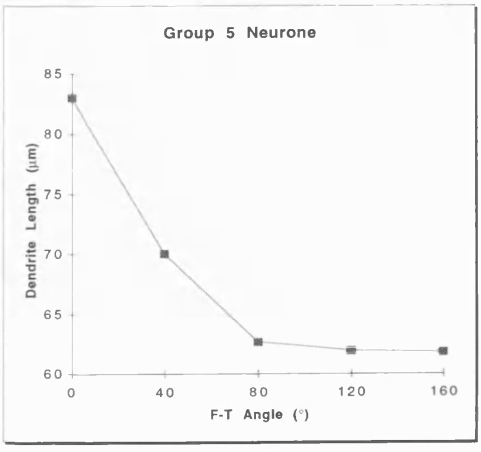
Group 5 Neurone
Dendrite Length (µm)
85
80
75
70
65
60
0
40
80
120
160
F-T Angle (°)

4

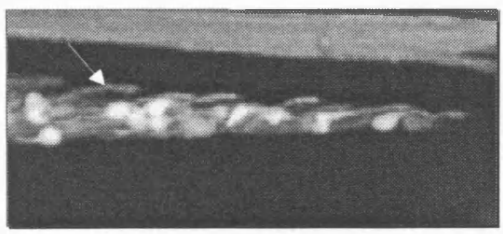

Figure 5.18

Figure showing the relationship between dendrite length and femoro-tibial angle for 7 group 6 dendrites (4 of which were located in the same preparation, graphs 4a, b). All the dendrites in this group show a tendency to shorten as the tibia is rotated from the fully flexed position before adopting a static length as the tibia approaches full extension. This is especially evident in neurones 2 and 3 whose dendrites have undergone their entire range of distortion over the range of femoro-tibial angles 0° - 100°. The distortion patterns of the four neurones in graph 4a are derived from 4 dendrites (indicated) in the same preparation. This allows their distortion patterns to be compared directly with one another and correlated with their proximo-distal locations. Graph 4b shows the same dendrite length data as shown in graph 4a, re-plotted so that the length of each dendrite at any particular femoro-tibial angle is expressed as a percentage of its maximum length at full tibial flexion (0°). This graph shows that the distortion patterns of the four dendrites are graded and reflect each neurone's position in the scoloparium. The dendrites of increasingly proximally located neurones are subjected to larger ranges of distortion. Arrows indicate neurones 1 - 7. Distal is to the right in all accompanying confocal micrographs

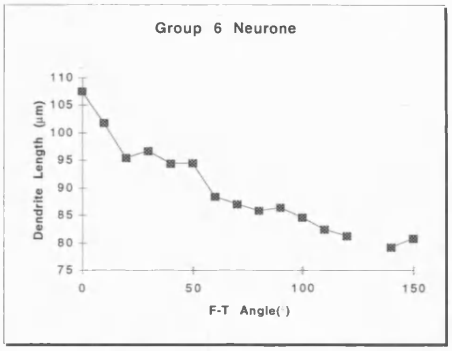
Group 6 Neurone
Dendrite Length (µm)
110
105
100
95
90
85
80
75
0
50
100
150
F-T Angle(°)

1

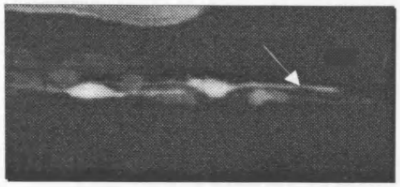

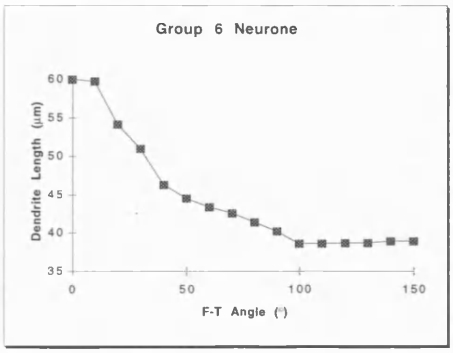
Group 6 Neurone
Dendrite Length (µm)
60
55
50
45
40
35
0
50
100
150
F-T Angle (°)

2

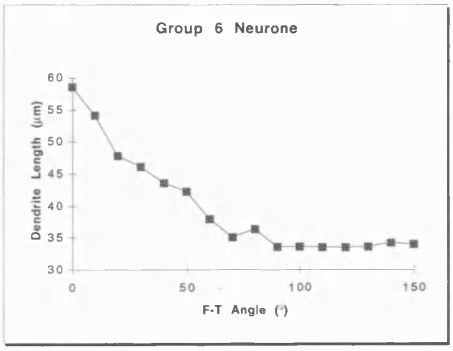
Group 6 Neurone
Dendrite Length (µm)
60
55
50
45
40
35
30
0
50
100
150
F-T Angle (°)

3

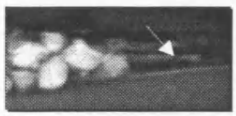

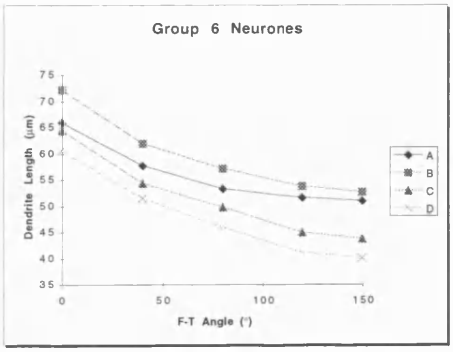
Group 6 Neurones
Dendrite Length (µm)
75
70
65
60
55
50
45
40
35
0
50
100
150
F-T Angle (°)
A
B
C
D

4a

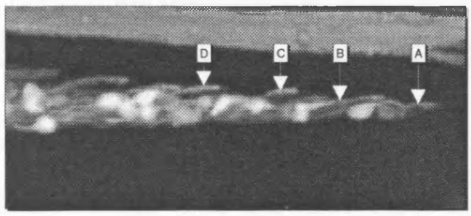
D
C
B
A

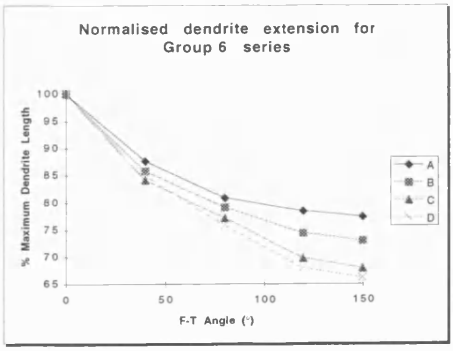
Normalised dendrite extension for Group 6 series
% Maximum Dendrite Length
100
95
90
85
80
75
70
65
0
50
100
150
F-T Angle (°)
A
B
C
D

4b

Figure 5.19a, b

These histograms show the mean rate of dendrite length change of the 6 neurone populations over the femoro-tibial range 0° - 150° (upper) and 0° - 40° (lower). The rate of length change was calculated as μm/10° tibial rotation. Over the full range of femoro-tibial extension (0° - 150°), the mean rates of dendrite extension ranged between 1 - 3 μm/10° femoro-tibial rotation. The dendrites of groups 1, 2 and 3 appear to be subjected to larger elongations/10° femoro-tibial rotation than those of the other more distally-located neurone groups. When the mean dendrite extension rates were calculated over the initial part of the range of tibial extension only (0° - 40°), the dendites of the group 1 and 2 neurones still appear to undergo larger elongations/10° femoro-tibial rotations than those of the remaining neurone groups. Groups 1 and 2 are subjected to particularly variable rates of dendritic distortion in both cases. The limited data set precludes detailed statistical analysis.

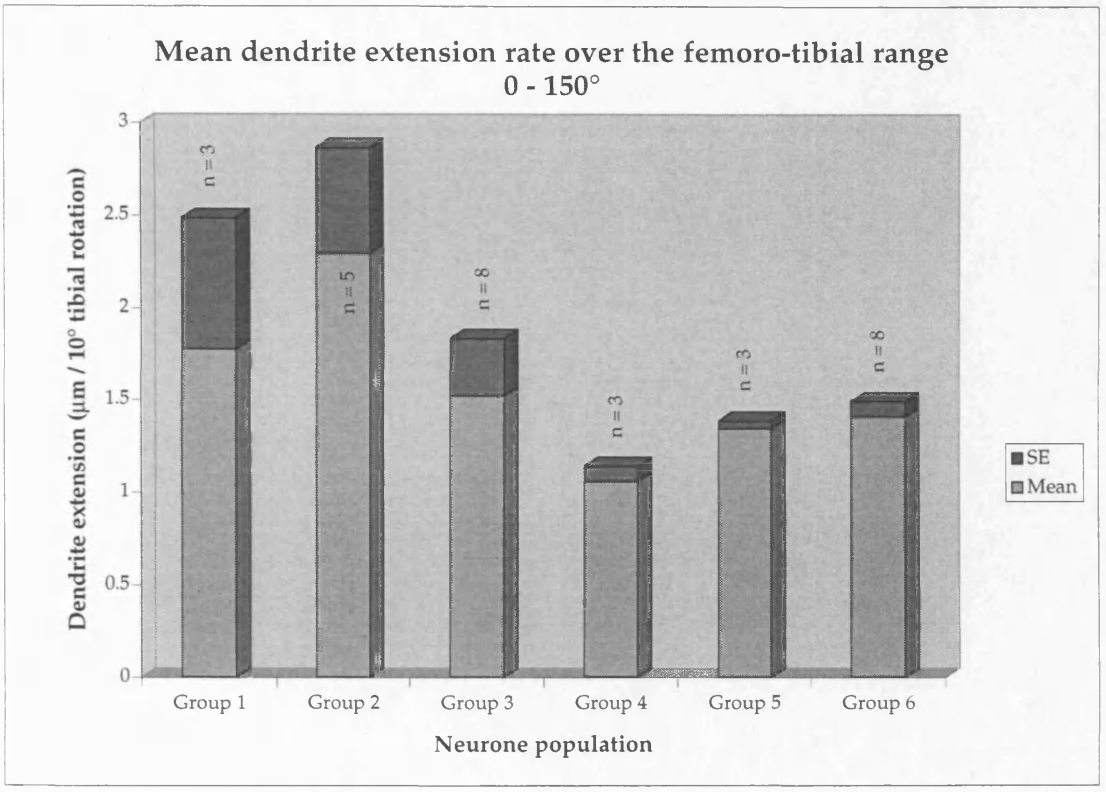
Mean dendrite extension rate over the femoro-tibial range
0 - 150°
Dendrite extension (µm / 10° tibial rotation)
3
2.5
2
1.5
1
0.5
0
n = 3
n = 5
n = 8
n = 3
n = 3
n = 8
SE
Mean
Group 1
Group 2
Group 3
Group 4
Group 5
Group 6
Neurone population

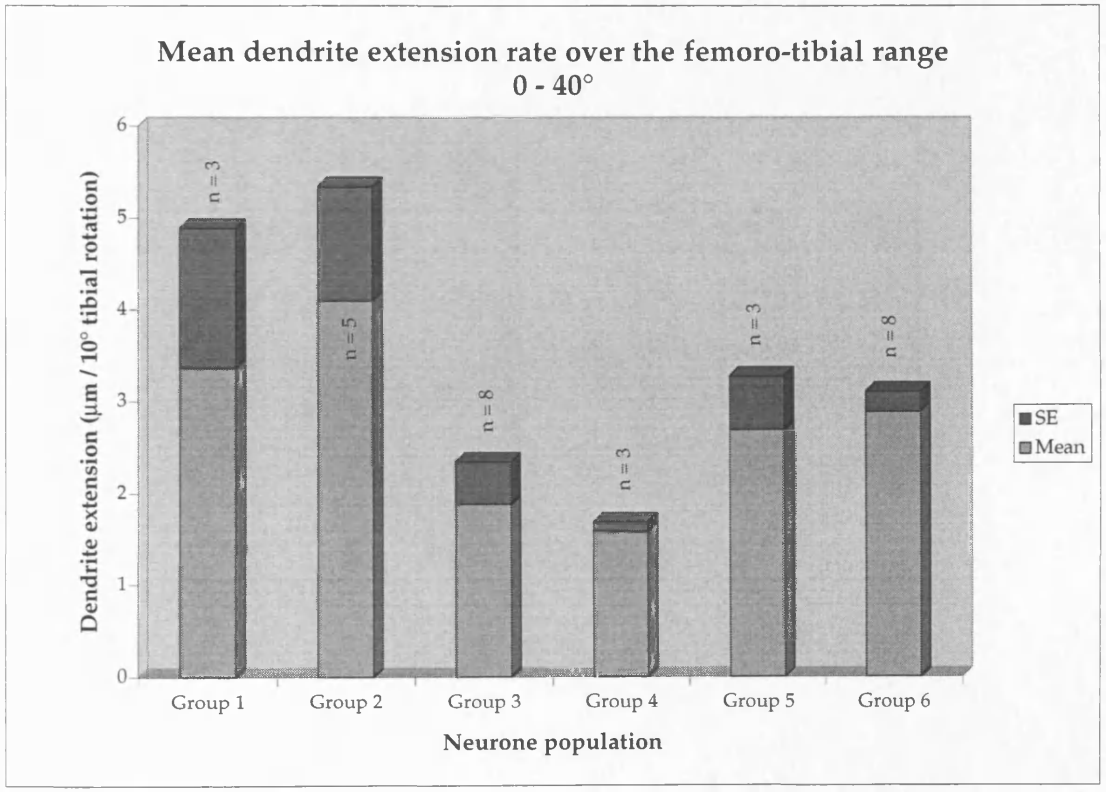
Mean dendrite extension rate over the femoro-tibial range
0 - 40°
Dendrite extension (µm / 10° tibial rotation)
6
5
4
3
2
1
0
n = 3
n = 5
n = 8
n = 3
n = 3
n = 8
SE
Mean
Group 1
Group 2
Group 3
Group 4
Group 5
Group 6
Neurone population

Figure 5.20

This diagram shows the displacement of 4 pairs of marker points at 30° intervals over the full range of femoro-tibial angles 0° - 150°. Each pair of markers consists of an internal point (red) located within the scoloparium and an external marker (blue) positioned upon the scoloparium surface. The external markers directly overlie their corresponding internal markers at a femoro-tibial angle of 150° (full femoro-tibial extension). The starting position of each marker pair is indicated relative to the scoloparium outline (arrows). As the tibia was flexed, the markers were displaced distally and their new positions were plotted at 30° intervals. The differential displacement between each pair of marker points shows the degree to which the mtFCO neurones are displaced relative to the scoloparium sheath. Pair 1 demonstrates that there is little differential displacement between the neurones and the scoloparium sheath at this proximal point. At the point where marker pair 2 are located, the marker located on the scoloparium sheath undergoès a smaller range of displacement, both proximo-distally and dorso-ventrally, than the marker located internally. Further distally (marker pairs 3 and 4) the relationship between the ranges of external and internal displacement is similar. As is the case for pairs 1 and 2, the dorsal pair of points (pair 3) appears to show a greater difference between external and internal displacement than the ventral pair (pair 4). In all cases there appears to be a greater degree of differential displacement between the corresponding pairs of markers in the dorso-ventral plane than the proximo-distal plane.

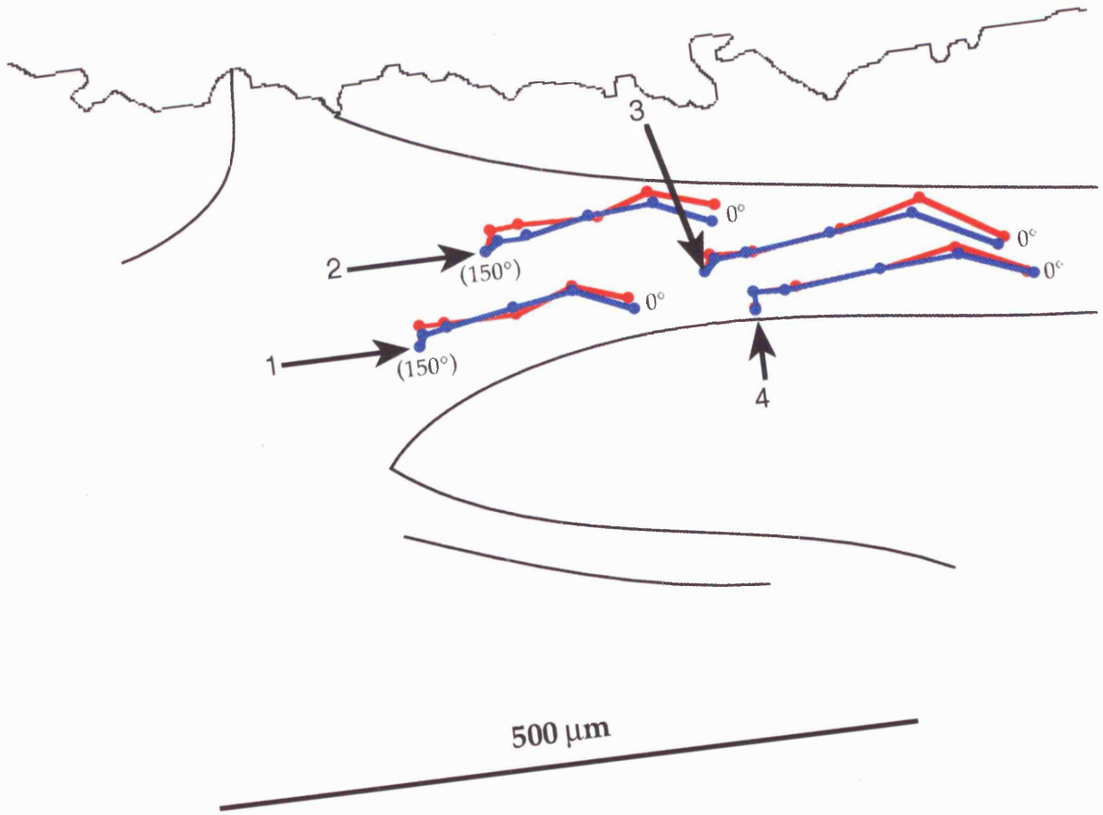
3
0°
0°
0°
2
(150°)
1
(150°)
4
500 µm

Chapter 6: Mechanical properties of the mtFCO linkages

6.1 SUMMARY

- *The mtFCO is a viscoelastic system whose resonant frequency lies between 1 - 2 Hz. The amplitude and phase of the tension oscillations resulting from a sinusoidal input of constant amplitude is frequency dependent. The system also exhibits stress-relaxation behaviour such that an imposed step displacement is followed by a characteristic decline in the resulting tension.*

6.2 INTRODUCTION

A receptor's sensory characteristics depend upon a sequence of three time-dependent mechanisms (French, 1988): the mechanical coupling of the site receiving the displacement stimulus with the site of sensory transduction, the process of mechano-electric transduction to produce a generator potential, and the sensory encoding of the electrical potential into action potentials.

The relatively large size of the locust mtFCO in comparison to other mechanoreceptors makes it possible to investigate the role of the first of these three mechanisms and to speculate concerning its likely contribution to the overall organ response. The nature of the mechanical connections of the mtFCO and the mechanical properties of the mtFCO system as a whole, determine the mechanical input reaching the membranes of the mtFCO sensory neurones. In the following experiments, the chordotonal organ's connection to the tibia was severed and was attached to a small strain gauge. The properties of the mtFCO were investigated by imposing deformations mimicking flexion or extension of the tibia whilst measuring the corresponding changes in tension.

An ideal elastic material will support a given load for any length of time and when the load is removed, the original dimensions will be restored rapidly. Viscous materials deform under load in a time dependent manner. Most biological materials combine elastic and viscous behaviours (Fung, 1984); viscoelasticity has been demonstrated to be a property of materials such as spider's silk (Weber, 1835, 1841; see Dorrington, 1980), insect cuticle (Brunet and Coles, 1974) including locust

tibial extensor muscle apodeme (Ker, 1977; see Vincent, 1980), and bone (Hulsen, 1896; Yokoo 1952; Burstein *et al.*, 1973; Bargren *et al.*, 1974).

Linear viscoelastic materials obey the law of proportionality between a stretching load and the resulting elongation (Hooke's Law), but only for a short time following the application of the load. If a constant load were to remain applied to such a material over a length of time, the elongation would continually increase (Dorrington, 1980). Authors have quantified viscoelastic phenomena using a variety of experimental techniques. In the case of 'creep' experiments, a rested specimen is rapidly loaded so as to bear a constant stress (= force/unit cross-sectional area) whilst the gradual increase in strain (= proportional change in length) is monitored with time (e.g. Alexander 1964). In 'stress-relaxation' experiments the strain on the specimen is rapidly increased and held constant whilst the force required to hold the deformation constant falls as a function of time (e.g. McCrum and Dorrington, 1976).

A characteristic of viscoelastic materials is that their stiffness is a function of the imposed strain rate. This phenomenon has been demonstrated in materials such as spider silk (Iizuka, 1965; Denny 1976). Its occurrence indicates the presence of a viscous component in a primarily elastic material. Denny (1976) and Mullins (1980) illustrated this phenomenon in spider's silk and synthetic rubber respectively, by the production of hysteresis curves in response to cyclical loading. The rate at which a material is stretched and unloaded determines the maximum tension developed and the size of the hysteresis loop. The magnitude of the loop reflects the limited 'flow' of the viscous components under the action of the load.

In the case of a forced vibration experiment, a continually oscillating sinusoidal strain is applied to the material whilst the resulting stress oscillations are monitored. In a perfectly Hookean material, the stress and strain remain perfectly in phase (Dorrington, 1980) whilst in a viscoelastic material the stress and strain appear out of phase with one another (e.g. whole arteries, Bergel, 1961; Learoyd and Taylor, 1966; Apter and Marquez, 1968, isolated elastin, Gotte *et al.*, 1968; Pezzin and Scandola 1976; Scandola and Pezzin, 1978; Gosline and French, 1979; and mesogloea, Gosline, 1971). In the case of a linearly viscoelastic material the difference in phase

between the applied strain and resulting stress oscillation varies in a characteristic manner with the frequency of oscillation (Dorrington, 1980).

In the current investigation both stress-relaxation and dynamic stress-strain tests have been used to demonstrate the viscoelasticity of the mtFCO's tissue and the consequent relationship between stress, strain and time when it is subjected to different types of deformation.

Hysteresis is a property of many viscoelastic systems (Chaplain *et al.*, 1971) and has been observed in the responses of many types of mechanosensory apparatus. In invertebrates, hysteresis has been reported in neural discharges of a variety of sense organs including: crayfish stretch receptors (Krnjevic and van Gelder, 1961; Brown and Stein, 1966; Chaplain *et al.*, 1971; Segundo and Diez Martinez, 1985), the propodite-dactylopodite joint proprioceptors of decapod crustaceans (Mill and Lowe, 1972), the femoral CO of the stick insect (Kittmann and Schmitz, 1992), the locust femoral CO (Burns, 1974; Zill, 1985a; Zill and Jepson-Innes, 1988, 1990; Field and Pflüger, 1989; Matheson, 1990, 1992b), and non-spiking local interneurones of the locust ventral nerve cord (Siegler, 1981). Hysteresis is also a property of proprioceptors in higher animals. In the cat it has been observed in the responses of muscle-spindle afferents and joint receptors (Lennerstrand, 1968; Kostyukov and Cherkassky, 1992), receptors in the mammalian vestibular system (Vidal *et al.*, 1971), Pacinian corpuscles (Alvarez Buylla and Ramirez de Arellano, 1953) and in primate joint receptors (Grigg and Greenspan, 1977).

In the locust, when the tibia is extended and returned to its original position the discharge of the mtFCO is depressed relative to the firing frequency before the change in joint angle was imposed (Burns, 1974; Matheson, 1990, 1992b). In this chapter it will be shown that because of its viscoelastic properties, the mtFCO system is subjected to mechanical hysteresis during cyclic extension and relaxation. This provides an explanation for the observed differences in sensory output during flexion and extension. Hysteresis implies that the mtFCO scoloparium can be subjected to two different tensions at the same femoro-tibial angle, depending upon the direction of joint rotation. It would seem to present a problem in the accurate encoding of information concerning joint position.

The typically non-linear viscoelastic properties of biological systems must present problems in proprioceptive circuits which ideally faithfully relay the peripheral condition irrespective of previous history (Hatsopoulos *et al.*, 1995). Possible compensatory mechanisms are discussed with respect to the observed results. Both physical and theoretical models are used to demonstrate the properties of simple viscoelastic systems and rationalise the stress-strain relationships of the mtFCO.

6.3 MATERIALS AND METHODS

6.3.1 Dissection

Isolated femora from *Schistocerca gregaria, Locusta migratoria* or *Tropidacris collaris* were dissected from either the posterior or anterior side to reveal the mtFCO. Dissection from the posterior side was favoured since this approach allows the femur to act as a natural haemolymph bath. In some preparations, the mtFCO itself was partially dissected. In these preparations one of the apodeme complex ligaments or the guy-rope fibres were severed using fine dissecting scissors.

6.3.2 Experimental setup

In order to measure the mtFCO's mechanical properties all experiments were performed upon an anti-vibration table. The cuticular rod of the apodeme complex was attached to a measuring device and tension within the mtFCO was monitored as the organ was deformed. The tibia was positioned in the flexed position during all experiments unless stated otherwise. Some mtFCO length-tension measurements were performed using glass filaments attached to the mtFCO apodeme. Deflection of the filament when the organ was displaced reflected the force to which the mtFCO was subjected. Deflection was measured using an eyepiece graticule. The forces causing filament deflection were calibrated using known weights. The majority of mechanical experiments were performed using a Sensinor X-18939 silicon beam force transducer incorporated into an electronic strain gauge (Fig. 6.1) designed and built by Dr R.O. Stephen (Dept. of Pre-clinical Sciences, Leicester University). The strain gauge was calibrated by the application of known weights. This allowed the output (mV) to be converted to units of force (N). The strain gauge was mounted upon a micromanipulator equipped with a vernier scale. Adjustment of the micromanipulator allowed the mtFCO to be displaced by precise increments. Adjustable buffered stops were positioned on either side of

the micromanipulator to restrict the range of travel to the mtFCO's physiological range. This arrangement also allowed the organ to be displaced manually over its entire physiological range in a single accurate rapid step. A fine tungsten needle formed the connection between the strain gauge and the cuticular rod of the apodeme complex (Figs 6.2a, b). A spot of glue on the end of the needle was used to cement the two together. A glass hook was used to manipulate the organ and to hold the cuticular rod clear of the haemolymph for approximately 30 s whilst the glue was allowed to dry. The tungsten needle was electrolytically sharpened in a bath of sulphuric acid and then the tip was shaped into a small hook. The tungsten hook passed beneath the cuticular rod to provide a good attachment to the strain gauge whilst the tapering limited any drag within the haemolymph when mechanical stimuli were applied. Complex stimuli were delivered to the mtFCO using a mechanical actuator (Brüel and Kjaer model 4810 minishaker) driven by either a programmable signal generator (Strathkelvin Instruments model 983) or a Signal Analyser (Brüel and Kjaer type 2032). Saw-tooth, sinusoidal, ramp and pink noise stimuli were applied. The strain gauge remained stationary during these experiments whilst the femur was displaced proximo-distally on a linear bearing race (Fig. 6.3). The displacement of the femur was measured directly using a laser displacement transducer (Microepsilon model LD 1605-20) accurate to ±10 μm. Using this system displacement of the femur resulted in similar displacement of the mtFCO rod. Thus, known length changes in the mtFCO system could be applied and the tension during such changes could be monitored. In some cases pink noise stimuli were used. Prior to administering pink noise stimulation, the frequency response of the apparatus before connection to the mtFCO was recorded and stored on the signal analyser. For this the strain gauge needle was positioned within the femur adjacent to, but not coupled with, the mtFCO. The resulting frequency response curve was then digitally subtracted from subsequent experimental runs used to measure the frequency response of the organ. This procedure removed any experimental error introduced by resonance of equipment or hydrostatic coupling between the strain gauge needle and the haemolymph in the femur.

6.3.3 Data acquisition

Displacement and tension data were acquired using either the Brüel and Kjaer signal analyser, a digital oscilloscope (Nicolet Pro-10), or a 'MacLab/4' digitiser in conjunction with a Macintosh 'Classic II'

microcomputer running 'Chart' (v3.3.6) software. The output signal was sampled at rates in excess of 512 samples/second. The records were either saved to disk or printed out as hard copy using a graphics plotter (Brüel and Kjaer model 2319).

6.3.4 Modelling

A model was constructed to examine the characteristics of a simple resonating system. The model consisted of a tapered mass suspended from a vertically oscillating support via a length of elastic. The components were chosen such that the model resonated at approximately 2 Hz, at which frequency small displacements (1 cm) of the movable beam resulted in large displacements (5 cm) of the mass. The displacement of the support, tension in the elastic and displacement of the mass were monitored via three transducers (a foil strain gauge (RS catalogue number 623-124), an eddycurrent probe (Emic transducer model C623) and a laser displacement transducer (Microepsilon model LD 1605-20)) (Fig. 6.4). Data was acquired using a Hewlett Packard microcomputer or the Brüel and Kjaer signal analyser.

6.4 RESULTS

6.4.1 mtFCO Displacement-tension relationship

The change in tension as the mtFCO is stretched from one extreme of its physiological range to the other demonstrates the range of axial forces to which the mtFCO scoloparium can be subjected. In the case of *S. gregaria*, the mtFCO is at a mean tension of 40 μN (s.d. = 19.5, n = 9) when the cuticular rod is held at a position equivalent to a femoro-tibial angle of 150° (full tibial extension). It reaches a tension of 398.2 μN (s.d. = 75.2, n = 9) when the rod is displaced to a position equivalent to a femoro-tibial angle of 0° (full tibial flexion). A typical mtFCO displacement-tension curve for *S. gregaria* measured using glass filaments is shown in Figure 6.5. As the organ is stretched in a series of equal steps, tension rises with increasingly large increments indicating that the mtFCO is not linearly elastic (Fig. 6.5a). This observation almost certainly reflects, in part, the recruitment of additional elastic components in the apodeme complex as the tibia is flexed (Field, 1991; Shelton *et al.*, 1992). Due to the eccentric nature of the mtFCO's distal attachment to the tibia there is a sinusoidal relationship between mtFCO displacement and femoro-tibial angle (see Chapter 2). When tension is plotted against equivalent femoro-

tibial angle the relationship is also found to be non-linear (Fig. 6.5b). Approximately 90% of the total possible mtFCO tension change occurs over the femoro-tibial range 0° - 80°. This may endow the mtFCO with increased angular resolution over this part of the femoro-tibial range. The mtFCO tension changes by approximately 100 μN over the mean walking cycle range (see Chapter 2).

The contributions of various elements of the mtFCO apodeme complex to the mechanical properties of the system were investigated by measuring the displacement/tension relationship before and after the different elements had been severed. The measurements described in the following sections were made using *S. gregaria*.

6.4.1.1 Effects of guy-rope ablation

First of all the role of the guy-rope fibres associated with the apodeme complex was investigated. Comparison of the displacement/tension curves before and after cutting, shows that the guy-rope fibres exert most influence upon the organ when the tibia is extended (Fig. 6.6a). Before they have been cut, these fibres take up some of the stress as the apodeme complex unloads during tibial extension. When they are severed this effect is lost causing the tension in the mtFCO to rise relative to that in the intact leg by the amount that was previously unloaded into the guy-rope fibres. The mean tension increase measured at a femoro-tibial angle of 0° following the cutting of the guy-rope fibres was 32 μN (s.d. = 19.7, n = 3). The functional consequences for the mtFCO are that the guy-rope fibres modulate the force to which the mtFCO sensory neurones are subjected. In particular, they maintain the scoloparium under tension when the tibia is extended and the apodeme complex is at its slackest.

6.4.1.2 Effects of the ventral attachment

Because the apodeme was detached from the tibia in order to measure tension at the level of the mtFCO rod, the tibia could be moved without displacing the mtFCO via the apodeme. This meant that the influence of the mtFCO's ventral attachment to the flexor muscle apodeme could be investigated. This was done by comparing displacement/tension curves measured whilst the tibia was flexed and extended, in which positions the ventral attachment is taut/slack respectively (Fig. 6.6b). Relative to the forces developed when the attachment was slack, the forces developed when it was taut were increased by similar amounts over the whole range

of femoro-tibial angles. When the apodeme was in the fully flexed position and the ventral attachment was at maximum tension (tibia held in the flexed position), the mean maximum tension developed was increased by 51.5 μN (s.d. = 24.8, n = 3). However, the mtFCO's ventral attachment to the flexor muscle apodeme is taut only over the 0° - 40° range of femoro-tibial angles (see Chapter 2). Thus, the ventral attachment modifies the mtFCO displacement/tension relations *in vivo* by increasing tension in only parts of the curve corresponding to femoro-tibial angles of 0° - 40° (0 μm - 300 μm apodeme displacement). In all subsequent experiments, the tibia was held at a femoro-tibial angle of 0°.

6.4.2 Mechanical hysteresis within the mtFCO

When viscoelastic materials are deformed, part of the energy is stored as potential energy (elastic response), and part is dissipated as heat (viscous response). If the tension in an extended mtFCO is measured as it is returned to its original length, the resulting displacement-tension curve does not follow the same course as that produced when the organ is extended. A hysteresis loop is generated, the area of which represents the loss of elastic energy in one extension-relaxation cycle (Figs 6.7a, b). In this case the tension was measured using glass filaments whilst the mtFCO was displaced in 120 μm increments. There was a pause of approximately 10 s between measurements. The occurrence of such hysteresis curves shows that the mtFCO has viscoelastic properties.

6.4.3 The viscoelasticity of the mtFCO

The effect of viscoelasticity upon mtFCO extension/tension dynamics was investigated by distorting the organ at different rates (Fig. 6.8). This was achieved by imposing saw-tooth displacements upon the end of the cuticular rod using a mechanical actuator driven by a signal generator. A standard displacement amplitude of 1000 μm was used to simulate rotation of the tibia over the majority of the femoro-tibial range. When the organ is displaced slowly, the resulting hysteresis loop is small. At increasingly high frequencies, the amount of energy dissipated per extension-relaxation cycle rises and so the areas of the hysteresis loops increase. Similar results were obtained for *S. gregaria* (n = 9) and *L. migratoria* (n = 5).

Because the area of each hysteresis loop represents the amount of energy dissipated during the displacement cycle, measuring this area enables the

amount of energy lost to be related to the velocity of displacement (Figs 6.9a, b). It was found that in the case of both *S. gregaria* and *T. collaris*, the amount of energy dissipated/cycle is not linearly related to the displacement velocity. Instead there is a rapid increase in energy dissipation up to a displacement velocity of $2x10^{-3}$ m s^{-1}, followed by a slower rate of increase at higher velocities which approximates to a linear relationship.

Comparing the relationship between energy dissipation/cycle and displacement velocity of intact and partially dissected mtFCOs, shows that if either of the apodeme complex ligaments are severed, the amount of energy dissipated per cycle approximately halves (Figs 6.10a, b). This indicates that the majority of energy dissipation observed is due to the viscosity of the mtFCO apodeme complex ligaments (and not more proximally situated mechanical linkages), and that both ligaments behave in a similar manner.

In a perfectly elastic material, the amount of energy dissipated per cycle is linearly related to the displacement velocity. Although the results were variable from specimen to specimen, results from *S. gregaria* (n = 9), *L. migratoria* (n = 4) and *T. collaris* (n = 6) were all similar in showing that at low frequencies the relationship was far from linear (Figs 6.9; 6.10). In at least half the cases there was a distinct peak or shoulder in the graph between 1 Hz and 2 Hz. The intact preparation in Figure 6.10b clearly demonstrates that there is a disproportionate amount of energy dissipated at a displacement velocity of $1x10^{-3}$ m s^{-1} in comparison to the higher velocity of $2x10^{-3}$ m s^{-1}. This pattern of velocity-dependent energy dissipation is characteristic of resonating systems (Holwill and Silvester, 1973; Bolton, 1986).

6.4.4 Sinusoidal stimulation

In viscoelastic systems, an oscillating sinusoidal input gives rise to a sinusoidal output that differs from the input in amplitude and phase. This reflects the material's ability to transmit vibrations at different frequencies. The mtFCO was subjected to sinusoidal oscillations over a constant amplitude of 200 μm (equivalent to ±10° tibial rotation) about a mean angle of 55° at a range of different frequencies whilst the resulting tension change was measured at the strain gauge (Fig. 6.11). A mean angle of 55° was chosen because this had been established as the mean femoro-

tibial angle during the locust walking cycle (see Chapter 2). It was found that the oscillation in mtFCO tension is phase-advanced with respect to the sinusoidal input (Fig. 6.11) and that the phase relations vary with frequency. In addition, the amplitude of the resulting oscillation in tension is frequency dependent with a peak in the amplitude plot at 1 Hz (Fig. 6.12). There is a corresponding trough in the phase advance plot indicating that the mtFCO system resonates at a frequency of approximately 1 Hz (Fig. 6.12).

6.4.5 Stress-relaxation

Figures 6.13a and 6.13b show the typical relationship between tension and time following a step displacement for the mtFCOs of *T. collaris* and *S. gregaria* respectively. In both species, the decay in tension following the imposition of a step displacement follows a similar time course. In all cases it was found that the tension fell as a logarithmic function of time. In two typical examples from *T. collaris* and *S. gregaria* (Figs 6.13a, b) it was found that the relationship was described by the formulae $y = -22.5 \log(x) + 639.4$ ($r^2 = 0.93$) and $y = -15.8 \log(x) + 330.2$ ($r^2 = 0.91$) respectively. Such relationships are typical of viscoelastic behaviour (e.g. McCrum and Dorrington, 1976; Ker, 1977; Dorrington, 1980) and means that the initial rate of tension drop is higher than at later stages. The initial mean rate of decrease in tension over the first 60 s is rapid in both species (*T. collaris*: 0.47 $\mu N\ s^{-1}$ s.d. = 0.24 $\mu N\ s^{-1}$, n = 12 and *S. gregaria*: 0.45 $\mu N\ s^{-1}$ s.d. = 0.16 $\mu N\ s^{-1}$, n = 9 rates measured at t = 30 s) whilst the remaining fall in tension is at a slower rate (*T. collaris*: 0.1 $\mu N\ s^{-1}$ and *S. gregaria*: 0.24 $\mu N\ s^{-1}$ at t = 5 mins). Stress-relaxation can still be detected 20 minutes after the imposition of the step displacement, at which time the rate of relaxation is of the order of 0.01 $\mu N\ s^{-1}$ in *S. gregaria*. Upon imposition of a step displacement simulating flexion over the entire femoro-tibial range the mtFCO of *T. collaris* is subjected to a greater maximum tension (744.4 μN s.d. = 171.8 μN, n = 7) than that of *S. gregaria* (405.8 μN s.d. = 81.4 μN, n = 9)(Fig. 6.14a).

Previous authors (e.g. Dorrington, 1980) illustrated differences between different viscoelastic biological materials by comparing their stress-relaxation curves. In his comparisons, % maximum stress was plotted against time, after the moment when the strain was applied. The stress-relaxation behaviours of *T. collaris* and *S. gregaria* were compared by measuring the % decrease in tension at a given time after the imposition

of the step displacement. Comparing the behaviour of the mtFCO between the two species following displacement shows that the mtFCO of *T. collaris* relaxes faster and to a greater extent than that of *S. gregaria* (Fig. 6.14b).

6.4.5.1 Comparing stress-relaxation between the two ligaments

In these investigations, the stress-relaxation behaviours of intact mtFCOs of *S. gregaria* were measured in response to an imposed step displacement. Each experiment was then repeated after cutting either the dorsal or ventral ligament of the apodeme complex. This enabled the properties of the individual ligaments to be compared with one another and with the behaviour of the intact organ (Figs 6.15a, b). The results show that following the imposition of a step displacement, the tension in either ligament declines over a comparable time period as was measured for the intact apodeme complex, showing typical tension-relaxation behaviour. However, the decrease in tension measured following the dissection of the apodeme complex depended upon which ligament was severed. A larger percentage decrease in tension was recorded after cutting the ventral ligament (39.0% s.d. = 11%, n = 4) than was found after cutting the dorsal ligament (27.4% s.d. = 9.6%, n = 5). Although the difference demonstrated between the mechanical properties of the ligaments in this small data set is not a significant one ($U = 5$; $P > 0.05$, Mann-Whitney U-test), these results are consistent with the observations of the quantity of Acid Fuchsin-staining found in each ligament (see Chapter 3) which indicated that the ventral ligament was the stiffer of the two.

6.4.5.2 Stress-relaxation over different parts of the femoro-tibial range

Displacements of similar magnitude imposed over different parts of the femoro-tibial range result in correspondingly different ranges of mtFCO tension change and degrees of stress-relaxation (Fig. 6.16). For example the imposition of identical 250 μm step displacements applied at the mtFCO cuticular rod at positions corresponding to the extremes of the femoro-tibial range (tibial extension and tibial flexion) elicit relaxations of 4 μN and 34 μN respectively over the following 100 s.

In linear viscoelastic systems, the ratio of stress to strain at any given time after the imposition of a step displacement remains the same for all displacement magnitudes (Dorrington, 1980). In such systems, plotting stress against strain for a range of step displacements results in a straight line 'isochronal', the gradient of which is equal to the relaxation modulus

of the material. In the current investigation, isochronal plots for *S. gregaria* were made by plotting force against displacement. As is the case in many biological materials (e.g. human tendon: Cohen *et al.*, 1976), the mtFCO produces markedly non-linear isochronal curves (Fig. 6.17). This indicates that the ligament system is not linearly elastic. The non-linearity is likely to be partly due to the recruitment of more and more attachment cells as the ventral ligament tightens.

6.4.6 Frequency response

The ability of the mtFCO to transmit mechanical power at different frequencies was measured using white-noise analysis. Band limited (0 - 25 Hz) pink noise displacement was applied to the organ and the mechanical power transmitted along the ligaments was measured at the strain gauge. The resulting mtFCO power spectra show that power is transmitted most efficiently by the mtFCO at frequencies of 1 - 2 Hz (Figs 6.18a, b). This finding is constant with the known frequency of metathoracic limb movement during walking. This was found to be 1.6 Hz (see Chapter 2).

6.4.7 A simple model to demonstrate resonance in a viscoelastic system

To demonstrate the effects of resonance in a viscoelastic system, a simple model system was constructed consisting of a mass attached to a moving support by a length of elastic. The components of the model were chosen so that it resonated at a frequency of about 2 Hz. The frequency response of the model was measured using a white-noise stimulus. The system transmitted power most efficiently at the resonant frequency (Figs 6.19a, b). In addition, a series of hysteresis curves was obtained from the model. The model showed frequency-dependent energy dissipation with maximum dissipation occurring at resonance (Fig. 6.20). The magnitude of the mass oscillation elicited by a sinusoidal stimulus of constant amplitude was also measured for the model system and plotted on the same graph as the model's energy dissipation characteristics (Fig. 6.21a). This shows that energy dissipation and amplitude of oscillation in a resonating system are not linearly related to frequency, but increase at resonance. Constant amplitude sinusoidal stimulation of the model also showed that the phase of the mass oscillation was frequency dependent. In a simple resonating system, the phase of the mass oscillation lags that of the stimulus by 90° at the resonant frequency (Fig. 6.21b).

Models such as these can be useful in understanding the mechanics of complex biological systems such as the mtFCO. Features of the present model that relate to the mtFCO include frequency-dependent phase relations and non-linear energy-dissipation with displacement velocity. Such a model demonstrates the way in which the tension in an elastic system can vary in a complex manner with the frequency of input. It also shows the limitations of extrapolating static tension and displacement measurements in an attempt to characterise the behaviour of a dynamic system.

6.5 DISCUSSION

The results in this chapter have shown that the mtFCO system has non-linear viscoelastic properties. The incorporation of viscoelastic components into an oscillating system results in several related phenomena which are likely to influence the organ's response characteristics. In particular, sensory adaptation (Usherwood *et al.*, 1968; Burns, 1974; Theophilidis, 1986b) and response hysteresis (Usherwood *et al.*, 1968; Matheson, 1990, 1992b) may be wholly or partly attributable to the mechanical properties of the mtFCO tissue.

6.5.1 Viscoelastic models

To help visualise and analyse viscoelastic behaviour, theoretical models can be constructed using elements representing simple mechanical analogues. Models are constructed using serial and parallel combinations of two basic elements used to define two types of idealised stress-strain behaviour. Perfect elastic behaviour is represented by the Hookean spring:

Text Figure 6.1

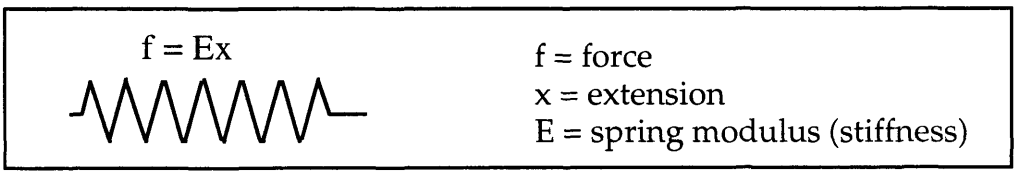

in which stress and strain are linearly related (Text Figure 6.1). The imposition of an instantaneous stress will result in instantaneous strain without time lag or inertia effects (no real materials are completely Hookean under all conditions). The viscous component is simulated by the Newtonian dashpot analogous to a shock absorber on a car whose

stress when deformed is proportional to the imposed strain rate (Text Figure 6.2).

Text Figure 6.2

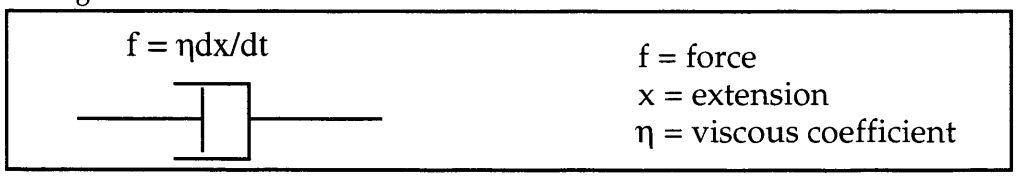

These two elements can be linked in a variety of configurations to simulate the mechanical properties of different materials. When coupled in series the arrangement is known as a Maxwell element (Text Figure 6.3):

Text Figure 6.3

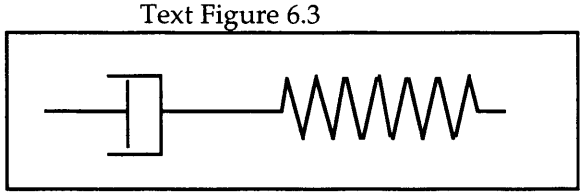

When they are joined in parallel with one another, they are referred to as a Kelvin or Voight model (Hall, 1968) (Text Figure 6.4):

Text Figure 6.4

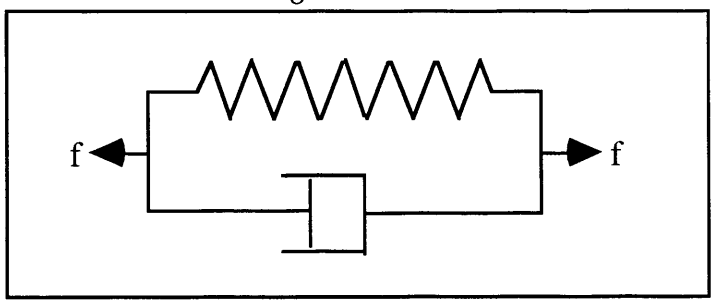

Neither of these arrangements alone can model both stress-relaxation and recovery types of behaviour. However, there is a third common combination of elements, known as the 'Standard Linear Solid' (Maxwell, 1868; Zener, 1948), 'Zener' or 'Three Element' model consisting of a spring (1) in parallel with a Maxwell element (2 and 3) (Text Figure 6.5):

Text Figure 6.5

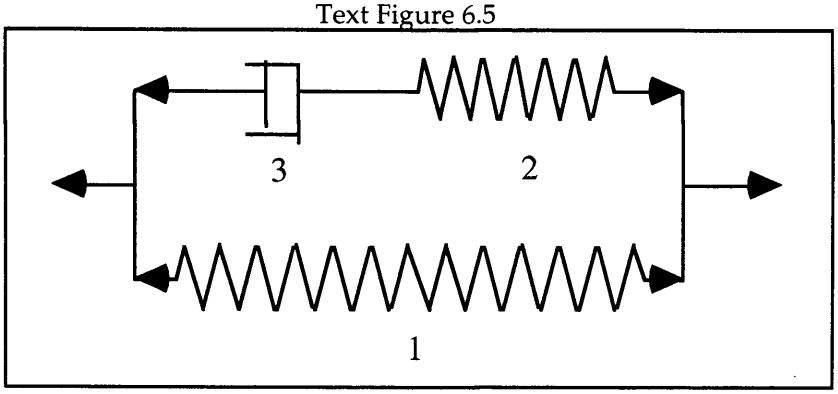

This model is capable of reproducing qualitatively similar behaviour to that observed in the case of the mtFCO when subjected to a stress-relaxation test (Text Figure 6.6):

Text Figure 6.6

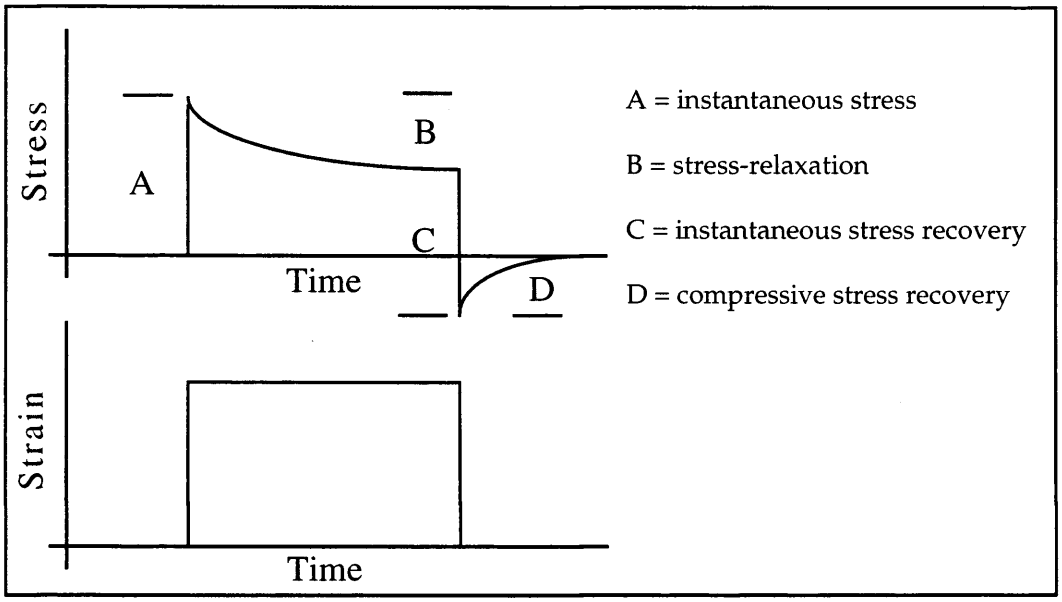

Upon imposition of a step elongation, the two springs (1 and 2) extend instantaneously resulting in a step increase in stress (A). Subsequently, the force exerted upon the dashpot by spring 2 causes it to extend, so unloading spring 2. This causes the force required across the model to maintain this elongation to fall at a decreasing rate (B), until spring 2 is completely unloaded. Upon returning the model to its original length, both springs change length instantaneously (C). Spring 1 becomes unloaded whilst spring 2 is now under compressive stress resulting from the extension of the dashpot whilst the model was elongated. This results in the overall stress measured across the model to undershoot its initial value. As the

dashpot subsequently closes, spring 2 extends and the force required to hold the model at its original length recovers to its initial value (D). In addition to showing stress-relaxation and recovery the standard linear solid (SLS) model also shows hysteresis characteristics similar to those observed in the mtFCO. Whilst Maxwell and Kelvin models show a progressive decrease or increase in hysteresis with increasing frequency respectively, the SLS shows a characteristic frequency at which hysteresis reaches a peak (Fung, 1984). However, this model cannot be used to mathematically characterise the observed stress-relaxation behaviour of the mtFCO by assigning real values to the constituent components. The relationship between the components of the model is such that any hypothetical stress-relaxation curve follows an exponential function with time. In the case of the mtFCO, tension does not decay exponentially with time; a single exponential function cannot describe both the initial (fast) as well as the later (slow) phase of stress-relaxation. Although the Standard Linear Solid describes some biological materials well (e.g. Alexander, 1962 described the properties of the body wall of the sea anemone), it is clear that the behaviour of the majority of biological materials needs to be represented by a broader spread of relaxation times than afforded by the exponential function of a standard linear solid (Dorrington, 1980). This problem can be addressed by coupling two SLS models and assigning appropriate values such that as one unit is completing its stretch relaxation, the second slower unit is still just beginning to relax. Taking the incorporation of additional units to its conclusion, results in a theoretical model proposed by Wiechert (see Dorrington, 1980) consisting of an infinite number of individual units each having slightly different relaxation characteristics. Investigators have used different combinations of such models to relate structure to observed behaviour in animal tissues (e.g. Loewenstein and Skalak, 1966 in representing the lamella layers of the Pacinian corpuscle; Fung, 1984 in mammalian artery and lung). In addition, authors have introduced additional elements to represent non-linear behaviours when necessary (e.g. Rydqvist *et al.*, 1990; Chaplain *et al.*, 1971; Nakajima and Onodera, 1969).

Although the mtFCO shows non-linear characteristics, it is possible in the light of the organ's morphology (Field, 1991; Shelton *et al.*, 1992; this thesis) to represent the mtFCO using a model in which a collection of linear components combines to produce non-linear behaviour. For example, the non-linear stress-strain curve produced as the organ is

extended may be explained by the recruitment of compliant components representing the sequential tightening of the apodeme complex loop fibres. Unit recruitment could be represented in a model by the addition of a 'frictionless' sliding component which slides up against a stop to represent the tightening of a loop fibre (Text Figure 6.7):

Text Figure 6.7

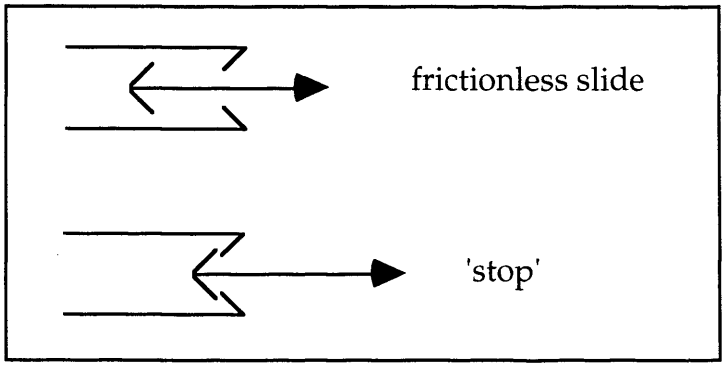

Any elements in series with these components would only be put under tension after the slide had reached its 'stop' position. This additional element could be used to produce a simplified model demonstrating the operation of the ventral ligament (Text Figure 6.8). The 'ventral ligament loops fibres' are depicted as being perfectly elastic for simplicity:

Text Figure 6.8

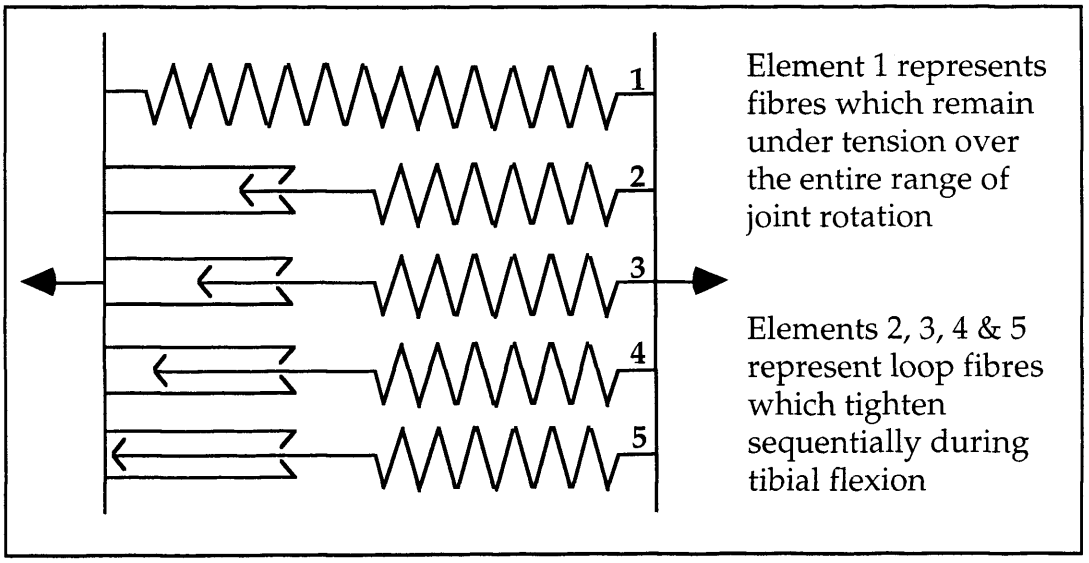

This hypothetical model would respond to extension as shown in Text Figure 6.9:

Text Figure 6.9

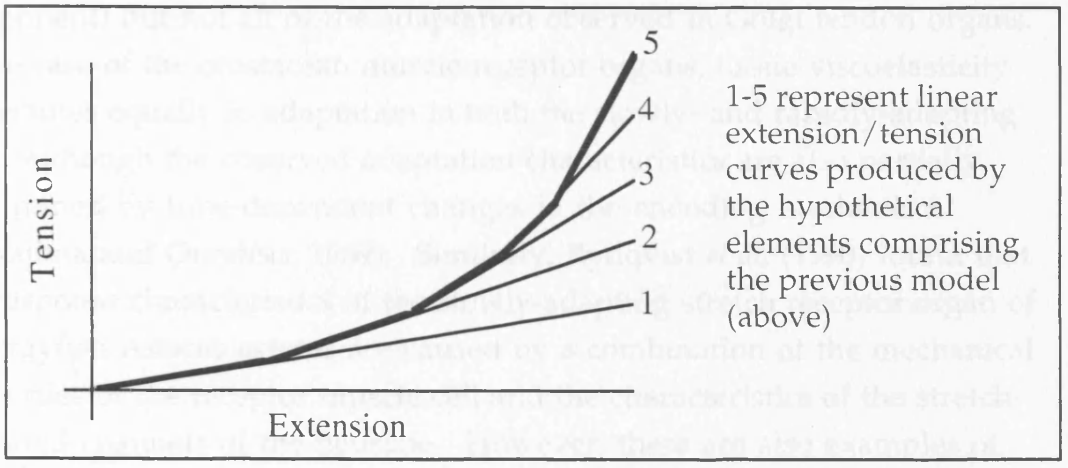

Thus, a non-linear stress-strain curve (bold line) can be produced by a combination of conventional linear components.

In addition to loop-forming characteristics, there are many other complicating factors, such as interaction between neighbouring attachment cells and interaction between the attachment cells and the mtFCO sheath, which prevent the mechanical behaviour of the organ being represented by a simple mathematical model. Dorrington (1980) emphasises that linear viscoelastic theory can be applied only if the material is linearly viscoelastic in the sense of having a single relaxation modulus. The non-linear isochronal curves (Fig. 6.17) show that this is not so in the case of the mtFCO. Measurements in this study were obtained by treating the entire mtFCO system as a 'black box'. In reality the properties measured result from the interaction of all the organ's mechanical attachments. Analysis of the properties of individual mtFCO attachment cells would be required to justify any further modelling speculation. The implications of the observed behaviour of the system as a whole are discussed below.

6.5.2 Adaptation

Viscoelasticity of the tissue elements that couple mechanical stimuli to the receptor transducer region has been proposed by several authors to account for part or all of observed sensory adaptation in a range of different mechanoreceptors. In the Pacinian corpuscle, viscoelasticity of the capsule determines the receptor's adaptation (Hubbard, 1958). Removal of the corpuscle lamella layers reduces the adaptation of the generator potential

(Loewenstein and Mendelson, 1965). Houk (1967) demonstrated that stress-relaxation of the attached muscle contributes some (the slow component) but not all of the adaptation observed in Golgi tendon organs. In the case of the crustacean muscle receptor organs, tissue viscoelasticity contributes equally to adaptation in both the slowly- and rapidly-adapting types although the observed adaptation characteristics are also partially determined by time-dependent changes in the encoding mechanism (Nakajima and Onodera, 1969). Similarly, Rydqvist *et al.* (1990) found that the response characteristics of the slowly-adapting stretch receptor organ of the crayfish *Astacus astacus* are caused by a combination of the mechanical properties of the receptor muscle cell and the characteristics of the stretch-activated channels of the neurone. However, there are also examples of mechanoreceptor systems in which response adaptation can be attributed entirely to neuronal factors. In the case of the tactile spine of the cockroach, in which the increased firing frequency following a step stimulus decays over approximately 1 s, adaptation takes place at the level of mechano-electric transduction. In this mechanoreceptor the receptor current does not show sensory adaptation (French, 1984c; Bohnenberger, 1981) and direct electrical stimulation of the action potential initiating region produces adaptation indistinguishable from that elicited by movement (French, 1984a, b). Therefore, the adaptation observed in the response of this receptor occurs during the encoding of the receptor current into action potentials. Further, French (1987) demonstrated that oxidising agents that affect sodium channel inactivation abolish the rapid adaptation. It was concluded that sensory adaptation in this case is likely to be due to sodium channel inactivation at the action potential initiating region of the neurone.

In the case of the mtFCO, sensory adaptation in the form of a decline in discharge rate following a step displacement has been demonstrated by Usherwood *et al.* (1968), Burns (1974) and Theophilidis (1986b). The adaptation consists of an initial rapid decline in firing rate over the first minute followed by a slower steady decline lasting in excess of 15 minutes. Following a step displacement to a femoro-tibial angle of 0°, the discharge rate decreased by approximately 30% over a period of 10 minutes (Usherwood *et al.*, 1968). Similarities between the time course of sensory adaptation and the observed viscoelastic behaviour of the mtFCO during stress-relaxation tests suggest that the organ's mechanical properties could contribute to adaptation over such a time period (a hypothesis also

suggested by Theophilidis (1986a) in the case of the femoral CO from the Tettigonid *Decticus albifrons*).

The results of the present study suggest that the two mtFCO ligaments have differing mechanical properties, the ventral ligament being stiffer than the dorsal ligament. This may reflect their presumed evolutionary origins in different scoloparia (Matheson and Field, 1990) optimised to respond to different stimuli (Field and Pflüger, 1989). The implications of this observation is that differing mechanical properties between the two ligaments may contribute to differences in response characteristics of the two sets of sensilla lying in series with them. Such functional specialisation is found in the case of the crayfish stretch receptor organ in which the viscoelastic properties of the mechanical couplings contribute to receptor adaptation. In this system, the rapidly-adapting and slowly-adapting receptors lie in series with two muscles which have different viscoelastic properties (Purali, 1997). The muscle associated with the rapidly-adapting receptor is more compliant than that associated with the slowly-adapting receptor.

6.5.3 Hysteresis

It seems likely that the observed hysteresis in mtFCO tension during cyclic extension-relaxation demonstrated in this study will contribute to the response hysteresis in mtFCO afferents documented by previous investigators (Burns, 1974; Matheson, 1990, 1992b). Both the mtFCO tension and firing frequency are elevated during joint flexion relative to extension. The fact that Matheson (1990) demonstrated that the degree of response hysteresis is variable amongst individual mtFCO neurones suggests that response hysteresis is likely to be due to both mechanical and neuronal factors. Hysteresis is potentially problematic in all proprioceptors in which firing frequency is used to encode information about the magnitude of peripheral variables such as joint angle. Ambiguities introduced by hysteresis would apparently degrade the resolution of such systems by reducing their ability to accurately encode position-dependent information.

When the tibia is extended and returned to its original position the discharge of the CO is depressed relative to the firing frequency before the change in joint angle was imposed (Burns, 1974; Matheson, 1990, 1992b). This implies that joint receptors can fire at two different frequencies at the

same joint angle. Despite this, the locust has the ability to reposition its leg at a predetermined angle (e.g. Zill, 1985b).

Whilst some authors have demonstrated theoretical models to explain how the CNS could extract accurate positional information from hysteretic inputs (e.g. Mill and Lowe, 1972 in the crustacean PD joint receptor) others have proposed mechanisms by which receptor hysteresis could be exploited to enhance proprioception by providing additional information (e.g. Zill and Jepson-Innes, 1988).

Certainly some of the locust mtFCO sensory afferent signals are subsequently processed in such a way as to suppress hysteresis. The site of primary integration of incoming mechanosensory signals is at the level of the interneurones of the metathoracic ganglia. They receive monosynaptic inputs from CO afferents (Burrows, 1987a). The interneurones show much less hysteresis than the incoming afferent discharge. Hatsopoulos *et al.* (1995) measured hysteresis ratios of tonic responses in opposing directions as large as 10:1 using the published records of Matheson (1992b), but ratios of only 1.1:1 to 1.2:1 were obtained in one carefully studied spiking interneurone in a study by Burrows (1985).

An example of a mechanism by which sensory afferent hysteresis could be modulated is that of presynaptic shunting inhibition. Presynaptic shunting inhibition was demonstrated to occur between the afferents at axon terminals by Burrows and Laurent (1993) and Burrows and Matheson (1994). Burrows and Matheson (1994) showed that such inhibition causes the amplitude of a spike-induced excitatory post synaptic potential to be reduced in postsynaptic neurones. Using mathematical modelling Hatsopoulos *et al.* (1995) demonstrated that presynaptic shunting inhibition between adjacent sensory afferents can reduce hysteresis in mechanosensory coding. Such a system acts as an automatic gain control mechanism modulating postsynaptic afferent-induced activity (Grosberg, 1973). However, previous authors (Zill and Jepson-Innes, 1988) demonstrated mechanisms which appeared to exploit mtFCO response hysteresis in the postural reflexes of *S. americana* and *S. gregaria*. To counter sudden shifts in joint position, tension in postural muscles should increase and subsequently return to levels set prior to disturbance. However, muscles in both vertebrates (Burke *et al.*, 1970) and invertebrates (Wilson and Larimer, 1968; Burns and Usherwood, 1978) have been shown

to exhibit 'catch' properties. Such properties mean that an increase in motor neurone firing rate, followed by return to initial frequency, produces a large residual increase in muscle tension. Whilst this phenomenon has the advantage that high levels of muscle tone can be maintained at low motor firing rates, it represents problems in reflex loops involved in posture and load compensation. Zill and Jepson-Innes (1988) proposed that hysteresis in sensory afferents and consequent hysteresis in motor firing serves to eliminate 'catch' muscle tension. In such a reflex arc, receptor hysteresis represents a mechanism of pre-patterning motor activity to compensate for residual muscle tension and allows the 'tuning' of the receptor properties to the characteristics of the muscles whose activity they reflexively excite.

The above strategies to cope with hysteresis in the mtFCO response need not conflict with one another. Hatsopoulos *et al.* (1995) pointed out that monosynaptic or bisynaptic pathways via the non-spiking interneurones may retain hysteresis to compensate for muscle catch, whilst multi-synaptic pathways reduce hysteresis to pass information to higher centres. There is also the possibility that, by combining information from hysteretic pathways with that from hysteresis-suppressing pathways, the animal may also be able to derive information about the joint's immediate history.

6.5.4 Resonance

In addition to showing that the mtFCO has viscoelastic properties, the relationship demonstrated between mechanical hysteresis and displacement velocity indicates the presence of resonance in the mtFCO system. In a simple resonating system, such as a mass suspended by elastic from a moving support, the amplitude of mass displacement in response to sinusoidal oscillation of the support is frequency dependent. At resonance, the energy dissipated per cycle increases with the amplitude of oscillation of the mass. This study has demonstrated that the mtFCO shows an analogous increase in energy dissipation at a frequency of 1 - 2 Hz (Figs 6.9a, b; 6.10a, b) coinciding with an increase in amplitude of tension oscillation (Fig. 6.12). Associated with resonance are changes in the phase relations between the input and resulting oscillations. In the case of the model (an undamped oscillator), the oscillation of the mass varies with frequency, lagging the input oscillation by 90° at resonance. In the case of the mtFCO, the phase of the tension oscillation is advanced relative to the sinusoidal input (Figs 6.11; 6.12) and is also frequency

dependent. The mtFCO frequency response spectrum also indicates that the system resonates at approximately 1 - 2 Hz (Fig. 6.18a, b). Power is transmitted through the mtFCO system most efficiently at these frequencies. Displacements of the mtFCO apodeme complex result in tension changes across the viscoelastic strand in which the mtFCO sensory neurones are embedded. The fact that the resulting tension changes vary in amplitude and phase relative to the input in a frequency-dependent manner has implications regarding the mtFCO's response characteristics.

Several authors have reported the phase advance of receptor response in mechanoreceptive systems and have presented hypotheses with respect to its implications. Maximum neuronal activity associated with the stick insect msFCO is phase advanced with respect to a sinusoidal stimulus (Kittmann and Schmitz, 1992). A similar phase relationship is also found in the cases of cockroach campaniform sensilla (Chapman *et al.*, 1979) and tactile hairs (Pringle and Wilson, 1951). In the context of a reflex arc the control sequence must incorporate the conduction delay to and from the CNS, in addition to any central and neuromuscular delays. In the analysis of the phase relationships round a complete reflex arc the time-dependent liberation of chemical transmitters at synapses and neuromuscular junctions whose concentrations are related to the frequency of arriving impulses, imply a phase lag (Pringle and Wilson, 1951). These authors proposed that variable phase may be employed within the control loop as some form of compensation, since a regulatory system with a finite delay in the control sequence is unstable and leads to oscillation or 'searching' behaviour. The authors point out that compensation becomes increasingly important in situations where a muscle is working against a load and that a phase advance in one of the control sequence components may supply the required compensation. This potential was also recognised by Merton (1951) who implicated the role of such phase relations in modulating the discharge of muscle spindles, preventing overshoot and oscillation when the spindle was disturbed. However, in the case of the mtFCO it seems that the observed phase advance would be too small to perform such a compensating role.

Resonance of the mtFCO system at 1 - 2 Hz may also serve to increase its sensitivity across these frequencies by increasing the magnitude of the tension changes that a given amplitude of input elicits. Thus, the organ could be 'tuned' to input displacements of a certain frequency such as that

associated with the locust walking cycle. Different authors have reported large differences in the natural frequency of leg movements during locust walking. Usherwood *et al.* (1968) observed leg movements of 2 - 4 Hz and Burns (1973) measured frequencies of 2 - 9 Hz, although his measurements may have been influenced due to the heating effect of his cinemaphotography lamps. In the present study leg movements with a mean frequency of 1.6 Hz were observed (see Chapter 2). These were similar to those observed by Burrows (1996). This frequency coincides with the frequency range over which the mtFCO shows disproportionally large amplitude tension oscillation (Fig. 6.12), disproportional energy dissipation (Fig. 6.10b) and peak power transmission (Fig. 6.18a, b).

In addition to possible receptor tuning and control loop compensation effects, resonating systems have a filtering action. Input displacements on either side of the resonance are not transmitted as efficiently as displacements applied at the resonant frequency and so are mechanically filtered out as they are transmitted to the site of transduction. Chapman *et al.* (1979) examined the viscoelastic coupling of the cockroach campaniform sensillum. These authors demonstrated that the sensillum showed mechanical stress relaxation and related adaptation of sensory discharge. They also showed that the viscoelastic properties of the system provided a natural filtering action in which the sensillum was selectively sensitive to certain frequencies.

Figure 6.1

Line diagram showing the mechanical components of the strain gauge used to monitor the tensions generated within the mtFCO. The strain gauge consisted of a Sensinor X-18939 silicon beam force transducer mounted within a brass chassis. The strain gauge was attached to the specimen via a thin tungsten needle (1) which was mounted upon a pivoting arm (2). The pivot (3) rotated on sapphire watch bearings (4), to minimise friction. Pivoting of the arm (5) caused deflection of the silicon beam (6) of the force transducer (7). The force transducer was held in place by a small locking screw (8). The transducer was wired to a small socket (9), via which the strain gauge was connected to form part of a Wheatstone bridge circuit. The relative positions of the pivoting arm and the silicon beam could be observed through an observation hole in the brass chassis (10). A locking screw (11) was used to prevent unnecessary loading of the silicon beam between experiments.

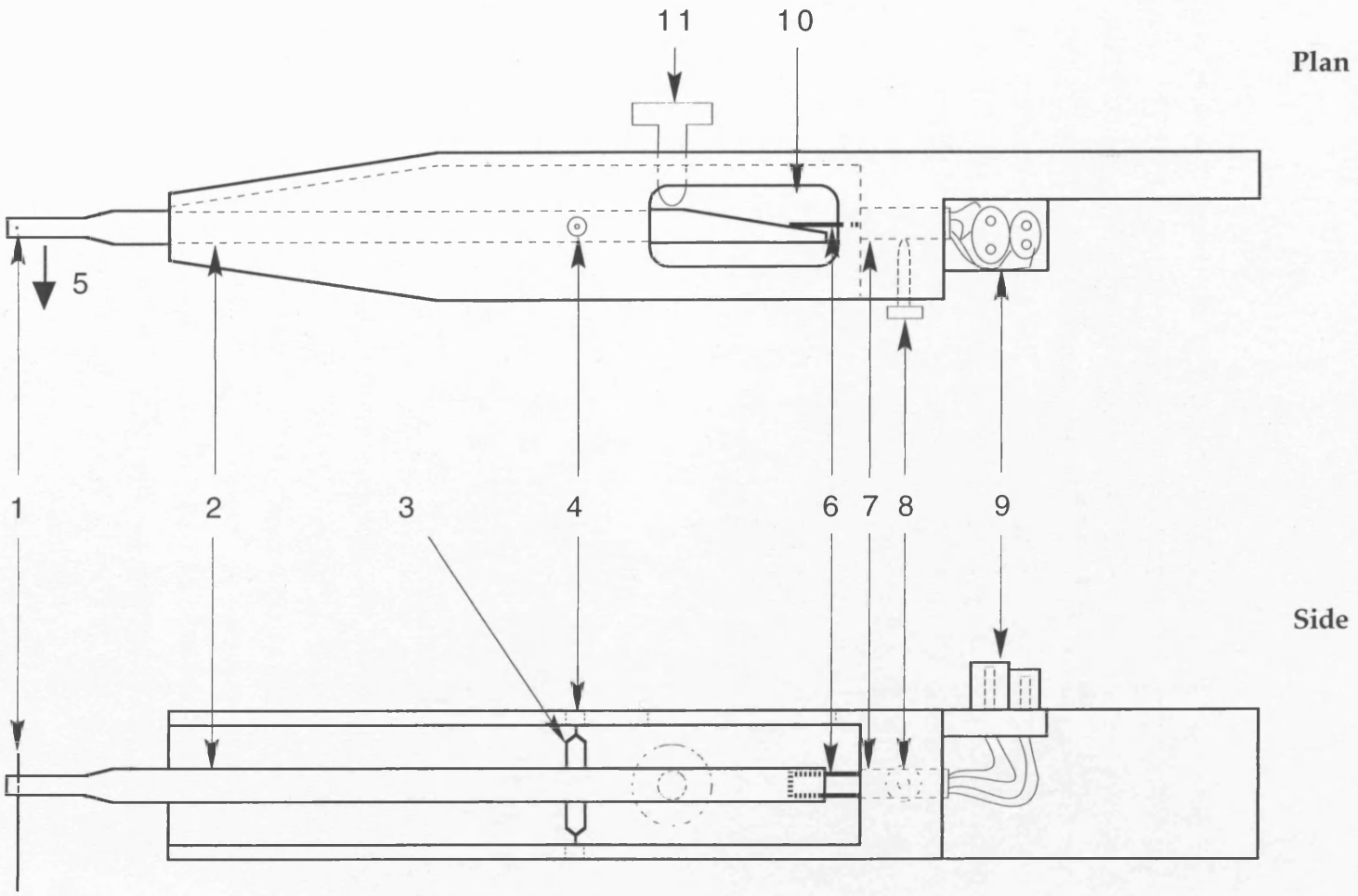
11
10
Plan
5
1
2
3
4
6
7
8
9
Side

Figures 6.2a, b

a

The strain gauge arm (s) was attached to the cuticular rod of the mtFCO apodeme complex with a spot of cyanoacrylic adhesive. To avoid any adhesive running into the haemolymph of the leg, the cuticular rod apodeme was raised slightly within the dissection using a fine glass hook (h) mounted on a micromanipulator. The tibia (t) was partially extended during this procedure to allow the glass hook to raise a portion of the cuticular rod clear of the haemolymph, without stretching the chordotonal organ system beyond its physiological limits.

b

When the glue had set, the glass hook was removed and the cuticular rod was cut immediately distal to the attachment point to the strain gauge (r). The tibia (t) was repositioned in the flexed position. The movement of the apodeme in response to flexion of the tibia from the extended position, could then be simulated by moving the strain gauge as indicated on the diagram. This allowed the tension of the chordotonal organ system corresponding to different femoro-tibial angles to be measured.

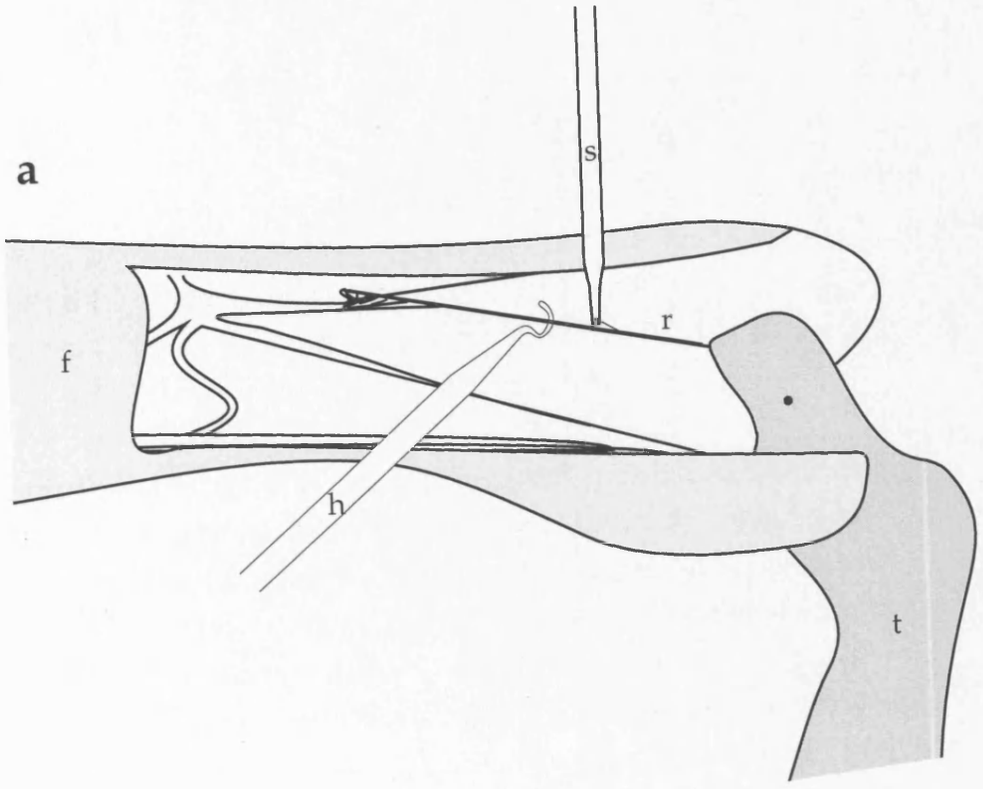
a
s
r
f
h
t

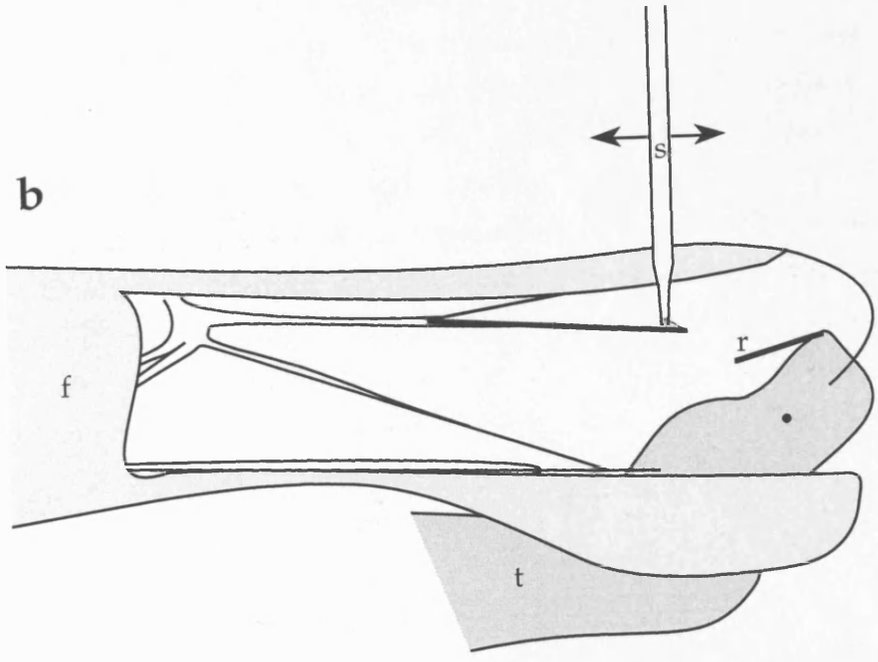
b
s
r
f
t

Figure 6.3

Semi-schematic diagram showing the way in which complex mechanical stimuli were imposed upon the chordotonal organ. To impose dynamic displacements upon the chordotonal organ, a mechanical actuator (a) was used to displace the leg as a whole, relative to the stationary strain gauge (sg). The proximal end of the chordotonal organ remained anchored within the femur (f) whilst the distal end (cuticular rod) was glued to the strain gauge arm (Figure 6.2b). The relative displacement between the femur and the strain gauge caused deformation of the compliant elements of the chordotonal organ. The femur was mounted upon a linear bearing-race trolley (br). The trolley was connected to the diaphragm (d) of the actuator (a) by a thin brass rod (r) secured with a locking screw (s). The actuator translated incoming signals from a programmable signal generator into proximo-distal displacements of the femur, indicated by the hollow arrows. The movement of the trolley was monitored using an optical displacement transducer (dt) which projected a laser spot (l) onto a white target (t) of the end of the moving trolley.

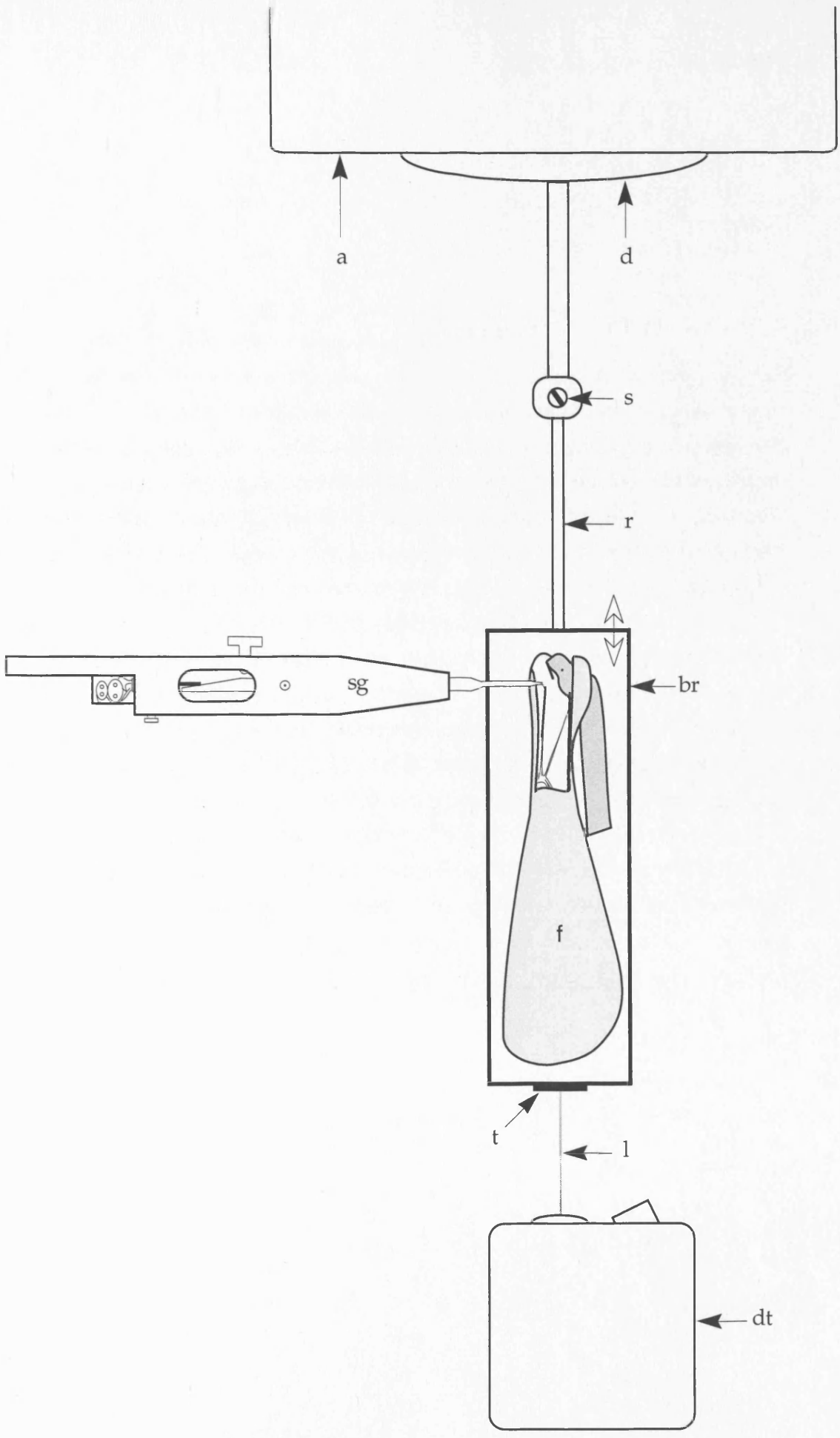
a
d
s
r
sg
br
f
t
l
dt

Figure 6.4

Semi-schematic diagram showing the experimental setup used to test the response of a simple model to different mechanical stimuli. The model consisted of a conical mass (m) suspended from a movable beam (b) by a length of elastic (e). The beam was mounted on a 20N 'Ling' mechanical actuator (a). Displacement stimuli (S) delivered to the actuator were translated into vertical displacements of the model. The input displacement to the model (D_i) was monitored independently using an eddy current probe (p). Displacement of the movable support resulted in vertical displacement of the conical mass relative to a stationary displacement transducer (d). Change in distance between the transducer and the conical side of the mass was used to measure vertical mass displacement (D_o). The changes in force to which the model was subjected during mechanical stimulation were measured using a strain gauge (s) mounted on the movable beam between its junction with the actuator and the attachment of the model. Output (T) from the strain gauge was calibrated to show the change in tension with time.

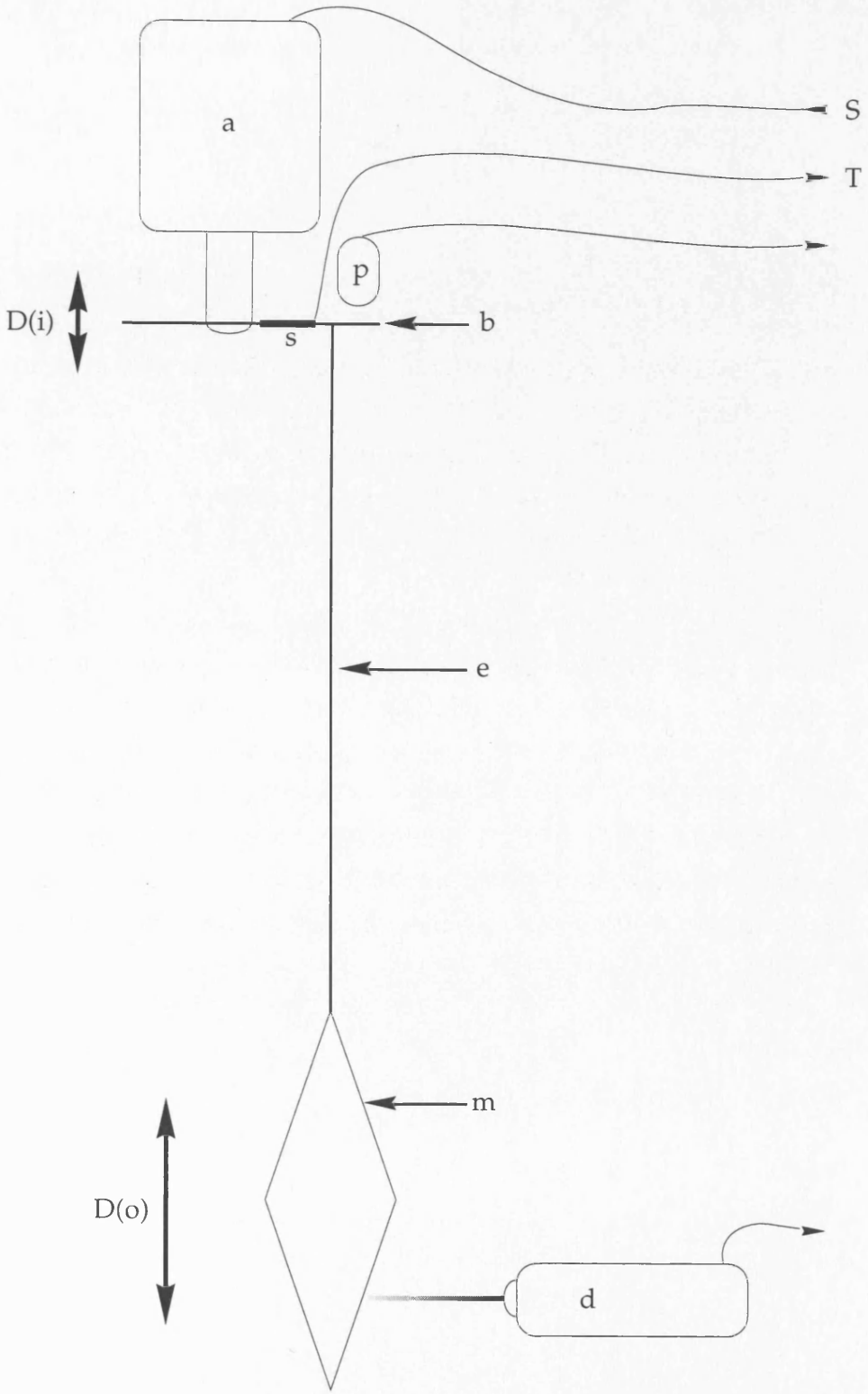
a
S
T
P
D(i)
s
b
e
m
D(o)
d

Figures 6.5a, b

An individual displacement-tension curve for the mtFCO in *S. gregaria,* showing the tension developed within the mtFCO as the organ is stretched. The tension is plotted against linear extension of the organ (**a**) and against equivalent femoro-tibial angle (**b**). MtFCO tension was measured in this case by observing the deflection of a glass filament attached to the organ using an eyepiece graticule.

a

Zero displacement corresponds to the proximo-distal position of the cuticular rod at a femoro-tibial angle of 150° (full tibial extension). In this preparation, the tension in the mtFCO is approximately 60 μN at this angle. As the cuticular rod is displaced distally, simulating flexion of the tibia, the tension in the mtFCO increases at an increasing rate. The position of the cuticular rod at maximum displacement (1200 μm) corresponds to its position at full tibial flexion (0°) in an intact femur. The tension in the mtFCO is approximately 400 μN at this position.

b

Proximo-distal displacement of the apodeme complex cuticular rod is sinusoidally related to femoro-tibial angle. This figure shows the displacement/tension data from Figure 6.5a plotted against equivalent femoro-tibial angle. The mean range of femoro-tibial rotation during the walking cycle is indicated on this plot. Error = ±5 μN = 1 epu

a

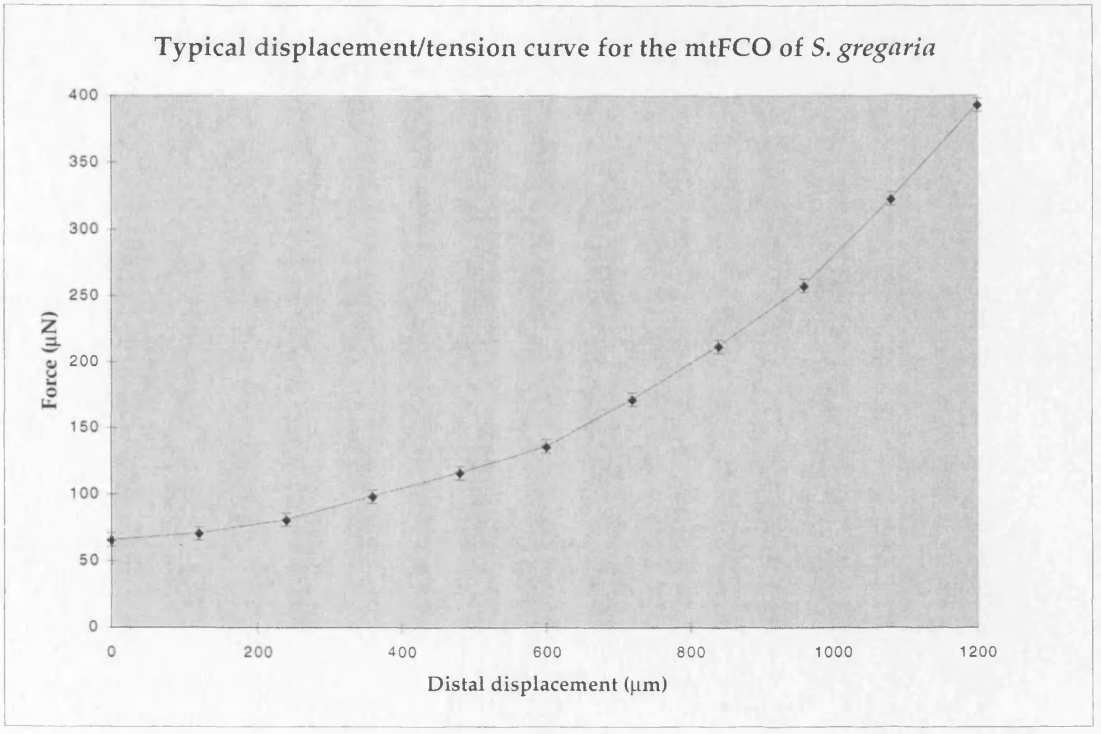
Typical displacement/tension curve for the mtFCO of S. gregaria
Force (µN)
400
350
300
250
200
150
100
50
0
0
200
400
600
800
1000
1200
Distal displacement (µm)

b

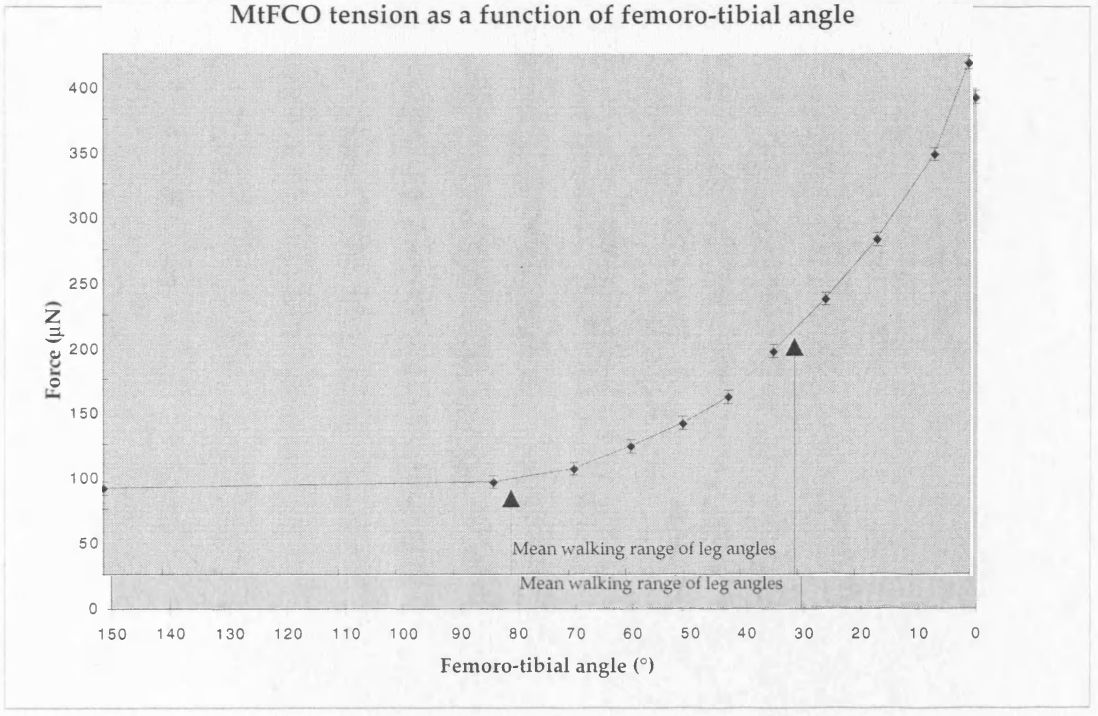
MtFCO tension as a function of femoro-tibial angle
Force (µN)
400
350
300
250
200
150
100
50
0
Mean walking range of leg angles
Mean walking range of leg angles
150
140
130
120
110
100
90
80
70
60
50
40
30
20
10
0
Femoro-tibial angle (°)

Figures 6.6a, b

These figures compare displacement/tension curves produced during the extension of the mtFCO with curves produced after the organs' mechanical attachments have been manipulated. As before, increasingly distal displacement is equivalent to tibial flexion. Each plot is obtained from a single example and is typical of a number of preparations.

a

This plot compares the displacement/tension curve of the mtFCO whilst the guy-rope fibres were intact with that obtained after they had been severed. The guy-rope fibres are most influential at minimal degrees of flexion. During extension (moving to the left on the graph) of the intact organ, the guy-rope fibres maintain the stress upon the mtFCO scoloparium as the apodeme complex buckles and becomes unloaded. Thus, as the guy-ropes are stretched they reduce the tension at the level of the cuticular rod. When the guy-ropes are severed, they are no longer able to perform this role which results in the tension measured at the level of the cuticular rod rising by approximately 20 μN. Error = ±5 μN = 1 epu

b

This figure compares the displacement/tension curves of the mtFCO when the organ's ventral attachment to the flexor tibiae muscle is held in the fully extended and fully flexed positions. When the tibia is fully extended, the ventral attachment remains slack. When the tibia is rotated to the fully flexed position, the ventral attachment becomes taut. When the ventral attachment is taut, the displacement/tension curve is vertically shifted such that the tension is greater than that in the curve produced when the ventral attachment is slack. In this example the difference in tension between the curves is of the order of 25 μN over most of the range. Error = ±5 μN = 1 epu

a

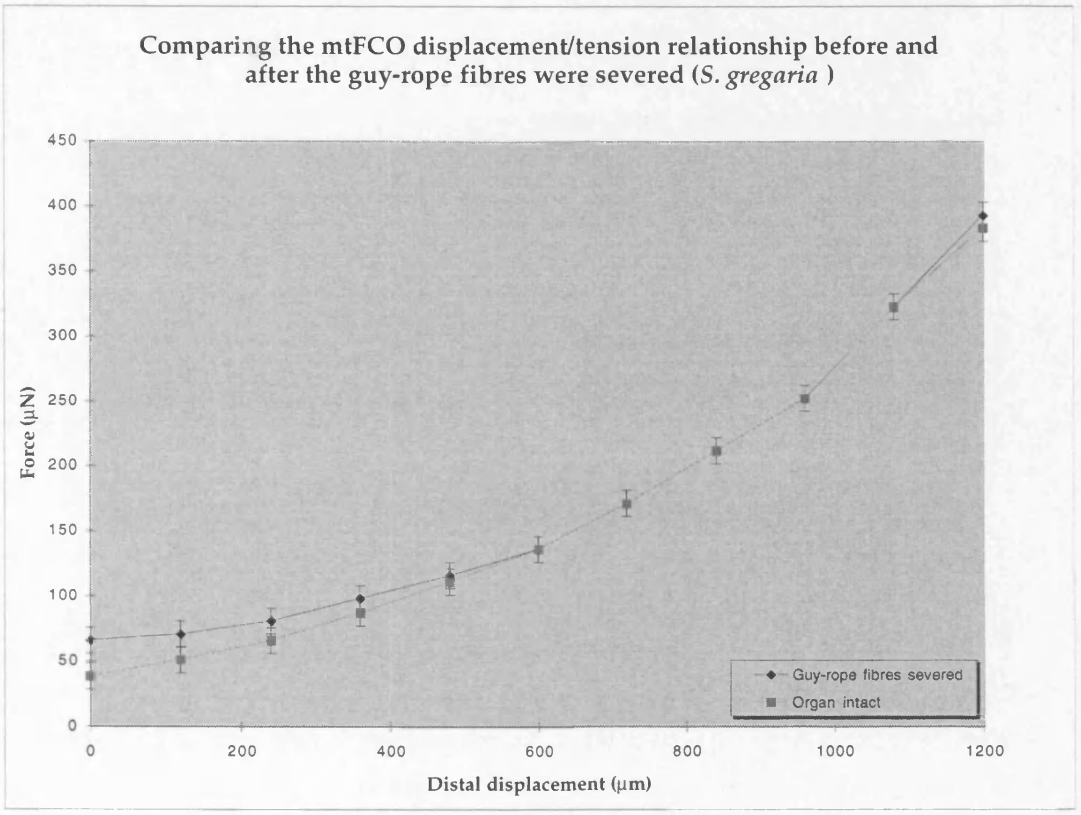
Comparing the mtFCO displacement/tension relationship before and after the guy-rope fibres were severed (S. gregaria)
Force (μN)
Distal displacement (μm)
Guy-rope fibres severed
Organ intact

b

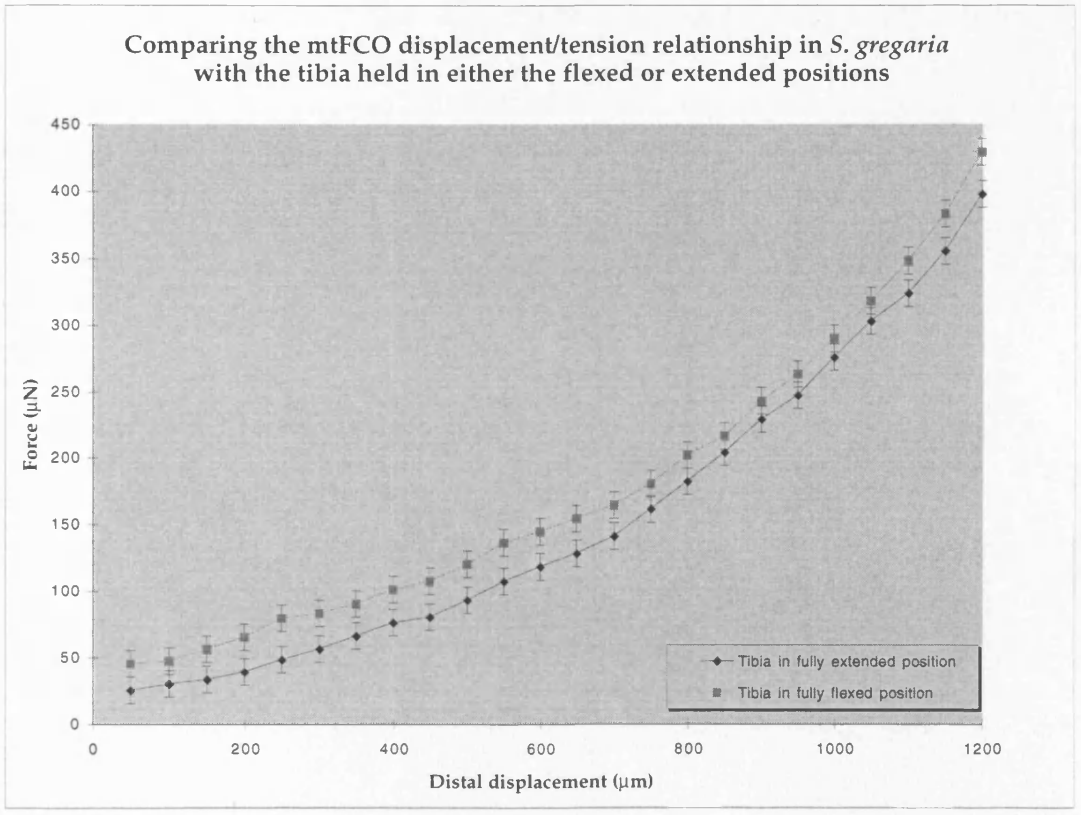
Comparing the mtFCO displacement/tension relationship in S. gregaria with the tibia held in either the flexed or extended positions
Force (μN)
Distal displacement (μm)
Tibia in fully extended position
Tibia in fully flexed position

Figures 6.7a, b

These figures show typical displacement-tension hysteresis curves from *S. gregaria* (**a**) and *L. migratoria* (**b**). The curves were generated by measuring the tension in the mtFCO at a series of displacement positions as the organ was stretched and returned to its original length. The displacement-tension curves appear similar in both species. In the case of *L. migratoria,* the tension at 0 μm displacement (equivalent to a femoro-tibial angle of 150°) falls to zero because the apodeme complex becomes fully unloaded at full extension of the tibia. Error = ±5 μN = 1 epu

a

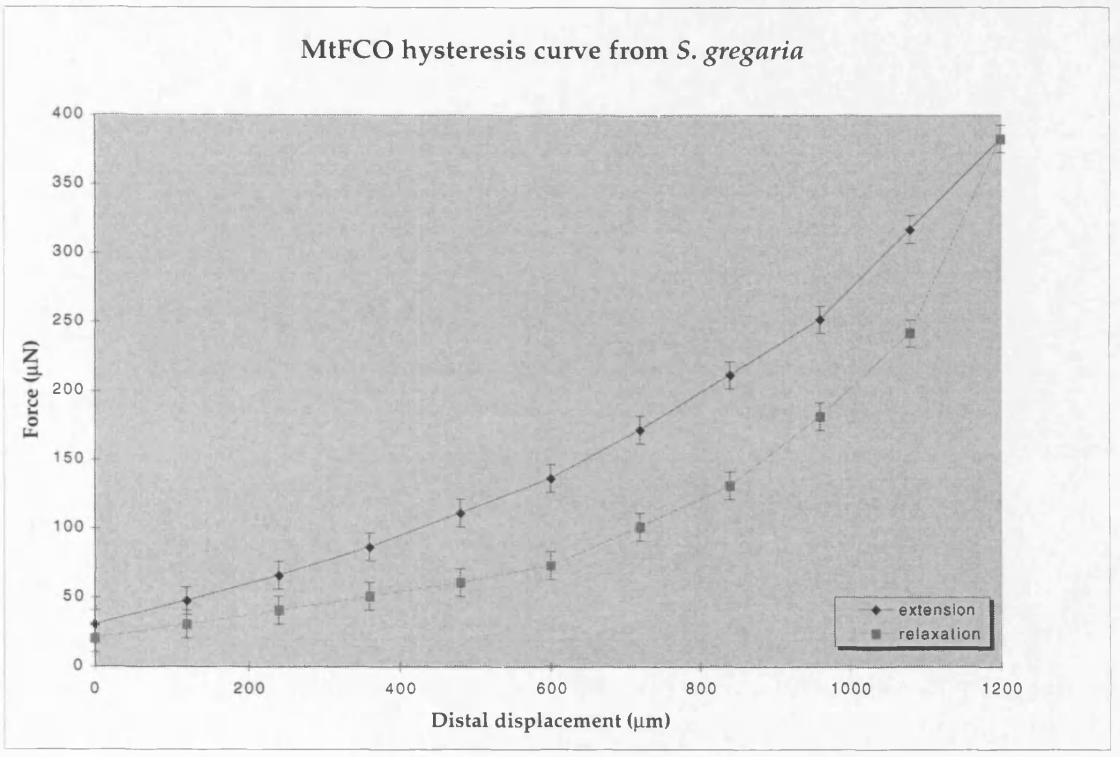
MtFCO hysteresis curve from S. gregaria
Force (µN)
Distal displacement (µm)
extension
relaxation
0
50
100
150
200
250
300
350
400
0
200
400
600
800
1000
1200

b

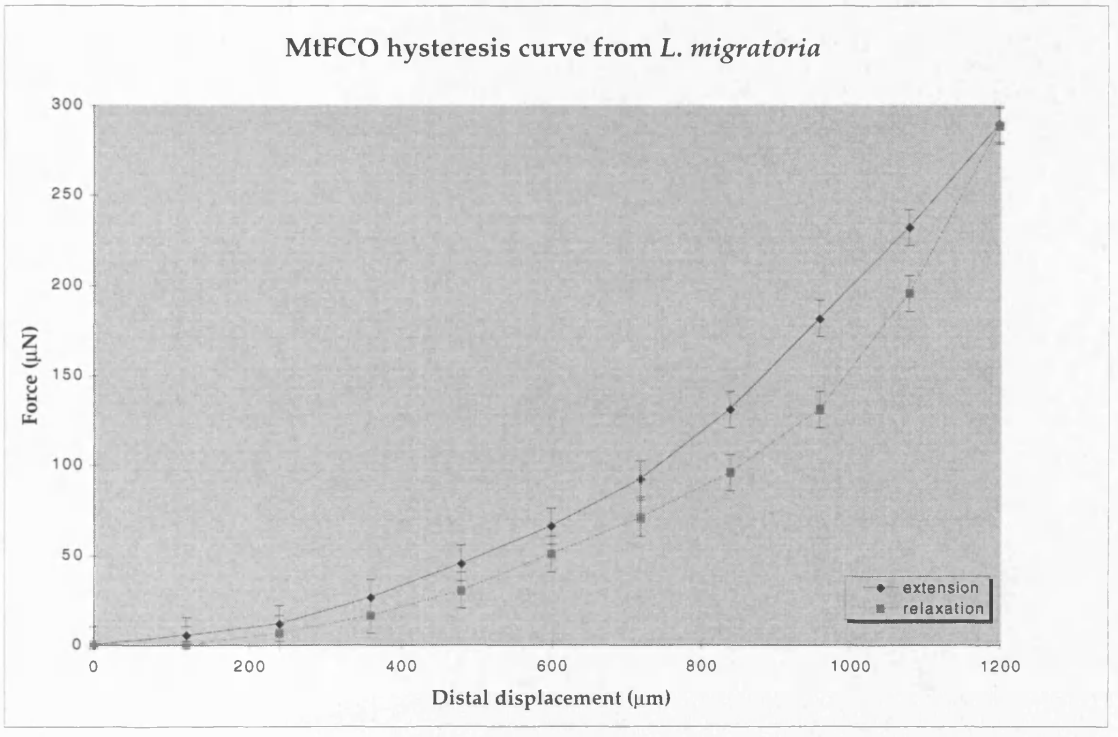
MtFCO hysteresis curve from L. migratoria
Force (µN)
Distal displacement (µm)
extension
relaxation
0
50
100
150
200
250
300
0
200
400
600
800
1000
1200

Figure 6.8

The three traces shown were measured from the mtFCO of *T. collaris* displaced at a frequencies of 0.1 Hz (upper), 1 Hz (middle) and 4 Hz (lower). The hysteresis loops in this figure were generated by stretching and returning the mtFCO over a distance of 1 mm. The displacement regime consisted of a saw-tooth delivered at different frequencies, so that the velocity of displacement could be calculated. The maximum tension developed varies from 0.75 mN at a displacement frequency of 0.1 Hz to 1.2 mN at a frequency of 4 Hz. The amount of work done per cycle is equal to the area of the hysteresis loops, and increases with the frequency of displacement.

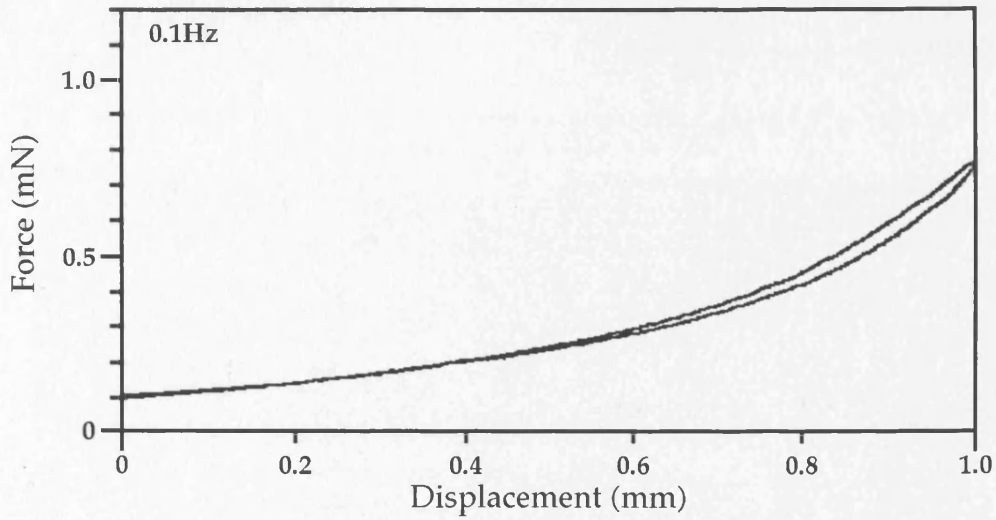
0.1Hz
Force (mN)
1.0
0.5
0
0
0.2
0.4
0.6
0.8
1.0
Displacement (mm)

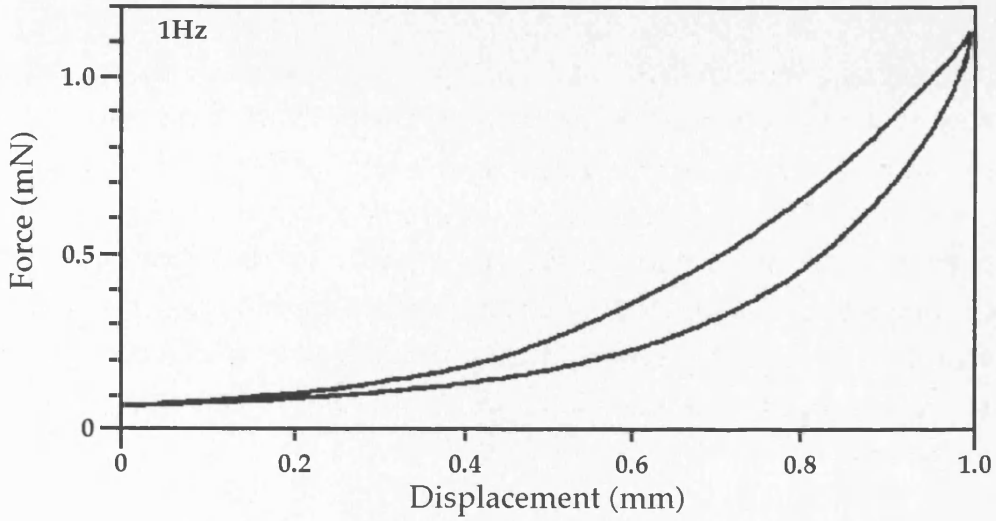
1Hz
Force (mN)
1.0
0.5
0
0
0.2
0.4
0.6
0.8
1.0
Displacement (mm)

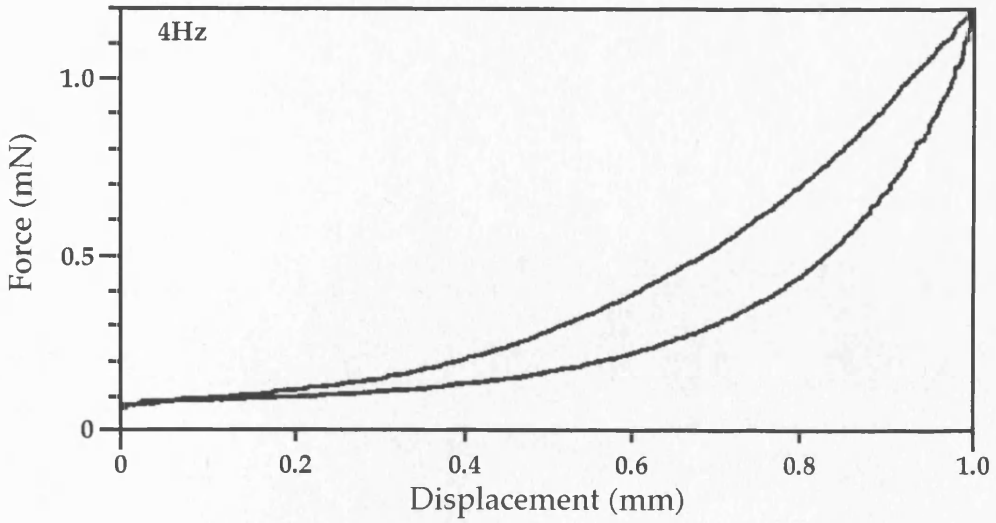
4Hz
Force (mN)
1.0
0.5
0
0
0.2
0.4
0.6
0.8
1.0
Displacement (mm)

Figures 6.9a, b

These figures show typical examples of the mean relationship between the amount of energy dissipated per cycle, expressed in (Nm), and the velocity of displacement (ms^{-1}) for *S. gregaria* (**a**) and *T. collaris* (**b**) . The mtFCOs of both species were displaced over a range of 1 mm from the position corresponding to a femoro-tibial angle of 150°. In both species, the amount of work done per cycle does not increase linearly with displacement velocity. There is a noticeable rapid increase in energy dissipation/cycle up to displacement velocities of $2x10^{-3}$ m s^{-1}. Thereafter there is a slower rate of increase. Error bars = standard deviation.

a

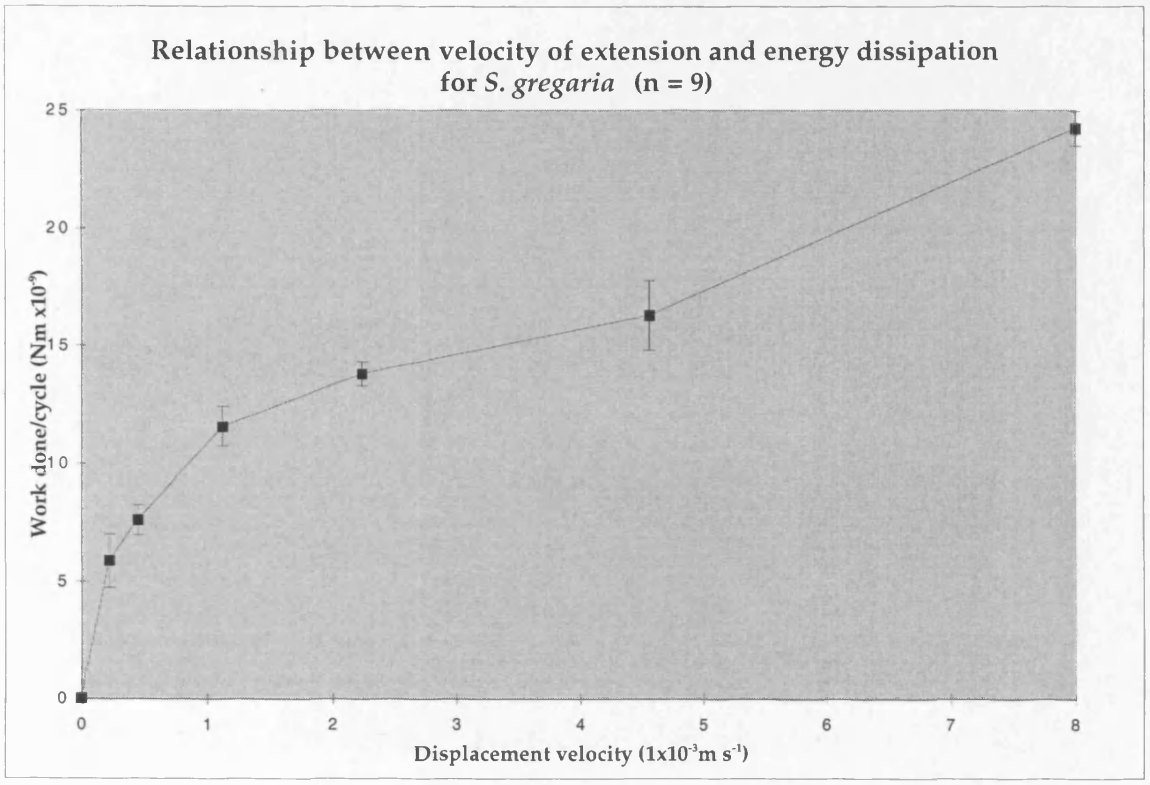
Relationship between velocity of extension and energy dissipation
for S. gregaria (n = 9)
Work done/cycle (Nm x10⁻⁹)
Displacement velocity (1x10⁻³m s⁻¹)
0
5
10
15
20
25
0
1
2
3
4
5
6
7
8

b

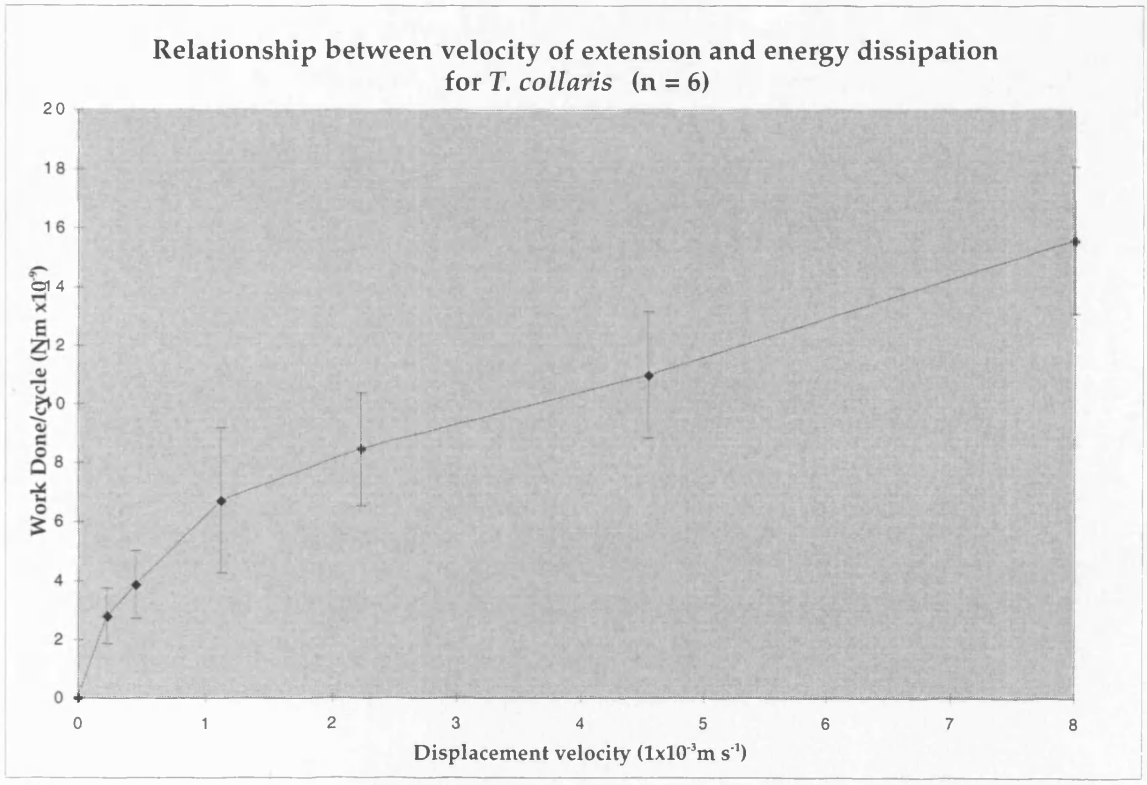
Relationship between velocity of extension and energy dissipation
for T. collaris (n = 6)
Work Done/cycle (Nm x10⁻⁹)
Displacement velocity (1x10⁻³m s⁻¹)
0
2
4
6
8
10
12
14
16
18
20
0
1
2
3
4
5
6
7
8

Figures 6.10a, b

These figures compare the relationship between work done/cycle and displacement velocity for two intact mtFCOs before and after their ventral (**a**) or dorsal (**b**) apodeme complex ligaments were severed. These graphs indicate that severing either of the ligaments has a similar effect, each ligament being responsible for dissipating approximately half of the total elastic energy lost/cycle in the intact organ. The energy dissipation curve of the intact organ in **b** indicates particularly clearly the likelihood of elastic resonance in the mtFCO. This organ dissipates more energy for each extension-relaxation cycle at an extension velocity of $1x10^{-3}$ m s^{-1} than it does at $2x10^{-3}$ m s^{-1}.

a

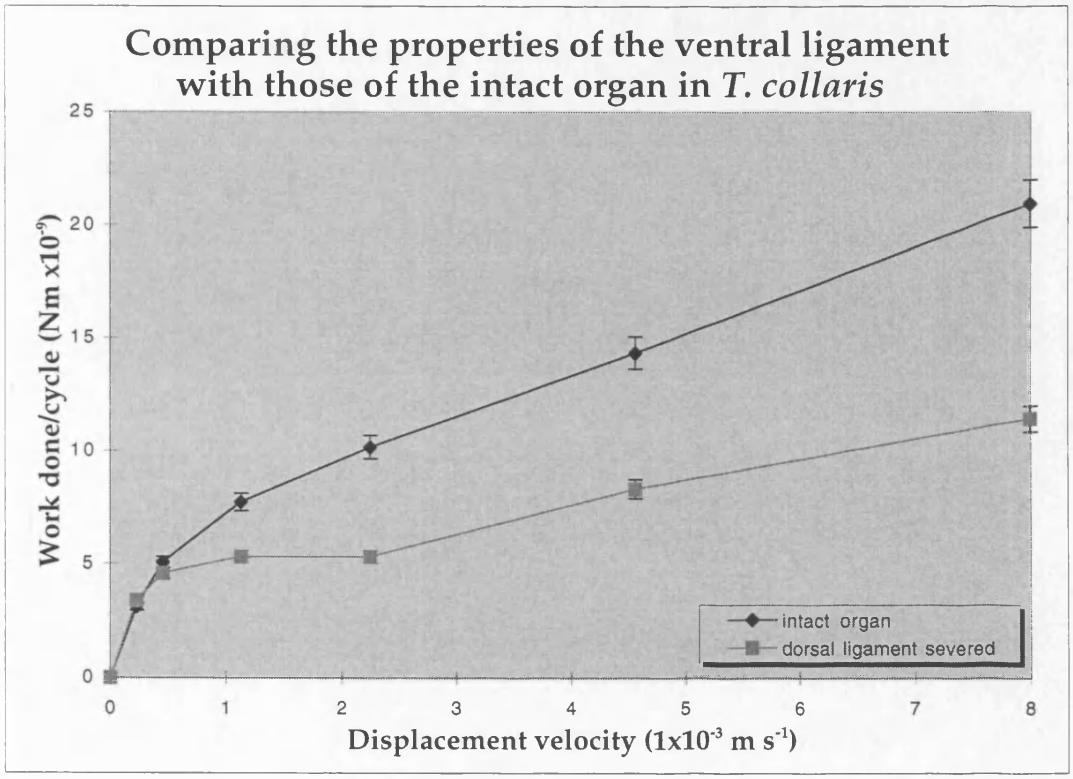
Comparing the properties of the ventral ligament with those of the intact organ in T. collaris
Work done/cycle (Nm x10⁻⁹)
Displacement velocity (1x10⁻³ m s⁻¹)
intact organ
dorsal ligament severed

b

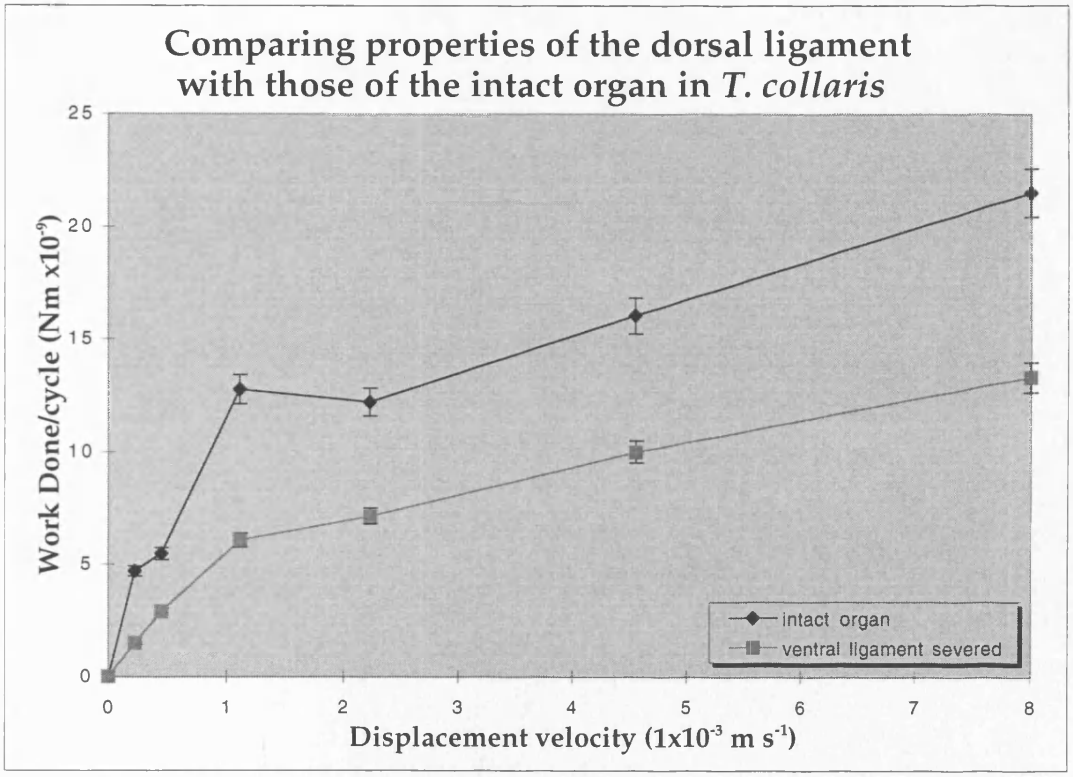
Comparing properties of the dorsal ligament with those of the intact organ in T. collaris
Work Done/cycle (Nm x10⁻⁹)
Displacement velocity (1x10⁻³ m s⁻¹)
intact organ
ventral ligament severed

Figure 6.11

This figure shows the amplitude and phase relationships between the imposed sinusoidal displacement (upper records) and the resulting mtFCO tension oscillation (lower records) at three different frequencies. The stimulus amplitude remained constant in all cases. At a stimulus frequency of 0.1 Hz, the amplitudes of the oscillation in tension is 55 μN. At frequencies of 2 Hz and 6 Hz, the amplitude of the tension oscillation elicited by the same amplitude of sinusoidal stimulation are 80 μN and 100 μN respectively. The sinusoidal changes in tension at each frequency are phase advanced with respect to the stimulus displacement (indicated by arrows).

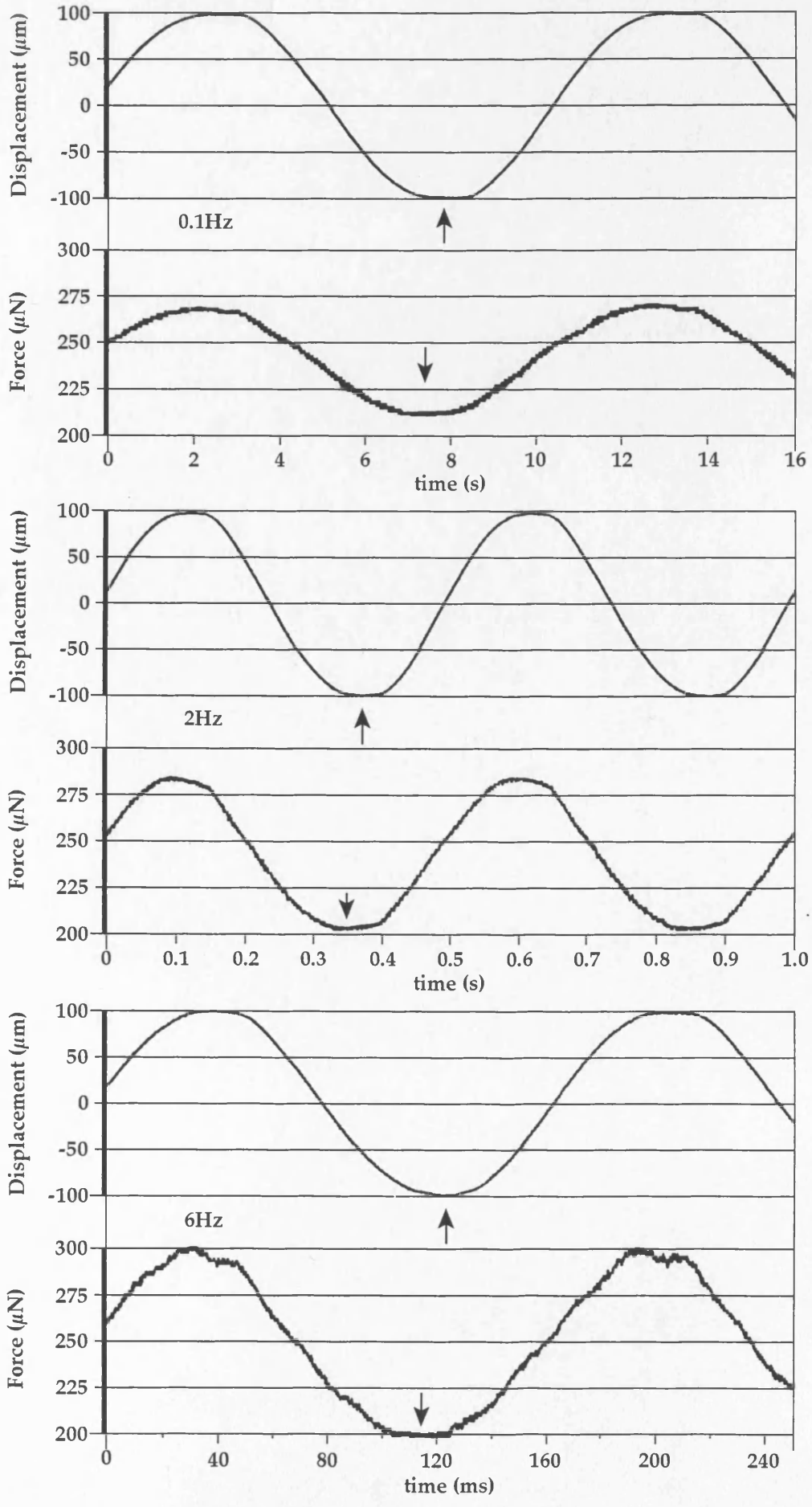
Displacement (μm)
100
50
0
-50
-100
0.1Hz
Force (μN)
300
275
250
225
200
0
2
4
6
8
10
12
14
16
time (s)
Displacement (μm)
100
50
0
-50
-100
2Hz
Force (μN)
300
275
250
225
200
0
0.1
0.2
0.3
0.4
0.5
0.6
0.7
0.8
0.9
1.0
time (s)
Displacement (μm)
100
50
0
-50
-100
6Hz
Force (μN)
300
275
250
225
200
0
40
80
120
160
200
240
time (ms)

Figure 6.12

This graph shows how both the maximum amplitude of the tension developed in the mtFCO and the phase of the tension with respect to the stimulus vary with stimulus frequency. The maximum tension elicited by the sinusoidal stimulus is smallest at low frequencies (60 μN at 0.1 Hz). It is highest at the upper frequencies (100 μN at 6 Hz). However there is a peak in the maximum amplitude of tension at a frequency of 1 Hz , indicating a resonance at this frequency. At 1 Hz there is also a 7° shift in the phase of the tension oscillation relative to the oscillation elicited at a frequency of 0.1 Hz. This is also indicative of resonance.

Phase and amplitude of the mtFCO tension oscillation in response to sinusoidal stimulation at a range of frequencies

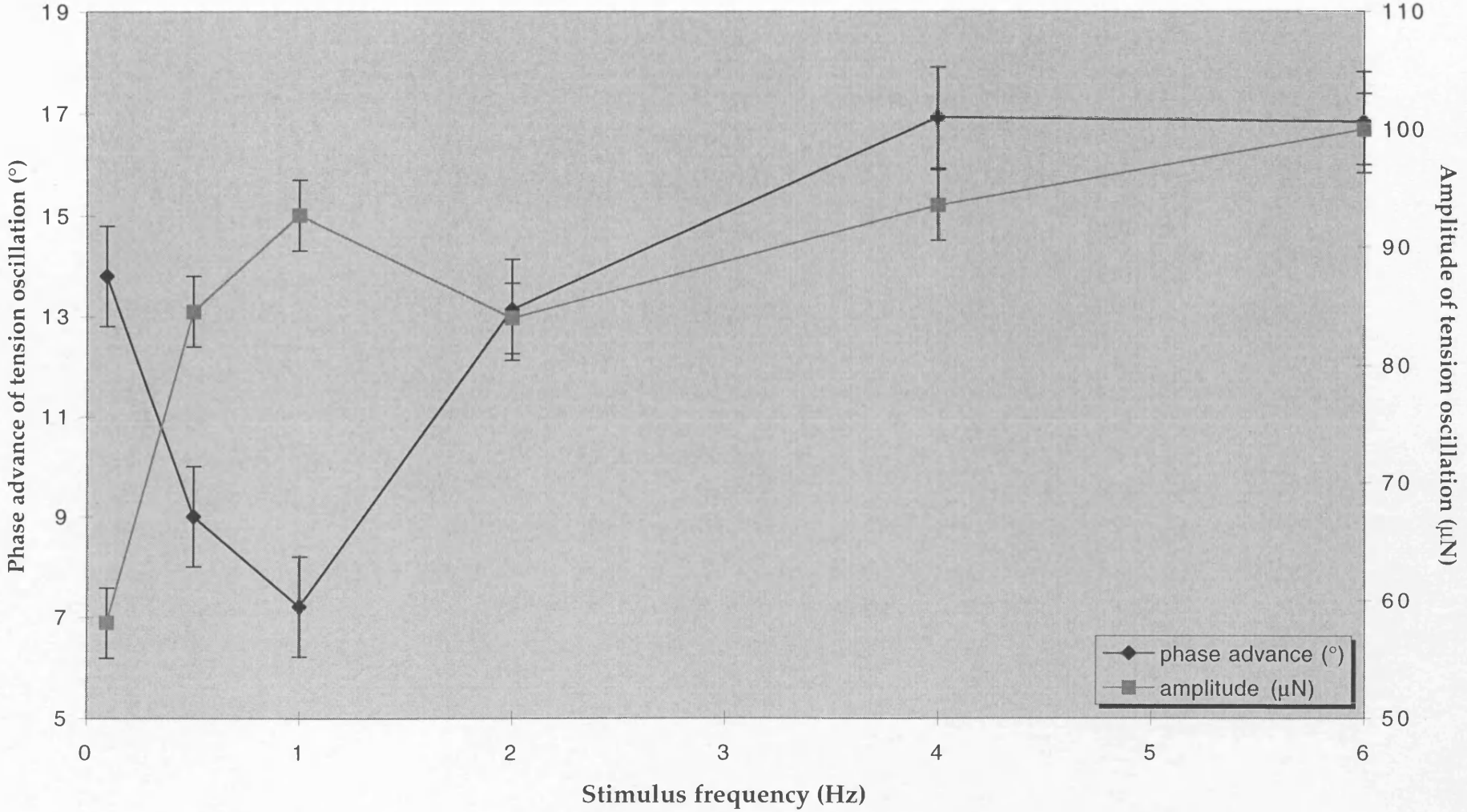

Figure 6.13a

This trace shows the mtFCO stress-relaxation behaviour of *T. collaris* in response to a step extension equivalent to tibial flexion over the entire femoro-tibial range. The upper trace shows the tension (force, μN) generated; the lower trace the displacement. When the step displacement is imposed at T1 (indicated), the tension rises to 700 μN (indicated by marker 'm'). The tension subsequently declines with time at a decreasing rate whilst the cuticular rod is maintained in its new position. When the step displacement is returned to 0 mm (T2), the tension initially falls to a level below that to which the organ was subjected before the displacement was imposed. The tension then increases with time and recovers to the original level during this recovery phase.

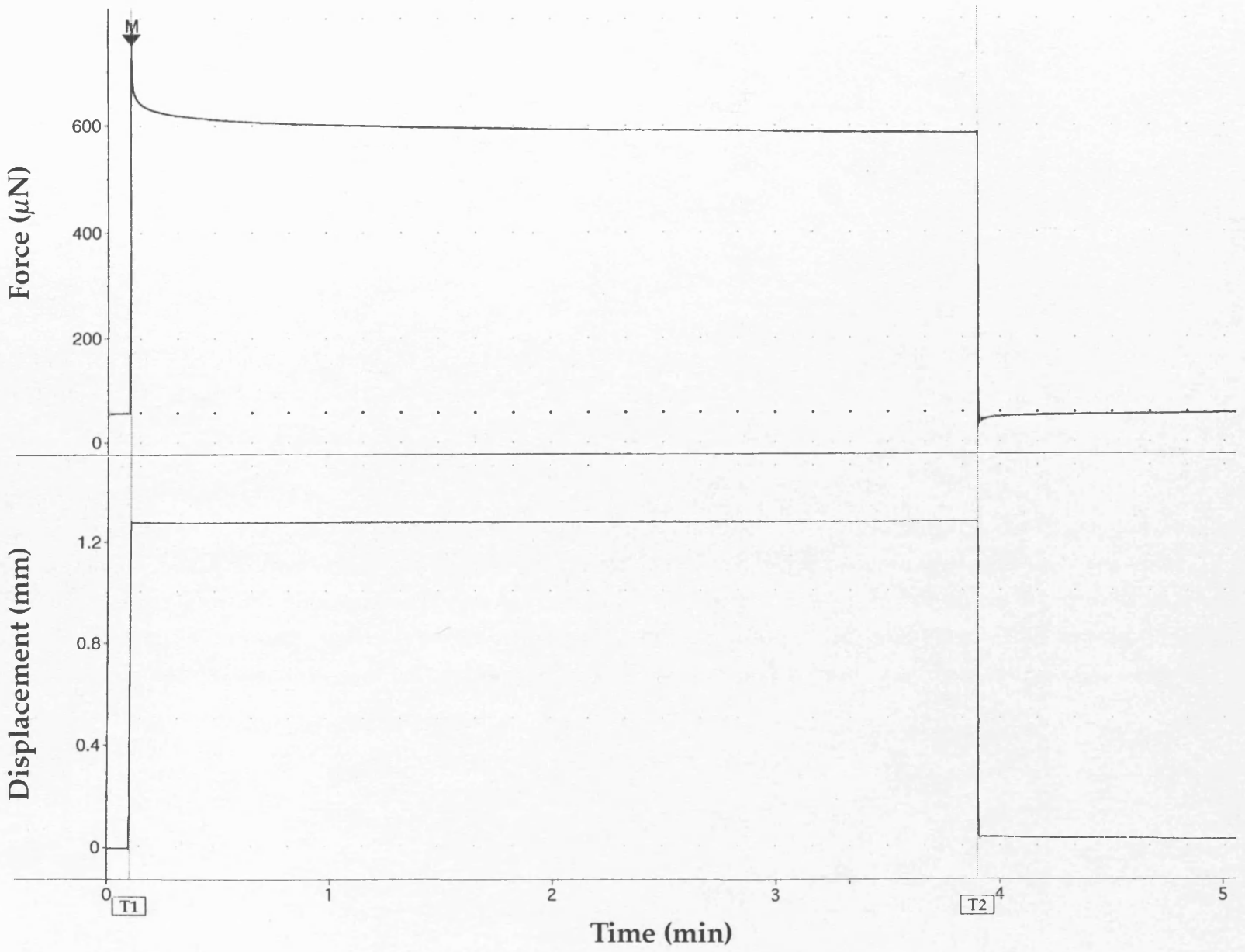
M
Force (μN)
600
400
200
0
Displacement (mm)
1.2
0.8
0.4
0
0
T1
1
2
3
T2
4
5
Time (min)

Figure 6.13b

S. gregaria shows similar stress-relaxation characteristics to *T. collaris* (Fig. 6.13a). The time-course of the fall in tension can be divided into two phases. There is an initial fast decrease in tension immediately following the application of the displacement, which lasts for approximately 60 s (indicated by the marker 'm'). This fast phase is followed by a prolonged slower phase during which the tension continues to fall gradually over several minutes. The step displacement is not fully returned to its original position (0 mm) in this preparation and the associated recovery phase (see figure 6.13a) is not present.

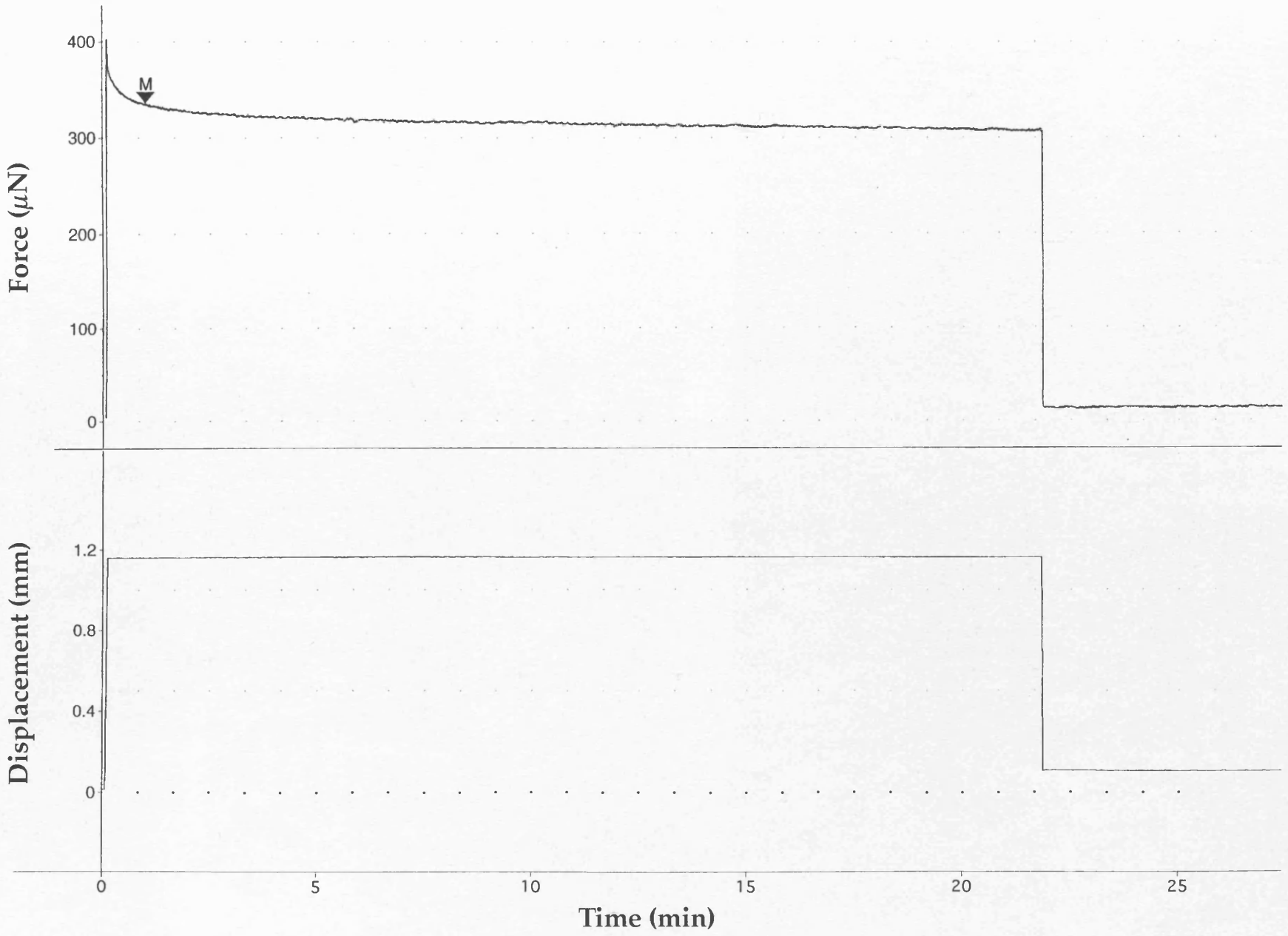
Force (μN)
400
300
200
100
0
M
Displacement (mm)
1.2
0.8
0.4
0
0
5
10
15
20
25
Time (min)

Figure 6.14a, b

These histograms compare the mechanical characteristics of the mtFCOs of *S. gregaria* and *T. collaris*

a

Histogram comparing the maximum tension developed following a step displacement of the mtFCO cuticular rod simulating tibial rotation from 150° - 0°. The mean maximum tension developed in the mtFCOs of a number of *S. gregaria* was 406 μN (s.d. = 81 μN; n = 9) whereas in *T. collaris*, the mean maximum tension was 747 μN (s.d. = 172; n = 7).

b

This histogram shows the percentage decrease of maximum tension developed which occurs over the initial 60 seconds following the imposition of a step displacement simulating tibial rotation from 150° - 0°. The mtFCO of *S. gregaria* shows a 17% (s.d. = 2.7; n = 9) mean decrease in tension over the initial 60 seconds of stress-relaxation, whilst that of *T. collaris* undergoes a mean decrease of 25% (s.d. = 2.8; n = 7) over the same period.

a

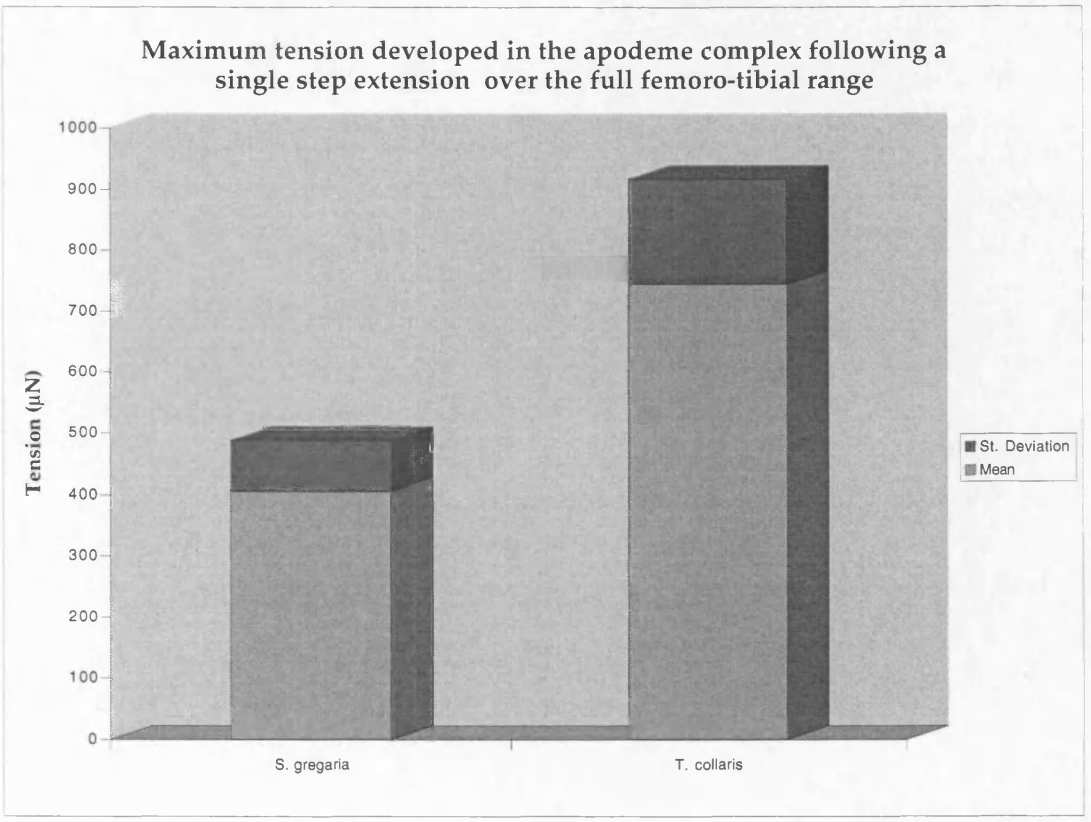
Maximum tension developed in the apodeme complex following a single step extension over the full femoro-tibial range
Tension (μN)
1000
900
800
700
600
500
400
300
200
100
0
S. gregaria
T. collaris
St. Deviation
Mean

b

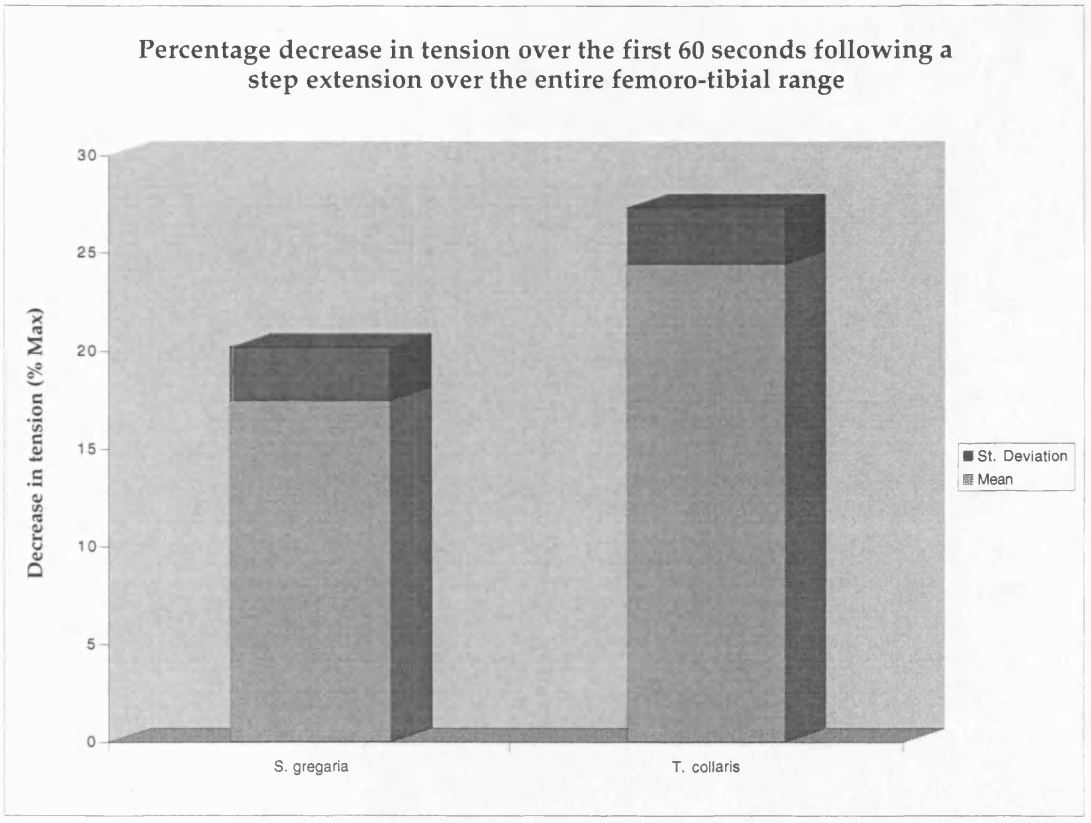
Percentage decrease in tension over the first 60 seconds following a step extension over the entire femoro-tibial range
Decrease in tension (% Max)
30
25
20
15
10
5
0
S. gregaria
T. collaris
St. Deviation
Mean

Figure 6.15a, b

a

These graphs compare the tension-relaxation curves of intact and partially dissected *S. gregaria* mtFCOs in response to step displacements equivalent to tibial rotations of 150° - 0°. Severing either the dorsal or ventral ligaments of the apodeme complex results in a reduction in the tension developed upon a step displacement. In these examples cutting the ventral ligament causes a larger drop in tension than does cutting the dorsal ligament. Typical relaxation of tension with time is seen in all instances.

b

This histogram compares the decrease in tension following the partial dissection of the apodeme complex in a number of *S. gregaria*. The percentage decrease in tension was calculated from the maximum tension developed following a step displacement equivalent to a change in femoro-tibial angle of 150° - 0° in the intact and partially dissected organs. The percentage decrease in tension was found to be 39.0% (s.d. = 11%) after cutting the ventral ligament and 27.4% (s.d. = 9.6%) after severing the dorsal ligament. The difference demonstrated between the mechanical properties of the ligaments in this small data set is not a significant one ($U = 5$; $P > 0.05$, Mann-Whitney U-test).

a

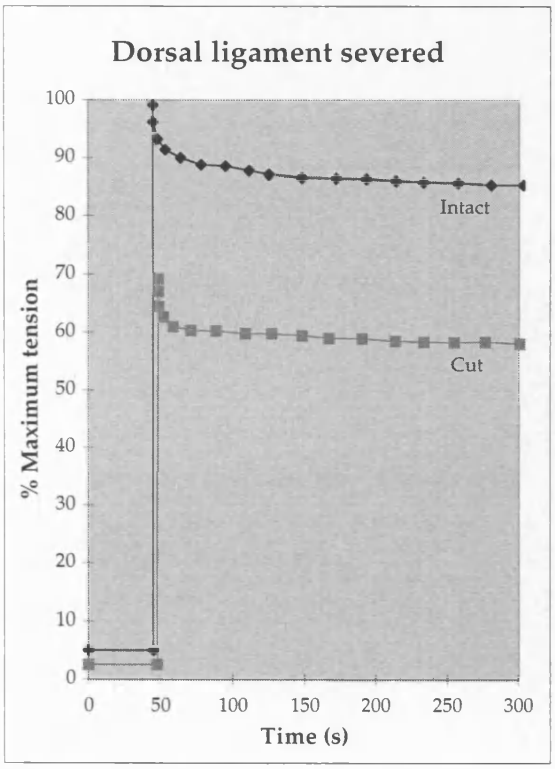
Dorsal ligament severed
% Maximum tension
Time (s)
Intact
Cut
0
10
20
30
40
50
60
70
80
90
100
0
50
100
150
200
250
300

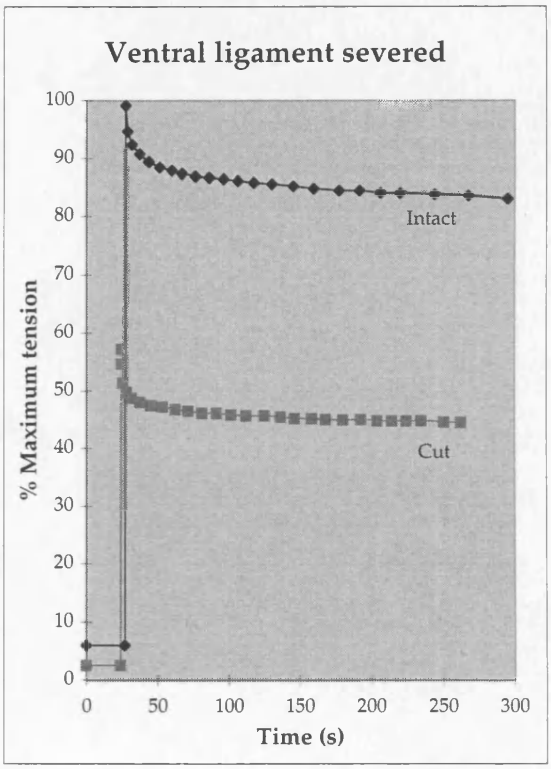
Ventral ligament severed
% Maximum tension
Time (s)
Intact
Cut
0
10
20
30
40
50
60
70
80
90
100
0
50
100
150
200
250
300

b

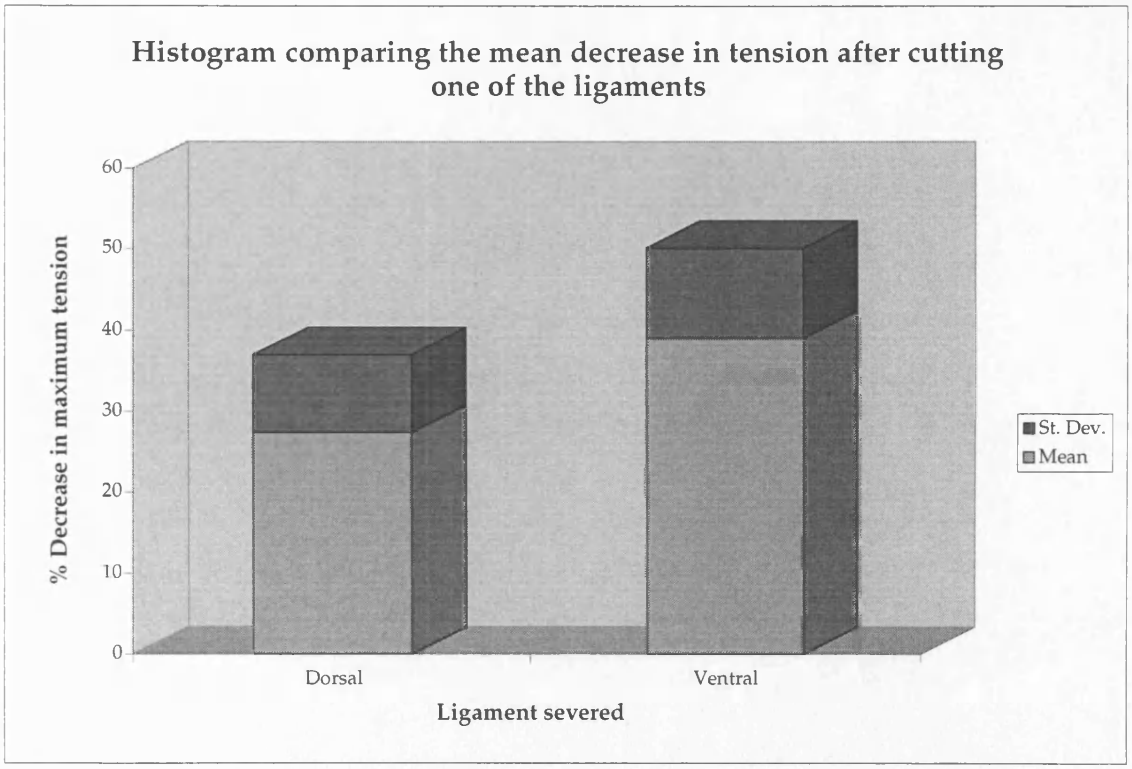
Histogram comparing the mean decrease in tension after cutting one of the ligaments
% Decrease in maximum tension
Ligament severed
Dorsal
Ventral
St. Dev.
Mean
0
10
20
30
40
50
60

Figure 6.16

This trace shows the tension developed in the mtFCO of *S. gregaria* (upper) when it is subjected to a series of step displacements (equivalent to flexion) of the cuticular rod (lower). The series of 5 step displacements (indicated) are each 240 μm in magnitude and together simulate tibial flexion over the full femoro-tibial range. Displacement of 0 mm corresponds to the position of the cuticular rod when the tibia is fully extended, whilst a displacement of 1.2 mm indicates the distal displacement of the rod as the tibia is rotated to the fully flexed position. Each step was held for 100 s duration. The imposition of each increment in the series elicits an increasingly large increase in mtFCO tension. The extent of tension-relaxation evident also increases with each step. The decrease in tension over the 100 s following each step ranges from 4 μN (T1) to 34 μN (T5), the observed stress-relaxation being maximal as the displacement simulates full tibial flexion (indicated by marker 'm').

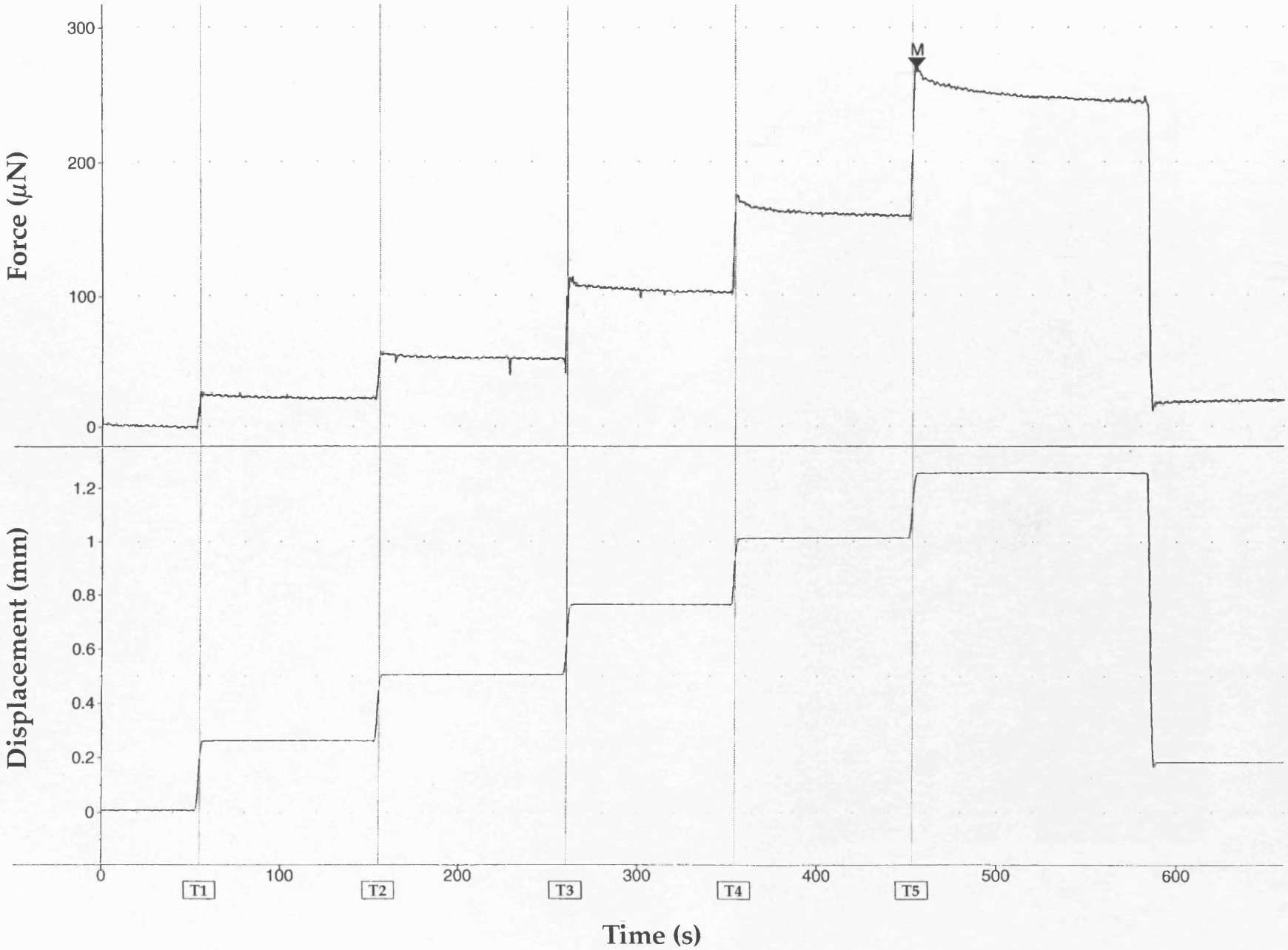
Force (μN)
300
200
100
0
M
Displacement (mm)
1.2
1
0.8
0.6
0.4
0.2
0
0
100
200
300
400
500
600
T1
T2
T3
T4
T5
Time (s)

Figure 6.17

Graph showing isochronal curves from two preparations of *S. gregaria*. Tension was measured 30 s after the imposition of each step displacement. Preparations were returned to their original length and rested for 2 minutes between successive steps. The non-linearity of the isochronal curves indicates that the mtFCO is not linearly viscoelastic. Error bars indicate experimental error estimated from 10 displacements upon the same preparation. The imposed displacement was subject to small amounts of error since it was difficult to impose small swift step displacements precisely.

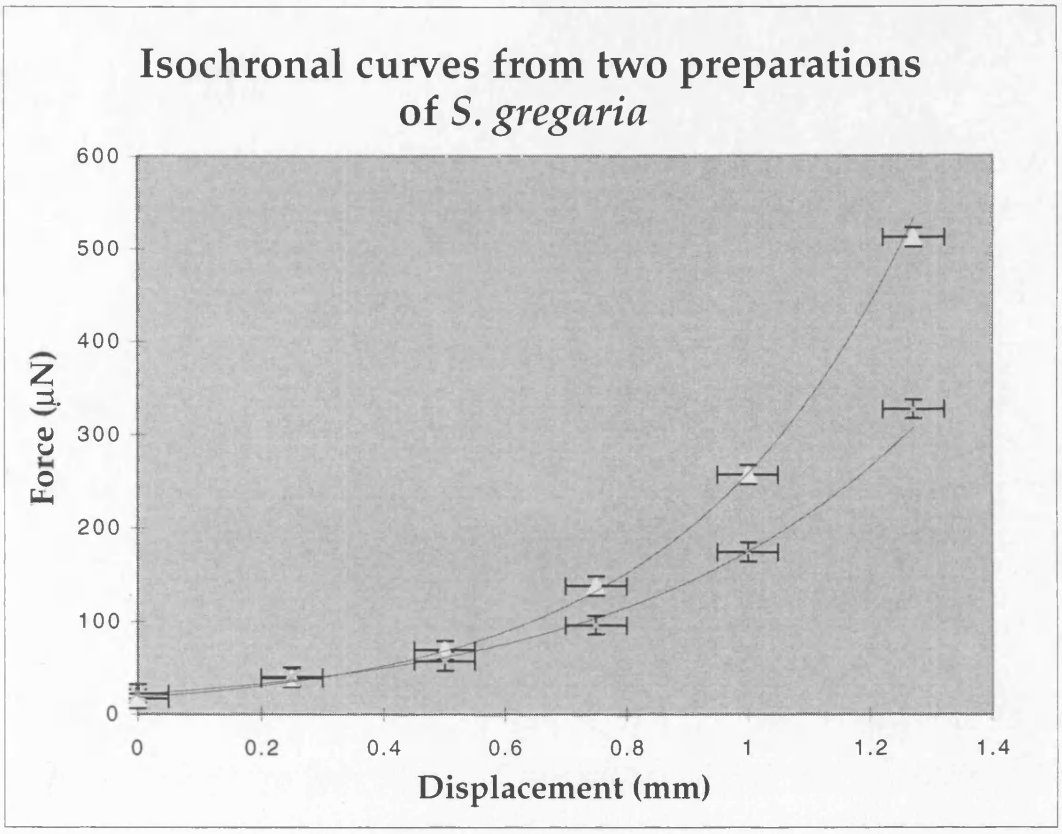
Isochronal curves from two preparations of S. gregaria
Force (µN)
600
500
400
300
200
100
0
0
0.2
0.4
0.6
0.8
1
1.2
1.4
Displacement (mm)

Figures 6.18a, b

Frequency response spectra from two preparations (**a**, **b**) of *S. gregaria* subjected to pink noise stimulation. Such power spectra show the frequencies at which maximum power is transmitted. Each trace is the average of 1000 32 second sweeps of the analyser. Both curves show that power is transmitted along the mtFCO most efficiently at approximately 1 - 2 Hz.

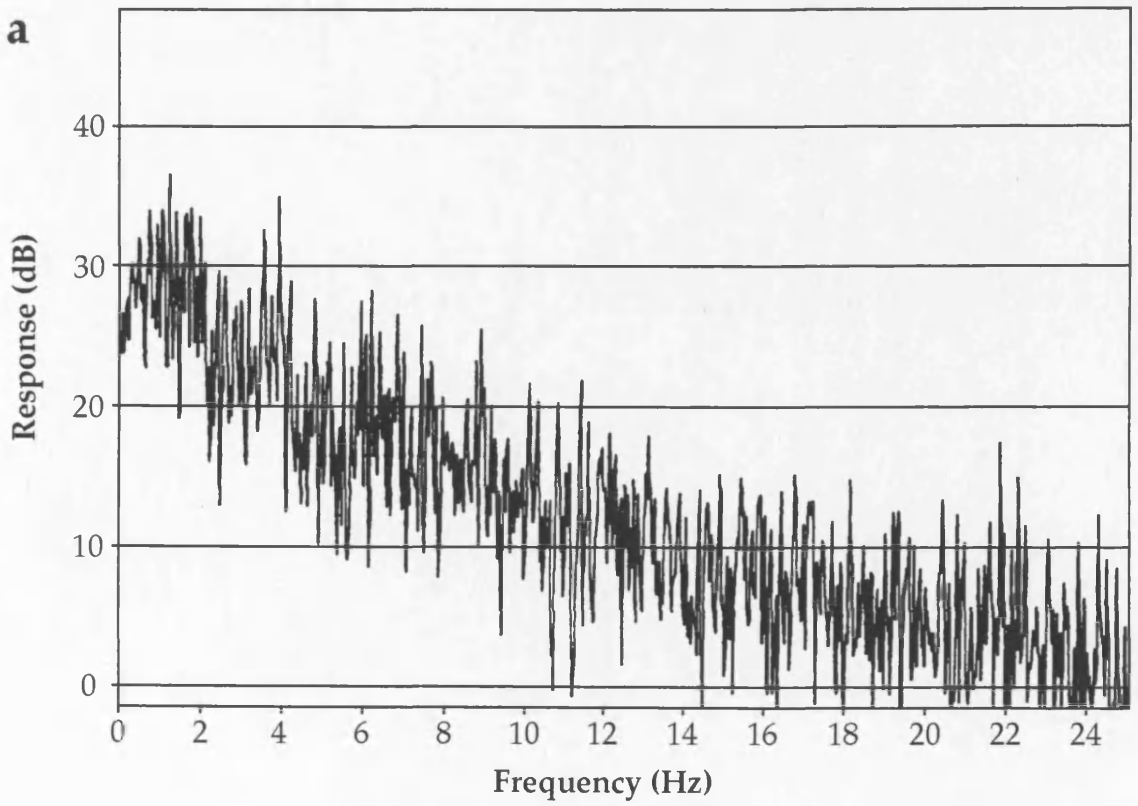
a
Response (dB)
40
30
20
10
0
0
2
4
6
8
10
12
14
16
18
20
22
24
Frequency (Hz)

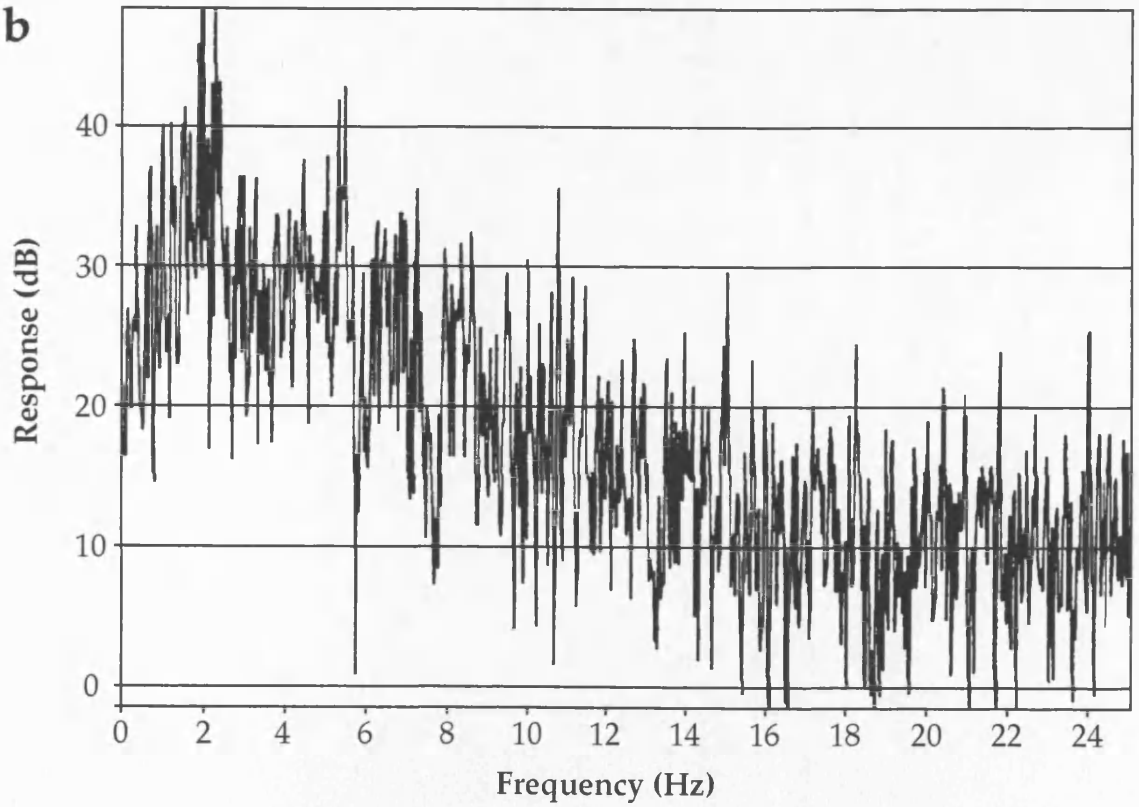
b
Response (dB)
40
30
20
10
0
0
2
4
6
8
10
12
14
16
18
20
22
24
Frequency (Hz)

Figures 6.19a, b

This figure shows that power is transmitted to the mass most efficiently at the natural frequency of a simple resonating system. Power spectra from the model system subjected to pink noise stimulation show that both the tension of the model (**a**) and the displacement of the mass (**b**) show peaks in power at the resonant frequency of 2.2 Hz. Each trace is the average of 1000 32 second sweeps of the analyser. The peak at 0.9 Hz (arrow) was artefact introduced by the pendulum motion of the mass relative to the displacement transducer.

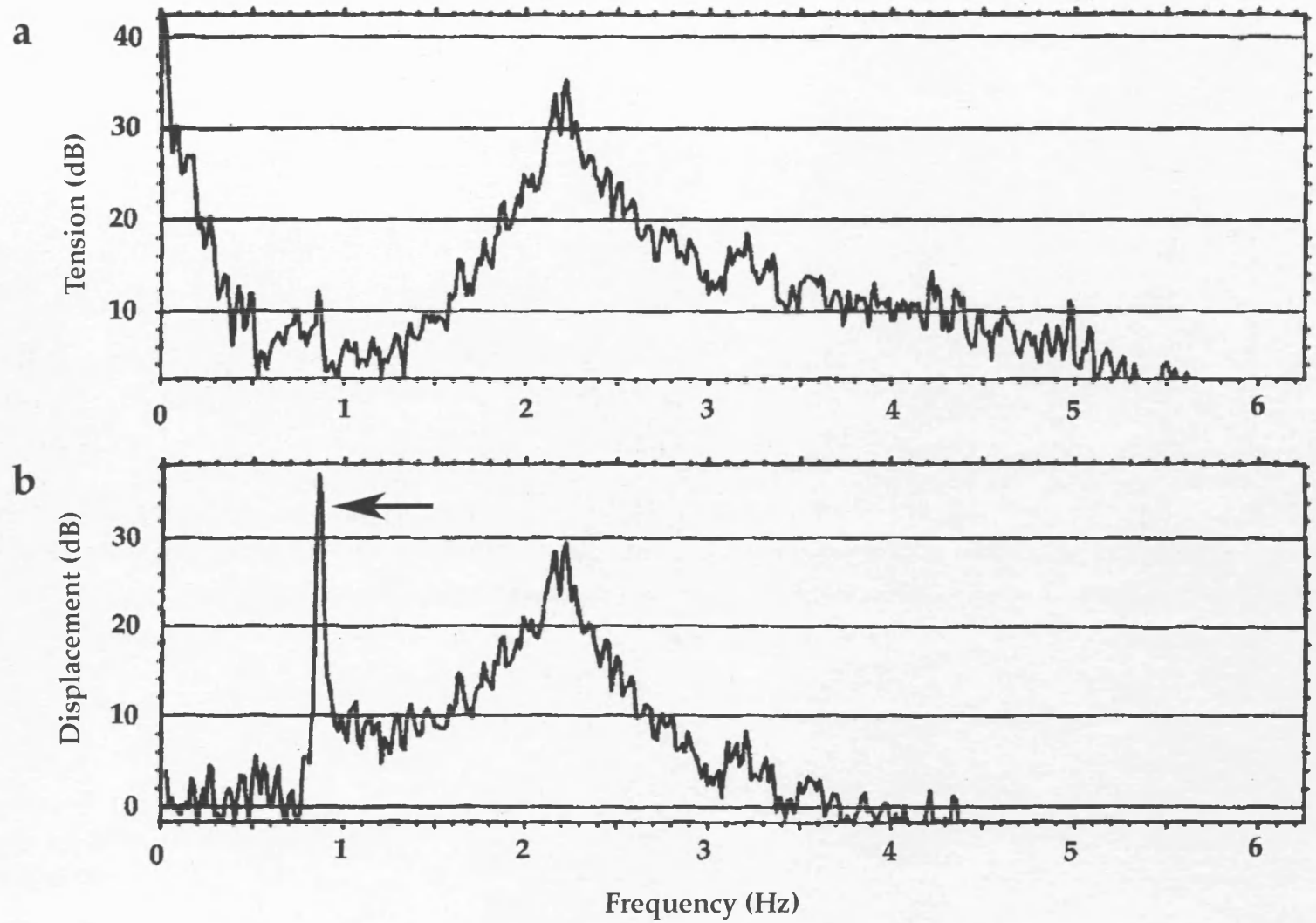
a
Tension (dB)
40
30
20
10
0
1
2
3
4
5
6
b
Displacement (dB)
30
20
10
0
0
1
2
3
4
5
6
Frequency (Hz)

Figure 6.20

Hysteresis curves measured from the model system at a range of frequencies (1 - 5 Hz). At each frequency the input displacement (x axis) was the same. This figure shows that the amount of energy dissipated per cycle is dramatically increased at the resonant frequency of 2 Hz.

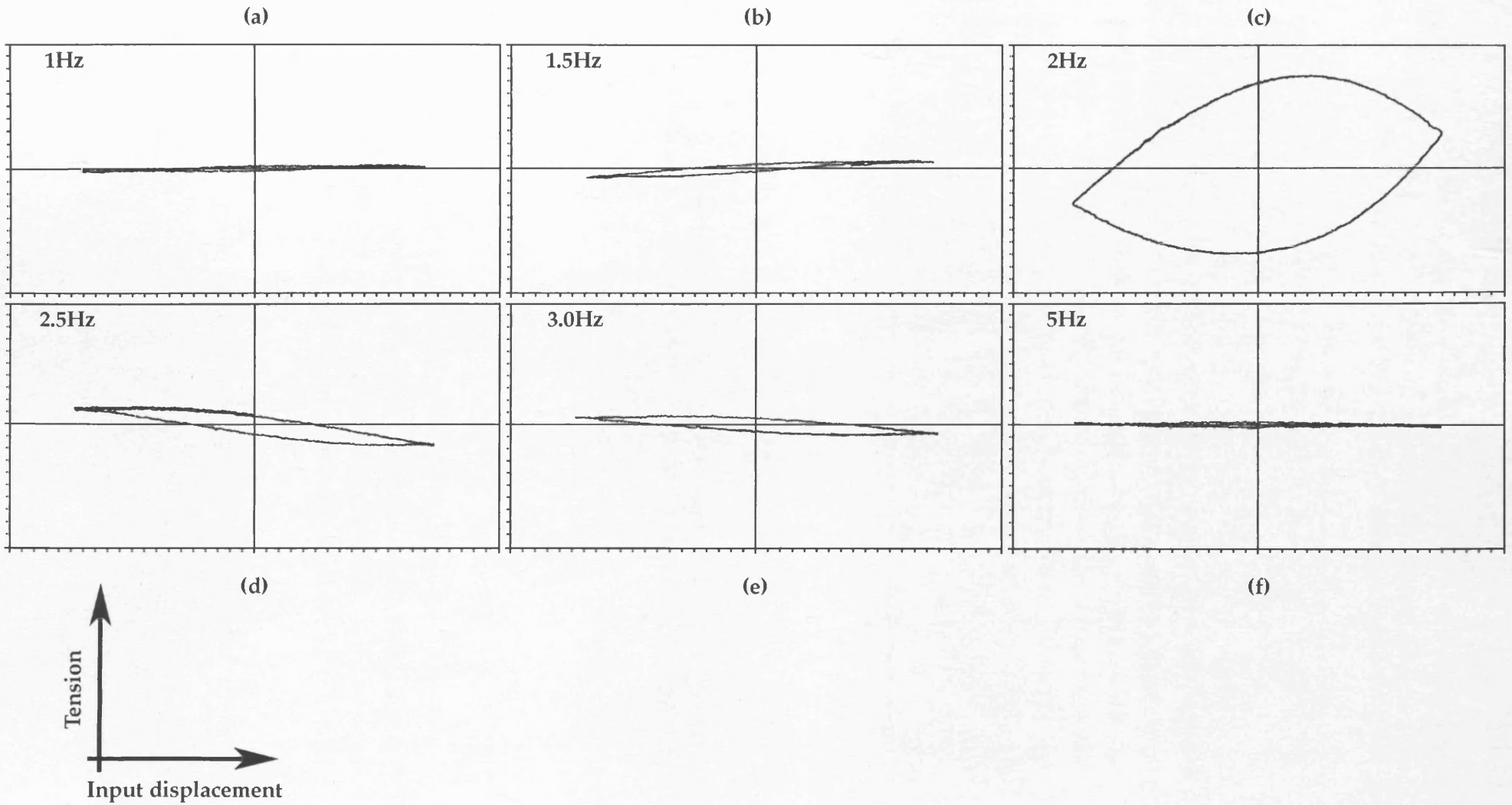
(a)
(b)
(c)
1Hz
1.5Hz
2Hz
2.5Hz
3.0Hz
5Hz
(d)
(e)
(f)
Tension
Input displacement

Figure 6.21a, b

a

This graph shows the energy dissipation and oscillation amplitude characteristics of the model system at a range of displacement velocities. Both the amplitude of oscillation and the amount of energy dissipated per cycle increase at the system's resonant frequency. The rate of displacement (velocity m s^{-1}) was calculated from the mean velocity of the sinusoidal stimulus at each frequency.

b

In a simple resonating model, the phase of the mass oscillation varies in a frequency dependent manner. The displacements of the mass lag those of the input by 90° at the resonant frequency. At this frequency the amplitude of the mass displacement is maximal.

a

Graph showing the oscillation amplitude and energy dissipation of a simple resonating model at a range of displacement velocities

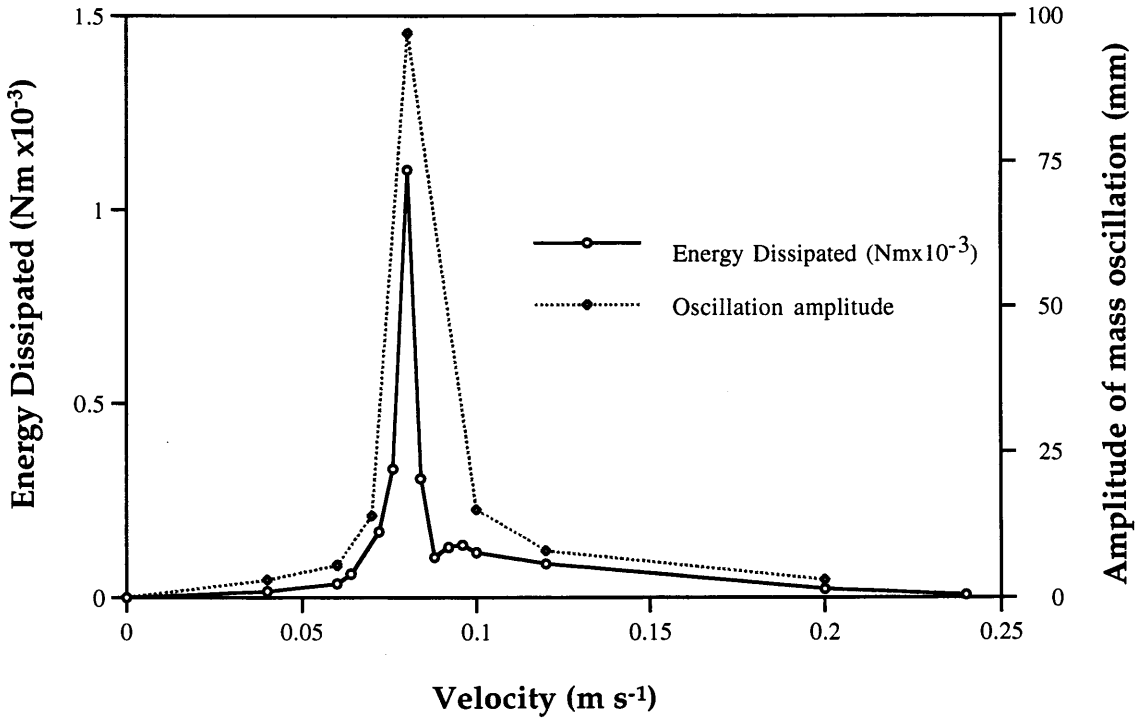

b

Graph showing the relationship between oscillation amplitude and phase in response to forced vibration of a simple resonating system at a range of frequencies

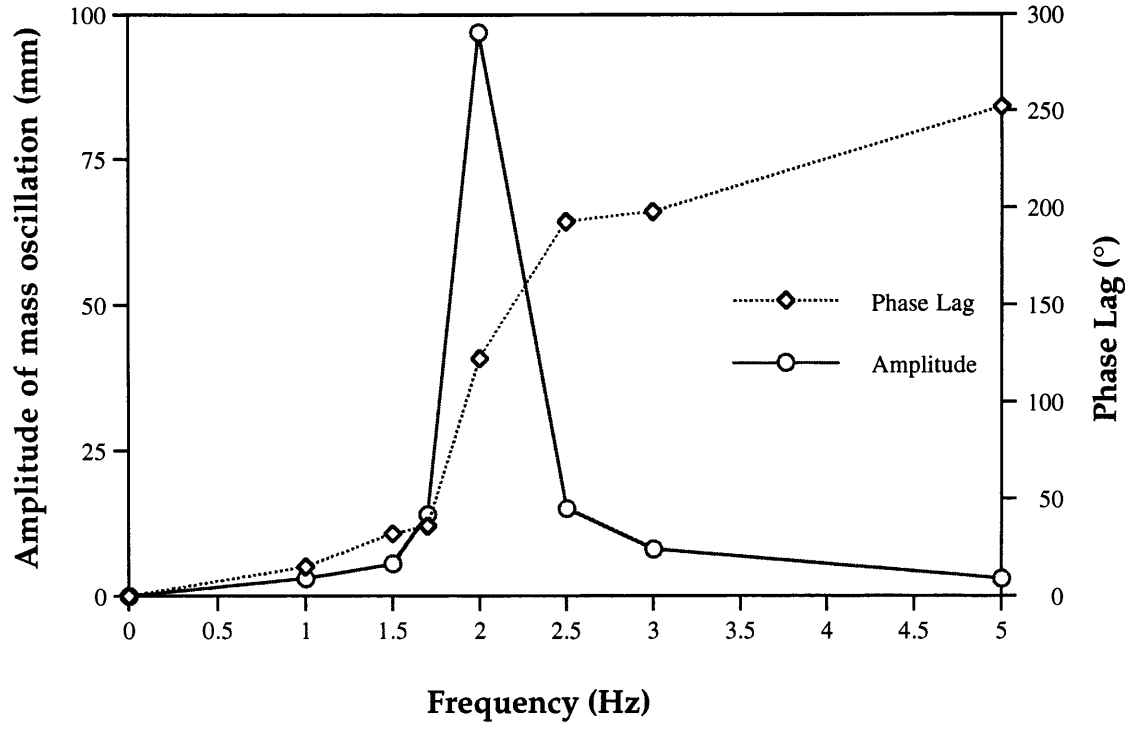

Chapter 7: Other Proprioceptors within the femur

7.1 SUMMARY

- *The femoro-tibial joint is monitored by two receptors of the strand-receptor type: the strand receptor organ associated with the mtFCO flexor strand, and a previously undescribed receptor located at the level of the femoro-tibial joint (femoro-tibial joint receptor, ftjR). Both receptors feature finely branched naked dendritic terminals embedded in connective tissue strands.*

7.2 INTRODUCTION

Associated with the femoro-tibial joint of all three pairs of locust legs are one chordotonal organ (Slifer, 1935; Usherwood *et al.*, 1968; Burns, 1974), five multipolar sensory neurones arranged in three groups (Coillot and Boistel, 1968; Williamson and Burns, 1978), one multipolar muscle tension receptor (Theophilidis and Burns, 1979; Matheson and Field, 1995) and a strand receptor (Bräunig, 1985). The strand receptor in the metathoracic leg was first described by Usherwood *et al.* (1968) as a 'ligament' joining the mtFCO to the apodeme of the flexor tibiae muscle. It was subsequently referred to as the 'flexor strand' (Field and Burrows, 1982) or the 'femoro-tibial strand receptor' (fetiSR) (Bräunig, 1985).

This chapter describes the ultrastructure of the flexor strand receptor for the first time. In addition, a second strand-type receptor is described which has been overlooked in previous studies. Strand organs always have a similar pattern of organisation. Typically, terminal dendrites arising from a centrally located nerve cell body (located in the metathoracic ganglion), branch extensively within a deformable ribbon of connective tissue (Bräunig, 1982b, 1985). In this study the term 'strand receptor' is used to describe the neural components of the flexor strand organ. The term 'flexor strand' is used to refer to the connective tissue component in which the neural elements are embedded.

The flexor strand receptor is sensitive to elongation (Bräunig, 1985) as are all other known strand receptors (Bräunig and Hustert, 1980; Hustert, 1983; Bräunig, 1983). It is stretched by tibial extension whereas the mtFCO is stretched during tibial flexion (Field and

Burrows, 1982). Thus, there is a reciprocal displacement pattern between the two organs.

The flexor strand discharges over the entire range of femoro-tibial angles. Sensory discharge is close to zero at the position of full tibial flexion; it increases as the tibia is extended (Bräunig, 1985). It exhibits both phasic and tonic properties so that step elongation elicits an increase in firing rate which adapts over approximately 5 s to a rate proportional to the degree of elongation. The angle of the femoro-tibial joint appears to be encoded by its tonic discharge frequency (Bräunig, 1985). Strand organ afferents synapse on a spiking local interneurone which has an inhibitory connection upon a local non-spiking interneurone which in turn has an excitatory connection to a slow extensor tibiae motor neurone (Pflüger and Burrows, 1987). Thus, extension of the strand organ prevents excitation of the extensor motor neurone and so inhibits tibial extension.

To date, four organs of the strand receptor-type have been identified in each locust leg; one in the subcoxal joint (Bräunig and Hustert, 1980; Bräunig *et al.*, 1981; Hustert, 1983), two in the coxo-trochanteral joint (Bräunig, 1982a, b) and one at the femoro-tibial joint (Bräunig, 1985). During the course of the present study, another strand receptor associated with the mtFCO was found. It appears to be associated with monitoring tibial displacements and its morphology and ultrastructure are described. This receptor has been named the femoro-tibial joint receptor (ftjR) and is located such that it can monitor changes in the orientation of the tibia with respect to the cuticular rod of the mtFCO. All previously described strand receptors in the locust leg are innervated by branches of nerve 3B (Bräunig, 1985). The new receptor appears to be innervated by a branch of nerve 5B.

7.3 MATERIALS AND METHODS

To examine the flexor strand organ and the ftjR, femora were first isolated from adult specimens of *S. gregaria*. For the flexor strand, mtFCOs were exposed by dissection and osmicated *in situ* before being dissected out and embedded between siliconised (Repelcoted) slides. This allowed the subsequent mounting of the organ, with the flexor strand lying at a suitable orientation, within plastic embedding stubs as described in Chapter 4. Preparations for examination of the ftjR were dissected to

reveal the femoro-tibial joint from the anterior side. These preparations were then osmicated, fixed and embedded conventionally in plastic embedding stubs. The resin stubs were orientated in an adjustable chuck on a Huxley ultramicrotome and sectioned at 0.1 μm. Sections were picked up on pioloform films and mounted on 0.25 mm slot grids using a binocular dissecting microscope. Sections were stained for TEM and viewed in the usual way. Preparations for viewing the ftjR using Scanning Electron Microscopy (SEM) were obtained and dissected as above. Specimens were then critical point dried, sputter coated using Gold/Paladium, and viewed using an Siemens (S.102) SEM.

7.4 RESULTS

7.4.1 Flexor strand

The gross morphology of the flexor strand was described in Chapter 3 whilst characterising the mechanical linkages of the mtFCO. Figure 7.1 is reproduced from this chapter to summarise the morphology of the flexor strand and to indicate the levels from which subsequent electron micrographs were obtained.

The following account describes the ultrastructure of the flexor strand and the way in which the strand receptor dendrite branches within it. Proximally the dendrite is single and unbranched (not shown) as it travels distally over the surface of the mtFCO to which it is attached (see Chapter 3, Fig. 3.34). Just distal to the mtFCO (level 1; Fig. 7.1) the dendrite branches into two (Fig. 7.2a). Each dendrite is surrounded by a thick glial wrapping which is in turn surrounded by a layer of extracellular matrix containing extracellular fibres of the type that stain with Acid Fuchsin at the light microscope level. In addition, the matrix contains bundles of dendritic processes that arise from the main dendritic branches. The whole structure is contained within a fatty sheath (Figs 7.1, 7.2a). Soon after the dendrite branches into two they remain separate from one another and an extracellular space separates each one from the overlying glial sheath (Figs 7.2b, 7.3a). The glial wrapping is a characteristic of the main dendrite branches. This distinguishes them from the finer dendritic processes. These are naked and are embedded within the extracellular matrix that contains both extracellular fibres and smaller fibrils (Fig. 7.3b). Distally (level 4; Fig. 7.1), the cross-sectional area of the strand receptor increases in size (Fig. 7.4) . Increasing numbers of naked dendritic

processes are present although the two main dendrite branches remain distinct. Approximately 600 μm distal to the point where the flexor strand leaves the mtFCO scoloparium (level 4; Fig. 7.1), the two main dendritic branches divide further (Fig. 7.5). At a distance of 1000 μm from its origin at the mtFCO (level 5; Fig. 7.1) both main dendrite branches have subdivided into larger numbers of smaller branches (Fig. 7.6). These dendrite branches still retain their glial wrappings unlike the naked dendritic processes (Figs 7.7a, b; 7.8a, b). The dendritic processes are organised into bundles of interdigitating membrane-bound cytoplasmic fingers (Fig 7.8a) which lie in parallel with extracellular fibres. The cytoplasmic fingers are separated from one another by a consistent extracellular gap (Fig. 7.8b). These bundles both taper and divide as they extend along the axis of the organ (Figs 7.9a-d). 1500 μm distal to the mtFCO scoloparium, the fatty sheath which surrounds the strand receptor is reduced (levels 6 - 8; Fig. 7.1). What are thought to be flexor strand sheath cells are situated both dorsal and ventral to the strand organ (Fig. 7.10). At this level the bundles of dendritic processes are fewer in number and smaller in cross-sectional area than those located further proximally within the strand organ. At the level of their distal terminations the dendritic processes are of the order of 0.4 μm in diameter and often contain vesicles and mitochondria (Figs 7.11a, b).

7.4.2 Femoro-tibial joint receptor (ftjR)

In addition to the strand organ in the mtFCO flexor strand, the mtFCO is associated with a second strand-type receptor at the level where the apodeme complex cuticular rod originates from the tibia at the femoro-tibial joint. This receptor has not been described previously and will be referred to as the femoro-tibial joint receptor (ftjR). Like the strand receptor within the flexor strand, the ftjR appears to consist of a single branching dendrite, the neurone cell body presumably also being located at a central site. The dendrite is located within the cuticular nerve which branches from the chordotonal organ nerve at the level of the mtFCO scoloparium (see Chapter 4, Fig. 4.2). The dendrite travels distally before branching ventrally from the cuticular nerve at the level of the femoro-tibial joint (Fig. 7.12). The receptor dendrite runs ventral to the cuticular rod to attach onto the tibia close to the centre of joint articulation. This arrangement means that the dendrite is not exposed to excessive stresses as it crosses the femoro-tibial joint. The ftjR is anchored to the tibia at this point via a short ventral attachment strand (Figs 7.13a, b). Rather than be

subjected to axial stretching during tibial rotation, the ftjR 'hinges' at the level of this ventral attachment strand as the tibia is extended from the flexed position (Fig. 7.14). The angle between the cuticular rod (upon which the ftjR terminates) and the proximal margin of the tibia changes by approximately 150° over the femoro-tibial range 0° - 150°. The dendrite is protected by a thick sheath (Fig. 7.15) which may help it withstand stretching during joint rotation. In addition, the glial-wrapped dendrite is surrounded by extracellular matrix which is heavily reinforced with extracellular fibrils. Once the dendrite has joined the tibia, the ftjR runs dorsally along its proximal margin. At this level the receptor dendrite is no longer subjected to excessive stresses and the reinforced sheath is lost. The dendrite branches into 8 - 10 bundles of dendritic processes (Figs 7.16a, b) characteristic of stretch receptors (Osborn 1963, 1969). Each bundle consists of a number of naked processes embedded in extracellular matrix. They are similar in appearance to the terminal dendritic processes of the mtFCO strand organ. Unlike in the case of the strand organ, the dendritic processes of the ftjR spread out across the surface of the tibia as they approach the distal origin of the mtFCO cuticular rod (Fig. 7.17). They spread out to terminate in the epidermis surrounding the distal attachment of the cuticular rod to the tibia (Fig. 7.18). Thus, over the femoro-tibial range 0° - 150°, the articulation of the cuticular rod relative to the tibia results in the ftjR dendritic processes being stretched.

7.5 DISCUSSION

7.5.1 Flexor Strand

Examining the mtFCO flexor strand using conventional light microscopy in conjunction with cobalt staining, Bräunig (1982b) identified proximal dendrite branches, replaced distally by increasingly fine higher order ramifications. He described the strand as having the 'typical peripheral branching pattern' of a strand receptor neurone (Bräunig, 1982a, b). The current study using transmission electron microscopy has confirmed these observations, and demonstrated that the flexor strand dendrite terminates with numerous naked neural processes embedded in extracellular matrix.

The fact that the proximal joints of orthopteran insects lack COs and instead rely exclusively upon strand receptors and multipolar sensilla as internal mechanoreceptors (Bräunig, 1982a, b), demonstrates that such receptors are potentially capable of encoding joint relations. For example,

the locust coxo-trochanteral joint contains only two strand receptors and one muscle receptor (Bräunig, 1982a). In contrast to the coxo-trochanteral joint, the mechanoreceptors of the femoro-tibial joint include: the mtFCO, the flexor strand, tactile hairs located around the femoro-tibal joint, campaniform sensilla (which signal cuticular stress), a muscle tension receptor (Theophilidis and Burns, 1979; Matheson and Field, 1995) and five multipolar sensory cells (referred to a multipolar joint receptors, Pflüger and Burrows, 1987) arranged in three groups (Coillot and Boistel, 1968).

Multipolar neurones (Coillot and Boistel, 1968, 1969; Williamson and Burns, 1978), the muscle tension receptors (Theophilidis and Burns, 1979; Matheson and Field, 1995), and some mtFCO units (Usherwood *et al.*, 1968; Burns, 1974; Zill, 1985a; Matheson, 1990) respond to tibial extension. The multipolar receptors encode information over restricted ranges of femoro-tibial angle, their sensory ranges often overlapping (Pflüger and Burrows, 1987). The flexor strand may encode some parameters of tibial extension that the other receptors cannot (Bräunig, 1985).

Zill (1985a) investigated the contributions of the mtFCO flexor strand and apodeme complex to the tonic discharge recorded from the CO nerve, and demonstrated that the mtFCO and flexor strand receptor have complementary roles. Severing the apodeme complex eliminates the increase in firing associated with tibial flexion but leaves the discharge in response to joint extension intact. Conversely, severing the flexor strand produces normal responses to joint flexion, but eliminates the increase in activity in response to joint extension. This implies that the flexor strand is almost completely responsible for the increase in tonic response seen during tibial extension.

Isolating the role of the flexor strand is complicated since responses of the mtFCO and flexor strand are inextricably linked. The mechanical connection between the flexor strand onto the mtFCO means that manipulation of one component must influence the other. This fact is highlighted by the presence of neurones situated ventrally within the mtFCO scoloparium which are capable of responding to either tibial extension, or to elongation of the flexor strand (Zill, 1985a).

However, the response of the flexor strand does complement that from the mtFCO scoloparium in other respects. Rotation of the femoro-tibial joint

causes reciprocal displacement of the mtFCO apodeme complex and flexor strand and so the two attachments consequently elicit different reflex effects (Field and Burrows, 1982). Displacement of either attachment to mimic tibial flexion excites extensor tibiae motor neurones whilst mimicking tibial extension excites the flexor tibiae motor neurones. In each case the strongest effects occurred during maximum stretching of either component; the flexor strand is most effective when the tibia is in the extended position whilst the apodeme complex is most effective at flexed positions. Despite the fact that displacement of the flexor strand can stimulate units in the mtFCO scoloparium (Zill, 1985a), qualitative differences between the reflexes elicited by either component convinced the authors (Field and Burrows, 1982) that the phenomena observed were not due to parallel mechanical stimulation of the same sensory units. These results indicate that the flexor strand plays an important role in femoro-tibial reflexes when the tibia is in extended positions.

The central connections of the strand receptor have been traced with respect to these reflexes. The strand receptor afferent makes an excitatory connection with a spiking local interneurone in the metathoracic ganglia (Pflüger and Burrows, 1987). The strand receptor does not synapse directly with motor neurones, unlike some CO afferents.

The current account has provided the first detailed description of strand receptor ultrastucture in the locust.

7.5.2 Femoro-Tibial Joint Receptor (ftjR)

Unlike other documented femoral mechanoreceptors the dendrite of the previously undescribed ftjR travels the length of the femur and crosses the femoro-tibial joint to associate with the tibia before inserting onto the cuticular rod. Its dendritic processes are elongated by articulation of the apodeme complex cuticular rod within the femur. The articulation between the distal end of the mtFCO cuticular rod and the tibia appears to be a favourable site to monitor femoro-tibial relations, the angle between the cuticular rod and the tibia increasing from approximately 30° to 180° over the entire femoro-tibial range. In addition, this situation means that both receptors are affected by the same stimulus. One receptor (ftjR) may monitor the input stimulus to a second mechanoreceptor (mtFCO). Such an arrangement has potential implications regarding the central processing of these signals. Comparing the discharge of the two receptors

at a central level may provide additional sensory information regarding femoro-tibial relations.

The mechanical problems associated with a dendrite crossing the femoro-tibial joint to innervate the ftjR are overcome in two ways. The ftjR is anchored near the joint articulation to avoid excess dendritic shearing. In addition the thick sheath with associated fibrils should protect the receptor dendrite from kinking/shearing.

Both the flexor strand and the ftjR share a similar ultrastructure with the crayfish stretch receptor (Tao-Cheng *et al.*, 1981). They all share: branching dendrites ('primary, dendritic branches and dendritic tips' (Tao-Cheng *et al.*, 1981)) which ramify within the surrounding tissue at distal levels, naked dendrite tips which are axially embedded in extracellular matrix, extracellular spaces associated with the dendrites at proximal levels, and similar associated clusters of dendritic tips with vesicles located within them.

Tao-Cheng *et al.* (1981) examined the ultrastructure of the crayfish stretch receptor fixed in either the stretched or relaxed positions. The authors proposed that the dendritic tip membrane is susceptible to stretch and may be the region where the generator potential is produced.

The ftjR further increases the already considerable potential for known sensory input into the mtFCO nerve from other receptors. This has implications regarding previous studies in which gross discharge recorded from the mtFCO nerve was attributed to the mtFCO alone but in fact may have included signals from other receptors. Crushing all distal nerves "by insertion of an insect pin up the shaft of the tibia" (Zill and Jepson-Innes, 1988) is not sufficient to ensure that all the afferent sensory discharge and subsequent modulation of motor activity can be attributed to the mtFCO .

It seems likely that discharge from the ftjR provides significant proprioceptive input additional to that derived from the flexor strand, the mtFCO and other femoral receptors. Cruse *et al.* (1984) demonstrated such integration of proprioceptive information from a range of mechanoreceptors in the stick insect *Carausius morosus*. They showed that the two coxal hairplates, the trochanteral hairplate, the coxal hair rows and the msFCO all supplied unique information to the central nervous

system which was used to calculate the target point for hind leg protraction during walking. It is probable that different proprioceptive outputs from the mechanoreceptors of the femur, including the flexor strand and ftjR, also combine together to produce to the total proprioceptive response.

The ftjR is a type of receptor that has never been described before. Unlike previously described stretch receptors (Osborn 1963, 1969; Tao-Cheng *et al.*, 1981), the terminal dendritic processes are not embedded within an elastic ligament but spread out to terminate individually, associated only by a thin sheet of extracellular matrix.

Figure 7.1

This figure, reproduced from Chapter 3, summarises the morphology of the mtFCO flexor strand at several proximo-distal levels. The flexor strand consists of a fatty sheath (fs) which contains the branching dendrite of a 'strand-type' receptor (sr).

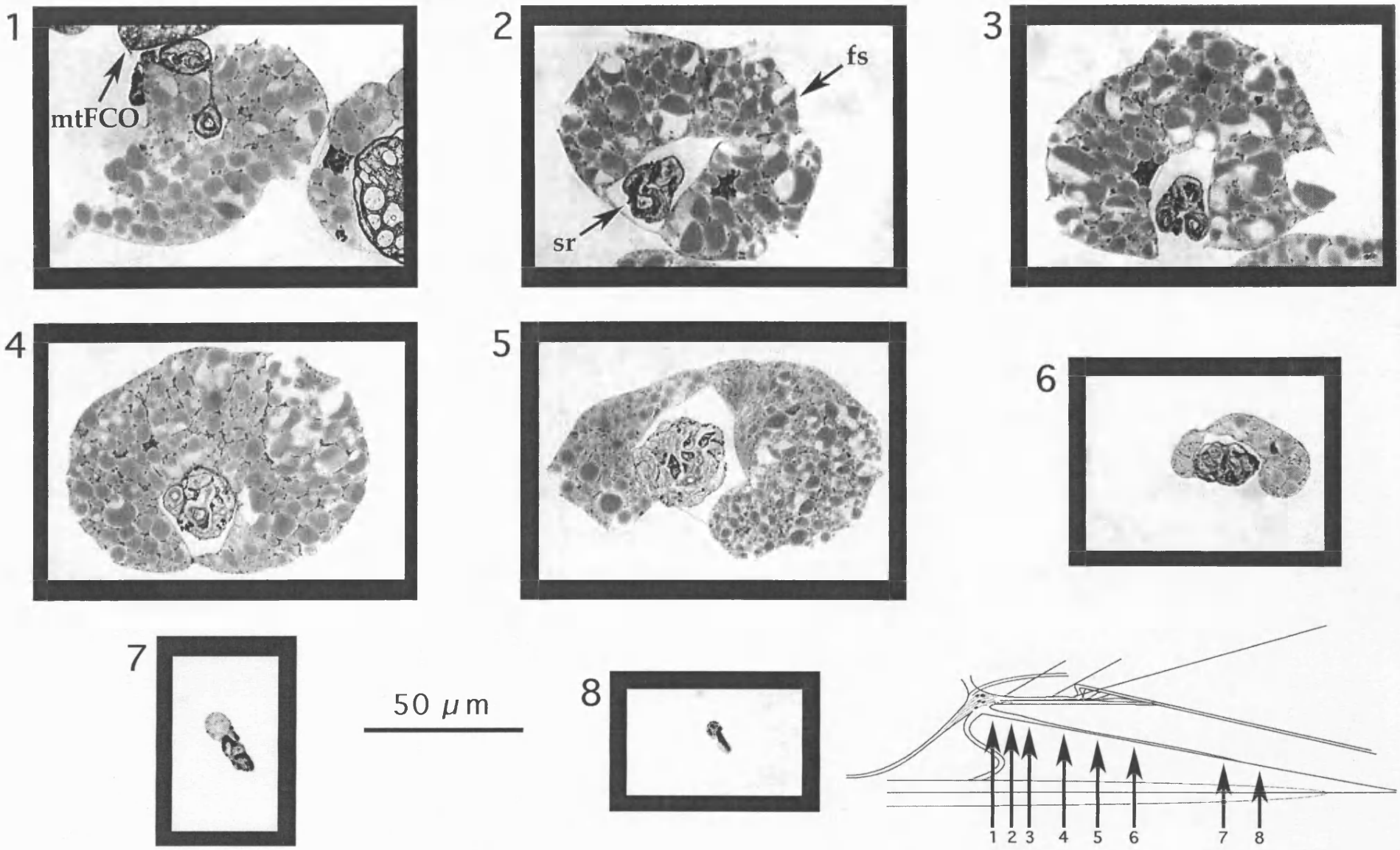
1
mtFCO
2
fs
sr
3
4
5
6
7
50 μm
8
1 2 3 4 5 6 7 8

Figure 7.2a, b

a

At the level at which the flexor strand leaves the mtFCO scoloparium, the strand receptor dendrite branches into two (d1 and d2), each branch being surrounded by glial wrappings (g). Acid Fuchsin-staining extracellular fibres (F) are located adjacent to the dendrite branches in a layer of extracellular matrix. The matrix also contains bundles of fine dendritic processes (arrows). The strand receptor is surrounded by a fatty sheath (s).

b

Cross section of the strand receptor immediately distal to the mtFCO scoloparium. At this level, extracellular spaces (ex) develop around the main dendrite branches (d1 and d2). The bundles of dendritic processes become larger and more numerous (arrows). g = glial wrappings; n = glial cell nucleus

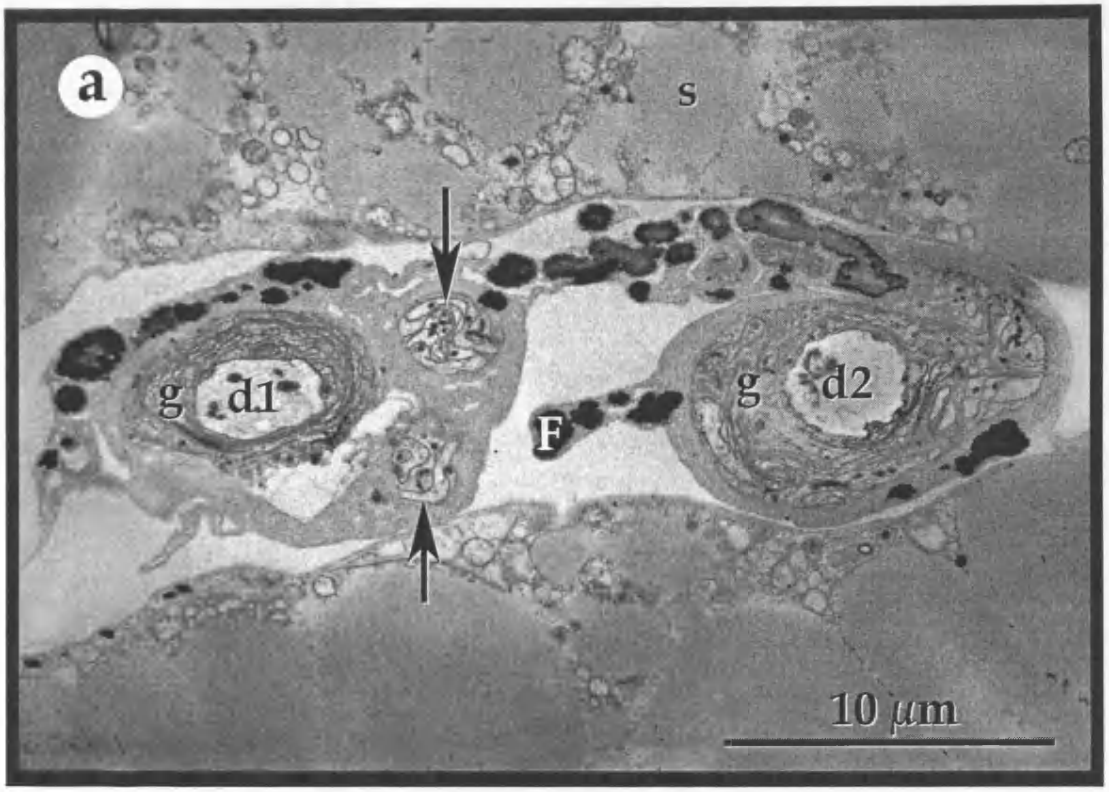
a
s
g
d1
F
g
d2
10 μm

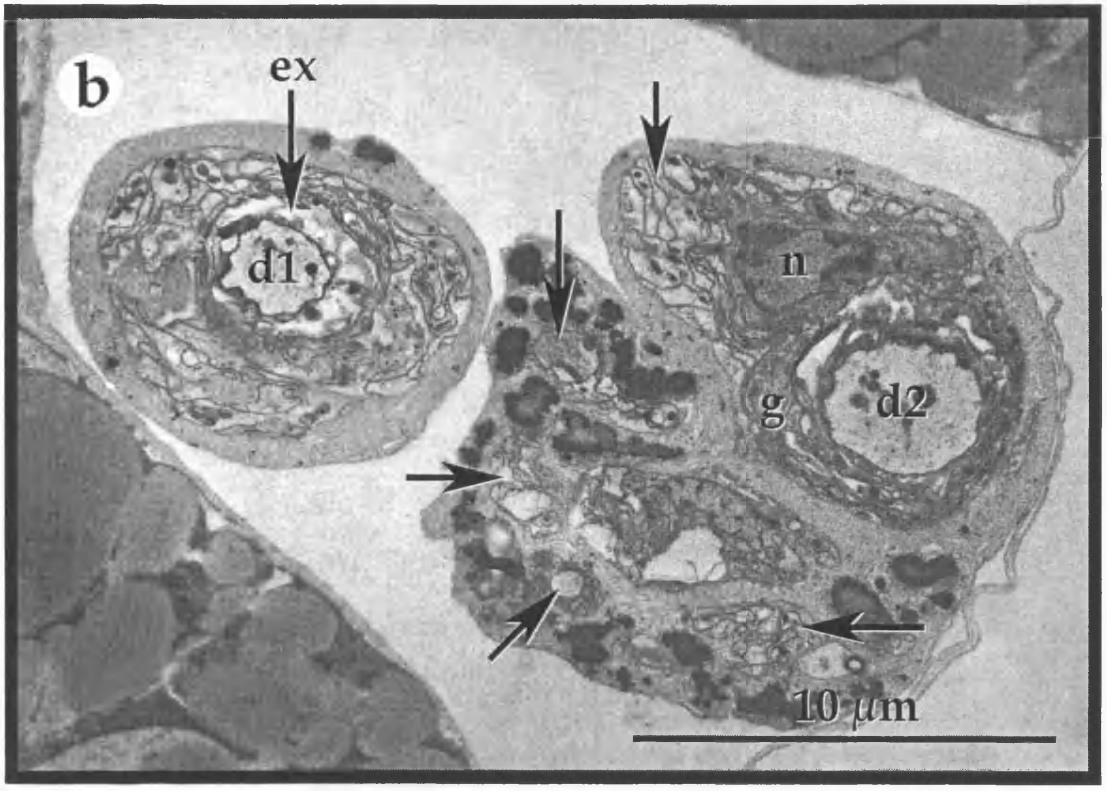
b
ex
d1
n
g
d2
10 μm

Figure 7.3a, b

a

Each main dendritic branch (d) is located within an extracellular space (ex) containing lightly-staining extracellular material. Glial wrappings (g) enclose the extracellular space and also form a continuous layer over the surface of the dendrite (arrowhead).

b

Bundles of dendritic processes (p) branch into the strand receptor's extracellular matrix (m) which contains both extracellular fibres (F) and fibrils (f). h = haemolymph space

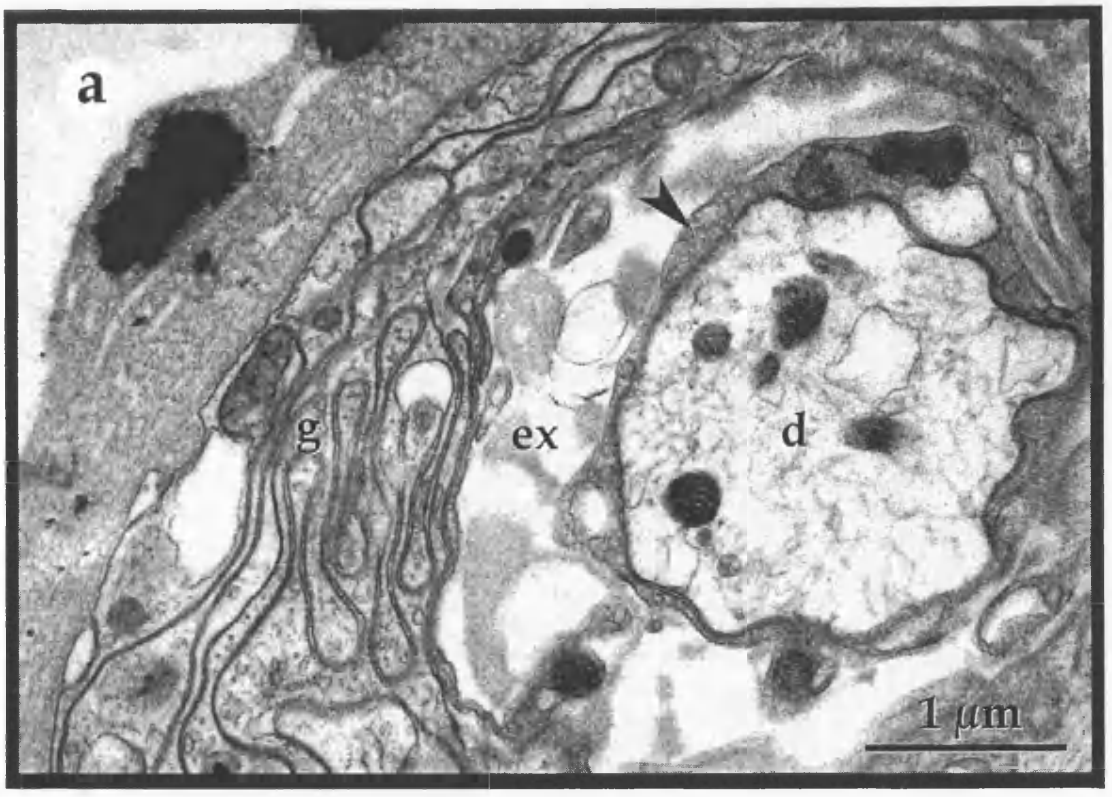
a
g
ex
d
1 μm

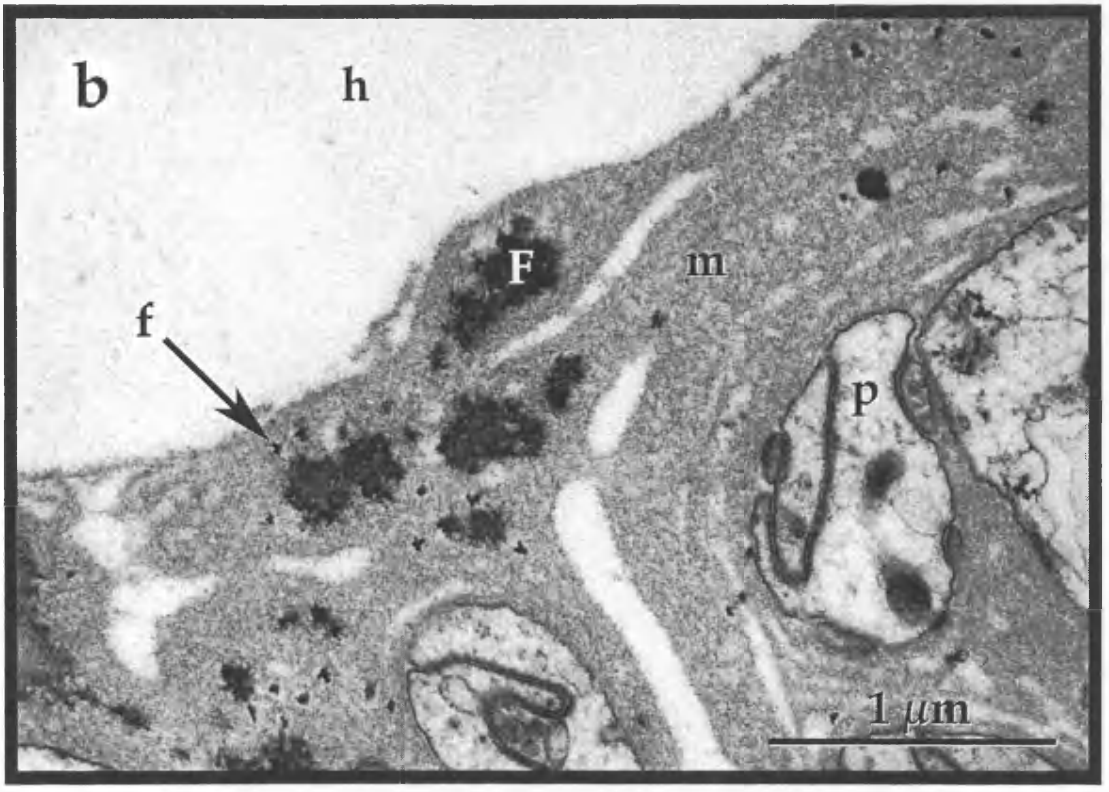
b
h
F
m
f
p
1 μm

Figure 7.4

The strand receptor increases in cross-sectional area as the dendrite branches (d1 and d2) send out bundles (b) of dendritic processes into the extracellular matrix (m). The dendritic processes lack glial wrapping and are often interdigitated in complex patterns. F = extracellular fibre; n = glial cell nucleus; ex = extracellular space

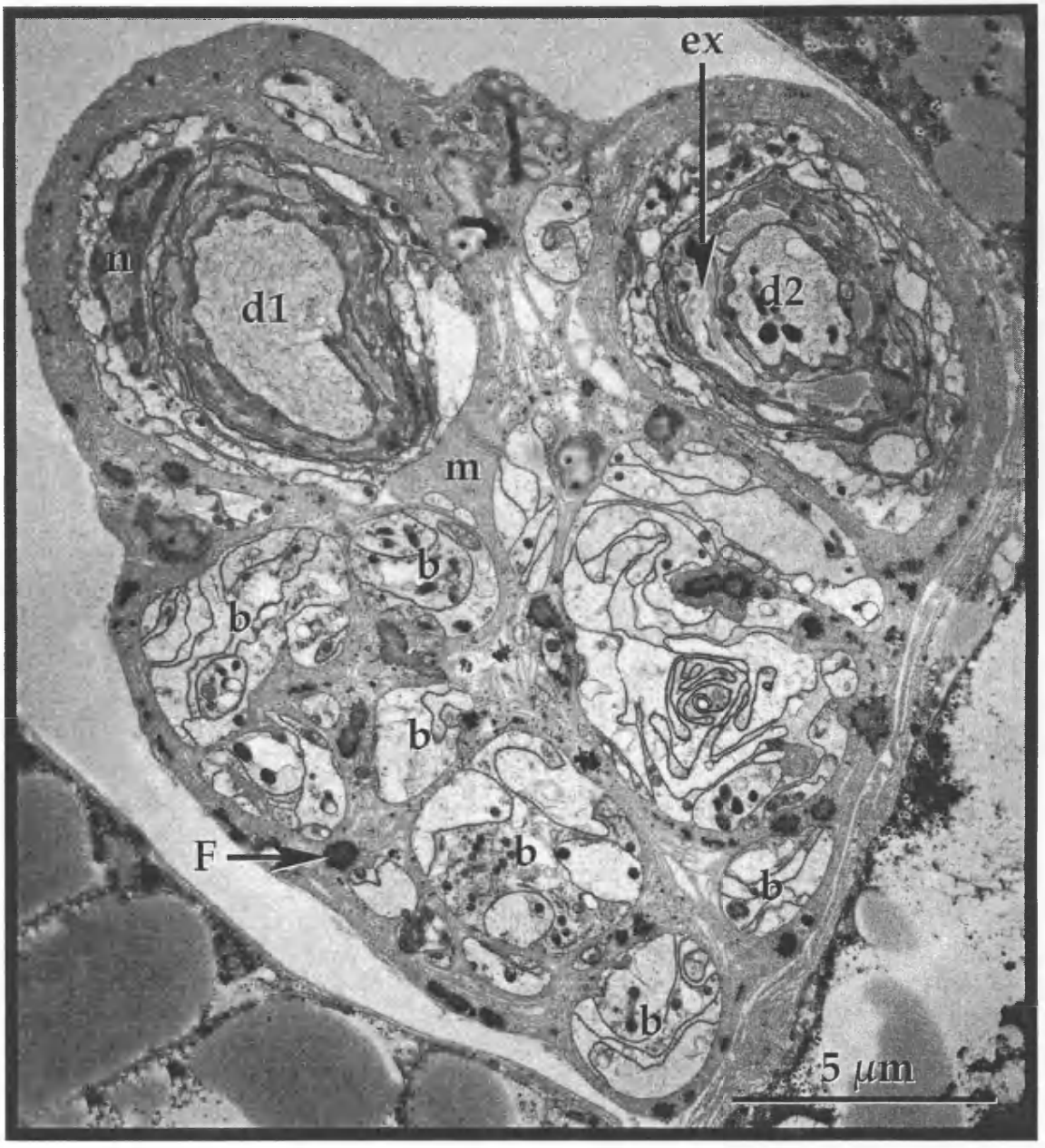
ex
n
d1
d2
m
b
b
b
F
b
b
b
5 μm

Figure 7.5

Distally the main dendrite branches become subdivided. At the level shown in this micrograph dendrite d1 can still be identified, whereas dendrite d2 has split into at least five branches (arrows). ex = extracellular space; n = glial cell nucleus

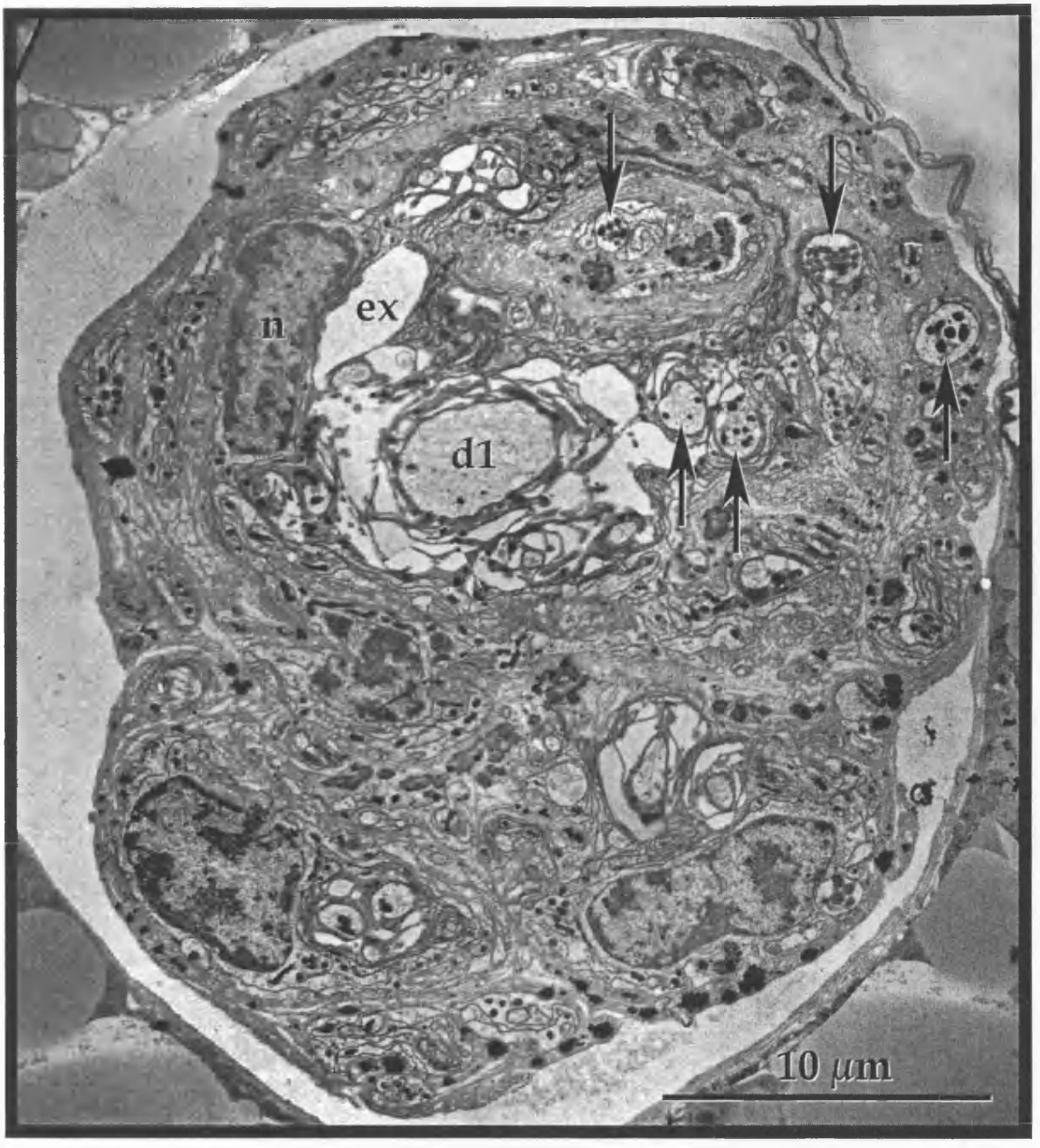
n
ex
d1
10 μm

Figure 7.6

At this proximo-distal level neither of the main dendrite branches can be identified, having subdivided into smaller dendrites. These remaining dendrites (d) are still sheathed by the glial cells (g) which ramify throughout the organ. No extracellular spaces remain within the strand receptor at this level. The bundles (b) of dendritic processes taper distally, resulting in a range of process cross-sectional areas. n = glial cell nucleus; F = extracellular fibre

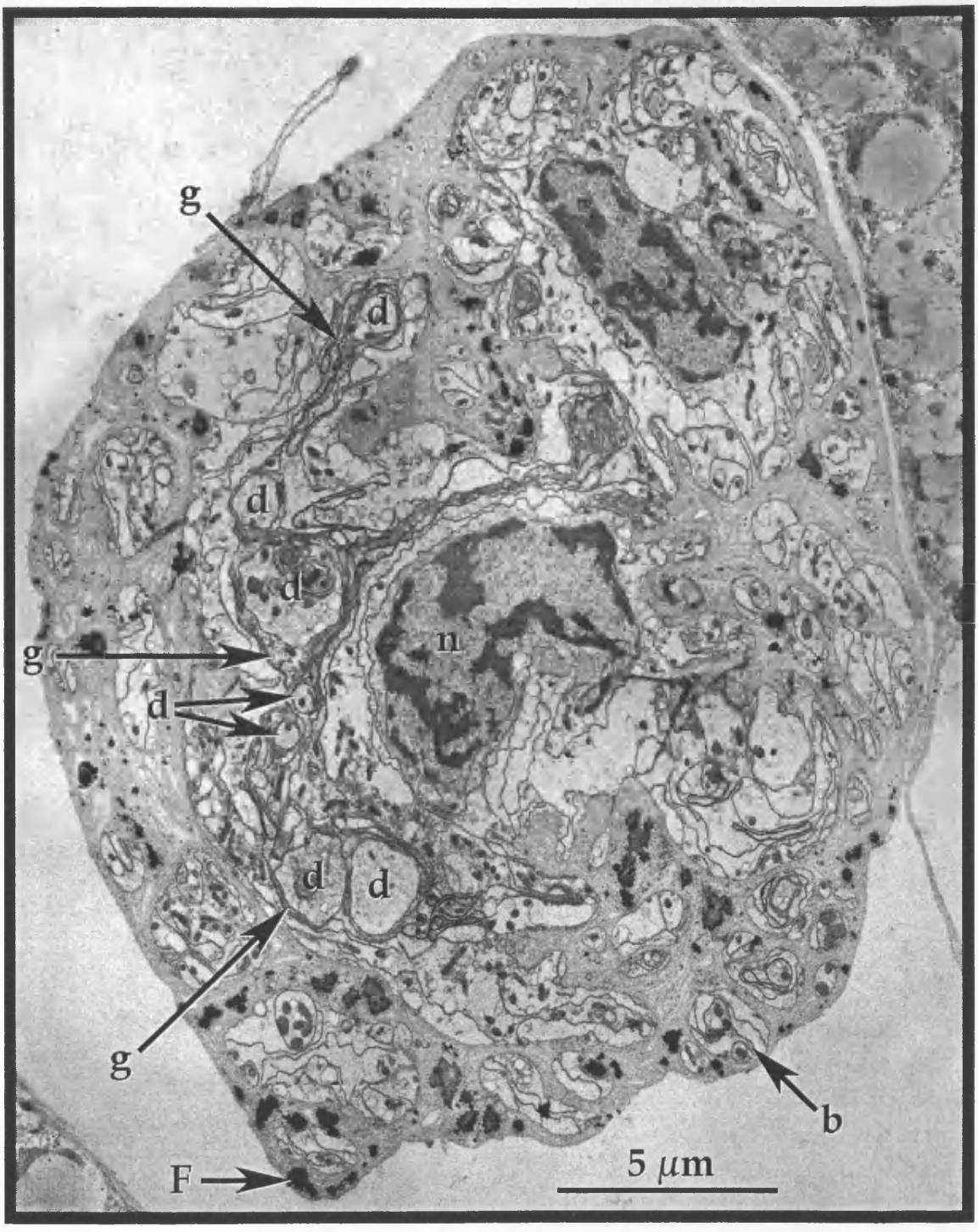
g
d
d
d
g
n
d
d
d
g
b
F
5 μm

Figures 7.7a, b

a

Dendrite branches (d) maintain their glial wrapping (g) as they split into smaller units.

b

The glial wrapping around the dendrites (d) is secured by septate desmosomes (arrows).

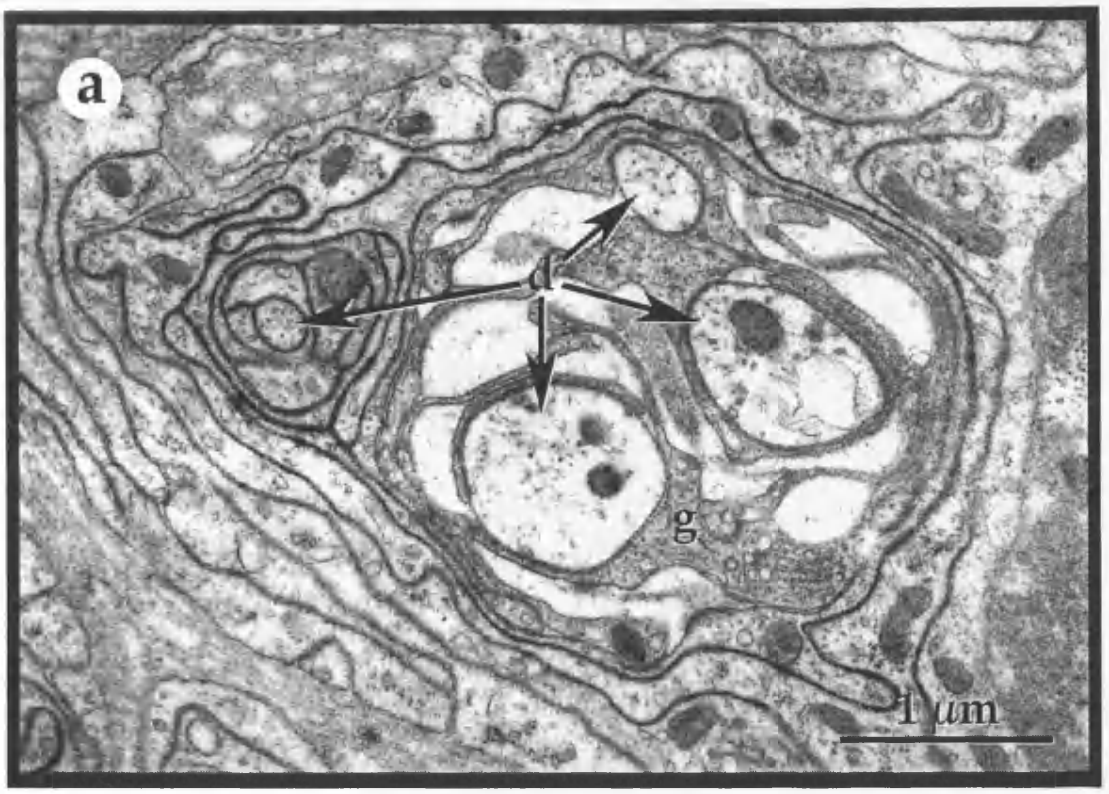
a
d
g
1 μm

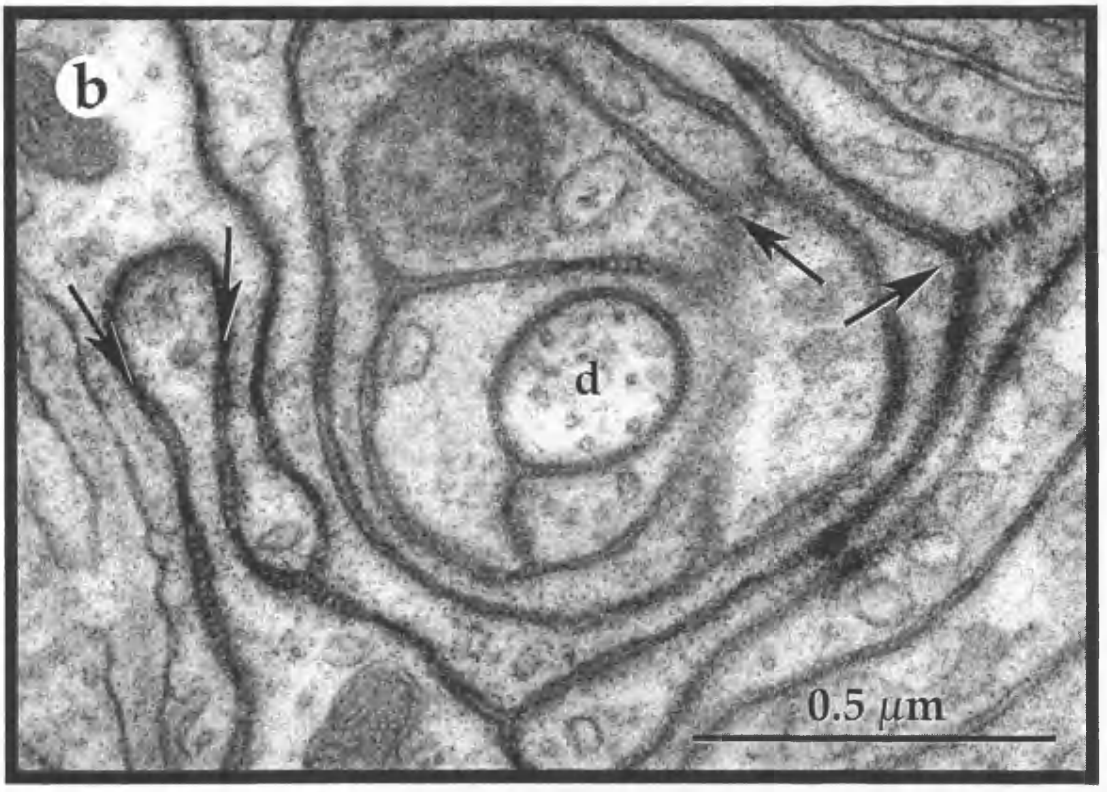
b
d
0.5 μm

Figures 7.8a, b

a

Bundles of dendritic processes are associated with both Acid Fuchsin-staining fibres (F) and extracellular fibrils (f) within the extracellular matrix (m). The processes contain both mitochondria (mtc) and vesicles (v). Each bundle of processes consists of approximately five interdigitating membrane-bound cytoplasmic fingers.

b

The cytoplasmic fingers or dendritic processes are separated by a consistent gap of 14.5 nm (±1.5 nm) which is continuous with the extracellular matrix (arrowheads).

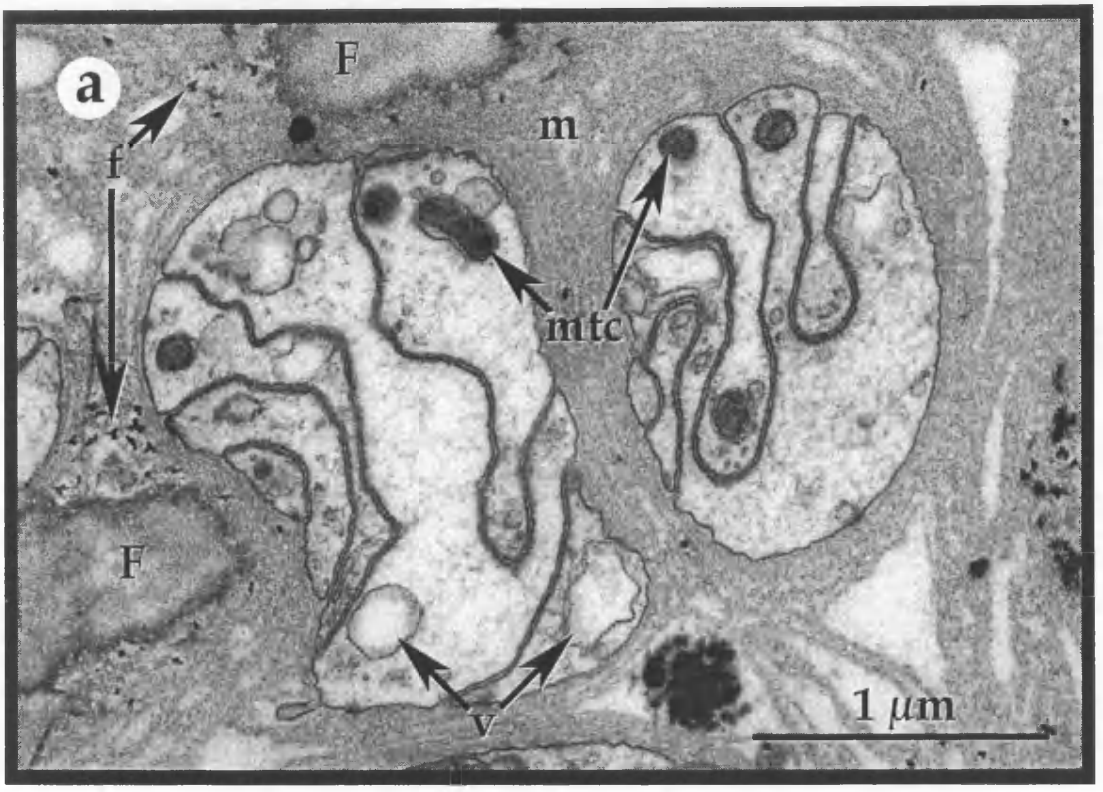
a
F
m
f
mtc
F
v
1 μm

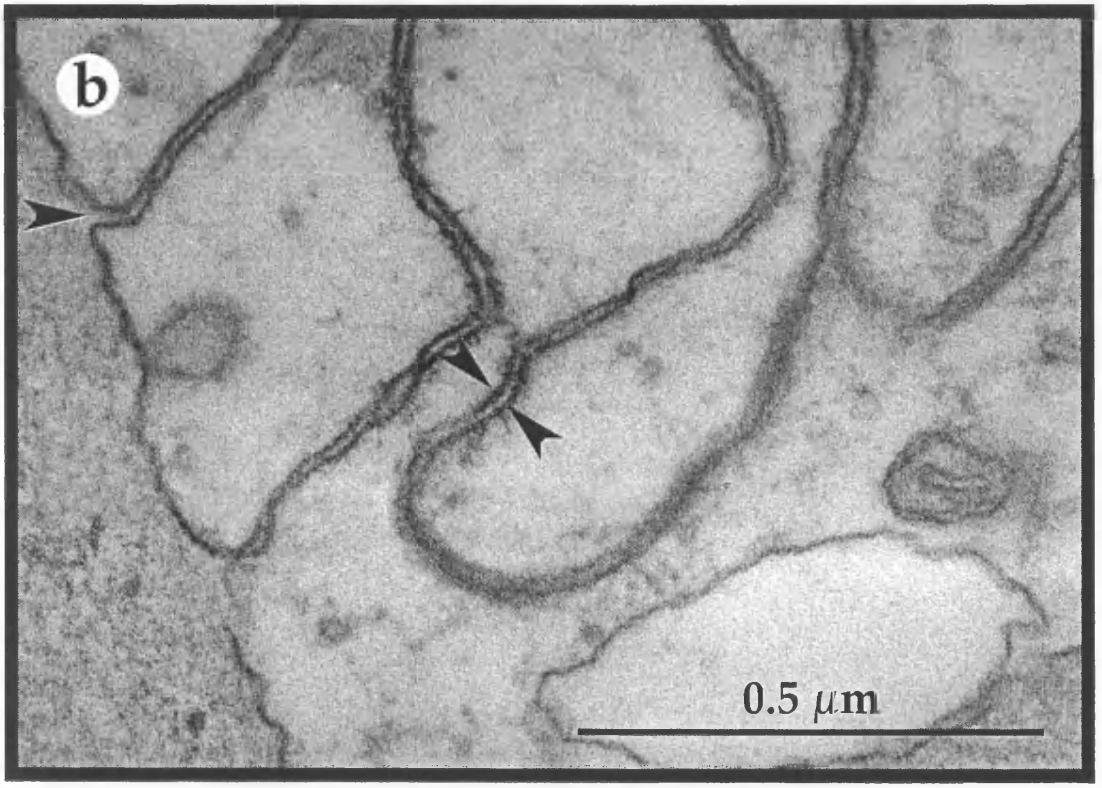
b
0.5 μm

Figures 7.9a-d

A consecutive series of electon micrographs showing the division of a bundle of dendritic processes (B1) into two as it travels distally (a-d) within the strand organ. In addition, a second bundle (B2) can be observed throughout the series. This bundle of processes tapers distally.

a

Two of the cytoplasmic 'fingers' (1, 2) comprising the dendritic bundle B1 start to move away from the rest of the bundle, pinching part of a third finger (3) between them.

b

As bundle B1 begins to split into two, the third dendritic finger (3) elongates to form a thin neck (arrow).

c

The third cytoplasmic finger branches as the bundle splits into two. One branch runs distally with the original process (3') whilst the second joins the new bundle (3'').

d

As new bundle continues to run distally, a new cytoplasmic finger (4) arises to augment it.

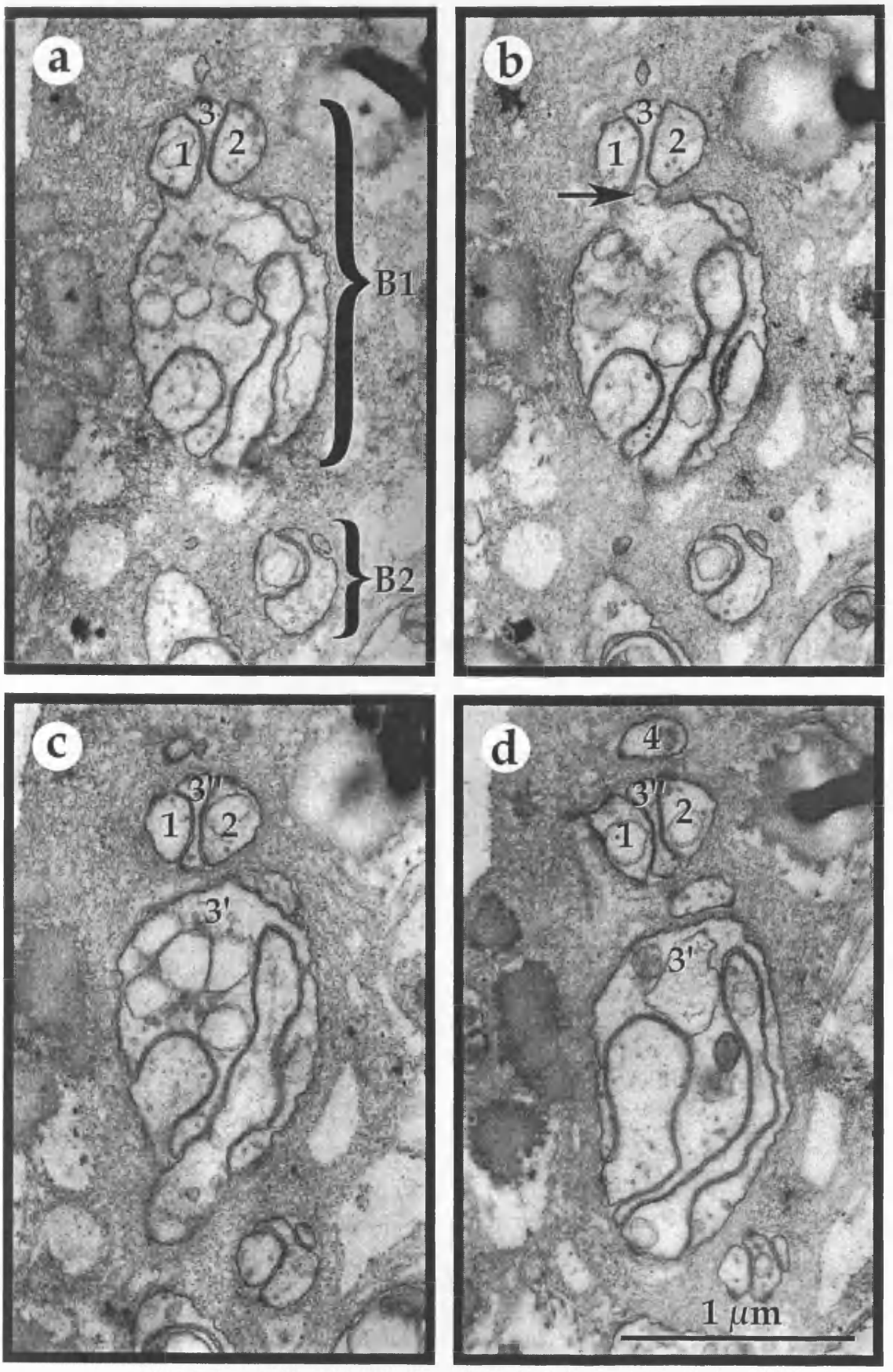
a
3
1
2
B1
B2
b
3
1
2
c
3''
1
2
3'
d
4
3''
1
2
3'
1 μm

Figure 7.10

At this proximo-distal level the cross-sectional area of the flexor strand is reduced. The remainder of the sheath is situated dorsally (Sd) and ventrally (Sv) relative to the strand receptor (sr). Two sheath cell nuclei (Sn) are visible at this level. Many of the dendritic process bundles have tapered to such an extent that they consist of two or three cytoplasmic fingers only (arrows). n = glial cell nucleus

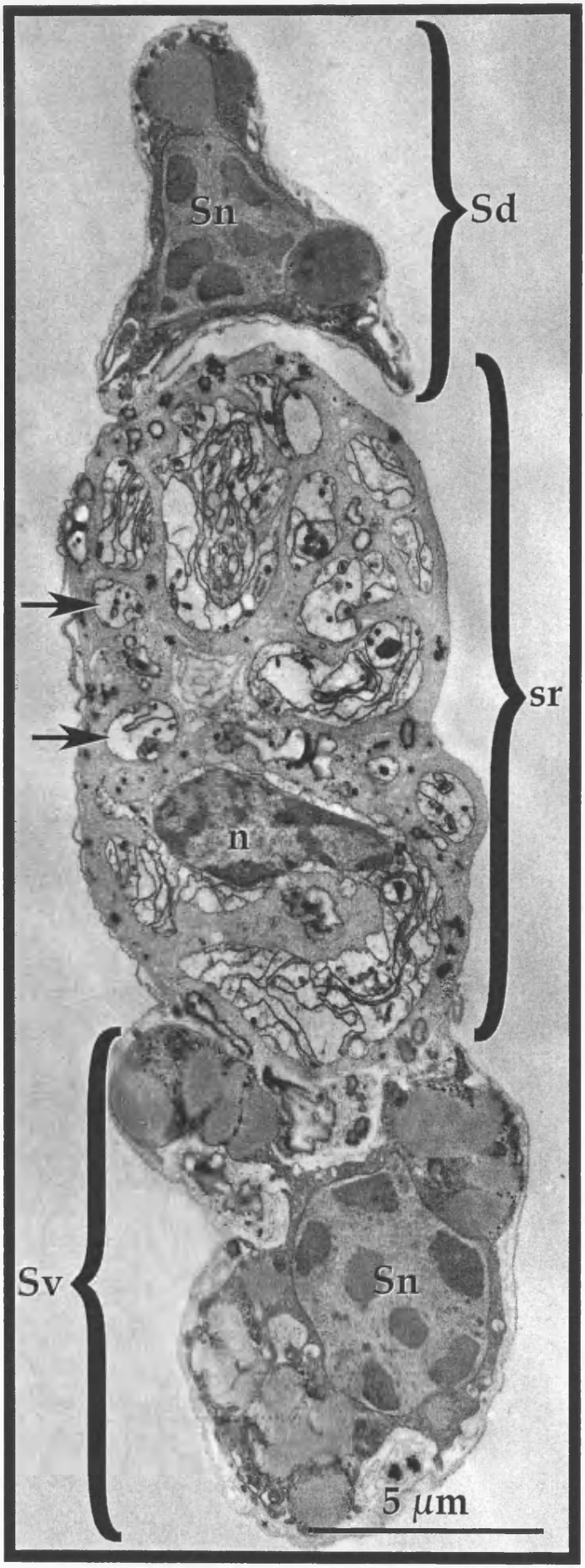
Sn
Sd
sr
n
Sv
Sn
5 μm

Figures 7.11a, b

These micrographs show dendritic processes immediately proximal to their distal terminations. At this level the processes often contain vesicles (v) (**a**) and/or mitochondria (mtc) (**b**). m = extracellular matrix

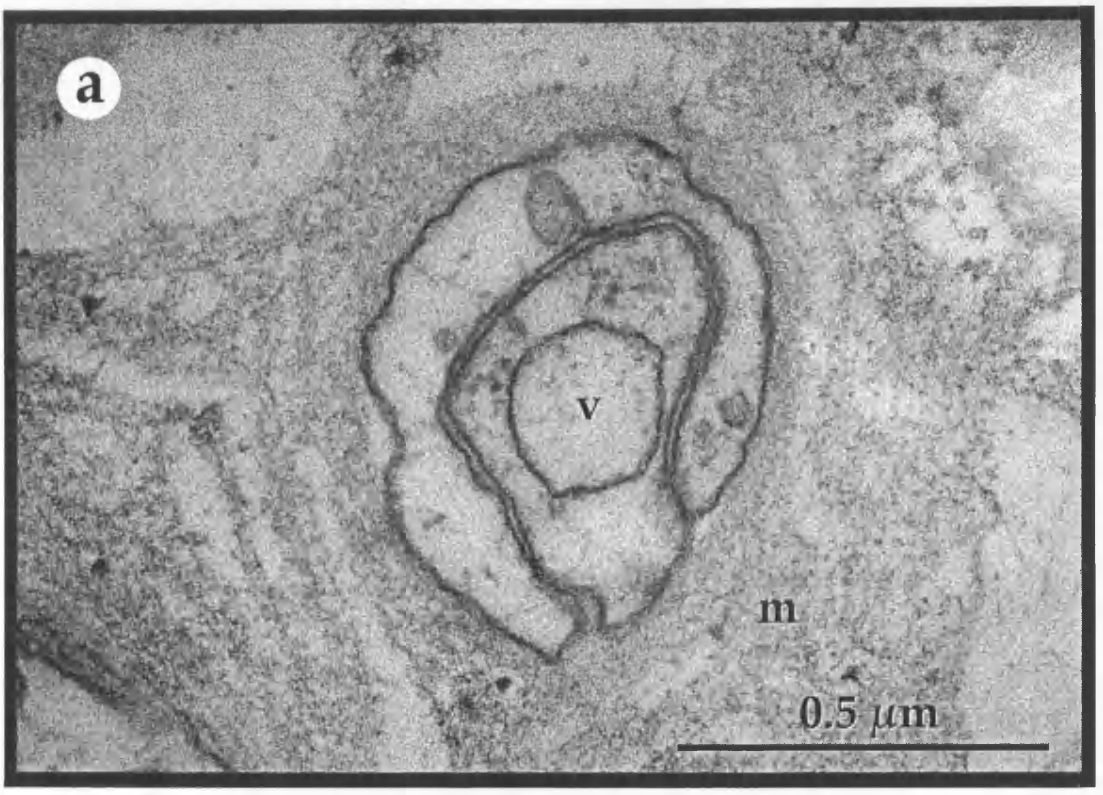
a
v
m
0.5 μm

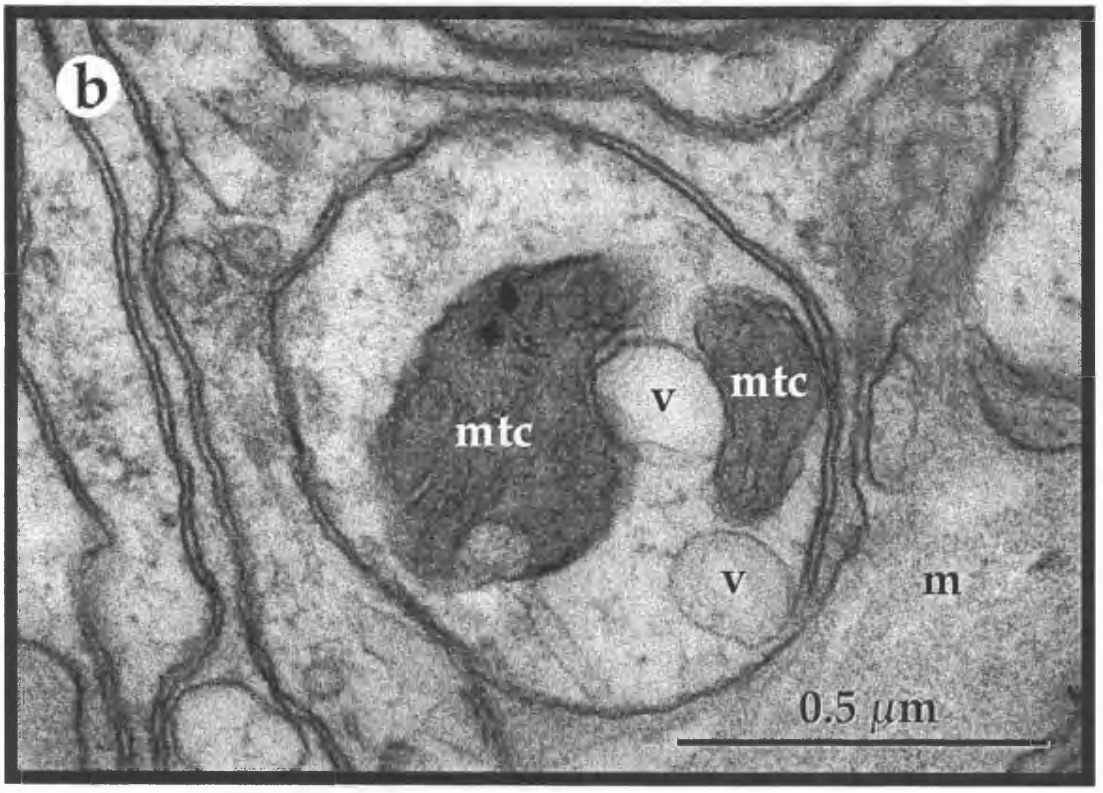
b
mtc
v
mtc
v
m
0.5 μm

Figure 7.12

This montage of digital images captured from an osmicated preparation, shows the morphology of the knee organ. Distal is to the right. The ftjR dendrite (d) branches ventrally from the cuticular nerve (c) and joins the tibia (t) ventral to the origin of the mtFCO cuticular rod. Dendritic processes (p) run dorsally along the proximal margin of the tibia to terminate upon the rod (r).

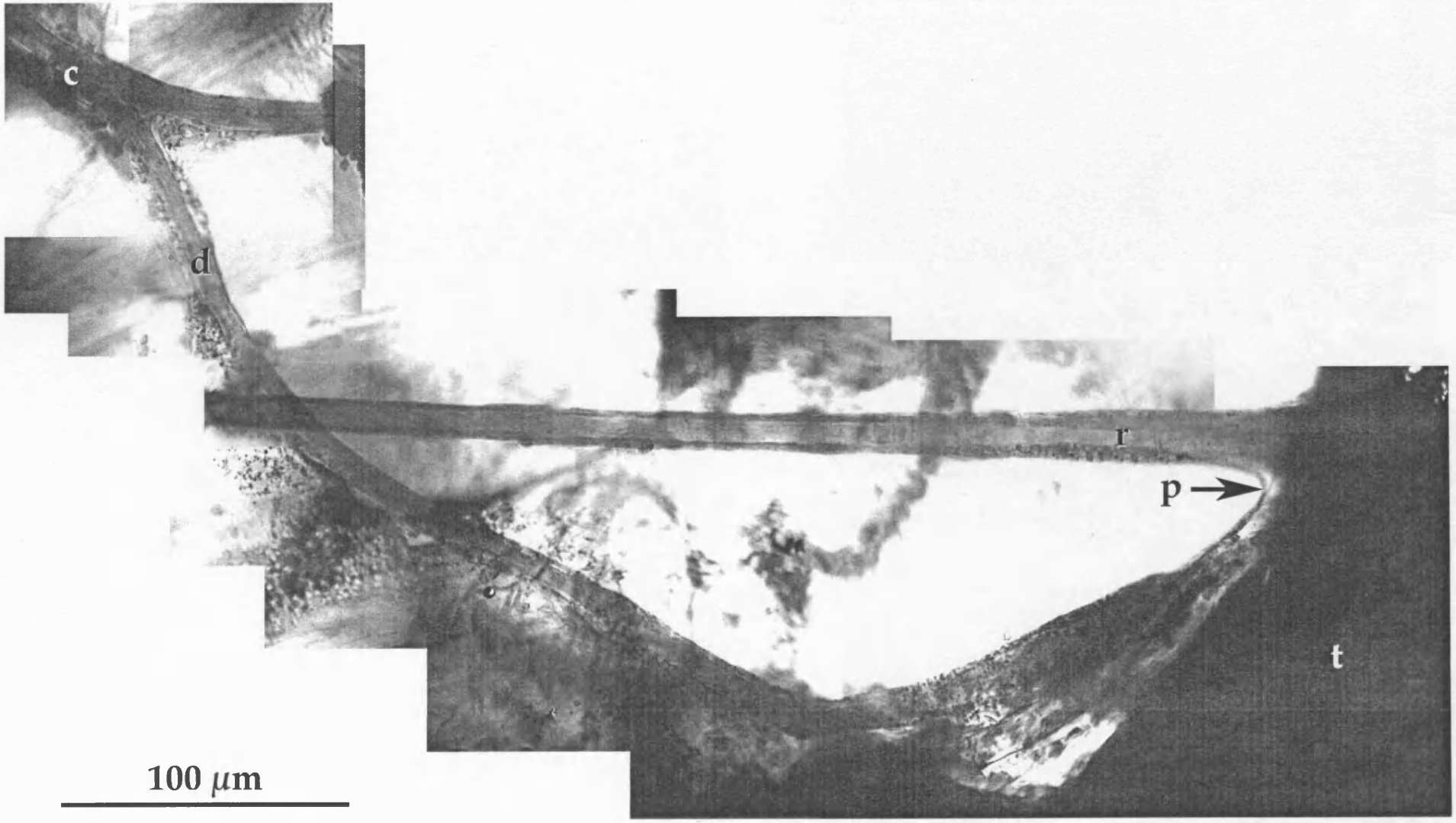
c
d
r
p
t
100 μm

Figures 7.13a, b

a

This scanning electron micrograph show the position of the ftjR in the distal femur. Distal is to the right. The cuticular nerve (cn) is located dorsally within the femur. Short branches of the nerve (b) run dorsally to innervate cuticular receptors. The ftjR branches from the cuticular nerve (arrow) approximately 500 μm proximal to the level of the femoro-tibial articulation. r = cuticular rod; t = tibia

b

This higher power micrograph, taken from the anterior side of the femur, shows that the ftjR dendrite (d) runs ventrally to the anterior side of the mtFCO cuticular rod (r). A short ventral attachment strand (v) anchors the knee organ dendrite to the tibia close to the centre of rotation of the femoro-tibial joint. The knee organ dendritic processes (p) extend dorsally along the proximal edge of the tibia to terminate at the distal origin of the mtFCO cuticular rod (r).

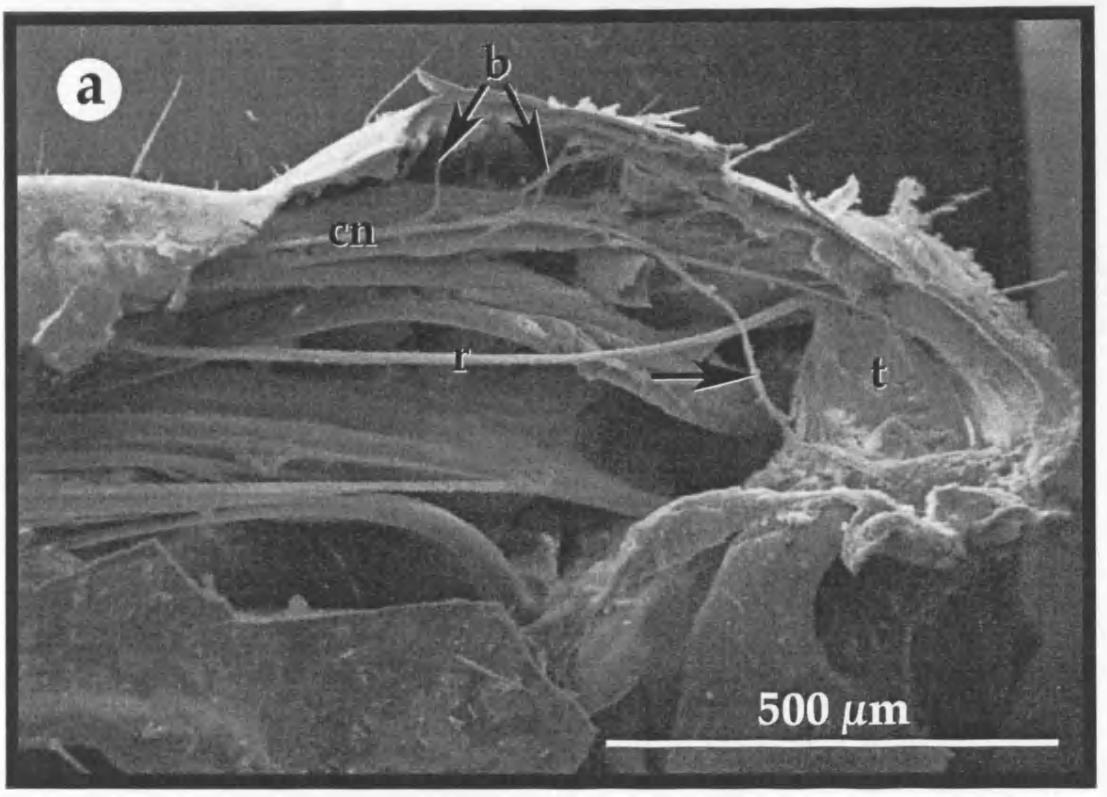
a
b
cn
r
t
500 μm

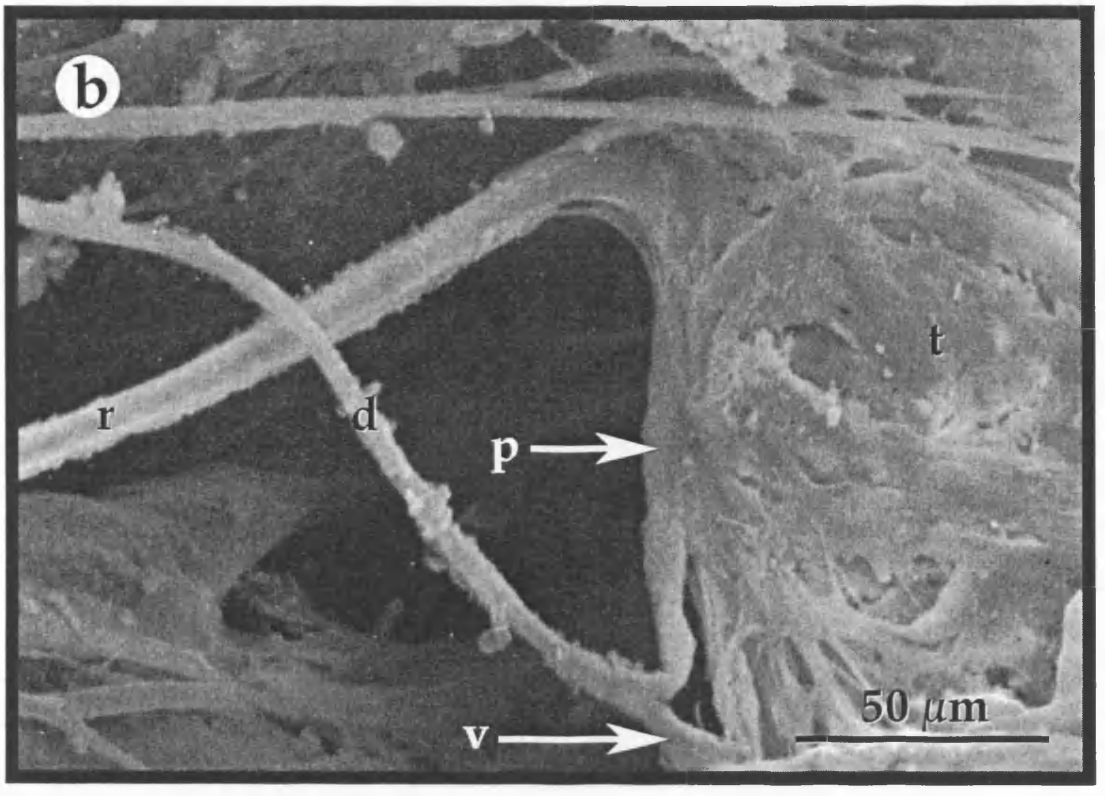
b
t
r
d
p
v
50 μm

Figure 7.14

These figures show the way in which the ftjR is stimulated by changes in femoro-tibial angle. Distal is to the right. At a femoro-tibial angle of 30° (**a**), the angle between cuticular rod (r) and the proximal margin of the tibia is approximately 70°. As the tibia is rotated to a femoro-tibial angle of 50° (**b**), the angle between the rod and the proximal margin of the tibia increases to approximately 90°. Thus, tibial extension causes elongation of the ftjR. d = ftjR dendrite; arrow = indicates the level at which the distal attachment of the ftjR inserts onto the rod

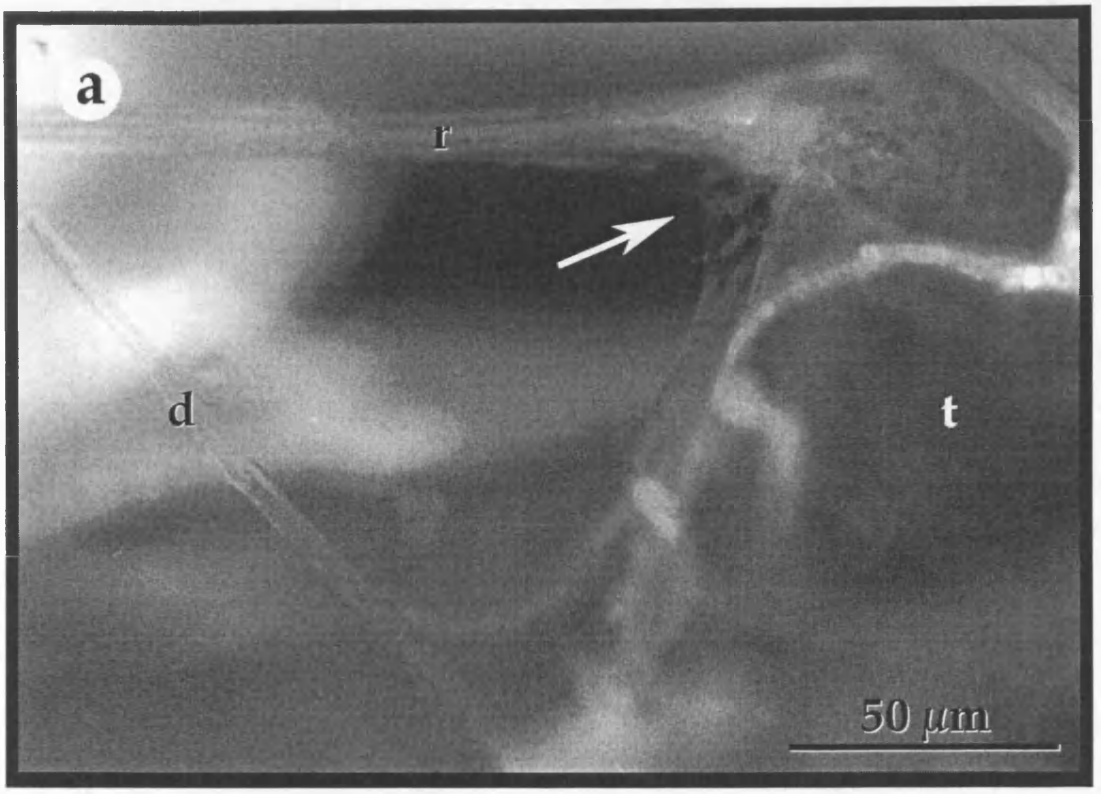
a
r
d
t
50 μm

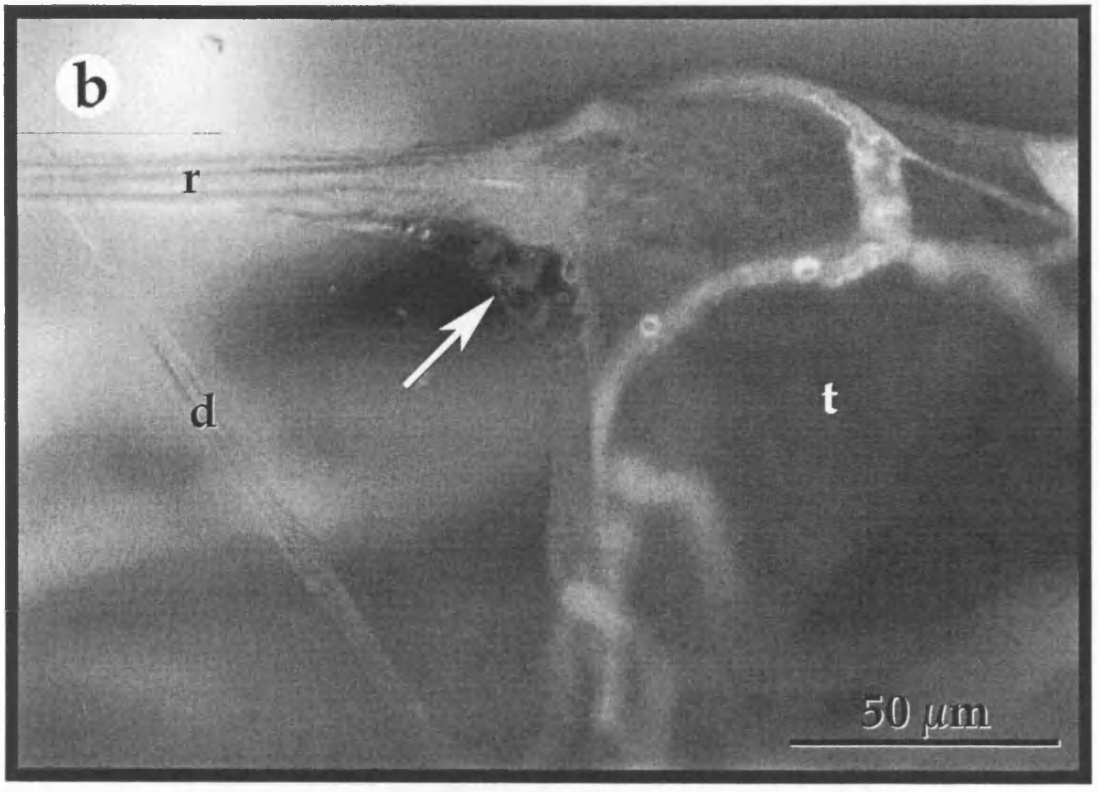
b
r
d
t
50 μm

Figure 7.15

Montage of transmission electron micrographs showing a transverse section through the ftjR. This section is taken at the level at which the ftjR crosses to the ventral femur prior to inserting onto the tibia. The ftjR consists of a single dendrite (d) at this level. The dendrite is surrounded by concentric layers of glial wrapping (g). The strand receptor is delimited by a thick layer of extracellular matrix (m) which is reinforced by electron dense extracellular fibrils (f). The organ is contained within a loosely fitting sheath (s) which is bound by an acellular layer of lightly-staining neural lamella (l). The dark objects within the cytoplasm of the sheath are in fact mitochondria. Extracellular spaces (ex) are visible both between concentric layers of glia, and between the strand organ and its outer sheath. n = sheath cell nucleus; h = haemolymph space

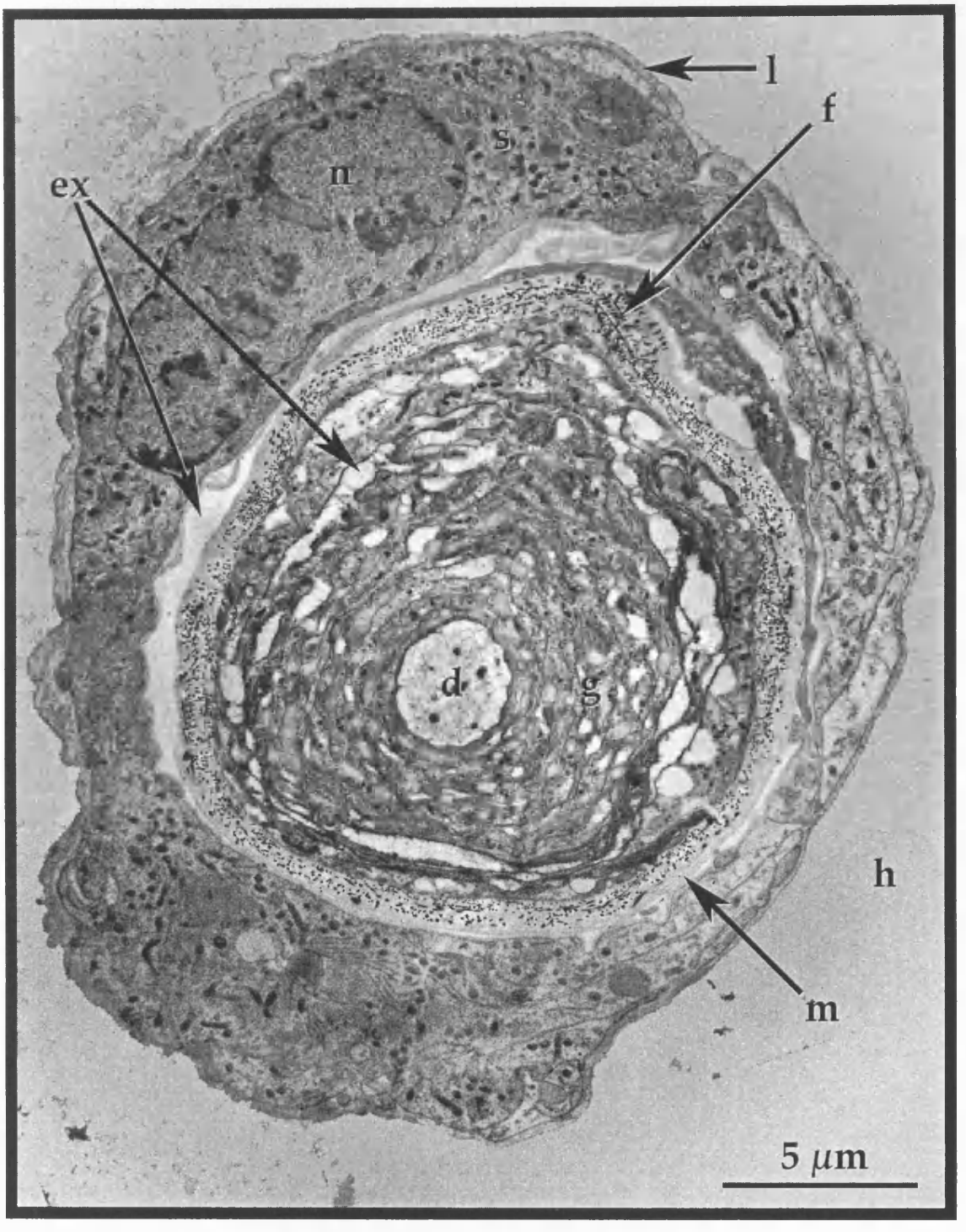
l
f
s
n
ex
d
g
h
m
5 μm

Figures 7.16a, b

a

As the ftjR runs up the proximal edge of the tibia, the single dendrite of the strand receptor branches into several bundles of dendritic processes. This transmission electron micrograph shows three bundles (b) of dendritic processes. Each bundle is surrounded by extracellular matrix (m) in which extracellular fibres (F) are embedded.

b

Each bundle takes the form of a group of membrane-bound cytoplasmic fingers which are tightly interdigitated with one another. m = extracellular matrix; F = extracellular fibres

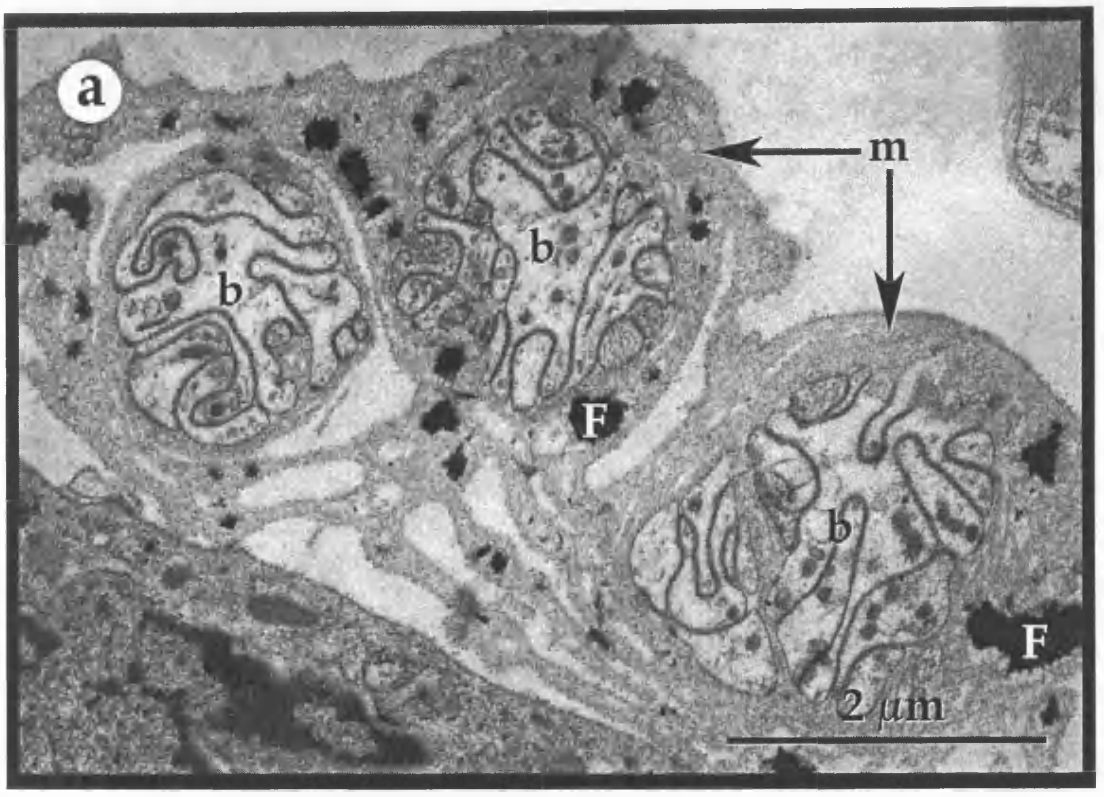
a
m
b
b
b
F
F
2 μm

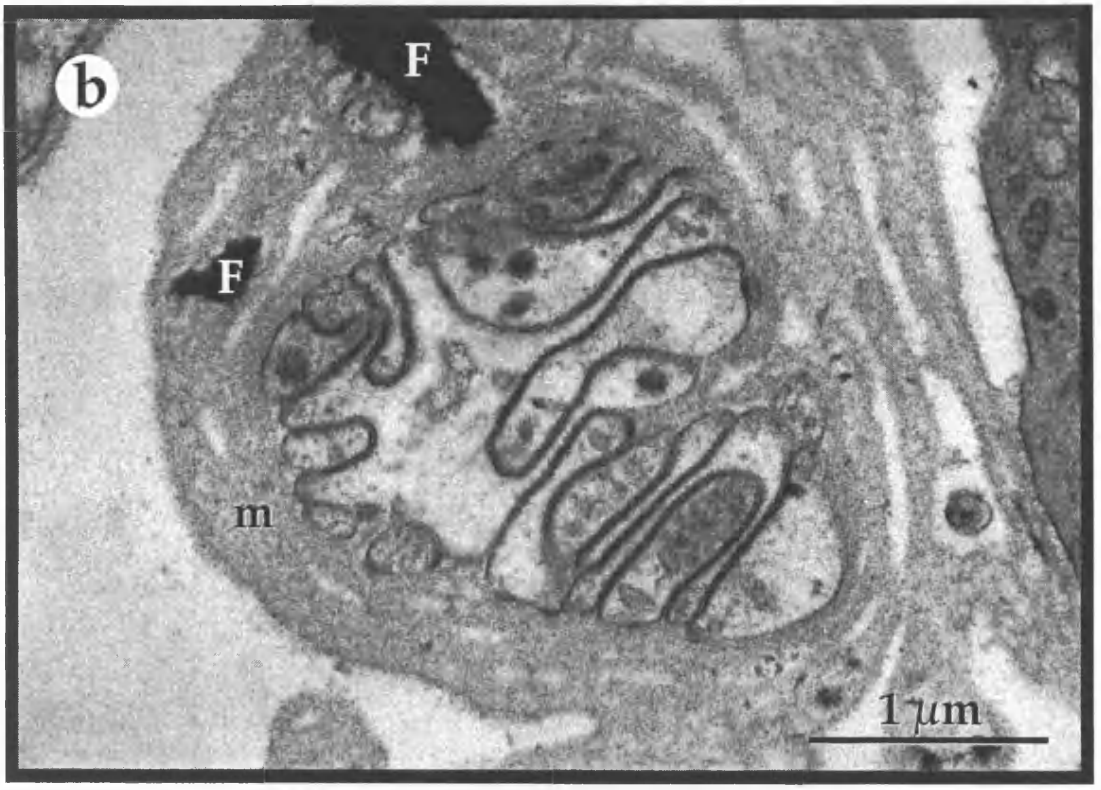
b
F
F
m
1 μm

Figure 7.17

This series of micrographs were taken at the level labelled 'p' in Figure 7.12. The bundles of dendritic processes (b) spread out laterally as they travel dorsally to the mtFCO cuticular rod. They remain interconnected by extracellular matrix strands (m). The tibia (distal) is to the right.

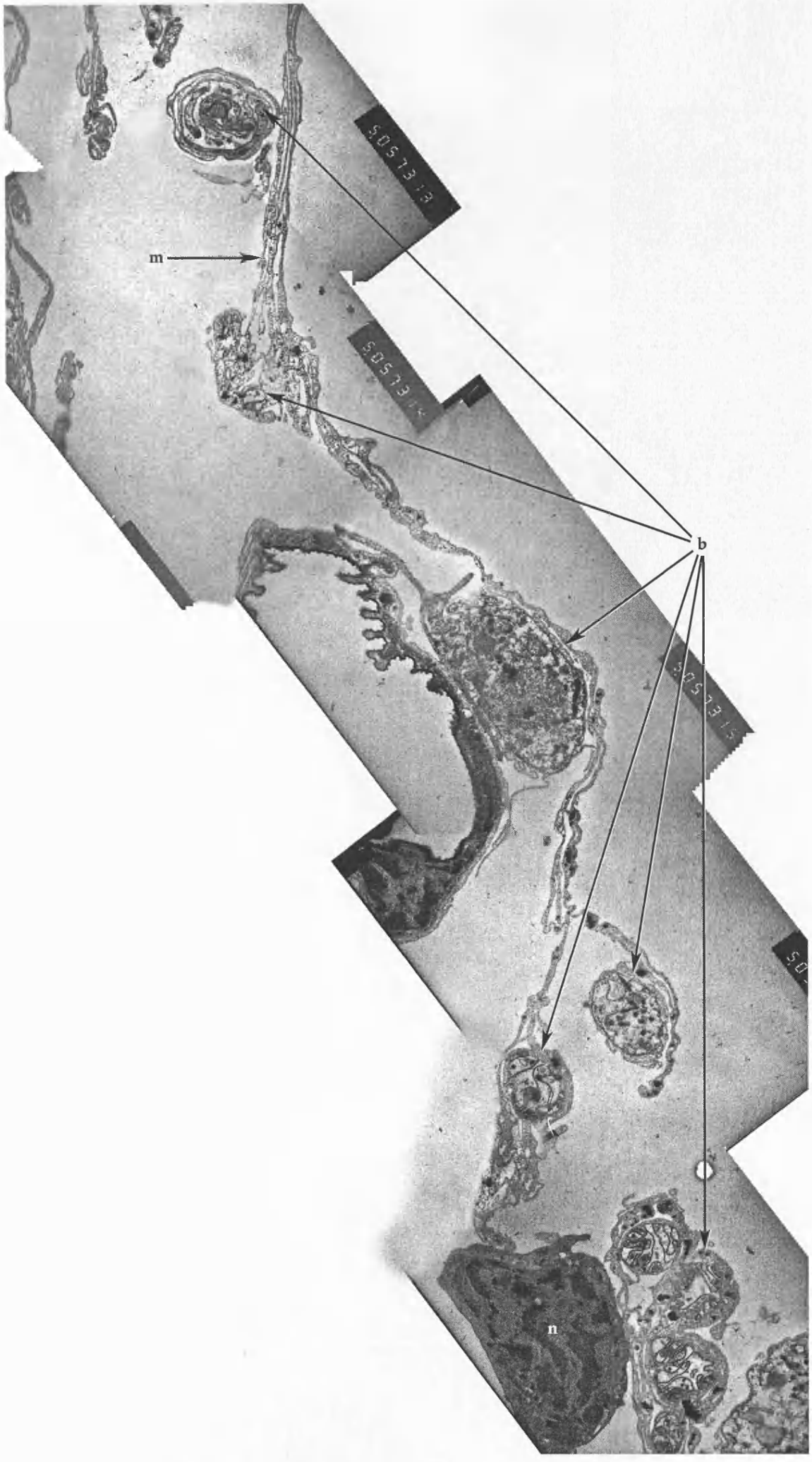
m
b
n

Figure 7.18

Longitudinal section showing the termination of a dendritic process (p) upon an epidermal cell (e) situated on the ventral side of the mtFCO cuticular rod. cf = cytoplasmic fingers of dendritic process

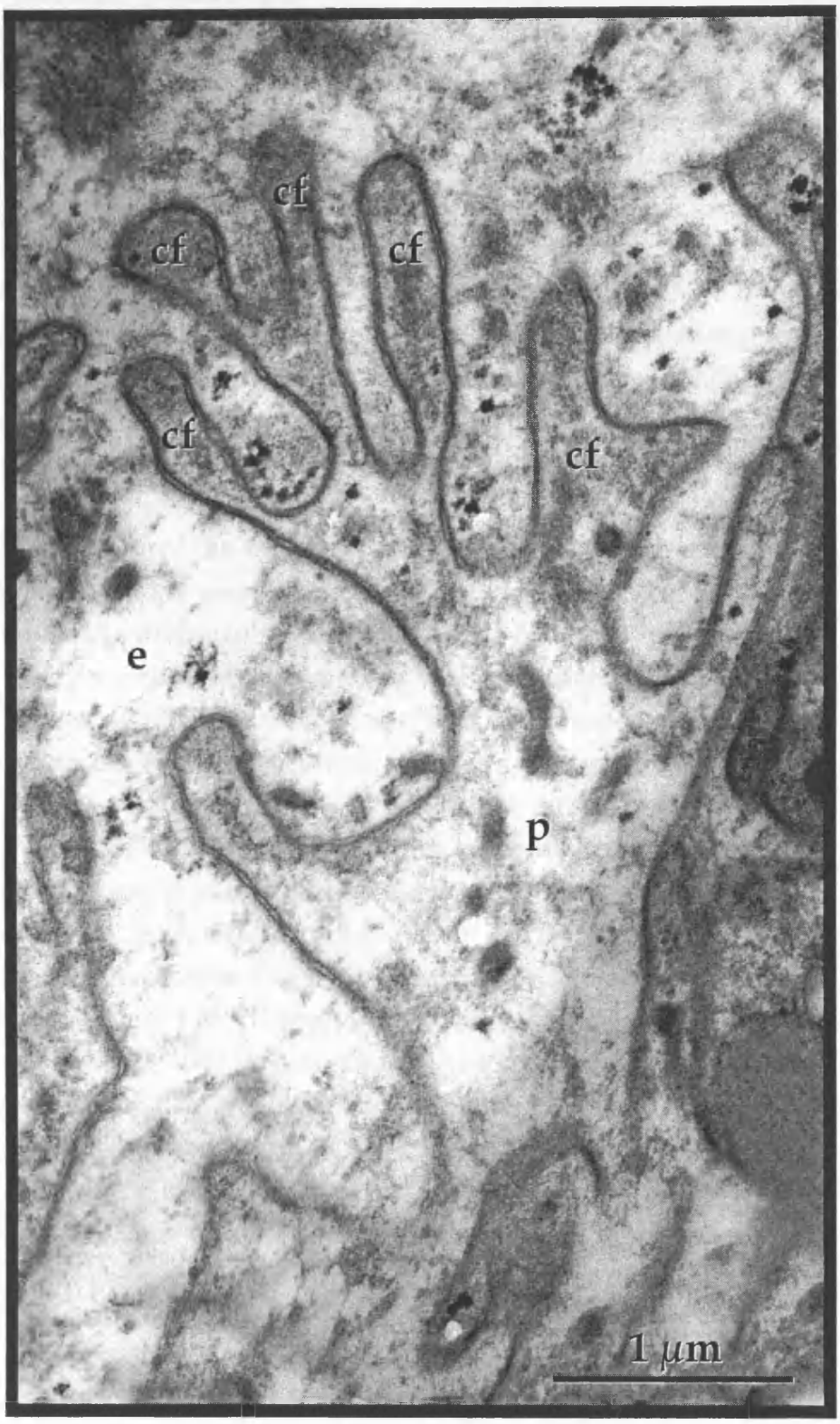
cf
cf
cf
cf
cf
e
p
1 μm

Chapter 8: General Disscusion

8.1 Implications of Scoloparium Organisation

This study confirms that the mtFCO scoloparium consists of twin fused scoloparia (Matheson and Field, 1990; Matheson, 1990, 1992a), and shows that each is innervated by one of two main branches of the mtFCO nerve (5b1). For the first time it has been shown that the mtFCO neurones can be further subdivided into at least 6 consistently-positioned discrete populations each innervated by its own nerve bundle. The positions and orientations of these populations are consistent with clusters of neurones identified on the basis of their physiological response characteristics (Matheson, 1990) and their central projection patterns (Matheson, 1992a).

Functional subdivision of the neurones within limb proprioceptors is not unique to the FCOs and is usually correlated with topographical representation at a central level (Mücke and Lakes-Harlan, 1995). Such subdivision at a peripheral level combined with topographical representation at a central level enables the integrated response of a number of individual sensilla to contain more information than could be encoded by the same sensilla considered individually. The benefits of such organisation can be demonstrated at three different levels of mechanoreceptor organisation: receptive fields, receptor aggregations and integrated organs. The femoral trichoid hairs of the locust metathoracic legs are arranged in receptive fields, their central projections being topographically organised at the level of the metathoracic ganglion (Burrows and Newland, 1993; Mücke and Lakes-Harlan, 1995) with denser receptor spacing around limb joints endowing their collective output with enhanced resolution over such key parts of the femur. The same is true of the locust mesothoracic legs (Mücke, 1991), with topographic representation within the mesothoracic ganglion (Mücke and Lakes-Harlan, 1995). In these situations there is no functional subdivision peripherally, all the receptors being physiologically alike. However, collectively they can encode not only the presence but also the position of a stimulus by virtue of their spatial distribution with respect to limb morphology. However, encoding the nature of the stimulus is limited by the characteristics of the particular receptor responding. Hairplates and hair rows, consisting of aggregations of tactile hairs (Tatar, 1976; Eliott, 1983; Cruse *et al.*, 1984; Dean 1984; Dean and Schmitz, 1992), possess

intermediate characteristics between those of isolated units arranged in receptive fields and of an integrated mechanoreceptive organ. Hairplates are used to transduce and modulate the feedback loops of the thoraco-coxal and coxo-trochanteral joints in stick insects and are both morphologically and functionally subdivided. Each hairplate consist of two subgroups of mechanoreceptive hairs (Tatar, 1976; Schmitz, 1986a, b) which are successively bent by the joint membrane during joint flexion. This morphological distribution of receptors allows similar mechanoreceptive units to respond differentially to the same stimulus, the sequential stimulation of hairs being due to the receptors relative positions with respect to the centre of joint rotation. However, only one subgroup of hairs functions as the transducer of the control loop and elicits the associated resistance reflexes (Schmitz, 1986a, b; Büschges and Schmitz, 1991). The second, larger group of hairs on each plate may play a role in the intersegmental coordination of leg movement (Dean and Schmitz, 1992). This diversity represents the functional subdivision of the hairplate.

Morphological and functional subdivision appears to have been conserved during the evolutionary integration of sensilla clusters to form internal proprioceptive organs. However, it is difficult to distinguish between morphological and functional factors contributing to the overall response of such an organ. It is unclear whether to attribute diversity in afferent response to functional factors (intrinsic properties of the receptive units) morphological factors (their positions relative to key structures), or a combination of the two. Previous authors have indicated the presence of functional organisation at a central level, the central projections of the mtFCO reflecting elements of both topographical (Burrows and Newland, 1993) and grouping of neurones by functional catagory (Nagayama and Newland, 1993). Mücke and Lakes-Harlan (1995) showed the same was true in the case of the scolopidial organs (including the proximal and distal scoloparia of the FCO; Field and Pflüger, 1989) of the mesothoracic leg of *S. gregaria*. Nagayama and Newland (1993) found that afferents from mtFCO units sharing particular physiological properties had similar morphologies. In particular, afferents had central projection areas dependent upon their velocity thresholds. However, it was not known whether such observations simply represented the central organisation of

afferents from neurones distributed randomly throughout the mtFCO, or reflected the functional subdivision of neurones at the peripheral level.

The description of the morphological subdivision of the mtFCO scoloparium in this thesis completes the understanding of the relationship between the peripheral and central CO projections. It shows that the mtFCO scoloparium is functionally subdivided and that the clusters of neurones sharing similar response characteristics identified by Matheson (1990) do correspond to consistently-positioned discrete neurone populations having characteristic anatomical features. This result, and the fact that the sensory cells of the proximal and distal scoloparia in the pro- and mesothoracic legs of the locust (Field and Pflüger, 1989) and the stick insect (Schmitz *et al.*, 1991) have different central projection areas, supports the hypothesis that neuronal pathways serving specific functions (such as the resistance reflex) are already separated at the level of the proprioceptive cells (Kittmann and Schmitz, 1992). The functional segregation found between the proximal and distal scoloparia of the pro- and mesothoracic legs (Field and Burrows, 1982; Burrows, 1987; Zill, 1987; Field and Pflüger, 1989) suggests that only group 1 and 2 neurones (presumed to be homologous with the pro- and mesothoracic distal scoloparia) may contribute to reflex mediation in the mtFCO. The remaining neurones may play a role in walking, jumping, sound production and vibration detection.

8.2 Why does the structure of the mtFCO differ from those of the other femoral COs in the locust

The mtFCO fulfils basic functional roles common to those carried out by the pro- and mesothoracic organs. Thus, it is involved in postural reflexes (Zill and Jepson-Innes, 1990), and proprioceptive output from the mtFCO modulates motor activity during the walking cycle (Burrows, 1996). It is possible to rationalise the way in which the proprioceptive requirements may have changed during the specialisation of the metathoracic limb for kicking and jumping by comparing the limb's morphology and function with those of the pro- and mesothoracic limbs. Thus, its specialised structure is assumed to be a product of selective pressures which resulted in the functional specialisation of the hind leg (Theophilidis, 1986a, b). The long metathoracic tibia allows increased mechanical leverage during a jump and a larger femur is required to contain the enlarged femoral

muscles. These muscles are capable of developing considerably larger forces than their pro- and mesothoracic counterparts. Occasionally the forces generated are sufficient to damage the knee joint or snap the extensor muscle apodeme during a jump (Burrows, 1996). In the light of these differences, the mtFCO may be expected to differ from the pro- and mesothoracic FCOs in several respects. The increased length of the metathoracic tibia, by a factor of 2 over those of the pro- and mesothoracic limbs (*S. gregaria* and *L. migratoria*), means that a given angular rotation of the femoro-tibial joint results in twice the displacement of the tarsus. As a result the mtFCO may be required to provide improved femoro-tibial angular resolution to allow the metathoracic tarsus to be positioned with the same accuracy that is achieved by the pro- and mesothoracic limbs during locomotion. Enhanced control of muscle tone may also be necessary to protect the femoro-tibial joint against the forces developed by the enlarged femoral muscles of the metathoracic limb. This study has shown that the mtFCO may be able to monitor the state of contraction of the flexor tibiae muscle by virtue of its mechanical connections to the flexor tibiae muscle apodeme.

The proprioceptive requirements from a jumping leg may differ from those of the pro- and mesothoracic limbs in other ways. Emphasis may be placed upon monitoring different parts of the femoro-tibial range, such as the fully flexed position held prior to a jump - a position rarely adopted by either the pro- and mesothoracic limbs. The metathoracic limbs are also involved in sound production (*L. migratoria*), which represents an additional role unique to the metathoracic limbs. Thus, the mtFCO may be required to monitor the high frequency joint movements which occur during sound production in addition to the lower frequency movements associated with locomotion. In addition, the mtFCO is located further from the central nervous system (CNS) than the pro- and mesothoracic COs. This may have implications for proprioceptive response time, proximity to the CNS being important for the fast activation of reflexes (Theophilidis, 1986a, b). In the other limbs, femoral COs are located at the extreme proximal ends of the femora, minimising the conduction distance between the site of signal transduction and the CNS. The increased distance for the signal to travel in the metathoracic femur (approximately 2 cm), combined with the limitations on action potential conduction speed due to the unmyelinated axons of the invertebrates (Pearson *et al.*, 1970;

Aidley, 1971), introduces the potential for a time lag between the detection of sensory input and the arrival of sensory information at the CNS. This may have implications regarding the receptor's role in reflex joint control loops and may require some form of compensatory mechanism.

8.3 Comparison with other systems

Now that a complete description of mtFCO anatomy has been provided it is possible to compare it with other systems. Comparing a wide range of COs reveals common themes in both the distribution of neurones within the scoloparia, and the way that the scoloparia themselves are mechanically anchored within the limb. A series of semi-schematic diagrams demonstrates that COs from a diverse range of species share two common characteristics which are exemplified in the locust mtFCO. These are a graded proximo-distal distribution of sensory neurones and the grouping of neurones of similar size or orientation (Fig. 8.1). The proximo-distal distribution of neurones shown in the above examples is often characterised by a population of the smaller neurones in a scoloparium extending distally along the ventral edge of the CO. For example the DP proprioceptor in the crab *Cancer pagurus* (not shown) contains smaller position-sensitive cells located in pairs along the ventral edge of the receptor strand (Lowe *et al.*, 1973). There also appears to be a trend towards generating a differential input across the scoloparia of chordotonal organs by having a variety of distal attachment sites and so attachment cells of different lengths. The bee tibio-tarsal organ (not shown) contains approximately 50 scolopidia arranged in graded length (Lukoschus, 1962). Graded lengths of attachment fibres are also found in the connective chordotonal organ of the cockroach leg (Young, 1970); its 14 scolopales are arranged into one main branch and two sub-branches. In the case of the locust mtFCO there is scope for the dorsal and ventral ligaments to be stretched differentially by the movement of the joint. This phenomenon has been suggested as a mechanical basis for range fractionation (Field, 1991).

The extent to which such apparent analogies reflect functional aspects of CO operation can be further illustrated by comparing the FCOs of the locust (middle leg: Field and Pflüger, 1989; hind leg: Matheson, 1990; Matheson and Field, 1990; Field 1991; Shelton *et al.*, 1992) and the stick insect (Füller and Ernst, 1973; Kittmann and Schmitz, 1992). Both locust

and stick insect COs consist of twin scoloparia (fused in the locust mtFCO) coupled to the joint by a common receptor apodeme. Kittmann and Schmitz (1992) suggested that, like those of the locust mtFCO, the neurones of the stick insect FCOs are also likely to be divided into small subpopulations of sensory cells with differing response characteristics. In the case of the locust pro- and mesothoracic legs, only the smaller distal scoloparium (approximately 40 cells) is responsible for known resistance reflexes in the extensor and flexor tibiae motor neurones, whilst the larger proximal scoloparium ('several hundred' cells) was presumed to be vibration sensitive (Field and Pflüger, 1989). The distal scoloparia in these COs are located ventrally within the femur relative to the proximal scoloparia. In the case of the stick insect too, only the smaller ventral scoloparium (approximately 80 neurones) is involved in control of the femoro-tibial angle in the femoro-tibial control loop, whilst the role of the larger dorsal scoloparium (approximately 400 neurones) remains unclear (Kittmann and Schmitz, 1992; Büschges, 1994). In addition to this functional analogy, there are also similarities between the behaviours of the mechanical connections of the two systems. The mtFCO dorsal ligament in the locust buckles to form a loop upon tibial extension as described in this study. In the case of the stick insect, Kitmann and Schmitz (1992) observed the dorsal scoloparium to unload fully at FT angles in excess of 150°, whilst the ventral scoloparium remained under tension across the full femoro-tibial range (range not given, 0° - approximately 170° personal observations). Thus, both systems feature slackening of one of their connective ligaments over part of the femoro-tibial range.

8.4 To what extent do the mtFCO's mechanical connections contribute to the organ's response characteristics ?

This thesis shows that sensory neurones can be subjected to different patterns of distortion by virtue of their positions within the scoloparium. This result implicates the role of the mtFCO mechanical linkages in contributing to the functional subdivision of the organ response. In particular, the graded attachment cell lengths of the ventral ligament have been demonstrated to be linked with graded dendritic distortion at the level of the scoloparium. This report has also demonstrated the range of forces to which the mtFCO is subjected. The tension developed within the mtFCO system increases in a non-linear fashion upon tibial flexion, a

phenomenon attributable to the sequential recruitment of ventral ligament fibres during joint flexion. Such an arrangement increases the range of forces to which the scoloparium is subjected over the full femoro-tibial range of joint rotation. Maximising the variation in tension over the femoro-tibial range may be a mechanism to increase the angular resolution of the mtFCO, a requirement anticipated considering the increased length of the metathoracic tibia compared with those of the pro- and mesothoracic limbs.

This study has also revealed differences between the dorsal and ventral mtFCO ligaments. Variations in attachment cell cross-sectional areas and elastic fibre distributions suggest the capacity for subtle mechancial differences between the linkages of different sensory scolopidia with the femoro-tibial joint. Evidence has been presented to suggest that attachment cells associate in bundles, bound by elastic fibres, which terminate upon discrete neurone populations. However, the demonstration of extensive cell-to-cell junctions between adjacent attachment cells indicates that individual cells are unlikely to be able to move completely independently from one another. This limits the potential for large differences in stimulus transmission between adjacent bundles.

8.5 Implications of the observed mtFCO mechanical properties

The results from this thesis suggest that the mechanical properties of the mtFCO are likely to be partly or wholly responsible for two documented phenomena common to all COs: hysteresis of the sensory output in response to cyclic elongation/relaxation (Burns, 1974; Matheson, 1990, 1992b) and adaptation in firing rate following a step displacement (Usherwood *et al.*, 1968; Theophilidis, 1986b). Viscoelasticity of the mtFCO's mechanical connections results in the force to which the scoloparium is subjected being dependent upon the rate of femoro-tibial rotation. This report has demonstrated both mechanical hysteresis in response to cyclic elongation/relaxation of the mtFCO and gradual stress-relaxation (creeping) following step displacements. The combined properties of the organ's mechanical connections have been shown to filter and modify the input stimulus. Displacements at the level of the femoro-tibial joint are modified such that displacements measured at the level of the scoloparium over the middle of the femoro-tibial range elicit

larger displacements at the level of the scoloparium than joint rotations near the extremes of the femoral-tibial range. This study has shown that displacements at the organ's natural frequency of 1 Hz - 2 Hz are transmitted most effectively to the scoloparium. Although resonant properties have been demonstrated to be physiologically useful in the heart muscles fibres of the crab *Cancer magister* (Meyhöfer, 1993), they have not previously been demonstrated in a chordotonal organ.

8.6 Transduction Mechanism

This thesis has provided the first descriptions of the dendritic distortions which occur when the mtFCO is stimulated. Studies of this type help to reveal the component of the stimulus to which the neurones respond (such as dendritic stretch, shear or compression) and provide insight into the likely regions of signal transduction. These descriptions complement and expand upon previous investigations which examined dendritic morphology after fixation in the stimulated and unstimulated states (e.g. Moran *et al.*, 1977). Relevant investigations into the nature of mechano-electric transduction have been carried out upon epithelial mechanosensilla (variously referred to as external/cuticular by different authors) for the experimental considerations of accessibility and the fact that isolated sensilla are easier to characterise.

The general organisation of epithelial sensilla may serve as a model for more complex sensory organs (Thurm and Küppers, 1980). The ability to transform cuticular sensilla to CO sensilla by the manipulation of a single gene (Blochlinger *et al.*, 1991) demonstrates that the two receptors and their accessory cells are homologous with one another. It is reasonable in the light of these observations to assume that both epithelial and chordotonal organ sensilla may share functional aspects of operation. The detailed ultrastructure of the mtFCO sensilla revealed in this thesis allows comparisons to be drawn between homologous structures in CO and epithelial sensilla and so to hypothesise how the model of electrophysiological operation devised for the external sensilla could be applied to mechano-electric transduction in a CO sensillum.

Thurm and Wessel (1979) revealed that in epithelial sensilla the apical dendrite is bathed in a fluid filled cavity known as the receptor lymph cavity. This cavity is maintained at a positive voltage with respect to the

haemolymph, in which the basal dendrite is bathed. Erler and Thurm (1981) were able to show that the elongated dendrite does have an apical spiking process. In epithelial sensilla, tight junctions exist between the cells forming the cavity and the sensory dendrite (Keil, 1984; Bernard *et al.*, 1980; Gnatzy, 1976; Moran *et al.*, 1976; Thurm and Küppers 1980) creating a high electrical resistance between the receptor lymph cavity and the haemolymph space. The electrical potential is generated and maintained by the transport of cations by the sensilla's accessory (tormogen) cell. The dependence of this sensillum-bound voltage source on oxidative metabolism (Küppers and Thurm, 1979) supports the hypothesis that the transmembrane voltage is maintained by active ion transport. A transporting role is also suggested by the invagination of the apical epithelial membrane (to provide a large surface area) and the presence of 5000 particles/μm^2 on the cytoplasmic side of the membrane with large numbers of mitochondria. Particle densities have been shown to be functionally correlated with specialised ion transport activity (Thurm and Küppers 1980).

Hartman and Boettiger (1967) deduced that in the case of the propus-dactylus CO in *Cancer irroratus*, the action potential spike is initiated at the apical dendritic terminations in the region of the scolopale. Zill (1985a) also thought action potentials originated in the distal dendritic process of the locust mtFCO neurones, although he did not rule out the spread of the generator potential into the soma. Oldfield and Hill (1986) provided evidence that the apical spikes are derived from the apex of the dendrite in the auditory organ sensilla in a tettigoniid. The extracellular space in which the apical dendrite tip is bathed in the locust CO sensillum appears to be analogous to this region. This cavity is formed and tightly sealed early in development (Juang *et al.*, 1996; Carlson *et al.*, 1997). The scolopale cell is also characterised by extensive invagination and vacuolisation. Evidence to support this hypothesis was provided by Carlson *et al.* (1997) who reported that CO functional competence did not occur in *Drosophila* in the absence of an intact blood-brain barrier capable of excluding sodium, chloride and potassium ions in the haemolymph from access the extracellular ion stores of the neurones. This blockage is achieved in the COs of *Drosophila* by occlusive scolopale cell septate junctions suggesting a functionally significant role of the scolopale cell.

8.7 Spike Production

In epithelial sensilla, the active transport of the accessory cell raises the potential of the receptor lymph cavity to approximately 70 mv relative to the haemolymph (Thurm and Wessel, 1979). Assuming the potential of the sensory dendrite to be -70mV with respect to the haemolymph, the apical dendrite is therefore exposed to a small potassium gradient but a transmembrane potential of approximately 140 mV. This situation would enable a small mechanical stimulation to elicit a large inward receptor current (French, 1988).

Thurm and Küppers (1980) and Erler and Thurm (1981) summarised this work by the production of a circuit diagram explaining how their electrical model was related to the structure of an epithelial sensillum. They also provided evidence to show that the transepithelial voltage in epithelial sensilla is maintained by a cation-outward-flux transport mechanism, which is K^+ dependent. The authors remark that despite the limited luminal space into which the ions are transported the transport works continuously whether the receptor cell is stimulated or resting.

Thurm and Küppers (1980) also measured large voltage amplitude differences (20 - 80mV) between sensilla in the same specimen, a phenomenon inversely correlated with the distance between neighbouring sensilla. Such differences may account for variation in threshold sensitivity throughout the mtFCO scoloparium.

8.8 Implications of such a mechanism

Atema (1973) suggested that the restoration of resting potential would be an expensive metabolic process, especially in the case of the tonic units which may fire repeatedly for long periods (e.g. Zill, 1985a). This problem is addressed by the above mechanism, in which the scolopale cell is responsible for the ionic composition of the lumen surrounding the apical dendrite, by putting the metabolic burden of restoring resting potential upon accessory (scolopale) cells. In many sensillum types, transepithelial current elicits impulses only during adequate stimulation of the receptor (Erler and Thurm, 1978; Maes, 1977). Thurm and Küppers (1980) speculated that the sensitivity of what they termed the 'pacemaker membrane' is so high that the opening of a single membrane channel may elicit a spike. If the sensilla are so sensitive, mechanical creep as

demonstrated in this thesis may represent a mechanism by which 'tonic' units are subjected to a low level of continuing stimulation following a step displacement of the tibia to a new position (Dr R. O. Stephen, personal communication). For mechanical creep to provide continuing low-level stimulation, the sensory units would need to be extremely sensitive. Evidence from similar mechanoreceptive systems suggests that such sensitivity is realistic. Various authors have reported that COs are capable of responding to displacements of the order of 1 nm (see French, 1988).

8.9 Differences in physiological properties of different mtFCO neurones

Ultrastructural modifications at the level of the of ciliary components or the number and localisation of ion channels could endow apparently similar sensory units with different response characteristics. Zill (1985a) demonstrated that the phasic and tonic units posses intrinsically different electrophysiological properties. In response to current injection, phasic units exibit only transient discharges whilst tonic units respond with sustained increases in activity, followed by periods of inhibition of background activity upon cessation of current injection. In addition, Matheson (1997) showed that the phasic and tonic units respond differently to the addition of the neurohormone octopamine, the firing frequency of tonic units being enhanced whilst the response of phasic units remains unaffected. The existence of sensory units having different physiological properties indicates that differential mechanical stimulation is not the only mechanism by which the mtFCO neurones are induced to fire differentially in reponse to a given tibial rotation.

8.10 Directional Sensitivity

The presence of directionally-sensitive units in chordotonal organs has been widely reported (Hartman and Boettiger, 1967; Usherwood *et al.*, 1968; Burns, 1974; Zill, 1985a; Theophilidis, 1986b; Matheson, 1990, 1992b; Bässler, 1993; Büschges, 1994). The basis and possible mechanisms of directional sensitivity in COs have been addressed by only a few authors.

Potentially, detection of the direction of joint rotation may depend upon either the peripheral level (a property of the transducer) or the central level (by the firing sequence of a range fractionated neurone series). The fact that Matheson (1990) found directional sensitivity whilst recording from individual CO afferents indicates that at least some directional

information is encoded at the peripheral level by individual units. The mechanism by which this might occur is unknown although dual innervation of each CO scolopale unit has been suggested to be indicative of directional sensitivity. There are examples of campaniform sensilla innervated by paired neurones which show directional sensitivity in response to cuticular distortion (Shelton and Laverack, 1968): one neurone active for each stimulus direction. Many hair sensilla are similarly innervated. Laverack (1976) argued that each CO scolopidium is homologous to one such hair sensillum, the innervation being consequently double and directionally sensitive. However, both campaniform sensilla and tactile hairs rely upon differential mechanical stimulation of the two neurones to derive directional information. Such stimulation has been shown to be provided by the arrangement of the associated structures such as the ultrastructure of the hair or campaniform sensillum socket (e.g. Laverack, 1976; Gnatzy and Tautz, 1980). It is difficult to see how such differential displacement could occur within the CO. Investigations by previous authors have suggested that dual innervation of each scolopidium is not indicative of directional sensitivity. For example, the pair comprising each scolopidium of the PD proprioceptor both respond to either extension or relaxation of the strand (Mill and Lowe, 1973). Each dendrite in a scolopidial pair, rather than conferring directional sensitivity as suggested by Laverack (1976), may instead have different threshold levels of excitability. This is true of the paired neurones in the PD organ of *Cancer irroratus* in which the paired neurones of each scolopidium both respond to the same stimulus, but one invariably has a lower threshold than the other (Hartman and Boettiger, 1967). A similar situation is found in the muscle receptor organs (MROs) of lobsters and crayfish which also consist of two neurones with different firing thresholds (Eyzaguirre and Kuffler, 1955). Different stimulation intensities are required to stimulate the two cells, so extending the range of sensitivity of each scolopidium whilst improving the discrimination of stimulus magnitude over different parts of the range.

Taylor (1967), studying the CO in the antennae of a hermit crab, suggested that dendritic shearing could occur if the dendrites crossed an interface between two connective tissues of different elasticities. Could such an arrangement endow COs with directional sensitivity by causing differential stimulation of similar units depending upon the mode of the

stimulus? Hartman and Boettiger (1967) suggested that the nature of the mechanical coupling of the dendritic terminal to the attachment strand may endow neurones with directional sensitivity in the case of the propodite-dactylopodite (DP) proprioceptor of *Cancer pagurus*. This receptor consists of approximately 80 bipolar neurones associated with a receptor strand (Mill and Lowe, 1973). The dendrites of relaxation-sensitive cells (RSCs) are inserted into the dorsal side of the elastic strand, whilst those sensitive to strand elongation (ESC) are inserted into a narrow band on the anterior side of the strand. In every case, the surface of dendrite insertion was indicative of a neurone's directional sensitivity. Mill and Lowe (1973) found that the dendritic terminals of the ESCs were surrounded by 'strand' cells whilst those of the RSCs were surrounded by collagen fibres, having very little contact with the strand cells themselves. These authors (Hartman and Boettiger, 1967; Mill and Lowe, 1973; Lowe *et al.*, 1973) suggested that interaction between the dendrite termination and the mechanical components of the elastic strand resulted in differential stimulation of the sensory dendrite during extension and relaxation. Specifically, Mill and Lowe (1973) proposed that energy stored in collagen fibres during strand elongation could be released during strand relaxation to distort dendritic terminals.

No evidence was found in this study to support the observations of Mill and Lowe (1973) who found each member of a dendrite pair in a scolopidium is associated with different structural components to its partner. However, there were indications that the twin neurones in each scolopidium may be proximo-distally offset from one another, although it is difficult to see how such an arrangement could confer directional sensitivity.

8.11 MtFCO role in the joint control loop

This thesis has provided a definitive account of the structure and mechanical properties of the mtFCO and shown that both the properties of its mechanical connection to the joint and the position of the neurones within the scoloparium are likely to play a significant role in influencing the discharge from individual CO units. However, the functional role played by the CO in the control of behaviour is also dependent on other factors and is ultimately determined by the way in which the afferent mtFCO discharge is centrally integrated and subsequently utilised. The

mtFCO signal is modulated at three different stages within the joint control loop: presynaptically (mtFCO afferents), centrally (interneurones within the metathoracic ganglion) and postsynaptically (motor neurones).

8.11.1 Presynaptic modulation

Presynaptic inhibition is the first level of modulation and occurs prior to CO afferents terminating upon their post-synaptic targets (Burrows and Matheson, 1994; Newland *et al.*, 1996). Depolarising inhibitory inputs onto the mtFCO afferents close to their terminals shunt action potentials, reducing transmitter release onto postsynaptic neurones. These presynaptic inputs are mediated by interneurones from three sources (Wolf and Burrows, 1995): central neurones involved in walking (Cattaert *et al.*, 1992; Sillar and Skorupski, 1986), signals from different mechanoreceptors in the same leg and other legs (Blagburn and Sattelle, 1987), and interaction between sensory neurones of the same organ signalling the same movement (Burrows and Laurent, 1993; Burrows and Matheson, 1994; Sauer *et al.*, 1997). The situation in which afferents activate interneurones which in turn presynaptically inhibit other neurones responding to the same signal represents an automatic gain control mechanism, regulating the flow of encoded information from CO afferents to postsynaptic targets. In such a mechanism, postsynaptic activity is dependent upon the pooled and weighted output of other active neurones (Matheson, 1997). Blocking presynaptic inhibition has been demonstrated to change the relative weighting of positional and velocity signals in the parallel interneuronal pathways between the CO afferents and motor neurones (Sauer *et al*, 1997). Thus presynaptic inhibition contributes to the 'tuning' of the femoro-tibial control system. As a method of modulation, it has the advantage of allowing selective control over the action of certain sensory neurones whilst leaving the excitability of the postsynaptic neurones unchanged (Wolf and Burrows, 1995).

8.11.2 Central modulation

The CO output is integrated to differing degrees within the metathoracic ganglion. The simplest situation consists of CO afferents synapsing directly upon motor neurones, whilst other groups of afferents synapse collectively upon banks of interneurones which act as sites of signal integration. The situation is complex; Burrows (1987) showed that mtFCO afferents synapse on both motor neurones and spiking local

interneurones. He demonstrated that each afferent synapses on several motor neurones and that in turn, each motor neurone and interneurone receives input from several afferents. Spiking and non-spiking local interneurones collectively transform the afferent signal prior to synapsing with motor neurones (Burrows, 1987; Burrows and Siegler, 1982; Burrows *et al.*, 1988). The local spiking interneurones organise large numbers of afferent axons into receptive fields, the interneurones themselves showing some functional segregation of proprioceptive and exteroceptive pathways (Burrows and Laurent, 1989; Schmidt and Rathmayer, 1993). The presence of tonic units in the mtFCO is reflected centrally, where the firing frequency of some interneurones reflects the position of the femoro-tibial joint (Burrows, 1988). As is the case in the mtFCO neurones, interneurones respond within discrete ranges of femoro-tibial angle such that information about joint position is range fractionated.

Wolf and Büschges (1995) identified interneurones in the mesothoracic leg of the locust having variable roles during walking. Some were involved with coordinating muscles driving leg swing, others have more of a trigger role at key points in the walking cycle. Reflex pathways are complicated by numerous interactions between each class of local interneurone (Burrows, 1979; Nagayama and Burrows, 1990) but there is evidence that non-spiking interneurones control the gain of the reflexes and act as sites for converging signals (Laurent and Burrows, 1989a, b). Non-spiking interneurones are the major pre-motor elements, their graded transmitter release allowing subtle control of motor neurone activity (Burrows and Siegler, 1978; Pearson and Fourtner, 1975; Siegler, 1985). Non-spiking interneurones, in addition to integrating local inputs (Burrows, 1987b; Burrows and Laurent, 1989; Büschges, 1990; Driesang and Büschges, 1993), also integrate inter-segmental signals allowing coordination of leg movement between segments (Büschges *et al.*, 1994; Laurent and Burrows, 1989b).

Büschges and Wolf (1995) demonstrated the significant role played by central processing by comparing the interneuronal pathways controlling mesothoracic femoro-tibial joint displacements in the locust (*L. migratoria*) and stick insect (*C. morosus*). The neuronal networks controlling the femoro-tibial joints are homologous in both species, receiving qualitatively similar inputs from their respective femoral COs

and driving corresponding pools of motorneurones. The authors showed that although the interneuronal pathways are sensitive to stimulus velocity in both species, the interneurones processed 'velocity' information from the respective COs in different ways, ultimately resulting in different characteristic behaviours between the two species. The stick insect, unlike the locust, showed a marked velocity dependence in the interneuronal responses which effected postural leg motor control sufficiently to elicit catalepsy behaviour. The stick insect joint control loop has low position-sensitivity and high non-linear velocity dependency and high gain (Bässler, 1993). This example puts the role of the COs into context, illustrating the influential role of afferent central processing in determining the behaviour elicited by CO stimulation.

The role of central processing is not confined to signal integration, there is also evidence that the afferent signal is split centrally to form two antagonistic proprioceptive pathways. Wolf and Büschges (1995) recorded simultaneous activity amongst local interneurones supporting and opposing leg movement in the locust mesothoracic ganglion, suggesting the operation of parallel antagonistic pathways. It seems likely that the resulting motor output which determines the movement to be executed is produced by the parallel action of antagonistic pathways of information processing (Büschges, 1990; Büschges and Schmitz, 1991; Bässler, 1993).

The complex interactions of the central neural network allow simple inputs to mediate complex and complementary responses simultaneously. For example, tibial extension produces bursts of afferent spikes which directly excite many flexor tibiae motor neurones resisting extension (Burrows, 1987a). In addition, local spiking interneurones are excited in parallel and inhibit the antagonistic extensor tibiae motor neurones (Burrows and Seigler, 1982; Büschges, 1989) and the non-spiking interneurones that excite them (Burrows, 1987b; Büschges, 1990).

The interneurone network also allows mtFCO-elicited reflexes to be executed in a behavioural context (Zill, 1985b). For example, the resistance reflex only occurs in resting animals. In active animals, mtFCO discharge elicits a flexion reflex (Zill, 1985b). The latter reflex can also be induced in a resting animal when the tibia is positioned close to the fully flexed position.

8.11.3 Motor modulation

Another level at which the joint control loop is modulated is during the transformation of sensory information into muscle activity.

The flexor tibiae muscle consists of both fast and slow muscle fibres (Bässler *et al.*, 1996) and is innervated by nine excitatory motor neurones. This motor pool is divided into three groups (Phillips, 1981), each of which contains a fast, an intermediate and a slow motor neurone which show variable activity in response to stimulation of the mtFCO.

Newland and Kondoh (1997a) analysed the response dynamics of the flexor tibiae motor neurones in response to stimulation of the mtFCO. They revealed that each individual motor neurone has specific dynamic response properties; within the motor pool some units respond best to position whilst others respond most strongly to velocity at discrete stimulus frequencies. This represents fractionation of the motor pool. In addition, Newland and Kondoh (1997a, b) illustrated differences in the response dynamics between antagonistic motor neurone pools, flexor tibiae motor neurones being predominently velocity-dependent and extensor motor neurones being position-dependent. They suggested that this may reflect the differing demands upon the two muscles during different behaviours.

In addition to the factors described above, properties of the motor neurones themselves may also affect the ways in which the reflex pathway leads to muscle contraction. Thus, some transformation of information has also been demonstrated to be exclusive to the motor units. As an example, not every spike evoked in a slow extensory tibiae motor neurone of the locust *L. migratoria* evokes a junction potential in the extensor muscle (Bässler *et al.*, 1996). It has been suggested that delayed inputs to the flexor motor neurones may be removed by processing within the motor neurones themselves and so may never be expressed at the muscles (Newland and Kondoh, 1997b). They concluded that the properties of individual neurones and their synapses can exert a marked influence on the way a signal is transmitted. Collectively the dynamics of the motor output, filter properties of the neuromuscular junction, the structure and innervation patterns of the muscles, the properties of force production

and the mechanics of movement of the femoro-tibial joint cause the muscle joint system to act as a low pass filter (Bässler and Stein, 1996).

8.11.4 Hormonal modulation

In addition to neuronal network properties the joint control loop may also be modulated by the release of neurohormones. Neurohumoural modulation has been demonstrated to occur at the level of signal transduction within the mtFCO. In insects, levels of circulating neurohormone octopamine are elevated during stress (Orchard *et al.*, 1981). Octopamine (or its agonist synephrine) increases the firing frequency of the tonic component but not the phasic component of the mtFCO's response (Matheson, 1997). The latter study also showed that tonic spiking of phaso-tonic units is also enhanced, whilst their phasic spiking remains unaffected. It is possible that increasing the firing frequency of the tonic response relative to the phasic component may result in increased femoro-tibial position sensitivity in times of stress.

8.12 Other mechanoreceptors associated with the femoro-tibial joint

In addition to the mtFCO, the metathoracic femora contain additional mechanoreceptors associated with the femoro-tibial joint, whose sensory discharge is likely to complement that of the mtFCO. Cruse *et al.* (1984) demonstrated integration of proprioceptive information from a range of mechanoreceptors in the stick insect *Carausius morosus.* In the stick insect, output from two coxal hairplates, the trochanteral hairplate, the coxal hair rows and the femoral CO of the mesothoracic leg all supply information to the CNS which is used to calculate the target point for hind leg protraction. All of these sense organs contribute some facet to the final signal, absence of any one changing the behaviour of the limb. On the basis of ablation experiments, Cruse *et al.* (1984) also proposed the mechanism of 'suppression of divergent signals', a phenomenon enabling the CNS to discard anomalous inputs which deviate from the majority of inputs from the other organs.

It is likely that a similar situation exists in the locust, such that information from several mechano-receptors is combined to give the total proprioceptive response. In the locust, changes in femoro-tibial angle are monitored by the mtFCO (Usherwood *et al.*, 1968; Burns, 1974; Field and Rind, 1977, 1981; Hofmann *et al.*, 1985; Hofmann and Koch, 1985; Field and

Pflüger, 1989; Matheson and Field, 1990; Matheson, 1990; Büschges, 1994; Kondoh *et al.*, 1995; Matheson, 1997; Newland and Kondoh, 1997a, b), the flexor strand (Zill, 1985a; Bräunig, 1985) and maybe the ftjR (this thesis). In addition, there are multipolar receptors associated with the femoro-tibial joint. The five multipolar sensory cells (referred to as multipolar joint receptors, Pflüger and Burrows, 1987) are arranged in three groups (Coillot and Boistel, 1968). The dorsal posterio-lateral receptor (RDPL) and ventral posterio-lateral receptor (RVPL) each contain two multipolar receptor cells, whilst the dorsal anterio-lateral (RDAL) consists of a single receptor cell. The RDPL and RDAL are stimulated by rotation of the tibia over the ranges 80° - 160° and 125° - 160° respectively. These units respond in a manner similar to that of the flexor strand, encoding joint position by tonic changes of frequency (Coillot and Boistel, 1969; Coillot, 1974, 1975). The RVPL is activated by tibial flexion and has been called the 'lump receptor' (Heitler and Burrows, 1977b) due to its proximity to the 'lump' of the flexor apodeme.

The precise role of the inputs from all of these receptors remains unclear and further work is required before a full understanding is reached

8.13 Final conclusion and suggestions for further work

The present thesis has provided a very full description of the anatomy of the mtFCO and has investigated its mechanical properties. It provides the basis upon which future investigations can be based.

The outstanding gap in our knowledge relates to the dynamic properties of the mtFCO neurones. The present investigation examined changes in neurone morphology resulting from static displacements. What is now needed is a comprehensive understanding of the response properties of individual neurones located in different regions of the mtFCO. Matheson's (1990) results were ambiguous because of the stimuli he used to characterise the neurones. These were ramp and step displacements. In such stimuli, the three components (position, velocity and acceleration) are not easily separable. Sinusoidal stimuli provide the ideal input with which to analyse the response properties of the system, because the three components (position, velocity and acceleration) vary predictably with time and so can be defined at any point during the stimulus cycle. The ideal study would record from individual mtFCO neurones whilst a

sinusoidal stimulus regime was applied. Subsequent injection with carboxyfluorescein would then allow the dendritic distortion pattern of each neurone to be characterised. It may be possible to use phase-locked imaging techniques in order to observe the dynamic displacement patterns of the neurones at different stimulus frequencies.

The role of the mtFCO's mechanical linkages to the flexor tibiae muscle apodeme is not completely understood. Stimulation of the flexor-tibiae muscle whilst clamping both the flexor muscle apodeme and the mtFCO cuticular rod, could provide evidence that the organ can respond to changes in flexor tibiae muscle tone.

The present investigation has investigated the mechanical properties of the mtFCO system as a whole. There is now a need to examine the mechanical properties of the individual components to see how they contribute to the overall properties of the organ. For instance, the non-linear properties of the apodeme complex demonstrated in this thesis may arise from the recruitment of individual components with linear viscoelastic properties. To resolve this matter, it would be necessary to isolate individual attachment cell bundles from the apodeme complex and subject them to stress/strain analysis.

The roles of different structural components within the system need further investigation. One approach that has been used in the investigation of other mechanoreceptors, but not chordotonal organs, is chemical dissection. For example, it is possible to dissociate microtubules using vinblastline or colchicine (e.g. Erler, 1983a, b). Similar approaches could be applied to the mtFCO. In such a study, the mechanical properties of the attachment cells would be monitored before and after microtubule dissociation. If the mechanical properties did not change, this would indicate that the microtubules play little part in determining its viscoelastic properties. If the mechanical properties do change, the interpretation would be more difficult, because chemical treatments almost certainly affect more than one cellular component.

At present it is unclear what proportion of the observed decrease in firing frequency following a step displacement is due to gradual creeping of the ligaments and how much is attributable to the adaptation properties of the

neurones themselves. Attempts could be made to characterise the effect of the stress-relaxation upon firing rate by maintaining a constant tension following a step displacement rather than observe it decline with time. Any decrease in firing frequency under these conditions would be attributable to factors other than the viscosity of the apodeme complex.

Fig. 8.1a-n

This series of diagrams (continued overleaf) shows that there is often a graded proximo-distal distribution of neurones within arthropodan proprioceptors and that neurones of similar sizes and orientations are often grouped together. In all cases distal is to the right.

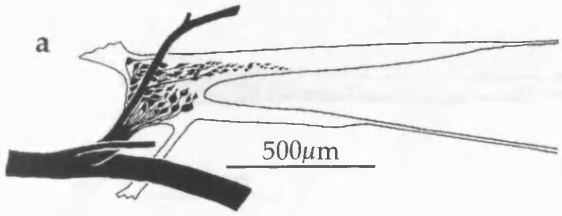

The mtFCO of the locust *Locusta migratoria*, the largest neurones are located proximally whilst a population of smaller neurones extends distally along the ventral edge of the ligament.
From Matheson and Field (1990)

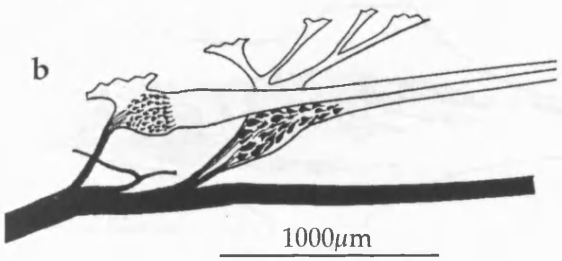

Morphological subdivision of the CO is clearly represented in the twin scoloparia of the msFCO of the locust *Locusta migratoria*, the CO with which the mtFCO is proposed to be homologous.
From Matheson and Field (1990)

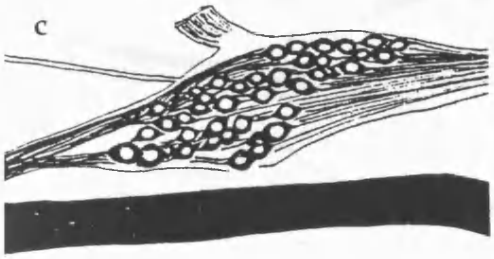

This diagram shows the neurone distribution within the distal scoloparium of the msFCO of the locust *Locusta migratoria* (see above). These neurones (responsible for mediating the femoro-tibial joint control loop) are proposed to be homologous with the group 1 and 2 neurones in this study, and are distributed in clusters.
From Field and Pflüger (1989)

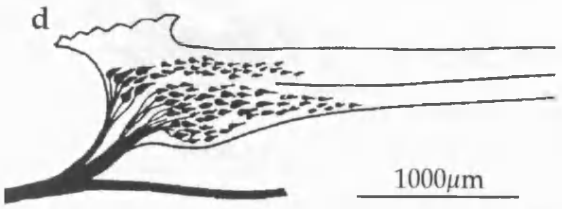

The mtFCO of the New Zealand Weta, like the locust mtFCO, is connected to the tibia via twin ligaments. The sensory neurones are divided into two populations, one associated with each ligament.
From Matheson and Field (1990)

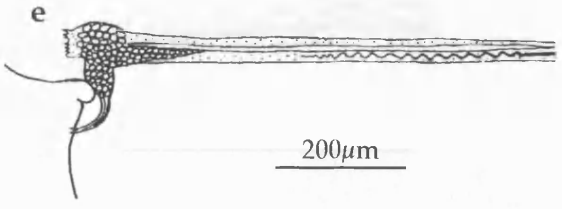

The mtFCO of the cricket *Acheta domesticus* is also attached to the femoro-tibial joint by twin ligaments. Sensory neurones extend distally along the ventral ligament. The dorsal and ventral ligaments have different structures; the ventral ligament containing a cuticular 'spring'.
From Nowel *et al.* (1995)

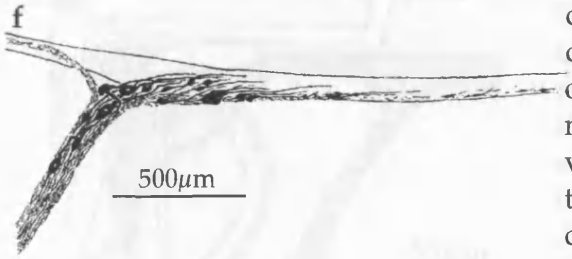

The coxo-propodite CO1 of the shore crab *Carcinus maenas* shares characteristics with the ventral ligament of the locust mtFCO. The sensory neurones extend distally along the ventral edge of the ligament, whilst their dendrites terminate at graded dorso-ventral levels.
From Whitear (1962)

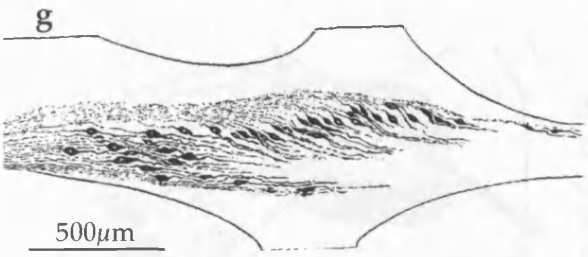

The neurones of the shore crab *Carcinus maenas* coxo-propodite CO2 are distributed in a proximo-distal series. There is also a range of cell orientations and graded dorso-ventral dendritic terminations analogous to those described in this study.
From Whitear (1962)

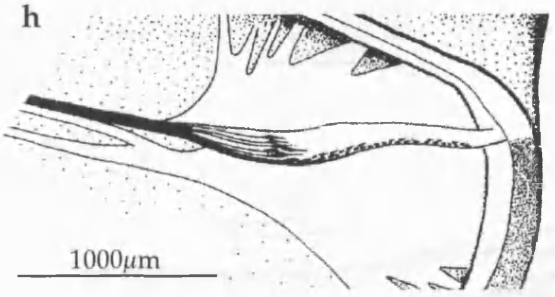

The 3rd maxilliped CO of the lobster *Homarus gammarus* shows similar neurone distributions to that of the locust mtFCO. A proximal group of large neurones is situated dorsal to a population of smaller neurones which extends distally along the ventral edge of the ligament.
From Wales *et al.*, (1970)

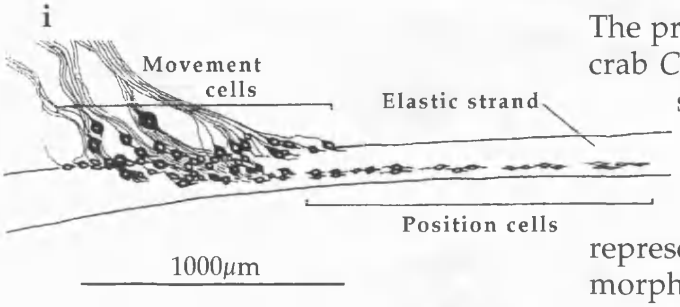

The propodite-dactylopodite CO of the crab *Cancer magister* also shows a similar neurone distribution to the locust mtFCO. In this CO the cells have been characterised, confirming that this distribution represents functional as well as morphological subdivision of neurones.
From Hartman and Cooper (1994)

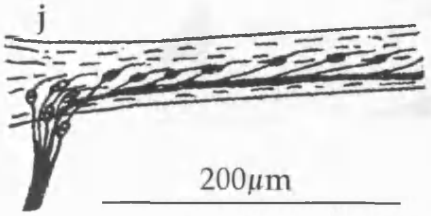

The scoloparium of the thoracic-coxal CO of the spiny lobster *Palinurus vulgaris* shares characteristics with the locust mtFCO in that it consists of a proximal neurone cluster and a neurone series extending distally along the ligament.
From Alexandrowicz (1967)

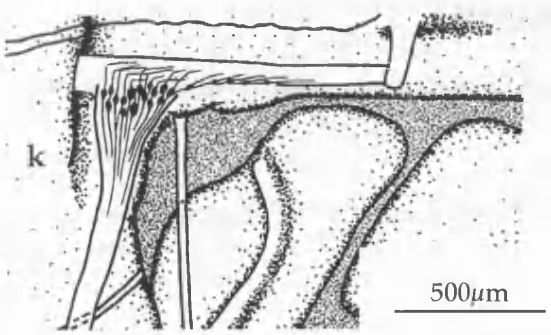

The 2nd periopod Cuticular Stress Detector (CSD) organ of the shore crab *Carcinus maenas* consists of two neurone populations: a proximal cluster and a distal group extending along the ventral edge of the ligament. The dendrites of this organ also terminate at a series of dorso-ventral levels within the ligament. From Wales *et al.* (1971)

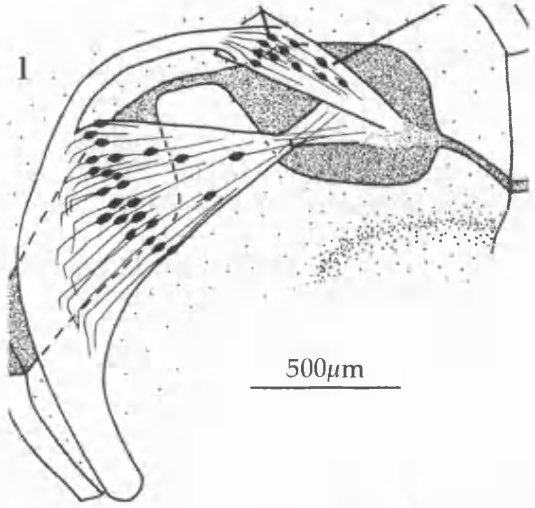

The neurones of the 2nd Periopod CSD2 of the crayfish *Astacus leptodactylus* are located in twin scoloparia, both of which have a range of proximo-distal neurone locations.
From Wales *et al.* (1971)

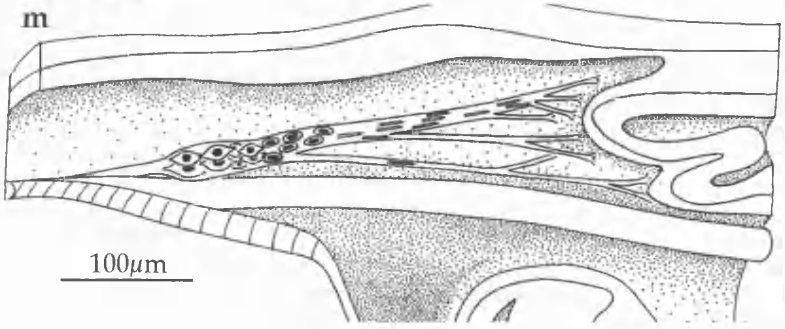

Tibio-tarsal CO of the cockroach *Periplaneta americana.* The scoloparium of this CO has a range of neurone sizes whose sensory dendrites terminate in one of two ligaments. From Young (1970)

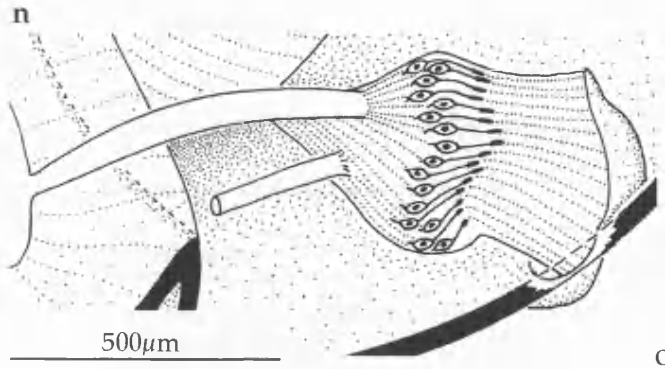

Auditory organ of the bladder cicada *Cystoma saundersii.* The neurones of this scoloparium are all similarly sized and comparably located. However, the neurones do show a range of dendritic orientations resembling those described in the locust mtFCO. From Doolan and Young (1981)

APPENDIX 1

Reagents used in the fixation, embbeding and staining of material

EM Grade Araldite

Regular

araldite epoxy resin (CY 212; Agar Scientific).....	20ml
DDSA.....	22ml
BDMA.....	1.1ml

Soft

araldite epoxy resin (CY 212; Agar Scientific).....	20ml
DDSA.....	22ml
BDMA.....	1.1ml
Dibutyl phthalate.....	1ml

Phosphate buffer

M/15 Na2HPO4.2H2O (5.933g in 500ml stock)...8ml
M/15 KH2PO4 (2.258g in 250ml stock) +2ml balanced to pH 7.2

Karnovsky (1965) fixative

2g paraformaldehyde in 25ml distilled H2O
+ 1-3 drops 1N NaOH & dissolve at 60-70°C
Add 10ml 25% glutaraldehyde when cool and top up to 50ml with phosphate buffer (pH 7.2)

Insect Saline

NaCl.....	180mM
KCl.....	10mM
$CaCl_2$.....	1-2mM
NaH_2PO_4.....	4mM
Hepes.....	10mM
Na_2HPO_4.....	6mM

Adjust to pH 6.8

Subbing Solution

Gelatine 0.1%
Chrome Alum (chromium potassium sulphate)..... 0.01%
Filter

Toluidine Blue

1% Toluidine blue in 1% Boric acid

Cobalt chloride

5% (saturated) solution of Hexamminecobalt III Chloride in distilled water
(Store at 4°C)
[Precipitated using Ammonium Polysulphide]

5(6)Carboxyfluorescein

C21H12O7 MW 376.32
5% (saturated) solution in distilled water
Balance to pH 7 with NaOH
(Store at 4°C)

APPENDIX 2

Image analysis macro routine used to characterise the sizes, shapes and orientations of the mtFCO neurones

This code executes using the public domain software NIH Image (vs. 1.6/ppc) (Mac OS) developed at the U.S. National Institutes of Health and available on the Internet at http://rsb.info.nih.gov/nih-image/.

```
{1. Modifications to 'best-fit-ellipse' implementation by M.E. Walker}
{Gets Selection
Fill black
Copy Selection
Fit ellipse, measure area, axes & orientation
Select "LOCATION"
Paste in Roi
Copies updated Locations
Return to camera and transparently pastes
Ellipse angles, value is >90, value -180 gives angle below horisontal ;distal to right}

{Ensure both 'LOCATION' and 'camera' windows;
1. SAME SIZE
2. SAME SCALING (Pix/µm = 1.525 at x10)}

macro 'Cell Parameters [L]';
var
  left,top,width,height:integer;

begin
    GetRoi(left,top,width,height);
  if width=0 then begin
     PutMessage('Selection required.');
    exit;
  end;
  SetForeground(255); {Black}
  Fill;
 Copy;

   SetOptions('Area; Ellipse Major Axis; Ellipse Minor Axis; Angle');
          Measure;
   SetOption; MarkSelection;

   SelectWindow('LOCATION');
   RestoreRoi;
   Paste;
   SetOption; MarkSelection;
    KillRoi;
    SelectAll;
   Copy;
    KillRoi;

  SelectWindow('camera');
   Paste;
```

```
  SetOption; DoReplace;
end;

macro 'Reset Count [R]';
begin
SetCounter(0);
end;


*****************************************************************


{2. Origional best-fitting ellipse routines by Bob Rodieck}
{  Department of Ophthalmology, RJ-10}
{  University of Washington, }
{  Seattle, WA, 98195}
{  (206) 543-2449}


implementation

        const
                HalfPi = 1.5707963267949;

        type
                TMoments= record
                                n: extended;
                                xm, ym,         { mean values }
                                u20, u02, u11: extended; { central moments }
                        end;

        var
                BitCount, xsum, ysum: LongInt;
                x2sum, y2sum, xysum: extended;
                Moments: TMoments;
                gMajor, gMinor, Theta: extended;
                gxCenter, gyCenter: integer;
                SaveRect:  rect;

        procedure DrawEllipse;

{ basic equations: }

{   a: major axis}
{   b: minor axis}
{    t: theta, angle of major axis, clockwise with respect to x axis. }

{   g11*x^2 + 2*g12*x*y + g22*y^2 = 1      -- equation of ellipse}

{   g11:= ([cos(t)]/a)^2 + ([sin(t)]/b)^2}
{   g12:= (1/a^2 - 1/b^2) * sin(t) * cos(t)}
{   g22:= ([sin(t)]/a)^2 + ([cos(t)]/b)^2}

{   solving for x:     x:= k1*y ± sqrt( k2*y^2 + k3 )}

{   where:  k1:= -g12/g11}
{         k2:= (g12^2 - g11*g22)/g11^2}
{         k3:= 1/g11}
```

```
{  ymax or ymin occur when there is a single value for x, that is when:  }
{       k2*y^2 + k3 = 0  }


            const
                    maxY = 1000;

            type
                    TMinMax = record
                                    xmin, xmax: Integer;
                            end;

            var
                    sint, cost, rmajor2, rminor2, g11, g12, g22, k1, k2, k3: extended;
                    xsave, y, ymin, ymax: Integer;
                    aMinMax: TMinMax;
                    TXList: array[0..maxY] of TMinMax;

            procedure GetMinMax (yValue: Integer; var xMinMax: TMinMax);
                    var
                            j1, j2, yr: extended;
            begin
                    yr := yvalue;
                    j2 := sqrt(k2 * sqr(yr) + k3);
                    j1 := k1 * yr;
                    with xMinMax do begin
                                    xmin := round(j1 - j2);
                                    xmax := round(j1 + j2);
                            end;
            end;

            procedure Plot (x: Integer);
            begin
                    MoveTo(gxCenter + xsave, gyCenter + y);
                    LineTo(gxCenter + x, gyCenter + y);
                    xsave := x;
            end;

        begin
            if not EqualRect(info^.RoiRect, SaveRect) then
                    exit(DrawEllipse);
            sint := sin(Theta);
            cost := cos(Theta);
            rmajor2 := 1.0 / sqr(gMajor);
            rminor2 := 1.0 / sqr(gMinor);
            g11 := rmajor2 * sqr(cost) + rminor2 * sqr(sint);
            g12 := (rmajor2 - rminor2) * sint * cost;
            g22 := rmajor2 * sqr(sint) + rminor2 * sqr(cost);
            k1 := -g12 / g11;
            k2 := (sqr(g12) - g11 * g22) / sqr(g11);
            k3 := 1.0 / g11;
            ymax := Trunc(sqrt(abs(k3 / k2)));
            if ymax > maxy then
                    ymax := maxy;
            ymin := -ymax;
 { Precalculation and use of symmetry speed things up }
            for y := 0 to ymax do begin
```

```
                        GetMinMax(y, aMinMax);
                        TXList[y] := aMinMax;
                end;
        xsave := TXList[ymax - 1].xmin; { i.e. abs(ymin+1) }
        for y := ymin to ymax - 1 do
                with TXList[abs(y)] do
                        if y < 0 then
                                Plot(xmax)
                        else
                                Plot(-xmin);
        for y := ymax downto ymin + 1 do
                with TXList[abs(y)] do
                        if y < 0 then
                                Plot(xmin)
                        else
                                Plot(-xmax);
end; { TraceOval }


procedure GetMoments;{changed n_}
        var
                x1, y1, x2, y2, xy: extended;
begin
        with moments, Info^ do begin
                        if BitCount = 0 then
                                exit(GetMoments);
                        x2sum := x2sum + 0.08333333* BitCount; {NIntegrate[x^2,
<x, centerx-0.5, centerx+0.5>]-center^2 = 0.08333333}
                        y2sum := y2sum + 0.08333333* BitCount; {=correction when
the mass of a pixel is seen as an area instead of a point}
                        n := bitcount;
                        x1 := xsum / n;
                        y1 := ysum * PixelAspectRatio/ n;
                        x2 := x2sum / n;
                        y2 := y2sum * sqr(PixelAspectRatio)/ n;
                        xy := xysum * PixelAspectRatio / n;
                        xm := x1;
                        ym := y1;
                        u20 := x2 - sqr(x1);
                        u02 := y2 - sqr(y1);
                        u11 := xy - x1 * y1;
                end;
end;


        procedure GetEllipseParam (var Major, Minor, angle, xxcenter, yycenter:
extended);{changed n_}
{Return the parameters of an ellipse that has the same second-order }
{moments as those specified by 'm'. }

{See Cramer, Mathematical Methods of Statistics, }
{Princeton Univ. Press 1945, page 283.}

{The elliptical parameters returned specify an ellipse that}
{has the the same second order moments as that of the profile}
{that generated the moments. This ellipse need not have the same}
{area as that of the profile, although its area will be close to}
{that of the profile. In order to refine our measure, we scale}
```

```
{the major and minor axes so as to make the area equal to that}
{of the profile. }
 const
  sqrtPi = 1.772453851;
 var
  a11, a12, a22, m4, z, scale, tmp, xoffset, yoffset: extended;
   width, height: integer;
  str1, str2, str3: str255;
   RealAngle: real;

begin
 with info^, info^.RoiRect do
 begin
   width := right - left;
  height := bottom - top;
  if RoiType = RectRoi then
  begin
   major := width / sqrtPi;
    minor := height / sqrtPi * PixelAspectRatio;
   angle := 0.0;
   if major < minor then
   begin
    tmp := major;
    major := minor;
    minor := tmp;
    angle := 90.0;
   end;
   xxcenter := left - 0.5 + width / 2.0;
   yycenter := top - 0.5 + height / 2.0;
    exit(GetEllipseParam);
  end;
 end;
                GetMoments;
                with moments do begin
                        m4 := 4.0 * abs(u02 * u20 - sqr(u11));
                        if m4 <0.000001 then

                        m4 := 0.000001;
                        a11 := u02 / m4;
                        a12 := u11 / m4;
                        a22 := u20 / m4;
                        xoffset := xm;
                        yoffset := ym/Info^.PixelAspectRatio;
                end;
                tmp := a11 - a22;
                if tmp = 0.0 then
                        tmp := 0.000001;
                theta := 0.5 * arctan(2.0 * a12 / tmp);
                if theta < 0.0 then
                        theta := theta + halfpi;
                if a12 > 0.0 then
                        theta := theta + halfpi
                else if a12 = 0 then begin
                        if a22 > a11 then begin
                                        theta := 0;
                                        tmp := a22;
                                        a22 := a11;
                                        a11 := tmp;
```

```
                                end
                        else if a11 <> a22 then
                                theta := halfpi;
                end;
        tmp := sin(theta);
        if tmp = 0.0 then
                tmp := 0.000001;
        z := a12 * cos(theta) / tmp;
        major := sqrt(1.0 / abs(a22 + z));
        minor := sqrt(1.0 / abs(a11 - z));
        scale := sqrt(BitCount * Info^.PixelAspectRatio/ (pi * major * minor ));
{equalize areas }
        major := major * scale;
        minor := minor * scale;
        RealAngle := 180.0 * theta / pi;{force rounding by using real}
        angle := RealAngle;
        if angle = 180.0 then
                angle := 0.0;
        if major < minor then begin
                tmp := major;
                major := minor;
                minor := tmp;
                end;
        with info^ do begin
                        with RoiRect do begin
                                        xxCenter := left + xoffset;
                                        yyCenter := top + yoffset;
                                end;
                        SaveRect := RoiRect;

                end;
        gxCenter := round(xxCenter);
        gyCenter := round(yyCenter);
        gMajor := major;
        gMinor := minor;
end;


procedure ComputeSums (y, width: integer; var MaskLine: LineType);{changed n_}
        var
                x: longint;
                BitcountOfLine: longint;
                xe, ye: extended;
                xSumOfLine: longint;
begin
  BitcountOfLine := 0;
  xSumOfLine:= 0;
        for x := 0 to width - 1 do
                if MaskLine[x] = BlackIndex then begin
                    BitcountOfLine := BitcountOfLine+1;
                                xSumOfLine := xSumOfLine + x;
                                x2sum := x2sum + sqr(x);
                        end;
        xsum := xsum + xSumOfLine;
        ysum := ysum + BitcountOfLine * y;
        ye := y;
        xe := xSumOfLine;
        xysum := xysum + xe * ye;
```

```
        y2sum := y2sum +  sqr(ye) * BitcountOfLine;
        bitCount := bitCount + BitcountOfLine;
end;


procedure ResetSums;
begin
        xsum := 0;
        ysum := 0;
        x2sum := 0.0;
        y2sum := 0.0;
        xysum := 0.0;
        bitCount := 0;
end;
```

REFERENCES

Adrian, E. D. (1926). The impulses produced by sensory nerve endings. *Journal of Physiology* **61,** 49-72.

Aidley, D. J. (1971). The Physiology of Excitable Cells. Cambridge: Cambridge University Press.

Alexander, R. M. (1962). Viscoelastic properties of the body wall of sea anemones. *Journal of Experimental Biology* **39,** 373-386.

Alexander, R. M. (1964). Viscoelastic properties of the mesogloea of jellyfish. *Journal of Experimental Biology* **41,** 363-369.

Alexandrewicz, J. S. (1967). Receptor organs in the coxal region of *Palinurus vulgaris*. *Journal of the Marine Biological Association, U.K.* **47,** 415-432.

Altman, J. S., Shaw, M. K. and Tyrer, N. M. (1980). Input synapses on to a locust sensory neurone revealed by cobalt-electron microscopy. *Brain Research* **189,** 245-250.

Alvarez Buylla, R. and Ramirez De Arellano, J. (1953). Local responses in Pacinian corpuscles. *American Journal of Physiology* **172,** 237-244.

Apter, T. and Marquez, E. (1968). A relation between hysteresis and other viscoelastic properties of some biomaterials. *Biorheology* **5,** 285-301.

Ashhurst, D. E. (1959). The connective tissue sheath of the locust nervous system: a histochemical study. *Quarterly Journal of Microscopical Science* **100,** 401-412.

Ashhurst, D. E. (1961a). The cytology and histochemistry of the neurones of *Periplaneta americana*. *Journal of Microscopical Science* **102,** 399-405.

Ashhurst, D. E. (1961b). A histochemical study of the connective-tissue sheath of the nervous system of *Periplaneta americana*. *Quarterly Journal of Microscopical Science* **102,** 455-461.

Ashhurst, D. E. (1964). Fibrilligenesis in the wax-moth, *Galleria mellonella*. *Quarterly Journal of Microscopical Science* **105,** 391-403.

Ashhurst, D. E. (1965). The connective tissue sheath of the locust nervous system: its development in the embryo. *Quarterly Journal of Microscopical Science* **106,** 61-73.

Ashhurst, D. E. (1968). The connective tissue of insects. *Annual Review of Entomology* **13,** 45-74.

Ashhurst, D. E. (1982). The structure and development of insect connective tissues. In *Insect Ultrastructure*, vol. 1 (ed. R. C. King and H. Akai). New York, London: Plenum.

Ashhurst, D. E. and Chapman, J. E. (1961). The connective-tissue sheath of the nervous system of *Locusta migratoria*: an electron microscope study. *Quarterly Journal of Microscopical Science* **102,** 463-467.

Ashhurst, D. E. and Richards, A. G. (1964). The histochemistry of the connective tissue associated with the central nervous system of the pupa of the wax moth *Galleria mellonella*. *Journal of Morphology* **114,** 237-246.

Atema, J. (1973). Microtubule Theory of Sensory Transduction. *Journal of Theoretical Biology* **38,** 181-190.

Baccetti, B. (1957). Observations by polerised light on the supporting stroma of some organs in insects. *Experimental Cell Research* **13,** 158-160.

Bacon, J. P. and Altman, J. S. (1977). A silver intensification method for cobalt filled neurones in wholemount preparations. *Brain Research* **138,** 359-363.

Barber, V. C. (1974). Cilia in sense organs. In *Cilia and Flagella* (ed. M. A. Sleigh), pp. 403-433. New York: Academic press.

Bargren, J. H., Bassett, C. A. L. and Gjelsvik, A. (1974). Mechanical properties of hydrated cortical bone. *Journal of Biomechanics* **7,** 239-245.

Barth, F. G. (1972). Die Physiologie der Spaltsinnesorgane. II. Funktionelle Morphologie eines Mechanorezeptors. *Journal of Comparative Physiology*, **91,** 159-186.

Bässler, U. (1976). Reversal of a reflex to a single motorneuron in the stick insect Carausius morosus. *Biological Cybernetics* **24,** 47-49.

Bässler, U. (1993). The walking (and searching) pattern generator of stick insects, a modular system composed of reflex chains and endogenous oscillators. *Biological Cybernetics* **69,** 305-317.

Bässler, D., Buschges, S., Meditz, S. and Bässler, U. (1996). Correlation between muscle structure and filter characteristics of the muscle-joint system in 3 Orthopteran insect species. *Journal of Experimental Biology* **199,** 2169-2183.

Bässler, U. and Stein, W. (1996). Contributions of structure and innervation pattern of the stick insect extensor tibiae muscle to the filter characteristics of the muscle-joint system. *Journal of Experimental Biology* **199,** 2185-2198.

Bear, R. S. (1942). Long X-ray diffraction spacings of collagen. *J. Am. Chem. Soc.* **64,** 727.

Bentley, D. and Caudy, M. (1983). Navigational substrates for peripheral poineer growth cones; Limb-axis cues, limb segment boundaries, and guidepost neurones. *Cold Spring Harbour, Symposium of Quantitative Biology* **48,** 573-585.

Bergel, D. H. (1961). The dynamic elastic properties of the arterial wall. *Journal of Physiology* **156,** 458-469.

Berlot, J. and Goodman, C. S. (1984). Guidance of peripheral pioneer neurones in the grasshopper: adhesive heirachy of epithelial and neuronal surfaces. *Science* **223,** 493-496.

Bernard, J., Guillet, J. C. and Coillot, J. P. (1980). Evidence for a barrier between blood and sensory terminal in an insect mechanoreceptor. *Comparative Biochemical Physiology* **67a,** 573-579.

Blagburn, J. M. and Sattelle, D. B. (1987). Presynaptic depolarization mediates presynaptic inhibition at a synapse between an identifed mechanosensroy neurone and giant interneurone 3 in the first instar cockroach, *Periplaneta americana. Journal of Experimental Biology* **127,** 135-157.

Blochlinger, K., Jan, L. Y. and Y.N., J. (1991). Transformation of sensory organ identity by ectopic expression of 'cut' in *Drosophila. Genes and Development* **5,** 1124-1135.

Bodmer, R., Barbel, S., Shepherd, S., Jack, J. W., Jan, L. Y. and Jan, Y. N. (1987). Transformation of sensory organs by mutations of the 'cut' locus of *Drosophila melanogaster. Cell* **51,** 293-307.

Bodmer, R., Carretto, R. and Jan, Y. N. (1989). Neurogenesis of the peripheral nervous system in *Drosophila* embryos. *Neuron* **3,** 21-32.

Bohnenberger, J. (1981). Matched transfer characteristics of single units in a compound slit sense organ. *Journal of Comparative Physiology* **142,** 391-402.

Bolton, W. (1986). Solids, Liquids and Gases. In *Patterns in Physics*, vol. 2nd Edition, pp. 325-359. London: McGraw-Hill Book Company (UK) Ltd.

Bradfield, J. R. G. (1950). Biochemical aspects of cell morphology. *Proceedings of the Linnean Society of London* **162,** 76-81.

Bräunig, P. (1982a). The Peripheral and Central Nervous Organisation of the Locust Coxo-Trochanteral Joint. *Journal of Neurobiology* **13,** 413-433.

Bräunig, P. (1982b). Strand receptors with central cell bodies in the proximal leg joints of Orthopterous insects. *Cell and Tissue Research* **222,** 647-654.

Bräunig, P. (1983). Morphology and physiology of locust jumping leg proprioceptors and their influence on the leg motor system, Doctoral thesis. University of Konstanz.

Bräunig, P. (1985). Strand receptors associated with the femoral chordotonal organs of locust legs. *Journal of Experimental Biology* **116,** 331-341.

Bräunig, P. and Hustert, R. (1980). Proprioceptors with central cell bodies in insects. *Nature, London* **283,** 768-770.

Bräunig, P., Hustert, R. and Pflüger, H. J. (1981). Distribution and specific central projections of mechanoreceptor in the thorax and proximal leg joints of locusts. I. Morphology, location and innervation of internal proprioceptors of pro-and mesothorax and their central projections. *Cell and Tissue Research* **216**, 57-77.

Brewster, R. and Bodmer, R. (1995). Origin and specification of Type II sensory neurons in *Drosophila. Development* **121**, 2923-2936.

Brewster, R. and Bodmer, R. (1996). Cell lineage analysis of the Drosophila periferal nervous system. *Developmental Genetics*, **18,** 50-63.

Brown, R. H. J. (1967). Mechanism of locust jumping. *Nature*, **214,** 939.

Brown, M. C. and Stein, R. (1966). Quatitiative studies on the slowly adapting stretch receptor of the crayfish. *Kybernetik*, **3,** 175-181.

Brunet, P. C. J. and Coles, B. C. (1974). Tanned silks. *Proceedings of the Royal Society of London, Series B* **187,** 133-170.

Burke, R. E., Rudomin, P. and Zajac, F. E. (1970). Catch property in single mammalian motor units. *Science* **1968,** 122-124.

Burns, M. D. (1973). The control of walking in orthoptera. I. Leg movements in normal walking. *Journal of Experimental Biology* **58,** 45-58.

Burns, M. D. (1974). Structure and physiology of the locust femoral chordotonal organ. *Journal of Insect Physiology* **20,** 1319-1339.

Burns, M. D. and Usherwood, P. N. R. (1978). Mechanical properties of locust extensor tibiae muscles. *Comparative Biochemistry and Physiology*, **61A,** 85-95.

Burrows, M. (1979). Graded synaptic interactions between local premotor interneurones of the locust. *Journal of Neurophysiology* **42,** 1108-1123.

Burrows, M. (1985). The processing of mechanosensory information by spiking local interneurons in the locust. *Journal of Neurophysiology* **54,** 463-478.

Burrows, M. (1987a). Parallel processing of proprioceptive signals by spiking local interneurones and motor neurones in the locust. *The Journal of Neuroscience* **7,** 1064-1080.

Burrows, M. (1987b). Inhibitory interactions between spiking and nonspiking local interneurones in the locust. *Journal of Neuroscience* **7,** 3282-3292.

Burrows, M. (1988). Responses of spiking local interneurones in the locust to proprioceptive signals from the femoral chordotonal organ. *Journal of Comparative Physiology* **164,** 207-217.

Burrows, M. (1989). Effects of temperature on a central synapse between identified motor neurons in the locust. *Journal of Comparative Physiology* . A **165**, 687-695.

Burrows, M. (1996). The Neurobiology of an insect brain: Oxford University Press.

Burrows, M. and Horridge, G. A. (1974). The organisation of inputs to motoneurones of the locust metathoracic leg. *Philosophical Transactions of the Royal Society of London B. Biological Science* **269,** 49-94.

Burrows, M. and Laurent, G. J. (1989). Reflex circuits and the control of movement. In *The Computing Neuron* (ed. R. Durbin, C. Miall and G. Mitchison), pp. 244-261. New York: Addison-Wesley.

Burrows, M. and Laurent, G. (1993). Synaptic potentials in the central terminals of locust proprioceptive afferents generated by other

afferents from the same sense organ. *Journal of Neuroscience* **13,** 808-819.

Burrows, M., Laurent, G. J. and Field, L. H. (1988). Proprioceptive inputs to nonspiking local interneurones contribute to local reflexes of a locust hindleg. *The Journal of Neuroscience* **8,** 3085-3093.

Burrows, M. and Matheson, T. (1994). A presynaptic gain control mechanism among sensory neurons of a locust leg proprioceptor. *Journal of Neuroscience* **14,** 272-282.

Burrows, M. and Newland, P. L. (1993). Correlation between the receptive fields of locust interneurons, their dendritic morphology, and the central projections of mechanosensory neurons. *Journal of Comparative Physiology* **329,** 412-426.

Burrows, M. and Siegler, M. V. S. (1978). Graded syaptic transmission between local interneurones and motor neurones in the metathoracic ganglion of the locust. *Journal of Physiology. London* **285,** 231-255.

Burrows, M. and Siegler, M. V. S. (1982). Spiking local interneurons mediate local reflexes. *Science. Washinton DC* **217,** 650-652.

Burstein, A. H., Reilly, D. T. and Frankel, V. H. (1973). Failure characteristics of bone tissue. In *Perspectives in Biomedical Engineering* (ed. R. M. Kenedi), pp. 131-134. Baltimore: University Park Press.

Büschges, A. (1989). Processing of sensory input from the femoral chordotonal organ by spiking interneurones of stick insects. *Journal of Experimental Biology* **144,** 81-111.

Büschges, A. (1990). Nonspiking pathways in a joint-control loop of the stick insect *Carausius morosus*. *Journal of Experimental Biology* **151,** 133-160.

Büschges, A. (1994). The physiology of sensory cells in the ventral scoloparium of the stick insect femoral chordotonal organ. *Journal of Experimental Biology* **189,** 285-292.

Büschges, A., Kittmann, R. and Schmitz, J. (1994). Identified nonspiking interneurones in leg reflexes and during walking in the stick insect. *Journal of Comparative Physiology A. Sensory Neural and Behavioural Physiology* **174,** 685-700.

Büschges, A. and Schmitz, J. (1991). Nonspiking pathways antagonize the resistance reflex in the thoraco-coxal joint of stick insects. *Journal of Neurobiology* **22,** 224-237.

Büschges, A. and Wolf, H. (1995). Nonspiking local interneurones in insect leg motor control I. Common layout and species-specific response properties of femur-tibia joint control pathways in stick insect and locust. *Journal of Neurophysiology* **73,** 1843-1860.

Campbell, J. I. (1961). The anatomy of the nervous system of the mesothorax of *Locusta migratoria migratorioides* R. and F. *Proceedings of the Zoological Society of London* **137,** 403-432.

Carlson, S. D., Hilgers, S. L. and Juang, J. L. (1997). First developmental signs of the scolopale (glial) cell and neuron comprising the chordotonal organ the *Drosophila* embryo. *Glia* **19,** 269-274.

Cattaert, D., El Manira, A. and Clarac, F. (1992). Direct evidence for presynaptic inhibitory mechanisms in crayfish sensory afferents. *Journal of Neurophysiology* **67,** 610-624.

Chaplain, R. A., Michaelis, B. and Coenen, R. (1971). Systems analysis of biological receptors. I. Quanititative description of the input-output characteristics of the slowly-adapting stretch receptor on the crayfish. *Kybernetik* **9,** 85-95.

Chapman, K. M. and Duckrow, R. B. (1975). Compliance and sensitivity of a mechanoreceptor of the insect exoskeleton. *Journal of Comparative Physiology* **100,** 251-268.

Chapman, K. M., Mosinger, J. L. and Duckrow, R. B. (1979). The role of distributed viscoelastic coupling in sensory adaptation in an insect mechanoreceptor. *Journal of Comparative Physiology* **131,** 1-12.

Cleaveland, D. W., Lopata, M. A., MacDonald, R. J., Cowan, N. J., Rutter, W. J. and Kirschner, M. W. (1979). Number and evolutionary conservation of a- and b- tubulin and cytoplasmic b- and g- actin genes using specific cloned cDNA probes. *Cell* **20,** 95-105.

Cohen, M. J. (1964). The peripheral organization of sensory systems. In *Neural Theory and Modeling* (ed. R. F. Reiss). Stanford: Standford University Press.

Cohen, R. E., Hooley, C. J. and McCrum, N. G. (1976). Viscoelastic creep of collagenous tissue. *Journal of Biomechanics* **9,** 175-184.

Coillot, J. P. (1974). Analyse du codage d'un mouvement périodique par des récepteurs á l'étirement d'un insecte. *Journal of Insect Physiology* **20,** 1101-1116.

Coillot, J. P. (1975). La conversion analogique numérique des récepteurs á l'étirement de la patte métathoracique du criquet *Schistocerca gregaria. Journal of Insect Physiology* **21,** 423-433.

Coillot, J. P. and Boistel, J. (1968). Localisation et description de recepteurs a l'etirement au niveau de l'articulation tibio-femorale de la patte sauteuse du criquet, *Shistocerca gregaria. Journal of Insect Physiology* **14,** 1661-1667.

Coillot, J. P. and Boistel, J. (1969). Etude de l'activite electrique propagee de recepteurs a l'etirement de la patte metathoracique du criquet, *Shistocerca gregaria. Journal of Insect Physiology* **15,** 1449-1470.

Condic, M. L., Lefcort, F. and Bentley, D. (1989). Selective recognition between embryonic afferent neurons of grasshopper appendages *in vitro. Developmental Biology* **135,** 221-230.

Cote, R. H., Bergen, L. G. and Borisy, G. G. (1980). Microtubules and Microtubule Inhibitors (ed. M. Brabander and J. Mey), pp. 325-328. Amsterdam: Elsevier.

Crouau, Y. (1980). Comparison of a new structure associated with the membrane of 9+0 cilia of chordotonal sensilla with the central structure of motile cilia and flagella. *Biology of the Cell.* **39,** 349-52.

Cruse, H., Dean, J. and Suilmann, M. (1984). The contributions of diverse sense organs to the control of the leg movement by a walking insect. *Journal of Comparative Physiology A.* **154,** 695-705.

Dean, J. (1984). Control of leg protraction in the stick insect: a targeted movement showing compensation for externally applied forces. *Journal of Comparative Physiology [A]* **155,** 771-781.

Dean, J. and Schmitz, J. (1992). The two groups of sensilla in the ventral coxal hairplate of *Carausius morosus* have different roles during walking. *Physiological Entomology* **17,** 331-341.

Denny, M. W. (1976). The physical properties of spiders' silk and their role in the design of orb-webs. *Journal of Experimental Biology* **65,** 483-506.

Doolan, J. M. and Young, D. (1981). The organisation of the auditory organ of the bladder cicada, *Cystosoma saundersii. Philosophical Transactions of the Royal Society of London* **291,** 525-540.

Dorrington, K. L. (1980). The theory of viscoelasticity in biomaterials. In *The mechanical properties of biological materials (34th Symposium of the Society for Experimental Biology)* (ed. J. F. V.

Vincent and J. D. Currey), pp. 289-314. Cambridge: Cambridge University Press.

Driesang, R. B. and Büschges, A. (1993). The neural basis of catalepsy in the stick insect. IV. The role of nonspiking interneurones. *Journal of Comparative Physiology A. Sensory Neural and Behavioural Physiology* **173,** 445-454.

Edwards, J. S., Chen, S.-W. and Berns, M. W. (1981). Cercal sensory development following laser microlesions of embryonic apical cells in *Acheta domesticus*. *Journal of Neuroscience* **1,** 250-258.

Elliott, C. J. H. (1983). Wing hair plates in crickets: physiological characteristics and connections with stridulatory motor neurones. *Journal of Experimental Biology* **107,** 21-47.

Erler, G. (1983a). Reduction of mechanical sensitivity in an insect mechanoreceptor correlated with destruction of its tubular body. *Cell and Tissue Research* **234,** 451-61.

Erler, G. (1983b). Sensitivity of an insect mechanoreceptor after destruction of dendritic microtubules by means of vinblastine. *Cell and Tissue Research* **229,** 673-684.

Erler, G. and Thurm, U. (1978). Die Impulsantwort epithelialer Receptoren in Abhängigheit von der transepithelialen Potentialdiffernz. *Verh. Dtsch. Zool. Ges* **71,** 279.

Erler, G. and Thurm, U. (1981). Dendritic impulse intiation in an epithelial sensory neuron. *Journal of Comparative Physiology* **142,** 237-249.

Eyzaguirre, C. and Kuffler, S. W. (1955). Processes of excitation in the dendrites and in the soma of single isolated sensory nerve cells of the lobster and crayfish. *Journal of General Physiology* **39,** 87-119.

Farrell, K. W., Kassis, J. A. and Wilson, L. (1979). Outer doublet tubulin reassembly: Evidence for opposite end assembly-disassembly at steady state and disassembly end equilibrium. *Biochemistry* **18,** 2642-2647.

Farrell, K. W., Morse, A. and Wilson, L. (1979). Characterisation of the *in vitro* reassembly of tubulin derived from stable *Strongylocentrotus purpuratus* outer doubled microtubules. *Biochemistry* **18,** 905-911.

Field, L. H. (1991). Mechanism for range fractionation in chordotonal organs of *Locusta migratoria* (L) and *Valanga* sp. (Orthoptera : Acrididae). *International Journal of Morphology and Embryology* **20,** 25-39.

Field, L. H. and Burrows, M. (1982). Reflex effects of the femoral chordotonal organ upon leg motor neurones of the locust. *Journal of Experimental Biology* **101,** 265-285.

Field, L. H. and Coles, M. M. L. (1994). The position-dependent nature of postural resistance reflexes in the locust. *Journal of Experimental Biology* **188,** 65-88.

Field, L. H. and Pflüger, H. J. (1989). The femoral chordotonal organ: a bifunctional orthopteran (*Locusta migratoria)* sense organ? *Compartive Biochemical Physiology* **93A,** 729-743.

Field, L. H. and Rind, F. C. (1977). The function of the femoral chordotonal organ in the weta. *The New Zealand Medical Journal* **86,** 451.

Field, L. H. and Rind, F. C. (1981). A single insect chordotonal organ mediates inter- and intra-segmental leg reflexes. *Comparative Biochemistry and Physiology A. Comparative Physiology* **68a,** 99-102.

Finlayson, L. H. (1968). Proprioceptors in the invertebrates. *Symposium of the Zoological Society of London* **23,** 217-249.

Forssberg, H., Grillner, S. and Rossignol, S. (1975). Phase dependent reflex reversal during walking in chronic spinal cats. *Brain Research* **85,** 103-107.

French, A. S. (1984a). Action potential adaptation in the femoral tactile spine of the cockroach *Periplaneta americana. Journal of Comparative Physiology* **155,** 803-812.

French, A. S. (1984b). Dynamic properties of the action potential encoder in an insect mechanosensory neurone. *Biophysical Journal* **46,** 285-90.

French, A. S. (1984c). The receptor potential and adaptation in the cockroach tactile spine. *Journal of Neuronscience* **4,** 2063-2068.

French, A. S. (1987). Removal of rapid sensory adaptation from an insect mechanoreceptor neurone by oxidizing agents which affect sodium channel inactivation. *Journal of Comparative Physiology* **161,** 275-282.

French, A. S. (1988). Transduction mechanisms of mechanosensilla. *Annual Review of Entomology* **33,** 39-58.

French, A. S. and Sanders, E. J. (1979). The mechanism of sensory transduction in the sensilla of the trochanteral hair plate of the

cockroach, *Periplaneta americana*. *Cell and Tissue Research* **198,** 159-174.

Friedman, M. H. (1972a). A light and electron microscopic study of sensory organs and associatad structures in the foreleg tibia of the cricket, *Gryllus assimilis*. *Journal of Morphology* **138,** 263-328.

Friedman, M. H. (1972b). An electron microscopic study of the tympanal organ and associated structures in the foreleg tibia of the cricket, *Gryllus assimilis*. *Journal of Morphology* **138,** 329-348.

Füller, H. and Ernst, A. (1973). Die ultrastruktor der femoralen chordotonalorgane von *Carausius morosus*. *Zool. Jb. Anat. Bd.* **91,** 574-601.

Fung, Y. C. (1984). Structure and Stress-Strain Relationship of Soft Tissues. *American Zoologist* **24,** 13-22.

Gaffal, K. P. and Theiss, J. (1978). The tibial thread hairs of *Acheta domesticus* L. (Saltatoria, Gryllidae). *Zoomorphology* **90,** 41-51.

Gaffal, K. P., Tichy, H., Theiss, J. and Seelinger, G. (1975). Structural polarities in mechanosensitive sensilla and their influence on stimulus transmission (Arthropoda). *Zoomorphology* **82,** 79-103.

Gnatzy, W. (1976). The ultrastructure of the thread-hairs on the cerci of the cockroach *Periplaneta americana* L.: the intermoult phase. *Journal of Ultrastrucure Research* **54,** 124-134.

Gnatzy, W. and Tautz, J. (1980). Ultrastructure and mechanical properties of an insect mechanoreceptor: stimulus-transmitting structures and sensory apparatus of the cercal filiform hairs of *Gryllus*. *Cell Tissue Research* **213,** 441-463.

Gosline, J. M. (1971). Connective tissue mechanics of *Metridium senile*. *Journal of Experimental Biology* **55,** 775-795.

Gosline, J. M. (1980). The elastic properties of rubber-like proteins and highly extensible tissues. In *The mechanical properties of biological materials*, vol. Symposia of the society for Experimental Biology no. 34, pp. 331-358. Cambridge: University Press.

Gosline, J. M. and French, C. J. (1979). Dynamic mechanical properties of elastin. *Biopolymers* **18,** 2091-2103.

Gossard, J.-P., Cabelguen, J.-M. and Rossignol, S. (1990). Phase-dependent modulation of primary afferent depolarization in single cutaneous primary afferets evoked by peripheral stimulation during fictive locomotion in the cat. *Brain Research* **537,** 14-23.

Gotte, L., Mammi, M. and Pezzin, G. (1968). Some structural aspects of elastin revealed by X-ray diffraction and other physical methods. In *Symposium of fibrous proteins, Australia, 1967* (ed. W. G. Crewther), pp. 236-245. London: Butterworths.

Gray, E. G. (1959). Electron microscopy of collagen-like connective tissue fibrils of an insect. *Proceedings of the Royal Society of London* **150,** 233-239.

Gray, E. G. and Pumphrey, R. J. (1958). Ultra-structure of the insect ear. *Nature* **181,** 618.

Gray, J. A. B. (1959). Mechanical into electrical energy in certain mechanoreceptors. *Progress in Biophysics and Biophysical Chemistry* **9,** 285-324.

Grigg, P. and Greenspan, B. J. (1977). Response of primate joint afferent neurons to mechanical stimulation of knee joint. *Journal of Neurophysiology* **40,** 1-8.

Grosch, A., Callender, F., Petersen, M., Cokl, A. and Kalmring, K. (1985). Vibration receptors of larvae and of imagines in locusts: location on the legs, central projections and physiology. In *Acoustic and Vibrational Communication in Insects* (ed. Kalmring, K. and Elsner, N.), pp 151-161. Berlin, Hamburg: Paul Parey.

Gross, J. (1950). Connective tissue fine structure and some methods for its analysis. *Journal of Gerontology* **5,** 343-360.

Gross, J. (1963). Comparative biochemistry of collagen. In *Comparative Biochemistry*, vol. 5 (ed. M. Florkin and H. S. Mason), pp. 307-346: Academic Press (New York and London).

Grossberg, S. (1973). Contour enhancement, short term memory, and constancies in reverberating neural networks. In *Studies of Mind and Brain* (ed. S. Grossberg). Dordrecht, Holland: Reidel.

Hall, I. H. (1968). Deformation of Solids: Nelson, London.

Harkness, R. D. (1961). Biological functions of collagen.*Biol. Rev.* **36,** 399-463.

Hartenstein, V. (1988). Development of Drosophila larval sensory organs: spatiotemporal pattern of sensory neurones, peripheral pathways and sensilla differentiation. *Development* **102,** 869-886.

Hartman, H. B. and Boettiger, E. G. (1967). The functional organization of the propus-dactylus organ in *Cancer irroratus* Say. *Comparative Biochemistry and Physiology* **22,** 651-663.

Hartman, H. B. and Cooper, R. L. (1994). Regeneration and molting effects on a proprioceptor organ in the dungeness crab, *Cancer magister*. *Journal of Neurobiology* **25,** 461-471.

Hatsopoulos, N. G., Burrows, M. and Laurent, G. (1995). Hysteresis reduction in proprioception using presynaptic shunting inhibition. *Journal of Neurophysiology* **73,** 1031-1042.

Heitler, W. J. and Burrows, M. (1977a). The locust jump I. The motor programme. *Journal of Experimental Biology* **66,** 203-219.

Heitler, W. J. and Burrows, M. (1977b). The locust jump II. Neural circuits of the motor programme. *Journal of Experimental Biology* **66,** 221-241.

Hofmann, T. and Koch, U. T. (1985). Acceleration receptors in the femoral chordotonal organ in the stick insect, *Cuniculina impigra*. *Journal of Experimental Biology* **114,** 225-237.

Hofmann, T., Koch, U. T. and Bässler, U. (1985). Physiology of the femoral chordotonal organ in the stick insect, *Cuniculina impigra*. *Journal of Experimental Biology* **114,** 207-223.

Holwill, M. E. and Silvester, N. R. (1973). Mechanics and the properties of solids. In *Introduction to biological physics*. London, New York, Sydney, Toronto: John Wiley and sons.

Houk, J. (1967). A viscoelastic interaction which produces one component of adaptation in reponses of Golgi tendon organs. *Journal of Neurophysiology* **30,** 1482-1493.

Howse, P. E. (1968). The fine structure and functional organisation of chordotonal organs. *Symposium of the Zoological Society of London* **23,** 167-198.

Hubbard, S. J. (1958). A study of rapid mechanical events in a mechano-receptor. *Journal of Physiology* **141,** 198-218.

Hulsen, K. K. (1896). Specific gravity, resilience and strength of bone. *Bulletin of Biological Laboratories* **1,** 7-35.

Hustert, R. (1983). Proprioceptor responses and convergence of proproceptive influence on motorneruones in the mesothoracic thoraco-coxal joint of the locust. *Journal of Comparative Phsiology* **150,** 77-86.

Iizuka, E. (1965). Degree of crystallinity and modulus relationship of silk threads from *Bombyx mori* and other moths. *Biorheology* **3,** 1-8.

Jan, Y. N. and Jan, L. Y. (1993). The peripheral nervous system. In: *The Development of Drosophila melanogaster* (ed. Bate, M and Arias, A. M.), pp 1207-1244. New York, Cold Spring Harbor Laboratory Press. (1993).

Juang, J. L., Carlson, S. D. and Hilgers, S. L. (1996). Dipteran blood-brain barrier: Current findings, future prospects. In *International Congress of Entomology (20th; Florence, Italy): Taxonomy of Dermaptera*, vol. August 25-31, pp. 110. Tokyo: Seiroku Sakai.

Karnovsky, M. J. (1965). A formaldehyde-glutaraldahyde fixative of high osmalarity for use in electron microscopy. *Journal of Cell Science* **27,** 137A-138A.

Keech, M. K. (1961). The formation of fibrils from collagen solutions. IV. Effect of mucopolysaccharides and nucleic acids: An electron microscope study. *Journal of Biophysical and Biochemical Cytology*, **9,** 193.

Keil, T. (1978). Die Makrochaeten auf dem Thorax von *Calliphora vicina* Robineau-Desvoidy (Calliphoridae, Diptera). Feinstruktur und Morphogenese eines epidermalen Insekten-Mechanorezepters. *Zoomorphologie* **90,** 151-180.

Keil, T. A. (1984). Very tight contact of tormogen cell membrane and sensillum cuticle: ultrastructural basis for high electrical resistance between receptor lymph and subcuticular spaces in silk-moth olfactory hairs. *Tissue and Cell* **16,** 131-135.

Kemphues, K. J., Raff, R. A., Kaufman, T. C. and Raff, E. C. (1979). Mutation in a structural gene for a b-tubulin specific to testis in *Drosophila melanogaster. Proceedings of the National Acadamy of Sciences U.S.A.* **76,** 3991-3995.

Kennedy, T. E., Serafini, T., Torre, J. R. d. l. and Tessier-Lavigne, M. (1994). Netrins are diffusible chemotropic factors for commissural axons in the embryonic spinal chord. *Cell* **78,** 425-435.

Ker, R. F. S., University of Oxford, U.K. (1977). Some structural and mechanical properties of locust and beetle cuticle, University of Oxford, U.K. *Unpbl D. Phil. thesis* .

Kirschner, M. W. (1980). Implications of treadmilling for the stability and polarity of actin and tubulin polymers in vivo. *Journal of Cell Biology* **86,** 330-334.

Kittmann, R. and Schmitz, J. (1992). Functional specialization of the scoloparia of the femoral chordotonal organ in stick insects. *Journal of Experimental Biology* **173,** 91-108.

Klose, M. (1996). Development of leg chordotonal sensory organs in normal and heat-shocked embryos of the cricket *teleogryllus-commodus* (walker). *Rouxs Archives of Developmental Biology* **205,** 344-355.

Kondoh, Y., Okuma, J. and Newland, P. L. (1995). Dynamics of neurons controlling movements of a locust hind leg - wiener kernel analysis of the responses of proprioceptive afferents. *Journal of Neurophysiology* **73,** 1829-1842.

Kostyukov, A. I. and Cherkassky, V. L. (1992). Movement-dependent after-effects in the firing of the spindle endings from the de-efferented muscles of the cat hindlimb. *Neuroscience* **46,** 989-999.

Krnjevic, K. and van Gelder, N. M. (1961). Tension changes in crayfish stretch receptors. *Journal of Physiology* **149,** 310-325.

Küppers, J. and Thurm, U. (1979). Active ion transport by a sensory epithelium. I. Transepithelial short circuit current, potential difference, and their dependence on metabolism. *Journal of Comparative Physiology* **134,** 131-136.

Kuster, J. E., French, A. S. and Sanders, E. J. (1983). The effects of microtubule dissociating agents on the physiology and cytology of the sensory neuron in the femoral tactile spine of the cockroach, *Periplaneta americana* L. *Proceedings of the Royal Society of London* **219,** 397-412.

Laurent, G. (1986). Thoracic intersegmental interneurons in the locust with mechanoreceptive inputs from a leg. *Journal of Comparative Physiology A.* **159,** 171-186.

Laurent, G. and Burrows, M. (1988). A population of ascending intersegmental interneurones in the locust with mechanosensory inputs from a hind leg. *Journal of Comparative Neurology* **275,** 1-12.

Laurent, G. and Burrows, M. (1989a). Distribution of intersegmental inputs to nonspiking local interneurones and motor neurones in the locust. *Journal of Neuroscience* **9,** 3019-3029.

Laurent, G. and Burrows, M. (1989b). Intersegmental interneurones can control the gain of reflexes in adjacent legs of the locust by their

action on nonspiking local interneurones. *Journal of Neuroscience* **9,** 3030-3039.

Laverack, M. S. (1976). External proprioceptors. In *Structure and Function of Proprioceptors in the Invertebrates* (ed. P. J. Mill), pp. 1-63. London: Chapman and Hall.

Learoyd, B. M. and Taylor, M. G. (1966). Alterations with age in the viscoelastic properties of human arterial walls. *Circulation Research* **18,** 278-292.

Lee, J. C., Frigon, R. P. and Timasheff, S. N. (1973). The chemical characterisation of calf brain microtubule protein subunits. *Journal of Biological Chemistry* **248,** 7253-7262.

Leibrock, C. S., Marchand, A. R. and Barnes, W. J. P. (1996). Force dependent response reversal mediated by low-threshold and high-threshold afferents from the same mechanoreceptor in a crayfish leg. *Journal of Neurophysiology* **76,** 1540-1544.

Lennerstrand, G. (1968). Position and velocity sensitivity of muscle spindles in the cat. I. Primary and secondary endings deprived of fusimotor activation. *Acta Physiologica Scandinavica* **73,** 281-299.

Locke, M. and Huie, P. (1972). The fiber components of insect conective tissue. *Tissue and Cell* **4,** 601-612.

Locke, M. and Huie, P. (1975). Staining of the elastic fibers in insect connective tissue after tannic acid/ glutaraldehyde fixation. *Tissue and Cell* **7,** 211-216.

Loewenstein, W. R. and Mendelson, M. (1965). Components of receptor adaptation in a Pacinian corpuscle. *Journal of Physiology* **177,** 377-397.

Loewenstein, W. R. and Rathkamp, R. (1958). The sites for mechano-electric conversion in a Pacinian Corpuscle. *Journal of General Physiology* **41,** 1245-1265.

Loewenstein, W. R. and Skalak, R. (1966). Mechanial transmission in a Pacinian corpuscle. *Journal of Physiology* **182,** 346-378.

Lowe, C. A., Mill, P. J. and Knapp, M. F. (1973). The fine structure of the PD proprioceptor of *Cancer pagurus* II. The position sensitive cells. *Proceedings of the Royal Society of London B.* **184,** 199-205.

Luduena, R. F., E.M., S. and Wilson, L. (1977). Homogeneous glycogen synthetase b from rat liver. *Journal of Biological Chemistry* **252,** 7006-7014.

Lukoschus, F. (1962). Über bau und entwicklung des chordotonalorgans am tibia-tarsus-gelenk der honigbiene. *Z. Bienenforsch*, **6**, 48-52.

Macmillan, D. L., Field, L. H. and Oakley, J. K. (1980). The relationship between muscle tension and output in a crustacean meropodite-carpopodite chordotonal organ (MC1). *Comparative Biochemical Physiology* **68A**, 331-335.

Macmillan, D. L., Field, L. H. and Oakley, J. K. (1982). The relationship between muscle tension and output in a crustacean meropodite-carpopodite chordotonal organ (MC2). *Comparative Biochemical Physiology* **72A**, 579-581.

Maes, F. W. (1977). Simulaneous chemical and electrical stimulation of labellar tast hairs of the blowfly *Calliphora vicina. Jounal of Insect Physiology* **23**, 453-460.

Mallory, F. B. and Parker, F. (1927). Reticulum. *American Journal of Pathology* **3**, 515.

Margolis, R. L. (1981). Role of GTP hydrolysis in microtubule treadmilling and assembly. *Proceedings of the National Acadamy of Sciences U.S.A.* **78**, 1586-1590.

Margolis, R. L. and Wilson, L. (1981). Microtubule treadmills- possible molecular machinary. *Nature* **293**, 705-711.

Matheson, T. (1990). Responses and locations of neurones in the locust metathoracic femoral chordotonal organ. *Journal of Comparative Physiology* **166**, 915-927.

Matheson, T. (1992a). Morphology of the central projections of physiologically characterised neurones from the locust metathoracic femoral chordotonal organ. *Journal of Comparative Physiology* **170**, 101-120.

Matheson, T. (1992b). Range fractionation in the locust femoral chordotonal organ. *Journal of Comparative Physiology A* **170**, 509-520.

Matheson, T. (1997) Octopamine modulates the responses and presynaptic inhibition of proprioceptive sensory neurones in the locust *Schistocerca gregaria. The Journal of Experimental Biology* **200**, 1317-1325.

Matheson, T. and Field, L. H. (1990). Innervation of the metathoracic femoral chordotonal organ of *Locusta migratoria. Cell and Tissue Research* **259**, 551-560.

Matheson, T. and Field, L. (1995). An elaborate tension receptor system highlights sensory complexity in the hind leg of the locust. *The Journal of Experimental Biology* **198,** 1673-1689.

Matthews, K. A., Miller, D. F. B. and Kaufman, T. C. (1990). Functional implications of the unusual spatial distribution of a minor α-tubulin isotype in *Drosophila:* a common thread among chordotonal ligaments, developing muscle, and testis cyst cells. *Journal of Developmental Biology* **137,** 171-183.

Maxwell, J. C. (1868). On the dunamic theory of gases. *Philosophical Magazine* **35,** 129-145.

McCrum, N. G. and Dorrington, K. L. (1976). The bulk modulus of solvated elastin. *Journal of Materials Science* **11,** 1367-1368.

McIver, S. B. (1985). Mechanoreception. In *Comprehensive Insect Physiology, Biochemistry and Pharmacology,* vol. 6 (ed. G. A. Kerkut and L. I. Gilbert), pp. 71-132. Oxford: Pergamon.

Mckinney, R. L. (1930). The development of reticulum into collagenous fibres in cultures of adult rabbit lymph nodes. *Arch. f. exp. Zellforsch.* **9,** 14.

Medalia, A. I. (1970). Dynamic Shape Factors of Particles. *Powder Technology* **4,** 117-138.

Merton, P. A. (1951). The silent period of a muscle in the human hand. *Journal of Physiology* **114,** 183-198.

Meyhöfer, E. and Daniel, T. (1990). Dynamic mechanical properties of extensor muscle cells of the shrimp *Pandalus danae*: Cell design for escape locomotion. *Journal of Experimental Biology* **151,** 435-452.

Meyhöfer, E. (1993). Dynamic mechanical properties of passive single cardiac fibers from the crab Cancer magister. *Journal of Experimental Biology,* **185,** 207-249.

Mill, P. J. and Lowe, D. A. (1972). An analysis of the types of sensory unit present in the PD proprioceptor of decapod crustaceans. *Journal of Experimental Biology* **56.**

Mill, P. J. and Lowe, D. G. (1973). The fine structure of the PD proprioceptors of Cancer pagurus. 1. The receptor strand and the movement sensitive cells. *Proceedings of the Royal Society B* **174,** 179-197.

Moran, D. T. (1971). Loss of the sensory process of an insect receptor at ecdysis. *Nature* **234,** 476-477.

Moran, D. T. and Rowley, J. C. (1975). High voltage and scanning electron microscopy of the site of stimulus reception of an insect mechanoreceptor. *Jounal of Ultrastructure Research* **50,** 38-46.

Moran, D. T., Rowley, J. C. and Varela, F. G. (1975). Ultrasturcture of the grasshopper proximal femoral chordotonal organ. *Cell and Tissue Research* **161,** 445-457.

Moran, D. T., Rowley, J. C., Zill, S. N. and Varela, F. G. (1976). The mechanism of sensory transduction in a mechanoreceptor. Functional stages in campaniform sensilla during the moulting cycle. *Journal of Cell Biology* **71,** 832-47.

Moran, D. T. and Varela, F. (1971). Microtubules and sensory transduction. *Proceedings of the National Academy of Science USA* **68,** 757-760.

Moran, D. T., Varela, F. G. and Rowley, J. C. (1977). Evidence for active role of cilia in sensory transduction. *Proceedings of the National Academy of Sciences, USA.* **74,** 793-97.

Moulins, M. (1976). Ultrastructure of chordotonal organs. In *Structure and Function of Proprioceptors in the Invertebrates* (ed. P. J. Mill), pp. 387-426. London: Chapman and Hall.

Mücke, A. (1991). Innervation pattern and sensory supply of the midleg of *Schistocerca gregaria* (Insecta, Orthoptera). *Zoomorphology* **110,** 175-187.

Mücke, A. and Lakes-Harlan, R. (1995). Central projections of sensory cells of the midleg of the locust, *Schistocerca gregaria. Cell and Tissue Research* **280,** 391-400.

Mullins, L. (1980). Theories of rubber-like elasticity and the behaviour of filled rubbers. In *The mechanical properties of biological materials (34th Symposium of the Society for Experimental Biology)* (ed. J. F. K. Vincent and J. D. Currey), pp. 273-288. Cambridge: Cambridge University Press.

Nagayama, T. and Burrows, M. (1990). Input and output connection of an anteromedial group of spiking local interneurones in the metathoracic ganglion of the locust. *Journal of Neuroscience* **10,** 785-794.

Nagayama, T. and Newland, P. L. (1993). A sensory map based on velocity threshold of sensory neurones from a chordotonal organ in the

tailfan of the crayfish. *Journal of Comparative Physiology A* **172,** 7-15.

Nakajima, S. and Onodera, K. (1969). Adaptation of the generator potential in the crayfish stretch receptors under constant length and constant tension. *Journal of Physiology* **200,** 187-204.

Newland, P. L., Aonuma, H., Sato, M. and Nagayama, T. (1996). Presynaptic inhibition of exteroceptive afferents by proprioceptive afferents in the terminal abdominal ganglion of the crayfish. *Journal of Neurophysiology* **76,** 1047-1058.

Newland, P. L. and Kondoh, Y. (1997a). Dynamics of neurons controlling movements of a locust hind leg .2. Flexor tibiae motor neurons. *Journal of Neurophysiology* **77,** 1731-1746.

Newland, P. L. and Kondoh, Y. (1997b). Dynamics of neurons controlling movements of a locust hind leg .3. Extensor tibiae motor neurons. *Journal of Neurophysiology* **77,** 3297-3310.

Nishino, H. and Sakai, M. (1997). Three neural groups in the femoral chordotonal organ of the cricket *Gryllus bimaculatus*: central projections and soma arrangement and displacement during joint flexion. *Journal of Experimental Biology* **200,** 2583-2595.

Nowel, M. S., Shelton, P. M. J. and Stephen, R. O. (1995). Functional organisation of the metathoracic femoral chordotonal organ in the cricket *Acheta domesticus. The Journal of Experimental Biology* **198,** 1977-1988.

Okabe, M. and Okano, H. (1997). Two-step induction of chordotonal organ precursors in *Drosophila* embryogenesis. *Development*, **124(5),** 1045-1053.

Okuno, M. and Hiramoto, Y. (1979). Direct measurements of the stiffness of echinoderm sperm flagella. *Journal of Experimental Biology* **79,** 235-243.

Oldfield, B. P. and Hill, K. G. (1986). Functional organisation of insect auditory sensilla. *Journal of Comparative Physiology* **158.**

Orchard, I., Loughton, B. G. and Webb, R. A. (1981). Octopamine and short-term hyperlipaemia in the locust. *General And Comparative Endocrinology* **45,** 175-180.

Osborne, M. P. (1963). An electron microscope study of an abdominal stretch receptor of the cockroach. *Journal of Insect Physiology* **9,** 237-245.

Osborne, M. P. (1969). Structure and Function of Neuromuscular Junctions and Stretch Receptors. In *Symposia of the Royal Entomological Society of London: Number Five; Insect Ultrastructure* (ed. A. C. Neville), pp. 77-100. Oxford and Edinburgh: Blackwell Scientific Publications.

Pearson, K. G. and Fourtner, C. R. (1975). Nonspiking interneurones in the walking system of the cockroach. *Journal of Neurophysiology* **38,** 33-52.

Pearson, K. G., Stein, R. B. and Mulhotra, S. K. (1970). Properties of action potentials from insect motor nerve fibres. *Journal of Experimental Biology* **53,** 290-316.

Pease, D. C. and Quilliam, T. A. (1957). Electron microscopy of the Pacinian Corpuscle. *Journal of Biophysical and Biochemical Cytology* **3,** 331-342.

Pezzin, G. and Scandola, M. (1976). The low-temperature mechanical relaxation of elastin. I. The dry protein. *Biopolymers* **15,** 283-292.

Pflüger, H. J., Bräunig, P. and Hustert, R. (1988). The organisation of mechanosensory neuropiles in locust thoracic ganglia. *Philosophical Transactions of the Royal Society of London* **321,** 219-276.

Pflüger, H. J. and Burrows, M. (1987). A strand receptor with a central cell body synapses upon spiking local interneurones in the locust. *Journal of Comparative Physiolgy A* **160,** 295-304.

Phillips, C. E. (1981). An arthorpod muscle innervated by nine exitatory motor neurones. *Journal of Exponential Biology* **88,** 249-258.

Pipa, R. L. and Cook, E. F. (1958). The structure and histochemistry of the connective tissue of the sucking lice. *Journal of Morphology* **103,** 353-85.

Pipa, R. L., Cook, E. F. and Richards, A. G. (1959). Studies on the hexapod nervous system II. The histology of the thoracic ganglion of the adult cockroach, *Periplaneta americana. Journal of Comparative Neurology* **113,** 401-423.

Ponstingl, H., Krauhs, E., Little, M. and Kempf, T. (1981). Complete amino acid sequence of a-tubulin from porcine brain. *Proceedings of the National Acadamy of Sciences U.S.A.* **78,** 2757-2761.

Pringle, J. W. S. (1955). The function of the lyriform organs of archnids. *Journal of Experimental Biology* **32,** 270-278.

Pringle, J. W. S. and Wilson, V. J. (1951). The response of a sense organ to a harmonic stimulus. *Journal of Experimental Biology* **29,** 220-234.

Purali, N. (1997). Mechanisms of adaption in mechanoreceptor: a study of mechanical and ionic factors in the crayfish stretch receptors. Thesis, Karolinska Institute, Stockholm.

Purves, D. (1986). The trophic theory of neural connections. *Trends in Neuroscience* **9,** 486-489.

Purves, D. and Lichtman, J. W. (1985). Principles of neuronal development, pp. 433. Sunderland: Sinauer Associates.

Rice, M. J. (1975). Insect mechanoreceptor mechanisms. In *Sensory physiology and behaviour* (ed. R. Galun, P. Hillman, L. Parnas and R. Werman), pp. 135-165. New York, London: Plenum Press.

Rice, M. J., Galun, R. and Finlayson, L. H. (1973). Mechanotransduction in insect neurones. *Nature, new Biol.* **241,** 286-288.

Richards, A. G. and Schneider, D. (1958). Über den komplexen Bau der Membranen des Bindegewebes von Insekten. *Z. Naturf.* **13,** 680-687.

Rohrer, H. (1990). The role of growth factors in the control of neurogenesis. *European Journal of Neuroscience* **2,** 1005-1015.

Runion, H. I. and Usherwood, P. N. R. (1966). A new approach to neuromuscular analysis in the intact free-walking preparation. *Journal of Insect Physiology* **12,** 1255-1263.

Rydqvist, B., Swerup, C. and Lännergren, J. (1990). Viscoelastic properties of the slowly adapting stretch receptor muscle of the crayfish. *Acta Physiologica Scadinavica* **139,** 519-527.

Sauer, A. E., Buschges, A. and Stein, W. (1997). Role of presynaptic inputs to proprioceptive afferents in tuning sensorimotor pathways of an insect joint control network. *Journal of Neurobiology* **32,** 359-376.

Scandola, M. and Pezzin, G. (1978). The low-temperature mechanical relaxation of elastin. II. The solvated protein. *Biopolymers* **17,** 213-223.

Scharrer, B. C. J. (1939). The differentiation between neuroglia and connective tissue sheath in the cockroach *Periplaneta americana*. *Journal of Comparative Neurology* **70,** 77-88.

Schmidt, J. and Rathmayer, W. (1993). Central organisation of common inhibitory motorneurones in the locust: role of afferent signals

from leg mechanoreceptors. *Journal of Comparative Physiology A. Sensory Neural and Behavioural Physiology* **172,** 447-456.

Schmidt, K. (1969). Der Feinbau der stiftführenden Sinnesorgane im Pedicellus der Florfliege *Chrysopa* LEACH (Chrysopidae, Planipennia). *Z. Zellforsch* **99,** 357-388.

Schmidt, M. and Gnatzy, W. (1984). Are the funnel-canal organs the 'campaniform sensilla' of the shore crab, *Carcinus maenas* (Decapoda, Crustacea)? II. Ultrastructure. *Cell and Tissue Research* **237,** 81-93.

Schmitt, F. O., Gross, J. and Highberger, J. H. (1955). States of aggregation of collagen. *Symposium of the society of Experimental Biology* **9,** 148-162.

Schmitt, F. O., Hall, C. E. and Jakus, M. A. (1942). Electron microscope investigations of the structure of collagen. *Journal of Cellular and Comparative Physiology* **20,** 11-33.

Schmitz, J. (1986a). The depressor trochanteris motorneurones and their role in the coxo-trochanteral feedback loop in the stick insect *Carausius morosus*. *Biological Cybernetics* **55,** 24-34.

Schmitz, J. (1986b). Properties of the feedback system controlling the coxa-trochanter joint in the stick insect *Carausius morosus*. *Biological Cybernetics* **55,** 35-42.

Schmitz, J., Dean, J. and Kittmann, R. (1991). Central projections of leg sense organs in *Carausius morosus* (Insecta, Phasmida). *Zoomorphology* **111,** 19-33.

Segundo, J. P. and Diez Martinez, O. (1985). Dynamic and static hysteresis in crayfish stretch receptors. *Biological Cybernetics* **52,** 291-296.

Serafini, T., Kennedy, T. E., Galko, M. J., Mirzayan, C., Jessel, T. M. and Tessier-Lavigne, M. (1994). The netrins define a family of axon out-growth-promoting proteins homologous to *C. elegans* UNC-6. *Cell* **78,** 409-424.

Shapiro, S. S. and Wilk, M. B. (1965). An analysis of variance test for normality (complete samples). *Biometrika* **52,** 591-611.

Shapiro, S. S., Wilk, M. B. and Chen, H. J. (1968). A comparative study of various tests for normality. *Journal of American Statistical Association* **63,** 1343-1372.

Shelton, P. M. J., Stephen, R. O., Scott, J. J. A. and Tindall, A. R. (1992). The apodeme complex of the femoral chordotonal organ in the

metathoracic leg of the locust *Shistocerca gregaria. Journal of Experimental Biology* **163,** 345-358.

Shelton, R. G. J. and Laverack, M. S. (1968). Observations on a redescribed crustacean cuticular sense organ. *Comparative Biochemistry and Physiology* **25,** 1049-1059.

Siegler, M. V. S. (1981). Postural changes alter synaptic interactions between nonspiking interneurons and motor neurons of the locust. *Journal of Neurophysiology* **46,** 310-323.

Siegler, M. V. S. (1985). Nonspiking interneurones and motor control in insects. *Advances in Insect Physiology* **18,** 249-304.

Sillar, K. T. and Skorupski, P. (1986). Central input to primary afferent neurones in crayfish, *Pacifasticus leniusculus,* is correlated with rhythmic output of thoracic ganglia. *Journal of Neurophysiology* **55,** 678-688.

Slifer, E. H. (1935). Morphology and development of the femoral chordotonal organs of *Melanoplus differentialis* (Orthoptera, acrididae). *Journal of Morphology* **58,** 615-637.

Slifer, E. H. and Sekhon, S. S. (1975). The femoral chordotonal organs of a grasshopper Orthoptera, Acrididae. *Journal of Neurocytology* **4,** 419-438.

Smith, D. S. (1969). The fine structure of haltere sensilla in the blowfly, *Calliphora erythrocephala* (Meig.), with scanning electron microscopic observations on the haltere surface. *Tissue and Cell* **1,** 443-484.

Smith, D. S. and Treherne, J. E. (1963). Functional aspects of the organization of the insect nervous system. In *Advances in Insect Physiology,* vol. 1 (ed. J. W. L. Beament, J. E. Treherne and V. B. Wiggelsworth), pp. 401-478: Academic Press (London and New York).

Smith, D. S. and Wigglesworth, V. B. (1959). The occurrence of collagen in the perilemma of insect nerve. *Nature* **183,** 127-128.

Smith, J. F. H., Canham, P. B. and Starkey, J. (1981). Orientation of collagen in the tunica adventitia of the human cerebral artery measure with polarized light and the universal stage. *Jounal of Ultrastructure Research* **77,** 133-145.

Spinola, S. M. and Chapman, K. M. (1975). Proprioceptive indentation of the campaniform sensilla of cockroach legs. *Journal of Comparative Physiology* **96,** 257-272.

Sugawara, T. (1996). Chordotonal sensilla embedded in the epidermis of the soft integument of the cricket, *Teleogryllus commodus*. *Cell Tissue Research* **284,** 125-142.

Taghert, P. H., Bastiani, M. J., Ho, R. K. and Goodman, C. S. (1982). Guidance of pioneer growth cones: Filopodial contacts and coupling revealed with an antibody to Lucifer Yellow. *Developmental Biology* **94,** 391-399.

Tao-Cheng, Jung-Hwa, Kazushige Hirosawa and Yasuko Nakajima (1981). Ultrastructure of the crayfish stretch receptor in relation to its function. *Journal of Comparative Neurology* **200,** 1-22.

Tatar, G. (1976). Mechanische Sinnesorgane an den Berinen der Stabheuschrecke *Carausius morosus*. *Diplomarbeit, Universität Köln* .

Taylor, R. C. (1967). The anatomy and adequate stimulation of a chordotonal organ in the antennae of a hermit crab. *Comparative Biochemical Physiology* **20,** 709-717.

Terry, B. J. and Purich, D. L. (1980). Assembly and disassembly properties of microtubules formed in the prosence of GTP, 5'-Guanylyl Imidodiphosphate, and 5'-Guanylyl Methylenediphosphate. *Journal of Biological Chemistry* **255**.

Theophilidis, G. (1986a). The femoral chordotonal organs of *Decticus albifrons* (Orthoptera: Tettigoniidae)-I. Structure. *Comparative Biochemical Physiology* **84A,** 529-536.

Theophilidis, G. (1986b). The femoral chordotonal organs of *Decticus albifrons* (Orthoptera: Tettigoniidae)-II. Function. *Comparative Biochemical Physiology* **84A,** 537-543.

Theophilidis, G. and Burns, M. D. (1979). A muscle tension receptor in the locust leg. *Journal of Comparative Physiology* **131,** 247-254.

Thurm, U. (1964). Mechanoreception in the cuticle of the honey bee: fine structure and stimulus mechanism. *Science* **145,** 1063-1065.

Thurm, U. (1965). An insect mechanoreceptor. Part I : fine structure and adequate stimulus. *Cold Spring Harbor Symposia on Quantitative Biology* **30,** 75-82.

Thurm, U. (1981). Mechanoelectric transduction. *Biophysics of structure and mechanism* **7,** 245-246.

Thurm, U. (1982). Mechano-elektrische Transduktion. In *Biophysik* (ed. W. Hoppe, W. Lohmann, H. Markl and H. Ziegler), pp. 691-696. Berlin.

Thurm, U., Erler, G., Gödde, J., Kastrup, H., Keil, T., Völker, W. and Vohwinkel, B. (1983). Cilia specialized for mechanoreception. *Journal of Submicroscopic Cytology* **15,** 151-155.

Thurm, U. and Küppers, J. (1980). Epithelial Physiology Of Insect Sensilla. In *Insect Biology In The Future* (ed. L. M. and S. D.), pp. 735-764. New York: Academic Press.

Thurm, U. and Wessel, G. (1979). Metabolism-dependent transepithelial potential differences at epidermal receptors of arthropods. *Journal of Comparative Physiology* **134,** 119-130.

Toh, Y. and Yokohari, F. (1985). Structure of the Antennal Chordotonal Sensilla of the Americal Cockroach. *Journal of Ultrastructure Research* **90,** 124-134.

Tonna, E. A. and Hatzel, G. (1967). Any changes in the distribution of connective tissue elements in human material studied with polerized light microscopy. *Journal of Gerontology* **22,** 281.

Usherwood, P. N. R., Runion, H. I. and Campbell, J. I. (1968). Structure and physiology of a chordotonal organ in the locust leg. *Journal of Experimental Biology* **48,** 305-323.

Valenzuela, P., Quiroga, M., Zaldivar, J., Rutter, W. J., Kirschner, M. W. and Cleveland, D. W. (1981). Nucleotide and corresponding amino acid sequences encoded by a and b tubulin mRNAs. *Nature* **289,** 650-655.

Varella, F. J., Rowley, J. C. I. and D.T., M. (1977). The control of ciliary movements; an application of the cusp catastrophe. *Journal of Theoretical Biology* **65,** 531-553.

Vidal, J., Jeannerod, M., Lifschitz, W., Levitan, H., Rosenberg, J. and Segundo, J. P. (1971). Static and dynamic properties of gravity-sensitive receptors in the cat vestibular system. *Kybernetik* **9,** 205-215.

Vincent, J. F. V. (1976). Design for living- the elastic-sided locust. In *The insect integument* (ed. H. R. Hepburn). Amsterdam: Elsevier.

Vincent, J. F. V. (1980). Insect Cuticle: A paradigm for natural composites. In *The mechanical properties of biological materials (34th Symposium of the Society for Experimental Biology)* (ed. J. F. V. Vincent and J. D. Currey). Cambridge: Cambridge University Press.

Wainwright, S. A., Biggs, W. D., Currey, J. D. and Gosline, J. M. (1976). Mechanical design in organisms. London: Edward Arnold Ltd.

Wales, W., Clarac, F., Dando, M. R. and Laverack, M. S. (1970). Innervation of the receptors present at the various joints of the pereiopods and third maxilliped of *Homarus gammarus* (L.) and other macruran decapods (crustacea). *Z. vergl. Physiologie* **68,** 345-384.

Wales, W., Clarac, F. and Laverack, M. S. (1971). Stress detection at the autotomy plane in decapod crustacea. 1. Comparative anatomy of the receptors of the basi-ischiopodite region. *Zeitschrift für vergleichende Physiologie* **73,** 357-382.

Warner, F. D. and Satir, P. (1974). The structural basis of cilliary bend formation. *Journal of Cell Biology* **63,** 35-63.

Weber, W. (1835). Über die Elasticität der Seidenfäden. *Annalen der Physik und Chemie* **34,** 247-257.

Weber, W. (1841). Über die Elasticität fester Körper. *Annalen der Physik und Chemie* **54,** 1-18.

Wensler, R. J. (1977). The fine structure of distal receptors on the labium of the aphid, *Brevicoryne brassicae* L, (Homoptera). Implications for current theories of sensory transductions. *Cell and Tissue Research* **181,** 409-422.

Whitear, M. (1962). The fine structure of crustacean proprioceptors. 1. The chordotonal organs in the legs of the shore crab, *Carcinus maenas*. *Philosophical Transactions of the Royal Society, London [B]* **245,** 291-325.

Whitten, J. M. (1962). Breakdown and formation of connective tissue in the pupal stage of an insect. *Quarterly Journal of Microscopical Science* **103,** 359-356.

Whitten, J. M. (1964). Connective tissue membranes and their apparent role in transporting neurosecretory and other secretory products in insects. *General Comparative Endocrinology* **4,** 176-192.

Wiechert, E. (1893). Gesetze der elastischen Nachwirkung für constante Temperatur. *Annalen der Physik und Chemie,* **50,** 335-348; 546-570.

Wiederhold, M. L. (1976). Mechanotransduction in sensory and motile cilia. *Annual Review of Biophysics and Bioengineering* **5,** 39-62.

Williamson, R. and Burns, M. D. (1978). Multiterminal receptors in the locust mesothoracic leg. *Journal of Insect Physiology* **24,** 661-666.

Wilson, D. M. and Larimer, J. L. (1968). The catch property of ordinary muscle. *Proceedings of the National Acadamy of Science* **61,** 909-916.

Wilson, V. J. and Peterson, B. W. (1980). The role of the vestibular system in posture and movement. In *Medical Physiology*, vol. 1 (ed. V. B. Mountcastle), pp. 813-836: The C. V. Mosby Company.

Wolf, H. and Burrows, M. (1995). Proprioceptive sensory neurons of a locust leg receive rhythmic presynaptic inhibition during walking. *Journal of Neuroscience* **15,** 5623-5636.

Wolf, H. and Büschges, A. (1995). Nonspiking local interneurones in insect leg motor control. II. Role of nonspiking local interneurons in the control of leg swing during walking. *Journal of Neurophysiology* **73,** 1861-1875.

Wolfrum, U. (1990). Actin filaments: the main components of the scolopale in insect sensila. *Cell and Tissue Research* **261,** 85-96.

Wolfrum, U. (1991a). Centrin- and α-actinin-like immunoreactivity in the ciliary rootlets of insect sensilla. *Cell and Tissue Research* **266,** 231-238.

Wolfrum, U. (1991b). Tropomyosin is co-localised with the actin filaments of the scolopale in insect sensilla. *Cell and Tissue Research* **265,** 11-17.

Wolman, M. (1970). On the use of Polerised Light in Pathology. *Pathology Annual* . **5,** 381-416.

Wright, B. R. (1976). Limb and wing receptors in insects, chelicerates and myriapods. In *Structure and Function of Proprioceptors in the Invertebrates* (ed. P. J. Mill), pp. 323-386. London: Chapman and Hall.

Yack, J. E. and Roots, B. I. (1992). The metethoracic wing-hinge chordotonal organ of an atympanate moth, *Actias luna* (Lepidoptera, Saturniidae): a light- and electron-microscopic study. *Cell and Tissue Research* **267,** 455-471.

Yokoo, S. (1952). The compression test upon the diaphysis and the compact substance of the long bone of human extremities. *Journal Kyoto Prefecture Medical University* **51,** 291-313.

Young, D. (1970). The structure and function of a connective chordotonal organ in the cockroach leg. *Philosophical Transactions of the Royal Society of London* **256,** 401-428.

Zar, J. H. (1984). Biostatistical Analysis. New Jersey: Prentice Hall.

Zener, C. (1948). Elasticity and Anelasticity of Metals: The University of Chicago Press.

Zill, S. N. (1985a). Plasticity and proprioception in insects. I. reponses and cellular properties of individual receptors of the locust metathoracic femoral chordotonal organ. *Journal of Experimental Biology* **116,** 435-461.

Zill, S. N. (1985b). Plasticity and proprioception in insects. II. Modes of reflex action in the locust metathoracic chordotonal organ. *Journal of Experimental Biology* **116,** 463-480.

Zill, S. N. (1987). Selective mechanical stimulation of an identified proprioceptor in freely moving locusts: role of resistance reflexes in active posture. *Brain Research* **417,** 195-198.

Zill, S. N. and Jepson-Innes, K. (1988). Evolutionary adaption of a reflex system: sensory hysteresis counters 'catch' tension. *Journal of Comparative Physiology A* **164,** 43-48.

Zill, S. N. and Jepson-Innes, K. (1990). Functions of a proprioceptive sense organ in freely moving insects - characteristics of reflexes elicited by stimulation of the locust metathoracic femoral chordotonal organ. *Brain Research* **523**, 211-218.